REMOTE SENSING OF CRITERIA AND NON-CRITERIA POLLUTANTS EMITTED IN THE EXHAUST OF ON-ROAD VEHICLES

Marc M. Baum[1], Eileen S. Kiyomiya[1], Sasi Kumar[1], Anastasios M. Lappas[1], and Harry C. Lord III[2].
[1]Department of Chemistry, Oak Crest Institute of Science, 13300 Brooks Dr, Suite B, Baldwin Park, CA 91706, [2]Air Instruments & Measurements, Inc, 13300 Brooks Dr, Suite A, Baldwin Park, CA 91706

INTRODUCTION

Emissions from mobile sources are well known to play a central rolc in urban air pollution (photochemical smog formation, violation of CO and ozone O_3 standards, and aerosol formation). The Clean Air Act Amendments of 1990 call for auto makers to reduce tailpipe emissions of hydrocarbons and nitrogen oxides by 35 % and 60 % respectively. CO emission standards of no more than 10 g mi^{-1} for light duty motor vehicles have also been set. Additional emission reductions for all three pollutants have been scheduled for the early 2000s. Data collected from remote sensing studies of large fleets of in-use vehicles indicate that approximately half of CO, hydrocarbon (THC), and NO emissions are generated by less than 10% of vehicles. Moreover, remote sensing data suggest that fleet dynamometer testing significantly underestimates tailpipe emissions, and contribute to errors in model predictions (e.g., U.S. EPA's MOBILE4). A knowledge of the chemical composition of the exhaust plume emitted by on-road vehicles on a car-by-car basis therefore is essential when developing effective pollution abatement strategies, and in helping meet Clean Air Act objectives.

EXPERIMENTAL

A remote sensor incorporating UV-vis and IR spectrometers in conjunction with an innovative optical design has been developed. The instrument was used to non-invasively measure over 20 pollutants in the exhaust of 19 in-use vehicles powered by a range of fuels – reformulated Phase II gasoline, diesel, compressed natural gas, and methanol blended with 15% gasoline. CO_2, CO, aldehydes, aliphatic and speciated aromatic hydrocarbons were identified along with NO_x, determined as the sum of NO, NO_2; N_2O and HONO was also measured, although their levels were typically below the instrument's detection limit.

RESULTS AND DISCUSSION

The results are summarized in Table 1 below.

Table 1. Effect of fuel type on vehicle exhaust emissions.

Fuel	$[HC]_{mean}$ (ppm)	$[CO]_{mean}$ (%)	$[NO]_{mean}$ (ppm)	$[NH_3]_{mean}$ (ppm)
Gasoline	126.5	1.92	475.6	317.0
Diesel	50.1	0	934.6	0.0
CNG	55.8	0.34	2041.3	12.1
M-85	25.5[§]	2.01	0.0	438.5

[§]Measured as methanol.

NH_3 levels in vehicle exhaust are reported for the first time on a car-by-car basis. The exhaust from gasoline- and methanol-powered cars was found to contain elevated levels of NH_3, in some cases over 1000 ppm, despite near stoichiometric air-to-fuel ratios, and were often significantly higher than corresponding NO levels. Catalyst efficiency is discussed as a function of NH_3 and NO concentrations in the exhaust of vehicles operating "cold" and "hot". In some of the tested vehicles, the three-way catalysts showed high reduction activity, but poor selectivity resulting in the formation of NH_3, and possibly other nitrogen-containing products other than N_2.

Remote sensing was also performed on the exhaust emissions from over 2,100 vehicles as they drove up a freeway on-ramp. Criteria pollutants, CO, THC, and NO, were found to follow a γ-distribution and agreed with data from previous remote sensing studies using a different technology; over half the total pollutant emissions are from 10 % of the fleet. Optical densities of the two principal aromatic hydrocarbon components of gasoline, toluene and xylene, were found to correlate well with THC measurements (Fig. 1), despite the fact that the measurements were made by different techniques; UV (aromatics) and IR (THC) absorption spectroscopy.

Figure 1.

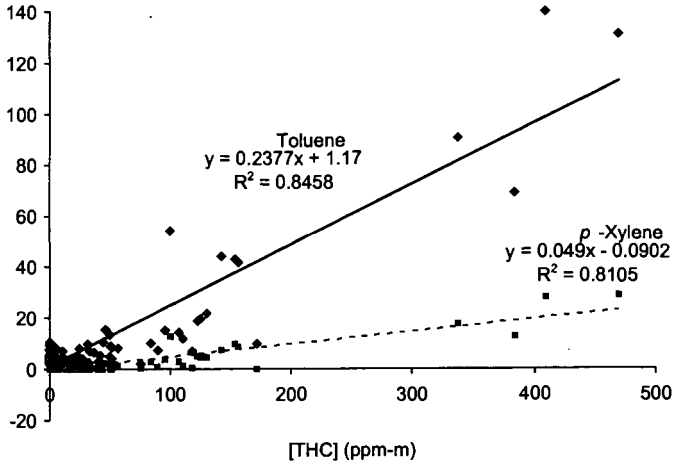

Note: concentrations are shown as column densities, not as levels in undiluted exhaust.

Emission rates of CO, THC, NO, toluene and xylene are shown in Table 2 below.

Table 2.

Pollutant X	Mean [X]/[CO_2]	Max. (ppm)	E_m (mg/km)
NO	0.00381	4963	940
NH_3	0.00056	3934	138
Toluene	0.00018	1620	44†
p-Xylene	0.000037	350	9†

†Based on relationship to THC emissions.

Figure 2.

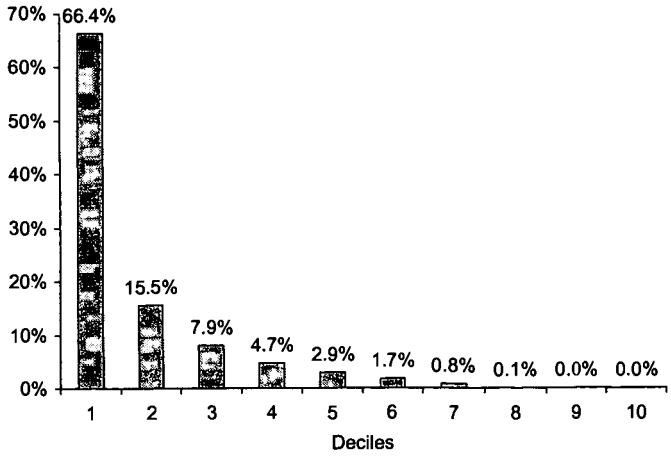

SUMMARY AND CONCLUSIONS

For the first time, remote sensing was used to measure NH_3 directly in the exhaust plume emitted by on-road vehicles. It was shown that 66.4 % of the emitted NH_3 was produced by 10 % of the fleet as illustrated by the decile plot given in Figure 2; the first decile represents the fraction of the total analyte produced by the 10 % dirtiest fraction of the measured vehicle fleet, and so on.

Mean NH_3 emission rates were calculated at 138 mg km^{-1}, nearly twice as high as previous estimates. However, it is expected that NH_3 generation in three-way catalysts is highly dependent on driving conditions and, therefore, NH_3 emission rates will probably vary as a function of the remote sensing test site. These observations could have significant implications on the formation of ammonium nitrate aerosol and on the acid-neutralizing capacity of urban air masses and NH3 emissions from motor vehicles may need to addressed in future amendments of the Clean Air Act.

ACKNOWLEDGEMENTS

We would like to acknowledge cooperation of the Gas Company and Rio Hondo in supplying us with natural gas-powered test vehicles and support, as well as CalTrans for issuing a permit in haste.

This research was supported by the South Coast Air Quality Management District under contract No. AB2766/96028. We gratefully acknowledge the valuable assistance provided by this program, as well as the loan of the M85 vehicle.

The statement and conclusions in this paper are those of the contractor and not necessarily those of the Mobile Source Air Pollution Review Committee (MSRC) or the South Coast Air Quality Management District (SCAQMD). The mention of commercial products, their sources or their uses in connection with material reported herein is not to be construed as either an actual or implied endorsement of such products.

CHARACTERIZATION OF FLY ASH CARBONS DERIVED DUE TO THE IMPLEMENTATION OF NOx CLEAN AIR ACT AMENDMENTS

M. Mercedes Maroto-Valer[1], Darrell N. Taulbee[2] and James C. Hower[2]

[1]The Energy Institute, The Pennsylvania State University,
405 Academic Activities Building, University Park, PA-16802
[2]University of Kentucky - Center for Applied Energy Research, 2540 Research Park Drive,
Lexington, KY-40511

Keywords: NOx Clean Air Act Amendments, fly ash carbons, properties.

One of the more extensively used approaches for meeting the Title IV of the 1990 Clean Air Act Phase-I has been the installation of low-NOx burners. Although these technologies have been proven effective in reducing NOx emissions, they have also resulted in an increase in the concentration of unburned carbon in the fly ash. This has restricted the principal use of ash in the cement industry, since the unburned carbon tends to adsorb the air-entrainment admixtures (AEAs), that are added to the cement to prevent crack formation and propagation. However, very little is known about the properties of fly ash carbons and any information regarding their properties is watched closely by the utility industry. Accordingly, the work reported here represents the first characterization of the bulk properties of unburned carbon concentrates that have been isolated to purities up to 86% by using density gradient centrifugation. The density of like carbon forms isolated from two fly ashes appears to be quite similar, regardless of the source of the fly ash. The H/C atomic ratios are ~ 0.028-0.016, indicating a high degree of condensation. The BET surface areas are relatively low, ranging from 10 to 60 m^2/g, and most of the pores are in the mesopore range (2-50 nm in width). For both series of fly ash samples, the surface area was found to increase linearly with increasing particle density.

INTRODUCTION

The Environmental Protection Agency (EPA) issued, under Title IV of the 1990 Clean Air Act Amendment, a two-phase strategy to reduce NOx emissions from coal-fired utility boilers. Phase I took effect on January 1996 and promulgated that emissions levels from Group-1 boilers should be reduced by over 400,000 tons/year between 1996-1999 [1]. Group-1 is formed by dry-bottom wall-fired boilers and tangentially fired boilers and their emissions levels were reduced to 0.50 and 0.45 lb NOx / MM Btu, respectively. Phase II, that began last January, will achieve an additional reduction of ~ 900,000 tons of NOx annually. Phase II has lowered the emission levels for Group-1 boilers to 0.46 - 0.40 lb NOx / MM Btu, and established limits for Group-2 boilers, that include cell, cyclones, wet bottoms and vertically fired boilers to levels down to 0.68, 0.86, 0.84, and 0.80 lb NOx / MM Btu, respectively [2]. Nevertheless, Phase II regulation has been dormant during a litigation process that was originated by eight upwind states and a number of utilities, that sued EPA's authority to issue the rule [3]. However, a federal appeals court has recently upheld EPA's rule and the administration has requested to reactivate the rule. It is expected that facilities in 19 states could be affected by the implementation of this regulation.

One of the more extensively used approaches for meeting the Title IV of the 1990 Clean Air Act Phase-I has been the retrofitting of several hundred existing boilers with low-NOx burners. Furthermore, EPA has projected that around 85-90% of the boilers in both Group-1 and 2 could meet the required NOx reduction levels by installing low-NOx burners [2], leaving other technologies, such as Selective Catalytic Reduction (SCR) and Selective Non-Catalytic Reduction (SNCR) suitable complimentary approaches to meet the required NOx reduction levels. The installation of low-NOx burners changes the flame-temperature profile as well as the flame chemistry since, in essence, a hot oxygen-rich flame is replaced by a cooler and longer, fuel-rich flame. While these modifications have proven effective in reducing NOx emissions, they have also resulted in a lower combustion efficiency, leading to an increase in the concentration of unburned carbon in the fly ash [4]. Although the unburned carbon is known to preclude the use of fly ash in the cement industry, very little is known about the properties of this material and any information regarding its properties is watched closely by the utility industry.

It is generally known that the ASTM LOI specification is not sufficient to identify the suitability of a fly ash for the cement industry, since this criterion only gives a rough approximation to the carbon content of a sample and does not directly correlate with the capacity to adsorb air entrainment admixtures (AEAs), that are added to the cement to prevent crack formation and propagation [5,6]. In fact, prior petrographic examinations of a number of high-carbon fly ashes have shown that the unburned carbon is not visually uniform [7]. Three microscopically distinct carbon types have been identified: (i) inertinite particles, which appear to have been entrained from the combustor prior to melting or combustion; (ii) isotropic coke; and (iii) anisotropic coke, the latter two being extensively reacted particles, which appear to have passed through a molten stage [7,8]. The above particle types can be further subdivided according to particle shape, pore volume and wall thickness [9]. Although several studies have been conducted on the characterization of

whole fly ash samples [5,6], very little is known about the relative properties of the three carbon types, as their isolation is not a trivial task. For example, it is not known whether a fly ash that contains mainly inertinite has the same capacity to absorb air entrainment agents as an otherwise equivalent fly ash containing predominantly isotropic carbon. If in fact the capacity to absorb air entrainment agents varies substantially for the differing forms of unburned carbon, it may be possible to establish a criterion based on the relative properties of the differing carbon types to identify suitable fly ashes for the cement industry, regardless of their LOI value. Accordingly, this work presents the first characterization of these differing forms of unburned carbon, that have been previously separated by Density Gradient Centrifugation (DGC). The authors have successfully developed a method to isolate the three differing forms of unburned carbon [10,11]. The methodology used includes a preliminary triboelectrostatic enrichment or acid digestion, followed by DGC with a high-density lithium polytungstate media (2.85 g cm^{-3} max). Two fly ashes, identified as Dale and WEPCO, obtained from different power plants, were separated by the above procedure. In this work, the highest purity fractions from these separations were extensively analyzed by several analytical techniques, including elemental and surface area analyses.

EXPERIMENTAL

Two fly ashes, identified as Dale and WEPCO, were examined in this study. For the Dale sample, approximately 12 kg of fly ash were collected from the mechanical precipitators of a 70 MW boiler (Dale unit #3) operated by Eastern Kentucky Power. The WEPCO (Wisconsin Electric Power Co.) sample was collected from the electrostatic precipitators of a 136 MW unit at Valley Power Station. A series of preliminary enrichments were conducted to increase the amount of carbon in the ash and thereby, minimize the number of DGC runs. These steps included an initial screening of the sample with a 140 mesh sieve (106 μm), with the 140+ fraction being triboelectrostatically separated to obtain a sample (Dale-TES) with an inorganic matter content below 10 %. This carbon-enriched fraction was then used as the feed for subsequent DGC separations. The WEPCO (Wisconsin Electric Power Co.) sample was processed directly through the triboelectrostatic separator without the initial screening step. Again, the carbon-enriched fraction (WEPCO-TES) was used as the feed material in a subsequent DGC separation, using a lithium heterolpolytungstate high-density media. Details of the DGC separation procedure can be found elsewhere [10, 11].

Petrographic analyses of the fly ash parent samples and DGC fractions were performed on epoxy-bound polished pellets using oil-immersion objectives at a final magnification of 500-625x. The elemental analyses were carried out on a Leco CHN-600 analyzer. The porosity of the samples was determined via N_2 adsorption isotherms at 77K using a Quantachrome adsorption apparatus, Autosorb-1 Model ASIT. The BET surface areas were calculated using the adsorption points at the relative pressures (P/Po) 0.05 - 0.25. The values reported were corrected to a mineral-free basis using the 6 m^2/g surface area measured for the 2.5 g cm^{-3} density fraction of the fly ash and the TGA-derived inorganic contents for the respective density fractions [11]. The total pore volume, V_{TOT}, was calculated from the amount of vapor adsorbed at the relative pressure of 0.95. The mesopore (pores 2-50 nm in width) volume was calculated using the BJH equation.

RESULTS AND DISCUSSION

Purities and densities of the fraction separated by DGC The petrographic data for the Dale and WEPCO parent samples and the carbon-enriched DGC feed samples (Dale-TES and WEPCO-TES) are presented in Table 1 on a volume % basis. The parent Dale fly ash contained approximately 64% glass, while its -140 fraction had ~91% glass. The glass content was reduced to ~ 59% in the +140 mesh fraction and to less than 10% following the triboeletrostatic separation. The predominant carbon type is anisotropic coke. The relative proportions of the three carbon types in the parent and the beneficiated Dale samples are very similar, with the exception of a slight reduction in inertinites in the +140 fraction and resultant subsamples. However, even these minor changes were not statistically significant as they stay within the experimental error of the petrographic measurements (±5%). The WEPCO sample was selected for this study for two reasons. First, to determine if like carbon forms exhibited the same densities regardless of the source of the fly ash. Second, the WEPCO sample contained a higher proportion of isotropic relative to anisotropic coke, which, assuming like carbon forms do in fact have the same density, should be reflected by the weight recovery curve. For the WEPCO sample, a similar reduction in the glass content was observed after the triboeletrostatic separation, going from ~ 60% to ~ 10% (Table 1). The predominant carbon form in the WEPCO sample is isotropic coke. However, there seems to be somewhat higher beneficiation of the anisotropic carbon, compared to the other carbon types, during the triboelectrostatic separation. Nevertheless, this difference stays within the experimental error. Whether triboelectrostatic separations truly discriminate certain carbon types has not been fully investigated.

Figure 1 shows the petrographic composition for all the density fractions recovered for the WEPCO-TES fractions. The highest enrichment is for inertinites (densities < 1.60 g cm^{-3} with purity of ~85%) and is similar to that found for Dale-TES. Isotropic coke particles partitioned predominantly at densities ~ 1.725-1.750 g cm^{-3}, similar to the Dale-TES sample, but presented higher purities (79% cf. 72%), due in part to the higher proportion of isotropic carbon present in the parent sample, as well as the smaller particle size and lower frequency of mixed particles. Anisotropic coke particles maximized at similar densities and purities to those observed for the Dale separations. The higher density fractions are dominated by inorganic particles, with spinel being the most dense mineral. This is consistent with the values reported for spinel and glass minerals, where the former has a specific gravity of 3.55 g cm^{-3}, while the latter is ~ 2.50 g cm^{-3}. Previous centrifugal separations have also reported a higher partition of non-glassy particles, consisting primarily of iron oxides, at densities > 2.40 g cm^{-3} [12, 13].

The petrographic analysis of the three highest purity carbon-type fractions from each separation along with the density range over which these highest purity fractions were recovered are also shown in Table 1. After DGC separation, enrichments ranged up to 85.5 vol% inertinite in the WEPCO separation, up to 78.5 vol% isotropic coke for the WEPCO separation, and up to 76 vol% anisotropic coke in the Dale and WEPCO carbon-enriched separations (Table 1). Note that the differences in the fraction number in which the highest purities were obtained for the three separations is due to changes made in the cut-point densities for the three separations and not necessarily to differences in particle density. Maximum purities were obtained at similar densities for both samples. That is, inertinite purity maximizes in the lowest density fractions (<1.65 g cm^{-3}), isotropic-coke purity maximizes between 1.72 and 1.78 g cm^{-3}, and anisotropic-coke purity maximizes between 1.88 and 1.94 g cm^{-3}. Thus, these data indicate that the density of the three unburned carbon types to be similar in these two fly ash samples despite the differences in the starting coal or the utility combustor from which they were derived.

Elemental analyses and atomic ratios CHN analyses were carried out only on the Dale carbon-enriched separation samples. The results of these analyses conducted on the DGC feed and selected higher-purity carbon-type fractions are shown in Table 2. The elemental analyses show that the three types of unburned carbon consist primarily of C, while the H content is below 0.23. The H/C atomic ratios range between 0.028 to 0.016, indicating a high degree of condensation. Any trends that may be present in the hydrogen data and atomic H/C ratios are masked by the error of the analysis stemming from the very low hydrogen concentrations coupled with potential interferences from adsorbed moisture. However, there does appear to be a correlation between nitrogen concentration and carbon type (or fraction density), where higher nitrogen concentrations and N/C atomic ratios are associated with increasing density. In addition, there also appears to be a higher level of oxygen in the isotropic coke particles (fraction nos. 5 and 6). FT-IR spectra were conducted on selected density fractions in an effort to determine if the isotropic-rich fractions were measurably greater in carbonyl (C=O) functional groups, the only oxygen functionality to which infra-red analysis would be sufficiently sensitive to detect, but these analysis were inconclusive. Nevertheless, similar trend has been found previously by other authors, where fly ashes with predominant isotropic coke presented higher oxygen levels than ashes with predominantly anisotropic coke [5]. In this previous study, diffuse reflectance FT-IR was also used, but again this technique did not detect carbonyl functional groups, implying that the oxygen was most likely bound as heterocyclic compounds. The reason for these trends in the nitrogen and oxygen levels is unclear, but these distinctive concentrations as a function of unburned carbon type may be reflected in differences in adsorption properties.

Surface area, pore volume and adsorption properties The N_2 adsorption isotherms of all the samples investigated were Type II according to the BDDT classification and they are typical for nonporous or macroporous adsorbents, on which unrestricted monolayer-multilayer adsorption can occur. BET surface area (N_2 at 77K) measurements were carried out on the Dale and WEPCO carbon-enriched separation samples. The surface areas are relatively low, ranging from 10 to 60 m^2/g. The WEPCO parent fly ash and subsequent subsamples present slightly higher surface areas than those observed for their counterparts of the Dale separations. For example, the inertinite fraction derived from WEPCO fly ash has a surface area of 25 m^2/g, compared to only 15 m^2/g for the inertinite fraction derived from Dale fly ash. For both series of fly ash samples, the surface area was found to increase linearly as a function of particle density, as illustrated in Figure 2 for selected density fractions from the Dale and WEPCO DGC separations. Inertinites exhibited the lowest surface area (15-25 m^2/g), isotropic coke particles presented intermediate surface areas (25-35 m^2/g), while anisotropic coke particles exhibited the highest surface areas (35-60 m^2/g). The fly ashes investigated here are class F and were derived from high volatile bituminous coals. Studies on class C fly ashes, that are generally derived from subbituminous coals, have shown much higher surface areas (200-400 m^2/g) [14], indicating that the properties of fly ashes are nor only dependent of petrographic composition, but also on the rank of the coal they are derived from. In a previous study, we showed that anisotropic coke, with the greatest BET surface area, appears to adsorb the greatest amount of Hg from the flue gas stream, while inertinite, derived from the coal with little alteration in the combustion process, is the least adsorptive carbon form. Although the relationship between sample density and BET surface area is essentially linear, for Hg adsorption while generally increasing with the density and surface area, does deviate from a simple, linear relationship [15].

Pore size distribution studies were also conducted on the above samples and the proportion of mesopore (pores 2-50 nm in width) volume over total volume is presented in Figure 3 for selected density fractions from the Dale separation. Figure 3 shows that for the three carbon types, the pore volume is mainly due to mesopores, with the mesopore volume accounting for over 60% of the total pore volume. This indicates that the extensive and rapid devolatilization that coal undergoes in the combustor, seems to promote the generation of meso- and macropores. There does appear to be a correlation between mesopore volume and carbon type, with inertinites exhibiting the highest proportion of mesopores (~90%), while isotropic coke particles present the lowest fraction of mesopore volume (~ 60%) and anisotropic coke presenting intermediate values (70-80%). A similar trend has been found for the WEPCO DGC fractions.

CONCLUSIONS

Concentrates of three microscopically identifiable forms of unburned carbon (inertinite, isotropic coke, and anisotropic coke) have been generated from two high-carbon-content fly ash samples using the technique of density gradient centrifugation (DGC). The density of like carbon forms isolated from the two fly ashes appears to be quite similar, regardless of the source of the fly ash. The H/C atomic ratios are ~ 0.028-0.016, indicating a high degree of condensation. The surface

areas are relatively low (10-60 m^2/g), and most of the pores are in the mesopore range (2-50 nm in width). For both series of fly ash samples, the surface area was found to increase linearly as a function of particle density. This work has shown that the three carbon types are not only visually different, but also present distinctive physical and chemical properties (density, nitrogen and oxygen concentrations, as well as surface area and mesopore volume). Furthermore, these distinctive properties may be reflected in differences in absorption properties, and therefore, the ASTM LOI specification, that is only based on the total carbon content, is not sufficient to identify the suitability of a fly ash for the cement industry. Our immediate goal is to measure the relative capacity of the different carbon types to adsorb air-entrainment reagents. For this purpose, we are developing a micro-technique to measure in-situ the adsorption of such agents directly. Finally, this characterization work has indicated that the unburned carbon can also be considered as a valuable precursor for the production of premium carbon products, since it consists basically of carbon and it has gone through a devolatilization process while in the combustor. Accordingly, we have investigated two potential routes for the generation of premium carbon products from the unburned carbon present in fly ash [16]. The first route focuses on the use of fly ash carbons as precursors for activated carbons by steam activation at 850°C, while the second route concentrates on the utilization of fly ash carbons as a replacement for calcined petroleum coke in the production of carbon artifacts.

ACKNOWLEDGEMENTS

The authors wish to thank Drs. H. Ban and J. M. Stencel (CAER-University of Kentucky) for conducting the triboelectrostatic separation and to the Research Council of the Basque Government for financial support.

LITERATURE CITED

1. The U.S. Department of Energy, 1996, Clean Coal Technology, Reducing emissions of nitrogen oxides via low-NOx burner technologies, Topic report no. 5.
2. U.S. Environmental Protection Agency, 2000, http://www.epa.gov/ardpublc.
3. Hogue, C., 2000, Chemical and Engineering News, **78**, 10.
4. Hower, J.C., Rathbone, R.F., Robl, T.L., Thomas, G.A., Haeberlin, B.O., and Trimble, A.S., 1997, Waste Management, **17**, 219.
5. Hill, R.L., Sarkar, S.L., Rathbone, R.F. and Hower, J.C., 1997, Cement and Concrete Research, **27**, 193.
6. Freeman, E., Gao, Y-M, Hurt, R.H. and Suuberg, E.M., 1997, Fuel, **8**, 761.
7. Hower, J.C., Rathbone, R.F., Graham, U.M., Groppo, J.G., Brooks, S.M., Robl, T.L. and Medina, S.S., 1995, Proceedings International Coal Testing Conference, 49.
8. Maroto-Valer, M.M., Taulbee, D.N. and Hower, J.C., 1998, Proceedings Conference on Unburned Carbon on Utility Fly Ash, 49.
9. Bailey, J.G., Tate, A., Diessel, C.F.K. and Wall, T.F., 1990, Fuel, **69**, 225.
10. Maroto-Valer, M.M., Taulbee, D.N. and Hower, J.C., 1999, Energy & Fuels, **13**, 947.
11. Taulbee, D.N., Maroto-Valer, M.M. and Hower, J.C., 1999, Proceedings 13th International Symposium on Use and Management of Coal Combustion By-Products, **1**, 24/1-15.
12. Ghosal, S., and Self, S.A., 1995, Fuel, **74**, 522.
13. Palmer, S.R., Sivanandan, S., and Huggett, W., 1997, Proceedings 1997 International Conference on Coal Science, **2**, 1999.
14. Kulatos, I., Gao, Y-M, Hurt, R.H. and Suuberg, E.M., 1998, Prepr. Am. Chem. Soc. Fuel Division, **43**, 980.
15. Hower, J.C., Maroto-Valer, M.M., Taulbee, D.N. and Sakulpitakphon, T., 2000, Energy & Fuels, **14**, 224.
16. Maroto-Valer, M.M., Andrésen, J.M., Andrésen, C.A., Morrison, J.L., and Schobert, H.H., 2000, Prepr. Am. Chem. Soc. Fuel Division, **45**, In Press.

Table 1: Petrographic analysis for the parent samples, carbon-enriched feeds and the highest purity carbon-type density fractions from each separation.

	Inertinite	Isotropic	Anisotropic	Glass
Dale Parent	3.8	13.4	19.2	63.6
-140 mesh Dale	1.2	2.6	5.2	91.0
+140 mesh Dale	2.0	13.0	25.5	59.5
Dale TES (DGC feed)	5.5	24.0	61.0	9.5
Fraction #2 (1.32-1.65 g cm^{-3})	76.5	7.0	1.0	15.5
Fraction #5 (1.72-1.75 g cm^{-3})	13.1	72.1	8.7	6.0
Fraction #12 (1.92-1.94 g cm^{-3})	<0.5	19.5	76.0	4.5
WEPCO parent	4.0	27.3	7.3	61.5
WEPCO TES (DGC feed)	8.5	51.5	27.5	12.5
Fraction #4 (1.50-1.60 g cm^{-3})	85.5	8.5	2.5	2.0
Fraction #8 (1.725-1.75 g cm^{-3})	9.5	78.5	11.5	0.5
Fraction #14 (1.875-1.90 g cm^{-3})	2.0	20.0	75.5	2.5

Table 2: Elemental analyses of selected density fractions from the Dale carbon-enriched separation.

Fraction #	Dominant carbon type (vol%)	%C (daf)	%H (daf)	%N (daf)	%O[a] (daf)	H/C	N/C
DGC feed	6%in; 24% iso; 61% ani	97.2	0.17	1.77	0.86	0.021	0.016
#2	Inertinite (77 v%)	98.4	0.21	1.44	< 0.01	0.025	0.013
#5	Isotropic (72 vol%)	95.7	0.22	1.55	2.53	0.027	0.014
#6	Isotropic (66 vol%)	96.5	0.13	1.55	1.82	0.016	0.014
#10	Anisotropic (71 vol%)	97.8	0.19	1.83	0.18	0.024	0.016
#11	Anisotropic (71 vol%)	98.1	0.16	1.77	< 0.01	0.019	0.015
#12	Anisotropic (76 vol%)	98.1	0.17	1.73	< 0.01	0.021	0.015
#13	Anisotropic (73 vol%)	97.6	0.23	1.86	0.31	0.028	0.016

[a] Determined by difference

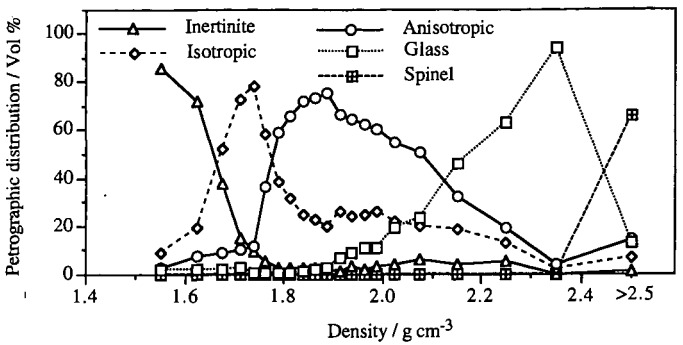

Figure 1: Petrographic distribution of the recovered density fractions for the separation of the WEPCO-TES sample.

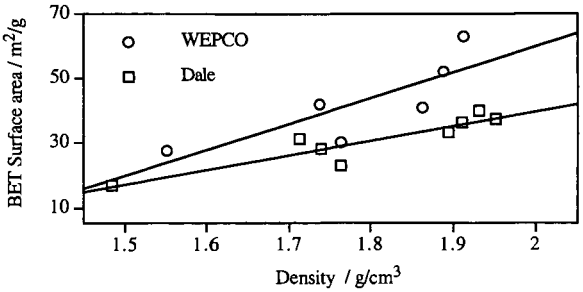

Figure 2: Relationship between surface area and density for selected density fractions from the Dale and WEPCO DGC separations.

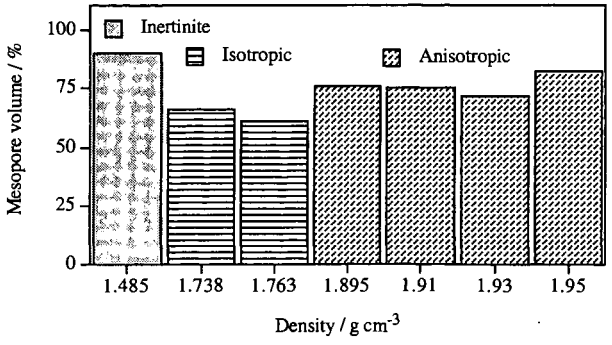

Figure 3: Proportion of mesopore (2-50 nm) volume for selected density fractions from the Dale DGC separation.

TECHNICAL CHALLENGES IN NO_x CONTROL: COST-COMPETITIVE COMPLIANCE FOR COAL-FIRED BOILERS

Stephen A. Johnson and Charles A. Lockert*
ADA Environmental Solutions, LLC
50 Nashua Road, Londonderry NH 03053
*Solvera Particulate Controls

ABSTRACT

In the decade since the Clean Air Act Amendments (CAAA) were enacted, the power generation business has undergone rapid change. In many parts of the U. S., utilities are being restructured into separate generating and distribution companies in preparation for a competitive market for wholesale and retail power. To survive in the emerging marketplace, generating companies are striving to produce the most power (high capacity and availability) for the lowest cost (3 to 3.5 cents per kWh).

At the same time that costs are being reduced, utilities are challenged with meeting tougher new NO_x emission limits imposed by Title IV (acid rain) and Title I (ozone non-attainment) of the CAAA. Title IV limits can generally be met by applying combustion NO_x controls (low-NO_x burners and overfire air) with additional flexibility provided by reburning and selective non-catalytic reduction (SNCR). The cost impacts of these technologies have been recognized and endured. Now Title I will require more drastic NO_x reductions in the 2003 to 2007 timeframe in the 19 eastern states where ozone is highest. The only technology capable of consistently meeting Title I limits is selective catalytic reduction (SCR). Competitive pressures may eventually force all coal-fired plants to meet Title I regulations. The utilities that are able to reduce emissions at the lowest cost will survive.

Since the CAAA were enacted, ADA Environmental Solutions (ADA-ES) has developed and implemented a suite of strategies to reduce the cost of low-NO_x operation through the use of sensors and controls. This paper will provide field data from several plants showing how cost savings were achieved by the test team and maintained by the utility. Examples of cost savings include reduced consumption of SNCR reagent, lower combustion NO_x via biased firing and burners out of service, system-wide NO_x averaging to minimize SCR, reducing the cost of SCR operation by controlling the NO_x going into the reactor, and monitoring and controlling flyash salability by preventing carbon or ammonia contamination.

BACKGROUND

Salem Harbor Station, now owned by PG&E Generating, installed both combustion NO_x controls and Non-selective Catalytic Reduction (SNCR) to meeting NO_x emission goals of 0.33 lb./M Btu for their three coal-fired units. Emission limits were met, but the consumption of urea was a significant operating cost. The original control system metered urea to pre-selected injectors based on a look-up table of inlet NO_x as a function of load generated during pre-retrofit testing by the plant. The urea flow rate was then adjusted to maintain the stack NO_x emission safely below 0.33 lb./M Btu over the load range of each unit. Unfortunately, this control scheme often cranked up the urea flow when furnace temperatures were high, leading to urea combustion instead of NO_x reduction. The author verified the high temperatures by measuring furnace exit gas temperatures (FEGT) with an accurate, on-line, continuous optical temperature monitor called GasTemp. Sootblowing practices had a lot to do with these high temperatures.

RESULTS AND DISCUSSION

First, testing was performed on Units #1 and #2; both 81-MW front-fired boilers equipped with low-NO_x burners and overfire airports. The tests yielded the following conclusions:

- Reagent was injected at the upper end of the temperature window at full load, resulting in only 15 to 22 percent reagent utilization (especially with a dirty furnace at the tail end of a sootblowing sequence).
- Utilization was higher (30-35 percent) at low loads.
- Ammonia slip was experienced, especially during load transients.
- Reagent utilization improved to 26 percent at full load when FEGT was below 2020 F.
- Reagent utilization could be increased to 42 percent at 70% load when FEGT was below 1880 F.

After the initial tests, the plant agreed to modify the control system and incorporate the temperature signal into the control logic for the SNCR system on Unit #3.[1]

Fuel Tech, the original equipment supplier, designed the control modifications and worked with the plant to install the new software. ADA-ES planned the demonstration tests, collected and analyzed the data, and interpreted the results. The program, results from which are described in reference 1, included 24 days of baseline measurements documenting the original system performance and 35 days of demonstrating the improvements.

Salem Harbor #3 is a front-fired boiler rated at 155 gross MW. The unit is equipped with four levels of urea injectors as well as low-NO_x burners and overfire air to control NO_x emissions below 0.33 lb./M Btu. A complete division wall divides the furnace into two chambers. After the burner retrofit, the unit has had difficulty achieving the designed steam temperature due to lower FEGT. Therefore, furnace sootblowing was only performed a few times a week prior to the test program as necessary to maintain primary superheater steam temperatures below 950 F.

Historical reagent consumption prior to the demonstration varied from 70 to 200 GPH, and averaged about 125 GPH in 1995 and 1996. On the first day of baseline testing, the reagent consumption averaged about 112 GPH over the 24-hour period. On the second test day, operators blew all 36 furnace sootblowers and watched as the reagent consumption at full load dropped to about 62 GPH (the minimum flow allowed by the original control system)! As a result, the operators immediately decided to change their sootblowing practices to better control NO_x. The initial drastic sootblowing decreased reheat steam temperatures by about 15-degrees F, but also reduced superheater attemperator spray flows from 52,000 to 15,000 lb./h. Reheat steam temperatures recovered in a matter of hours, but the reagent consumption continued at the minimum level for another day. Further experience indicated that frequent sootblowing using only a few blowers at a time could maintain low reagent consumption without any adverse effects on boiler performance.

FEGT at full load varied from 1950 to 2100 F, depending on sootblowing, as shown on Figure 1. As a result of this "baseline" testing experience, the FEGT signal was incorporated into the revised control system.

Fig. 1 Relationship of FEGT to Steam Flow at Salem Harbor #3

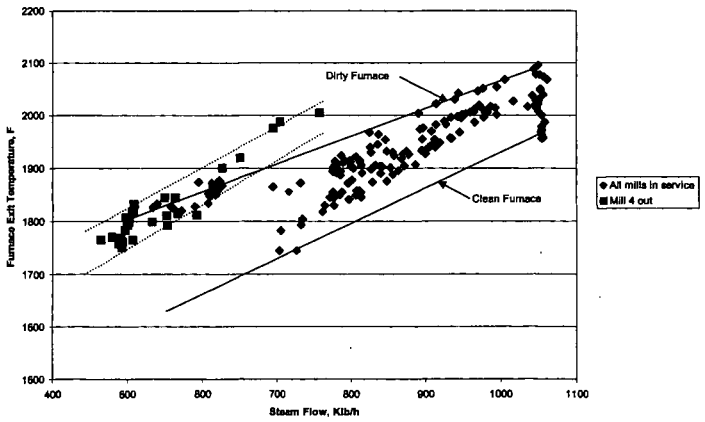

The changes to the SNCR system included mechanical upgrades, new instrumentation, and software replacement. Fuel Tech first installed a remote pressure regulator on each reagent metering module so that atomizing pressure and reagent flow could be controlled across the load range at each injection elevation. This modification allowed flexibility to use temperature to dictate system operation. Then Fuel Tech updated the Allen-Bradley and FactoryLink software to include the temperature signal among other changes listed in Table 1.

The results achieved with the new control system were dramatic. Figure 2 shows daily reagent consumption for both the baseline and demonstration periods. Historical reagent usage had been over 3000 gal/day based on Unit #3's share of the total station consumption. During the baseline test period, consumption ranged from 1500 to 2700 gal/day, depending on how the operators

chose to apply the IR sootblowers. Sootblowing schedules were formally introduced in order to maintain FEGT at full load in the range of 1950 to 2000 degrees F during the demonstration period in conjunction with the control system modifications. As a result, the reagent consumption was reduced to 600-1500 gal/day (less than half of the historical level). Moreover, these savings were sustainable after the test crew had gone home. The resulting cost savings was estimated by the plant to be about $600K/y at a urea price of $0.90/gallon.

Table 1. Software Changes

Original Control System	Upgraded Control System
Initial reagent flow rate selected from look-up tables based on steam flow and mills in service.	Initial reagent flow rate calculated from curves based on steam flow and FEGT.
Look-up table values for reagent flow were established during tests when sootblowers were not used.	The reagent flow curves extended to much lower values based on the sootblower performance data.
Injector liquid pressure constant.	Injector pressure varied with rate of temperature change. Rapid FEGT decrease results in reduced atomizer pressure, thus reducing both reagent flow rate and droplet size.
NO_x set point selected automatically, but operator override possible.	Included a new screen showing average daily NO_x and projected NO_x if current set point is maintain. Operators could then adjust set point to reduce reagent flow at the end of the day and still assure compliance.
System response time set to avoid instabilities given original inputs.	System response time shortened to take advantage of new inputs.

Figure 2. Daily Reagent Use at Salem Harbor #3

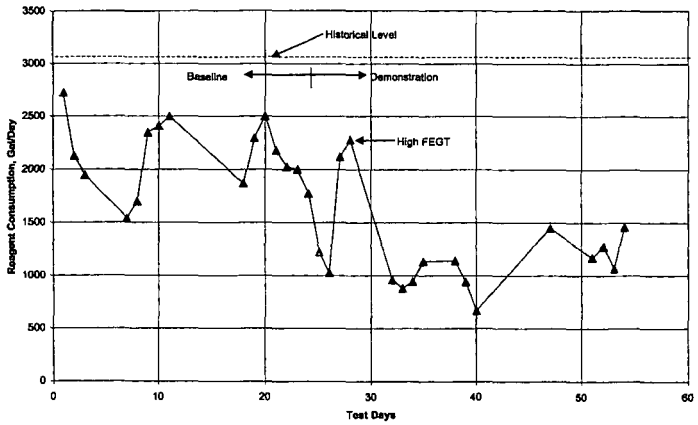

Biased Firing and BOOS: a Poor Man's OFA.

Another low-cost step for reducing NO_x from existing boilers is to increase the amount of staged combustion that the boiler can achieve. Figure 3 shows a general relationship between NO_x emissions and stoichiometric ratio at the lower burners. The background data for this curve are somewhat complicated to explain [2,3,4], but the main points are that NO_x can be further reduced when:

1. The SR approaches 0.7
2. The OFA ports are located well above the top burner elevation.

The poor-man's way to achieve these low-NO_x conditions is to try biased firing and burners out of service. Biased firing increases the size of locally fuel-rich regions within the flame zone by

redistributing the air and fuel within the furnace. To best reduce NO_x, the fuel should be biased lower or toward the middle of the furnace, while the air is biased upward and toward the furnace sidewalls. The result is to decrease the SR for the lower (or center) burners, and increase the SR for the upper (or wing) burners and OFA ports. Since NO_x emissions decrease more drastically at low SR than they increase at high SR, the overall result is usually a substantial NO reduction. The only trick is choosing fuel-rich burners such that their flames will contact enough combustion air in the upper furnace to complete burnout.

Biased firing taken to the extreme is taking burners out of service entirely. In this case, the lower burners are operated fuel-rich, while the upper burners are operated on air only and essentially become a second set of OFA ports. Flame-zone NO_x reduction is maximized at a SR of 0.7, the additional residence time between active burners and OFA ports enhances NO_x reduction, and very little NO_x is formed in the burnout zone as long as burnout is slow.

To take advantage of BF/BOOS, the operator must have accurate control over fuel and airflow to each burner. On-line measurement of both air and fuel can be achieved by installing flow sensors in the burner lines. Alternatively, combustion optimization software has been used to help operators maintain BF/BOOS conditions. The software will often select biased firing conditions from the normal operating range as lowest possible NO_x. Given total airflow to the burners and overfire air ports, the software can learn to control biased firing, even if fuel distributions are not well characterized. If the fuel flow to each burner is measured, the system is even more robust.

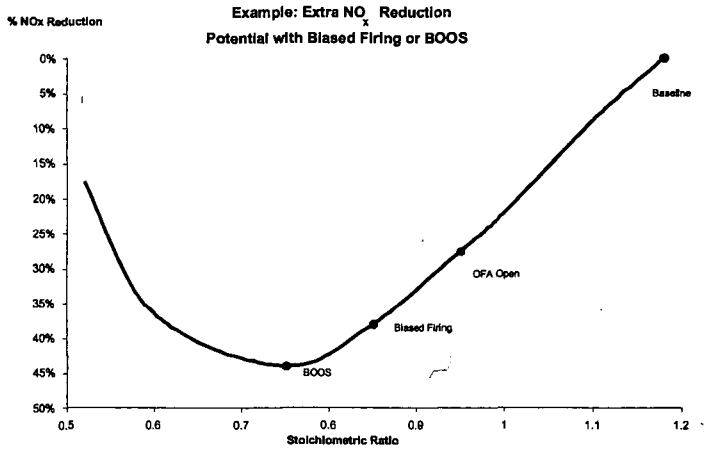

Figure 3. NO_x Reduction from Staged Combustion.

ADA-ES has recently completed a test series on a 180-MW tangentially fired boiler already equipped with closed-coupled OFA ports. Figure 4 shows the trends of NO_x with load before and during the tests. The situation at this utility is that they need to meet Title IV NO_x limits now while looking ahead to Title I. Low-cost NO_x control will partially offset the cost of credits in the nearterm, and reduce the cost of SCR (if required) in the long term. It can be seen that BF/BOOS can achieve up to 50% reduction in low-load NO_x, and 20% NO_x reductions are sustainable at full load. BF/BOOS operation has been adopted by the operators and is now the preferred mode of operation.

Figure 4.
NOx Emissions Vs. Load at a 180 MW Tangential Unit

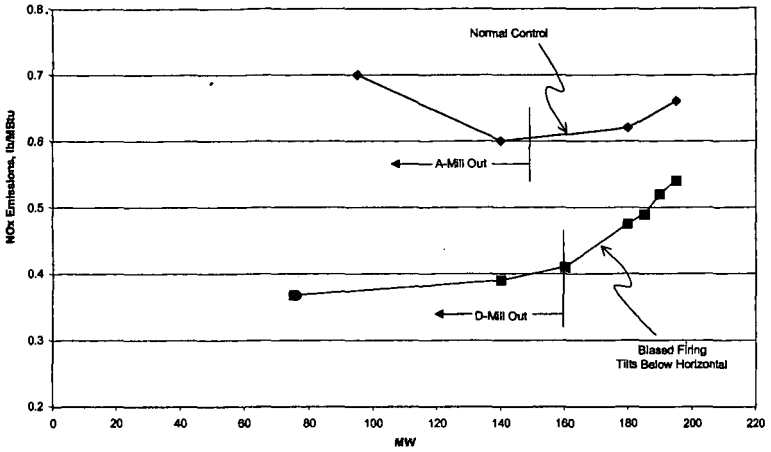

System-Wide NO_x Averaging.
Title I NO_x controls will be enforced within each state on a system-wide basis. Therefore, another way to save money on NO_x control is to over-control NO_x on units that have advantages and under-control NO_x on other units where there are barriers to NO_x control. Since SCR is the most expensive control method in terms of $/ton of NO_x removed, the objective of this strategy is to juggle the suite of NO_x-control technologies such that the fewest number of SCR units are required.

One utility company that we have worked with operates 24 boilers in two states. Since most of these boilers already used low-NO_x burners and overfire air for NO_x control, they only needed 10 SCR units on their largest boilers to achieve a system-wide average NO_x of 0.15 lb./M Btu. Accordingly, high performance SCR treats flue gas from equipment that generates 72% of the seasonal power production. However, this was not the least-cost scenario.

To reduce compliance costs, ADA-ES walked down each unit and examined design and operating data to determine additional NO_x reduction potential. Technologies considered included:

- Biased firing/burners-out-of-service
- Low-NO_x burners (if not already there)
- Overfire air booster fan for deeper staging
- Optimization software and sensors for temperature, LOI, per-burner coal flow
- Conversion to natural gas
- Reburning with coal or natural gas
- Fuel lean gas reburning
- Amine-enhanced gas reburning
- Selective non-catalytic reduction

Several units in this system have spare mill capacity and sufficient furnace volume to take maximum advantage of BF/BOOS. Therefore, it was not surprising that some combination of BF/BOOS, optimization software, and SNCR for the smaller megawatt units saved considerable money. In addition, by applying these techniques in all 24 boilers, the NO_x emission limit could be met using only seven SCR units. The overall savings were about $17M/y.

SCR Control Improvements.
There are now ten Selective Catalytic Reduction (SCR) NO_x control systems operating in the United States on coal-fired boilers. Within the next year, SCR technology will be adopted by many other utilities faced with meeting low NO_x emission limits driven by Title I of the Clean Air Act Amendments. Currently, there are an estimated 40 SCR units either under construction or in procurement within the Ozone Transport Region. Estimates of the number of SCR units to be built between now and 2007 in the US range from 80 to 200.

SCR systems employ relatively simple instrument and control (I&C) schemes to meter the correct amount of ammonia into the flue gas to maintain NO_x below the regulated value. System designs contain some margin of safety to account for the range of temperature, inlet NO_x concentration, or particulate matter expected under steady-state conditions. However, these parameters can change very quickly during transient operation (load swings, start-up, shutdown) or off-design operation (mills or burners out of service, feedwater heaters out of service). Also, the local NO_x or temperature distributions can change at the ammonia injection point, even though the total NO_x or heat input remains the same. The results could be wasted reagent or worse, the formation of ammonium sulfate or bisulfate that can foul air preheater surfaces, contaminate flyash that the utility may want to sell, and increase stack opacity above regulated limits.

Weaknesses in conventional SCR control systems, as described by operators, include:

- Unreliable NO_x analyzer sampling system upstream of the SCR reactor.
- Slow ammonia reagent flow response based on a 5 to 10 minute lag time in the feedback NO_x signal from the stack CEM.
- Over-feeding ammonia reagent when the SCR inlet NO_x concentration undergoes a step change decrease (as occurs when a top mill is taken out of service or a lower mill is put into service).
- Reagent flow reverts to default values during CEM calibration.

ADA Environmental Solutions, LLC (ADA-ES) was contracted by EPRI to evaluate SCR design and operating data from US SCR installations in order to quantify the extent of any adverse impacts from the problems listed above. We then evaluated whether improvements can be made to existing control systems to manage potential side effects of SCR, which could include air heater fouling, flyash contamination, catalyst poisoning, or stack opacity.

Control system upgrades devised by ADA-ES were described in two papers given at the recent EPRI/EPA/DOE Mega Symposium [5,6]. However, one of the most effective ways to reduce the cost and risk of SCR operation is to minimize the NO_x concentration going into the reactor. Lower inlet NO_x means lower ammonia consumption and lower ammonia/NO_x ratios. The ammonia/NO_x ratio defines the risk of ammonia slip: if the ratio can be held less than 0.8, then the ammonia slip will not exceed 1 PPM. The catalyst lifetime (defined as the time until ammonia slip exceeds 2 PPM) can also be increased significantly when the inlet NO_x is low. Biased firing was one technique recommended by ADA-ES to reduce ammonia/NO_x ratio.

Recent operating experience at Stanton has incorporated many of the improvements suggested by the results of this EPRI project. In their third year of operation, Stanton experienced higher than expected catalyst deactivation, which motivated operators to modify combustion to reduce NO_x going into the SCR. One change that worked well was operating with the top mill (out of five) out of service to increase the staging effect. This allowed Stanton to reduce boiler outlet NO_x from 0.4 to as low as 0.26 lb./M Btu, and consistently maintain this value below 0.32 lb./M Btu! Another change was to move the NO_x emission set point closer to the permitted NO_x value. As a result of these improvements, reagent consumption has dropped to about 200 lb./h at full load, saving about 25%, and ammonia slip episodes have been less frequent. Further efforts are underway to improve the feedback NO_x signal from the stack CEM to achieve faster response to load swings.

Improved Flyash Sales

Before the CAAA, utilities found it easy to meet unburned carbon specifications for flyash sold to use in cement and concrete products. Flyash loss-on-ignition (LOI) must be below 3-5% in order to prevent absorption of air entrainment chemicals used in the cement industry to control the strength and prevent cracking of concrete products. Flyash sales also represent a significant revenue stream for some utilities. The difference between landfill costs and flyash sales can be as much as $25/T. A 500 MW coal-fired unit firing a bituminous coal will produce about 280 tons/day of flyash, which could represent about $2M/y in revenues and avoided costs.

ADA-ES has been working with Solvera Particulate Controls, Inc to help utilities realize these cost benefits. Solvera has obtained the rights to the CAMRAC online LOI monitor[7], and has applied this monitor to determine whether flyash removed from the precipitator is saleable or not. In this application, the LOI monitor takes an ash sample from the pneumatic line under each collection hopper. Solvera has also mounted the LOI monitor in the economizer outlet duct and

developed reliable procedures to extract a representative, isokinetic sample for analysis every ten minutes. The resulting LOI readings are accurate and close enough to real time to make online combustion tuning feasible.

ADA-ES has recently installed the CAMRAC on a 50 MW coal-fired boiler to measure and reduce LOI that impairs precipitator performance. First, the instrument will be used to troubleshoot the root cause of the LOI problem. The problem developed after installation of low-NO_x burners, but changes to burner operation (airflow distribution, primary airflow) or sealing windbox leaks into the furnace may help alleviate the problem. We will also try biased firing for simultaneous NO_x and LOI reduction. We have already talked about the NO_x benefits of BF/BOOS. Sometimes this technique can also reduce LOI by injecting more coal lower into the furnace, thus extending combustion burnout time for more of the fuel. As of this writing, no data are available from this test but results should be ready to incorporate into the presentation of this paper in August.

CONCLUSIONS

Meeting the NO_x emission limits required by Title IV and Title I of the CAAA can be costly, but cost improvements are possible for most boiler operators. The key to achieving cost savings is to monitor and control those factors that can be related to cost. For SNCR installations, the furnace temperature at the point of reagent injection can be monitored and controlled to maximize reagent utilization. In the example given above, utilization was doubled from less than 20 percent to over 40 percent. For SCR, it is cost-effective to monitor and minimize the NO_x concentration coming into the reactor to save on reagent cost. For both these technologies, reducing NH_3/NO_x ratios will also cut back on ammonia carryover, a major cause of air heater pluggage and possible source of flyash contamination.

Combustion NO_x controls (low-NO_x burners, overfire air, reburning) slow down the combustion process, often leading to more unburned carbon in the flyash unless operators can make adjustments. Combustion NO_x controls also decrease the margin of error for maintaining per-burner air-fuel ratios, since a single burner can produce enough carbon to contaminate the flyash product. Sensors are available to monitor LOI and furnace temperature. LOI provides direct feedback for combustion tuning and other firing strategies to reduce NO_x. It is also a required input for optimization software systems that provide operators with operating settings for maintaining NO_x within compliance while not exceeding LOI or heat rate constraints. Furnace temperature can also be used by these optimization systems as a way to measure and control boiler heat balance.

Payback for sensor-driven systems can be very rapid. The reward is reliable emission compliance and more power sales in a competitive market.

REFERENCES

1. R Afonso, A Sload, D Miles, S Johnson, and J O'Leary, "Enhanced NOxOUT Control at Salem Harbor Unit #3, presented at the EPRI-DOE-EPA Mega Symposium, Washington, DC, August 1997.
2. Johnson, S. A., "NO_x Control by Burner and Furnace Design," Chapter in Energy Technology Handbook edited by Douglas Considine, McGraw-Hill Publishers, NY, NY 1978.
3. Johnson, S. A. and Sommer, T. S., "Commercial Evaluation of a Low-NO_x Combustion System as Applied to Coal-Fired Utility Boilers," Proceedings of the Joint Symposium on Stationary Combustion NO_x Control, Volume 1, EPRI Report WS-79-220, Palo Alto, CA, May 1981.
4. Lisauskas, R. A., Snodgrass, R. J., Johnson, S. A., and Eskanazi, D., "Experimental Investigation of Retrofit Low-NO_x Combustion Systems," Presented at the 1985 Joint Symposium on Stationary Combustion NO_x Control, May 1985.
5. Johnson, S. A., Zammit, K. D., and Engelmeyer, A. J., "Improved SCR Control to Reduce Ammonia Slip", presented at the EPRI-DOE-EPA Mega Symposium, Atlanta, GA, (EPRI Report TR-113187-V2) August 1999.
6. Comer, J. P. and Johnson, S. A., "SCR Sootsniffers: a New NO_x Process-Monitoring Tool", presented at the EPRI-DOE-EPA Mega Symposium, Atlanta, GA, (EPRI Report TR-113187-V2) August 1999.
7. DiGioia, A. and Trerice, D., "In-Duct Monitoring of Flyash LOI for Ash Quality and NO_x Control" presented at the Southeastern Electric Exchange, November 1996.

A NEW PATH TO "PROMPT" NO: CH + N_2 = H + NCN STUDIED BY AB INITIO MO AND STATISTICAL THEORY CALCULATIONS

M. C. Lin, L. V. Moskaleva, And Wensheng Xia
Department of Chemistry
Emory University, Atlanta, GA 30322, USA

ABSTRACT

In the past two decades, the $CH(^2\Pi) + N_2 \rightarrow HCN + N(^4S)$ reaction has been routinely employed for kinetic modeling of NO_x formation in hydrocarbon combustion. The reaction has been studied by many investigators[1-17] since Fenimore[18] suggested it to be a potential "prompt" NO precursor process in 1971. The result of a recent comprehensive study by Morokuma and co-workers,[19,20] however, indicated that the theoretically predicted rate constant for the formation of the spin-forbidden HCN + N products is about two orders of magnitude lower than experimentally measured values.[1,2,7,8] The result of our high-level molecular orbital study aided by a statistical-theory calculation reveals that the spin-allowed H + NCN products occurring by the ground electronic doublet surface is the dominant CH + N_2 process under combustion conditions.

INTRODUCTION

The kinetics of the reaction available prior to 1983 were first interpreted in terms of the global mechanism involving an intemally excited HCNN adduct:

$$CH(^2\Pi) + N_2 \underset{b}{\overset{a}{\rightleftharpoons}} HCNN^{\dagger} \xrightarrow{c} HCN + N(^4S) \quad (1)$$

$$HCNN^{\dagger} \xrightarrow[+M]{d} HCNN \quad (2)$$

by Berman and Lin,[4] who measured the pressure-dependent bimolecular rate constant (k_2) by laser-induced fluorescence, monitoring the decay of CH at temperatures between 297 and 675 K. Their low-temperature, pressure-dependent data, which have been corroborated in subsequent independent studies,[9,10] were correlated with high-temperature NO formation results by Blauwens et al.[1] with the Rice-Ramsperger-Kassel-Marcus (RRKM) theory. More recently, there have been two shock-tube studies at high temperatures, monitoring either CH decay by laser absorption spectroscopy or N production by atomic resonance absorption spectroscopy, providing the much needed high-temperature kinetic data.[7,8]

Theoretically, the production of N atoms by reaction (1) has been investigated by Manna and Yarkony[13,14] on the nature of the doublet-quartet curve crossing and by Walch[15] and Seideman and Walch[16] on the potential energy surface (PES) involved. Miller and Walch[17] recently calculated k_1, ignoring the retarding effect of the doublet-quartet crossing, with the RRKM theory above 1000 K and concluded that the high-temperature shock-tube data of Hanson, Roth and co-workers[7,8] can be satisfactorily accounted for. On the other hand, the result of a more comprehensive calculation by Morokuma and co-workers[20], based on a more detailed PES[19] with the inclusion of the curve crossing effect, indicated a rather poor agreement between theory and experiment as alluded to above.

RESULTS AND DISCUSSION

In this work, we study the mechanism of the CH + N_2 reaction, centering on the reaction path over the ground electronic doublet PES. The result of this high-level *ab initio* molecular orbital calculation, aided by a multichannel RRKM analysis and kinetic modeling for CH decay and N production reveals unambiguously that the prompt NO observed in hydrocarbon flames actually arises primarily from the spin-allowed reaction,

$$CH(^2\Pi) + N_2 \rightarrow H + NCN(^3\Sigma_g^-). \quad (3)$$

The reaction occurs via two NC(H)N ring intermediates and the HNCN radical. The prompt NO can be formed by the facile, exothermic oxidation of NCN by O, OH and O_2 present in the flame.

The PES of the ground electronic doublet state, shown in Fig. 1 with a relevant portion of the quartet state leading to HCN + N, has been computed with the G2M method.[21] The method employed is the same as previously used by Cui and Morokuma.[19] The geometries were

optimized at the B3LYP level (Becke's three parameter density functional[22] with the nonlocal correlation functional of Lee, Yang, and Parr[23]) with the standard 6-311G(d,p) basis set. The vibrational frequencies used for characterization of stationary points, ZPE corrections and RRKM calculations, were computed at the same level of theory. All MO calculations were performed with the Gaussian 94[24] and MOLPRO96[25] program packages.

The quartet portion of the potential energy surface is entirely taken from ref. 19. On the doublet surface we found a concerted path connecting a ring intermediate, INT2, with the HNCN radical, the latter can dissociate to H + NCN. The endothermicity of this channel is 21.5 kcal/mol at the G2M level, while the concerted transition state, TS3, is 11.7 kcal/mol above the reactants at the same level of theory. The connections of this transition state to respective minima on the PES were established by an IRC test.[26]

Since for the last part of the potential energy surface (HNCN dissociation) no distinct transition state could be found, we mapped out a one dimensional dissociation profile at the B3LYP level and fitted it with Morse potential, adjusting D_e to the respective G2M value afterwards. The resulting potential can be effectively represented by the equation, $V(r) = D_e(1-e^{-\beta(r-r_0)})^2$, where D_e = 84.01 kcal/mol, β = 3.27, r_0 = 1.160 Å. A canonical variational RRKM calculation was performed based on the G2M energies and calculated B3LYP molecular parameters at each point along the dissociation curve for HNCN → H + NCN.

Although the doublet product channel, NCN + H, is 18.1 kcal/mol higher than HCN + N, it is 0.8 kcal/mole lower than the last barrier leading to the formation of the latter products on the quartet surface. The apparent barrier for the HNCN dissociation would be much lower at high temperatures because of the entropic contribution, which reduces the values of $\Delta G^{\ddagger}$ as the temperature increases. The theoretically predicted heat of formation for the NCN radical at 0 K based on reaction (3), 111.0 kcal/mol, is in good agreement with the recently reported experimental values: by Neumark and co-workers[27], 111.3 kcal/mol, and by Clifford et al.[28], 107.4 ± 3.2 kcal/mol.

The rate constant for the production of NCN by reaction (3) was calculated with a multichannel RRKM program previously used in our study of the NH_2 + NO reaction.[29] The result of the calculation compares closely with those measured at high temperatures purportedly for k_1, based on either the decay of CH[8] or the formation of N.[7] In the temperature range, 1500-4000 K, the predicted k_3 at 0.88 atm can be represented by the modified Arrhenius expression, $k_3 = 2.22 \times 10^7 T^{1.48} \exp(-11760/T)$ cm^3/(mol·s).

SUMMARY AND CONCLUSIONS

To conclude, we have demonstrated that the CH + N_2 → H + NCN reaction, which occurs over the ground electronic doublet PES, is spin-allowed and more favorable than the accepted, spin-forbidden path producing HCN + N. The computed rate constant for CH decay agrees quantitatively with experimentally measured values.[8] In addition, the predicted N-atom production rate also agrees fully with expeimental result[7] within the scatter of typical shock-tube data. Under combustion conditions, NO can be formed readily by the rapid oxidation of NCN by O, OH and O_2.

ACKNOWLEDGEMENTS

LVM thanks the Division of Chemical Science, U.S. Department of Energy, for the support. WX and MCL acknowledge the support from the Caltech MURI project through the Office of Naval Research.

REFERENCES

1. Blauwens, J., Smets, B. & Peeters, J. *Combust. Inst.* **16**, 1055-62 (1977).
2. Matsui, Y. & Nomaguchi, T. *Combust. Flame*, **32**, 205-14 (1978).
3. Butler, J. E., Goss L. P., Lin, M. C. & Hudgens, J. W. *Chem. Phys. Lett.* **63**, 104-7 (1979).
4. Berman, M. R., Lin, M. C. *J. Phys. Chem.* **87**, 3933-42 (1983).
5. Duncanson, J. A., Jr., Guillory, W. A. *J. Chem. Phys.* **78**, 4958-62 (1983).
6. Matsui, Y. & Yuuki, A. *Jpn. J. Appl. Phys.* **24**, 598-603 (1985).
7. Lindackers, D., Burmeister, M., Roth, P. *Combust. Inst.* **23**, 251-57 (1991).
8. Dean, A. J., Hanson, R. K. & Bowman, C. T. *Combust. Inst.* **23**, 259-65 (1991).

9. Becker, K. H., Engelhardt, B., Geiger, H., Kurtenbach, R., Schrey, G. & Weisen, P. *Chem. Phys. Lett.* **195**, 322-328 (1992).
10. Medhurst, L. J., Garland, N. L. & Nelson, H. H. *J. Phys. Chem.*, **97**, 12275 (1993).
11. Morley, C. *Combust. Flame*, **27**, 189-204 (1976).
12. Miller, J. A., Bowman, C. T. *Prog. Energy Combust. Sci.*, **15**, 287-338 (1989).
13. Manna, M. R. & Yarkony D. R. *J. Chem. Phys.* **95**, 1808-1816 (1991).
14. Manna, M. R. & Yarkony D. R. *Chem. Phys. Lett.* **188**, 352-358 (1991).
15. Walch, S. P. *Chem. Phys. Lett.* **208**, 214-18 (1993).
16. Seideman, T. & Walch, S. P. *J. Chem. Phys.* **101**, 3656-61 (1994).
17. Miller, J. A., Walch, S. P. *Int. J. Chem. Kinet.* **29**, 253-259 (1996).
18. Fenimore, C. P. *Proc. Combust. Inst.* **13**, 373-79 (1971).
19. Cui, Q., Morokuma, K. *Theor. Chem. Acc.* **102**, 127-133 (1999).
20. Cui, Q., Morokuma, K., Bowman, J. M., and Klippenstein, S. *J. Chem. Phys.* **110**, 9469-82 (1999).
21. Mebel, A. M., Morokuma, K. & Lin, M. C. *J. Chem. Phys.* **103**, 7414-21 (1995).
22. Becke, A. D. *J. Chem. Phys.* **98**, 5648-52 (1993).
23. Lee, C., Yang , W. & Parr, R. G. *Phys. Rev. B*, **37**, 785-9 (1998).
24. M. J. Frisch, G. W. Trucks, H. B. Schlegel, P. M . W. Gill, B. G. Johnson, M. A. Robb, J. R. Cheeseman, T. Keith, G. A. Petersson, J. A. Montgomery, K. Raghavachari, M. A. Al-Laham, V. G. Zakrzewski, J. V. Ortiz, J. B. Foresman, J. Cioslowski, B. B. Stefanov, A. Nanayakkara, M. Challacombe, C. Y. Peng, P. Y. Ayala, W. Chen, M. W. Wong, J. L. Andres, E. S. Replogle, R. Gomperts, R. L. Martin, D. J. Fox, J. S. Binkley, D. J. Defrees, J. Baker, J. P. Stewart, M. Head-Gordon, C. Gonzalez and J. A. Pople, *GAUSSIAN 94, REVISION A.*1; Gaussian, Inc., Pittsburgh PA, 1995.
25. MOLPRO is a package of *ab initio* programs written by H.-J. Werner and P. J. Knowles, with contributions from J. Almlöf, R. D. Amos, A. Berning, D. L. Cooper, M. J. O. Deegan, A. J. Dobbyn, F. Eckert, S. T. Elbert, C. Hampel, R. Lindh, A. W. Lloyd, W. Meyer, A. Nicklass, K. Peterson, R. Pitzer, A. J. Stone, P. R. Taylor, M. E. Mura, P. Pulay, M. Schütz, H. Stoll and T. Thorsteinsson.
26. Gonzalez, C. Sosa, C., and Schlegel, H. B. *J. Phys. Chem.* **93**, 2435-40 (1989).
27. Bise, R. T., Choi, H., Neumark, D. H. *J. Chem. Phys.* **111**, 4923-32 (1999).
28. Clifford, E. P., Wenthold, P. G., Lineberger, W. C., Petersson, G., and Ellison, G. B. *J. Phys. Chem.* **101**, 4338-45 (1997).
29. Diau, E. W., Wagner, M. A. G. & Lin, M. C. *J. Phys. Chem.* **98**, 4034-42 (1994).

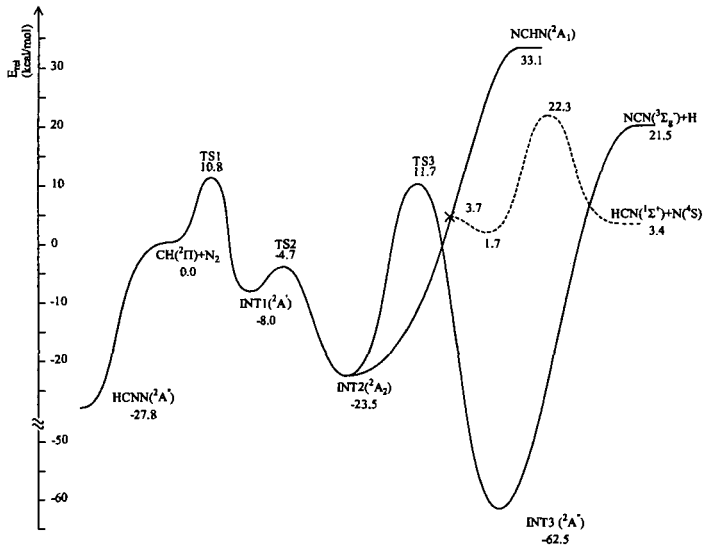

Figure 1. Potential energy diagram for reaction (3) combining the result of Cui and Morokuma[19] for the quartet state given by the dotted curve where "×" indicates curve crossing with the present work for the doublet state given by the solid curve. The relative energies are calculated at the G2M(RCC) level including B3LYP/6-311g(d,p) ZPE correction.

PREDICTING AROMATICS FORMATION FROM PROPARGYL REACTIONS: DEVELOPMENTS IN AROMATICS-FORMATION MODELING IN THE 1990'S

Phillip R. Westmoreland* and George E. Oulundsen
Department of Chemical Engineering; University of Massachusetts Amherst
Amherst, MA 01003-3110; westm@ecs.umass.edu

KEYWORDS: propargyl, soot, combustion, chemical activation, benzene, phenyl

ABSTRACT

Predicting the formation of aromatics and soot is a long-sought goal for combustion design, and propargyl (C_3H_3) chemistry appears to be a key. Self-combination reactions and addition to propyne or propadiene have all been proposed to form aromatic rings. Some of these proposals have been based on careful calculations or on clean experimental data. However, the picture is quite complex and in dispute because of the complex rearrangements that can result from chemical activation. Using theory and experiment, I will discuss the controversy over the various proposed kinetics. In the next ten years, we should be able to establish the correct kinetics and use it for engineering analysis and design.

INTRODUCTION

Clean air was one of the central concerns as the environmental movement grew though the 1960's, and sooty air has been one of the worst offenders throughout time. Percival Pott's recognized in the 18th century that combustion-generated soot was linked to cancer, but this insight only led to better personal hygiene requirements for chimney sweeps, not to reduced amounts of soot. Indeed, coal use in the 19th century's Industrial Revolution exacerbated the problem. Reduction began in the 20th century, spurred by an increased scale of industry and increased acceptance of individual rights relative to those industries, and aided by the use of natural gas and new environmental control technologies. A US landmark was the 1970 formation of the Environmental Protection Agency.

Twenty years later, the Clean Air Act of 1990 pushed industry to reduce emissions of smog-forming chemicals, carbon monoxide, and particulates up to 10 μm in size, such as soot. Incentives were mixed with regulation. Subsequent 1997 amendments led to tightening by adding specific standards for particulate matter smaller than 2.5 μm.

The US Department of Energy, Department of Defense, and Environmental Protection Agency, as well as government agencies around the world, have long supported research to identify the chemical pathways that form soot. The guiding hypothesis is that by knowing the pathway, it can be interfered with to prevent or destroy soot. Wagner's 1980 review [1] concluded that soot was made of small graphitic domains of polycyclic aromatic hydrocarbons (variously acronyms as PAH, PCA, or PNA). A large body of work, most notably the daring model of Frenklach *et al.* in 1984 [2], pointed to formation of the first aromatic ring as being the rate-determining step for growth toward soot.

Propargyl (linear C_3H_3, $CHCCH_2$) has gained wide support as the key precursor to aromatic hydrocarbons in flames, but its dominance, reaction pathway(s), and kinetics are still controversial. This paper examines the competing ideas in the context of recent calculations and data.

BACKGROUND: LITERATURE ON AROMATICS FORMATION

In 1989, Westmoreland *et al.* [3] reviewed the precursors and routes to single-ring aromatics which had been proposed to date. Previous mechanistic proposals had focused on molecular pathways (polyacetylene bridging, Diels-Alder additions), ion-molecule reactions, and radical addition or combination. Modeling their acetylene flame data [3] showed that only the radical routes:

- n-C_4H_5+C_2H_2 (·CHCHCHCH$_2$, route proposed by Cole *et al.* [4]);
- n-C_4H_3+C_2H_2 (·CHCHCCH, proposed by Stehling et al. [5] and by Frenklach et al. [2]), and/or
- C_3H_3+C_3H_3 (proposed in the literature by Kern and co-workers [6-7])

could be fast enough, necessarily proceeding by chemically activated isomerizations rather than thermal steps. However, they could not establish which of the three reactant pairs dominated, nor whether the detected C_4H_5 and C_4H_3 were the proper isomers.

Several possible propargyl paths then were proposed around the early 1990's:

- In 1989, we subsequently proposed [8] and later tested [9] a chemically activated pathway from C_3H_3 via chemically activated 1,5-hexadiyne and 1,2,4,5-hexatetraene, isomerizing to 3,4-dimethylenecyclobutene (DMCB). Corresponding thermal isomerizations are recognizable as a Cope rearrangement and a 2+2 sigmatropic ring closure. We proposed that DMCB might isomerize to fulvene (methylenecyclopentadiene) and then to benzene, possibly decomposing to phenyl + H. Chemical activation at the low-pressure (adiabatic) limit could allow reaction above all these intrinsic barriers. Reaching any well would require bimolecular collisions. This hypothesized route was based on thermal pyrolyses of the intermediates. Our reaction modeling [9] implied that phenyl would be an important product at high temperatures.
- Stein and co-workers [10] developed a similar route independently and at about the same time, using their VLPP data and the flame data of Ref. [1]. It proposed that DMCB might isomerize directly either to fulvene or benzene.
- Alkemade and Homann proposed another route [11] involving cyclopropenyl intermediates.
- Miller *et al.* [12] had proposed formation of benzene from propargyl, and Melius, Miller, and Evleth [13] later proposed a variety of routes based on singlet carbene intermediates, BAC-MP4//MP4/6-31G(d,p)//UHF/6-31G(d) potential energy surfaces, and adiabatic RRKM calculations. The end products were phenyl + H.

These promising proposals do not mean that we know that aromatics are formed from propargyl or that we know by what rate. Modeling by Frenklach *et al.* [14] in 1997 implied that the C_4H_3 route might be more important than the C_3H_3 route in some flames and at lower temperatures. Likewise, $C_3H_3+C_3H_4$ is still discussed, and $C_5H_5+C_5H_5$ routes have been proposed and supported by using assumed rate constants in large-mechanism modeling of shock-tube and flame data [15]. Finally, the different possible channels from $C_3H_3+C_3H_3$ will have different pressure dependences. In lieu of clean, direct measurement of rates and products at high temperatures, we must make use of more complex flame data and of calculations.

EXAMINING FLAME DATA

Recent MBMS measurements in an allene-doped ethylene flame by Oulundsen [16] allow comparisons to species in a matching undoped flame of Bhargava and Westmoreland [17]. Although most species are unperturbed, C_3's and C_6H_6 are affected.

Molecular-beam mass spectrometry (MBMS) was used to measure profiles of free-radical and stable-species mole fractions in one-dimensional flames (Table 1). Both flames had the same fuel-rich equivalence ratio $\phi = 1.90$ (fuel-rich), pressure of 2.666 kPa (20.00 Torr), and velocity at the burner of $u_{b\text{-}300} = 62.5$ cm/s. The doped flame was composed of 0.50 % allene, C_2H_4, O_2, and 49.7 % Ar, in comparison to the undoped flame with only C_2H_4, O_2, and 50.0 % Ar. The profiles were mapped between 0.5 mm and 45.0 mm above the burner surface. Mole fraction profiles were moved 0.9 mm (5 times the orifice diameter) towards the burner surface to account for probe perturbations. The temperature profile and area-expansion ratio were measured in the first study [17].

Calibration uncertainties affect the comparison of profiles. Among the C_3's, propene (C_3H_6) was calibrated directly, and C_3H_4 in the allene-doped flame was calibrated directly with allene. Other species were calibrated by the method of relative ionization cross-sections, C_3H_2 and C_3H_3 relative to C_3H_4, and C_3H_5 relative to C_3H_6, and C_3H_4 in the undoped flame (a mixture of propyne and allene) relative to C_3H_6. Direct calibration has an uncertainty of <10%, while the indirect calibration should be within a factor of two.

The surprise is that C_3H_3 remains constant within experimental uncertainty (Fig. 1), while C_6H_6 rises more than an order of magnitude (x20) in the allene-doped flame. C_6H_6 also peaks almost 4 mm earlier than propargyl and 3 mm earlier than its maximum in the undoped flame, which had been almost at the same position as that of propargyl.

Roughly, if propargyl were the sole reactant making benzene higher by a factor of twenty, we would have expected its mole fraction to be higher in the doped flame by a factor of 4-5 (square root of 20), but it is unchanged. A difference in rate of benzene destruction would affect this simple analysis. However, the temperatures and the mole fractions of H, O, and OH hardly change at all, so the oxidative environment for C_6H_6 is unchanged. Another contribution might be $C_3H_3+C_3H_4$ reaction, seeing that C_3H_4 is high and C_3H_3 is unchanged before the peak in C_6H_6, but the C_3H_4 mole fractions would have to be a factor of twenty higher in this region, and they are not.

A second interesting observation is that mass 41, assigned to C_3H_5, peaks at the same position as C_6H_6 (Fig. 2). Mass 41 probably has some contribution from HCCO, as mass 42 appears to be dominated by CH_2CO rather than C_3H_6. However, modeling implies that allyl and 2-propenyl

are formed easily from H+allene, and we propose that CH_2CO is formed from the chemically activated reaction O+allene = H+CH_2CO.

Table 1. Species measured in low-pressure flat flames of ethene/oxygen/50.0% argon and 0.50% propadiene/ethene/oxygen/49.7% argon at fuel-rich (ϕ=1.90) conditions.

Species	Ethene	Propadiene/ethene	Species	Ethene	Propadiene/ethene
H	Profile	Profile	CH_2CO	Profile*	Profile
H_2	Profile	Profile	CH_2CHO **	Profile	Profile
CH_2	Profile	Profile	CH_3CHO	Profile	Profile
CH_3	Profile	Profile	CO_2	Profile	Profile
CH_4	Profile	Profile	C_4H_2	Profile	Profile
OH	Profile	Profile	C_4H_3	-	Profile
H_2O	Profile	Profile	C_4H_4	Profile	Profile
C_2H_2	Profile	Profile	C_4H_5	-	Profile
C_2H_3	Profile	Profile	C_4H_6	-	Profile
C_2H_4	Profile	Profile	C_3H_3O/C_4H_7	-	Profile
CO	Profile	Profile	C_3H_4O/C_4H_8	Profile	Profile
HCO	Profile	Profile	C_3H_6O/C_4H_{10}	Profile	Profile
H_2CO	Profile	Profile	C_5H_4	Profile	Profile
O_2	Profile	Profile	C_5H_6	Profile	Upper bound
HO_2	-	Profile	C_4H_3O/C_5H_7	Profile	Upper bound
H_2O_2	-	Profile	C_4H_4O/C_5H_8	Profile	-
C_3H_2	Profile	Profile	C_4H_6O/C_5H_{10}	Profile	-
C_3H_3	Profile	Profile	C_4H_8O/C_5H_{12}	Profile	-
C_3H_4	Profile	Profile	C_6H_2	Profile	Profile
Ar	Profile	Profile	C_6H_4	Profile	Profile
HCCO	-	Postflame profile	C_6H_5	Profile	Profile
C_3H_5	Profile	Profile	C_6H_6	Profile	Profile

*Reported previously as C_3H_6. **Possibly CH_2CHO^+ ionization fragment of CH_3CHO.

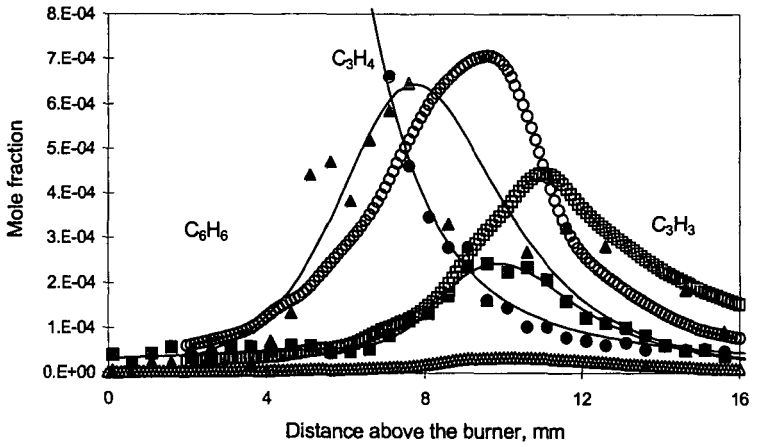

Figure 1. Species profiles in the ethene flames, undoped (open symbols) and allene-doped (filled symbols and lines): C_3H_4 (circles), C_3H_3 (squares) and C_6H_6 (triangles) in ethene flames.

Allyl has long been proposed as a precursor to benzene [18]. Stoichiometry works against it, though; its combination product C_6H_{10} has much hydrogen to lose. Also, it is not cyclic, and the weak allyl-allyl bond donates little energy for subsequent chemically activated reactions of C_6H_{10}.

Other explanations could that mass 78 might not be benzene or that benzene is a side product formed from phenyl. Ionization potentials are the basis of identification. They match literature values well for benzene and phenyl, although the IP measurement with electron-impact ionization is not so precise as to distinguish them definitively among hydrocarbon isomers. In the allene-doped flame, phenyl reaches its maximum slightly before benzene (Fig. 2). It is a factor of 10 higher and occurs 2.5 mm earlier than in the undoped flame.

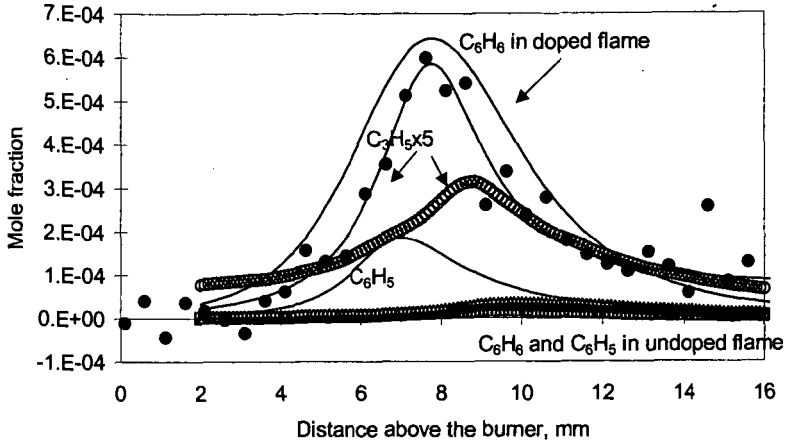

Figure 2. Species profiles in the ethene flames, undoped (open symbols) and allene-doped (filled symbols and lines): C_3H_5 (circles), C_6H_5 (squares), and C_6H_6 (triangles) in ethene flames.

C_4H_3 and C_4H_5 additions to C_2H_2 seem fairly plausible ways to reach aromatics here. Maximum mole fractions occur for C_2H_2 at 9 mm; C_2H_3 at 8.5 mm; C_4H_3 at about 9.5 mm; and C_4H_5 at 7 mm. All these are in the neighborhood of the C_6H_6 maximum. The C_4 radical peaks are both an order of magnitude higher in the doped flame.

CONCLUSIONS

There is strong evidence in many systems that propargyl combination is an important route to forming single-ring aromatics. It does not appear to explain the changes in benzene formation comparing MBMS profiles in a fuel-rich ethane flame with those in a near-identical flame doped with a small amount of allene. In the allene-doped flame, C_4H_3 and C_4H_5 routes may be dominant, despite the potential of allene as a C_3H_3 precursor.

With the correct kinetics, likely to be worked out in the next ten years, we will be able to use soot prediction from flame modeling for engineering analysis and design. To predict soot formation, we must be able to model flames of all sorts of fuels. There is no reason to think that propargyl combination should be the sole route to make aromatics, although it may often be the dominant one. Modeling of these and other flames will be used as an aid to interpreting the roles of the different routes, and new approaches are being applied to tighten the uncertainty of calibration factors.

ACKNOWLEDGEMENT

We gratefully acknowledge the support of the US Department of Energy, Basic Energy Sciences / Chemical Physics for support of this work under grant DE-FG02-91ER14192.

REFERENCES

1. Wagner, H.Gg., *18th Symposium (International) on Combustion*, The Combustion Institute, Pittsburgh, 1 (1980).
2. Frenklach, M., D.W. Clary, W.C. Gardiner, Jr., and S.E. Stein, *20th Symposium (International) on Combustion*, The Combustion Institute, Pittsburgh, 887 (1984).
3. Westmoreland, P.R., A.M. Dean, J.B. Howard, and J.P. Longwell, *J. Phys. Chem.* **93**, 8171-8180 (1989).
4. Cole, J.A., J.D. Bittner, J.B. Howard, and J.P. Longwell, *Combustion and Flame* **56**, 51 (1984).
5. Stehling, F.C., J.D. Frazee, and R.C. Anderson, *Sixth Symposium (International) on Combustion*, The Combustion Institute, Pittsburgh, 247 (1956).
6. Wu, C.H.; Kern, R.D. *J. Phys. Chem.* **91**, 6291 (1987).
7. Kern, R.D.; Singh, H. J.; Wu, C.H. *Int. J. Chem. Kin.* **20**, 731 (1988).

8. Thomas, S.D.; Westmoreland, P.R. "Role of C_3H_3 in Aromatics and Soot Formation," Paper 130g, 1989 Annual Meeting of AIChE, San Francisco CA, November 5-10, 1989.
9. Thomas, S.D., F. Communal, P.R. Westmoreland, "C_3H_3 Reaction Kinetics in Fuel-Rich Flames," *Preprints of Div. of Fuel Chemistry,* American Chemical Society, **36**, No. 4, 1448-1455 (1991).
10. Stein, S.E., J.A. Walker, M.M. Suryan, A. Fahr, *23rd Symposium (International) on Combustion*, The Combustion Institute, Pittsburgh, 85 (1991).
11. Alkemade, U., K.H. Homann, *Z. Phys. Chem. N.F.* **161**, 19 (1989).
12. Miller, J.A., R.J. Kee, C.K. Westbrook, *Ann. Rev. Phys. Chem.* **41**, 345 (1990).
13. Melius, C.F., J.A. Miller, E.M. Evleth, *24th Symposium (International) on Combustion,* The Combustion Institute, Pittsburgh, 621 (1992).
14. Wang, H., M. Frenklach, *Comb. Flame* **110**, 173 (1997).
15. Marinov, N.M., W.J. Pitz, C.K. Westbrook, A.M. Vincitore, M.J. Castaldi, S.M. Senkan, C.F. Melius, *Comb. Flame* **114**, 192 (1998).
16. Oulundsen Jr., G.E., "Measurements and Kinetics for Hydrocarbon-Chlorine and Allene-Doped Ethylene Flames," Ph.D. dissertation, Chemical Engineering, U. Massachusetts (2000).
17. Bhargava, A., P. R. Westmoreland, *Combustion and Flame* **113**, 333 (1998).
18. Kinney, R.E., D.J. Crowley, *Ind. Eng. Chem* **46**, 258 (1954).

MICROWAVE DESTRUCTION OF TRICHLOROETHYLENE IN A H_2O - O_2 - AR PLASMA

Youngsam Ko[1] , GoSu Yang[2], Daniel P. Y. Chang[3] and Ian M. Kennedy[4]

[1] Department of Environmental Engineering, Yosu National University, Korea

[2] Department of Mechanical Engineering, Chonbuk National University, Korea

[3] Department of Civil and Environmental Engineering, University of California Davis

[4] Department of Mechanical and Aeronautical Engineering, University of California Davis

INTRODUCTION

As of 1997, total U. S. emissions of volatile organic compounds (VOC) had fallen to an estimated 19 X 10^6 tpy (tons per year) while total NO_x emissions continued to rise to about 24 X 10^6 tpy [1]. Among VOC categories, solvent usage increased to roughly to 6.5 X 10^6 tpy [2]. Of especial concern are those compounds that are toxic air contaminants (TAC), or that may produce toxic by-products while undergoing capture and treatment. Chlorinated solvents, chlorofluorocarbons and sulfur hexafluoride fall into such a category because of their higher activation energies and low biodegradability under oxidative conditions. In terms of millions of U.S. tons of carbon equivalents, i.e., a measure of greenhouse gas potential, an increase of about 67% (16 X 10^6) tpy has occurred in the emissions of HCFCs, PFCs, and SF_6 during the decade of the 1990's [2]. Although increases in emissions have occurred, concentrations of emitted streams may actually be decreasing because of improved production methods or capture of these pollutants. Control costs generally increase as concentrations decrease, e.g., the cost of catalytic incineration of VOCs increases from about $5,000/ton to $50,000/ton for a compound such as benzene as its concentration drops from 100 ppm_v to 10 ppm_v resulting in even the least costly of combustion control measures impractical for low concentration streams. Control costs for NO_x range from roughly less than about $1000/ton for advanced burner technologies to over $5,000/ton for exhaust gas treatments [3]. Development of efficient control strategies for low concentrations of these compounds while avoiding NO_x formation is highly desirable.

Conventional methods for removing volatile organic compounds (VOC's) from gas streams include absorption, adsorption, condensation, and incineration (including thermal and catalytic). Among these technologies, adsorption is an efficient and economical method for moderate to low concentration streams. Nevertheless, adsorbates (such as VOCs) must be removed periodically after they saturate the adsorbents (e.g., activated carbon or zeolites) and require further treatment.

There are two conventional regeneration methods: steam and hot gas regeneration. The former requires a steam generation facility while leaving the adsorbent bed wet with condensate, thus requiring that time and equipment be available to dry out the bed before its reuse. Moisture in the condensate can also lead to undesirable chemical reactions between the VOCs and bed materials. Regeneration with a hot gas is accomplished by heating the adsorbent (and adsorbate) to a temperature sufficient to desorb the adsorbate. The flow of hot gas not only heats the adsorbent, but also purges the adsorbate as it is desorbed resulting in a lower final concentration factor. Effective adsorbents also create a problem in regeneration, since generally, the more effective the adsorbent the more difficult it is to remove the adsorbate. Thus, a long regeneration time and large purge gas volumes are required. Moreover, the heating requirements are large since not only the adsorbent, but also the adsorbent support, the adsorbent column, associated conduits and the purge gas itself often must be heated. If a higher temperature purge gas was used, the desorption could be more rapid, but thermal degradation could yield undesirable intermediate by-products and shorten the life of the adsorbent reducing its capacity. In the case of activated carbon the potential for a fire exists.

Microwave regeneration utilizes "dielectric heating" which eliminates many of the above drawbacks and provides benefits unobtainable with conventional regeneration. In the microwave regeneration process, heat is generated internally, i.e., within the adsorbent bed either by heating the adsorbate directly and/or the adsorbent. It does not need to be conveyed through a fluid; therefore a minimal amount of purge gas is used and large concentration factors can be obtained. Minimal heating of ancillary mass occurs, reducing over all energy requirements and cooling time. As a result, a microwave regeneration process makes it possible to desorb VOCs from adsorbents rapidly and efficiently. In addition, the microwave system can be used for the destruction of the desorbed waste stream.

Microwave technology for waste treatment

Plasma processing for environmental remediation applications is a developing technology. The primary interest in plasma processes has been in the area of combustion, due to the ability to generate extremely high temperatures, approaching 10,000 K, in the gas phase. By comparison,

most chemical thermal processes, such as incineration, operate at temperatures ranging from 2000 to 2500 K. The higher temperatures attainable in a plasma process minimize the potential for the *in situ* formation of polynuclear aromatic hydrocarbons(PAH), dioxins and furans, that are major concerns of incineration processes. The cooling of a plasma is rapid and not conducive to molecular growth processes that yield complex molecules. However, thermal systems that are operated with air suffer from a common problem - the production of oxides of nitrogen (NO_x).

Recently there has been a growing interest in potential applications of high-frequency plasmas. For example, Wang et al. [4] reported the use of a RF plasma system to convert dichlorodifluoromethane to methane and acetylene in a hydrogen environment. Microwave plasmas may also be applied to the remediation of off-gas streams. Microwave plasmas possess a number of advantages over plasmas generated by other types of electrical excitation which make them attractive for this application: (1) production of high ionization levels and molecular dissociation without excess heating of the contained gas; (2) construction of reaction vessels which are simple, free from contamination and less subject to damage because of the absence of internal electrodes; (3) production of little electrical interference; (4) absence of high voltages which can be easily contacted by operating personnel, i. e., absence of shock hazardous; (5) potentially lower power consumption; (6) and the ability to tolerate high concentrations of water. The latter feature is particularly important because it means that energy can be fed directly into a flow with high water concentration and a stable plasma can be established.

Although the microwave plasma process has been successfully applied in the metals [5] and microelectronics industries [6], the application of microwave plasma technology to hazardous waste treatment is very limited. Bailin et al. [7] first investigated the decomposition of organic compounds by passage through a microwave-induced oxygen plasma. The basic idea in their study was to apply microwave discharge energy to break chemical bonds of organic compounds under reduced pressure conditions. Hertzler et al. [8] oxidized halocarbons with molecular oxygen directly in a low-pressure tubular flow microwave plasma discharge reactor. Although conversion of parent compounds exceeded 99.99%, a complete product analysis was not provided, and, therefore effluent toxicity could not be determined. Moreover, in the above studies, the organic compounds were introduced in liquid form into the plasma reactor. In other words, a microwave plasma was used to treat liquid organic wastes.

Researchers in Japan have been particularly active in promoting plasma technology for waste remediation. They have included microwave plasma systems in their studies. Suzuki et al. [9] investigated the use of a microwave heated oxygen plasma for the conversion of metal chlorides into oxides. The method was shown to be successful in the conversion of a wide range of metals, from transition metals to lanthanides, with results that were consistent with an equilibrium analysis. Shimizu et al. [10, 11] studied the decomposition of trichlorotrifluoroethane with a microwave induced argon plasma. They used SiC fibers to assist in the generation of the plasma. The plasma was operated at one atmosphere pressure with small amounts of O_2 added to ensure complete conversion of C to CO_2. Somewhat surprisingly, they found that pulsed microwave operation achieved better destruction of the waste feed than DC operation. However, the reason for this behavior was not discovered.

Chlorine that is present in waste materials is most conveniently sequestered as HCl. When Cl is bonded to H it is effectively removed from participation in all further reactions, except at very high temperatures. Ultimately, HCl needs to be handled with devices such as wet scrubbers where it can be neutralized. Dechlorination of wastes is an important first step in reducing the toxicity of remediation by-products through the prevention of formation of compounds such as tetra-chloro-dibenzo-dioxin (TCDD).

The dechlorination of these compounds is thermodynamically favored by reaction in a reducing environment. Barat and Bozzelli [12] showed that an overall reaction of the form

$$CCl_4 + 2H_2O = 4HCl + CO_2$$

exhibited large equilibrium constants

T, *K*	K_p
300	3.8×10^{43}
800	7.6×10^{25}

When oxygen is present in the system, O competes with Cl for bonding with H atoms. Hence, the ideal conditions for dechlorination are reducing, not oxidative. Barat and Bozzelli used a quartz flow reactor, driven by a microwave plasma, to examine the reaction of H_2 and H_2O with chlorocarbons. Reactions with H_2 yielded non-parent chlorocarbons, low molecular weight hydrocarbons, and soot. Reactions with water yielded only carbon monoxide and carbon dioxide.

The production of carbon monoxide was a necessary side effect of the stoichiometry that was used; insufficient oxygen was available to ensure complete oxidation of the available carbon. Ravindran et al. [13] have shown from thermodynamic arguments that a similar dechlorination in hydrocarbon rich environments is also possible.

EXPERIMENTAL

A continuous microwave generator(low ripple magnetron, 1.5 KW, 2450 MHz; Gerling Laboratory) and a plasma tuner (ASTEX) were used to generate a steam plasma. A schematic diagram illustrating the gas flow paths is shown in figure 1. The main components of the system consisted of a plasma reactor (AX 7200), a plasma tuner, microwave generator and microwave wave-guide. Continuous microwave power from the magnetron was conducted through a waveguide to the plasma torch. The forward and reflected powers from the plasma torch could be maximized and minimized by adjusting the tuning stubs on the plasma tuner. The forward power was maintained at 600W and the reflected power was maintained below about 100 W. The plasma reactor consisted of a 1/4" O.D. ceramic tube through which the mixture to be reacted was passed, and an outer quartz tube housing.

Argon, oxygen and steam were used as gases from which a plasma was generated. The Ar was utilized as a basic carrier and reference gas, the O_2 provided stoichiometric oxidation requirements for the chlorinated hydrocarbon tested and steam provided a reactive atmosphere containing additional hydrogen. Steam was generated by a coiled-tubing heater and was carried by Ar gas. All plasma gas flow rates were controlled by rotameters meters and were introduced to the plasma torch as shown in Figure 1. The total flow rate of gases was held constant at 10 lpm. The proportion of steam was established by trial-and-error to obtain an intense plasma. All the lines from the flow meter to the torch were heated to prevent steam condensation.

A solvent, trichloroethylene(TCE) was selected as the target compound and introduced through the ceramic tube in the plasma reactor. Destruction and removal efficiency (DRE) for TCE was calculated from measured concentrations remaining and the known flow rates to determine the efficiency of the steam plasma. The effluent gas from the plasma reactor was passed through two traps. The first trap consisted of a coiled water concentrator and an Erlenmeyer flask, in which the most of the steam was condensed. A second back-up trap was used to condense the remaining water vapor. Gas samples were collected on an adsorbent bed of Carbotrap C. A gas sampling loop and switching valve were used to inject gas samples to the GC from a by-pass line exiting the second trap. Liquid samples were also collected from the first and the second traps. The reactor effluents were analyzed with an on-line GC equipped with a TCD detector (TCE) and by GC/MS (adsorbent tubes - TCE and other by-products), and a specific ion meter for chloride. The Carbotrap samples were soxhlet extracted for 20 hours with methylene chloride with deuterated phenanthrene and terphenyl added as internal standards. The samples were evaporated down to 0.5 mL prior to injection into a HP GC/MS system.

RESULTS AND DISCUSSION

The DRE for TCE was evaluated in the microwave system for a series of microwave powers at a condition of 30% steam with an O_2 flow rate of 0.5 lpm and an argon flow rate of 6 lpm. The concentration of TCE in the input flow to the plasma was 1700 ppm. The small amount of O_2 was added to ensure that sufficient O_2 was available in the system to complete the oxidation of TCE. The post plasma gases were analyzed on a GC. The results are shown in Table 1.

Table 1. DRE and Cl ion concentration in post plasma gases at different operating powers

Power (W)	DRE (%)	Cl^- (ppm)
200	58	10800
300	99.8	38700
400	100	52000
500	100	56200
600	100	56900

It is apparent that the plasma system is quite capable of achieving significant destruction at operating powers as low as 400 W. The chloride ion concentration is a measure of the HCl that is formed and is second measure of the accuracy of the sampling system and analysis. The constant Cl^- concentration at powers above 400 W confirms the conclusion that all the input chlorine was sequestered as HCl under these conditions.

Experiments were also conducted with a power of 600 W and a TCE input concentration of 1700 ppm but with varying concentrations of steam in the plasma. The results of those tests are shown in Table 2.

The presence of steam is seen to have an important impact on the effectiveness of the microwave destruction process. The effect of steam that is shown in Table 2 is consistent with the observation of Barat and Bozzelli that at the temperatures of the microwave plasma, thermodynamics favors the dechlorination of chlorinated hydrocarbons.

Finally, the Carbotrap samples were analyzed on a GC/MS system for products of incomplete combustion. The microwave power was 600 W with 30% steam and 1700 ppm of TCE. This analysis did not find any evidence of dioxins or furans, showing that a high DRE can be achieved without the production of other products of incomplete reaction.

Table 2. DRE at 600 W of input microwave power with varying steam concentrations

Steam fraction of flow (%)	DRE
0	99.78
5	99.9
10	100
20	100
30	100

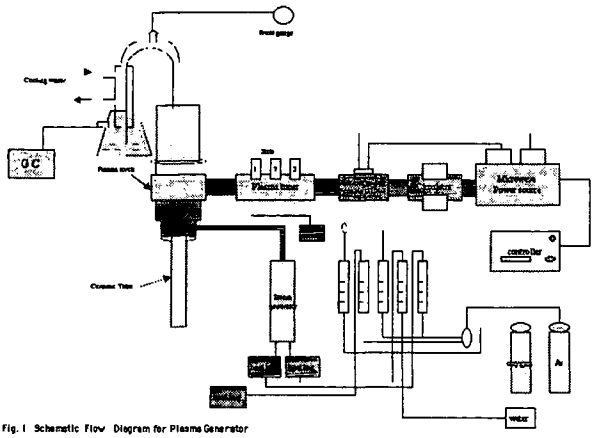

Fig. 1 Schematic Flow Diagram for Plasma Generator

REFERENCES

1. U.S. EPA, National air pollutant emission trends: 1900 - 1998, Technology transfer network chief database, http://www.epa.gov/ttn/chief (2000).

2. U.S. EPA, Inventory of U.S. Greenhouse gas emissions and sinks: 1990 – 1997, technology transfer network chief database, http://www.epa.gov/ttn/chief (1999).

3. U.S. EPA, Cost-effective nitrogen oxides (NOx) reasonably available control technology (RACT). Memorandum from D. Kent Barry, Air Quality management Division, Office of Air Quality Planning and Standards, Washington D.C., (1994).

4. Wang, Y., Lee, W., Chen, C. and Hsieh, L., Decomposition of dichlorodifluoromethane by adding hydrogen in a cold plasma system, *Environmental Science and Technology,* **33**, 2234-2240 (1999).

5. Zanetti, R. J., *Chemical Engineering,* **90**, 14-16 (1983).

6. Fraser, D. B., Westwood, W.D. (1990) in , , Eds.,, *Handbook of plasma processing technology,* in (eds. S. M. Rossnagel, J. J. Cuomo and W. D. Westwood), Noyes Park Ridge, NJ (1990).

7. Bailin, L. J. and Hertzler, B. L., *Detoxification of pesticides and hazardous wastes by the microwave plasma process*, ACS Symposium Series 73 Chicago, August 29 - September 2. (1977).

8. EPA, Development of microwave plasma detoxification process for hazardous wastes (phase iii), (1979).

9. Suzuki, M., Komatsubara, M., Umebayashi, M. and Akatsuka, H., Conversion of chloride waste into oxide by microwave heated oxygen plasma, *Journal of Nuclear Science and Technology,* **34**, 1159-1170 (1997).

10. Shimizu, Y., Ogawa, K., Takao, Y. and Egashira, M., Decomposition of trichloroethylene by microwave-induced ar plasma generated from SiC ceramics under atmospheric pressure, *Denki Kagaku,* **66**, 1018-1025 (1998).

11. Shimizu, Y., Akai, Y., Hyodo, T., Takao, Y. and Egashira, M., Decomposition of trichlorotrifluoroethane by microwave-induced ar plasma generated from SiC ceramics under atmospheric pressure, *Journal of the Electrochemical Society,* **146**, 3052-3057 (1999).

12. Barat, R. B. and Bozzelli, J. W., Reaction of chlorocarbons to HCl and hydrocarbons in a hydrogen-rich microwave-induced plasma reactor, *Environmental Science Technology,* **23**, 666-671 (1989).

13. Ravindran, V., Pirbazari, M., Benson, S. W., Badriyha, B. N. and Evans, D. H., Thermal destruction of chlorinated hydrocarbons by reductive pyrolysis, *Combustion Science Technology,* **122**, 183-213 (1997).

ZEOLITE-BASED MERCURY SORBENT-
LABORATORY TESTING AND MODELING

Thomai Panagiotou, Joseph R. Morency and Constance L. Senior

Physical Sciences Inc., 20 New England Business Center, Andover, MA 01810

KEYWORDS: mercury removal, zeolites, air pollution

INTRODUCTION

Mercury is one of the 11 toxic metals recognized by the Title III of the Clean Air Act Amendments as Hazardous Air Pollutants and has received special attention because of its high volatility combined with high toxicity and bioaccumulation. In the United States 21% of the total mercury emissions are attributed to coal-fired utility boilers.[1] The forms of mercury vapor in power plant flue gases are elemental Hg and oxidized Hg (probably $HgCl_2$, and in some cases, HgO), with elemental mercury being the predominant form.[2-6]
Generally, $HgCl_2$ can be removed from the flue gases easier than elemental Hg, either through wet scrubbing, dry injection or fixed bed using activated carbon.[3-10] However, removal of elemental mercury is more challenging, since it is practically insoluble in water and can be removed to a certain extend with expensively treated activated carbons

PSI has developed and tested mercury sorbents for enhanced removal of both elemental and oxidized mercury based on a natural zeolite. The sorbents were injected to mercury containing flue gases from combustion of coal, which were at 150 or 230°C. Three different forms of this zeolite were used, plain zeolite and two types of modified zeolited treated with proprietary agents.

EXPERIMENTAL

Combustion of coal took place at PSI's electrically heated Entrained Flow Reactor (EFR). This apparatus, which can achieve a maximum gas temperature of 1723 K, has been used extensively on many of PSI's combustion research projects. Fuel, air, other gases and coal are injected at the top of the reactor. The combustion section is an externally heated ceramic tube that is 8.57 cm in internal diameter and 158 cm in length.

Once the flue gas exited the furnace, it entered a quartz tubular reactor where sorbent injection took place. The reactor temperature was kept constant to 130 or 200°C. To ensure that no additional mercury removal took place downstream the reactor, the flue gases passed through a series of particulate removal devices, including an impactor, two cyclones and finally a filter, see Fig. 1. The particle removal devices were kept at about 150°C.

After leaving the filter assembly, the gas stream passed into a series of impingers designed to collect any mercury left in the flue gases and determine the mercury species, as specified by Ontario Hydro Method. The sorbent injection system consisted of a syringe with the sorbent loaded on driven by a syringe pump into a tube. The air flowing in the tube was used to carry the sorbent. The injection rate was controlled by the speed of the syringe pump.

Coal was burned in the EFR to more closely approach the conditions found in power plant flue gases. For this program, a bituminous coal, Pittsburgh seam, was used. The mercury content of the coal as determined by Neutron Activation Analysis is 0.11 ppm. To maintain 10-70 $\mu g/m^3$ levels of Hg concentration, a mercury laden stream of oxygen was added to the top of the EFR.

Two types of treated zeolite were used, TZ1 and TZ2, and also untreated zeolite, UZ, with particle size in the range of 1 to 5 μm. In addition, a high-surface-area activated carbon, AC, CL-213, from Barneby and Sutcliffe was used as a comparison.

The normal operating conditions were:

- Coal flow rate: 1.7 g/min
- Furnace temperature: 1700 K
- Equivalence ratio: 1.2
- Mercury reactor residence time: 2-3 s
- Mercury reactor temperature: 130 and 230°C.

At the end of each experiment six samples were collected and analyzed for mercury concentration: the ash/sorbent from the impactor and the two cyclones, the filter with any collected material, the three liquid samples from the Ontario-Hydro sampling train and the rinse of the glassware.

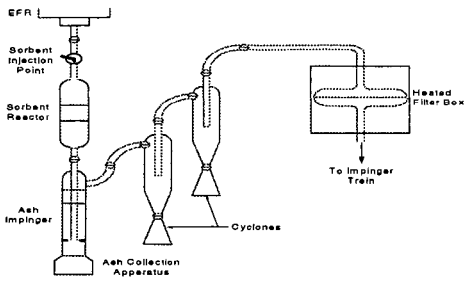

Figure 1. Sorbent injection, reactor and particulate collection apparatus for sorbent injection experiments.

RESULTS

Sorbent Injection Data

Figure 2 shows a plot of mercury capture as a function of sorbent:Hg ratio. For all sorbents capturing efficiency increased with sorbent to mercury ratio. The removal efficiencies of a treated zeolite (TZ2) and activated carbon (AC) were well over 90% even for modest sorbent to Hg ratios in the range of 25,000. The other treated zeolite (TZ1) exhibited removal efficiencies 45-55% for average sorbent to mercury ratios and up to 85% for high sorbent to mercury ratios, of about 90,000. The temperature did not appear to affect the capturing efficiency of the sorbents.

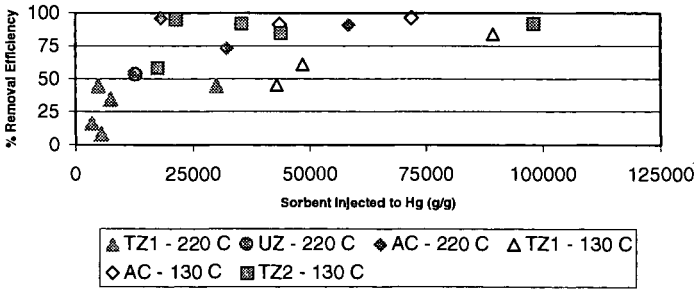

Figure 2. Mercury removal efficiency as a function of sorbent to mercury ratios.

Figure 3 shows the amount of mercury removed per unit mass of sorbent (sorbent utilization) plotted against the sorbent to mercury ratio present in the effluent stream. As the sorbent to mercury ratio increases, the amount of mercury removed per unit mass of sorbent decreases for all sorbents.

Figure 4 shows the percentage of oxidized mercury in the remaining mercury (was not removed by the sorbents) as a function of sorbent to mercury ratio. For low sorbent to mercury ratios, oxidized mercury decreases from 25% to less than 5% at a sorbent to mercury ratio of 25,000. Then it increases to about 50% for a sorbent to mercury ratio of 50,000 and decreases to less than

Mercury mass balance closure was determined for all runs by adding the mercury from each of the analyzed samples and dividing by the sum of the theoretical mercury from the combustion of the coal and the added mercury from the permeation tube as determined by the Jerome analyzer. The mercury mass balance for most of the runs was in the range of 70-110%.

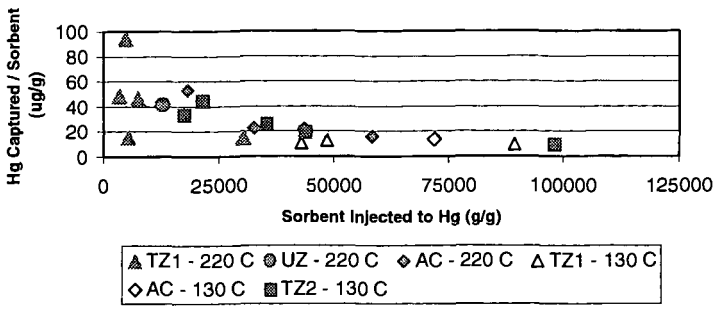

Figure 3. Sorbent utilization as a function of sorbent to mercury ratio.

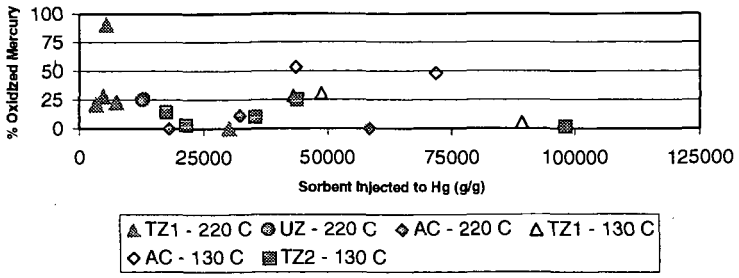

Figure 4. Percentage of oxidized mercury in the remaining (not removed) mercury.

Baseline Runs

In order to characterize the experimental apparatus and explain experimental data, three types of baseline runs were conducted. In all cases additional mercury was added to the system.

(A) No coal combustion took place and no sorbent was injected. The purpose of these experiments was to determine the amount of mercury that may be lost while flowing through the furnace.

(B) No coal combustion took place but treated zeolite was injected. The purpose of these experiments was to determine the amount of mercury captured by the treated zeolite when no coal combustion products are present.

(C) Coal combustion took place but no sorbent was injected. The purpose of these experiments was to measure the amount of mercury removed by the fly ash alone.

For baseline A runs, over 98% of the total amount of mercury injected is recovered in the impingers at the end of the baseline A runs. This indicates that there is no substantial amount of mercury lost or unaccounted for while flowing through the furnace. Also for these runs, greater than 95% of the mercury is collected as elemental mercury.

In baseline type B, TZ1 was injected into the sorbent reactor at 130°C (266°F), with no coal combustion taking place. The sorbent to Hg ratio was 89,000 and the removal efficiency was 85 %. Similar removal efficiencies of the same sorbent were found in presence of combustion products, see Fig. 2.

Removal efficiencies from ash, as measured in baseline C runs (ash baseline) are shown in Fig. 5. Removal efficiencies increase from about 35% to 65% as the ash to mercury increases from 50,000 to 120,000.

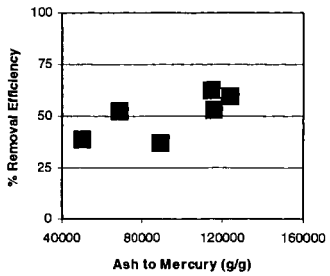

Figure 5. Ash removal efficiency as a function of ash to mercury ratio.

Modeling

The impact of speciation of mercury on activated carbon performance has been quantified in laboratory fixed bed experiments[11] and these data can be applied to models for the performance of sorbents in duct injection mode.[12] Figure 6 shows a calculation of the mercury removal at 130 °C for 5 micron activated carbon particles and a mercury concentration of 35 $\mu g/m^3$. The calculation assumes plug flow conditions with a two second residence time. Using fixed bed data to determine the reactivity of a single activated carbon to elemental mercury and mercury chloride, the figure shows the removal efficiency for both species. Mercury chloride shows a higher removal rate for a fixed sorbent to mercury ratio. Figures 2 and 6 show a good agreement between theory and experiments.

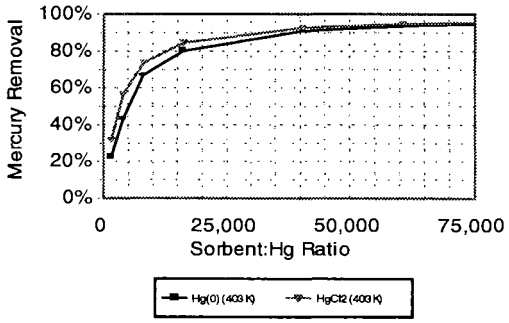

Figure 6. Calculated mercury removal for 2 seconds residence time at 130°C, assuming 5 micron activated carbon and concentration of 35 $\mu g/m^3$.

DISCUSSION

The ash baseline runs, see Fig. 5, indicate that ash can remove substantial amounts of mercury, as long as sorbent is not present. However, in the presence of sorbent, ash appears to lose its ability to remove mercury. If we assume that the removal efficiency of ash is independent of the presence of sorbent, then the removal efficiencies in presence of sorbent would have to be much higher than those indicated in Fig. 2.

Results indicate that oxidation of mercury takes place in presence of ash and/or sorbent. Baseline A suggests that only 5% of the injected mercury is oxidized in the furnace when no combustion products are present. However, in the presence of combustion products and/or sorbents, oxidized mercury can be 25-50% of the remaining (not removed) total mercury. Taking into account the removal efficiency, there is a net production of oxidized mercury from elemental in those experiments.

Physical Sciences Inc. (PSI) is developing mercury sorbents using a zeolite material treated with proprietary agents for improved capture of elemental as well as oxidized mercury. The performance of these sorbents was compared with that of activated carbon tested at similar conditions. To identify removal mechanisms of mercury, the mercury removal process was modeled using an adsorption/diffusion model.

The mercury removal efficiencies of sorbents varied in the range of 45-96% for sorbent to Hg ratios in the range of 5,000-96,000. A treated zeolite (TZ2) and the activated carbon exhibited removal efficiencies well over 90% at modest sorbent to Hg injection ratios of 25,000.The sorbent utilization, expressed as the amount of mercury removed per unit mass of sorbent, decreased from 80 μg Hg/g of sorbent to 6 μgHg/g of sorbent as the sorbent to Hg ratio increased from 5000 to 96,000. When no sorbent was injected, ash did remove some mercury, but in the presence of sorbent the role of ash in mercury removal appeared to diminish, presumably due to the higher reactivity of the sorbent with respect to the ash. Also, when no sorbent was present ash appeared to oxidize mercury, but in the presence of sorbent no substantial oxidation of mercury appeared to have taken place.

Results from the modeling effort suggest that at low sorbent injection rates mercury removal is highly influenced by adsorption kinetics. At higher concentrations diffusion becomes more pronounced. Also, modeling results indicate that most mercury is removed very shortly after injection, while long injection times do not substantially increase the removal rate.

ACKNOWLEDGMENTS

This work was supported by the Department of Energy under Grant # DE-FG02-97ER82456.

REFERENCES

1. *Mercury Study Report to Congress*, EPA-452/R-96-001g, 1996.
2. Tumati, P.R.; DeVito, M.S. "Partitioning Behavior of Mercury During Coal Combustion," presented at the Joint ASME/IEEE Power Gen. Conf., Kansas City, KS (October 1993).
3. DeVito, M.S.; Jackson, B.L. "Trace Element Partitioning and Emissions in Coal-Fired Utility Systems," presented at the 87th Annual Meeting and Exposition of the Air and Waste Management Association, Cincinnati, OH (June 1994).
4. Meij, R. "Distribution of Trace Species in Power Plant Streams: A European Perspective," presented at American Power Conf., Chicago (April 1994).
5. Nordin, A.; Schager, P.; Hall, B. "Mercury Speciation in Flue Gases: A Comparison of Results from Equilibrium Calculations with Results from Laboratory Experiments," Swedish Flame Days, Turkoo, Finland (September 1990).
6. Young, B.C.; Miller, S.J.; Laudal, D.L. "Carbon Sorption of Trace Mercury Species," proceedings of the 11th Annual Pittsburgh Coal Conference (September 1994), pp. 575-580.
7. Gorishi, B.; Gullet, B.K. "Sorption of Mercury Species by Activated Carbon and Calcium Based Sorbents: Effect of Temperature, Mercury Concentration and Acid Gases," *Waste Management & Research* **1998**, *6*, 582-593.
8. Guijarro, M.I.; Mendioroz, S.; Munoz, V. "Effect of Morphology of Sulfurized Materials in the Retention of Mercury from Gas Streams," *Ind. Eng. Chem. Res.* **1998**, *37*, 1088-1094.
9. Mendioroz, S.; Guijarro, M.I.; Bermejo, P.J.; Munoz, V. "Mercury Retrieval from Flue Gas by Monolithic Absorbents Based on Sulfurized Sepriolite," *Environ. Sci. Technol.* **1999**, *33*, 1697-1702.
10. Karatza, D.; Lancia, A.; Musmarra, D. "Fly Ash Capture of Mercuric Chloride Vapors From Exhaust Combustion Gas," *Environ. Sci. Technol.* **1998**, *32*, 3999-4004.
11. Carey, T.R., Hargrove, O.W., Richardson, C.F., Chang, R., and Meserole, F.B., "Factors Affecting Mercury Control in Utility Flue Gas Using Sorbent Injection," Paper 97-WA72A.05, presented at Air & Waste Management Association" 90th Annual Meeting, June 8-13, 1997, Toronto, Ontario, Canada.
12. Meserole, F.B., Chang, R., Carey, T.R., Machac, J., Richardson, C.F., "Modeling Mercury Removal by Sorbent Injection," *J. Air Waste Manage. Assoc.*, **1999**, *49*, 694-704.

PREDICTION OF MERCURY AIR EMISSIONS FROM COAL-FIRED POWER PLANTS

Constance L. Senior
Physical Sciences Inc.
20 New England Business Center
Andover, MA 01810

KEYWORDS: mercury, hazardous air pollutants, coal-fired power plant

INTRODUCTION

A recent report by the Environmental Protection Agency (EPA) on emission of hazardous air pollutants by electric utilities predicted that emissions of air toxics from coal-fired utilities would increase by 10 to 30% by the year 2010.[1] Mercury from coal-fired utilities was identified as the hazardous air pollutant of greatest potential public health concern. Anthropogenic emissions of mercury account for 10 to 30% of the world-wide emissions of mercury.[2] EPA has estimated that during the period 1994-1995 annual emissions of mercury from human activities in the United States were 159 tons.[2] Approximately 87% of these emissions were from combustion sources. Coal-fired utilities in the U.S. were estimated to emit 51 tons of mercury per year into the air during this period.

The form of mercury emitted from point sources is a critical variable in modeling the patterns and amount of mercury deposition from the atmosphere.[1,3] Both elemental and oxidized mercury are emitted to the air from combustion point sources. Elemental mercury has a lifetime in the atmosphere of up to a year, while oxidized forms of mercury have lifetimes of a few days or less[6] as a result of the higher solubility of Hg^{+2} in atmospheric moisture. Elemental mercury can thus be transported over long distances, whereas oxidized and particulate mercury deposit near the point of emission. Once mercury has deposited on land or water, it can transform into methylmercury, an organic form, and thereby enter the food chain. Humans are most likely to be exposed to methylmercury through consumption of fish.

Measurements of the concentration of mercury species taken in the stacks of pilot and full scale coal combustion systems show more than half of the vapor phase mercury as an oxidized form which is likely to be $HgCl_2$. Current measurement methods cannot identify specific oxidized species of mercury.[4-9] The range of observed values is broad: one study consisting of mercury speciation measurements from fourteen different coal combustion systems reported anywhere from 30% Hg^{+2} to 95% Hg^{+2} upstream of the air pollution control device (APCD).[4]

Although we can identify the major reaction pathways for mercury in coal combustion flue gas with some degree of confidence, we cannot yet make quantitative predictions of the emissions of specific mercury species from coal-fired power plants. The goal of this work is to advance the state of knowledge such that a predictive model for emissions of total mercury and for speciation of mercury can be formulated.

MERCURY EMISSIONS

A simple mass balance model for emissions of mercury from coal-fired power plants was devised to test our current understanding of mercury transformations in flue gas. The post-combustion region of the boiler was divided into three parts: 1) convective section to air heater (AH); 2) electrostatic precipitator (ESP); and 3) flue gas desulfurization unit (FGD). Concentrations of mercury species (gaseous and condensed) in each section were either calculated from equilibrium or plant parameters, or assigned based upon limited observations available from field data. All of the mercury is assumed to start as gaseous elemental mercury (Hg^0). In the AH section, elemental mercury can oxidize to Hg^{+2}, nominally the sum of HgO and $HgCl_2$. In addition, both Hg^0 and Hg^{+2} can be adsorbed on particulate matter in the AH section, converting them to Hg_p. No change of mercury speciation or partitioning was calculated in the ESP because there are not enough data available to deduce mechanisms (or clear trends). In the FGD section, both Hg^0 and Hg^{+2} can be absorbed into the scrubber solution. In addition, a fraction of the adsorbed Hg^{+2} can be converted to gaseous Hg^0. The model therefore predicts the speciation and emissions of mercury from the boiler based upon coal mercury content, equilibrium at elevated temperatures, assumed mercury partitioning coefficients in the various sections of the boiler, and scrubber operation as outlined in Table 1.

Recent DoE-sponsored field studies have been conducted to measure mercury speciation and mercury mass balances on coal-fired power plants using the Ontario Hydro method for gaseous mercury sampling. These data provide the best set for testing the model. In one study,[8] six

power plants were sampled which all burned Eastern bituminous coal. The plants all had wet scrubbers and ESP's. In another study,[9] a power plant burning a Western lignite was sampled. This plant also had a wet scrubber and an ESP.

Table 1. Mercury Model Parameters

Parameter	Value	Notes
Fraction of Hg^0 Oxidized in AH	**	Calculated from Equilibrium at 825 K
Fraction of Hg^0 Adsorbed in AH	0%	Assumed
Fraction of Hg^{+2} Adsorbed in AH	**	Calculated from LOI for bituminous coals
Fraction of Hg^0 Oxidized in ESP	0%	Assumed
Fraction of Hg^0 Adsorbed in ESP	0%	Assumed
Fraction of Hg^{+2} Adsorbed in ESP	0%	Assumed
Collection Efficiency of ESP	**	Input from Plant Operation
Fraction of Hg^0 Absorbed in FGD	0%	Assumed
Fraction of Hg^{+2} Absorbed in FGD	**	Calculated from scrubber type and operating parameters
Fraction of Adsorbed Hg^{+2} Reduced to Hg^0 in FGD	**	Calculated from scrubber type and operating parameters

Since there is not currently enough information on the gas-phase reactions of mercury in flue gas, a simple approach was taken to predict the amount of mercury oxidation that takes place in the convective pass. When detailed kinetic information is available, this will be incorporated into the model. The amount of oxidation was calculated assuming that the chemical composition is frozen, equal to the equilibrium composition at 825 K. The results of equilibrium calculations at 20% excess air for a number of different coals were used to derive this correlation, shown in Figure 1. A range of chlorine contents, from 25 to 4500 ppm, were used in the calculation. At very low chlorine contents (< ~50 ppm), most of the gas-phase oxidized mercury is predicted to be HgO. Many western fuels fall into this low-chlorine category. The adsorption behavior of HgO on fly ash may be different from $HgCl_2$.

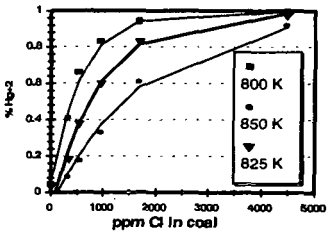

Figure 1. Predicted percentage of oxidized Mercury as a function of coal chlorine content.

Although, the oxidation of elemental mercury in the convective pass was assumed to proceed entirely via gas-phase reaction, experimental evidence suggests that some fly ash can catalyze oxidation of elemental mercury. Iron oxide is thought to be responsible for this oxidation.[28] Subsequent versions of the model may thus need to include a contribution from catalytic oxidation by fly ash. In this case, the iron content of the coal (and perhaps mineralogy) would be needed as input data.

At this time, it is not possible to generalize and conclude that high carbon in ash will always give high levels of particulate-bound mercury. However, in the case of similar coals, there may be a relationship as illustrated in Figure 2. The figure shows mercury measured in the ash, as sampled directly from the flue gas using the Ontario Hydro method, for nine different bituminous coals, all from the Northern Appalachian or Illinois Basins. The data were taken either at full scale power plants[8] or at a large pilot scale unit.[7] For these coals, there is a relationship between carbon content of ash (as measured by loss-on-ignition) and mercury content. However, the coals represented in the data are all very similar. Data will have to be obtained from a wider range of bituminous coals in order to generalize this relationship.

Western sub-bituminous coals produce fly ash which is very high in calcium. In some cases, ash from these coals has been observed to adsorb large amounts of mercury in the particulate collection device.[10] Calcium silicate sorbents also adsorb mercury chloride.[11] However, western coals are generally low in chlorine and produce very little mercury chloride. Some

component of the ash from these coals appears to adsorb elemental mercury. At this time, the mechanism by which elemental mercury is removed by the ash from western sub-bituminous ash is not known.

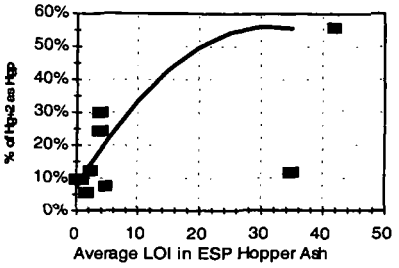

Figure 2. Mercury content of ash sampled at ESP inlet as a function of loss-on-ignition (LOI) of ESP hopper ash for nine different bituminous coals (References 7 and 8)

The majority of utility plants use an electrostatic precipitator (ESP) for particulate control; approximately 10 per cent use a fabric filter or baghouse instead. In the laboratory, fly ash has been observed to act as a catalyst for oxidation of elemental mercury.[12] In other laboratory work,[13] oxidized mercury has been observed to desorb from carbon-based sorbents and this may also occur for mercury adsorbed on fly ash in particulate control devices.[7,9]

Much of the discussion of adsorption of mercury by ash in the convective section applies to the behavior of mercury in the particulate control device. Unfortunately, little recent data on the removal of mercury species across ESPs and baghouses exist. (Older data taken with EPA Method 29 have been shown to speciate mercury incorrectly.) In a pilot scale study conducted by McDermott Technologies and involving combustion of three different Ohio bituminous coals,[7] gas-phase elemental mercury was removed by both a baghouse and an ESP, while oxidized mercury increased across both devices. This was also observed in a full scale power plant burning a North Dakota lignite.[9] As mentioned previously, ash from certain western sub-bituminous coals has been shown to remove elemental mercury from flue gas, particularly at lower temperatures.[14] Higher amounts of removal have been observed in baghouses relative to ESPs.

Since there are not enough data on the removal of mercury species across particulate control devices, no correlations have been developed for the preliminary model. Once a larger set of data has been assembled, it may be possible to derive relationships that take into account temperature, coal type, and particulate control device type.

A portion of the mercury may be adsorbed on the fly ash at the inlet to the particulate control device.[7,12] Combustion of bituminous coals can result in unburned carbon which has been suggested to adsorb mercury. Mercury has been found to concentrate in the carbon-rich fraction of fly ash.[15] Preliminary experimental work on adsorption of gaseous mercury on coal char[16] showed that $HgCl_2$ was adsorbed more efficiently than Hg^0, with two to fifty times more $HgCl_2$ adsorbed than Hg^0 under the same conditions, and the adsorption of the former was correlated with char surface area. This would also indicate that adsorption of $HgCl_2$ is a physical adsorption process. Adsorption of elemental mercury depended on the rank of the coal from which the char was derived. These results suggest that the nature of the unburned carbon, in terms of morphology and surface chemistry, strongly affects mercury adsorption.

Recent sampling campaigns on full scale utility boilers[8,9] and a large pilot scale unit[7] have provided data on the speciation of mercury before and after the FGD. Scrubbers have been observed to efficiently remove oxidized mercury, but not elemental mercury. Based on a detailed study of the behavior of mercury in a pilot scale wet scrubber,[7] the adsorption of oxidized mercury appears to be strongly correlated with the mass transfer in the scrubber. The liquid-to-gas ratio (L/G) was a good indicator for the amount of Hg^{+2} removed by the scrubber. The composition of the scrubber liquid and design of the scrubber are also important in determining the removal of Hg^{+2} and the nature of the scrubbing solution must be known in order to model mercury removal.

Pilot scale data have been taken on the effect of scrubber slurry pH on mercury removal in limestone scrubbers.[7] These suggest that the type of scrubber and the L/G ratio, not the pH, are the two key variables for modeling adsorption of Hg^{+2} across FGDs. Under some conditions, limestone scrubbers have been observed to reduce adsorbed mercury back to Hg^0 giving rise to higher concentrations of elemental mercury at the outlet than at the inlet. Assuming that no Hg^0

is adsorbed by the scrubber, the amount of adsorbed Hg^{+2} that is reduced can be calculated from the ratio of the increase in elemental mercury to the decrease in Hg^{+2} across the scrubber. Based on very limited data, this also appears to be related to the L/G ratio in the scrubber, although the effect is slight.

Figures 3 and 4 show a comparison of the measured and calculated values for mercury speciation (denoted by the fraction of mercury as Hg^{+2}) and total mercury emissions from the stack, respectively. The model predicts the stack emissions very well (r^2=0.94). Although the model is simple in its current form, it also predicts speciation well (r^2 = 0.59) using only limited information about the coal composition and operation of the air pollution control equipment. The model is able to predict a range of speciation from less than 5% Hg^{+2} to more than 30% Hg^{+2}.

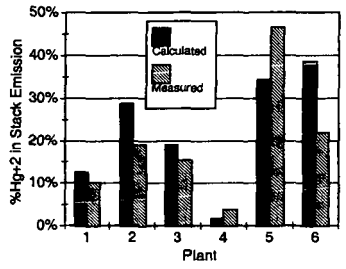

Figure 3. Predicted vs. measured stack speciation.

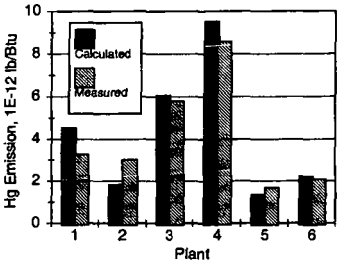

Figure 4. Predicted vs. measured emissions of mercury.

REFERENCES

1. Keating, M.H., et al. *Mercury Study Report to Congress, Volume I: Executive Summary*, EPA-452/R-97-003, December 1997.

2. Stein, E.D., Cohen, Y., and Winer, A.M. *Critical Rev. Environ. Sci.Technol.*, **1996**, *26*, 1-43.

3. Pai, P., Karamchandani, P., and Seigneur, C. "Uncertainties in Modeling Long-Range Transport and Fate of Mercury Emissions in North America," presented at EPRI Managing Hazardous Air Pollutants, Fourth International Conference, Washington, DC, November 12-14, 1997.

4. Meij, R. (1994), *Fuel Processing Technology* **39**: 199-217.

5. Prestbo, E.M. and Bloom, N.S. *Water, Air, Soil Poll.*, **1995**, *80*, 145-158.

6. Fahlke, J. And Bursik, A. *Water, Air, Soil Poll.* **1995**, *80*, 209-215.

7. Holmes, M.J., Redinger, K.E., Evans, A.P., and Nolan, P.S., "Control of Mercury in Conventional Flue Gas Emissions Control Systems," presented at the Fourth International Conference on Managing Hazardous Air Pollutants, Washington, D.C., November 12-14, 1997.

8. DeVito, M.S and Rosenhoover, W.A., "Flue Gas Mercury and Speciation Studies at Coal-Fired Utilities Equipped with Wet Scrubbers," presented at 15th International Pittsburgh Coal Conference, Pittsburgh, PA, September 15-17, 1998.

9. Laudal, D.L., "Mercury Speciation Sampling at Cooperative and United Power Associations' Coal Creek Station," Final Report, Energy & Environmental Research Center, University of North Dakota, January 1999.

10. Senior, C.L., Sarofim, A.F., Taofang, Z., Helble, J.J., and R.Mamani-Paco, *Fuel Processing Technology*, , **63**, 197-214 (2000).

11. Ghorishi, S.B. and Sedman, C.B.," *J.Air Waste Management Assoc.* **48**, 1191-1198 (1998).

12. Ghorishi, S.B., "Fundamentals of Mercury Speciation and Control in Coal-Fired Boilers," EPA-600/R-98-014, February 1998.

13. Miller, S.J., Dunham, G.E., Brown, T.D., and Olson, E.S., "Controlling Mechanisms That Determine Mercury Sorbent Effectiveness," presented at the Air & Waste Management Association 92nd Annual Meeting, St. Louis, Missouri, June 21-24, 1999, paper 99-898.

14. Sjostrom, S., Smith, J., Hunt, T., Chang, R., and Brown, T.D., "Demonstration of Dry Carbon-Based Sorbent Injection for Mercury Control in Utility ESPs and Baghouses," presented at the Air & Waste Management Association 90th Annual Meeting, Toronto, Ontario, Canada, June 8-13, 1997, paper 97-WA72A.07.

15. Li, Z. and Hwang, J.-Y., "Mercury Distribution in Fly Ash Components," presented at the Air &Waste Management Association 90th Annual Meeting, Toronto, Ontario, Canada, June 8-13, 1997, paper WP72B.05.

16. Wu, B., Peterson, T.W., Shadman, F., Senior, C.L., Morency, J.R., Huggins, F.E., and Huffman, G.P.," *Fuel. Proc. Technol.*, **63**, 93-108 (2000).

ATMOSPHERIC TRANSPORT, TRANSFORMATION, AND DEPOSITON OF MERCURY IN THE NORTHEASTERN UNITED STATES

Xiaohong Xu, Xiusheng Yang, David R. Miller, Joseph J. Helble, Robert J. Carley, and Hugo Thomas
University of Connecticut
Storrs, CT 06269-4087

KEYWORDS: mercury deposition, mercury transport.

INTRODUCTION

The health risks associated with consumption of mercury contaminated fish are a widespread concern. It is generally believed that the atmospheric deposition of mercury is a major source of the observed elevated concentrations of mercury in fish. Atmospheric deposition is therefore directly related to mercury-based health concerns, but is a problem that cannot be addressed locally. Because of the complexity of the Hg cycle that involves the atmosphere, geosphere, and biosphere, Hg must be viewed in either a regional or global scale. This is particularly important due to its long atmospheric lifetime and ability to re-enter the atmosphere. In this study, methods described in Xu (1998) and Xu et al. (1999) were used to estimate the atmosphere-surface exchange of elemental Hg including emission and dry deposition. In this model, atmospheric transport and transformation of mercury were incorporated into a three-dimensional Eulerian air quality model that included soot and ozone and was fully coupled to in-cloud processes. The model was used to predict Hg concentration and deposition in the northeastern United States for one summer and one winter week during 1997. Additional simulations were also conducted to study the sensitivity of regional Hg deposition to the partitioning of Hg(II) between particulate and non-particulate forms.

MODEL DEVELOPMENT

The atmospheric transport and transformations of mercury were incorporated into SAQM (Sarmap Air Quality Model, Chang et al. 1987; 1996), a three-dimensional regional scale air quality model. A one-dimensional cloud module based on Chang et al. (1987), Dennis et al. (1993) and Tsai (1996) was incorporated into SAQM. Three mercury species were considered: elemental [Hg(0)], divalent [Hg(II)], and particulate [Hg(p)]. Soot particles were also considered. The major aqueous chemical processes included oxidation of dissolved Hg(0) by ozone, reduction of Hg(II) by sulfite, and adsorption of Hg(II) onto soot particles. The aqueous phase chemical reactions largely followed Petersen et al. (1995), but included three types of clouds: precipitating, co-existing non-precipitating, and fair weather clouds. The interaction between the in-cloud transformation of Hg(0) and direct scavenging of ambient Hg(II) was also considered. The air-surface exchange of Hg(0) was treated by explicitly considering both dry deposition and re-emission from bare soil, vegetation, and water surfaces (Xu et al., 1999).

Simulation periods and domain

Simulations were conducted for two weeks during the year 1997. The winter week simulation started at 1900 hours eastern standard time (EST) on Feb. 13 1997 and lasted 96 hours. For the summer week, the simulation started at 1900 EST on Aug. 20 1997 and lasted 120 hours. The domain of the simulation covered the northeastern U.S. and part of the Atlantic Ocean as shown in Fig. 1. Grid spacing considered 34×41 grids in the horizontal direction, with grid size of 12 km $\times$ 12 km, and 15 layers in the vertical direction with the center of the lowest layer located approximately 30 m above the ground. The top of the modeling domain was approximately 15.5 km. Meteorological data were taken from Pennsylvania State University (PSU), generated by the PSU/NCAR (National Center for Atmospheric Research) Mesoscale Model, Version 5 (MM5). The regional average precipitation predicted by MM5 was 4.67 cm and 1.94 cm for the summer and winter week, respectively.

Model input for the base case simulations

A baseline simulation was conducted using measured or estimated concentrations for the major pollutants. Hourly ozone concentrations were taken from near-surface measurements in the USEPA (United States Environmental Protection Agency) database with horizontal and vertical interpolation. Ambient soot concentrations were estimated from ozone and $PM_{2.5}$ measurements by the USEPA. Mercury emissions from combustion sources in Connecticut (CT) were provided by the Connecticut Department of Environmental Protection (CTDEP). Anthropogenic Hg emissions from other parts of the modeling domain were based on the USEPA study (USEPA, 1996). Speciation of Hg from combustion sources followed Petersen et al. (1995). Mercury

initial and boundary concentrations were set at 1.3 ng/m^3 for Hg(0), and 0.01 ng/m^3 for each of Hg(II) and Hg(p).

Sensitivity simulations

Additional simulations were conducted by changing the speciation of Hg emission from anthropogenic sources or including adsorption of Hg(II) onto soot particles. The alternative emission speciation assumed all Hg(II) emissions were attached to particles. For the partitioning between ambient Hg(II) and Hg(p), an adsorption coefficient of $K = 3 \times 10^9 \times [\text{soot}]$ was adopted from Seigneur et al. (1998).

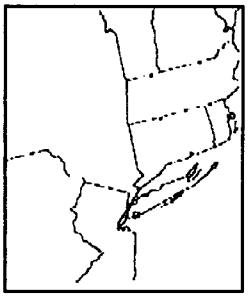

Figure 1. The domain of simulation.

Data analysis

For the baseline runs, the predicted weekly average ambient Hg concentrations and Hg concentrations in precipitation in CT were compared with weekly observations conducted by CTDEP and The University of Connecticut Environmental Research Institute (ERI). For comparing the sensitivity simulation results with those in the base case, the normalized deposition rates were calculated and presented by dividing the predicted regional daily average dry, wet, and total deposition with the corresponding value of the base case.

RESULTS AND DISCUSSION

Modeling results (base case) in comparison with monitoring data

Fig. 2 compares the model estimated summer week ambient concentrations of gaseous Hg [Hg(0)+Hg(II)] and Hg(p) with measured values at eight monitoring stations in CT during the same time period. For gaseous Hg, the model was able to recapture the spatial variation as observed by the monitoring stations. The modeled values agreed well with monitoring data except at site WB where the measured Hg concentration was higher than at all other sites, for that week and throughout the year of 1997 (ERI, 1998). There are two possible reasons for the underprediction by the model at WB: the exclusion of several undocumented Hg emission sources in the emission inventory, or the location of the monitoring site too close to these or other local Hg sources.

The model overpredicted the ambient Hg(p) concentration at all eight monitoring sites (Fig. 2b). The modeled values were also higher than Hg(p) concentrations measured in other regions, which ranged from 0.011 ng/m^3 in Underhill Center, VT (Burke et al., 1995) to 0.094 ng/m^3 in Detroit, MI (Keeler et al., 1995). This might have reflected the limitation of the model in handling the broad distribution of particle sizes. Because the largest particles will be poorly mixed and will deposit close to the stack, it is likely that the model would underestimate dry deposition and hence overestimate ambient concentrations of Hg(p).

The predicted summer week precipitation results agreed reasonable well with measurements (Fig. 3a). The modeled total Hg concentrations in precipitation, ranging from 7.68 to 11.7 ng/l, were higher than observations in general, as shown in Fig. 3b. The model estimates were comparable with published measurements (e.g. Fitzgerald et al., 1991; Rea et al., 1996; Keeler and Hoyer, 1997).

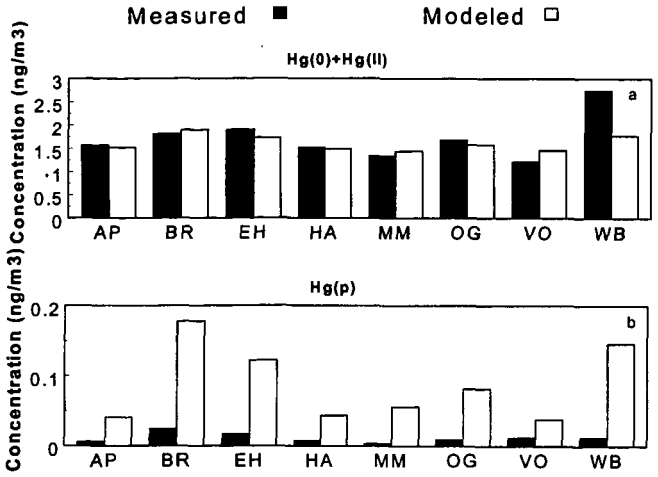

Figure 2. Comparison of modeled gaseous Hg concentrations (a) and Hg(p) concentrations (b) with monitored values in CT stations, during the summer week simulation. AP-Avery Point, BR-Bridgeport, EH-East Hartford, HA-Hammonassett, MM-Mohawk Mountain, OG-Old Greenwich, VO-Voluntown, WB-Waterbury.

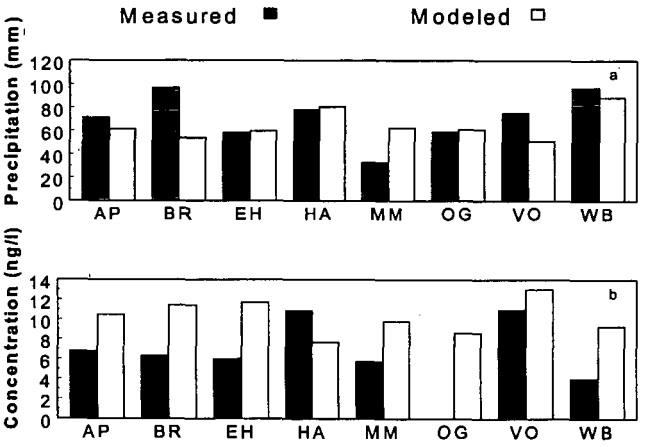

Figure 3. Comparison of modeled weekly precipitation (a) and Hg concentrations in precipitation (b) with monitored values in CT stations, during the summer week simulation. Concentration measurement was not available at OG.

The comparison between winter week simulation and measurements was similar to that of the summer week, with good agreement in gaseous concentration and precipitation concentration, but overprediction of ambient Hg(p) concentration.

Effects of emission speciation and Hg(II) adsorption to soot on Hg deposition

Table 1 lists normalized wet, dry, and total deposition of the region for the summer and winter week. By assuming all Hg(II) emissions were attached to particles, the ambient concentrations of Hg(p) increased, and concentrations of Hg(II) decreased. There was a significant decrease in dry deposition of Hg(II), but a large increase in the dry deposition of Hg(p). The total dry deposition decreased dramatically. This is because the dry deposition velocity of Hg(p) was much lower than that of Hg(II). The total wet deposition increased over the base case, as reported by Bullock et al. (1997), primarily due to a significant increase in wet deposition of Hg(p) and Hg(0). The resulting total deposition was less than in the base case.

When Hg(II) adsorption to soot particles was considered, the resulting partitioning between ambient Hg(II) and Hg(p) caused a decrease in the dry deposition of Hg(II) and an increase in the dry deposition of Hg(p), but to a lesser extent than in the case of alternative emission speciation. Similarly, the gas phase partitioning led to less wet deposition of Hg(II), and more wet deposition of Hg(p) and Hg(0). Compared with the alternative emission speciation, the Hg(II) adsorption to particles resulted in less reduction of total deposition because the alternative emission speciation influenced heavily concentrations near the surface where point sources were located. Thus, Hg(II) dry deposition was largely reduced, leading to much lower dry deposition.

As can be seen from Table 1, deposition during the winter was more sensitive to changes in ambient Hg(II) concentration compared with the summer week. This can be largely attributed to the different Hg species that predominate the deposition during warm and cold seasons. In the winter week, approximately 65% of total deposition was from Hg(II), in comparison with 40% in the summer week.

Table 1. Normalized regional deposition from model simulation during the summer and winter weeks.

	Summer			Winter		
Simulation	Dry dep.	Wet dep.	Total	Dry dep.	Wet dep.	Total
Alternative emission speciation	0.57	1.14	0.76	0.27	1.19	0.52
Adsorption of Hg(II) to soot, gas phase	0.78	1.10	0.89	0.48	1.16	0.67

SUMMARY AND CONCLUSIONS

Model predictions of surface level gaseous Hg concentrations were close to measured levels, agreeing to within 12% on average, about half the estimated error in measurements. The predicted Hg concentrations in precipitation were 50% higher than measured values on average, slight lower than the estimated 60% error in measurements. The modeled ambient particulate Hg concentrations, on the other hand, were much higher than measurements made in CT and other places, suggesting an underestimation of dry deposition in the source grids.

Both the alternative emission speciation and the adsorption of ambient Hg(II) onto soot particles resulted in less total deposition of Hg, indicating the dependence of total deposition on the fraction of gaseous mercury bound to particles. It is therefore important to determine accurately the emission speciation and transformation during transport.

In conclusion, the model was shown to be capable of producing acceptable results, and useful in analyzing the effects of various environmental factors on the atmospheric transport, transformation, and deposition of Hg. More simulations to address seasonal variations and to further evaluate the model are being conducted.

ACKNOWLEDGMENTS

This study was jointly supported by the Connecticut Department of Environmental Protection, the University of Connecticut Environmental Research Institute, and The Research Foundation of the University of Connecticut. The authors would like to thank Dr. Julius S. Chang at State University of New York at Albany, for providing SAQM and advising its modification, and Dr. Nelson L. Seaman and Mr. Glenn Hunter at the Pennsylvania State University for providing the meteorology data.

REFERENCES

Bullock Jr. O. R., Benjey W. G. and Keating M. H, 1997: The modeling of regional-scale atmospheric mercury transport and deposition using RELMAP. pp 323-347. In *Atmospheric Deposition of Contaminants to the Great Lakes and Coastal Waters*. Ed. J. E. Baker. SETAC Press. Pensacola, Florida.

Burke, J., M. Hoyer, G. Keeler, and T. Scherbatskoy, 1995: Wet deposition of mercury and ambient mercury concentration at site in the Lake Champlain basin. *Water, Air, and Soil Pollution*. 80, 353-362.

Chang, J. S., R. A. Brost, I. S. A. Isaksen, S. Madronich, P. Middleton, W. R. Stockwell, and C. J. Walcek, 1987: A three-dimensional Eulerian acid deposition model: physical concepts and formation. *Journal of Geophysical Research*. 92(D12), 14681-14700.

Chang, S. J., Y. Li, M. Beauharnois, H. Huang, C. Lu, and G. Wojcik, 1996: *SARMAP Air Quality Model.* Atmospheric Science Research Center, University at Albany, State University of New York, 100 Fuller Road, Albany, New York 12205.

Dennis, R. L., J. N. McHenry, W. R. Barchet, F. S. Binkowski, and D. W. Byun, 1993: Correcting RADM's surface underprediction: discovery and corrections of model errors and testing the corrections through comparisons against field data. *Atmospheric Environment.* 27A(60), 975-997.

ERI, 1998: *Annual Progress Report of Connecticut Atmospheric Mercury Monitoring Network.* Environmental Research Institute, The University of Connecticut. Storrs, Connecticut.

Fitzgerald, W. F., R. P. Mason, and G. M. Vandal, 1991: Atmospheric cycle and air-water exchange of mercury over mid-continental lacustrine regions. *Water, Air, and Soil Pollution.* 56, 745-767.

Keeler, G., G. Glinsorn, and N. Pirrone, 1995: Particulate mercury in the atmosphere: its significance, transport, transformation and sources. *Water, Air, and Soil Pollution.* 80, 159-168.

Keeler, G. J., and M. Hoyer, 1997: Recent measurements of atmospheric mercury in the Great Lakes region. pp305-321. In *Atmospheric Deposition of Contaminants to the Great Lakes and Coastal Waters.* Ed. J. E. Baker. SETAC Press. Pensacola, Florida.

Northeast Regional Climate Center, 1997: *New England Climate.* 97(8). Ithaca, New York.

Petersen, G., A. Iverfeldt, and J. Munthe, 1995: Atmospheric mercury species over central and northern Europe. Model calculations and comparison with observations from the Nordic Air and Precipitation Network for 1987 and 1988. *Atmospheric Environment.* 29(1), 47-67.

Rea, A. W., G. J. Keeler, and T. Scherbatskoy, 1996: The deposition of mercury in throughfall and litterfall in the Lake Champlain watershed: a short term study. *Atmospheric Environment.* 30(19), 3257-3263.

Seigneur C., Abeck H., Chia G., Reinhard M., Bloom N. S., Prestbo E., and Saxena P, 1998: Mercury adsorption to elemental carbon (soot) particles and atmospheric particulate matter. *Atmospheric Environment.* 32(14/15): 2649-2657.

Tsai, Y., 1996: *Evaluation of two one-dimensional cloud models used in air quality models.* Thesis. Department of Atmospheric Science, University at Albany, State University of New York, 100 Fuller Road, Albany, New York 12205.

USEPA, 1996: *Mercury study report to congress. Vol. II: An inventory of anthropogenic mercury emission in the United States.* Office of air quality Planning and Standards, Research Triangle park, NC, U.S.A.

Xu, X., 1998: *A modeling study of regional scale atmospheric transport and transformation of mercury.* Ph.D. Dissertation. The University of Connecticut. Storrs, CT 06269.

Xu X., Yang, X., Miller D. R., Helble J. J., and Carley R. J, 1999: Formulation of bi-directional air-surface exchange of elemental mercury. *Atmospheric Environment.* 33(27), 4345-4355.

STRUCTURE OF PRIMARY $PM_{2.5}$ DERIVED FROM DIESEL TRUCK EXHAUST

G. P. Huffman, F. E. Huggins, N. Shah and S. Pattanaik
University of Kentucky, CFFLS, 111 Whalen Building,
533 S. Limestone St., Lexington, KY 40506

H. L. C. Meuzelaar and Sun Joo Jeon,
Department of Chemical & Fuels Engineering,
University of Utah, Salt Lake City, UT

D. Smith and B. Harris
U.S. Environmental Protection Agency, National Risk Management Res. Lab.,
Research Triangle Park, NC 27711

M. S. Seehra and A. Manivannan,
Physics Department, West Virginia University, Morgantown, WV

Key-Words: Particulate matter, $PM_{2.5}$, Diesel engine exhaust, thermal desorption GC/MS, XAFS spectroscopy, SQUID magnetometry

INTRODUCTION

The U.S. Environmental Protection Agency is currently considering regulations on airborne particulate matter < 2.5 microns in mean diameter ($PM_{2.5}$). It is important that the molecular structure and microstructure of $PM_{2.5}$ from various sources be thoroughly characterized in order to identify structural features that may be important for source apportionment and health effects. Two of the primary sources of $PM_{2.5}$ from petroleum are combustion of residual fuel oil and diesel engines. In previous papers, we have discussed the structure of $PM_{2.5}$ derived from the combustion of residual fuel oil.[1,2] In the current paper, we report some preliminary results on the molecular structure of primary $PM_{2.5}$ from diesel vehicle tests. The techniques employed included thermal desorption (TD) GC/MS, x-ray absorption fine structure (XAFS) spectroscopy, and SQUID magnetometry.

SAMPLE GENERATION AND COLLECTION

The sample generation experiments were conducted by Harris and Smith at the EPA National Risk Management Research Laboratory (NRMRL). The samples were collected on teflon and quartz filters from the exhaust stack of a heavy-duty diesel truck. The total distance traveled by the truck during the sampling run was 191 miles at an average speed of 60.4 MPH. Diesel exhaust gas was sampled via a heated probe located two feet below the top of the exhaust stack. Hot exhaust gas passed through a $PM_{2.5}$ cyclone and was subsequently cooled and diluted with ambient air. The average total stack gas exhaust rate over the duration of the sampling period was 15.5 Lpm. Four samples were collected simultaneously by establishing different gas flow rates to each of four filters, each 48 mm in diameter. This yielded two heavily loaded quartz filters (B and C, 6.2 mg of PM), one lightly loaded quartz filter (D, .5 mg of PM), and one lightly loaded Teflon (PTFE) filter (A, .6 mg of PM). Two additional filters (labeled PM1 and PM2) with intermediate loading (~2mg) were collected in a separate experiment.

ANALYTICAL CHARACTERIZATION

Thermal desorption GC/MS methodology

Filter strips (1.5 x 18 mm^2) are positioned inside a special glass reaction tube that is lined with a ferromagnetic foil with a Curie temperature of 315°C. The tube is placed into a Curie-point reactor for desorption of volatile (VOC) and semivolatile organic compounds (SVOC). In Curie-point desorption, a high frequency coil surrounds the glass tube and heats the foil by induction. The foil heats up till its Curie point is reached and its energy intake drops, thus holding the temperature of the foil at this point. Flash desorption of organic compounds from the particles immobilized by the filter strips is achieved using a total heating time of 10 s under a continuous flow of He carrier. The continuous flow of He transfers the analytes from the reaction zone into a fused silica capillary column of a gas chromatograph, coupled to a mass spectrometer. A more detailed description of the apparatus is given elsewhere.[3]

Conventional solvent-based extraction method has been used for extraction of soluble analytes from a more or less insoluble matrix. However, there are several practical problems with the application of solvent-based GC/MS techniques to ambient PM filter sample characterization,

compared to the TD method. Solvent-based GC/MS analysis of filter samples requires relatively large sample masses and the laboratory methods involved are laborious and use large quantities of solvents. Solvent extracts can include significant quantities of large soluble or even polymeric molecules that are unsuitable for direct GC/MS analysis but may contaminate the GC inlet.

The two heavily loaded quartz filters (B and C), produced qualitatively and quantitatively similar TD-GC/MS profiles. The data for sample B are shown in Figures 1 and 3. The TIC are marked by a strong n-butylbenzenesulfonamide peak, together with some of the ubiquitous alkyl-phthalate contaminants, notably dimethylphthalate. Hopanes and steranes are virtually absent.

Compared to the high flow samples B and C, the lightly loaded quartz fiber filter D produces approx. 40 % of the long chain alkane signal intensities and 25 % of the PAH intensities. Since the "total PM mass" of sample D should only be 10 % of samples B and C, there is an obvious nonlinear response within the five-step analytical procedure (i.e. sample collection + sample preservation during storage and transportation + filter subaliquotting + thermal desorption + GC/MS response).

The TIC of the lightly loaded Teflon (PTFE) filter sample A shows a drastic reduction in the first "hump", which represents an unresolved complex mixture, and an increase in the yield of the highly polar and labile n-alkanoic acids (Figure 2). Perhaps the most surprising finding is the strong even vs. odd predominance among the long chain alkanes (Figure 4). The opposite phenomenon (odd vs. even predominance) is well known among geochemical samples and is generally attributed to decarboxylation of biogenic fatty acids with even carbon numbers. A highly speculative interpretation could be that the even vs. odd n-alkane predominance shown by the PTFE filter desorbate is in fact the correct relative abundance for the particle-borne long chain alkanes, as is the even vs. odd n-alkanoic acid abundance. Both observations might be explained by synthetic, 2-carbon pathways in the soot formation process. During desorption of alkanoic acids from the quartz filter, however, a substantial amount of decarboxylation may occur, thereby turning the dominant, even carbon number, alkanoic acids in to odd carbon number n-alkanes, thereby smoothing out the dips in the n-alkane distribution profile.

XAFS spectroscopy analysis

XAFS spectra were obtained at the S K-edge at beam line X-19A at the National Synchrotron Light Source (NSLS) and at the Cr, Fe, Ni and Zn K-edges at beam line 4-3 at the Stanford Synchrotron Radiation Laboratory (SSRL) and at beam line X-18B at NSLS. The concentrations of Fe and Zn (800 - 2000 ppm) were significantly higher than those of other metals in the samples and gave correspondingly better quality spectra. All spectra were collected in the fluorescent mode, using a Lytle detector for the sulfur spectra and a 13 element solid-state Ge detector for the metal spectra. Experimental procedures are described in detail elsewhere.[4,5]

Figure 5 shows a typical S K-edge XANES spectrum, deconvoluted into its component peaks. The locations of the peaks are used to assign each feature to a particular molecular form of valence state of sulfur, as indicated by the labels in Figure 5. Then, using previously developed methodology,[4] the areas under the various peaks can be converted into percentages of the total sulfur contained in each of the molecular forms or valence states identified. The results of this analysis for the diesel $PM_{2.5}$ samples are summarized in Table 1. It is seen that sulfate is the dominant sulfur form, followed by a sulfone species (most probably the n-butylbenzene sulfonamide identified by TD/GC/MS), and a small amount of thiophenic sulfur.

Although the XAFS spectra of the metals were quite noisy given the small amount of material under irradiation, useful XANES spectra were obtained from iron and zinc. Whereas the iron XANES spectra appeared to be similar to ferric sulfate, the zinc XANES spectra were quite different from that of zinc sulfate. Chromium sulfate was identified in sample C2.

SQUID magnetometry

A SQUID magnetometer (Quantum Design Model MPMS) was used to measure the temperature variation of the magnetization, M, from 5 K to 350 K of several of the diesel $PM_{2.5}$ samples. The data are corrected for the diamagnetic contribution (measured in separate experiments) from the filter and the polyethylene sample holder.

The variations observed for the samples PM1 and PM2 are nearly identical, both in magnitude as well as in temperature variation. In these cases, there is a rapid increase in M below 25 K, above which M is nearly temperature independent. For sample B, the rise in M at lower temperatures is spread over a larger temperature range, whereas for sample C, M is nearly temperature independent, with only a hint of an increase below 10 K.

The increase in M at lower temperatures can be described by the Curie-law $M = M_0 + CH/T$ where $C = N\mu^2/3k_B$ is the Curie constant, N is the concentration of impurities each with magnetic moment μ, and k_B is the Boltzmann constant.[6] The plots of $(M - M_0)$ versus 1/T are linear below ~25 K for samples PM2, PM1 and B. Using $\mu = 1.7\ \mu_B$ for spin S = ½ yields N = 10, 5 and 2 (in units of 10^{19}/g) for PM2, PM1 and B, respectively. These levels of impurities have been observed from similar analysis in high purity activated carbon.[7] The nature of these impurities including free radicals by low temperature electron spin resonance spectroscopy in the near future.

Acknowledgement: Support of this research under U.S. Department of Energy (FE/NPTO) contract No. DE-AC26-99BC15220 is gratefully acknowledged. The XAFS experiments were conducted at the Stanford Synchrotron Radiation Laboratory and the National Synchrotron Light Source, which are also supported by the U.S. DOE.

REFERENCES

1. G. P. Huffman, F. E. Huggins, N. Shah, R. Huggins, W. P. Linak, C. A. Miller, R. J. Pugmire, and H. L. C. Meuzelaar, *ACS Div. Fuel Chem. Preprints,* **45(1)**, 6-10 (2000).
2. G. P. Huffman, F. E. Huggins, N. Shah, R. Huggins, W. P. Linak, C. A. Miller, R. J. Pugmire, H. L. C. Meuzelaar, M. Seehra, and A. Mannivannan, "Characterization of Fine Particulate Matter Produced by Combustion of Residual Fuel Oil," *J. Air & Waste Management Assoc.*, **50,** (2000), in the press.
3. Dworzanski, J.P.; McClennen, W.H.; Cole, P.A.; Thornton, S. N.; Arnold, N.S.; Snyder, A.P.; Meuzelaar, H.L.C., *Environ. Sci. Technol.*, **31,** 295-305 (1997).
4. G.P. Huffman, S. Mitra, F.E. Huggins, N. Shah, S.Vaidya, and F. Lu, *Energy & Fuels*, **5**, 574-581 (1991).
5. F.E. Huggins, N. Shah, J. Zhao, F. Lu, and G.P. Huffman, *Energy & Fuels*, 7, 482-489 (1993).
6. V. S. Babu, L. Farinash and M. S. Seehra, *J. Mater. Res.*, **10,** 1075 (1995).
7. A. Manivannan, M. Chirila, N. C. Giles and M. S. Seehra, *Carbon,* **37,** 1741 (1999).

Table 1: Sulfur forms in diesel PM samples

Sample	Elemental S	Thiophene	Sulfone*	Sulfate
Diesel Filter PM1	< 1	3	7	90
Diesel Filter PM2	< 1	6	8	86
Diesel B2 9/99	< 1	< 1	2	98
Diesel C2 9/99	< 1	5	11	84

*Probably n-butylbenzenesuylfonamide contaminant (see text)

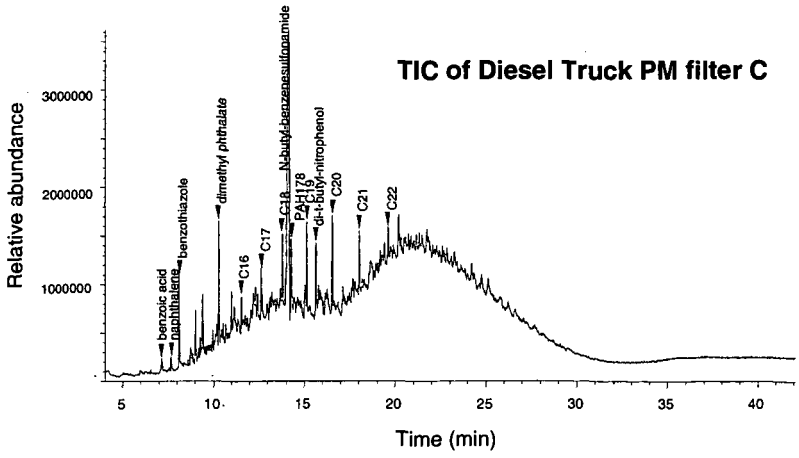

Figure 1: TIC of a heavily loaded diesel exhaust $PM_{2.5}$ filter.

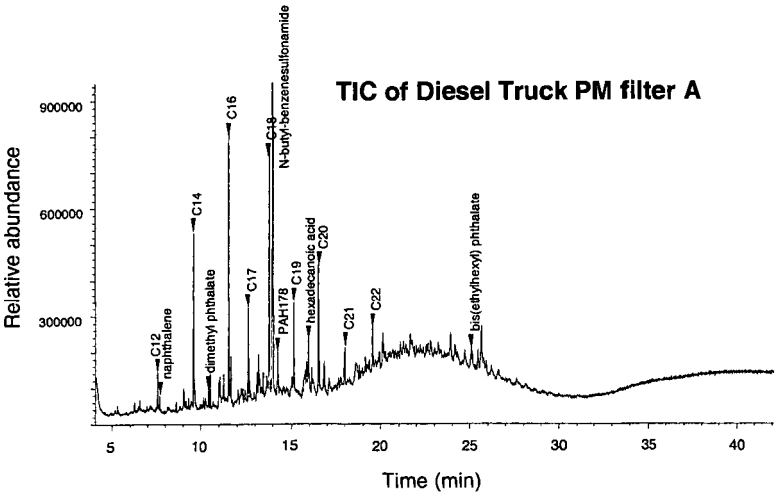

Figure 2. TIC of a lightly loaded diesel exhaust $PM_{2.5}$ filter.

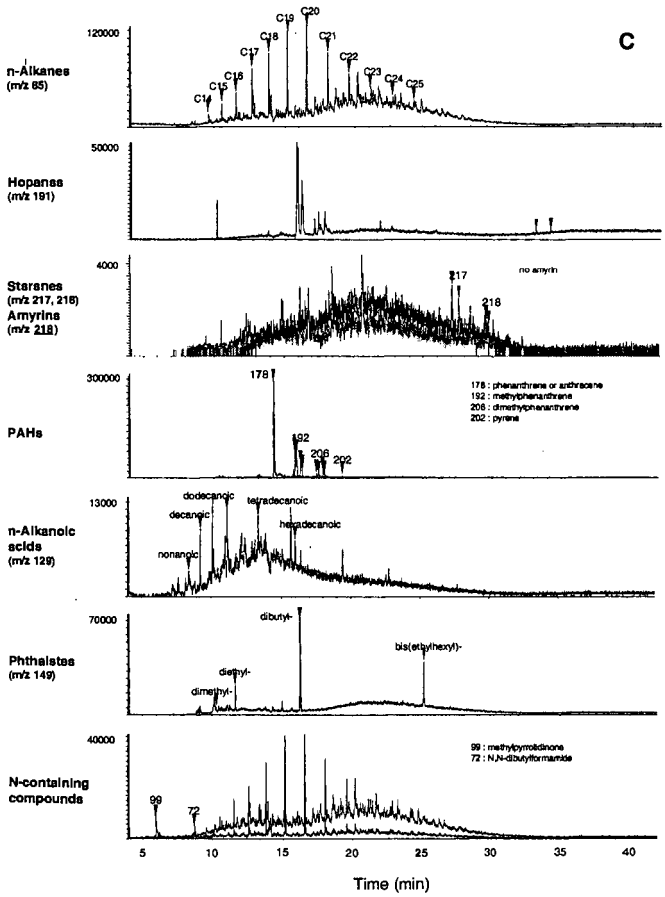

Figure 3: MS data for heavily loaded diesel exhaust $PM_{2.5}$ filter sample B

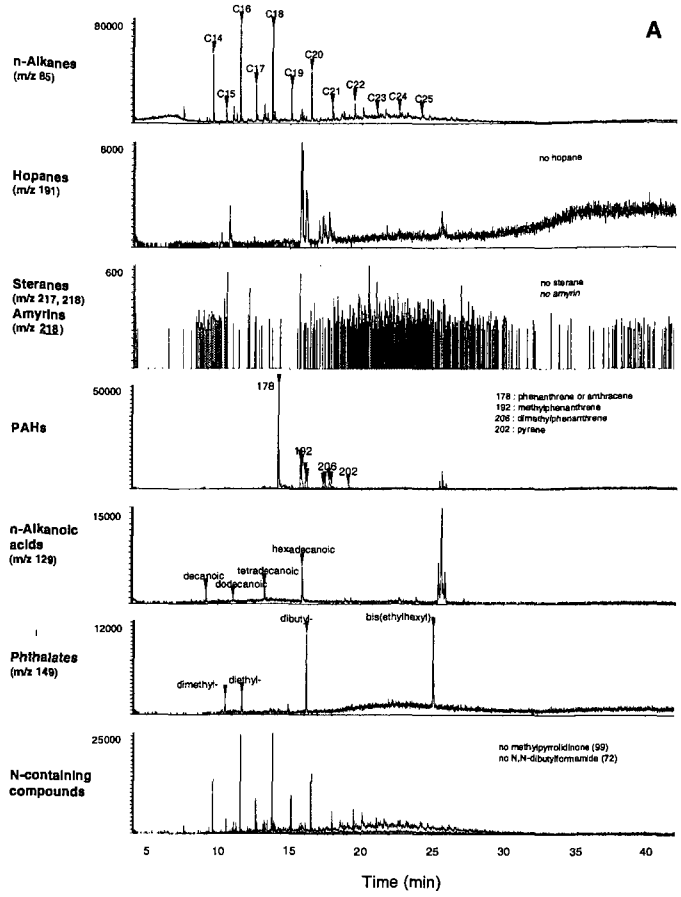

Figure 4. MS data for lightly loaded diesel exhaust PM2.5 filter sample.

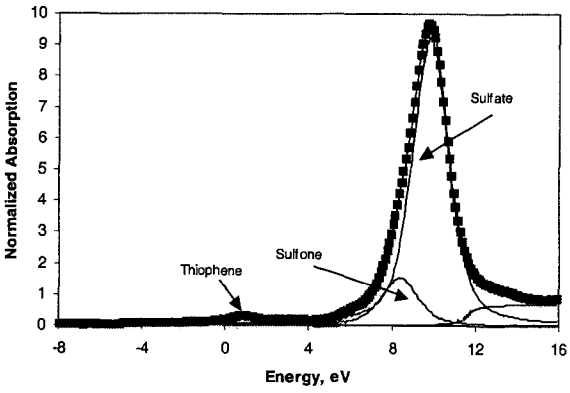

Figure 5: Least-squares fitted Sulfur K-edge XANES spectrum of Diesel PM sample "C2". The sulfone component is probably due to the n-butylbenzenesulfonamide contamination (see test).

IDENTIFICATION OF INORGANICS IN THE NIST SRM1648 SAMPLE OF URBAN PARTICULATE MATTER

A. Manivannan and M. S. Seehra
Physics Department, West Virginia University,
PO Box: 6315, Morgantown, WV 26506-6315

KEYWORDS: Particulate Matter, X-ray Diffraction, Electron Spin Resonance, Magnetometry

ABSTRACT

X-ray diffraction, electron spin resonance (ESR) and magnetometry studies are reported on the urban particulate matter sample NIST1648. This is a time-integrated sample of urban particulate matter collected over 12 months in St. Louis. We have identified major chemical compounds present in this sample. In XRD, the sharp lines match the spectra of the following crystalline compounds: gypsum ($CaSO_4.2H_2O$), quartz (SiO_2), illite (K-Al-Si-O-OH), kaolinite (Al-Si-O-OH), zinc sulfite hydrate ($ZnSO_3.2H_2O$), zinc sulfate sulfite hydrate ($Zn_2(SO)_3(SO_4).3H_2O$), zinc arsenate hydrate ($Zn_3(AsO_4)_2.4H_2O$), and iron sulfate ($Fe_2(SO_4)_3$. Magnetometry measurements indicate the presence of Mn_3O_4, Fe_3O_4 and alpha-Fe_2O_3. In ESR spectroscopy, lines due to Fe_3O_4 and Fe^{2+} have been identified.

INTRODUCTION

Air-borne ambient particulate matter (PM) is a mixture of particles directly emitted into the air from fossil fuel combustion such as coal, oil, electrical power plants and automobile exhausts. According to the US Environmental Protection Agency (EPA), particulate matter less than 10 microns in diameter (PM_{10}) and more recently less than 2.5 microns (fine PM or $PM_{2.5}$) is of particular concern [1]. The implementation of this new rule requires the acquisition of important scientific information regarding the effects of $PM_{2.5}$ on public health and welfare. These adverse health effects include premature mortality, aggravation of respiratory and cardiovascular symptoms, change in lung structure, and altered respiratory defense mechanisms [2-4]. Two controversial studies (the Harvard University six-city study and the American Cancer Society study) have linked the presence of fine particular matter to premature mortality [5]. Generally, fine particles are considered to be more hazardous than coarse particles. Therefore, the analysis have to be done at molecular levels. In order to understand the molecular speciation and its parameters such as valency, solubility, acidity, and composition, it is essential to identify and analyze the elements and compounds present accurately by employing several analytical tools. Huggins et al., [6] have carried out x-ray absorption fine structure (XAFS) and proton induced x-ray emission (PIXE) analysis to investigate several elements in the SRM1648 urban particulate matter sample supplied by NIST (National Institute of Standards and Technology). The emphasis is placed on those elements that are either transition metals or elements defined as hazardous air pollutants in the 1990 Amendments to Clean Air Act [7].

In this paper, we present results of our investigations on the determination of the chemical compounds in the NIST standard reference material SRM1648. This sample is used as the control material in the evaluation methods used in the analysis of atmospheric particulate matter and materials with similar matrix. One of the main focus in the present work is to identify the chemical formulae of the compounds present in PM. Information on the nature of chemical compounds present in this material is essential in understanding the chemical pathways that leads to their formation. We have employed x-ray diffraction (XRD), magnetometry and electron spin resonance (ESR) spectroscopy to identify the various components present in SRM1648. Details of these results and their discussion are presented below.

EXPERIMENTAL

The sample SRM1648 of urban PM [8] was obtained from NIST. It was collected in St Louis, MO area over a 12-month period in a bag-house designed especially for the purpose. The collected particulate material was removed from the filter bags, combined into a single lot, screened through a fine-mesh sieve to remove extraneous materials and thoroughly blended in a V-blender and then packed into bottles [8].

The PIXE (proton-induced X-ray emission) spectroscopy of this sample reported by Huggins et al [6] showed the presence of Al (2.33%), Si (7.92%), S (4.55%), Ca (5.52%), Fe (3.29%) and

the elements (C,H,O,N) = 70%. Other elements present in ppm levels (shown in parenthesis) are Na (5000), Mg (5300), P (7700), Cl (4000), K (8300), Ti (3500), Zn (4130) and Pb (6720), with even smaller amounts of Cr, Mn, Ni, Cu, Br, and Sr.

The X-ray anslysis was performed using a Wide Angle X-ray Diffractometer (WAXD) from Rigaku (Model D/MAX) using Cu K ra diation with = 1.542 Å. The other experimental conditions include ½ degree divergence and scatter slits, 0.15mm receiving slits, step scans with 0.04 degree steps and 30sec counting time at each step, and intensity measured in counts. This relatively slow scan process enabled us to obtain the diffraction pattern with resolved sharp lines due to various compounds. The analysis of the x-ray patterns was carried out using Jade software package supplied by MDI (Materials Data Inc.) and the JCPDS data files. Magnetization measurements were done in the 5K to 350K range using a SQUID magnetometer (Quantum Design Model MPMS). ESR spectroscopy of the sample was carried out using a standard reflection type X-band spectrometer.

RESULTS AND DISCUSSION

In Figure 1 we show the x-ray diffraction pattern of the NIST SRM1648 sample. In this pattern, sharp lines due to crystalline components are superposed on a broad peak centered around 2θ = 25°. This broad peak around 25° is characteristics of amorphous carbon [10]. Using the search/match program of the Jade software together with the help of JCPDS data base, we have identified almost all the observed crystalline peaks shown in Fig. 1. They are due to gypsum (CaSO4. $2H_2O$), quartz (SiO_2), kaolinite (Al-S-Si-O-OH), illite (K-Al-Si-O-OH), zinc arsenate hydrate ($Zn_3(AsO_4)_2$. $4H_2O$), zinc sulfite hydrate ($ZnSO_3$. $2H_2O$), zinc sulfate sulfite hydrate ($Zn_2(SO)_3(SO_4).3H_2O$), and iron sulfate ($Fe_2(SO_4)_3$. The major contribution of the present investigation using x-ray diffraction is that we are able to identify various compounds and their water content in this sample. In making the identifications, we compared the diffraction patterns of all apprppriate compounds available in the JCPDS files. The concentrations of the elements Al (2.33%), Si (7.92%), S (4.55%), Ca (5.52%), and Fe (3.29%) can be explained by the strong crystalline peaks in x-ray diffraction for their respective compounds mentioned above. In addition to the elemental data reported by Huggins et al. [6], x-ray diffraction analysis identifies the possible compounds present in the sample as a complimentary study. One important observation is the presence of gypsum ($CaSO_4$. $2H_2O$) which is not reported in the NIST certificate of analysis. All of the compound reported here can affect human health. Quartz and the arsenic compounds may be specially hazardous [11].

Since the sensitivity of WAXD for detecting elements and compounds in a mixture is at best limited to individual concentrations of 1% or more, we have employed magnetometry and ESR spectroscopy for possible detection of other materials. In Fig. 2, temperature variation of the magnetization of the sample SRM 1648 is shown. The arrows indicate the positions where magnetic transitions due to Mn_3O_4 (T_c= 43 K[12]), Fe_3O_4 (T_c = 120 K) and alpha-Fe_2O_3 (T_c =260 K) are known [13]. In order to confirm these assignments, a laboratory prepared mixture of Fe_3O_4, Mn_3O_4 and alpha-Fe_2O_3 in 1:1:1 ratio by weight was investigated (Fig. 2) by magnetometry. The transition temperatures observed in SRM1648 match with the three oxides, confirming our identifications. The concentration of Mn_3O_4 is relatively small in SRM1648 as indicated by the weakness of the peak near 43K. The results obtained by magnetometry provide evidence for the usefulness of this technique for detecting ferrimagnetic and ferromagnetic materials in quantities too small to be detected by x-ray diffraction.

The ESR spectroscopy of SRM1648 carried out room temperature and at 9.2GHz shows several lines (Fig.3). The main line with g = 2.2 and linewidth ΔH = 688 G is probably due to Fe_3O_4. The line at g = 3.57 (Fig.4) matches the location expected for Fe^{2+} species in octahedral symmetry [14]. The remaining lines are clearly a part of the byperfine structure. However because of lack of resolution, we are not able to identify all the lines and hence their origin at this time remains unresolved. Perhaps, with variable temperature ESR spectroscopy, we might be able to resolve this issue in the near future.

In summary, with the combined use of WAXD, magetometry and ESR spectroscopy, we have been able to identify a significant number of chemical compounds present in the NIST SRM1648 sample of urban particulate matter. This information combined with the data available from PIXE and XAFS on the elemental concentrations [6] provides a nearly complete analysis of the major constituents of this sample.

ACKNOWLEDGEMENT

Support of this research under the U.S. Department of Energy contract No. DE-AC26-99BC15220 is gratefully acknowledged. We thank Dr. G. P. Huffman and Dr. F. E. Huggins for useful consultations and for providing a copy of their paper [Ref.6] prior to publication.

REFERENCES

1. Federal Register, 62 FR 38652, July 18, 1997.
2. D. W. Dockery, C. A. Pope, X. Xu, J. D. Spengler, J. H Ware, M. E. Fay, B. G. Ferris, and F. E. Speizer, New England J. Med., 329 (1993) 1753.
3. R. T. Burnet, R. Dales, D. Krewski, R. Vincent, T. Dann, and J. R. Brook, Am. J. Epidemiology, 142 (1995) 15.
4. J. Schwartz, and R. Morris, Am. J. Epidemiology, 142 (1995) 23.
5. Chemical Engineering News, Particulate Matter Health Studies to be Reanalyzed August 18, (1997) 33.
6. F. E. Huggins, G. P. Huffman, and J. D. Robertson, J. Haz. Mat. (in press)
7. Amendments to Clean Air Act, U.S. Public Law 101-549, U.S. Gov. Printing Office, 1990, 314 pp.
8. National Institute of Standards & Technology, Certificate of Analysis, Standard Reference Material 1648, Urban Prticulate Matter, August 30,1991, 5 pp.
9. V. S. Babu, L. Farinash and M. S. Seehra, J. Mater. Res., 10, 1075 (1995).
10. A. Manivannan, M. Chirila, N. C. Giles and M. S. Seehra, Carbon 37 (1999) 1741.
11. R.S. Pandurangi, M. S. Seehra, B. L. Razzaboni and P. Bolsaitis: Environ. Health Perspectives, 86 (1990) 327.
12. G. S. Chaddha, and M. S. Seehra, J. Phys D: Appl. Phys. 16 (1983) 1767.
13. G. Srinivasan and M. S. Seehra, Phys. Rev. B (1983) 1.
14. Paramagnetic Resonance in Solids by W. Low (Academic Press, NY 1960) p. 87.

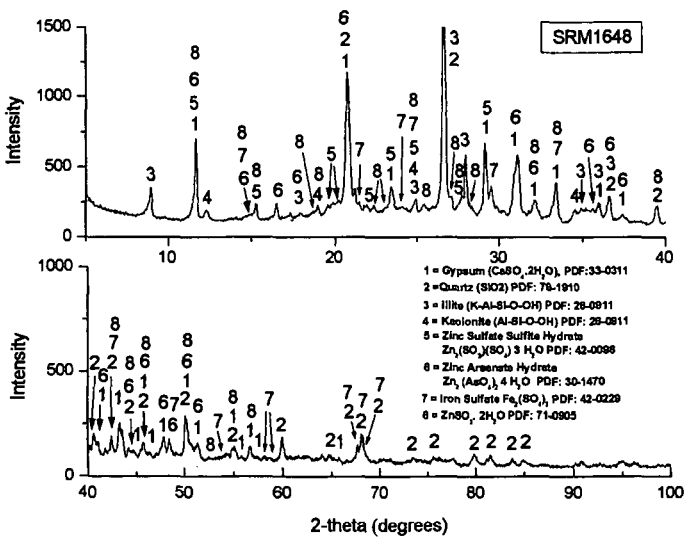

Figure 1. Room temperature x-ray diffractogram of the NIST SRM1648 sample. Lines due to various crystalline components are identified. The broad background near $2\theta \sim 25°$ is due to amorphous carbon.

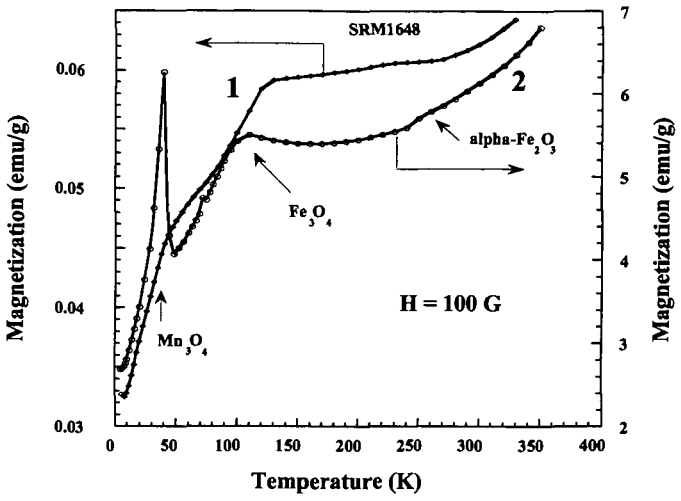

Figure 2. Temperature variation of the magnetization for SRM1648 (data 1)and for a laboratory prepared mixture of Fe_3O_4, Mn_3O_4 and alpha-Fe_2O_3 (1:1:1) (data 2). The transition temperatures indicated by arrows observed for the mixture are also observed in SRM1648.

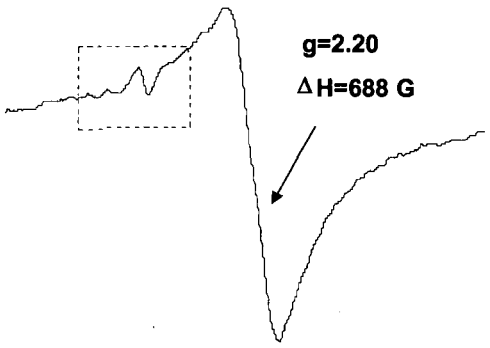

Figure 3. Room temperature ESR spectrum of SRM1648. The line shown by arrow at g = 2.2 is probably due to ferrimagnetic Fe_3O_4.

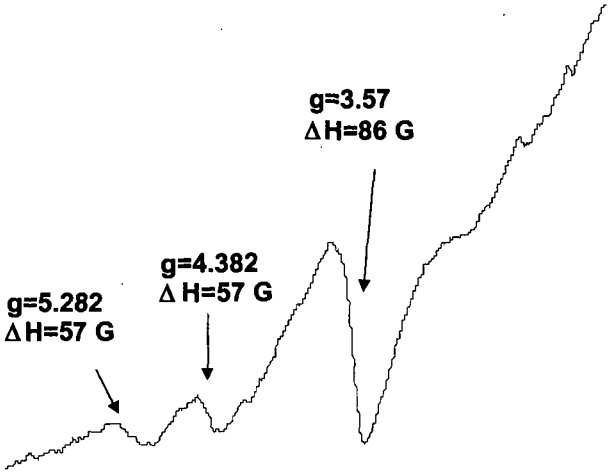

Figure 4. Expanded ESR spectrum of the box area shown in Figure 3. For some of the lines g and ΔH values are indicated. See text for details.

NANO-DMA/THERMAL DESORPTION PARTICLE BEAM MASS SPECTROMETRIC ANALYSIS OF NANOPARTICLES PRODUCED IN DIESEL EXHAUST

Herbert Tobias, Derek Beving, and Paul Ziemann
Air Pollution Research Center, University of California-Riverside, Riverside CA 92521
Hiromu Sakurai, Miriam Zuk, and Peter McMurry
Department of Mechanical Engineering, University of Minnesota, Minneapolis MN 55455
Darrick Zarling, Robert Waytulonis, and David Kittelson
Center for Diesel Research, University of Minnesota, Minneapolis MN 55455

KEY WORDS. diesel exhaust, nanoparticles, nucleation

ABSTRACT

Due to recent epidemiological studies that have found a correlation between atmospheric fine particle (diameter < 2.5 μm) mass concentrations and increased human morbidity and mortality, the chemistry of particles produced from diesel engines are of special concern. Diesel engines are known to emit high concentrations of nanoparticles (diameter < 50 nm), but due to their relatively small mass, chemical analysis is difficult. Here, a nano-differential mobility analyzer (Nano-DMA) was used to size select nanoparticles produced from diesel engine exhaust for subsequent chemical analysis by thermal desorption particle beam mass spectrometry (TDPBMS). A number of organic compound classes and sulfuric acid have been identified and the approximate molecular weights and vapor pressures determined from calibrated desorption temperatures. The effect of particle size and engine operating conditions on the composition of diesel nanoparticles was also studied.

INTRODUCTION

Recent epidemiological studies have found a correlation between atmospheric fine particle (diameter < 2.5 μm) mass concentrations and increased human morbidity and mortality. The chemistry of particles produced from diesel engines are of special concern since some laboratory studies suggest a stronger link between adverse health effects and smaller particles.[1] Diesel engines are known to emit high concentrations of nanoparticles (diameter < 50 nm) and analysis of total diesel aerosol has identified the presence of a number of toxic compounds.[2] A knowledge of nanoparticle composition is important for understanding the physical and chemical mechanisms by which they are formed in diesel exhaust. Such information can be used to establish the criteria for modifications of diesel engine design or operation, fuel, and lubricating oil that will help reduce nanoparticle formation. Due to the relatively small mass of nanoparticles, chemical analysis is difficult. In principal, an inertial impactor, such as a MOUDI, could be used to sample diesel nanoparticles for chemical analysis. However, in practice this is problematic because the diesel particle mass distribution is heavily weighted towards larger particles since nanoparticles typically compose a few percent of the total aerosol mass. Therefore, even a small amount of bounce from upstream impactor stages contributes a significant amount of contaminant mass to the lower nanoparticle stages. Other sampling artifacts that arise during collection are adsorption and volatilization of compounds. No data has been available for chemical composition of diesel nanoparticles for these reasons.

Here, we use a nano-differential mobility analyzer (Nano-DMA) to size-select nanoparticles produced from diesel engine exhaust for subsequent chemical analysis by thermal desorption particle beam mass spectrometry (TDPBMS). The Nano-DMA provides high concentrations of size-selected diesel nanoparticles without any contamination from larger particles. A number of organic compound classes and sulfuric acid have been identified and the approximate molecular weights and vapor pressures determined from calibrated desorption temperatures. The effect of particle size and engine operating conditions on the composition of diesel nanoparticles was also studied.

EXPERIMENTAL

Diesel particles were generated using a 4-cylinder, 4-cycle John Deere model 4045 TF250 diesel engine rated at 415 N-m @ 1400 rpm, but for which only 350 N-m can be achieved. All experiments were performed at a steady state at an engine speed of 1400 rpm in four modes: 15% load (50 N-m), 25% load (88 N-m), 40% load (140 N-m), and 50 % load (175 N-m). The fuel used was commercial EPA on-highway DF2 with 410-ppm sulfur. The lube oil used was John Deere +50 Supreme 15W-40 motor oil. The engine exhaust particles were sampled under constant conditions that closely simulate those in the ambient environment using a two stage air injector, variable residence time, micro-dilution system (VRTDS) previously described in detail.[3] A primary dilution ratio of ~16, a secondary dilution ratio of ~4, and a residence time of ~1700 ms was used for generation of high concentrations of nanoparticles with sufficient mass so that subsequent chemical analysis could be performed above the detection limits of the TDPBMS downstream of the VRTDS.

After diesel exhaust sampling through the VRTDS, three different modes of particle size selection were used before chemical analysis using a TDPBMS. In one mode, total particles were analyzed without size selection by sampling diesel exhaust directly from the VRTDS into the TDPBMS and is referred to as the total mode. In the second mode, which is referred to as the 40 nm mode, the diesel exhaust was sampled from the VRTDS into a unipolar charger for high efficiency, high throughput particle charging, followed by a Nano-DMA for size selection of charged nanoparticles with a diameter of average mass of ~40 nm. In the third mode, which is referred to as the 30 nm mode, diesel particles were sampled into a radioactive bipolar charger, followed by a Nano-DMA for size selection of charged nanoparticles with a diameter of average mass of ~30 nm.

Temperature-programmed thermal desorption (TPTD) analysis using TDPBMS[4] was used for diesel nanoparticle chemical analysis. Particles of ~20-500 nm in diameter are sampled into a high-vacuum chamber with ~40-100% efficiency using aerodynamic focusing techniques. All focused particles impact onto the inside walls of a v-shaped molybdenum foil. The particles were either continuously vaporized for real-time analysis by resistively heating the foil at ~250°C, or cryogenically collected over time for fast-TPTD analysis by cooling the foil to -50°C. The desorbing molecules are ionized by impaction with 70 eV electrons and mass analyzed using a quadrupole mass spectrometer.

Particles sampled in all three modes were cryogenically collected onto the cold foil over times ranging from 15-70 min. After collection, the components of the sample were quickly desorbed according to their vapor pressures and therefore separated to some degree in time. During desorption, the foil is resistively heated from approximately -50 to + 300°C over ~6 min. The non-linear temperature ramp rate is about 150, 100, and 50°C/min in the first, second, and third minutes of the desorption. A portion of the evaporating molecules is sampled into the mass spectrometer for mass analysis over the desorption period. Particles generated at each of the four engine conditions (15%, 25%, 40%, 50% load) were chemically analyzed from all three sampling modes (total, 40 nm, 30 nm) using the fast-TPTD procedure. Mass spectral analysis was conducted either by scanning over an appropriate mass range or single-ion monitoring (SIM) of five mass-to-charge ratios (*m/z*) during the fast-TPTD process.

At certain conditions where considerably less nanoparticle mass was available (e.g. the 30 nm mode, 50% load), full mass spectral analysis was not possible with 60 min sample collections. Increasing collection times to enhance S/N wasn't feasible, therefore SIM of five *m/z* signals was used instead to provide sufficient S/N to distinguish low nanoparticle signal from the background. With this enhanced S/N, vapor pressure measurements from well defined desorption profiles (*m/z* signal versus temperature) were also possible. The five masses used in the SIM method were chosen to represent the major organic compound classes identified from the full mass spectra (*m/z* 69, 85, 95), and sulfuric acid (*m/z* 81, 98). Diesel particles were collected for 60 min for all fast-TPTD analyses performed using the SIM method. Measurements of signal due to background gases were performed by sampling diesel under the same conditions as the 30 nm Mode and 40 nm

Mode, except that the Nano-DMA was set at 0 volts to allow only diesel exhaust gases to pass through the classifier.

The TDPBMS was calibrated with known standards so that the approximate molecular weights and vapor pressures of the diesel particle components could be estimated. Solutions of pure organic compound, diesel fuel, or lubricating oil in hexane or sulfuric acid in water was atomized using clean air, then dried and sent though a bipolar charger and DMA. The aerosol standard was cryogenically collected on the foil in the TDPBMS high-vacuum chamber and then analyzed using fast-TPTD in the same manner as for the diesel exhaust particles.

RESULTS AND DISCUSSION

Full mass spectra were obtained at the signal peak during desorption for all the 40 nm and 30 nm particle modes at the 15% engine load condition and for total mode particles at the 50% engine load condition. The mass spectra are very similar to each other and by themselves show no major difference in chemical composition as particle size and engine load change; however, desorption profiles using the five mass method reveal compositional differences and will be discussed below. Mass spectra for standards of the fuel and lubricating oil were also obtained using the same fast-TPTD analysis and are very similar to the diesel particle spectra. The fragmentation patterns within the mass spectra of the diesel particles analyzed in this work verify the presence of at least a few of the major organic compound classes found in other studies of diesel exhaust particles that involved filter collection of particles, solvent extraction, and GC-MS analysis.[5] Our results indicate branched alkanes and cycloalkanes are probably the greatest contribution to the diesel particles. It was not possible to ascertain the presence or absence of PAH in the diesel nanoparticles.

Figures 1 and 2 show a few of the desorption profiles or mass thermograms (*m/z* signal versus vaporizer temperature) of *m/z* 69 and 98, respectively, from the matrix of fast-TPTD experiments performed using the five mass method. These plots provide information on the relative volatilities of the particle components, since compounds with lower volatility desorb at higher vaporizer temperatures. For example, analysis of total mode particles at 15% engine load reveals a peak in the *m/z* 69 signal at ~37°C (Figure 1A), while total mode particles at 50% engine load peak out at ~107°C (Figure 1B). This desorption peak generally shifts to higher temperatures as engine load is increased in all particle modes, indicating a decrease in average compound volatility with increasing engine load. Analysis of *m/z* 85 and 95 reveal the same trend as for *m/z* 69. When engine load is held constant, the *m/z* 69, 85, and 95 desorption peaks also shift to higher temperatures for smaller particle sizes. This temperature difference is indicative of large increases in average compound volatility with increasing particle size. This observation is consistent with particle growth theory, where a compound adds to a particle depending on the difference between rates of compound condensation and evaporation, which in turn depends on the difference between the partial pressure and equilibrium vapor pressure of the compound. Because of the Kelvin effect, the equilibrium vapor pressure of a compound increases with decreasing particle size. Therefore, it is expected that diesel nanoparticles will initially grow by addition of lower volatility compounds, with growth by condensation of higher volatility components increasing with particle size.

For all particle modes at 15% engine load, the desorption profiles of *m/z* 81 and 98 contain single peaks at the same temperatures as in the profiles of *m/z* 69, 85, and 95 indicating an organic contribution to these *m/z*'s. However, for the 40 nm mode at 40% and 50% engine loads (Figure 2A and 2B), in which *m/z* 69, 81, 85, 95, and 98 all peak at temperatures higher than 150°C, a second peak appears in the desorption profiles of *m/z* 81 and 98 at 22-43°C, which was determined to be due to sulfuric acid. These results suggest that the nanoparticles form by nucleation of sulfuric acid and water, and that organics subsequently condense onto these nuclei to form the bulk of the particulate mass. At lower loads, more of the higher volatility organics are present in the exhaust and add to the mass of the particles.

ACKNOWLEDGEMENTS

We thank the Coordinating Research Council and the California Air Resources Board for funding this research.

REFERENCES

1) Donaldson, K.; Li, X. Y.; MacNee, W. *J. Aerosol Sci.* **1998**, *29*, 553-560.
2) Kittelson, D. B. *J. Aerosol Sci.* **1998**, *29*, 575-588.
3) Khalek, I. A.; Kittelson, D. B.; Brear, F. *SAE Tech. Pap. Ser.* **2000**, *No. 2000-01-0515.*
4) Tobias, H. J.; Ziemann, P. J. *Anal. Chem.* **1999**, *71*, 3428-3435.
5) Schauer, J. J.; Kleeman, M. J.; Cass, G. R.; Simoneit, B. R. T. *Environ. Sci. Tech.* **1999**, *33*, 1578-1587.

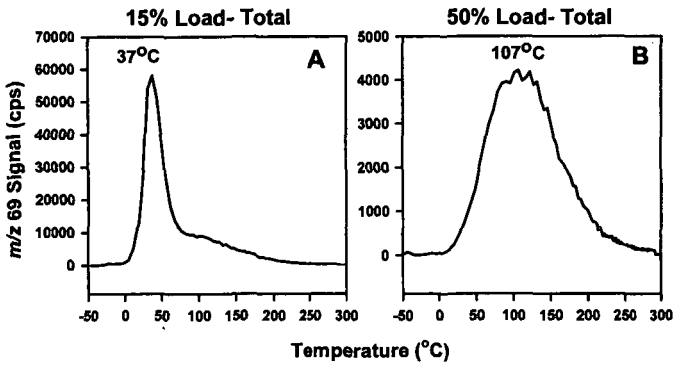

Figure 1- *m/z* 69 mass thermograms from fast-TPTD analysis of diesel particles.

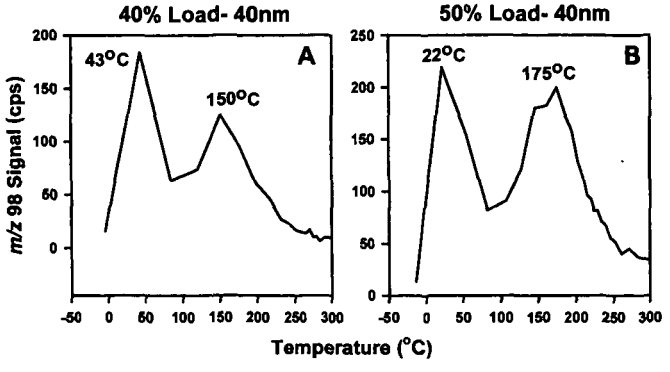

Figure 2- *m/z* 98 mass thermograms from fast-TPTD analysis of diesel particles.

NOVEL USES FOR TIRE PYROLYSIS CHAR

William Petrich

United Carbon Corporation

KEYWORDS: Carbon black, char, pyrolysis

Introduction

Char produced from the thermal conversion of used automobile tires contains a blend of the carbon blacks used in the manufacture of the tire as well as "ash" constituents formed in the pyrolitic process. This mixture provided a challenge to determine possible secondary and tertiary uses. Early work attempted to separate the "ash" fraction from the carbon black species.(1). Subsequent effort uncovered the relationship between the carbon black and the ash fractions and suggested a reverse method of formulation. Because all of the materials found in the char were derived from the recipes used in building the tread, side-wall and bead of the tire, it was anticipated that these materials, in ratio, could be used for other blended engineering materials. The idea of using the char as a "basic" starting material for formulated chemical specialties outside of the rubber industry was supported by two factors:

1. The potential volume of the char material was calculated at sixty tons per day.(2)
2. The composition the char did not vary by more than 0.5% in ratio of items.

These two considerations prompted further study and application evaluations.

Materials and Methods

One ton of shredded used automobile tires were processed using the Svedala Pyrolysis System (3), The shreds were reduced to a gas, "oil" and char. The char fraction is one third of the feed weight ,six hundred sixty seven pounds yield per ton of tires. Of the six hundred and sixty seven pounds of char, eighty five percent is carbon black and fifteen percent is ash. The char was ground to a uniform mesh size (4) to allow blending and dispersion to occur more easily in subseqnent formulations. The char was used in the following applications in order to determine the value added.

Results

Simultaneous Mercury, Sulfur Dioxide and Nitrous Oxide control in coal combustion by adsorption. The tire derived char was compared to silver impregnated activated carbon at laboratory level to ascertain the sorbent performance. Early tests showed that the char derived from pyrolysis of used automobile tires was equal to the silver impregnated activated carbou, indeed Mercury sorption on tire-derived activated carbon was identified as the most promising application.(5).

Carrier media for distillation of wastes derived from ink, paint, coatings and dry cleaning processes. The char derived from the pyrolysis of used automobile tires was evaluated as a "carrier" for mixed wastes generated by the paint, ink and coatings industries. The wastes evaluated contained aliphatic, aromatic solvents dispersed with pigment, filler, plasticizer and resins. Addition of 7.0 to 11.0% of the char created a mixture that allowed complete evolution of the solvents and absorbed the remaining ingredients of the waste creating a dry solid matrix. The dry solid was then re-ground to a uniform size and evaluated as an extending material for adhesives, synthetic lumber.(6)

Char may be used as an extender in adhesives, coatings and cements. Additions of 3.0 to 7.0% of char to blends of vinyl or rubber cements resulted in lower raw material cost with no loss of physical or chemical properties. The modified cements were tested in floor adhesives, tile adhesives and panel-stick compounds. Neither tack nor drying characteristics are affected by the addition. A stiffening of the finished adhesive bond was determined but did not affect the permanence of the bond.(7)

Discussion

Each application outlined above has been evaluated by no less than three investigators. Work done by others, including Advanced Fuel Research, Rohm & Haas, Morton International Automotive Finishes Group and others confirm that the inclusion of tire derived char, when properly ground and classified, can be nsed as a pre-engineered extender and physical property modifier. Extensive aging tests are being conducted on products utilizing the char. Among the properties within new rubber products that are affected include hardness, elongation, tensile and compression set.(8)

Conclusions.

The investigation of pyrolysis systems appears meaningful in light of the various uses found for the char produced through thermal conversion of used automobile tires. The economic model (9) represents an average value of the char at no less than $0.18 per pound. This "value" coupled with the value of the collected oil product and the energy value provides the support for re-evaluating pyrolysis as one technology to diminish the stockpiles of used tires.

Acknowledgements

We are grateful to Advanced Fuel Research and especially thankful for the meaningful assistance of our colleague Dr. Marek Wojtowicz. We would also like to thank Dr. Mark A. Petrich who was instrumental in the early work on tire char characterization. Special assistance was also provided by Marshall J. Field, President of United Carbon Corporation.

References

(1) Dr. Mark A. Petrich, Northwestern University, Chemical Engineering Department, Evanston Illinois.
(2) United Carbon Corporation, planned facility at California City California, Business Plan and conversation with Marshall J. Field, President.
(3) Michael H. Weinecke, Senior Development Engineer, Svedala Industries, Test Center, Oak Creek Wisconsin; Results of On-Going Production of char product.
(4) Ibid. Svedala Grinder Division Equipment
(5) Marek Wojtowicz, Advanced Fuel Research, SBIR Phase I study, East Hartford Connecticut
(6) David Miklos, Environmental Manager, Morton Automotive Group, Rohm & Haas Corporation, Lansing Illinois, Results of testing and production results.
(7) Gary Post, Applied Recycling Technologies Inc. St. Petersburg Florida. Current use of char in composite lumber production.
(8) Steve Mobley, ProTurn Corporation, Oregon City Oregon, Urethane Foam Rubber mechanical parts used in construction equipment.
(9) Economic model available upon request to author.

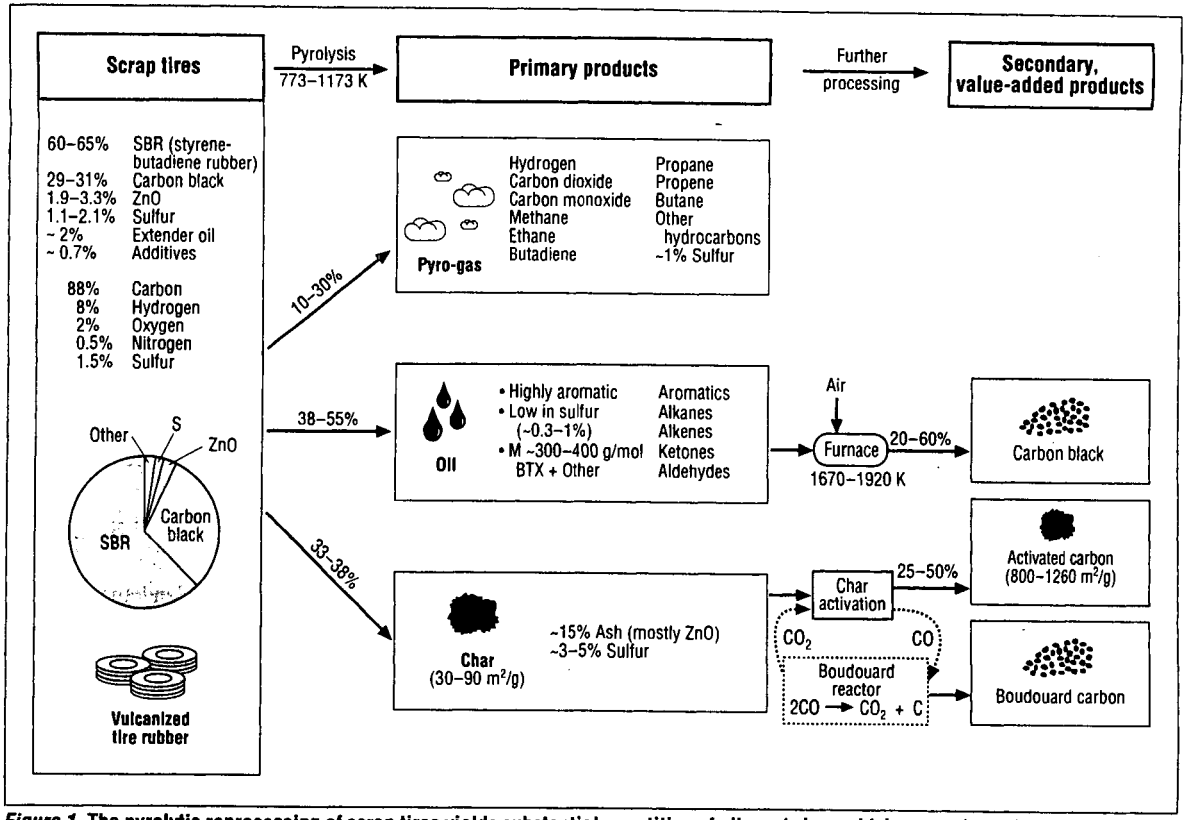

Figure 1. **The pyrolytic reprocessing of scrap tires yields substantial quantities of oils and char, which can undergo further processing to secondary, value-added products.** Char upgrading results in producing high-surface-area activated carbon and Boudouard carbon. Ash-free oils are turned into high-quality carbon black, or the oils can be separated into valuable chemical feedstocks by distillation.

IMPROVED WOMBAT METHOD FOR PROCESSING SCRAP TIRES INTO USEFUL MATERIALS

by
David L. Wertz
Department of Chemistry and Biochemistry, The University of Southern Mississippi,
Hattiesburg, MS 39406
david.wertz@usm.edu
and
Chris D. Deaton
WOMBAT Technologies International, Inc.,
Biloxi, MS 39531
info@omniinstruments.com

Keywords: Scrap tire degradation, economics

The Wertz Oxidative Molecular Bombardment at Ambient Temperature (WOMBAT) process is a sequence of redox reactions which has been used for several years to degrade scrap tires. This process has, to date, been conducted in adiabatic chemical reactors constructed either from poly-vinyl chloride and/or stainless steel. It has the potential to impact the scrap tire inventory in the United States (and elsewhere) which now has reached about three billion and is increasing by 250-300 million annually just in the United States. As previously shown, the WOMBAT process degrades the tire into four recoverable component parts: (a) the steel from its tread and its bead wire sections, (b) the rubber backing(s), (c) the fibers, and (d) a particulate which is dispersed in the reactor fluid. These results are summarized in Figure 1. After washing the steel, the rubber mats, and the fibers, these components may be separated and then used without further treatments. The particulate has typically been removed from the reactor fluid and then collected by centrifugation and/or filtration. After washing the collected particulate with water and drying in a convection oven, the resulting gel is converted to a carbon-based powder by light grinding. The resulting powder has highly irregular particle surfaces and a high, but somewhat variable, oxygen content.

These high carbon particles are effective as sequestering agents for several divalent cations, eg. Ca(II), Cu(II), Pb(II), Hg(II), etc. In addition, the black powder has a heat content ca. 30% higher than the heat content of the typical bituminous coal and a sulfur content in the 0.3 - 1.0% weight percent range even though this powder contains 10-15% oxygen by mass. The economic potential of the black powder recovered from degrading the tire is being explored based on its potential use as a sequestering agent and as a high energy, low ash, low polluting fuel. Both of these potential uses impact the economic model for the WOMBAT process (Figure 2). While the WOMBAT process has achieved its initial goal of degrading the tires into useful end products while generating no hazardous waste, the current reaction procedures have two drawbacks -- the process is quite slow, and the process requires too much reactor fluid (i.e., catalyzed nitric acid).

These limitations have been due, at least in part, to limitations in the design and the operation of our previous reactors. The WOMBAT IV reactor is now available and is being utilized in studies designed to minimize the process problems noted above. In addition, the WOMBAT IV reactor is a significant step forward in a concept of "complete" process

automation.

In an attempt to accelerate the reactor sequences and to improve the requisite fluid/tire materials ratio, several new reactor parameters have been introduced into our process procedures. To date, the effect(s) of controlling and increasing temperature, adding compressed air, and improving the fluid circulation within the reactor have all been studied using our new WOMBAT IV reactor (see Figure 3). In addition, the degradation of the reactor fluid is being studied in an attempt to develop a sensor which will allow for control of the entire process by microprocessor(s).

CONCLUSION. The rate(s) of at least some of the key reactions involved in the WOMBAT process have been accelerated by one order of magnitude.

ACKNOWLEDGMENT. The sponsorship of the United States Department of Agriculture (Small Business Innovative Research Phase I grant), the Mississippi Department of Environmental Quality, two phase 0 SBIR grants from the State of Mississippi, and The University of Southern Mississippi is gratefully appreciated.

SCHEMATIC OF THE WOMBAT PROCESS

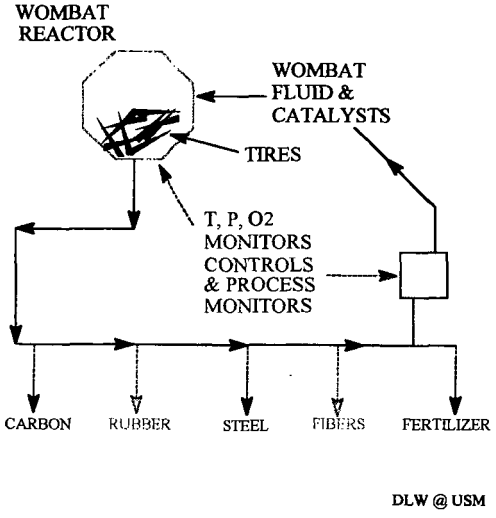

Figure 1

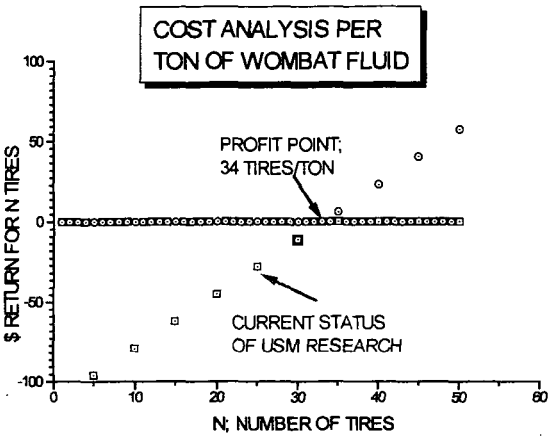

Figure 2

SCHEMATIC OF WOMBAT REACTOR

FLOW OF WOMBAT FLUID

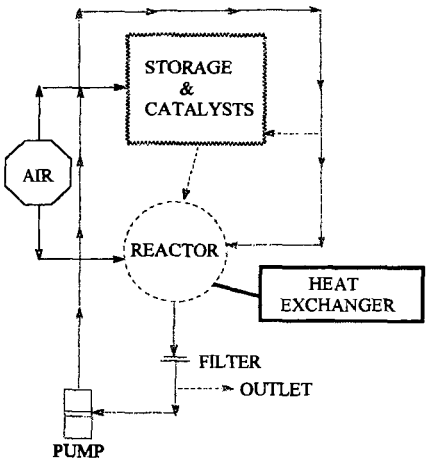

DLW@ USM

Figure 3

The Nature of Porosity in Carbons Derived from Scrap Automobile Tires

Eric M. Suuberg and Indrek Aarna
Division of Engineering, Brown University
Providence, RI 02912 USA
Tel. (401) 863-1420, E-mail *Eric_Suuberg@Brown.edu*

Keywords: activated carbon, porosity, surface area

Introduction

The use of scrap automotive tires for the production of activated carbons has been proposed by many investigators [e.g., 1-4]. The conversion of a problematic waste product to a potentially valuable industrial material has been the basis of possible commercial interest. It is, however, very clear that the ability to produce a material which is a legitimate replacement for currently utilized activated carbons is a prerequisite for moving towards actual commercialization. One of the key criteria for evaluating the potential of these materials concerns the nature of the porosity developed during their activation. This paper presents some detailed evaluations of the porosity developed under certain activation procedures. The research was not specifically aimed at identifying practical processing conditions, but instead sought to provide general insights concerning the development of porosity in this class of materials.

Experimental

The char used in this work was prepared from shredded tire crumb provided by Advanced Fuel Research (AFR) of East Hartford, Connecticut. The original tire particle diameter was about 1 cm, and its ash content was approximately 5%. All samples were initially pyrolyzed in a tube furnace at 973 K for five minutes, in a flow of high purity nitrogen. The yields of char ranged from 35 to 40% and averaged 36%. This is typical of yields from such tire pyrolysis experiments and is in excellent agreement with the results obtained by Teng et al. for the same material pyrolyzed at the same temperature [4]. Following pyrolysis, the char was ground to a powder in a mortar and sieved to a particle size between 320-420 μm. For the activation experiments reported here, the char was further pyrolyzed under nitrogen for one hour at 1173 K prior to activation. Following this second period of pyrolysis, the ash content of the char averaged 15% by mass.

Adsorption isotherms were determined in an automated volumetric gas adsorption apparatus (Autosorb 1, Quantachrome Co.). Adsorption of N_2 was performed at 77 K and adsorption of CO_2 at 195 K. Before measurements, samples were outgassed at 573 K for at least four hours in vacuum. Many were outgassed at 673 K for even longer times. This had no apparent effect on the results.

Char reactivity measurements and activation were performed in an Online Instruments TG-plus thermogravimetric analyzer. The reactions were performed in a mixture of helium and reactant gas (O_2, NO or CO_2), flowing at a rate of about 220 cm^3/min. Samples of 30-50 mg were dispersed on a circular platinum pan with a large flat surface and raised sides, resulting in a particle beds of about 1 mm thickness. Temperatures between 773-973 K were used for gasification with NO and CO_2, and temperatures between 573-748 K for O_2. The variation in temperature had no effect on the development of porosity. The partial pressures of oxidizing gases were 0.82, 2.02 and 4.80 kPa for NO, O_2 and CO_2, respectively. Char samples were outgassed at 1173 K for 30 minutes prior to reactivity measurements or activation. Burnoff is expressed on a dry-ash free basis.

Results and Discussion

The freshly pyrolyzed tire char is not a suitable for most activated carbon applications, due to its very low surface area. The materials that we produced had BET surface areas in the range from 54 to 87 m^2/g, which is typical of such unactivated materials. Thus it was clear that some activation of the material necessary. In the present paper, only the results of physical activation in oxygen, carbon dioxide and nitric oxide are presented.

The nitrogen isotherms on the unactivated material are unremarkable. A typical isotherm is shown on a logarithmic scale in Figure 1. Only very modest microporosity is observed, and there is no hysteresis observed in any portion of the isotherm. Standard Dubinin-Radushkevich (DR)

micropore analysis [5] of these data provides an estimate of micropore volume of 0.027 cc/g. This value was roughly a factor of three greater than the estimate of microporosity from an analysis of carbon dioxide isotherms on the same material. We have interpreted this as evidence for the existence of fairly wide microporosity which can be filled by nitrogen at 77 K, but not by carbon dioxide at 195 K.

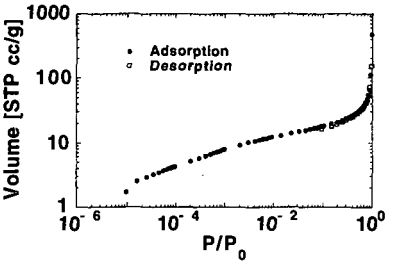

Figure 1. Typical N_2 isotherms on unactivated tire char.

The data of Fig. 1 may also be analyzed to provide an estimate of average pore radius. Assuming for simplicity cylindrical pores, the average radius r may be calculated from:

$$r = 2 * V_{pores} / S$$

where S represents the measured surface area. The values thus obtained for the raw chars range from 170 to 230 Å. It has been earlier noted that the yields of char from tire pyrolysis are generally quite comparable to the content of carbon black in the original tires. This is logical, since the rubber components themselves are quite volatile, and the carbon black can be expected to be nonvolatile. Electron microscopy has shown that our tire chars have a "grape cluster" appearance, consistent with the preservation of non-volatile carbon black particles in the char. In an aggregate solid made up of nearly spherical grains, the size scale of porosity is comparable to the diameter of the grains, i.e., the carbon black particles that constitute the raw tire char. The above average pore radius, thus implies a grain size typical of ASTM group 4 or 5 carbon blacks. These carbon blacks, in the raw state, typically exhibit a (purely external) surface area of around 35 to 70 m^2/g. This is clearly comparable to the values measured for these chars. Thus it may be concluded that the original char particles exhibit porosity determined by the residual carbon black grains. Again, such carbons are of little practical interest as activated carbons.

Upon activation, there is a very large increase in porosity. The adsorption isotherms for the oxygen activated material are shown in Figure 2.

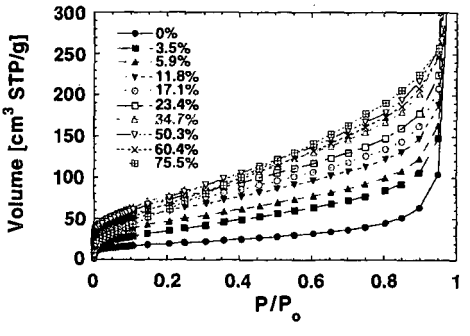

Figure 2. Nitrogen 77 K isotherms for samples activated in 2% oxygen.

It made little difference whether the chars were burned off in 2 % oxygen or in air (21 % oxygen) - the isotherm depended only upon level of burnoff, not the oxygen partial pressure used to achieve it. Likewise, temperature of activation made no difference to the development of porosity with burnoff in a range from 673 K to 773 K (400°C to 500°C). Naturally, both the oxygen partial

pressure and temperature did significantly affect the rates of activation. The similarity of porosity development observed under this wide range of conditions implied that the activating reactions were not taking place in a transport controlled regime, at least on the scale of porosity being developed.

Figure 3 shows the variation of nitrogen DR micropore volume with burnoff. Apart from re-emphasizing that the porosity development was not sensitive to activation conditions in oxygen, these results also indicate an apparent maximum in micropore volume at a burnoff of around 40%. On the other hand, the standard BET analysis [5] of the isotherm data show no significant decline in area with burnoff over 40% (see Figure 4). Generally, the BET surface area is associated with microporosity, so there is an apparent inconsistency between the results of Figures 3 and 4. The apparent contradiction is resolved by a density functional theory [6,7] analysis of the isotherm data. The results of the DFT analysis are shown in Figure 5.

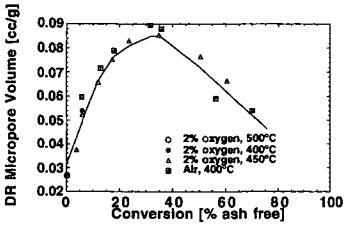

Figure 3. DR analysis of microporosity in tire chars activated in oxygen.

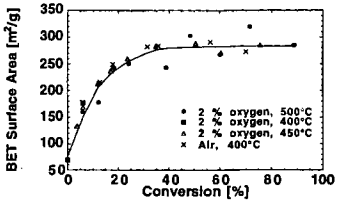

Figure 4. BET surface area of chars activated in oxygen.

The cumulative pore size distribution, on a pore volume basis, is shown in Figure 5. These results were obtained from DFT theory. They show that above 38.8% burnoff, there is a very significant loss of microporosity with burnoff (pores with halfwidths less than 10Å). By 88.7% burnoff, the micropores have virtually disappeared.

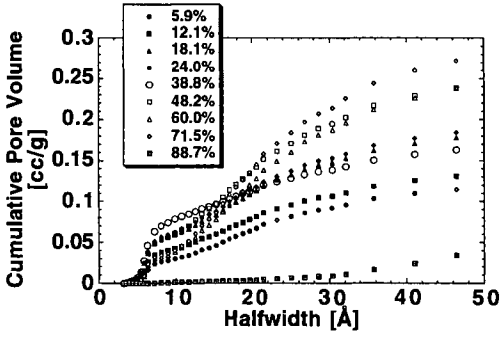

Figure 5. DFT pore size distributions as a function of burnoff in oxygen.

The decrease in micropore volume with burnoff above 38.8% burnoff is consistent with Figure 3. On the other hand, DFT theory can also be used to calculate surface area. The results of the calculation are shown in Figure 6. There is good agreement between the BET areas and those from DFT theory, with one notable exception (the sample at highest burnoff). Leaving this one exception aside, it is clear that the reason for the apparent discrepancy between the trends in micropore volume and BET area is that there is actually a significant contribution of mesopores to surface area, at high burnoffs. That is, the original assumption that surface area is dominated by micropores is not correct. The exceptional point at 88.7% burnoff exhibited a rather more curved BET plot than did the other samples. Therefore the fact that this point appeared to give the same surface area as the other lower burnoff samples is regarded as merely fortuitous. A similar high burnoff decline in DFT surface area was observed in another series of samples activated in air, so it is believed that the trend suggested by this point is real.

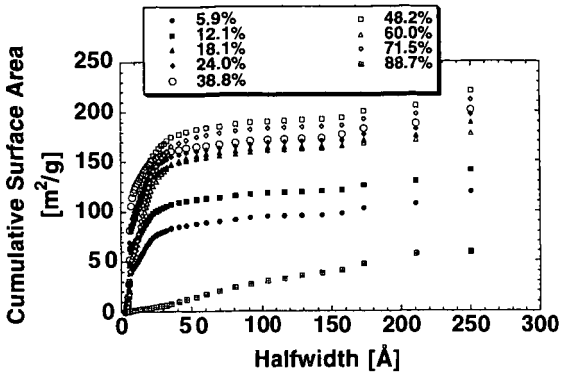

Figure 6. DFT cumulative surface areas for tire chars activated in 2% oxygen.

The development of surface area with activation follows a different pattern in different oxidizing gases. The results are shown in Figure 7. In this case, an attempt was made to match the initial gasification rates as closely as possible, so as to avoid differences in any possible role of mass transport. The oxygen activated samples appear to follow a different course than do the CO_2 and NO activated samples; the latter two gases appear much more effective in opening up surface area.

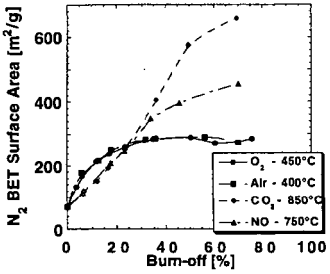

Figure 7. The development of BET surface area in oxygen, CO_2 and NO.

The ability of CO_2 to develop microporosity is explored in more detail, using DFT methods, in Figure 8. It is apparent that the difference between CO_2 and O_2 activation has to do with the absence of micropore-destroying processes at higher burnoffs. The CO_2 activation processes continue to develop micropores up to much higher burnoffs. This is reflected in the higher BET surface areas observed at high burnoffs.

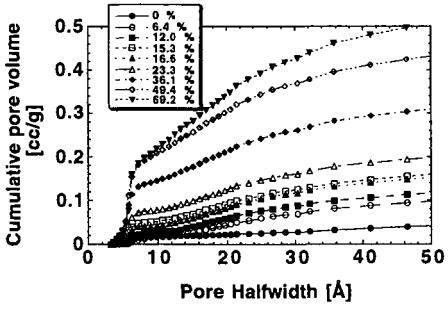

Figure 8. The development of porosity in CO_2 activation, examined using DFT.

It is interesting to compare the development of porosity in oxygen and carbon dioxide at lower

burnoffs. This is done, again using DFT methods, in Figure 9.

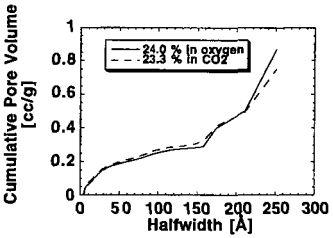

Figure 9. A comparison of porosity development during oxygen and carbon dioxide activation, at low burnoffs.

Figure 9 shows remarkable agreement in the pore size distributions obtained at already significant extents of burnoff. This would not have been anticipated, based upon the very different high burnoff behaviors of the samples activated in these two gases. The results with NO are also virtually identical in this range of burnoff (not shown here). It is as though up to a certain burnoff, the activation processes are being forced to follow a very similar pathway, but beyond that point, the differences in the nature of the reacting processes begin to manifest themselves. It may be that there is a certain fraction of carbon that is very much more reactive than the remaining carbon, and is removed first. This carbon would have to be associated with the carbon black particles, for the reasons noted above. It should be however noted that the accompanying reactivity studies gave no evidence of an abrupt change in carbon reactivity at burnoffs between 30 and 40% in either oxygen or carbon dioxide. Thus what drives the preferential removal of certain carbon atoms over others must be associated with subtle differences in reactivity. We have examined the possible role of catalysis in determining this behavior [8]. It is clear that the gasification is catalyzed by the inorganic impurities in the original tire material, but that this does not particularly influence the behavior of interest here. The catalysts appear to drive the formation of somewhat larger porosity in these samples.

Consequently, it appears as though the tire chars have an inherent propensity to form a certain amount of micro- and small mesoporosity. This tendency must be associated with the original carbon black particles in the tire, but it is not clear from the present work whether this tendency can be influenced by pyrolysis conditions. Beyond a certain burnoff, different oxidizing gases promote different types of porosity development, and can heavily influence the product carbon characteristics.

Acknowledgment

The support of the National Science Foundation under grant BES-9523794 and the US DOE under grant DE-FG22699-FT40582 are gratefully acknowledged.The encouragement and assistance of various personnel at Advanced Fuel Research, particularly Drs. Michael Serio and Marek Wójtowicz, is also gratefully acknowledged. Thanks are also due to Dr. Anil Prabhu of Quantachrome Corporation, for kindly allowing us to utilize a pre-release version of their DFT software.

References

1. Williams, P.T., Besler, S., Taylor, D.T., Fuel, 69, 1474 (1990).
2. Merchant, A. A., Petrich, M., AIChEJ, 39, 1370 (1993).
3. Ogasawara, S., Kuroda, M., Wakao, N., I&EC Res., 26, 2552 (1987).
4. Teng, H., Serio, M., Wojtowicz, M., Bassilakis, R., Solomon, P., I&EC Res., 34, 3102 (1995).
5. Gregg, S., Sing, K., *Adsorption, Surface area and Porosity*, Academic Press, 1982.
6. Evans, R., Marconi, U.M.B. and Tarazona, P. *J. Chem. Soc. Faraday Trans. II 82*, 1763 (1986).
7. Lastoskie, C., Gubbins, K.E. and Quirke, N. *J. Phys. Chem., 97*, 4786 (1993).
8. Suuberg, E.M. and Aarna, I., paper prepared for the *3rd Joint China/USA Chemical Engineering Conference,*, Beijing, September, 2000.

PYROLYSIS PROCESSING OF MIXED SOLID WASTE STREAMS

Michael A. Serio, Yonggang Chen, and Marek A. Wójtowicz

Advanced Fuel Research, Inc., 87 Church Street, East Hartford, CT 06108, USA

Eric M. Suuberg

Division of Engineering, Brown University, Providence, RI 02912 USA

KEYWORDS: Solid Waste, Pyrolysis, Life Support

ABSTRACT

The NASA objective of expanding the human experience into the far reaches of space will require the development of regenerable life support systems. A key element of these systems is a means for solid waste resource recovery. The objective of this work was to examine the feasibility of pyrolysis processing as a method for the conversion of solid waste materials in a Controlled Ecological Life Support System (CELSS). A composite mixture was made consisting of 10% polyethylene, 15% urea, 25% cellulose, 25% wheat straw, 20% Gerepon TC-42 (space soap) and 5% methionine. Pyrolysis of the composite mixture produced light gases as the main products (CH_4, H_2, CO_2, CO, H_2O, NH_3) and a reactive carbon-rich char as the main byproduct. Significant amounts of liquid products were formed under less severe pyrolysis conditions, but these were cracked almost completely to gases as the temperature was raised. A primary pyrolysis model was developed for the composite mixture based on an existing model for whole biomass materials.

INTRODUCTION

A key element of a CELSS is a means for solid waste resource recovery. Solid wastes will include inedible plant biomass (IPB), paper, plastic, cardboard, waste water concentrates, urine concentrates, feces, etc. It would be desirable to recover usable constituents such as CO_2, H_2O, hydrogen, nitrogen, nitrogen compounds, and solid inorganics. Any unusable byproducts should be chemically and biologically stable and require minimal amounts of storage volume. Many different processes have been considered for dealing with these wastes: incineration, aerobic and anaerobic biodigestion, wet oxidation, supercritical water oxidation, steam reforming, electrochemical oxidation and catalytic oxidation [1-13]. However, some of these approaches have disadvantages which have prevented their adoption. For example, incineration utilizes a valuable resource, oxygen, and produces undesirable byproducts such as oxides of sulfur and nitrogen. Incineration also will immediately convert all of the waste carbon to CO_2, which will require storing excess CO_2.

"Pyrolysis," in the context of this paper, is defined as thermal decomposition in an oxygen free environment. Primary pyrolysis reactions are those which occur in the initial stages of thermal decomposition, while secondary pyrolysis reactions are those which occur upon further heat treatment. A pyrolysis based process has several advantages when compared to other possible approaches for solid waste resource recovery: 1) it can be used for all types of solid products and can be easily adapted to changes in feedstock composition; 2) the technology is relatively simple and can be made compact and lightweight and thus is amenable to spacecraft operations; 3) it can be conducted as a batch, low pressure process, with minimal requirements for feedstock preprocessing; 4) it can produce several usable products from solid waste streams (e.g., CO_2,CO, H_2O, H_2, NH_3, CH_4, etc.); 5) the technology can be designed to produce minimal amounts of unusable byproducts; 6) it can produce potentially valuable chemicals and chemical feedstocks; (e.g., monomers, hydrocarbons, nitrogen rich compounds for fertilizers) 7) pyrolysis will significantly reduce the storage volume of the waste materials while important elements such as carbon and nitrogen can be efficiently stored in the form of pyrolysis char and later recovered by gasification or incineration when needed. In addition to being used as the primary waste treatment method, pyrolysis can also be used as a pretreatment for more conventional techniques, such as incineration or gasification. A summary of the pyrolysis processing concept is shown in Figure 1.

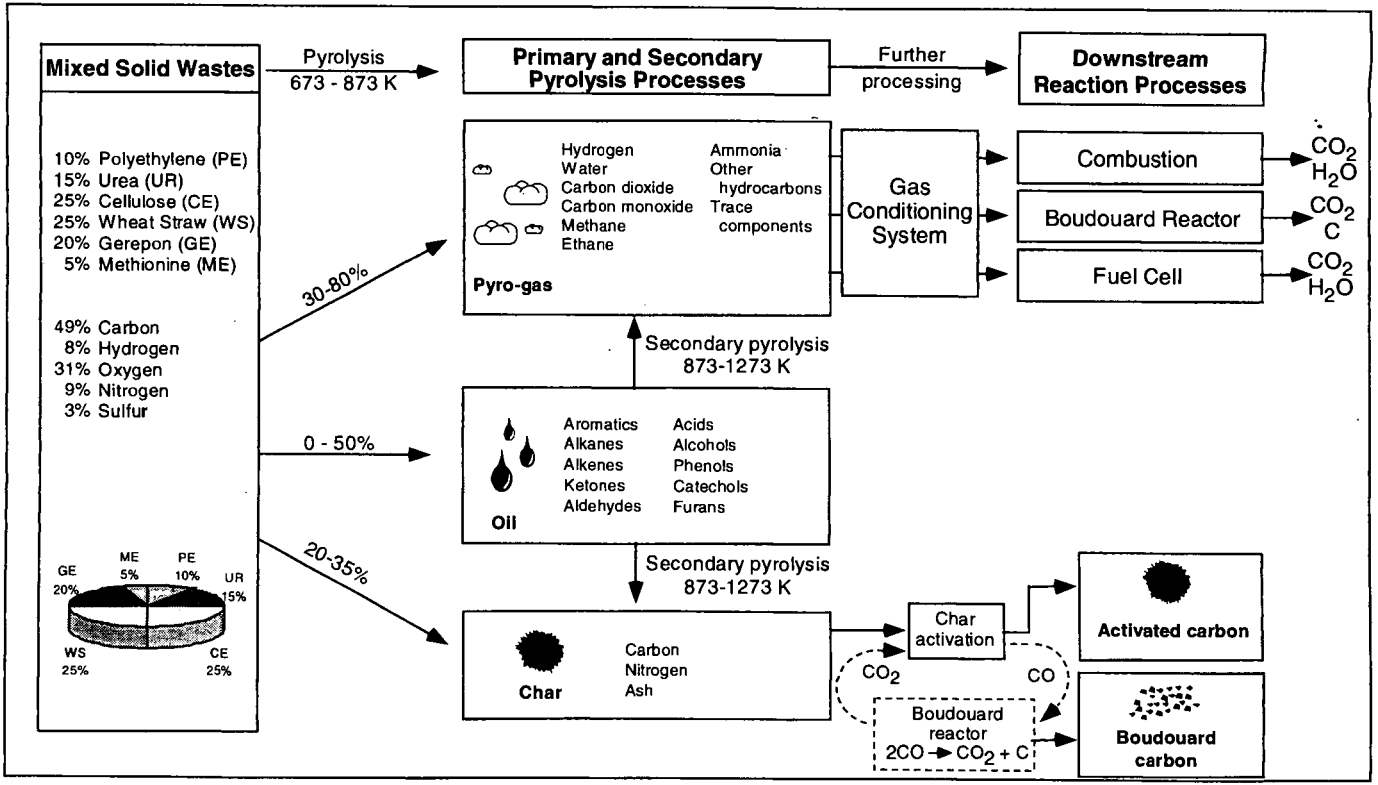

Figure 1. Summary of proposed pyrolysis-based solid waste processing scheme.

The primary disadvantages of pyrolysis processing are: 1) the product stream is more complex than for many of the alternative treatments; 2) the product gases cannot be vented directly in the cabin without further treatment because of the high CO concentrations. The former issue is a feature of pyrolysis processing (and also a potential benefit, as discussed above). The latter issue can be addressed by utilization of a water gas shift reactor or by introducing the product gases into an incinerator or high temperature fuel cell.

EXPERIMENTAL METHODS

Sample Selection - It was decided to use a model waste feedstock similar to what was used in a previous study at Hamilton Standard [11], the so-called "Referee mix." That study used 10 wt. % polyethylene, 15% urea, 25% Avicel PH-200 cellulose, 25% wheat straw, 10% Gerepon TC-42 (space soap) and 5% methionine. The materials that were obtained and the elemental compositions of each (on a DAF basis) are given in Table 1. A different sample of Avicel cellulose was used (PH-102), as a supply was already on hand and significant amounts of data had been generated with this material for a private client in a previous study. It was thought that the difference between these two cellulose samples would be small and that there was an advantage to using a material whose individual pyrolysis behavior had already been characterized. The NIST wheat straw sample was previously studied under a USDA project [14]. The Gerepon TC-42 is the same as the Igepon TC-42, but the name was changed since the product line was sold to a new company (Rhône-Poulenc). It is a soap which is made from coconut oil, so its exact formula is unknown. The composition was estimated by assuming that most of the fatty acids were C_{12}. The technical name for Gerepon TC-42 is sodium methyl cocoyl taurate.

TG-FTIR System - The samples in Table 1 were obtained and subjected to thermogravimetric analysis with FT-IR analysis of evolved gases (TG-FTIR) at 10 °C/min and 30 °C/min. Details of the TG-FTIR method can be found in references [15] and [16]. The apparatus consists of a sample suspended from a balance in a gas stream within a furnace. As the sample is heated, the evolving volatile products are carried out of the furnace directly into a 5 cm diameter gas cell (heated to 150 °C) for analysis by FT-IR. In the standard analysis procedure, a ~35 mg sample is taken on a 30 °C/min temperature excursion in helium, first to 150 °C to dry, then to 900 °C for pyrolysis. After cooling, a small flow of O_2 is added to the furnace and the temperature is ramped to 700 °C (or higher) for oxidation in order to measure the amount of inorganic residue. The TG-FTIR system can also be operated with a post pyrolysis attachment to examine secondary pyrolysis of the volatile species (see below).

During these excursions, infrared spectra are obtained approximately once every forty-one seconds. The spectra show absorption bands for infrared active gases, such as CO, CO_2, CH_4, H_2O, C_2H_4, HCl, NH_3, and HCN. The spectra above 300 °C also show aliphatic, aromatic, hydroxyl, carbonyl and ether bands from tar (heavy liquid products). The evolution rates of gases derived from the IR absorbance spectra are obtained by a quantitative analysis program. The aliphatic region is used for the tar evolution peak. Quantitative analysis of tar is performed with the aid of the weight-loss data in the primary pyrolysis experiments.

The TG-FTIR method provides a detailed characterization of the gas and liquid compositions and kinetic evolution rates from pyrolysis of materials under a standard condition. While the heating rates are slower (3-100 °C/min) than what is used in many practical processes, it is a useful way of benchmarking materials and was used in this study for characterizing both the primary and secondary pyrolysis behavior of the model waste samples and the individual components. In addition, Advanced Fuel Research, Inc. (AFR) has developed kinetic models based primarily on TG-FTIR data which can be extrapolated over a wide range of conditions.

Differential Scanning Calorimetry (DSC) - Measurements of the thermodynamics of the pyrolysis process, were made using differential scanning calorimetry (DSC) at Brown University. Samples of each of the materials in Table 1 were sent to Brown. The DSC experiments were done by heating at 10, 30 and 60 °C/min. These heating rates were the same or similar to the heating rates used in the TG-FTIR experiments, so a direct comparison could be made. A TA Instruments 2910 DSC system, with a maximum operating temperature of 600 °C, was employed in the DSC work. The sample cell was operated under a nitrogen flow rate of 100 cm^3/min in order to keep the cell free of oxygen during the measurements. In preliminary work,

this was noted to be important. Small amounts of oxygen, participating in a combustion reaction, can significantly influence the thermal characteristics of the process.

Table 1. Elemental Analysis of Individual and Composite Samples (DAF wt.%)

Sample	C	H	O	S	N
Polyethylene[a] (Aldrich)	85.7	14.3	0.0	0.0	0.0
Cellulose[b] (Avicel PH-102)	44.0	6.2	49.8	~0.0	~0.0
Wheat Straw[b] (NIST)	48.0	6.2	44.9	0.2	0.7
Urea[a] (Aldrich)	20.0	6.7	26.6	0.0	46.7
Gerepon[c] TC-42 (Rhône -Poulenc)	60.5	11.5	11.5	11.5	5.0
Methionine[a] (Aldrich)	40.3	7.4	21.4	21.5	9.4
Composite	48.7	8.2	31.0	3.4	8.7

Notes: DAF = Dry, Ash Free
a = determined from chemical formula
b = determined by Huffman Laboratories (Golden, CO)
c = estimated from approximate chemical formula

Aluminum sample pans were used for the DSC experiments in a partially sealed mode. This was done by pushing down the top sample pan cover gently onto the bottom pan containing the sample. Following this, three small pinholes were poked into the sample pan to allow a limited amount of mass loss from the pan. This configuration has been used previously in work on cellulose samples [17], and gives results which are consistent with pyrolysis in a confined system with a slow rate of mass bleed out of the system. It was felt that this would be reasonably representative of a pyrolysis processing system. Typically, about 10 mg of sample was used in an experiment.

In many cases, particularly with charring samples, the initial DSC run was followed by a cooling of the sample back down to room temperature, followed by a retrace of the original heating profile. This procedure provided a background trace attributable to the heat capacity of the char residue. In cases involving formation of a char residue, the mass loss of the sample during the first heating was also established. These values were compared with the TG-FTIR results, to verify whether the pyrolysis was occurring in a consistent manner, or in a different manner due to the increased mass transport resistance in the DSC pans.

RESULTS AND DISCUSSIONS

TG-FTIR Results for Primary Pyrolysis - An example of some representative data is shown in Table 2, which includes the average results of all the runs done at heating rates of 30°C/min. Similar results were obtained at 10°C/min [18,19]. For all of the samples, data from primary pyrolysis experiments for the same nominal pyrolysis conditions for each sample are generally in good agreement. For example, in the case of cellulose, there are differences in CO_2 yields that can probably be attributed to small air leaks in the system. For polyethylene, the material experiences a rapid and essentially complete depolymerization to tar which drives the balance pan below zero weight. Since the tar yields are ultimately determined by difference, this phenomenon results in integration errors which lead to tar yields above 100%. For the minor (trace) species for all of the samples, integration errors are also a concern and the results which are thought to be influenced mainly by noise are indicated by italics in Table 2.

For each of the samples, the data include moisture, total volatiles, fixed carbon, and ash. The yields of tar, CH_4, water, CO_2, and CO are reported as major pyrolysis products. In most cases, the minor pyrolysis products which are quantified include SO_2, C_2H_4, CS_2, NH_3, COS, and olefins and the amounts of these latter product are usually barely above the noise level. Hydrogen is not reported since the gas is not IR active. However only small amounts of

hydrogen are formed in primary pyrolysis experiments (<1 wt.%). It can be an important product from secondary pyrolysis experiments and for these experiments, the FT-IR measurements were supplemented by GC (see below).

The selection of the minor species to report is somewhat arbitrary and the current set of gases is historically based on our extensive work on coal pyrolysis. For some of the samples, (urea, methionine, composite), the selection of species was changed in order to reflect the important major and minor pyrolysis products. Obviously, any gas can be quantified that is IR active and for which a calibration exists. In the case of the cellulose, wheat straw and Gerepon TC-42, the results could be made quantitative without any new calibrations since the major products were in our existing reference library. However, for the urea, methionine, and composite mixture, some additional calibrations had to be done in order to describe the evolution of some of the important products.

Table 2 - Average Results from Primary Pyrolysis Experiments in TG-FTIR System at 30°C/min (wt.%, As-Received Basis)

Sample	Cellulose	Wheat Straw	Polyethy-lene	Urea	Gerepon TC-42	Methion-ine	Composite Mix
Moisture	3.5	5.2	0.6	1.8	67.1	0.0	0.6
Volatiles	94.4	69.4	99.2	98.2	27.2	99.2	87.0
Fixed Carbon	1.3	17.5	0.0	0.0	2.0	0.0	12.4
Ash	0.5	7.8	0.0	0.0	4.8	0.8	0.0
Tars	91.2	30.0	101.4+	0.00	20.8	46.55	30. 9
CH_4	0.23	0.88	0.11	0.00	0.13	0.00	0.56
C_2H_4	0.04	0.32	0.0	4.54	*0.14*	0.00	0.40
H_2O	7.81	22.74	1.30	21.94	3.12	3.74	23.30
CO_2	2.72	10.50	0.54	1.83	2.42	6.96	9.80
CO	1.04	6.56	0.00	1.66	0.85	0.00	5.58
NH_3	*0.05*	*0.07*	0.00	13.89	*0.26*	0.58	0.86
COS	0.00	*0.00*	0.00	0.00	*0.13*	0.00	0.60
SO_2	0.00	0.24	0.00	0.00	0.3	0.06	1.10
Cyanic acid (CHNO)				22.43			0.40
Cyanuric acid ($C_3H_3N_3O_3$)				0.56			
Biuret				32.70			
Methionine						27.77	
Methylthiopropyl amine						13.05	11.87

Notes: Yields are given on an as-received wt.% basis; numbers in italics are influenced by noise and may not be reliable; + indicates numbers that are influenced by balance errors due to very rapid devolatilization; all runs done at standard carrier gas flow rate of ~400 cm^3/min helium.

Both the cellulose and the polyethylene undergo nearly complete devolatilization to 100% tar plus gas. As expected, the cellulose and wheat straw produce oxygenated gases in addition to tar. However, the wheat straw produces about 20-25 wt.% char (fixed carbon plus ash) on an as-received basis. The formation of fixed carbon from whole biomass is known to result primarily from the aromatic lignin component of the plant, which typically comprises 20-25% by weight, with the remainder being primarily cellulose and hemicellulose [20]. Previous work at AFR and elsewhere has shown that the weight loss from pyrolysis for whole biomass samples can be understood as a linear superposition of these three main components to a first approximation [14]. However, one can not predict the yields of individual gas species using this approach, probably due to the catalytic effects of the trace minerals present in whole biomass.

Aside from NH_3 and small amounts of H_2O, the pyrolysis products from urea (N_2H_4CO) include cyanic acid, CHNO, and another compound that is probably biuret, $NH_2CONHCONH_2$. The latter two products were initially identified by a target factor analysis program that separates real component spectra from FTIR data. The cyanic acid was verified by pyrolyzing cyanuric acid

($C_3H_3N_3O_3$) a ring compound made essentially of three cyanic acid groups. Cyanuric acid produces cyanic acid and some cyanuric acid (either by evaporation or recombination of the cyanic acid) during pyrolysis. Biuret was tentatively identified by absorption peak positions, and comparison to solid phase spectra in the Aldrich Spectal Library book. The formation path for biuret is most likely from combination of cyanic acid with urea. All the products start evolving at fairly low temperatures, 125 to 145 °C but do not finish until around 420 °C.

Most of the mass loss from Gerepon TC-42 is from drying, due to the large moisture content. Additional water, along with CO_2, tars and small amounts of CO are produced from pyrolysis of the organic part of the soap.

Methionine ($C_5H_{11}O_2N_S$) pyrolysis proceeds in a much simpler fashion than in the case of urea. There is one basic weight loss event centered around 300 °C, producing mostly CO_2 and 3-(methylthio) propylamine. This is probably from decarboxylation of the methionine. To identify which other bonds in the methionine might be breaking, absorption spectra from the TG-FTIR runs were checked for some simple molecules that might result. For example, if the end C-S bond were to break, CH_4 would result. None was found, however. Similarly, there was no C_2H_4, NO, N_2O, NO_2, CH_3SH, CH_3SCH_3, SO_2, or CO and very little NH_3, indicating that the C-S bonds remained intact as did the bonds between the alpha and beta C. The only other thing that happened was a little bit of deamination and some dehydrolysis (as evidenced by water loss) which may have led to a polymerized high molecular weight product (tar). A compound, not yet identified, evolves around 220 to 270°C and accounts for about 25% of the methionine's weight loss. The material does not coincide with any release of other small gases. This means the product is either from direct evaporation of the methionine or some rearrangement is taking place. The hydrogen bonding in the methionine keeps the melting point high (and therefore the vapor pressure low) at around 275°C. Rearrangement could alter the hydrogen bonding and lead to a more easily evaporated material. The remainder of the sulfur mass must be distributed between the tar and this early pyrolyzate.

For the composite mixture, most of these unknown products are inconsequential, because of the relatively small contribution of urea and methionine to the overall product distribution and the product transformations that occur in the mixture due to chemical interactions and catalytic effects. Consequently, it was decided to limit the amount of effort devoted to identification of the products of pyrolysis of pure urea and methionine.

The results for TG-FTIR runs with the composite ("referee") mixture are also shown in Table 2. It can be seen that, in terms of product distribution (char, tar, gas), the results are much more similar to the NIST Wheat Straw sample than the cellulose, polyethylene, Gerepon, methionine, or urea samples. This result makes sense in that the wheat straw is also a composite mixture which consists of cellulose, hemi-cellulose, and lignin, while the composite mixture is made up of 25% cellulose and 25% wheat straw as the largest components. The wheat straw sample also has an elemental composition which is relatively close to that of the composite mixture (see Table 1). Therefore, one might expect similar pyrolysis behavior.

DSC EXPERIMENTS

The general conclusion which can be drawn from these measurements is that the composite mixture pyrolysis is only mildly endothermic (of order 100 J/g), under conditions in which a significant amount of mass loss is permitted to occur during pyrolysis. Confining pyrolysis more completely might be expected to drive the process in an even more exothermic direction, as it does in the case of pure cellulose [17]. In any event, it may be noted that, in comparison to this relatively modest enthalpy of pyrolysis, the sensible enthalpy for heating the sample is quite a bit larger. For example, using a "typical" average heat capacity for cellulose of 2 J/g-K to represent the composite mixture, it can be determined that heating from room temperature to 600°C will itself require 1150 J/g of sample. Additionally, the heat required to evaporate any residual moisture content could also far outweigh this small pyrolysis thermal demand. Thus it may be concluded that the heat of pyrolysis will not be of significant design concern unless conditions far removed from these are to be explored. Most of the heat input required will be to overcome heat losses from the reactor.

RESULTS OF CHAR CHARACTERIZATION STUDIES

Much of the work on char characterization was also done at Brown University. The work at Brown included characterization of the gasification reactivity of the char using a TGA system and pore structure measurements using the Autosorb instrument made by Quantachrome. Char forming experiments were performed under conditions comparable to those at AFR. In addition, samples of char generated at AFR were supplied to Brown.

At both AFR and Brown, reactivity measurements were made using indices known as $T_{critical}$ and T_{late}. These measure the temperature at which a char heated at 30 °C/min in air achieves a reaction rate of 6.5% per min in the early stage of reaction and where it returns to that value in the later stages. Low values of $T_{critical}$ and T_{late} indicate a reactive material and vice versa. The results indicated that these chars are very reactive and would be easy to gasify or combust in order to recover additional carbon and nitrogen. The same conclusions were reached in the more extensive char characterization studies that were done at Brown, which also included characterization of pore structure [18].

TG-FTIR EXPERIMENTS WITH THE POST PYROLYZER (TG-FTIR/PP)

The TG-FTIR system, was used as discussed above, to characterize the primary pyrolysis behavior of the individual components and the composite sample. Under this study, the system was also equipped with a post-pyrolysis system (isothermal secondary pyrolysis unit) in order to study the cracking of the heavy liquids (tars) and other volatiles that are formed during pyrolysis of these materials. This post pyrolysis unit can be operated from 500-1000 °C with an average volatile residence time of 0.4-2.6 seconds at atmospheric pressure. Under the right pyrolysis conditions, the liquids are cracked to produce primarily CO, CO_2, CH_4, H_2, H_2O, and small amounts of carbon.

In the current study, experiments were done with the TG-FTIR/PP system over the temperature range from 600 – 1000 °C in the post pyrolyzer. The helium gas flow rate through the 14 cm^3 volume post pyrolyzer for the "fast" runs was ~400 cm^3/min (at standard conditions). Additional runs were done at lower flow rates (~100 cm^3/min) in order to test the effect of this variable and also to provide gas concentration levels that would allow for simultaneous measurements by FT-IR and GC. Over a temperature range of 600 – 1000 °C, these gas flow rates correspond to a range of residence times for the fast flow conditions of 0.4 to 0.6 seconds and 1.8 to 2.6 seconds for the slower flow conditions, i.e., the flow rates were not adjusted to equalize the residence times at each temperature.

The TG-FTIR/PP experiments were done for both the composite mixture sample and the wheat straw sample. A set of results for the composite mixture, shown in Figure 2, demonstrate the

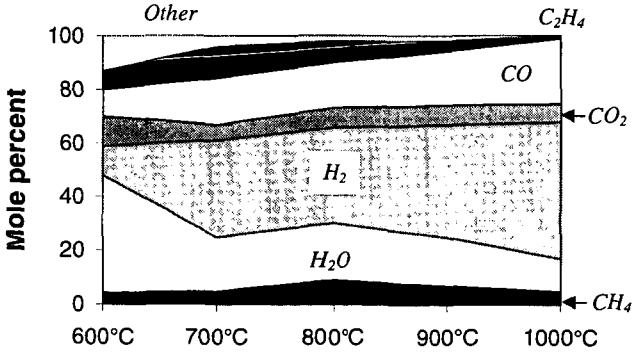

Figure 2. Estimated gas phase composition (mole %, excluding helium carrier) from TG-FT-IR pyrolysis experiments at 30°C/min with the composite mixture followed by secondary pyrolysis over a range of isothermal temperatures.

very strong effect of the post pyrolysis temperature on the product composition. As the post pyrolysis temperature increases, the tar yields decline to zero and the CO yields increase dramatically. The CH_4, H_2O and CO_2 yields go through a maximum. Similar results are observed for post-pyrolysis runs done with the pure wheat straw sample [18]. In order to get yield data on H_2, the GC system was used to take periodic samples.

The data shows that with increasing pyrolysis temperature, the gas composition becomes rich in H_2 and CO and that CH_4, CO_2 and H_2O are also key components. While tars and minor heterotomic species are present at low temperatures, these are largely eliminated as the temperature increases.

These results underscore the significant effect of primary and secondary pyrolysis conditions on the final product mix. There are many variables that can be manipulated for pyrolysis that can be used to compensate for changes in the feedstock composition and/or the desired product yields (e.g., time-temperature history, pressure). This provides a much greater degree of control over the solid waste processing step than is possible for either gasification or incineration. Changing the pyrolysis conditions allows one to effect significant changes in the pyrolysis product distribution (char, tar, gas) and the gas composition. Liquids can be produced if desired (under mild conditions) or cracked to form carbon oxides and fuel gases under severe conditions, depending on what is required for the life support system.

SUMMARY AND CONCLUSIONS

This project demonstrated that it is possible to pyrolyze a representative composite mixture of mixed solid waste materials and produce usable gases as the main products (CH_4, H_2, CO_2, CO, H_2O, NH_3) and a reactive carbon-rich char as the main byproduct. Significant amounts of liquid products were formed under less severe pyrolysis conditions, but these were cracked almost completely to gases as the secondary pyrolysis temperature was raised. A primary pyrolysis model was developed for the composite mixture based on an existing model for whole biomass materials, while an ANN model was used successfully to model the changes in gas composition with pyrolysis conditions [18].

This work has demonstrated that pyrolysis processing meets the requirements of solid waste resource recovery in space, i.e., it produces usable byproducts, with minimal side products, can be tailored to meet changes in the feedstock composition and the product requirements, significantly reduces storage volume, requires low maintenance can be conducted as a batch, low pressure process, and is compatible with the utilities that are present on board a spacecraft (electricity and small amounts of O_2 and H_2O). It should be noted that the pyrolysis gases will require further treatment, such as water gas shift conversion to remove CO, before they can be vented into the cabin. However, these gases could also be introduced into an incinerator or a high temperature fuel cell system with minimal pretreatment.

In future work, a prototype waste pyrolysis system will be developed in collaboration with NASA, Hamilton Sunstrand Space Systems International and Brown University and delivered to NASA. This pyrolyzer will be useful to NASA in at least four respects: 1) it can be used as a pretreatment for an incineration process; 2) it can be used as a more efficient means of utilizing oxygen and recycling carbon and nitrogen; 3) it can be used to supply fuel gases to fuel cells for power generation; 4) it can be used as the basis for the production of chemicals and materials in space.

ACKNOWLEDGEMENTS

The support of this work by the NASA-Ames Research Center under contracts NAS2-99001 and NAS2-00007 is gratefully acknowledged. The COTR was John Fisher and we are very grateful for his support and technical guidance. The authors also wish to acknowledge the contributions of David Marran, Rosemary Bassilakis, and Miriam Leffler of AFR to the experimental work and Robert Carangelo, an independent consultant to the interpretation of the TG-FTIR results. We are also grateful for comments and advice we have received from our colleagues at Hamilton SunStrand Space Systems International, Inc., Joseph Genovese, Philip Birbara, Harold Couch, and Kathy Ferner.

REFERENCES

1 Tri, T.O., Edeen, M.A., and Henninger, D.L., SAE 26th International Conference on Environmental Systems, Monterey, CA, Paper #961592, 8p. July 8-11,1996.

2 Budenheim, D.L. and Wydeven, T., Advances In Space Research (ISSN 0273-1177), Vol. 14, No. 11, P.113-123, Nov. 1994.

3 Flynn, M. and Budenheim, D., Space Technology and Applications International Forum (STAIF-98); Proceedings of The 2nd Conference on Applications of Thermophysics In Microgravity and 3rd Conference on Commercial Development of Space, Albuquerque, NM, P. 835-839, Jan. 25-29, 1998.

4 Ferrall, J.F., Ganapathi, G.B., Rohatgi, N.K., and Seshan, P.K., Technical Report - NASA-TM-109927; NAS 1.15:109927, Jet Propulsion Lab., Pasadena, CA.

5 Bilardo, V.J., Jr. and Theis, R.L.A., Engineering, Construction, and Operations In Space III: Space '92, Vol. 2, P. 1748-1764, May 31-June 4, 1992.

6 Ferrall, J., Rohatgi, N.K., and Seshan, P.K., SAE Paper 921119.

7 Marrero, T.R., NASA/ASEE Summer Faculty Fellowship Research Program Research Reports N86-14078 04-85), 1983.

8 Smernoff, D.T., Wharton, R.A., Jr., and Averner, M.M., Sales Agency and Pricing - HC A99/MF A04, P 263-280.

9 Spurlock, P., Spurlock, J.M., and Evanich, P.L., 21st Conference on Env. Systems, San Francisco, 1991.

10 Roberson, B.J., Lemay, C.S., NASA American Society For Engineering Education (ASEE) Summer Faculty Fellowship Program, Vol. 2, 1993.

11 NASA, Advanced Waste Management Technology Evaluation, Contract NASW - 5005, Final Report, June 1996.

12 Pisharody, S., Borchers, B., Schlick, G., "Solid Waste Processing in a CELSS: Nitrogen Recovery," Life Support & Biosphere Science, 3, pp. 61-65 (1996).

13 Bubenheim, D.L., Wydeven, T., "Approaches to Resource Recovery in Controlled Ecological Life Support Systems," Adv. Space Res., 14 (11), 113-123 (1994).

14 Serio, M.A., Wójtowicz, M.A., Chen, Y., Charpenay, S., Jensen, A, Bassilakis, R., Riek, K., "A Comprehensive Model of Biomass Pyrolysis," Final Report USDA 96-33610-2675, (1997).

15 Carangelo, R.M., Solomon, P.R., and Gerson, D.G., Fuel, 66, 960 (1987).

16 Carangelo, R.M., Solomon, P.R., Bassilakis, R., Gravel, D., Baillargeon, M., Baudais, F., and Vail, G., American Laboratory, P. 51, (1990).

17 Milosavljevic, I., Oja, V. and Suuberg, E.M., "Thermal Effects in Cellulose Pyrolysis-Relationship to Char Formation Processes," I&EC Research, 35, 653-662 (1996).

18 Chen, Y., DiTaranto, M., Kroo, E., Wójtowicz, M.A., Suuberg, E.M., and Serio, M.A., "Pyrolysis Processing for Solid Waste Resource Recovery in Space," Final Report submitted under contract NAS2-99001, June 1999.

19 Serio, M.A., Chen, Y., and Wójtowicz, M., "Pyrolysis Processing for Solid Waste Resource Recovery in Space," Submitted to 30th International Conference on Environmental Systems, Toulouse, France, July 10-13, 2000.

20 Klass, D.L., Biomass for Renewable Energy, Fuels and Chemicals, Academic Press, New York (1988).

PROPERTIES AND POTENTIAL ENVIRONMENTAL APPLICATIONS OF CARBON ADSORBENTS FROM WASTE TIRE RUBBER

Christopher M.B. Lehmann[1,2], David Rameriz[2],
Mark. J. Rood[2], and Massoud Rostam-Abadi[1,2]

[1] Energy and Environmental Engineering Section
Illinois State Geological Survey
Champaign, IL 61820

[2] Department of Civil and Environmental Engineering
University of Illinois at Urbana-Champaign
205 N. Mathews Ave.
Urbana, IL 61801

KEYWORDS: carbon adsorbent, pyrolysis, tire recycling, air pollution

ABSTRACT

The properties of tire-derived carbon adsorbents (TDCA) produced from select tire chars were compared with those derived from an Illinois coal and pistachio nut shells. Chemical analyses of the TDCA indicated that these materials contain metallic elements not present in coal- and nut shell-derived carbons. These metals, introduced during the production of tire rubber, potentially catalyze steam gasification reactions of tire char. TDCA carbons contained larger meso- and macopore volumes than their counterparts derived from coal and nut shell (on the moisture- and ash-free-basis). Adsorptive properties of the tire-derived adsorbent carbons for air separation, gas storage, and gas clean up were also evaluated and compared with those of the coal- and nut shell derived carbons as well as a commercial activated carbon. The results revealed that TDCA carbons are suitable adsorbents for removing vapor-phase mercury from combustion flue gases and hazardous organic compounds from industrial gas streams.

INTRODUCTION

The issue of disposing of waste tires in industrialized nations has become a pervasive issue that requires remedy. Data from a U.S. EPA study in 1993 indicates that 242 million waste tires are generated in the United States each year, corresponding to approximately one tire per US citizen per year[1]. The trend of one tire generated per person-year is generally applicable to industrialized nations. Tire stockpiles have created significant environmental concerns: the open shape of tires allows rainwater to collect, making them ideal breeding grounds for mosquitoes and vermin; tire stockpile fires are of concern since used tires are readily combustible and are difficult to extinguish; and finally, tire stockpiles are an aesthetic concern, since they are frequently located near densely-populated areas where large numbers of tires are generated. The millions of metric tonnes of waste tires are a potential feedstock for the production of new materials. However, data from the U.S. EPA indicates that only ~20% of waste tires are utilized in a given year, and the rest are disposed of in tire stockpiles or landfills; two to three billion tires were stored thusly as of 1993[1].

Pyrolysis has been proposed as a method for decomposing some of the tire rubber to salable oil, gas, and char (principally carbon black). The yield of char from tire pyrolysis is about 30 wt%, which could be upgraded into a value-added tire-derived carbon adsorbent (TDCA). Producing TDCA from waste tires may potentially provide an economic incentive for commercializing tire pyrolysis as a recycling process.

The work presented in this paper summarizes the results from an ongoing collaborative research program between the Illinois State Geological Survey and the University of Illinois at Urban-Champaign to prepare and evaluate the applications of TDCA for gas purification and clean up. TDCA samples were prepared in both laboratory- and pilot-scale reactors. The properties of TDCAs were compared to those derived from a high-sulfur bituminous Illinois coal and pistachio nut shells. These adsorbents were evaluated for removal of vapor-phase mercury species (Hg^0 and $HgCl_2$) from simulated coal combustion flue gases and for capture of gaseous organic solvents, including acetone and methyl-ethyl-ketone (MEK). These compounds are of concern due to their large source strength to the atmosphere (Table 1).

Adsorption processes are widely utilized in air pollution control operations for removing hazardous gases from industrial flue gas streams. A porous solid with large surface area and micropore volume is key for efficient removal of pollutants in any adsorption process. Adsorbents produced from different precursor materials will have differing properties due to inherent variations in the chemical and physical nature of precursor materials.

METHODOLOGY

Carbon adsorbents were prepared by heating the tire, coal, or pistachio shell in a fixed-bed reactor to 850°C under a nitrogen purge. The char was then activated in steam at 850°C. Activation rates of the precursor chars were obtained with a thermogravimetric analyzer (CAHN TG-131) in either a 100% CO_2 or (50% CO_2)/(50% steam) mixture at 850°C. The precursors were analyzed for their moisture, ash, carbon, hydrogen, nitrogen, and total sulfur contents using standard ASTM methodology (Table 2).

The surface structure and morphology of prepared adsorbents were evaluated via nitrogen adsorption (at 77 K) and scanning electron microscopy. Nitrogen adsorption isotherms were determined via an adsorption apparatus (Micromeritics ASAP 2400). Surface areas were determined via the standard BET equation. Total pore volumes were determined at $P/P_0 \approx 0.98$ and micropore volumes were evaluated using the 3-D pore size distribution model developed at ISGS/UIUC.[3] Scanning electron micrographs (SEM) were collected from prepared samples (Amary 1830).

Elemental mercury (Hg^0) and mercuric chloride ($HgCl_2$) equilibrium adsorption capacities for prepared samples were completed by Radian International LLC (Austin, TX). Tests were carried out in a simulated flue gas containing 1600 ppm, SO_2, 50 ppm, HCl, 12% CO_2, 7% H_2O, 6% O_2 and 40-60 $\mu g/N\text{-}m^3$ Hg^0 or $HgCl_2$. Adsorption capacities were measured using cold-vapor atomic adsorption. Equilibrium acetone and MEK capacities were determined in a gravimetric analyzer (CAHN 2000) using standardized gas cylinders diluted with nitrogen.

RESULTS AND DISCUSSION

Proximate analyses of the adsorbent precursor materials indicate that the principle differences are in the ash, sulfur, and carbon contents (Table 2). The ash content of pistachio shells is negligible in comparison with coal and tire-based materials. Ash contents are of interest since concentrations of trace species, especially metals, likely influence gasification rates and adsorption properties of materials. Total sulfur contents of precursor adsorbents also differed, again with pistachio having a negligible sulfur content in comparison to the coal and tire precursors. Sulfur contents are of interest, since they likely influence the adsorption of mercury species.

The steam gasification rate (on the total mass basis) of tire char was larger than the coal char (Figure 1). Its CO_2 gasification rate was, however, much smaller than the pistachio char. Properties of select carbon adsorbents prepared in the fixed-bed reactor are presented in Table 3. The data are shown for test conditions that resulted in about 15% yield in adsorbent prepared from tire and pistachio shell, and about 30% yield from the coal. The surface area of the TDCA (389 m^2/g) was about one-half of the coal and pistachio carbons. The TDCA , however, had 32% larger total pore volume (0.670 vs 0.505 cc/g) than the coal and pistachio carbons. Pistachio and coal carbons were more microporous than TDCA; more than 50% of the pores in the coal and pistachio carbons were in the micropore range as compared to 34% for the TDCA. TDCAs with surface areas as large as 1000 m^2/g, and micropore volumes as large as 0.5 cc/g have been prepared (Figure 2). The reactivity and pore structure data suggest that there should not be any difficulties in developing porosity in tire-derived char using steam.

Scanning electron micrographs of the pistachio-derived carbon revealed that it had a more heterogenous and "rougher" surface than coal-derived carbon (Figures 3 and 5). The surface texture of the TDCA was intermediate between the coal and the pistachio-derived carbons (Figure 4) with various rod-like and clusters of matters present on its surface. EDS revealed that the rod-like matters were typically composed of zinc and sulfur species, and that the jagged "globs" were generally composed of calcium and Si. It appears that ZnO (an additive added to tire) is converted to ZnS during the activation of tire char with steam.

Air pollution applications of adsorbents. Coal -derived carbon had the largest capacity (2718 $\mu g/g$) for adsorption of Hg^0 from the simulated coal combustion flue gas followed by tire- (872 $\mu g/g$) and pistachio-derived (500 $\mu g/g$) carbons (Figure 6). The TDCA and pistachio carbon, however, had about five times larger capacity for adsorption of $HgCl_2$ than their coal-derived counterpart. The presence of larger micropore volume and larger concentration of organic sulfur in the coal-derived carbon was potentially responsible for the large Hg adsorption capacity of this sample.[4] Since tire rubber contains organically bound sulfur from the vulcanization process, it could potentially be a suitable precursor for preparing effective Hg adsorbent. Indeed, the results from extensive mercury testing with several TDCAs, using five different compositions of simulated coal combustion flue gas, revealed that TDCA is an effective sorbent for removal of both Hg and $HgCl_2$.[5]

Plots of capacity of TDCA for adsorption of acetone and MEK as a function of the adsorbate concentration (ppm_v) at select temperatures are shown in Figure 7. As expected, the adsorption capacity increased with increasing adsorbate concentration, and decreased with increasing temperature. In the case of acetone, the adsorption capacity ranged from 15 to 41 mg/g to 59 to 125 mg/g as temperature varied from 20°C to 50°C. For MEK, the adsorption capacity ranged from 43

to 101 mg/g to 93 to 197 mg/g as temperature varied from 20°C to 50°C. The adsorption of MEK was larger than the adsorption of acetone at the same conditions of temperature and adsorbate concentration. Equilibrium adsorption capacities for acetone were also determined for a commercial carbon (Calgon BPL, surface area = 965 m^2/g) in a previous study.[6] The equilibrium acetone capacities for TDCA was about 70% of the capacity observed for BPL, 225 mg/g at 10000 ppm_v.

CONCLUSIONS

The work presented here showed that carbon adsorbents with adequate surface area and pore volume could be prepared from waste tire rubber. Furthermore, adsorption studies indicated that TDCAs were suitable sorbents for removal of trace amounts of vapor-phase mercury from coal combustion flue gases, and for purification of gas streams containing hazardous organic compounds. Further work is required to identify the potential application of TDCA for other pollution control operations. In addition, research in identifying the roles of various metals in the waste tire during thermal processing, pore structure development, and any catalytic properties during adsorption/desorption processes should be investigated. Finally, the commercial success for producing TDCA depends on the market size and the selling price for both the tire-derived oil and the TDCA.

ACKNOWLEDGMENTS

Support from the Office of Solid Waste Research at the University of Illinois at Urbana-Champaign made this research possible.

REFERENCES

1. Clark, C.; Meardon, K.; Russell, D., *Scrap Tire Technology and Markets*; Pollution Technology Review No. 2ll; U.S. Environmental Protection Agency: Park Ridge, NJ, 1993.
2. U.S. Environmental Protection Agency; *Toxic Release Inventory*; TRI Explorer; http://www.epa.gov/triexplorer/reports.htm.
3. Sun, J.; Chen, S.; Rood, M.J.; Rostam-Abadi, M.; *Energy & Fuels*; **1998**; *12*, 1071.
4. Hsi, H.C.; Chen, S.; Rostam-Abadi, M.; et al.; *Energy & Fuels*; **1998**; *12*, 1061.
5. ***Development and Evaluation of Low Cost Mercury Sorbents***, EPRI, Palo Alto, CA: TE-114043.
6. Lehmann, C.M.B.; Rostam-Abadi, M.; Rood, M.J.; Sun, J.; *Energy & Fuels*; **1998**; *12*, 1095.

Table 1. Total air emissions (million kg per year), 1988-1998.

	1988	1989	1990	1991	1992	1993	1994	1995	1996	1997	1998
MEK	64.3	63.9	61.2	49.6	42.5	39.4	36.4	31.9	27.4	24.2	21.1
acetone	96.5	96.2	88.5	74.3	63.4	59.0	---	---	---	---	---
mercury	0.010	0.011	0.010	0.008	0.006	0.005	0.005	0.006	0.006	0.006	0.006

Source: U.S. EPA (http://www.epa.gov/triexplorer/trends.htm)
Note: Acetone removed from TRI in 1994

Table 2. Properties of raw sorbent materials.

	coal	raw tire	tire char	pistachio shell
moisture	9.3	0.5	0.3	4.4
ash[a]	11.5	3.0	15.4	0.2
carbon[a]	68.1	87.2	78.8	48.0
hydrogen[a]	4.8	7.6	0.8	6.1
nitrogen[a]	1.2	0.2	0.2	0.1
oxygen[a,b]	10.5	0.9	2.0	45.5
total sulfur[a]	3.7	1.6	2.9	0.2

[a] moisture-free values
[b] oxygen content determined by difference

Table 3. Properties of prepared adsorbents.

	coal	tire	pistachio shell
ash [wt. %]	27.0	---	---
sulfur content	1.6	---	---
yield [%]	30.0	14.7	14.8
surface area [m^2/g]	787	389	775
total pore volume [cc/g]	0.504	0.670	0.505
micropore volume [cc/g]	0.265	0.230	0.312

— = not measured

Figure 1. Gasification rate of select precursor materials in CO_2 or steam/CO_2 mixture at 850°C.

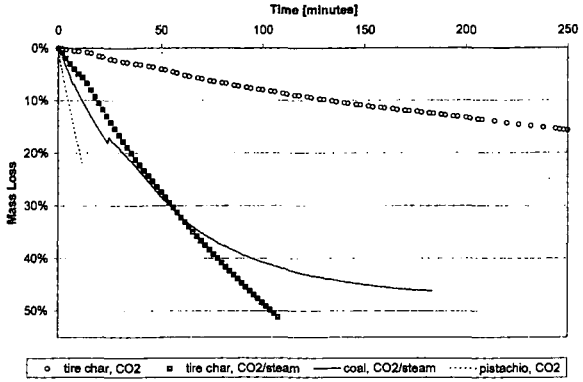

Figure 2. (A) BET-N_2 surface area and (B) micropore volume vs. yield for TDCA.

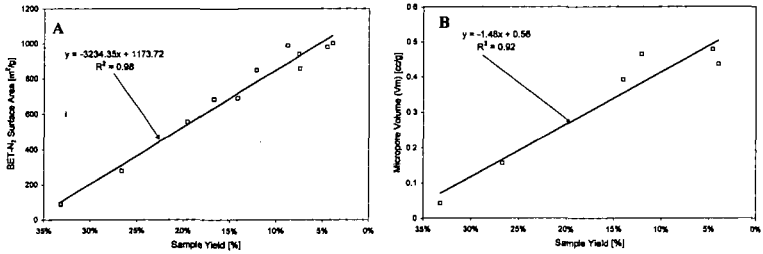

Figure 3. SEM of Illinois coal-derived adsorbent (4780x magnification).

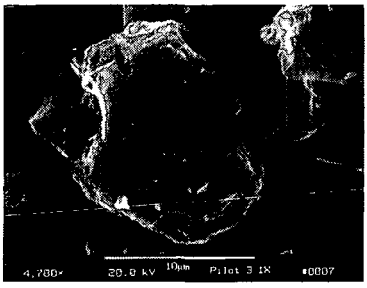

Figure 4. SEM of tire-derived adsorbent (3800x magnification).

Figure 5. SEM of pistachio shell-derived adsorbent (3800x magnification).

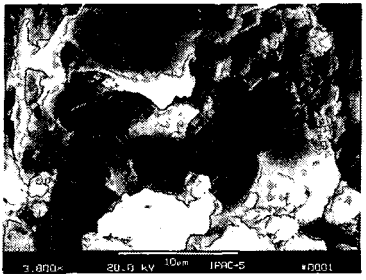

Figure 6. Hg^0 and $HgCl_2$ equilibrium capacities of adsorbents at 135°C.

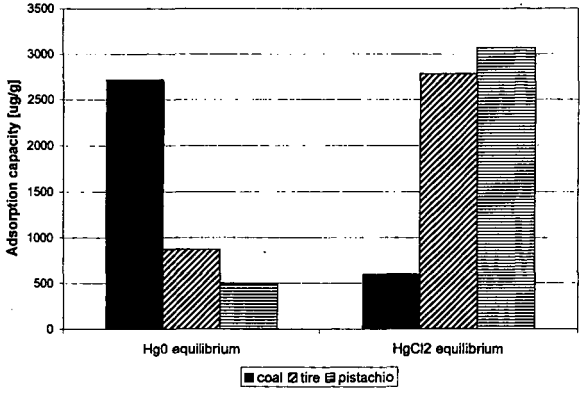

Figure 7. (A) Acetone and (B) MEK capacities of TDCA at 20-50°C.

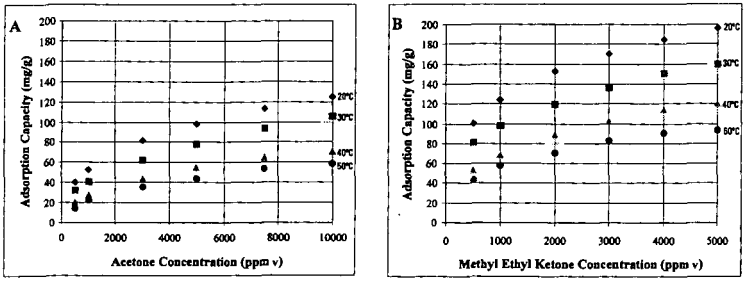

TERTIARY RESOURCE RECOVERY FROM WASTE POLYMERS VIA PYROLYSIS: POLYPROPYLENE

Hsi-Wu Wong, Todd M. Kruse, Oh Sang Woo and Linda J. Broadbelt
Department of Chemical Engineering
2145 Sheridan Road, Northwestern University
Evanston, IL 60208

ABSTRACT

Polypropylene is a significant component of mixed plastic waste from which fuels and chemicals can be recovered via thermal or catalytic degradation. Pyrolysis of polypropylene was investigated at a temperature of 420°C and reaction times ranging from 10 to 180 minutes. Total conversion reached approximately 60% at 90 minutes, and no significant change was observed for longer reaction times. The selectivity to monomer, propylene, achieved a plateau at approximately 10% after a reaction time of 90 minutes. The overall product distribution can be explained by the typical free radical mechanism with the dominant products as alkenes in the form of C_{3n}, alkanes in the form of C_{3n-1}, and dienes in the form of C_{3n-2}.

I. INTRODUCTION

In recent years, post-consumer wastes have caused increased concern because of the escalation of municipal solid wastes (MSW) generated. In 1995, 208 tons of MSW were generated, and it increased to 340 tons in 1998, with more than 60% of MSW landfilled. The decreasing availability of landfill space and the inefficient use of post-consumer products through landfilling, have heightened the attention paid to recycling of MSW over the past decade.

Plastics make up a significant portion of post-consumer products. In the United States alone, over 70 billion pounds of plastics are manufactured annually, while only 10% of this amount is recycled or incinerated. In 1995, 9.1 weight percent of MSW was composed of plastics, with a total of 30% by volume. Among the plastic waste, 15.3 weight percent contained polypropylene.

Currently, the recycling of plastics can be divided into four categories – primary, secondary, tertiary, and quaternary. Primary recycling simply reuses the plastics as products that have similar properties to the discarded materials. Secondary recycling, also known as material or mechanical recycling, is achieved by melting, grinding, and reforming plastic waste mixtures into lower value products. Tertiary recycling converts discarded plastic products into high-value petrochemical or fuel feedstocks. Quaternary recycling uses combustion or incineration to recover energy from plastic products. Since primary and secondary recycling have limitations on the properties and uses of the final products, and quaternary recycling is an insufficient use of resources and has a negative public image because of release of CO_2 and airborne particles, tertiary recycling promises the best long-term solution. However, tertiary recycling is not economical at present. One of the biggest costs is the sorting of the original polymers. Therefore, processing of multicomponent polymeric wastes may provide a potential solution. To establish a baseline to which pyrolysis of mixed plastic wastes containing polypropylene can be compared, the thermal degradation of neat polypropylene was examined.

II. EXPERIMENTAL

Batch pyrolysis experiments were carried out by loading 20 mg of polypropylene (PP) into a 3.1-ml glass ampoule (Wheaton). The polypropylene was obtained from Aldrich Chemical (M_w=127,000, M_n=54,000) in powder form. After purging with argon for 2 minutes, each ampoule was sealed using an oxygen/propane flame, and then the sample was reacted in an isothermal fluidized sand bath at 420°C. Reaction times ranged from 10-180 minutes. Upon completion of the reaction, the ampoule was removed from the sand bath and quenched in another sand bath set at ambient temperature. Three replicates were performed for each reaction time.

Gaseous products were analyzed by putting the ampoule inside a 53-ml flask with a Tygon tube on one end and an injection port on the other. Both ends were then sealed with septa. The flask was purged with helium for 10 minutes and, after the ampoule was broken, allowed to equilibrate for 30 minutes. Two ml gas samples for the 10 minute reaction runs and 1 ml samples for the other runs were then taken using a gas-tight syringe. Gaseous products were then identified and quantified against known standards using a Hewlett Packard 5890 Series II Plus Gas Chromatograph equipped with a thermal conductivity detector (TCD) and a 6 ft stainless steel Porapak Q column (Supelco).

Liquid and solid products were extracted with 1.5 ml HPLC grade methylene chloride overnight. The product solution was first passed through a 0.45-μm polypropylene filter (Alltech) attached to a syringe and then passed through a Waters Gel Permeation Chromatograph (GPC). Products with molecular weights less than ~400 g/mol were collected with the fraction collector attached to the GPC outlet. An external standard (biphenyl) was added after fraction collection. Product identification and quantification were achieved using a Hewlett Packard 6890 Series Gas Chromatograph-Mass Spectrometer and a Hewlett Packard 6890 Series Gas Chromatograph with a flame ionization detector (FID), each equipped with a Hewlett Packard 30 m crosslinked 5% Ph Me Silicone capillary column.

The percent conversion of PP, X, was defined according to the equation:

$$X = \frac{W_g + W_l}{W_o} \times 100\%$$

where W_g is the weight of gaseous products, W_l is the weight of liquid products with carbon number less than or equal to 25, and W_o is the initial weight loading of PP. Selectivity, S, of a certain species A was based on the following equation:

$$S = \frac{W_A}{W_g + W_l} \times 100\%$$

where W_A is the weight of species A. Product yields were normalized by dividing the millimoles of each product by the initial molar loading of propylene repeat units. Finally, error bars shown in the figures represent the standard deviations of experiments that have been triplicated.

III. RESULTS

The overall conversion of neat pyrolysis of polypropylene increased with respect to reaction time, as illustrated in Figure 1. After 90 minutes of reaction, the conversion reached approximately 60%, and no significant change was observed at longer reaction times. This suggests that little additional conversion can be achieved even for very long reaction times at this temperature in a closed batch reactor of 3.1 ml. The selectivity of polypropylene monomer, propylene, showed similar behavior, achieving a selectivity of approximately 10% after 90 minutes of reaction as shown in Figure 2.

If the products were divided into three fractions, C_1-C_4, C_5-C_{10}, and C_{11}-C_{25}, respectively, the yields of these fractions behaved differently. As shown in Figure 3, the yield of the C_1-C_4 fraction increased with reaction time, whereas the C_5-C_{10} fraction reached a maximum around 120 minutes and no significant change was observed at 180 minutes. Finally, the C_{11}-C_{25} fraction reached a maximum around 60 minutes. These results suggest that as reaction time increased, the heavier products decompose to lighter ones.

The reaction products of polypropylene pyrolysis consisted of four major categories - alkanes, alkenes, dienes, and aromatic compounds. Lower molecular weight species were found in higher yields whereas there were notable decreases in the yields with carbon numbers greater than ten. For alkanes, the most dominant product was ethane (C_2). In addition, pentane (C_5), 4-methylheptane (C_8), C_{11}, C_{14}, and C_{17} were found in the highest yield; the alkanes were thus dominated by products with carbon numbers C_{3n-1}, with n=1, 2, 3, 4,..., as shown in Figure 4. The yields of the majority of the alkanes increased with respect to reaction time. For alkenes, propylene was the most dominant product with propylene oligomers (C_6, C_9, C_{12}, C_{15}, C_{21}, and C_{24}), i.e., C_{3n}, n=1, 2, 3, 4,..., as the other major olefinic products. As shown in Figure 5, yields of alkenes with carbon numbers greater than five all reached maximum values then decreased when reaction time increased. However, yields of lighter alkenes (with carbon numbers less than five) increased monotonically with reaction time. Dienes, which were found beginning with C_7 and were present in relatively low yields, appeared as C_7, C_{10}, C_{13}, C_{16}, C_{19}, C_{22}, and C_{25}, i.e., C_{3n-2}, n=3, 4, 5, 6,...(not shown). They also appeared to reach maximum values then decrease except for C_7. Finally, aromatic compounds were also found as minor products. Their yields were comparable in magnitude to the diene yields. The yields of aromatic compounds generally increased with respect to reaction time (not shown).

As noted above, the product distribution showed that most alkenes appeared in the form of C_{3n}, whereas alkanes and dienes appeared in the form of C_{3n-1} and C_{3n-2}, respectively. This product distribution is in agreement with observations reported in the literature [1-2] and can be explained by the mechanism illustrated in Figure 6, which was based on the one proposed by Tsuchiya et al. [3]. The initiation step of the free radical mechanism is simply to break any of the PP long chains into two shorter end-chain radicals. The end-chain radicals (or mid-chain radicals formed subsequently) may abstract hydrogen from a PP long-chain to form a tertiary radical, as shown in Figure 6(a). Upon undergoing β-scission, the tertiary polymer radical is broken into two parts, one with a double bond on the end (denoted as I), and the other with a secondary free radical (denoted as II). When the polymer chain I is attacked by another free radical and β-scission occurs, dienes (in the form of C_{3n-2}) and alkenes (in the form of C_{3n}) can be formed, as shown in Figure 6(b). On the other hand, polymer chain II can undergo three kinds of reactions such that alkanes (in the form of C_{3n-1}) and alkenes (in the form of C_{3n}) can be formed. Figure 6(c) shows three possible reaction pathways of polymer chain II. Although other steps not explicitly drawn are possible, the formation of C_{3n} alkenes, C_{3n-1} alkanes and C_{3n-2} dienes as the dominant products suggests that the mechanism in Figure 6 captures the major reaction pathways.

ACKNOWLEDGMENT

The authors are grateful for financial support from the Department of Energy (DE-FG22-96-PC96204), the CAREER Program of the National Science Foundation (CTS-9623741), and the MRSEC program of the National Science Foundation (DMR-9632472) at the Materials Research Center of Northwestern University.

REFERENCES

[1] Uemichi, Y., Kashiwaya, M., Tsukidate, M., Ayame, A., and Kanoh, H., *Bull. Chem. Soc. Jpn.*, 1983, **56**, 2768-2773.

[2] Audisio, G., Silvani, A., Beltrame, P. L., and Carniti, P., *Journal of Analytical and Applied Pyrolysis*, 1984, **7**, 83-90.

[3] Tsuchiya, Y., Sumi, K., *Journal of Polymer Science: Part A-1*, 1969, **7**, 1599-1607.

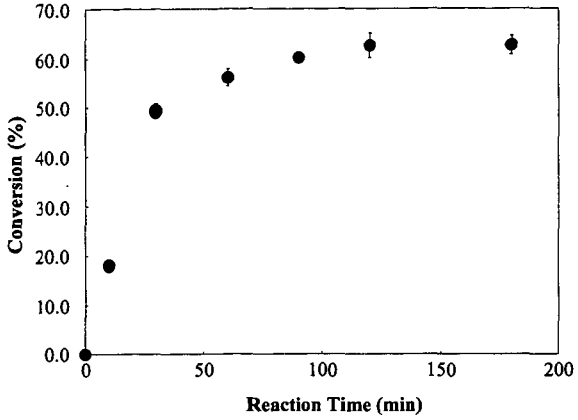

Figure 1 : Conversion of polypropylene as a function of reaction time.

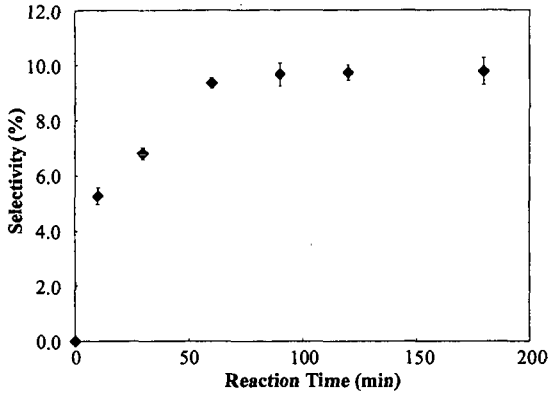

Figure 2 : Selectivity of propylene as a function of reaction time.

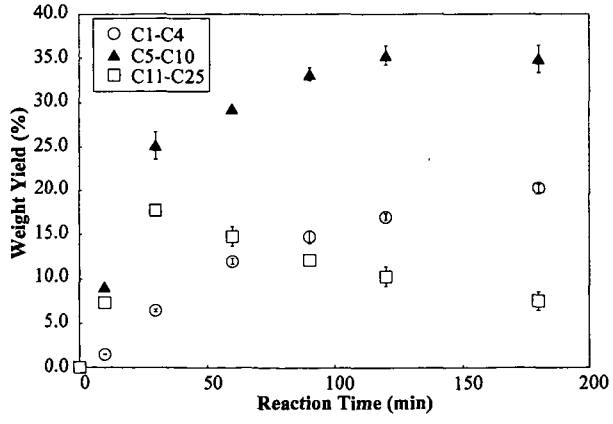

Figure 3 : Weight yields of different product fractions as a function of reaction time.

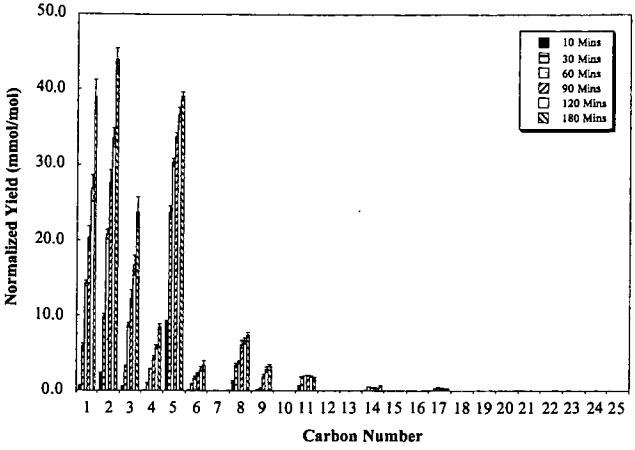

Figure 4 : Comparison of normalized yields of alkanes as a function of reaction time and carbon number.

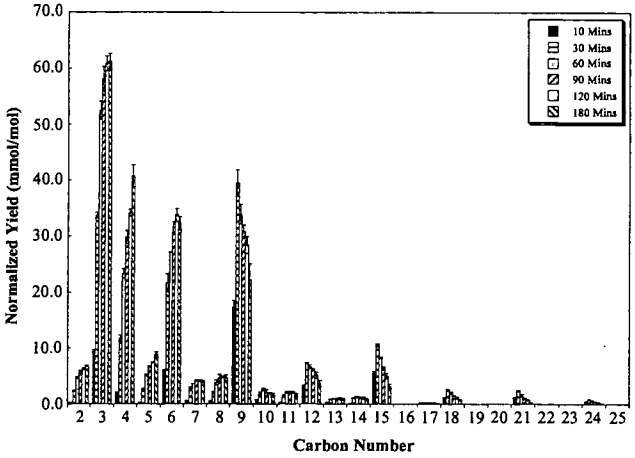

Figure 5 : Comparison of normalized yields of alkenes as a function of reaction time and carbon number.

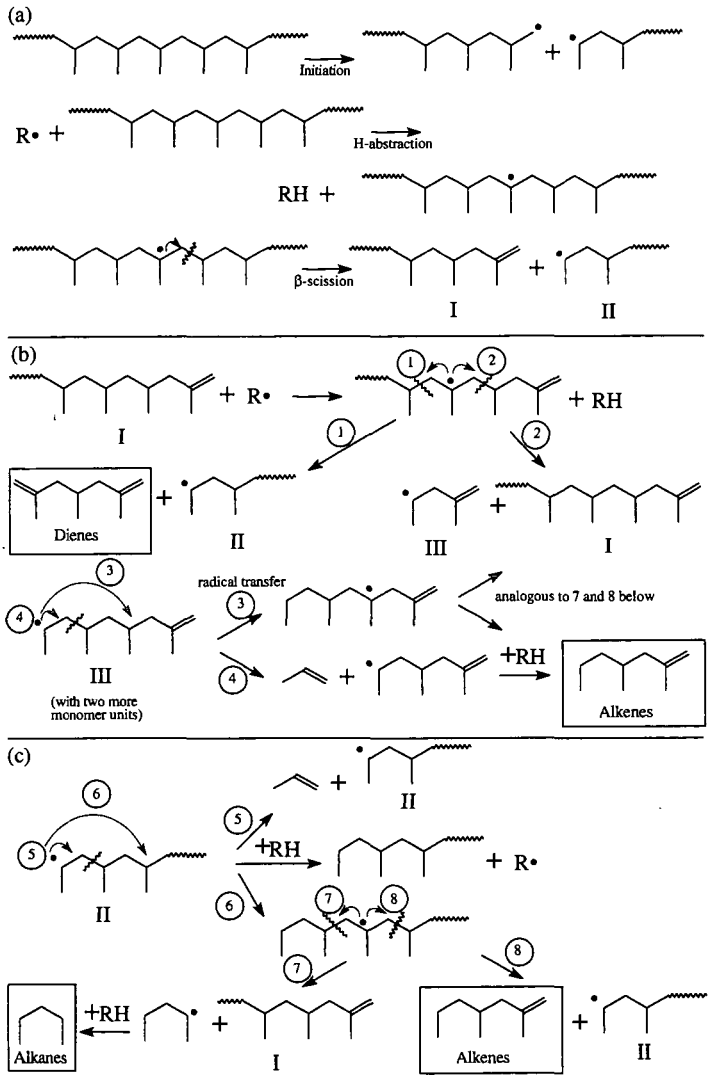

Figure 6: (a) Formation of two kinds of polymer chains (I and II) through bond fission, hydrogen abstraction and β-scission and proposed reaction mechanisms of polymer chains (b) I and (c) II.

Combustion of Coal Washery Rejects in a Circulating Fluidized Bed

By Lufei Jia, E.J. Anthony and R.E. Talbot
CANMET Energy Technology Centre, Natural Resources Canada
1 Haanel Dr., Nepean, Ont

KEYWORDS: Fluidized bed combustion, washery rejects, coal

INTRODUCTION

The CANMET Energy Technology Centre, sponsored by Luscar Ltd and the Alberta Government, carried out a series of combustion trials on a number of washery rejects, to determine whether they could be burned in an environmentally acceptable manner using both conventional and advanced combustion technologies - namely fluidized bed combustion (FBC). The facilities used were a pilot-scale research boiler (PSRB) and CANMET's 0.8 MWth circulating fluidized bed boiler (CFBC). The program was sponsored by the Alberta Government (Western Diversification) and Luscar Ltd. This paper presents details of the CFBC pilot plant trials only.

EXPERIMENTAL

Test Materials

The three fuels burned in the reactor were: raw coal (Obed No.4), Obed Jig Rejects (Obed No.7) and Obed Jig Middlings (Obed No. 10). These fuels required a sorbent, Cadomin limestone (Genstar Cement Ltd), to achieve the allowable SO_2 emissions levels recommended under the National Guidelines for Stationary Sources. This particular limestone had been previously tested by CANMET using a TGA and was shown to be only a moderately reactive sorbent. As some difficulties were experienced in achieving adequate sulphur capture under the test conditions employed, a trial was also carried out using Havelock limestone (a relatively reactive eastern Canadian limestone).

Test Methods

The pilot-scale CFBC unit used has been described extensively elsewhere [1]. The major features of this versatile facility include a refractory lined combustor 405 mm in diameter and 7 m high, a refractory lined hot cyclone and an inclined L-valve loop seal system for recirculation of solids (Fig. 1). Four retractable bayonet type vertical cooling tubes permit the control of the combustor temperature during operation at various test conditions. It is complemented by a comprehensive instrumentation and control system, which is described elsewhere [1]. The combustor is designed to operate at temperatures up to 1100 °C and at a superficial gas velocity of up to 8 m/s.

CFBCs typically operate at combustion temperatures between 800 °C and 950 °C. Lower temperatures normally reduce combustion efficiency to unacceptable levels, decrease sulphur capture and increase products of incomplete combustion. Higher temperatures by contrast, run the risk of producing bed agglomeration, increasing NO_x emissions to unacceptable levels, and also reducing sulphur capture.

Initial operation of the facility has demonstrated a satisfactory performance of the combustor and ancillary equipment. In addition, the unit has been successfully used with high sulphur petroleum coke and pitch. The unit has also been used to generate ash from the CFBC combustion of high sulphur coals in order to study various ash management applications.

The research facility generates a database useful for the design and process optimization of full-scale units, study of emissions of pollutants, and prediction of the combustion performance of feedstocks.

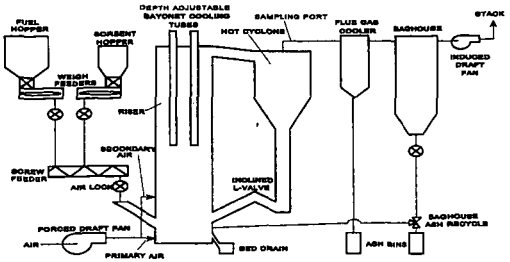

Figure 1. Schematic of CANMET's 0.8 MW(th) CFBC pilot plant

RESULTS

Table 1. Combustion results

Test and Date	Bed Temperature (°C)	Ca/S	NO_x (ng/J)	SO_2 (ng/J)	Sulphur Capture Efficiency (%)	Combustion Efficiency (%)
Obed No. 4 Oct. 29-30/ 92	850	0	155.3 ± 8.7	370.3 ± 31.9	26	99.0
	850	2.2	151.8 ± 7.7	354.1 ± 53.7	28	-
Obed No. 7 Nov. 3-4/92	850	0	149.5 ± 10.1	562.5 ± 34.9	14	98.2
	850	4.9	144.9 ± 11.7	377.9 ± 74.3	32	98.9
	800	4.9	100.9 ± 5.5	224.1 ± 31.5	49	97.7
Obed No. 10 Nov. 5-6/92(*)	850	0	117.8 ± 8.6	422.0 ± 69.0	14	99.0
	850	2.8	107.2 ± 5.1	313.5 ± 25.2	30	98.8
	800	2.8	72.7 ± 8.0	185.7 ± 9.2	63	98.0
	900	2.8	135.1 ± 4.1	395.2 ± 24.4	38	99.1
Obed No. 4 Nov. 10/92	800	0	103.6 ± 10.4	316.8 ± 65.6	26	98.5
	800	2.7	97.6 ± 10.4	264.3 ± 62.4	31	98.3
Obed No. 7 Nov. 12/92	800	0	113.2 ± 14.7	218.4 ± 79.2	-	-
	900	5.5	187.9 ± 4.9	403.7 ± 50.4	44	99.0

(*) Trial with Havelock limestone

Table 1 (above) presents results from the CFBC combustion trials.

DISCUSSION

Sulphur Capture Results

As indicated in Table 1, the natural Ca/S molar ratio of all of the fuels tested is relatively high. These high levels of alkali metals versus fuel sulphur content could potentially result in a significant inherent capture if the calcium was present in a suitable form. Sulphur removal without limestone addition observed by CANMET for FBC combustion of Canadian fuels appears to average about 28% [2], and captures of over 90% have been observed for one Western Canadian subbituminous coal using both circulating and bubbling FBC technology [3,4]. Similar data have been reported elsewhere, e.g., inherent captures of up to 75% have been reported for British coals [5].

However, one important difference between capture due to ash components and limestone in FBC systems was that the optimum capture temperature for ash appears to be about 750 °C. This is a full hundred degrees below the optimum temperature for most limestones [5].

Combustion Efficiency

The combustion efficiency data follow the expected trend increasing with increasing bed temperature. No other experimental parameter over the range used in this test series seems to have a significant effect on the combustion efficiency. The variation in combustion efficiency from 97.7 to 99.1% is very small, with typical combustion efficiency being about 99% for bed temperature of 850 °C.

Nitrogen Oxides Emissions

NO_x emissions vary from 73 to 188 ng/J, which are well below levels typically seen from conventional combustion. Surprisingly there appears to be no effect associated with the addition of limestone, which might have been expected to increase NO_x emissions. Limestone is well known to be able to increase NO_x emissions in CFBC's due to its ability to catalyze NH_3 oxidation (from fuel volatiles) [6]. Perhaps the explanation is that limestone is simply not present in sufficiently high absolute quantities to have a significant impact, despite the high Ca/S molar ratios used in this study. However, the data clearly show that NO_x appears to increase with bed temperature which is as expected.

Sulphur Dioxide Emissions

For the most part, the National Guideline for Stationary Sources (258 ng/J) is exceeded (Table 1). However, the use of Cadomin limestone with Ca/S molar ratio of greater than 5 does allow this guideline to be met at 800 °C and SO_2 emissions should not be a problem for sufficiently high Ca/S molar ratios.

CONCLUSIONS

Three fuels, Obed No. 4, Obed No. 7 and Obed No. 10, have been burned in a CFBC combustor. All of these fuels are highly reactive and at typical CFBC operating conditions (850 °C and 3% O_2), it appears that combustion efficiency (based on unburned carbon loss) is 99.0% which is typical of such very reactive fuels. Inherent sulphur capture was shown to be small and to decrease with bed temperature, and appeared to be directly related to the degree of pyritic sulphur in the fuel which suggests that the "apparent capture" is due to carryover of unreacted pyritic sulphur. Cadomin limestone is only likely to be effective in achieving emission guidelines when it is used at Ca/S molar ratios of greater than 5. NO_x emissions are all below the current guidelines. Other emissions such as CO and N_2O appear to be low and are unlikely to pose problems. CO and N_2O emissions decrease with increasing bed temperatures as expected and interestingly, limestone appears to have a small positive effect in reducing CO levels. CFBC appears to be an entirely satisfactory technology for burning these fuels and based on these results would have no problem in achieving

good combustion performance and low emissions.

REFERENCES

1. Desai, D.L. "The 0.8 MWth circulating fluidized bed combustion research facility at the Combustion and Carbonization Research Laboratory, CANMET: Its design and initial operating experience", Proceedings of the 1991 CANMET CFBC Management Seminar, eds. E.J. Anthony and F. Preto, Halifax, Nova Scotia, July 2-3, 1991.

2. Zhang, J.Q. and Jones, W.E. "Evaluation of SO_2 and NO_x emissions in fluidized bed combustion ", Final Report to Energy, Mines and Resources under contract 007SQ-234400-8-9213, August 1990.

3. Grace, J.R., Brereton, C.M.H., Lim, C.J., Legros, R., Zhao, J., Senior, R.C., Wu, R.L., Muir, J.M. and Engman, R. "Circulating fluidized bed combustion of Western Canadian fuels", Final Report to Energy, Mines and Resources Canada under contract 52.SS23440-7-9136, August 1989.

4. Becker, H.A., Code, R.K. and Stephenson, J.R. "Pilot scale trials on atmospheric fluidized bed combustion of a Western Canadian Sub-bituminous coal (Highvale)", Final Report to Energy, Mines and Resources Canada QFBC.TR.87.3, March 1987.

5. Raymant, A.P. "Sulphur capture by coal and freeboard processes during fluidized bed combustion", Proceedings of the Tenth International Conference on FBC, ed. A. Manaker, pp. 597-602, San Francisco, CA, April 30-May 3, 1989

6. Lyngfelt, A. and Leckner, B. "The effect of reductive decomposition of $CaSO_4$ on sulphur capture in fluidized bed boilers", Proceedings 10th International Conference on FBC, p. 675-684, San Francisco, CA, 1989.

Combustion of Pig Lard in an Industrial Boiler

Mark Badger and Bruce G. Miller
The Energy Institute
C211 Coal Utilization Laboratory
The Pennsylvania State University
University Park, Pennsylvania. 16802-2323

Keywords: Combustion, boiler fuel, pig lard, low emissions.

INTRODUCTION

The changing or loss of markets for lard and grease is a major concern for the hog processing industry. The U.S. capacity for the daily processing of hogs in July 1999 was 389,820 hogs per day [1]. After rendering, each hog will produce an average of 2.60 gallons of choice white grease (CWG) and 1.43 gallons of lard [2]. This equates to nearly 600 million gallons of combined products a year. Of the total animal product entering the slaughterhouses and meat processing and packing plants, some 60% leaves as appropriate for human use; the remaining 40% goes to the rendering plant, and 80% of the rendered material returns to animal feedstuffs [3]. Should legislative action prohibiting feeding animal by-products to animals consumed by humans occur, lard and CWG will then have to compete with the other non-food markets. It should be noted that not all of the lard and grease is currently used in the animal feed industry; hog by-products are sources of chemicals that are used in the manufacture of a wide range of products, e.g., cosmetics, insecticides, weed killers, lubricants, etc. [1].

In the study Penn State worked closely with Hatfield Quality Meats and Lehigh University. Although Hatfield currently has markets for the lard and CWG, they wanted to explore options should they lose their current markets through the changing demographics of lard consumers, or legislative action banning the use of animal by-products in animal feed for animals that are consumed by humans. Should these occur, then Hatfield will have a potentially massive and difficult disposal problem.

One option is to use the lard and the CWG as boiler fuels. Hatfield has three No. 6 fuel oil boilers in their main processing plant. The watertube boilers are of D-type design with one rated at 800 Hp and two rated at 650 Hp. Cleaver Brooks manufactured the 800 Hp boiler while the 650 Hp boilers were manufactured by Keeler Dorr-Oliver. Typically, when the 800 Hp boiler and one 650 Hp boiler are in operation they consume about 35,000 gallons of No. 6 fuel oil per week. Therefore, should lard and/or CWG prove to be an adequate fuel for firing industrial boilers, Hatfield would produce enough products in-house to meet their weekly fuel quota.

The objective of this study was to perform the analysis of CWG, semi-finished lard, finished lard and No. 6 fuel oil, and to compare the firing and handling characteristics of semi-finished lard, finished lard and No. 6 fuel oil in Penn State's research boiler. Should lard and CWG be candidates for boiler fuels, then they could be utilized in Hatfield's boilers and marketed to other boiler operators, both industrial and utility. From the utility perspective, the lard and CWG could be used as the start-up fuel in coal-fired boilers as a direct replacement for No. 6 in oil-fired boilers [4].

EXPERIMENTAL

Fuel Characterization

Ultimate analysis was performed on all feedstocks using a LECO CHN-600 instrument for total carbon, hydrogen, and nitrogen contents, and a LECO SC-132 sulfur determinator was used for total sulfur determination. As-fired heating values (in Btu/lb) were determined using a Parr Adiabatic Calorimeter. Viscosity measurements were taken using a Brookfield DVIII viscometer with a #21 spindle, at 100, 120, 140 and 160°F for the No. 6 fuel oil, CWG, and lard samples. Spindle speed rate was varied to establish whether the samples exhibited Newtonian or non-Newtonian fluid characteristics. Simulated distillation gas chromatography (SimDis GC) was performed on all samples using a Hewlett Packard 5890 plus gas chromatograph fitted with an FID and a Restek MXT-500 Sim Dist column (6 meter x 0.53 mm ID x 0.15μm df).

Research Boiler and Ancillary Components

The design and operation of the research boiler used in this study has been described previously [2]. The typical operating procedure of the boiler involved preheating the system with natural gas until the refractory-lined quarl (divergent burner throat) reached a predetermined temperature. This took approximately four hours. The natural gas flow was then reduced, and the No. 6 fuel oil and lard flow increased until the required thermal input was obtained with satisfactory flame appearance. Tests were conducted for three, six, and three hours, firing No. 6 fuel oil, finished lard, and semi-finished lard, respectively. Approximately 100 gallons (2 drums) of the finished lard and 100 gallons of the semi-finished lard were used during the testing.

The lard was heated and mixed before being transported to the feed tank where it was heated continuously to maintain a temperature of ≈130°F. The following information was collected:

- Fuel firing rate;
- Fuel pressure;
- Combustion air flow and temperature;
- Atomizing air mass flow rate and pressure;
- Flame character, stability, and quality (quantitative;)
- Boiler and system operating temperatures and pressures;
- Steam flow rate and pressure; and
- Continuous stack gas composition (O_2, CO_2, CO, NO_x, and SO_2).

RESULTS AND DISCUSSION

Fuel Characterization

The data from the determination of the fuel characteristics are shown in Table 1. The lard samples contained less carbon and more oxygen than the No. 6 fuel oil. In addition, the lard samples contained essentially no sulfur. The heating value of the lard samples was ≈16,900 and 17,000 Btu/lb for the semi-finished and finished lard samples, respectively, compared to ≈18,500 Btu/lb for the No. 6 fuel oil sample.

The CWG sample contains slightly more sulfur than the lard samples (0.2% vs. ≤0.1%) but much less than the No. 6 fuel oil. The heating value of the CWG is similar to the lard samples.

Table 1. Fuel Analysis

	Semi-Finished Lard	Finished Lard	Choice White Grease	No. 6 Fuel Oil
Ultimate Analysis (%, as fired)[a]				
Carbon	77.7	77.4	77.9	85.8
Hydrogen	12.0	11.5	13.6	12.1
Nitrogen	0.4	0.6	0.2	0.6
Sulfur	0.0	0.1	0.2	1.5
Oxygen (by difference)	9.9	10.4	8.1	-
Heating Value (Btu/lb, as fired)	16,941	16,990	16,977	18,454
Viscosity (cSt)[b]				
100°F	70	97	91	1,357
120°F	23	25	26	520
140°F	17	17	17	232
160°F	-	-	13	128
Boiling Points (°C)[c]				
<260	0.7	0.8	0.5	8.9
280 to 450	5.1	1.9	20.9	29.3
450 to 540	1.8	1.1	11.6	12.5
540 to 700	91.6	95.3	65.6	38.3
>700	0.3	0.3	0.9	9.8

[a] Fuel oil analysis normalized to 0% oxygen because oxygen, by difference, was –0.6%

[b] Measured using a Brookfield DVIII viscometer, a #21 spindle.

[c] Measured using a Hewlett Packard 5890 plus gas chromatograph fitted with a FID and a Restek MXT-500 Sim Dist column.

Figure 1 is a plot of viscosity (in centistokes) as a function of temperature for the samples analyzed in this study. For comparison, the viscosities of Nos. 4 and 5 fuel oils at 100°F are also shown [5]. The CWG and lard samples became very fluid over a small temperature rise and exhibited signs of being shear-thinning fluids, i.e. when more force is applied (faster spindle speed), the lower the measured viscosity. Semi-finished lard exhibited the lowest viscosity values; however, the viscosities for the CWG and lard samples fell in a narrow range. The differences in measured viscosity were mainly due to the relative concentrations of the components, e.g. the finished lard had proportionately more of the higher boiling constituents than the semi-finished lard

(95.3% to 91.6% in the 540-700°C boiling range). This is due to the fact that higher boiling constituents are usually more viscous than the lower boiling constituents. The viscosities of the lard and CWG samples indicate that they should handle and atomize easier than No.6 fuel oil and are probably more like No. 5 fuel oil.

SimDis GC was performed on each of the samples to determine their boiling point distributions (see Figure 2). This was done to compare the boiling characteristics of the lard and CWG samples with No. 6 fuel oil. The SimDis GC of the semi-finished lard shows that 91.6 wt.% of the sample boils between 540-700°C, and that there is a smaller proportion (5.1 wt.%) boiling between 260-450°C. Further refining to produce the finished lard reduces the quantity of constituents that boil below 540°C by 50% from 7.6 to 3.8 wt.%. Consequently, the proportion of 540-700°C boiling constituents increases to 95.3 wt.%.

The CWG has two distinct regions with different boiling points (see Figure 2a). Two thirds of the sample boils between 540-700°C. The majority of the rest boils between 300-540°C, while the entire sample boils below 750°C.

Figure 2d shows that No. 6 fuel oil has constituents that cover a wide range of boiling points. Over 50 wt.% boils below 540°C, and almost 10 wt.% boils above 700°C (for the lard and CWG samples < 1 wt.% boiled in the +700°C range). In addition 1 wt.% of the No. 6 fuel oil did not elute from the column, and thus had a boiling value of +770°C.

It is the presence of the very high boiling material and their physical interactions with the lower boiling constituents, that causes the high viscosity in the No. 6 fuel oil.

Materials Handling and Combustion

No. 6 fuel oil

The No. 6 fuel oil was heated to 130°F in the feed tank before firing in the boiler. Although No. 6 fuel oil is typically preheated to 200°F [5], it was heated to 130°F in order to have a direct comparison with the lard tests.

The research boiler was fired on natural gas for a period of four hours before switching over to the No. 6 fuel oil. The transition from natural gas to No. 6 fuel oil occurred over approximately a 20-minute period until the desired air and fuel flow rates were obtained. The No. 6 fuel oil was burned for a period of three hours. During this period, the operating conditions were varied to establish the lowest O_2 level the boiler would operate at without adverse impact on CO emissions. This was found to be ≈ 2.0%; consequently, the lard tests were then conducted at similar O_2 levels. The combustion data listed for the No. 6 fuel oil in Table 2 are for a 0.65 hour period of steady-state testing with 2.0% O_2 in the flue gas. No problems related to the handling or combustion of the No. 6 fuel oil were encountered.

Finished and Semi-Finished Lard

Both the finished and semi-finished lard had similar handling characteristics. The samples were heated to above ≈105°F, in order to 'melt', and homogenize them into a consistent liquid mixture. The lard samples were then transported into the feed tank where the temperature was maintained at ≈130°F. Except for heating, no processing of the lard was needed before combustion.

When firing the lard samples (which were done on separate days) the boiler was fired on natural gas for 4-4.5 hours before switching over to the lard. The transition from natural gas to lard required approximately ten minutes until the desired air and fuel flow rates were obtained. The finished lard was burned for six hours and the semi-finished lard was burned for three hours. No problems related to the handling or combustion of the lard samples was encountered.

The lard flames can best be described as having a small initial blue 'natural gas-like' flame followed by an 'oil-like' bright, central jet, surrounded by a grayish flame. The distinct separations in the flame are likely a result of the combustion differences of the discrete constituents of the lard.

The lard flames were well anchored during the tests. There was no change in the flame character over the time each fuel was tested. The lard flames were significantly longer than either the natural gas or No. 6 fuel oil flames, and were self-sustaining.

The emissions remained fairly steady throughout the tests. Interestingly, the NO_x and SO_2 emissions from the lard tests were lower than when firing the No. 6 fuel oil. The nitrogen content of the lard samples is similar to that of the No. 6 fuel oil; hence, the lower NO_x emissions are likely due to the presence of water or other constituents in the fuel, which resulted in a different flame structure (i.e., longer flame), and possibly a lower flame temperature. No flame measurements were taken during the tests. There is no appreciable sulfur in the lard samples; therefore, no SO_2 emissions were observed. The CO emissions when firing the lard were slightly higher than when firing the No. 6 fuel oil. This is because the O_2 level was not optimized for the lard tests. Instead the O_2 levels were kept to that of the No. 6 fuel oil test.

SUMMARY

In comparison with No. 6 fuel oil, the lard samples evaluated in this study possess very good materials handling and combustion characteristics. During combustion, the lard samples produced no sulfur emissions, and two thirds less NO_x than No. 6 fuel oil. With the correct firing system reconfigurations, lard and possibly CWG could be used as fuels for industrial-scale boilers, or as start-up fuel for utility boilers.

Table 2. Combustion Data

	#6 Fuel Oil	Finished Lard (Overall)	Semi-Finished Lard (Overall)
Length of Test (h)	0.65	5.90	2.53
Fuel Injection Temperature (°F)	140	130	130
Fuel Firing Rate (million Btu/h)	1.74	1.74	1.72
% O_2	2.2	2.0	2.2
% CO_2	14.4	14.7	14.6
ppm CO @ 3% O_2	111	145	147
ppm NO_x @ 3% O_2	395	137	135
ppm SO_2 @ 3% O_2	784	0	0

ACKNOWLEDGEMENTS

The authors would like to thank Hatfield Quality Meats and The Pennsylvania Ben Franklin Program for their financial support of this project, and acknowledge Professor John Larsen, Lehigh University, Bethlehem, PA, for his help and discussions.

REFERENCES

1. "Pork Facts Booklet-1999/2000", Booklet # 04057. Published by National Pork Producers Council, 2000.
2. Miller, B. G., Badger, M. W., Larsen, J. W., Clemens, T, Moyer, D., and Wehr, T., Proceedings of the 24th International Technical Conference on Coal Utilization and Fuel Systems, Clearwater, Florida. p. 734, March 1999.
3. Whittemore, C. in "The Science and Practice of Pig Production. Second Edition.", Blackwell Science, London. p. 254, 1998.
4. Battista, J.J., personal communiqué, October 1998.
5. " Combustion Fossil Power Systems" Singer, J.G. (Ed.), Combustion Engineering, Inc., pp. 2-27 - 2-33, 1981.

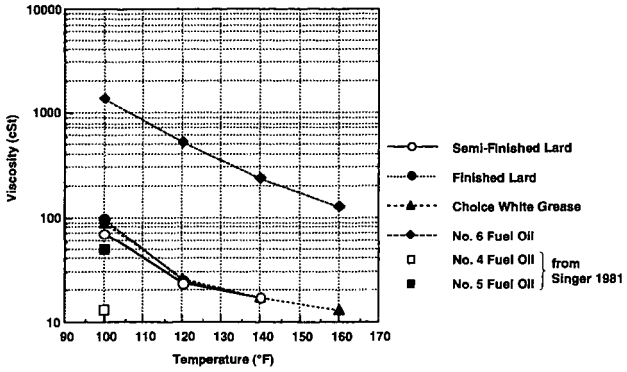

Figure 1. Viscosity as a function of temperature using a Brookfield DVIII viscometer with a #21 spindle.

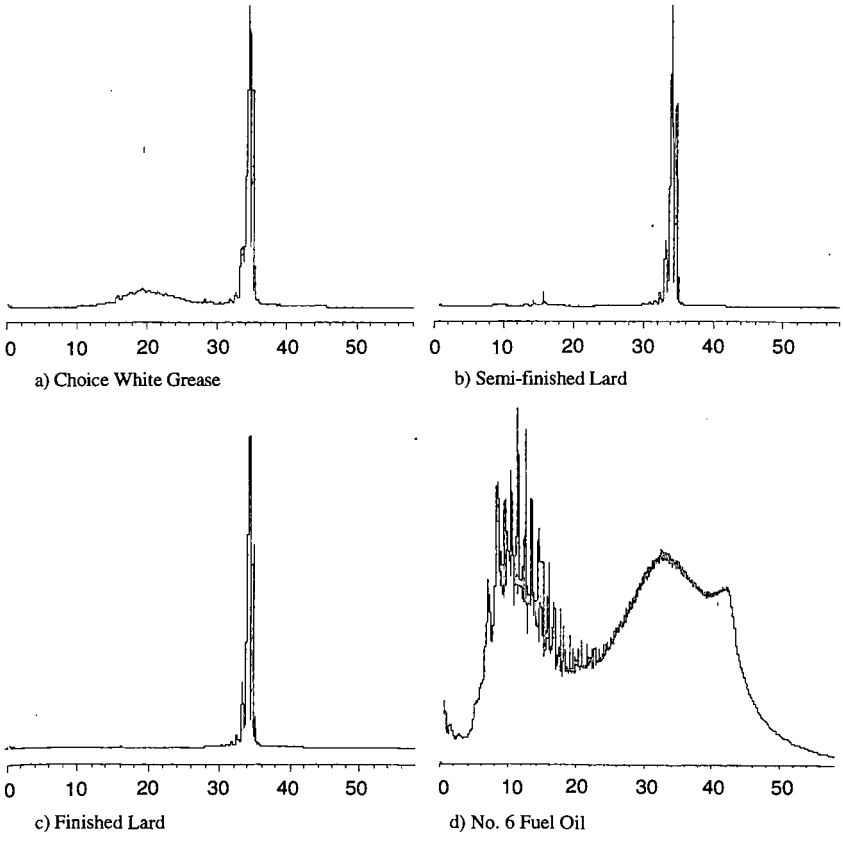

Figure 2. Simulated distillation chromatograms of samples evaluated in this study

CONSTRUCTION/DEMOLITION WOOD AS FUEL FOR COFIRING

James T. Cobb, Jr. and William W. Elder
Department of Chemical and Petroleum Engineering
University of Pittsburgh
Benedum Hall, Pittsburgh, PA 15261

Key words: cofiring of wood and coal, stoker boiler, urban wood waste

INTRODUCTION

National interest in the combustion of wood and wood/coal mixtures is growing rapidly in response to the world-wide concern for global warming, the U.S. concern for SO_2 and NO_x emissions, and regional interest in expanding the utilization of forest products and byproducts. The wood/coal cofiring program at the University of Pittsburgh has focused its early work on the use of clean urban waste. A design requirement of the program was that the cofiring be accomplished by providing a wood-coal fuel blend that could be utilized by the boilerhouses as a regular fuel shipment without modification or capital expenditures. Three demonstrations of cofiring wood and coal, up to 12% wood by BTU content, have been conducted at two local boilerplants. The first project, conducted in 1997, under this program was a demonstration at the traveling-grate stoker boiler of a Pittsburgh Brewing Company (PBC)[1]. In May 1999, a second demonstration was completed at a federally owned spreader stoker operated by the National Institute of Occupational Safety and Health (NIOSH)[2]. The third demonstration was conducted at PBC in October 1999. The principal wood used in all the demonstrations was broken pallets tub-ground to a mulch-like in its consistency. Combustion has been very acceptable, but further development work is underway to achieve acceptable feeding characteristics of the mixture through the receiving grill and pit of the boilerplants. The prime objective of the University of Pittsburgh's wood/coal cofiring program is the successful introduction in western Pennsylvania of commercial cofiring fuel for stoker boilers. This paper summarizes the results of the demonstrations at PBC and NIOSH along with observations on the identification of specific sources of urban wood, and the processing required to produce a cofiring fuel.

PROJECT DESCRIPTION

PBC Demonstration I Steam for brewing, bottling and space heating is produced at the boilerhouse, which contains a gas-fired boiler and two traveling-grate stokers. The stokers are rated at 42,000 lb steam/hr (140 psig) and do not have emissions control equipment. Allegheny County Health Department (ACHD) has primacy for air quality assurance. ACHD generally requires that coal-fired boilers (above 0.5 MMBtu/hr thermal input) emit less than 1.2 lb/MMBtu of SO_2 with an allowable opacity of less than 20%. ACHD performs visible inspections of stack plumes to check opacity and ensure that boilerhouses do not become nuisance problems for neighbors. Stoker coals used in Allegheny County usually arrive by river barge from low-sulfur mines in the Virginia/West Virginia/Kentucky region. Such low-sulfur, stoker-sized coals can cost up to $56/ton when delivered to the boilerplants.

Junior pea stoker coal - ¾ inch by ¼ inch - is delivered to the PBC by tri-axle truck (25 tons) from the Colona Terminal, a transfer station twenty miles west of the plant. Coal is dumped directly into a feed pit, which has a bucket elevator to convey the coal to one of two day bins located above the operating boiler. The feed pit is covered by a grizzly, for vehicle and personnel access, with openings of about 7-inches square. A paddle wheel feeder directs coal from the pit to the bucket elevator, which then transports it to the chute that supplies the day bin. Two chutes of about two feet square convey at the fuel from the day bin to a small hopper. Fuel is then fed by gravity from the small, open hopper onto the traveling grate that has an adjustable gate to set the initial fuel bed height above the grate. The fuel firing rate, set by the grate speed, is determined by a Bailey PID controller.

The first wood obtained for testing was screened tub-ground pallet pieces. Early in the test program, the size consist of this material was 1¼ inch by zero, but later it was changed to 1¼ inch by ¼ inch. The test was expanded to include a second urban wood waste – a 1 inch by zero chipped clearance wood. Fifteen 3-4 hour tests of 5% to 40% wood fuel blends (by volume) were conducted to evaluate the fuel flow/handling characteristics with PBC's existing conveying system. The blended fuels were prepared from wood and coal stored in two open piles near the boilerhouse, using a small front-loader bucket to assist with mixing, before the coal/wood fuel blends were loaded into the day bin. In addition, several 24 hour tests and a 72 hour test with flue gas monitoring provided by the Federal Energy Technology Center (FETC) were conducted to evaluate the boilerplant's ability to operate at steady state with a wood/coal mixture. These mixtures were prepared at Colona Terminal by layering the coal and wood onto the bed of a regular tri-axle delivery truck.

NIOSH Demonstration The NIOSH boilerhouse produces steam for the center's district heating system. The boilerhouse contains two gas-fired boilers and a spreader stoker Keeler boiler. The boiler is rated at 55,000 pph at 200 psig (but normally operates at 100 psig) with a baghouse for emissions control. As at PBC, ACHD has primacy for air quality assurance at the boilerplant and requires the use of low-sulfur compliance coal.

The junior pea stoker coal comes by barge from eastern Kentucky to a transfer station on the river and is trucked from the transfer station to the plant in 25-ton loads. Coal is dumped directly into a receiving

hopper. The coal receiving hopper is situated below a steel grate with openings a minimum of 5" by 8". A Syntron coal feeder picks up the coal onto a belt conveyer, which takes the coal up an elevation of 20 feet to a bucket elevator. The bucket elevator elevates the coal six stories to hoppers. From these hoppers the coal goes down through ducts onto a horizontal paddle conveyer that unloads the coal into a bunker. There are twelve gates at the bottom of the bunker. Another horizontal conveyer receives the coal from any one of the selected gates and delivers the coal to the Detroit Roto Grate stoker spreader feeder system.

There are three 18" feeders with a capacity of 500 to 2000 pounds per hour each. The boiler is also designed with an overfire air system to reburn the flyash. The stokers throw the coal to the back of the boiler, while a moving grate travels from back to front. The coal burns both above the grate in suspension and on the grate. A large number of fine fuel particles leave unburned from the firebox. The finer particles go through the economizer while the heavier ones are reinjected into the boiler by a stream of over fire air. The bottom ash falls into a hopper.

The wood for all test burns was a nominal 1¼ inch by ¼ inch tub-ground pallet waste. The screen and outlet of a tub grinder were modified from the settings used in the PBC demonstration to produce more "chunks" and fewer "stringers" from that used at PBC. Four-hour test burns of 10%, 20%, 30% and 40% wood by volume were conducted in mid-May 1999. The 10% and 20% wood fuel blends were prepared by mixing the wood and coal on the pad, while the 30 and 40% blends were prepared by layering the coal and wood onto the bed of the delivery truck. A 48-hour test burn was conducted using a fuel blend of approximately 33% wood by volume.

PBC Demonstration II In October 1999, two 4-ton mixtures of wood/coal fuel blend were test fired in one of PBC's stoker boilers. The wood component of the fuel blend was prepared by a modified method that produced a more cubic wood particle. Additionally, the wood and coal were mixed at the wood processor's site with a with a FECON blender to 50% wood by volume or about 12% by BTU content.

ACCOMPLISHMENTS

Fuel Conyeyance: PBC Demonstration The demonstration showed that fuel conveyance plays a critical role in the ability of a stoker boiler to handle and feed wood/coal blends. With the exception of a few large pieces, the flow properties of the wood chip/coal blends was similar to junior pea stoker coal. The same held true for the flow properties of the tub-ground wood/coal mixture when properly mixed at relatively low wood percentages.

The critical bottleneck for handling fuel blends with a tub-ground wood content greater than approximately 33% occurred at the grizzly and feed pit. First, the fuel blend bridged the openings in the grizzly to the point that regular intervention was required to maintain flow. Intervention by the operators was acceptable to the manager of this plant. Second, transport of the fuel blend from the feed pit to the entrance of the bucket elevator was erratic and required occasional prodding to sustain flow.

In the initial stages of the first demonstration at PBC, a second problem with conveyance developed. The second, and more important, effect was on fines segregation in the bin. A mixture of wood and coal fines built up rapidly in the day bin. When the pile of fines slumped, a "plug" of fines passed down the chutes and eventually onto the grate, causing significant adverse shifts in burning characteristics, especially when the fuel was soaking wet.

Two adjustments to fuel preparation were made to limit this second problem. The tub-ground material received a second bottom screening to reduce fines, and the method of blending wood/coal mixture was altered. In early tests, the wood and coal were mixed on the ground with a front-end loader to ensure that homogeneous mixture would be delivered. However, this method crushed the coal somewhat and generated excess coal fines. After this problem was recognized, coal and wood were layered onto the truck without any mixing. It was then observed that conveyance through the PBC system components mixed the wood/coal sufficiently while reducing fines production.

At all wood/coal percentages, the green wood chips, when free of large pieces and "plates", flowed through the conveyance system in a manner similar to the stoker coal, with no observed change in fines segregation. However, the wood chips delivered to both PBC and the terminal did contain a small number of long, thin pieces (up to several feet long) and plate-like chips (up to eight inches across). The material delivered to PBC had to be hand-sorted before blending with coal to prepare a mixture that would pass through the grizzly and paddlewheel feeder. Such sorting was not possible in preparing fuel at Colona terminal. The grizzly acted as a screen for oversized pieces that required heavy manual effort for removal. The oversized pieces were attributed to operating problems with the chipper, which should be corrected with proper adjustment.

Fuel Conveyance: NIOSH Demonstration Just as in the PBC demonstration, the NIOSH demonstration showed that fuel conveyance plays the critical role in the ability of a stoker boilerplant to utilize a wood/coal fuel blend. The wood used was principally mulch-like. Long stringers had been screened out as planned, but the grinder had not yet been refitted to produce principally chip-like material, rather than mulch-like material. This led to a difference between expected and delivered processed wood to the project. The resulting wood/coal blend did flow reasonably well from the bunker to the boiler, and it burned well in the boiler, but it

needed considerable assistance to pass through the grate into the outside fuel-receiving hopper. Providing this assistance is unacceptable to this plant's superintendent.

Combustion Both at PBC and at NIOSH, once fed to the grate, properly prepared wood/coal mixtures of both ground pallets and green wood chips met the demonstration's goals for combustion characteristics. As expected, there were no occurrences of flame propagating back into the fresh fuel across the gate, or discharge of still-burning ash particles into the ash pit or out of the boiler during any test.

Compared to coal, wood is a high volatile, low heat content and low density fuel. The lower heat content of the wood can be compensated for by a higher rate of feed (on both a volumetric and weight basis) to achieve a satisfactory heat release rate. The heat content on a volume basis for a 33% tub-ground pallet/coal blend was 85% of that for the coal, while the 33% green wood chip/coal blend was 61% of that for the coal. This difference in volumetric heat contents required higher gate openings and faster grate and stoker speeds during wood/coal test burns relative to normal boiler operation on coal only.

Emissions/Opacity Flue gas emissions were continuously monitored during the PBC demonstrations with standard process gas analyzers that were installed by FETC. Emissions were low, with average levels of 685 ppm SO_2 and 333 ppm NO_x (corrected to 3% dry O_2) that correspond to about 1.1 lb SO_2/MMBtu and 0.4 lb NO_x/MMBtu. These results were consistent with the low sulfur content of the pallets, while NO_x levels were similar, if not slightly lower, than levels reported for other stoker boilers. A slight reduction in NO_x when firing a biomass/coal fuel is expected given the higher volatile and lower nitrogen content of the pallets as compared to the stoker coal. CO emissions were reasonable with an average 363 ppm (corrected to 3% dry O_2), which is indicative of good combustion, particularly given the load swings and other operational changes, and the fact that the boiler does not utilize any overfire air.

Opacity is monitored continuously by instrument at the NIOSH boilerplant and visually monitored at PBC. Opacity was normal during all the test burns at the NIOSH boiler and during the test burns of the tub-ground pallet fuel blend at the PBC. When a 50% by volume green wood chip blend was tested at the PBC, some smoking was observed, indicating an incomplete combustion of volatiles, perhaps due to high-moisture fuel pieces and/or an uneven distribution of air through the fuel bed. This may represent the upper limit to the percent of green wood that can be used.

WOOD FOR CO-FIRING IN STOKER BOILERS

Types, Sources There are numerous systems for categorizing the types of wood residues. Below is a listing for urban wood residues developed by C.T. Donovan and Associates, Inc[3].

Urban wood residue is composed of highly heterogeneous woods. It is most simply defined as all the wood residue generated within a metropolitan area and may be sub-categorized into urban tree residues and post-consumer wood residue. Urban tree residue consists of residues from tree maintenance, utility right-of-way, and urban site conversion activities. This material is derived mainly from tops, limbs, and whole (small) trees. The material is composed of wood, needles, bark and leaves. Moisture content ranges from 35% to 50%.

Post-consumer wood residue consists of residues derived from secondary wood products. These residues may be further sub-categorized into:

- Pallet and Wooden Container residues – Each year, 16% to 18% of all the timber harvested in the US goes into the manufacture of pallets and wooden containers. Because of their number and bulk, pallets and wooden containers present significant disposal problems and are increasingly collected for reuse or repair. Pallets have a very low moisture content of 5% to 15% and are generally free of paints, stains or other treatments.
- Construction and Demolition (C/D) Wood residues – The wooden components of the debris generated during construction, renovation and demolition of buildings, roads and other structures. The amount of wood in the debris varies from 15% to 85%. 40% of new residential construction residue is believed to consist of wood and wood products. C/D residue wood can be treated or untreated. The wood may also contain laminates and have other waste (such as asphalt shingles, insulation and dry wall) attached. The average moisture content is 12% to 15%.
- Dunnage and Bracing Wood residues – Similar to pallet and wooden container wood residue.
- Urban Secondary Wood Products Manufacturing residues – The residues consist of chips, ends, sawdust, shavings and slabs. The moisture content ranges from 15% to 45%. The residues may contain preservatives, paint, glue and non-wood material such as plastic laminates. Also included are pallet recycling residues. Over 85 million pallets are received for recycling each year. 74% are repaired and reused (or reused without repair); 15% are dismantled for repairs; and the remaining go directly to disposal or are processed for mulch, fuel or fiber.
- Municipal Solid Waste (MSW) Wood residues – All types of urban wood, other than those types listed above, that are conveyed to a landfill for disposal. The average moisture content is 15% to 25%.

Characteristics Although the heat content for all hardwoods is approximately 8,500 Btu/lb on a moisture, ash-free basis (MAF) and MAF softwood has a heat content approaching 9,500, the physical and chemical

characteristics of wood residue varies widely depending on the type and source of the material. The most important characteristics of wood as it relates to its use as a fuel in stoker boilers are (i) moisture content, (ii) ash characteristics, (iii) post-harvest treatment/contamination, (iv) particle size/fuel blending, and (v). price/availability

Moisture Content: The moisture content for freshly harvested "green" wood is approximately 50%. Over time the moisture content declines to between 5% and 15%. The high moisture content of green wood poses several problems related to its use as fuel: (1) It represents a weight with no caloric value that can increase the transportation and handling cost. (2) It will increase the volume of flue gas generated in combustion requiring an increase in draft fan output. (3) It will lower the furnace exit temperature, which will lower the heat transfer rate in the connective sections of the boiler. (4) It will lower the heating value of the fuel due to un-recovered energy in the flue gases that represents the heat used to vaporize the moisture in the fuel. Stoker boilers are designed for a given fuel moisture content (and fuel size distribution). Usually moisture content should be kept within 10% of design.

Ash characteristics: One of the major concerns associated with adding a biomass co-firing fuel to a boiler originally dedicated to coal firing is the possibility for a change in the ash fusion characteristics of the blended fuel. In a properly operating chain-grate stoker boiler, the individual ash particles fuse together in a porous mass that permits he passage of air and allows for uniform combustion across the bed. Adding wood to the coal has had a deleterious effect on the slagging and fouling characteristics with certain wood/coal fuel blends.

The clear stemwood of most species of trees contains very little ash, generally less than 1%. Stemwood is the inner wood from the trunk and larger branches. Actively growing portions of a tree such as the leaves and inner bark are higher in ash and the ash is high in "alkali" content. Alkali content refers to the sum of the potassium oxide (K_2O) and sodium oxide (Na_2O) in the ash. This high alkali content is the source of many of the problems with biomass ash.

Using indices originally developed to predict coal ash behavior, the elemental ash analyses of bottom and fly ashes from a stoker boiler burning Eastern Kentucky compliance coal, and published data on hardwood and urban wood residue ashes, mathematical predictions of the ash characteristics for two possible 20% wood / 80% coal fuel blends were calculated. The results of the comparisons indicate that the combustion on the grate of either urban wood residues or hardwood alone would likely cause severe fouling problems and a possible slagging problem. These calculations also indicate that slagging and fouling should not be a problem when co-firing urban wood residues at 25% mass input with compliance coal in stoker boilers. Slagging and fouling problems were not observed during any of the demonstration test burns.

Post-harvest treatment/contamination: Treatment may be as a (1) surface coating (paint, stain, etc.), (2) manufacturing agent such as resin, glue, or binder used as adhesive; or (3) impregnated preservative. The treatments which cause the greatest environmental concern in relation to their combustion are chromated copper arsenate (CCA) pressure treated lumber and lead-based paint. Wood with these treatments may be found in C/D wood, and makes the uses of C/D problematic. The most common type of contamination is dirt. Dirt will be found in the bark of harvested wood and urban wood residues. Dirt can have a negative impact on the slagging and/or fouling behavior of the ash. Much of the contaminating dirt can be removed by screening out the fines.

Particle size/fuel blending: Stoker boilers are designed for a given fuel size distribution. The wood provided to the first PBC and the NIOSH cofiring demonstration was refined tub-ground mulch. A tub grinder shatters the wood to produces a splinter material. This material is stringy with frayed ends and is subject to bridging at the delivery grill. When a wood chip produced from green whole-tree stems was tested at the PBC, no bridging was observed even when mixed to over 40% wood by volume. The superior behavior at the delivery grill of a wood chip is due to the chip's more cubic shape and sharp, knife-cut edges. Unfortunately, urban wood waste with nails and other hard contaminates causes rapid wear on a wood chipper's knife blades. Therefore, chippers cannot be used for primary size-reduction.

Three methods of fuel blending have been used in the demonstrations: mixing on the ground using a front-end loader, layering on the bed of the delivery truck and mixing in a FECON blender. Mixing with front-end loaders can produce a homogeneous fuel blend but the process generally creates excessive fines. Layering on the bed of truck can be sufficient to produce a reasonably uniform mixture on the grate if the layering is performed with care. In the first PBC demonstration, uniform layers several feet thick were found to pass through the delivery grill and reach the boiler grate mixed in a manner indistinguishable from the blends made on the ground. In the NIOSH demonstration, less care was used in layering the fuels in several deliveries and the wood formed large clumps on the delivery grill. These clumps interrupted the delivery and were never completely mixed into the coal by the boilerhouse conveyances. Wood and coal were simultaneously loaded into a FECON blender to produce a very uniform blend. The blend retained its consistency through the boilerhouse conveyances onto the boiler grate. However, the frayed ends of the tub-ground wood led to occasional interruptions of flow through the delivery grill of even the well-blended mixtures.

Price/availability. In order for a wood/coal fuel blend to gain commercial success it must be offered to the boilerplant at a cost equal to or below the plant's current cost of coal. Size reduction is the major cost in marketing urban wood residues as a boiler fuel. The processing costs for a commercial operation are expected to be approximately $20 per ton. This is only marginally less than a wood processor can receive for the product from a coal vendor. In the current market in order to make wood to stoker boiler fuel processing profitable, the wood processor must capture a tipping fee for the waste residues that are collected. In 1996 at the beginning of the University's research program, wood processors in the Pittsburgh region were receiving a tipping fee for pallet wastes that they were tub grinding to produce a colored-mulch. Since then the highly profitable color-mulch market has expanded and all the readily available pallet residue is being collected for processing to colored-mulch without a tipping fee.

Nationally, it is estimated that 43.8 million tons of C/D waste are generated each year with 24.5 million tons available for cofiring[4]. This material is currently being landfilled with a tipping fee in the Pittsburgh region of approximately $30 per ton. Regionally this amounts to more than 125,000 tons per year.

CONCLUSIONS /FUTURE PLANS

While working toward the introduction in western Pennsylvania of commercial cofiring fuel for stoker boilers, the University has learned much about the problems associated with seeking specific sources of urban waste wood and its processing into boiler fuel. The project team has concluded that use of a properly prepared blend of processed pallet residue and coal as stoker fuel with up to 12% wood by BTU content is technically feasible and environmentally desirable. Unfortunately in the Pittsburgh region pallet residue will not be available for processing to a stoker boiler cofuel. C/D wood residue will be required for the fuel blend.

In future planned demonstrations, the University will use C/D wood for the wood component of the fuel blend. ACHD has been supportive of the use of pallet residue as a cofiring fuel and has readily granted air quality variances for the demonstrations. Improperly source-segregated C/D wood has the potential of being contaminated with material that will cause toxic air emissions when combusted. The University and the wood processor plan to develop a quality assurance plan that will satisfy ACHD that the fuel is free of hazardous contamination. If a variance is granted to burn construction wood, then the University, through local builders organizations, will locate construction contractors that wish to supply source-segregated construction wood (and avoid a portion of their normal waste tipping fee for this material). The wood processor will locate a roll-off container at one or more of these sites. If a variance is also granted to burn demolition wood then wood processor will locate roll-offs at one or more demolition sites identified by the University with the aid of the Pennsylvania Department of Environmental Protection. The emissions from demolition waste combustion will be monitored for lead, arsenic and chromium.

Although standard tub-ground wood has been acceptable in the boiler as the wood component of the cofiring fuel at some boilerplants, the bridging it causes at the delivery grill will be unacceptable at most plants. For future demonstration the wood processor will develop two methods for producing a "chip" from urban wood waste. In the first method the processor will extend the work started for the second PBC demonstration on producing chip-like mulch from tub grinding. The processor will install a cut-off plate behind an over sized screen on the tub grinder that will sheer off the long wood splinters to a more cubic wood fragment than is normally produced. The wood will be sized to 1¼ inch by ¼ inch. In the second method, the wood will be very briefly tub ground to liberate the nails. Passing the wood through a standard knife-bladed chipper will follow this tub grinding. The wood will be sized to 1½ inch by ¼ inch.

ACKNOWLEDGMENTS

This work has been performed with the financial support of USDA Grant No. NA-99-0078. The demonstration at the Bruceton Research Center was conducted under the provisions of a Memorandum of Understanding PRL-99-MOU103 between the U.S. Department of Health and Human Services (DHHS), Public Health Service (PHS), Centers for Disease Control and Prevention (CDC), National Institute for Occupational Safety and Health (NIOSH), and the University of Pittsburgh, Energy Resources Program.

REFERENCES

1. Cobb, James T., Jr., Gene E. Geiger, and William W. Elder, "Wood/Coal Cofiring in Industrial Stoker Boilers," *Proceedings of the of the Air and Waste Management Association's 1999 Annual Meeting and Exhibition*, St. Louis, Missouri, June 20-24, 1999.
2. Cobb, James T., Jr., William W. Elder, Mark C. Freeman, Robert A. James, Nathan J. Campus, Wayne F. Miller and Lew R. McCreery, "Wood/Coal Co-Firing in a Spreader Stoker," *Proceedings of Stoker Boiler's 99*, Stoker Efficiency Network, Greensboro, North Carolina, September 15-16, 1999
3 Fehrs, Jeffery, E., "Overview of Wood Waste Availability and Characteristics," in *Co-firing Wood with Coal in Utility Boilers*, CONEG -North Regional Biomass Program, 1994.
4 Garland, George, "Co-Firing Wood and Paper Waste," *Proceedings of the Biomass Interest Group of the Electric Power Research Institute*, January 20-21, 2000

NO_x REDUCTION IN PULVERIZED COAL COMBUSTORS USING WASTE COAL AS COAL-WATER SLURRY

Sarma V. Pisupati and Vlad Zarnescu

Energy and Geo-Environmental Engineering Department,
and The Energy Institute, Penn State University
110 Hosler Building
University Park PA 16802
Email: sxp17@psu.edu

Keywords: waste coal, coal-water slurry combustion, NO_x reduction,

INTRODUCTION

In order to comply with the regulations for nitrogen oxides emissions, various abatement strategies have been developed. These strategies can be divided into the following categories: 1) modification of the combustion configuration, 2) injection of reduction agents into the flue gases, and 3) treatment of the flue gas by post-combustion de-nitrification processes. A determination of the most effective and least expensive abatement technique depends on specific boiler firing conditions and the emission standards. A combination of techniques may be necessary to achieve certain mandated limits. Hence, the best NO_x control strategy for a certain unit is highly site dependent.

No definite rules exist to determine which nitrogen oxide formation mechanism dominates for a given stationary combustor configuration because of the complex interactions between burner acrodynamics, and both fuel oxidation and nitrogen species chemistry. But in general, fuel nitrogen has been shown to dominate pulverized coal fired boilers, although thermal NO is also important in the post-flame regions where over-fire air is used. Pershing and Wendt [1] showed that thermal NO contributions only become significant at temperatures above 2,500 °F in coal flames. Prompt NO] is not a major source during coal combustion. Coal-water slurry (CWS) prepared from waste coal has a potential to reduce NO_x emissions [2, 3]. Reburning is proposed as a general mechanism for lower NO_x emissions when cofiring coal-water slurry with PC [3]. Coal-water slurry reburning is applicable to all types of coal-fired boilers and offers electric utilities a potential option to achieve significant NO_x emissions reduction [4].

OBJECTIVES

The main objective of this study was to gain insight into the mechanism by which NO, emissions are lowered when cofiring coal and CWS as compared to coal firing by examining the extent of reburning in the gas phase, and understanding the heterogeneous char NO contribution to the reduction of NO.

EXPERIMENTAL

The study was conducted in the 0.5 MMBtu/h Down fired combustor (DFC) located at the Energy Institute of Penn State. Figure 1 provides a schematic diagram of the 0.5 MMBtu/h DFC. Detailed description of the facility can be found elsewhere [5]. Coal was fired through the central pipe of the burner, and slurry fuel was injected in Port 2 to simulate the reburn conditions. CWS was cofired with coal at 0, 10, 20, and 30 % of the total thermal input. A total of fifteen tests were performed in the DFC. Compositional analysis of the coal and CWS are provided in Table 1. Baseline flue gas concentration and temperature profile along the combustor was obtained when firing 100% coal. A continuous emission monitoring (CEM) system was used to measure O_2, NO, and CO at various Port levels. Axial oxygen concentration measurement was also obtained.

Table 1. Compositional analysis (wt%, dry basis) of PC and CWS

Fuel	Fixed Carbon	Volatile Matter	Ash	HHV (Btu/lb	C	H	N	S	O
Coal	62.94	24.17	12.89	13,339	76.10	4.66	1.37	1.59	3.39
CWS	60.06	30.29	9.65	13,353	77.07	4.51	1.34	1.32	6.11

A nominal firing rate of approximately 0.5 MMBtu/hr was used in the study. Ports were installed as per EPA methods for stack gas sampling for the sulfur oxides evaluation. The coal-water slurry fuel atomization gun was placed at Port 2 for all tests. Combustion air for coal-water slurry fuel during all reburn tests was introduced in Port 3 of the DFC. An air pressure of 100 psig was used for atomizing the CWS.

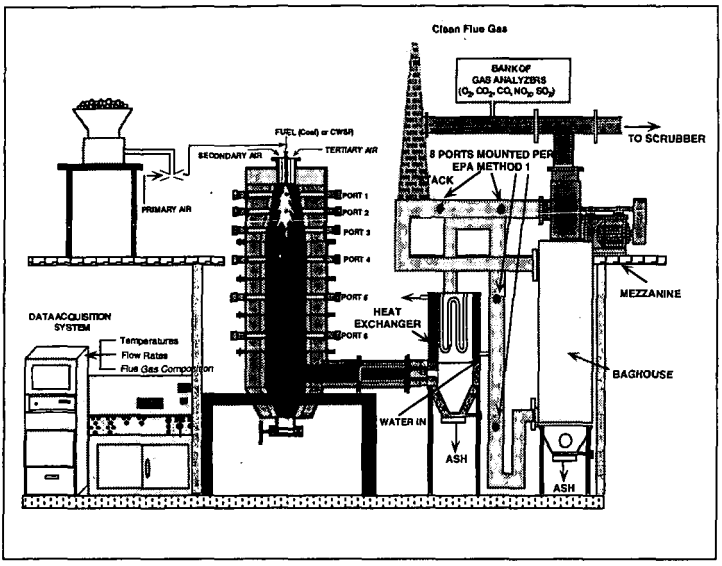

Figure 1. Schematic diagram of the down fired combustor (DFC).

Data on the gas temperatures using LAND suction pyrometer, and oxygen, CO, and NO_x concentration profiles using continuous emission monitoring system (CEM) in the combustor were also obtained during the tests. Char samples were collected from various Ports in the DFC using an isokinetic sampling probe. The char samples were collected in wet condition by washing the probe after each test and were analyzed for carbon, hydrogen, nitrogen, and carbon burnout.

RESULTS AND DISCUSSION

The gas composition (O_2, CO and NO_x) at various Port levels was measured at the center of the combustor, midway between the center and the wall (called "Mid") and at the wall. The results, when firing 100% PC with all the air though the burner (Figure 2), show that the NO_x concentration in the gas phase was maximum near the burner and as the flue gases pass down the combustor, the NO_x levels decrease. This suggests that the rate of destruction exceeded the rate of production of NO_x. This increase in the destruction is possibly accomplished by the reburn mechanism. Reburning can take place either by homogeneous gas phase reactions or by the NO_x - char reactions. Upon heating a coal particle, nitrogen is also distributed between the volatile and char phases. NH_i and HCN species in the volatiles depending on the temperature, concentration and mixing can form NO_x or N_2. Simultaneously the char nitrogen will be released to form either NO_x or finally to N_2. Depending on the

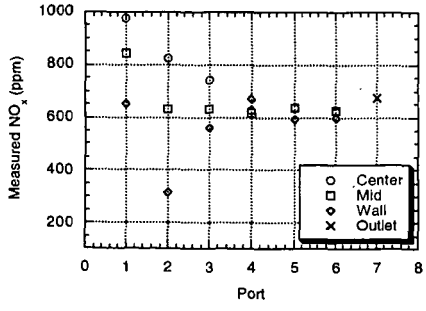

Figure 2. NO_x Profile in the DFC when firing 100% coal with all the air through the burner

net difference between the two processes, an increase or a decrease in the NO_x emissions occurs. It can be seen from Figure 3 that the initial NO_x levels when cofiring coal-water slurry are lower than the values for 100% PC. This suggests that the formation of NO_x in the initial phases is lower. Subsequently there is a minor decrease in the NO_x concentration for the tests with CWS cofiring tests. These results indicate that the NO_x production and destruction rates after the primary zone are almost equal leading to no net increase in NO_x levels. Conceptually, the reburning process can be divided into three zones: a) Primary Combustion Zone: This is the main heat release zone which accounts for approximately 80 % of the total heat input to the system and is operated under fuel-lean conditions. The level of NO_x exiting this zone is defined to be the input to the reburning process; b) Reburning Zone: The reburning fuel (10-30 % of the total fuel input) is injected downstream of the primary zone to create a fuel-rich, NO_x reduction zone. Reactive nitrogen enters this zone from two sources: the primary NO_x input and the fuel nitrogen in the reburning fuel. These reactive nitrogen species react with hydrocarbon radicals, primarily CH, from the reburning fuel, to produce intermediate species like NH_3 and HCN [6]. The HCN then decays through several reaction intermediates and ultimately reaches N_2; c) Burnout Zone: In this final zone, air is added to produce overall lean conditions and oxidize all remaining fuel fragments. The total fixed nitrogen species (TFN = NH_3 + HCN + NO + Char N) will either be oxidized to NO_x, or reduced to molecular nitrogen.

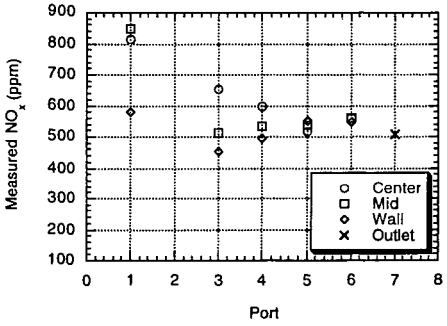

Figure 3. NO_x profile when firing 70% PC and 30% CWS with all the air flowing through the burner

The amount of nitrogen from the fuel into volatiles and char will change as a function of temperature, nitrogen content and size of the coal particle. Figure 4 shows the wall temperature profiles for various cofiring configurations. A test was performed with 100% PC but water, equivalent to 30% CWS test, injected in Port 3 to separate the effect of NO_x changes due to temperature decrease and any reburning reactions. Since all the fuel and combustion air was admitted through the burner the resulting temperature in the case of 100% PC was higher than the rest of the tests. This contributes to higher thermal and fuel NO_x during primary combustion zone. Partitioning of nitrogen between volatile and char phase is a function of temperature, heating rate and coal type and equipment used. It has been shown in the literature that total volatile and nitrogen yields are approximately proportional at comparatively low pyrolysis temperatures (1800 °F) and short heating times, but pyrolysis at temperatures > 2500 °F, results in the evolution of significant amount of additional nitrogen [7]. Since the temperature for 100% PC in the Port 1 region is high (>2500 °F), it is likely that more nitrogen is released into gas phase which, with more air tends to form higher amounts of NO_x and thereby higher concentration of NO_x. However, there is a reduction in NO_x concentration between Ports 1 and 3. This is primarily due to gas phase reaction involving hydrocarbon species from the volatiles.

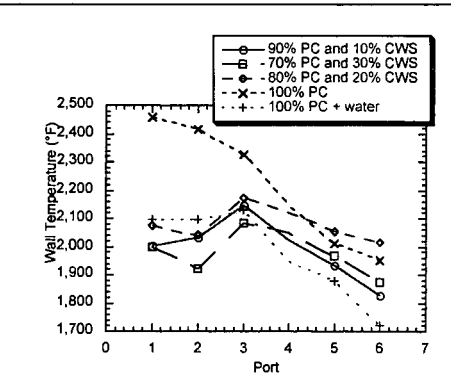

Figure 4. Temperature profile for various cofiring configurations

Carbon burnout data as a function of distance from the burner was obtained from the isokinetic char samples that were collected during the tests. The data show that that the carbon burnout during cofiring runs was lower than that of 100% PC run. As a result, lesser amount of carbon was available in the form of HC radicals during the initial stages of cofiring than the 100% PC run. From Figure 5, it can be seen that the chars collected show higher amounts of carbon, and up to 18% of total nitrogen remaining in the char phase at Port 3. Wendt [8] has shown that under rich conditions, HCN plays a critical role in driving the nitrogen cycle to form N_2 and that one source of HCN formation is the destruction of NO by hydrocarbon radicals, which is the main reburning reaction destroying NO. In addition, it has been shown [6, 9] that the Fenimore N_2 fixation reaction also produces HCN, especially under natural gas reburning conditions. Mereb and Wendt [10] confirmed the fact that reburning with pulverized coal is also effective but less than with gas because natural gas produces more hydrocarbon species in the NO_x reduction zone and reactions between NO and hydrocarbons are important. Their data showed that with coal reburning, HCN was destroyed more rapidly than it was being formed and its values decayed to levels below 20 ppm within 0.6 seconds. This result supported their hypothesis that it is important to maintain HCN formation rates during long time scales in order to keep N_2 formation mechanisms going, that this formation is mostly due to hydrocarbon reactions with NO or N_2 and that any slow release of nitrogen from the coal residue is a minor contributor to the process. The results in this study also confirm these observations since the residence time between Ports 1-4 is approximately 0.6-0.7 seconds. The gas phase reburning after this Port appears to be insignificant.

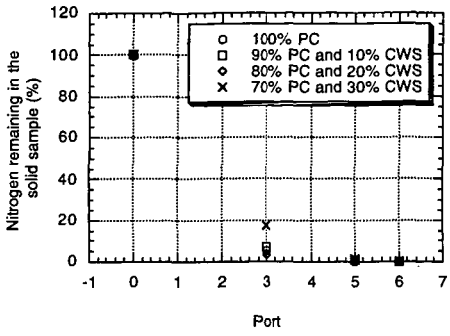

Figure 5. Percent nitrogen remaining in the solid sample as a function of distance from the burner

NO is expected to be the primary product of char nitrogen combustion [11]. However, the NO-carbon reaction can reduce the NO to N_2. NO reduction is enhanced by the presence of CO [11]. From the CO measurements in the combustor in this study, no significant difference in the CO in the gas phase emissions was observed. In most of the tests the CO concentration was around 100-120 ppm. Therefore, it is likely that the NO produced from oxidation of char nitrogen reacts with the carbon in the pore structure. Char produced from the coal-water slurry is texturally different from the char from PC combustion [12]. Therefore, local NO-char reactions are believed to be responsible for the small reduction in NO above and beyond the reduction obtained due to temperature reduction caused by water addition.

It was also seen from the data that there was a significant difference between the NO_x concentrations measured at the center and the wall. This indicates the lack of mixing in the combustor up to about 7-8 feet in the combustor. If the NO_x molecules do not mix with hydrocarbon radicals, the reduction in NO_x will be reduced. It has been shown [9] that the reburning mechanisms occur in two regimes: one in which fast reactions between NO and hydrocarbons are usually limited by mixing; the other in which reactions have slowed and in which known gas phase chemistry controls.

CONCLUSIONS

The results of the study showed that NO_x formation occurs during initial phases in the pulverized coal flames. The NO_x concentration profile indicated that the concentration decreases rapidly by reburning in the gas phase by the radicals in the volatile phase. Excess air levels (air staging), and mixing appeared to be the most important parameters in reducing the NO_x in the primary zone. When coal-water slurry was cofired with coal the temperature in the upper part of the combustor was lower because of water addition. The NO_x concentration near the Port 1 region of the combustor was also lower. This reduction was attributed to the lower temperature and lower fuel nitrogen split into the gas phase. The reduction of NO_x due to reburn in the primary zone was not observed for coal-water slurry cofiring tests. The carbon burnout was lower for the CWS cofiring tests. Therefore, lower amount of carbon was available in the volatile phase to

reduce NO_x initially. It is believed that gas phase reactions did not play a significant role in the reduction of gas phase NO_x that was produced initially.

Char contained higher amounts of nitrogen because of the char structural differences, the nitrogen oxides that are formed are believed to react on the char surface on their way out through the pore structure.

ACKNOWLEDGEMENTS

The financial support for this work was provided by the United States Department of Energy under the cooperative agreement DE-FC22-92PC92162. The assistance of Energy Institute staff is gratefully acknowledged.

REFERENCES

1. Pershing, D.W., and Wendt, J. O. L. "*Pulverized coal combustion: The influence of flame temperature and chemical composition on thermal and fuel NO_x*". in *Sixteenth Symposium (International) on Combustion*. 1977: The Combustion Institute, Pittsburgh, PA.

2. Miller, S.F., Morrison, J. L., and Scaroni, A.W. "*The effect of cofiring coal-water slurry fuel formulated from waste coal fines with pulverized coal on NO_x emissions*". in *21st International Technical Conference on Coal Utilization & Fuel Systems*. 1996. Clearwater, FL: Coal Water Slurry Association, Washington, D.C.

3. Miller, B.G., Miller, S. F., Morrison,J. L. and Scaroni, A.W. "*Cofiring coal water slurry with pulverized coal as a NO_x reduction strategy*". in *Fourteenth Annual International Pittsburgh Coal Conference & Workshop*. 1997. Taiyuan, Shanxi Province, China: University of Pittsburgh, Pittsburgh.

4. Ashworth, R.A., Melick, T.A. and Morrison, D.K. "*Co-firing coal water slurry fuel on a tangentially-fired boiler*". in *23rd Technical Conference on Coal Utilization and Fuel Systems*. 1998. Clearwater, FL: Coal water Slurry Association and US Department of Energy.

5. Pisupati, S.V., Simons, G. A., Oehr, K. H. and Zhou, J. "*Use of biomass-based product for simultaneous NO_x and SO_2 capture in pulverized coal combustion systems*". in *9th International Conference on Coal Science,*. 1997. Essen, Germany: P & W Druck und Verlag GmbH, Germany.

6. Lainer, W.S., Mulholland, J.A., and Beard, J.T. "*Reburning thermal and chemical processes in a two-dimensional pilot-scale system*". in *Twenty-First (International) Symposium on Combustion*. 1986: The Combustion Institute, Pittsburgh, PA.

7. Gibbons, J.R., Lockwood, F.C., Man, C.K. and Williamson, J. "*No release during char combustion*". in *Eighth International Coal Science Conference*. 1995. Oviedo, Spain: Elsevier, Amsterdam.

8. Wendt, J.O.L., "*Mechanisms governing the formation and destruction of NO_x and other nitrogenous species in low NO_x coal combustion systems*". Combustion Science and Technology, 1995. **108**: p. 323-344.

9. Mereb, J.B., and Wendt, J. O.L. "*Reburning mechanisms in a pulverized coal combustor*". in *Twenty-Third (International) Symposium on Combustion*. 1990: The Combustion Institute, Pittsburgh, PA.

10. Mereb, J.B., and Wendt, J.O.L., "*Air staging and reburning mechanisms for NO_x abatement in a laboratory coal combustor*". Fuel, 1994. 73(7): p. 1020-10276.

11. Thomas, K.M., "*The release of nitrogen oxides during char combustion*". Fuel, 1997. 76(6): p. 457-473.

12. Pisupati, S.V., Sharifi, R., Liu, Y. and Scaroni, A.W. "*Measurements of temperature, particle size distribution and particle speed in an industrial boiler*". in *Thirteenth Annual Pittsburgh Coal Conference*. 1996. Pittsburgh, PA: University of Pittsburgh, Pittsburgh, PA.

FABRICATION OF AUTOMOTIVE BRAKE COMPOSITES FROM UNBURNED CARBON

V. M. Malhotra[#], P. S. Valimbe[#], and M. A. Wright[*]
Department of Physics
* Center for Advanced Friction Studies
Southern Illinois University, Carbondale, IL62901-4401.
E-mail: vmalhotra@physics.siu.edu

KEYWORDS: Unburned Carbon, Coal Combustion By-Products, Friction Materials

ABSTRACT

In pursuit of our goal of finding additional uses for those fly ashes that are rich in unburned carbon, we evaluated how fly ash, bottom ash, sulfate-rich flue gas desulfurization (FGD) scrubber sludge, and unburned carbon affected the frictional properties of composites. We extracted unburned carbon-rich fractions from a fly ash, which was known to have a high carbon content. The unburned carbons were characterized by scanning electron microscopy (SEM), and their oxidative resistance was probed at $30°C < T < 710°C$ using differential scanning calorimetry (DSC) technique. The frictional composites formulated from coal combustion by-products, containing 38-volume percent by-product concentration, were evaluated using Friction Assessment and Screening Test (FAST). Our results suggested that the unburned carbon, being highly porous and resistant to oxidation, had the traits of being an excellent additive for automotive brakes. The composites formed from unburned carbon gave stable frictional behavior and reduced wear and noise.

INTRODUCTION

A substantial portion of the electric power generated in the USA comes from burning coal. However, coal burning by the power plants brings about a huge production of solid residues, mainly fly ash and bottom ash. In an effort to meet the environmental concerns of coal burning, various technologies are employed by electric power utilities, which further add to the solid materials formed, e.g., fluidized bed combustion (FBC) spent bed ash and flue gas desulfurization (FGD) scrubber sludge. It is estimated that about 90 million tons of these solid residues, typically known as coal combustion by-products (CCBs), are produced annually in the USA. Presently, only about 25% of the CCBs generated are utilized [1], with the rest going to landfill or surface impoundments. Most of the CCBs have been largely used in the construction industry, though many additional uses have been proposed [1-4], e.g., ultra-lightweight aggregates for the insulation industry, Portland cement-based FBC mixes, highway and street construction, construction bricks, roofing or paving tiles, pipe construction, artificial reefs for marine wildlife habitat, and aluminum-fly ash composite materials.

In an effort to further mitigate the environmental concerns of coal burning, many utilities have or are installing low-NO_x burner systems [5]. Unfortunately, the fly ash produced by the low-NO_x burner systems has substantially larger unburned carbon in it [5,6]. The higher concentration of unburned carbon in ash stream has a deleterious effect on the utilization of fly ash, especially in the concrete industry. Therefore, intense research is underway by various groups to seek alternative uses of unburned carbon.

The frictional materials used in automobile brake linings are complex composite materials, which generally contain a large number of ingredients, i.e., both organic and inorganic [7]. Typically, brake linings are either organic pads or semi-metallic pads. More than twenty components have been reported for certain brake formulations, though the five major constituents are organic resin as a binder, fibrous reinforcement, filler materials, sliding materials, and friction modifiers. The fillers added into automotive brakes are low cost materials like barytes ($BaSO_4$), char, and clays. The sliding materials have a hexagonal crystal structure and are incorporated into the frictional materials to alter their lubrication by forming debris on the frictional materials' surface. Asbestos fibers because of their thermal and structural characteristics were frequently used in the recent past as a preferred fibrous support for brake pads. However, they no longer are used due to environmental and health considerations. Slag, mineral, kevlar, or carbon fibers are now used in automotive brakes, depending on the targeted market. Frictional modifiers and abrasives are typically metal oxides. It was felt from our characterization measurements [3,8-9] on CCBs and certain types of carbon extracted from CCBs that the combustion by-products could act as friction modifiers and fillers for automotive brake composites. Moreover, certain fractions of CCBs might help in controlling the thermal properties of brake composites. Therefore, we formed frictional composites from PCC fly ash,

PCC bottom ash, FGD scrubber sludge, and unburned carbon, which was extracted from a high LOI fly ash. These materials' structural, thermal, mechanical, and frictional behaviors were evlauated to probe the suitability of these materials for automotive brake composites.

EXPERIMENTAL TECHNIQUES

The CCBs, i.e., PCC fly ash (Baldwin Unit #3), high LOI PCC fly ash (Southern Illinois Power Co. IL (SIPC)), PCC bottom ash (City Water, Light and Power, Springfield, IL), and sulfate-rich FGD scrubber sludge (City Water, Light and Power, Springfield, IL), samples were obtained from the coal combustion by-product bank maintained in the Mining Engineering department of Southern Illinois University at Carbondale. We used the centrifugation and flotation approach to extract unburned carbon from the high LOI fly ash. Unburned carbon was extracted from two different batches of fly ash obtained from the same power plant, and henceforth, these fractions are called unburned carbon-1 and unburned carbon-2. We blended various CCBs or unburned carbon with polymer binder, slag fibers, and sulfate-rich scrubber sludge to form our composites (see table 1) using a high shear mixer. To minimize the effect of binder on the evaluation of frictional behavior of CCBs, we chose a binder, which is typically used for commercial brake formulations. The blended powders were hot-pressed at 170°C in a 5.72 cm diameter stainless steel die for 1 hour. The hot-pressed composites were further post-cured in air for 8 hours in an oven whose temperature was ramped to 170°C from room temperature at a rate of 3°C/min.

Table 1
Fractions used to form friction composites.

Composite ID	Polymer Binder (volume %)	Slag Fibers (volume %)	Scrubber Sludge (volume %)	By-Product (volume %)
Basic Matrix	45	22	33	
Fly Ash	42	20	30	8 (fly ash)
Bottom Ash	42	20	30	8 (bottom ash)
Carbon-1	42	20	30	8 (unburned carbon-1)
Carbon-2	42	20	30	8 (unburned carbon-2)

Microscopic measurements were undertaken on the as-received fly ash as well as on the unburned carbon fractions by acquiring their SEM microphotographs. The SEM images were obtained using a Hitachi S-570 scanning electron microscope. To record the SEM pictures, a thin layer of fly ash or unburned carbon was sprinkled on a SEM high resolution stub. The samples were then heated at 60° C for 24 hours. These steps were necessary to ensure that ash particles would not detach from the stubs when under electron beam and also would not decompose when under electron bombardment. The fly ash particles were sputter coated with a 40 nm thin layer of gold to reduce sample charging. Generally, the SEM microphotographs were collected using an accelerating voltage of 20 kV. The working distance used was in the range of 8 mm to 12 mm.

The resistance to oxidation of unburned carbon was an important parameter in controlling the oxidative wear of the brake lining formed from CCBs. Therefore, we evaluated the oxidation potential of the unburned carbon by conducting DSC measurements at 30°C < T < 720°C under flowing oxygen conditions. The DSC data were acquired on a Perkin-Elmer DSC7 system, interfaced with a PC 486 computer using a UNIX operating system. The DSC was calibrated for temperature and enthalpy [10,11]. The accuracy in temperature between 30°C and 420°C, based on our calibration procedure, was estimated to be ± 1°C. The conditions under which the instrument calibration were performed exactly matched the experimental run conditions, namely the scan rate of 20°C/min, oxygen gas purge at 30 psi pressure.

The frictional behavior of our composites, as well as of a commercial automotive brake pad, was obtained with the help of a FAST machine (see Fig. 1). The main elements of the FAST machine are the drive motor and friction cast iron rotor disk, the pivot and load arm, the clamping assembly, and the control valve assembly. FAST test samples of dimensions 12.7 mm X 12.7 mm X 4 mm were placed in contact with a rotor disk. The motor rotated the rotor disk at a constant speed of 875 rpm. A constant frictional force of 0.61 MPa was maintained on the sample as it rotated against the rotor disk throughout the FAST test.

RESULTS AND DISCUSSION

Figure 2 reproduces the SEM microphotograph of the as-received high LOI fly ash sample. As can be seen from this figure, the physical structure of this fly ash had a typical appearance of

PCC fly ashes, i.e., spherical particles of various sizes. Our attempts to locate and probe the physical structure of unburned carbon particles in as-received high LOI fly ash were not successful since no distinct carbon particles could be recognized in Fig. 2. The FTIR

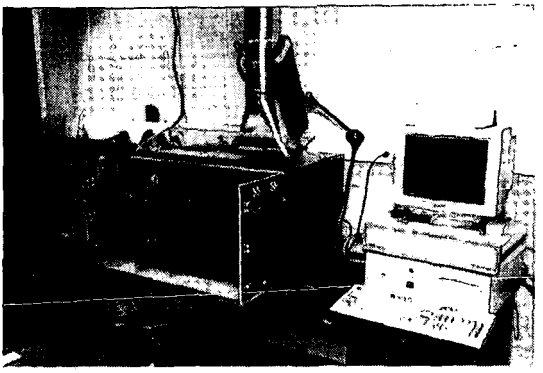

Figure 1. This figure shows the Friction Analysis and Screening Test (FAST) machine used to acquire frictional behavior of our composites.

measurements on as-received fly ash were not helpful either in identifying unburned carbon. Perhaps there were no functional groups in the unburned carbon. It is generally believed that the density of the unburned carbon particles is lower than the spherical fly ash particles. Therefore, we attempted to separate the high carbon particles from as-received fly ash by centrifugation and flotation. Figure 3 shows the SEM microphotograph of the fraction which floated. It has been suggested that the nature of the unburned carbon in fly ash could be different depending upon the utilities which produce them and the initial structure of coal which undergoes combustion. In fact, Graham et al. [12] proposed that the unburned carbon in fly ashes was actually composed of three petrographically fractions, i.e., inertinite, isotropic coke, and anisotropic coke. The inertinite fraction in the unburned carbon represents that part of coal which remained unchanged on combustion. The isotropic and anisotropic fractions of unburned

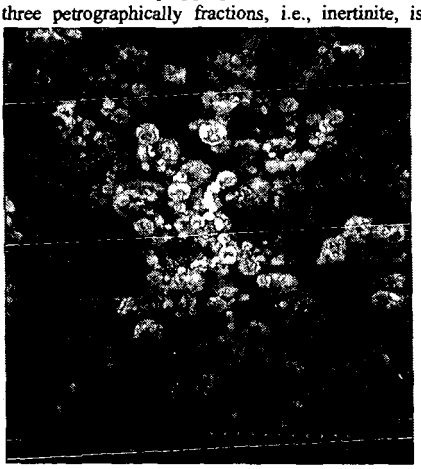

Figure 2. SEM microphotograph of as-received, high LOI PCC fly ash sample. It should be noted that it is difficult to discern the carbon particles in the fly ash.

carbon were those fractions of coal which underwent melting, devolatilization, swelling, and re-solidification during combustion. The isotropic carbon is that carbon which had a high degree of microscopic disorder in its structure, while anisotropic carbon displayed a higher degree of molecular alignment. It is clear from Figure 3 that it is difficult, if not

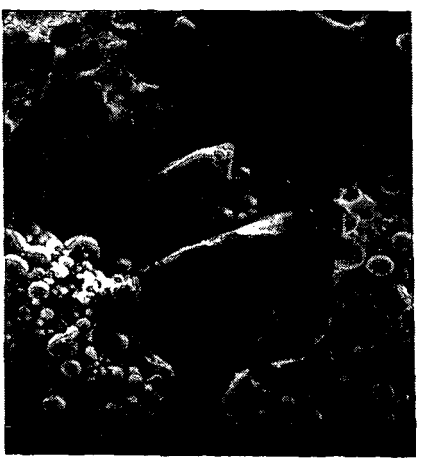

Figure 3. SEM microphotograph of the particles which were recovered from high LOI fly ash by centrifugation and flotation.

impossible, to distinguish these fractions in the unburned carbon. However, our SEM results did suggest that the unburned carbon in the high LOI fly ash was highly porous and had rough-textured spherical particles. Therefore, unburned carbon particles in frictional composites would facilitate breathing of the material especially under frictional application when the overall brake temperature could be as high as 400°C. The easier escape of the gases, which would be produced at T > 200°C in frictional materials due to the decomposition of organic fractions, could reduce the thermal wear of the frictional materials.

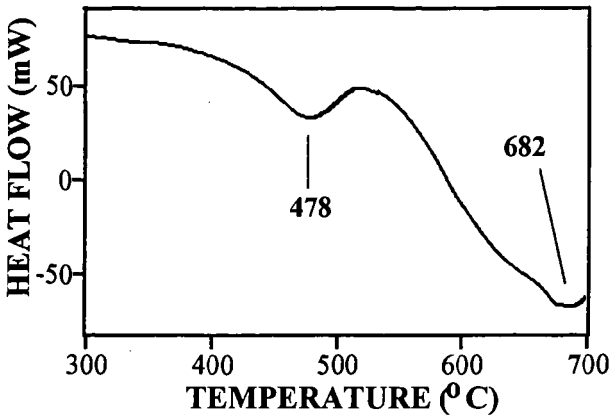

Figure 4: This figure shows the DSC thermograph observed for unburned carbon extracted from high LOI PCC fly ash. The DSC data were collected under flowing oxygen gas conditions.

An important consideration for using unburned carbon in frictional materials would be its resistance to oxidative degradation, especially at temperatures attained by automotive brakes during braking, i.e., T > 250°C. Our DSC measurements, conducted under oxygen gas environment, showed no exothermic reactions at T < 300°C. In the second batch of runs, we first heated the ash samples to 275°C under nitrogen gas purge environment to ensure the samples were free of water. After soaking the samples at 275°C for 10 minutes, the purge gas was switched to oxygen and the sample's temperature was ramped at the aforementioned heating rate. The typical DSC curve observed from extracted unburned carbon is depicted in Fig. 4. The unburned carbon concentrates, extracted from SIPC fly ash, showed four distinct exothermic reactions, i.e., at 478°C, 610°C, 640°C, and 682°C. The exothermic peaks of 610°C and 640°C overlapped between themselves as well as with the main exothermic peak located at 682°C. At present, it is difficult to assign the exact mechanism of the 478°C exothermic peak. Comparative DSC measurements on other fly ashes suggested that the peak at 478°C orginated due to the oxidation of unburned carbon. Since the exothermic reaction of the unburned carbon did not begin until at around 380°C, it appeared that carbon concentrates extracted from fly ashes might be useful additives for automotive brakes.

FAST test results observed for our Basic Matrix composite as well as for a commercial aftermarket automotive brake composite are reproduced in Fig. 5. Generally, unused brake composites show strong variation in the coefficient of friction (μ) in the initial phases of the friction test as material breaks in and its surfaces align with that of the cast iron rotor. Therefore, the variation in μ-value observed in Fig. 5 at time < 10 minutes was attributed to the break in phase. It should be noted that the commercial brake composite μ–value stabilized around 0.3 though it continued to slightly decrease as FAST test time increased. However, this was not the case for our Basic Matrix composite which showed strong variations in the μ-value. The spikes observed in the μ--value could be attributed to the generation of chips from the surface of Basic Matrix composite. The μ–value decreased to about 0.15 towards the end of the FAST run for Basic Matrix.

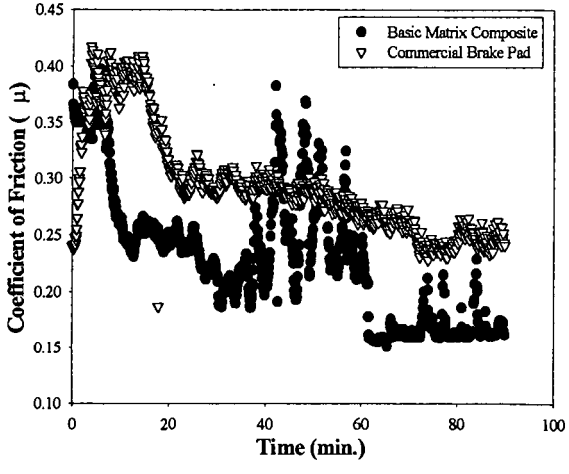

Figure 5. FAST test results obtained from a commercial automotive brake and our Basic Matrix composite.

How the incorporation of 8 volume percent of PCC fly ash, PCC bottom ash, or unburned carbon affected the

frictional behavior of our Basic matrix composite is shown in Fig. 6. After the break in period, the μ–value of composites containing fly ash or bottom ash increased to 0.7. As the time of the test increased beyond 60 minutes, the coefficient of friction decreased for both fly ash and

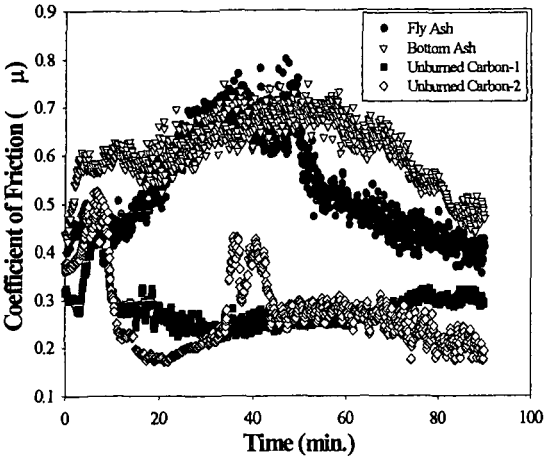

Figure 6. This figure shows how the incorporation of fly ash, bottom ash, or unburned carbon affected the frictional behavior of our composites.

bottom ash containing brake composites. It is important to note that no fade was observed from either of these composites even after 90 minutes of FAST test. The unburned carbon gave much lower μ–value than those observed from fly ash or bottom ash composite. However, the unburned carbon concentrates not only induced considerable stability in the frictional behavior of our composites but also substantially reduced the noise and wear of the brake composites formulated from CCBs.

CONCLUSIONS

The following was concluded: (a) Our SEM experiments on unburned carbon, extracted from a high LOI PCC fly ash, suggested that the unburned carbon from this ash was highly porous and had rough-textured spherical particles. (b) The unburned carbon was resistant to substantial oxidation at $T < 380°C$, with the major oxidation occurring around 480°C. The porous nature and oxidation resistant traits of unburned carbon made them excellent candidates for automotive brake composites. (c) The incorporation of fly ash, bottom ash, or unburned carbon had a strong effect on the frictional behavior of composites formed from coal combustion by-products. The unburned carbon composites gave desired frictional stability and considerably reduced noise.

ACKNOWLEDGMENTS

This work was supported in the initial stage by the Illinois Clean Coal Institute. Authors also acknowledge the support of this work in part by the Center for Advanced Friction Studies (NSF supported center).

REFERENCES:

1. G. J. McCarthy, F. P. Glasser, D. M. Roy, and R. T. Hemmings, (eds.) *Mater. Res. Soc. Sympos. Proc.* Vol. **113**, 1988.
2. L. B. Lee, "Management of FGD Residues: An International Overview.", Proc. 10th Annual Int. Pittsburgh Coal Conf, pp. 561-566, 1993.
3. P. S. Valimbe, V. M. Malhotra, and D. D. Banerjee, D. D., *Am. Chem. Soc. Prep., Div. Fuel Chem.*, 40(4), 776, 1995.
4. J. W. Goodrich-Mahoney, "Coal Combustion By-Products Field Research Program at EPRI: an overview" EPRI (Environmental division), 1994.
5. E. Freeman, Yu-M. Gao, R. Hurt, and E. Suuberg, *Fuel* 76, 761, 1997.
6. R. H. Hurt and J. R. Gibbins, *Fuel* 74, 471, 1995.
7. A. Radisic, P. S. Valimbe, and V. M. Malhotra, *Materials Research Soc. Symp. Series*, **542**, 13, 1999.
8. S. P. Kelley, P. S. Valimbe, V. M. Malhotra, and D. D. Banerjee, *Am. Chem. Soc. Prep. Div. Fuel Chem.*, 42(3) 962, 1997.
9. P. S. Valimbe, V. M. Malhotra, and D. D. Banerjee, *Am. Chem. Soc. Prep. Div. Fuel Chem.*, 42(4), 1123, 1997.
10. R. Mu and V. M. Malhotra, *Phys. Rev. B* 44, 4296, 1991.
11. S. Jasty and V. M. Malhotra, *Phys. Rev. B* 45, 1 (1991).
12. U. M. Graham, T. L. Robl, J. Groppo, and C. J. McCormick, "Utilization of Carbons from beneficiated High L.O.I. Fly Ash: Adsorption Characteristics", 1997 Ash Utilization Symposium, Lexington, Kentucky, USA.

RECOVERY AND UTILIZATION OF FLY ASH CARBONS FOR THE DEVELOPMENT OF HIGH-VALUE PRODUCTS

M. Mercedes Maroto-Valer[1], John M. Andrésen[1], Christian A. Andrésen[2],

Joel L. Morrison[1] and Harold H. Schobert[1]

[1]The Pennsylvania State University, The Energy Institute, 405 Academic Activities Building, University Park, PA 16802-2303, USA

[2] Norwegian University of Science and Technology, N-7491 Trondheim, Norway

Keywords: Fly ash carbons, activated carbons, carbon artifacts.

The implementation of increasingly stringent Clean Air Act Regulations by the coal utility industry has generally resulted in an increase in the concentration of unburned carbon in coal fly ash due to the installation of low-NOx burners. Although nowadays the fate of the unburned carbon is mainly disposal, this carbonaceous material is a very attractive precursor for the production of premium carbon products, since it contains >99% carbon and it has gone through a devolatilization process while in the combustor at temperatures well above 1300°C. Accordingly, this work has investigated two potential routes for the generation of premium carbon products from the unburned carbon present in fly ash. The first route focuses on the use of fly ash carbons as precursors for activated carbons by steam activation at 850°C, while the second route concentrates on the utilization of fly ash carbons as a replacement for calcined petroleum coke in the production of carbon artifacts.

INTRODUCTION

The implementation of increasingly stringent Clean Air Act Regulations by the coal utility industry has resulted in an increase in the concentration of unburned carbon in coal combustion fly ash. In 1998, around 5-8 million tons of unburned carbon were disposed, due to the present lack of efficient routes for its utilization. However, the increasingly severe regulations on landfill and the limited access to new disposal sites with the subsequent rise in the cost of disposal, may demand the utility industry to begin offsetting coal combustion with natural gas, or require additional coal cleaning to remove the ash prior to combustion, or simply start utilizing the unburned carbon. The authors have previously conducted extensive studies on the characterization of unburned carbon and showed that its properties are similar to those of conventional precursors for the production of premium carbon materials [1, 2]. Accordingly, this research program focuses on the development of routes for the generation of premium carbon products from the unburned carbon present in fly ash.

The utilization of fly ash carbons can bring enormous economical and environmental benefits to both the coal and utility industries. Although several technologies have been successfully developed to separate the unburned carbon from the fly ash, only a few power plants have installed a beneficiation process on their sites. This is due to the low value of the resultant separated materials, since a ton of fly ash is generally sold for as little as $10-20, and the unburned carbon is simply disposed or re-routed to the combustor. However, the economics of this process can be greatly enhanced if both separated materials can be used as precursors for value-added products. In fact, this is the case for the unburned carbon, which can be used as an excellent precursor for the generation of premium carbon products, like activated carbons and carbon artifacts. Therefore, the added value generated from the fly ash carbon utilization would clearly offset the cost of the separation process. For instance, the average price for a ton of activated carbon ranges from $500 up to $4000, which implies a potential 25-200 fold increase compared to the price of the ash (<$ 20/tonne). For the case of carbon artifacts, the calcined petroleum coke used for their manufacture usually costs ~ $ 220-250 / ton.

EXPERIMENTAL

Procurement of fly ash samples The fly ashes were collected from Portland station Unit #2 (Northampton County, PA) with a net capacity of 243 MW and operated by GPU Genco. Samples were collected all the way from the economizer through the hoppers to the stack, amounting to a total of 16 samples. The hoppers were emptied prior to collection in order to obtain fresh ash. The carbon contents of the fly ashes were determined according to the ASTM C311 procedure and the fly ash with the highest carbon concentration was chosen as feedstock for the production of the carbon products.

Activation of fly ash carbons The activation of the samples was carried out in an activation furnace, that consists of a stainless steel tube reactor inside a vertical tube furnace, as previously described [3]. Typically 3 g of sample was held isothermally at 850°C for periods of 60 minutes in flowing steam. The porosity of the samples was characterized conducting N_2 adsorption isotherms at 77K using a Quantachrome adsorption apparatus, Autosorb-1 Model ASIT. The BET surface areas were calculated using the adsorption points at the relative pressures (P/P_0) 0.05 - 0.25. The total pore volume, V_{TOT}, was calculated from the amount of vapor adsorbed at the relative pressure of 0.95. The mesopore (pores 2-50 nm in width) and micropore (pores <2 nm in width) volumes were calculated using the BJH and DR equation, respectively.

Manufacture of carbon artifacts The fly ashes with the highest carbon levels (40-50 wt%) were chosen as feedstocks for the beneficiation step conducted prior to the manufacture of carbon pellets. The beneficiation protocol was performed to be able to elucidate the interactions between the unburned carbon and the pitch, that otherwise may be masked by the high ash concentrations, and included first a flotation separation followed by an acid digestion step using a HF/HCl solution to reduce the inorganic content to ~3 wt%. The carbon pellets were produced from mixtures of this concentrated fly ash carbon (CFAC), a petroleum coke (PC) and a coal tar binder pitch (CTBP). The mixtures were heated to ~130°C and pressed into pellets. The absolute densities of the precursors and the pellets were measured by using a Quantachrome MVP-1 Multi Pycnometer with helium as density medium.

RESULTS AND DISCUSSION

Carbon variations between hoppers Fly ash samples were collected from each of the hoppers and Figure 1 shows the configuration and gas flow for the hoppers, and the carbon values of the corresponding fly ashes. The hot-side bins (1-2) present LOI contents of only 10-12%, that become higher for hoppers 5-6 (15 and 19%, respectively) and 9-10 (32 and 36%, respectively) and reach a maximum for the cool-side hoppers 13 and 14 (36 and 50%, respectively). Although this trend also prevails for the train of hoppers 3-7-11-15, it is not so clear, since the LOI values vary only between 14-18%. This "hot-side" and "cool-side" terminology has been adopted from former studies and it is based on characteristics of the respective ashes, where fly ashes from hot-side collectors present characteristics associated with higher temperatures (lower carbon content and larger fly ash sizes) compared to those of their cool-side counterparts [4].

Activation of fly ash carbons Figure 2 shows the N_2-77K adsorption isotherms for three fly ash carbon samples, designated as FAC-A, FAC-B and FAC-C, and illustrates the inherent porosity of these materials. All the adsorption isotherms are Type II according to the BDDT classification and they are typical for nonporous or macroporous adsorbents, on which unrestricted monolayer-multilayer adsorption can occur [2].

Table 1 lists the BET surface areas (SA) and total pore volume (V_{TOT}) for the precursors. The three samples have surface areas between 30-40 m^2/g. Previous studies conducted by the authors on a range of fly ashes and Density Gradient Centrifugation concentrates have shown that the extensive and rapid devolatilization that coal undergoes in the combustor, seems to promote the generation of meso- and macropores [2]. Pore size distribution studies were also conducted and showed that the pore volume is mainly due to mesopores, with the mesopore volume accounting for over 60% of the total pore volume [2]. The solid yields of the three FAC samples activated for 60 minutes are also listed in Table 1. Despite the low particle size of the FAC samples, the solid yields are relatively high, since the FAC has already undergone devolatilization in the combustor. This makes the UC an attractive precursor for the production of activated carbons, since they present much higher solid yields than conventional precursors, such as wood. FAC-A presents higher solid yields than FAC-B (73% vs. 55%), due to their larger particle size (200 μm vs. 45 μm). Previous studies have shown that the particle size of the precursor strongly affects the solid yields of the resultant activated samples, with higher yields for bigger particle size fractions [5].

Figure 3 shows the N_2-77K adsorption isotherms for the three steam activated FAC samples. Although the isotherms now look more like Type I, concave to the P/P_0 axis, that are typical for microporous materials, they do not reach a plateau at high relative pressures, indicating the presence of some meso- and macro-porosity. The activated carbons generated from the samples FAC-A and FAC-B present higher adsorption isotherms than that of FAC-C. This is reflected in FAC-A-Act and FAC-B-Act exhibiting surface areas and pore volumes higher than that of FAC-C-Act (332 and 443 m^2/g vs 110 m^2/g, Table1). This may be due to the lower steam flowrates used for the first two samples, resulting in more favorable conditions for the production of activated carbons. The higher ash content of FAC-C compared to that of FAC-A and FAC-B may also play a detrimental role in the activation of this sample. Further activation studies are being conducted to ascertain the role of the ash in the activation process of the unburned carbon.

Figure 4 compares the meso- and micropore volume for the precursors and the activated samples. As previously described, the inherent porosity of the UC samples is highly mesoporous, with the

mesopore volume accounting for ~ 66% of the total pore volume. The activation process promotes the development of micopores, with the micropore volume now accounting for over 60% of the total. Pore size distribution studies and CO_2 porosity measurements are in progress.

Properties of carbon pellets prepared with fly ash carbons In the preparation of conventional carbon materials, the petroleum coke is used as filler and it is normally separated into at least three different particle size fractions: fine (<200 mesh); intermediate; and coarse (>20 mesh), to obtain improved packing densities. Due to the nature of the combustion process, most fly ashes are milled to the size of the fine fraction or less used for the production of carbon materials. Hence, this study concentrated on the production of carbon pellets, where the fine fraction of petroleum coke was replaced by unburned carbon. Table 2 lists the absolute densities for the carbon pellets produced with the concentrate of fly ash carbon (CFAC), the conventional calcined petroleum coke (PC) and coal tar binder pitch (CTBP). As expected, the density of the carbon pellet A, consisting of 20 wt% coal tar binder pitch and 80 wt% petroleum coke, is slightly lower than that of the petroleum coke itself (1.76 g cm^{-3} vs. 1.89 g cm^{-3}). This is due to the lower density of the CTBP (1.25 g cm^{-3}), and can be derived from direct calculation of the two fractions (0.2*1.25 g cm^{-3} + 0.8*1.89 g cm^{-3} = 1.76 g cm^{-3}). Therefore, for conventional carbon pellets, the CTBP seems to mostly be filling the vacant voids between the PC particles. For pellet B, where all the fine fraction of petroleum coke has been replaced by concentrate unburned carbon, there was a difference between the observed and calculated densities (1.76 g cm^{-3} vs. 1.65 g cm^{-3}). This indicates that there is a synergistic filling effect between the unburned carbon and the coal tar binder pitch, that is reflected in a densification of the carbon pellets produced. This could presumably be related to the higher surface area of the concentrated unburned carbon of ~50 m^2/g compared to that of 5 m^2/g for the calcined petroleum coke, and we are presently conducting further studies to characterize this interaction. These results are very encouraging for further baking of the pellets into artifacts, that is now underway in our laboratory.

CONCLUSIONS

The present work has investigated novel routes for the use of unburned carbon as a high value product. The detailed study of a series of fly ash hoppers has revealed that cool-side bins present the highest LOI values (50%) and therefore they could be suitable hoppers for the collection of high carbon content ashes as precursors for carbon materials. This work has demonstrated the ability of unburned carbon from coal combustion waste to generate activated carbons by steam activation, where after 60 minutes activation time, the unburned carbon samples generated activated carbons with microporous structure and surface areas up to 443 m^2/g. Despite the low particle size of the samples investigated, the solid yields are relatively high, since the unburned carbon has already gone through a devolatilization process in the combustor. The activation process can tailor the inherent mesoporosity of these materials into the desired porosity for a specific application. For the case of the carbon artifacts, although the fly ash carbon presents lower density than petroleum coke, the density of the carbon pellets prepared with unburned carbon is comparable to that using only petroleum coke, probably due to a strong interaction between the unburned carbon and the coal tar binder pitch.

ACKNOWLEDGEMENTS

The authors wish to thank the Consortium for Premium Carbon Products from Coal (CPCPC) at The Pennsylvania State University and GPU-Genco/Sithe Energies for financial support.

LITERATURE CITED

1. Maroto-Valer, M.M., Taulbee, D.N. and Hower, J.C., 1999, Energy & Fuels, **13**, 947.
2. Maroto-Valer, M.M., Taulbee, D.N. and Hower, J.C., 2000, Fuel, In Press.
3. Maroto-Valer, M.M., Andrésen, J.M., and Schobert, H.H., 1999, Prepr. Am. Chem. Soc. Fuel Division, **44**, 675.
4. Hower, J.C., Rathbone, R.F., Robl, T.L., Thomas, G.A., Haeberlin, B.O., and Trimble, A.S., 1997, Waste Management, **17**, 219.
5. Maroto-Valer, M.M., Taulbee, D.N. and Schobert, H.H., 1999, Prepr. Am. Chem. Soc. Fuel Division, 44, 101.

Table 1. Solid yield, BET surface area and total pore volume for the fly ash carbon samples and their activated counterparts.[a]

Sample	Activation time / min	Solid yield / % weight	BET S.A. / m^2/g	V_{total} / cc/g
FAC-A	--	--	40	0.03
FAC-B	--	--	38	0.03
FAC-C	--	--	30	0.02
FAC-A-Act	60	73	332	0.15
FAC-B-Act	60	55	443	0.14
FAC-C-Act	60	79	110	0.04

[a] The solid yields and surface areas are expressed in ash free basis.

Table 2. Absolute densities of the carbon pellets prepared.

Pellet	Composition	Density / g cm^{-3}	
A	20% CTBP, 40% intermediate CFAC, 40% fine PC	1.76[a]	1.76[b]
B	20% CTBP, 40% intermediate CFAC, 40% fine UC	1.76[a]	1.65[b]

[a] Density measured by helium pycnometry.
[b] Calculated density.

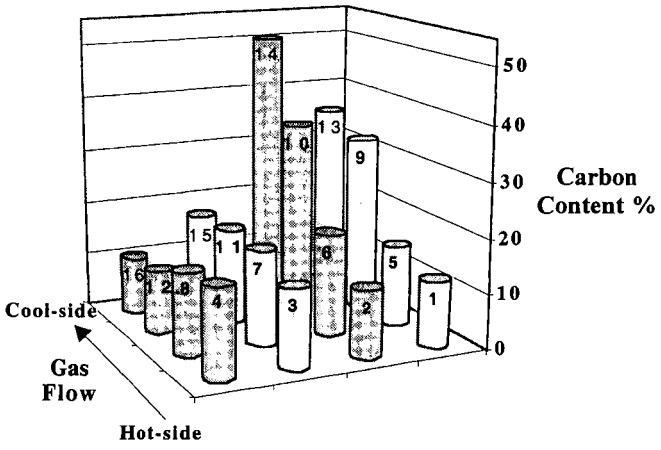

Figure 1. Variation in carbon contents of the fly ashes collected from the different hoppers. The numbers on the bars indicate hopper no.

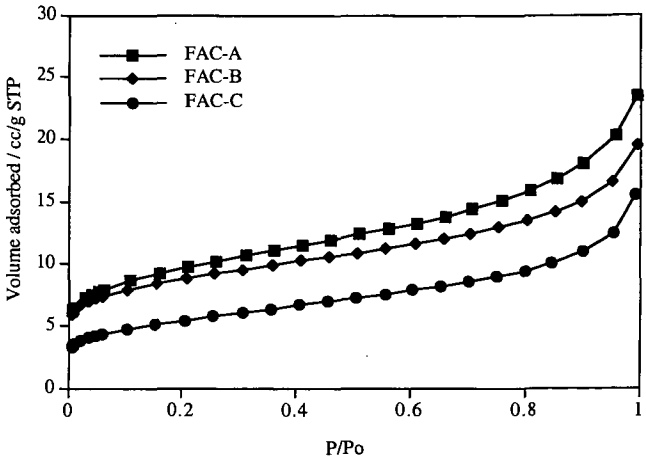

Figure 2. N_2-77K adsorption isotherms for the fly ash carbons.

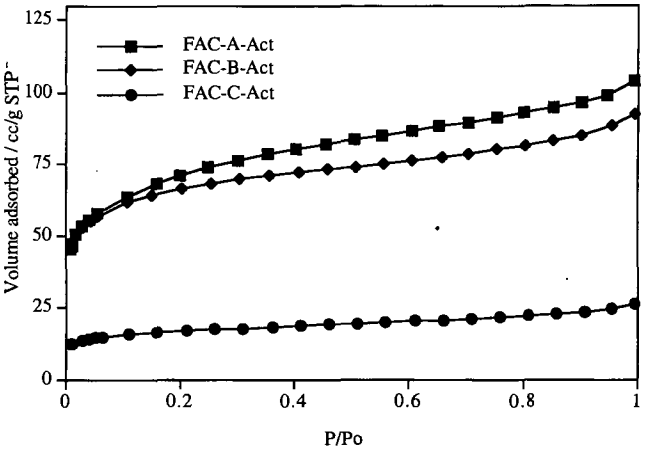

Figure 3. N_2-77K adsorption isotherms for the activated samples.

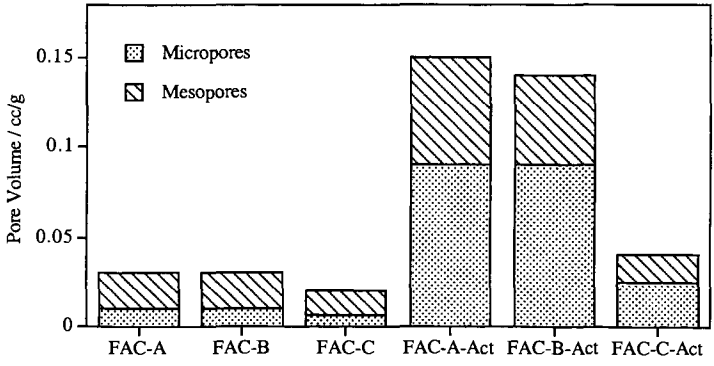

Figure 4. Distribution of the micro- and mesopore volume of the FACs and their activated samples.

Separation and Utilization of Value-Added Products from Combustion Fly Ash

Yee Soong*, McMahan L. Gray, Daniel J. Fauth, Thomas A. Link, J. Richard Jones, James P. Knoer, Kenneth J. Champagne, Michael. R. Schoffstall and Steven S. C. Chuang[1]

U.S. Department of Energy, National Energy Technology Laboratory,
P.O. Box 10940, Pittsburgh, PA 15236
[1]Chemical Engineering Department, University of Akron, Akron, OH 44325

KEYWORDS: fly ash, separation, and utilization

INTRODUCTION

The utilization of power-plant-derived fly ash has an impact on the cost of power production from coal. The usage has been hindered by recent shifts to low NO_x burners which can increase the carbon content of the ash above the specification (ASTM) for its use in cement applications. Due to the drastic changes in the carbon content in the fly ash, post-combustion beneficiation has been a recent focus of research. Beneficiations processes can generate a valuable unburned organic product and inorganic fly ash product, and these two constituents can be collected and used as commercial products. The unburned organic fraction can be recycled back to the burner as a fuel or used as a catalyst, activated carbon, or catalyst support. The purified inorganic fraction can be utilized as a cement additive or the material for synthesizing molecular sieves. Improved beneficiation and utilization schemes for fly ash can transform it from a waste material, with associated disposal costs, to a valuable product.

Researchers at National Energy Technology Center (NETL) over the last several years have developed a dry triboelectrostatic separation technology for the removal of mineral impurities from pulverized coal and fly ash [1]. In addition, NETL's researchers have extended the agglomeration method utilized for coal beneficiation for the recovery of unburned carbon from fly ash [2]. These techniques have recently been applied to the separation of carbon from fly ash to yield an ash rich product that meet specifications for use in cement applications as well as carbon rich products for other novel applications. The focus of current research is to take the resulting separated fractions, from both dry triboelectrostatic and wet agglomeration processes developed by NETL to explore their potential applications (i.e., activated carbon, molecular sieves, catalytic application, and catalyst supports).

One possible application for fly ash is the synthesis of zeolite products: a process analogous to the formation of natural zeolites from volcanic deposits [3]. Both volcanic ash and fly ash are fine-grained and contain a large amount of aluminosilicate. Amorphous aluminosilicates are the major mineral compounds present in Class F fly ash along with other crystalline minerals, including quartz, mullite, hematite, lime, and feldspars. These chemical and mineralogical features make fly ash a good candidate for zeolite synthesis. In natural conditions, these volcanic deposits may be converted into zeolites by the influence of percolating hot groundwater. This process may take tens to thousands of years under natural conditions. Acceleration of this natural process could result in a cost effective, large scale industrial application for fly ash. Within laboratory conditions, this conversion can be expedited to days. The goal of current research is to establish the optimal conditions for the formation of zeolite products from fly ash.

Carbon materials have been used for a long time in heterogeneous catalysis, because they can act as direct catalysts or, more importantly they can satisfy most of the desirable properties required for a suitable support [4]. Among many types of carbon-supported catalysts (graphite, carbon black, activated carbon, etc.), high surface area activated carbon and carbon black are the carbon materials of choice for most carbon-supported catalysts. Thus, novel applications of carbon derived from fly ash are the focus of current research. Carbon as a catalyst support for the NOx reduction reaction and carbon as a catalyst for dehalogenation applications are examined.

Farcasiu et al., [5] reported the catalytic activity of carbon black in selective dehydroxylation and dehalogenation reactions under reductive conditions in the presence of a hydrogen donor. Their work has shown that carbon black can catalyze dehydroxylation and dehalogenation reactions of aromatic compounds only in the presence of a hydrogen donor. Within this study, the catalytic reactivity of the carbon concentrates derived from fly ash was examined for hydrodehalogenation of 1-Bromo naphthalene reactions.

EXPERIMENTAL

The details of the dry triboelectrostatic separators and wet agglomeration column were described elsewhere [1,2]. Fly ash (carbon content of 7.74 wt.%) derived from the combustion of a Black Creek Pittsburgh seam coal was utilized for the preparation of carbon concentrates. The 2 wt.%. Rh on carbon catalysts were prepared by the impregnation of $RhCl_2$ over fly ash derived carbon. The NOx reduction study was conducted in an in-situ infrared cell reactor which was reported elsewhere [6]. Three reaction temperatures, 400, 500 and 650 °C were tested for NOx reduction activities over the Rh catalysts. The dehalogenation reactions were performed in sealed glass reaction tubes, following the previous described procedures [5]. Ratios of substituted aromatic to solvent to catalyst were 1 : 4: 0.1. The H-donor solvent was 9,10-dihydrophenanthrene (9,10-DHP). The reaction was conducted at 350 °C for one hour and the products were identified by GC-MS and quantified by GC, using a procedure described elsewhere [5]. The zeolitization process in its simplest form is a relatively straightforward process. Fly ash from Ohio #6A and Meigs Creek coals were mixed with a hydroxide solution in a Teflon reaction vessel and incubated at ambient pressure and various temperatures. At the end of the experiment, mixtures were quenched and the reaction products recovered by filtration.

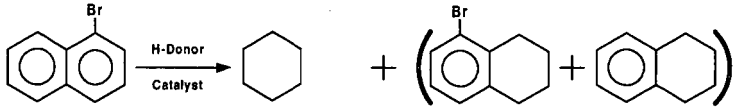

1-Bromonaphthalene

RESULTS AND DISCUSSIONS

Zeolite synthesis

An initial study using fly ash focused on synthesizing zeolites/zeolitic materials by hydrothermal activation heating. Samples of fly ash were collected by electrostatic precipitation during the combustion of Ohio #6A and Meigs Creek coals. Each sample was sieved through a 100 mesh Tyler screen and calcined at 750°C in air before being analyzed by atomic absorption spectroscopy. SiO_2 and Al_2O_3 were the major components and are the most important reagents for zeolite synthesis. Other crystalline phases identified included mullite ($Al_6Si_2O_{13}$), quartz (SiO_2), hematite (Fe_2O_3), and lime (CaO).

Each fly ash was activated by NaOH and KOH solutions in a closed system. The activations were conducted using a number of Parr digestion bombs equipped with Teflon reactors. Table 1 shows the zeolite synthesis route investigated. Typically, 10.0 g of fly ash was combined with 12.0 g of alkali hydroxide and placed into a covered platinum crucible and slowly heated to 550°C in a muffle furnace. After one hour, the resultant fused fly ash/NaOH mixture was then cooled to ambient temperature and re-ground. About 6 g of fused fly ash/NaOH powder was added to 30 mL of deionized water in a closed Teflon reactor and agitated for 24 hours at room temperature. After aging the solution, the Teflon reactor was then sealed and heated to 100°C without stirring for 48 hrs. The precipitates were filtered, washed repeatedly with deionized water, and dried overnight at 105 °C.

Table 1. Zeolite Synthesis Route

1. Fly Ash - 1.0 part by weight + NaOH or KOH - 1.2 part by weight
2.Treated in air at 550 degrees C for 1 hour
3. Ground fused fly ash to powder
4. Dissolution in distilled water
5. Aging of solution with stirring for 24 hours
6. Heat treatment and precipitation of zeolitic material

Physical synthesis of converted Ohio #6A and Meigs Creek fly ashes into zeolite by utilizing only the supernatant of the dissolved fused powder solutions was completed. Alternate zeolite synthesis path (Table 2) illustrates the systematic approach taken to create a higher surface area material.

Table 2. Alternate Zeolite Synthesis Route

1. Fly ash 1.0 part by weight + NaOH or KOH 1.2 part by weight
2. Treated in air at 550°C for 1 hour, ground to powder, fused fly ash powder
3. Dissolution of fused fly ash powder in distilled water
4. Separation of fused fly ash from supernatant
5. Addition of aluminum hydroxide
6. Aging of supernatant/aluminum hydroxide solution with stirring for 24 hours
7. Heat treatment of supernatant/aluminum hydroxide solution
8. Precipitation of pure zeolite material

Fusion of NaOH (or KOH) with either the Ohio #6A or Meigs Creek fly ash prior to the aging and heat treatment steps produce high amounts of silicates and aluminosilicates, which can be easily dissolved in aqueous solutions. In utilizing the separate •Separation of Fused Fly Ash from Supernatant• step, the formation of zeolite-P is desired. A pre-determined amount of aluminum hydroxide was added after the separation of the mother liquor from the fused fly ash powder sediment. Previous studies by others have shown that Al species may be the controlling parameter in the synthesis. In comparison to the products (NaP-type zeolite) synthesized earlier, the crystalline materials obtained from this alternate synthesis path are significantly lighter in appearance (white in color), due to the absence of unreacted fly ash in solution (green in color).

The specific surface areas of the original Ohio #6A fly ash and its fused NaOH-treated counterpart produced previously were also characterized. The Ohio #6A fly ash was found to have no appreciable surface area, i.e., less than 1 m^2/g. Alternatively, the NaOH-treated fly ash/zeolitic material had a specific surface area of 81 m^2/g. Surface areas obtained from the KOH-treated fly ash/zeolitic and Meigs Creek samples were very similar (74 m^2/g for synthesized zeolite) in comparison to the treated Ohio #6A ash. It is envisioned that the fusion of Meigs Creek ash with KOH will result in zeolite formation at lower temperatures and in less time than with NaOH. Also, the increased effectiveness of KOH should contribute largely to increasing nucleophilicity as the counter cation increases, resulting in a greater dissolution of amorphous aluminosilicates and silicates in the fused fly ash solutions.

Hydrodehalogenation

Carbon concentrates generated from NETL fly ash along with a commercial activated carbon (Black Pearl 2000) were examined for the catalytic activity in hydrodehalogenation of bromine from 1-bromonapthalene. Five samples received from an oil agglomeration column with carbon concentrations from 37.7 % to 67.3% along with five commercial activated carbons with similar carbon concentrations by diluting with SiO_2 beads were used in the study. The results are illustrated in Figure 1. It appears that the activities of the carbon samples generated by agglomeration and the commercial activated carbon samples are comparable. The increase in carbon concentration correlates with an increase in dehalogenation activity.

NOx reduction

The investigation of unburned carbon material as a catalyst support was conducted in collaboration with the University of Akron. NETL laboratory produced carbon samples from the fly ash derived from the combustion of a Pittsburgh bituminous coal. The University of Akron explored the catalytic properties of the carbon concentrated for NOx reduction.

A 2 wt.% Rh on NETL carbon catalyst was prepared by impregnation of $RhCl_2$ over the carbon support. The Rh-Carbon catalyst was first reduced in H_2 at 400 °C then exposed to He before exposed to the reactant (1% NO in He). Three reaction temperatures 400, 500 and 650 °C were tested for NOx reduction activities. As illustrated in Figure 2, the immediate production of N_2 (m/e:28), N_2O (m/e:44) and O_2 (m/e:16) after the introduction of NO to the reactor suggest the reactivity of the catalyst. Almost 100 % conversion of NO was observed after exposing to NO at 650 °C. Preliminary results from the University of Akron indicate that the carbon samples from

NETL do show the catalytic activities for NOx reduction.

CONCLUSIONS

Products derived from fly ash were explored for their potential applications as molecular sieves, catalytic applications, and catalyst supports. The fly ash derived zeolite with up to 75% conversion was prepared by the developed zeolite synthesis technique. X-ray diffraction analyses from the prepared zeolite are in accord with that of the natural zeolite-P. The fly ash derived carbon demonstrated good activities for hydrodehalogenation of bromine from 1-bromonapthalene. Furthermore, the NETL carbon based Rh catalyst showed a good activity for NOx reduction.

REFERENCES

1. Soong, Y., Schoffstall, M. R., Irdi, G. A., and Link, T. A., Proceedings of the 1999 Int. Ash Utilization symposium, pp 548-553, Oct. 18-20, 1999, Lexington, KY.
2. Gray, M. L., Champagne, K. J., Soong, Y., and Finseth, D. H., Proceedings of the 1999 Int. Ash Utilization symposium, pp 603-608, Oct. 18-20, 1999, Lexington, KY.
3. G. Steenburggen and G. G. Hollman, J. of Geochemical Exploration, 62, 305-309 (1998)
4. F. Rodriguez-Reinoso., Carbon Vol. 36, No. 3, 159-175 (1998)
5. M. Farcasiu, S. C. Petrosius, and E. P. Ladner , J of Catalysis 146, 313-316 (1994)
6. Chuang, S. S. C., Brundage, M. A., Balakos, M. W., and Srinivas, G., Applied Spectroscopy, vol. 49, 1152 -1163 (1995)

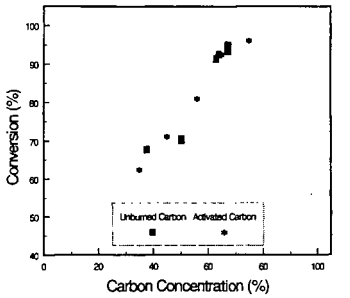

Fig. 1. The Effects of Carbon Concentrates on Dehalogenation Activities

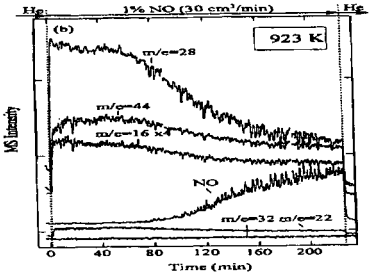

Fig. 2. The reaction of NO over Rh-Carbon catalyst

VALUE ADDED TECHNOLOGY FOR STRIPPER OIL AND GAS WELL BRINES

Robert W. Watson
The Pennsylvania State University
Petroleum and Natural Gas Engineering
125 Hosler
University Park PA 16802

Introduction

The Appalachian Basin oil and gas industry is composed primarily of independent producers operating stripper oil and gas wells in New York, Ohio, Pennsylvania and West Virginia. The wells operated by these independents produce very small quantities of crude oil and natural gas and small volumes of brine. This brine has historically been viewed as a waste product and proper disposal of it is a significant portion of the cost attendant to well operation. In many areas of the United States the brine is disposed of by injecting it into hydrocarbon and/or non-hydrocarbon bearing formations that are both porous and permeable. The Environment Protection Agency (EPA) regulates this subsurface disposal of brine using well injection. EPA categorizes these injection wells to be either Class I or Class II wells. Class I wells according to EPA guidelines[1] are considered to be "technically sophisticated wells that inject large volumes of hazardous and non-hazardous wastes into deep, isolated rock formations that are separated from the lowermost underground source of drinking water (USDW) by many layers of impermeable clay and rock." Class II wells inject fluids (brines) associated with oil and natural gas production. This category of injection wells includes wells that are used for enhanced recovery of oil and gas. The process of enhanced recovery amounts to the injection of fluids such as brine, gas or steam into hydrocarbon bearing zones and thereby recovering oil and gas that would otherwise be unrecoverable. The prerequisite for both Class I and II wells is a formation with adequate permeability and porosity. Permeability is the rock property that defines the rate at which fluid can be injected into a formation. In theory, higher-pressure differentials between the well bore and the formation result in higher injection rates. Limits with respect to pressure differential are imposed by regulations set forth by the EPA. Porosity is a measure of the capacity or voidage space of a rock and along with formation thickness and areal extent define the capacity of the formation. In many areas, there exist no formations that can be used with either Class I or Class II wells and as a consequence alternative methods of disposal are used.

One such alternative method is to treat produced brines in a wastewater treatment facility to remove suspended oils and greases, suspended solids, and heavy metals such as iron prior to discharge into surface water. Commercial brine treatment facilities[2] of the type located near Franklin, Pennsylvania, and Indiana, Pennsylvania, provide this service to local producers in southern New York and Central Pennsylvania. Transport of the brine to these facilities is by over-the-road tanker. This method of brine disposal is expensive and from an environmental management viewpoint, recovery of this resource is a more desirable alternative. For example, approval has been received to use these brines for stabilizing unpaved rural roads and in conjunction with State Transportation Departments, deicing[3]. There is no charge to the producer for the disposal of brines used in these applications. Efforts to find other uses for these brines that would result in at least a break-even proposition for producers are underway at The Pennsylvania State University.

Use of Produced Water in Hydrofracturing

Hydrofracturing is a technique of stimulating oil and gas wells. Economides et al.[4] describes it as consisting of injecting fluid into the formation with such pressure that it induces the parting of the formation. After failure of the rock, the sustained application of the hydraulic pressure extends the fracture outward from the point of failure. Proppants are added to the fracturing fluid to hold open the created fracture after the hydraulic pressure used to generate the fracture is relieved. The fluid used in this process can be very simple or quite complex and the amount of fluid used in the process can vary from a 1,000-gallons to over a 500,000-gallons. Fluids commonly used include water, diesel oil and gases such as Nitrogen and Carbon Dioxide. Material used for propping the fracture include well-sorted sand and spheres composed of ceramic or Bauxite. The amount of proppant used depends on the formation to be fractured. The

capability of the fluid to carry proppant is dependent upon the viscosity of the transport fluid. If the fluid used is water, a guar-derivative such as hydroxypropyl guar (HPG) or carboxymethylhydroxypropyl guar (CMHPG) is added to produce the appropriate viscosity. Other materials added to this fluid can include:

- Biocides – these materials are added to treatment water to control bacterial contamination. There are two types of microorganisms found in water base fluids: aerobic, which consume water base polymers during surface storage, and aerobic, sulfate reducing microorganism that destroy the polymer and produce hydrogen sulfide down hole.
- Gel breakers – used to chemically degrade the guar polymer and thereby reduce its viscosity.
- Surfactants – added to the fluid to reduce surface tension and capillary pressure in pore spaces.

The equipment necessary to hydrofracture a well is significant. Typically, positive displacement pumps capable of moving large volumes of fluid-sand slurries at high pressures are used. These pumps discharge the fluid-sand slurry into a network of high-strength steel piping that is attached to the wellhead. Additional equipment includes trucks to transport and feed the proppant. The capital, operating and maintenance costs associated with this equipment are significant. Consequently, the typical producer purchases the process and materials as a turnkey service.

A gas well drilled in the Appalachian basin penetrates multiple pay zones. These pay zones are Devonian age porous and permeable sandstones. Geologically, these sandstone reservoirs are separated by impermeable shale. The operator typically will select as many as five pay zones in each well for completion. Each pay zone is then isolated and hydrofractured as a separate unit. After drilling to the target depth, casing is run into the well and the annulus space between the casing and drilled hole is filled with cement. The casing adjacent to the zone to be completed is perforated. Perforating is accomplished by lowering into the well a perforator that fires electrically detonated shaped charges from the surface. Clean up of the perforation is accomplished by spearheading the hydrofracturing process with Hydrochloric acid.

The fluid of choice in the Appalachian basin for hydrofracturing is fresh water. Fresh water is used for economic reasons and generally; it is readily available from ponds, streams and/or rivers. Recently however, the Appalachian basin has experienced a regional drought. Independent producers have experimented with using untreated produced brine as a total substitute for fresh water or by mixing the fresh water with brine. Preliminary studies have indicated that it can be used as a replacement for freshwater and the results of the hydrofracturing have been positive.

There are significant questions with respect to the impact of the use of these brines on the productivity of formations. This is particularly true if the brine is used in repeated applications. It is reasonable to expect that the brines will reach a point where their effectiveness will be reduced and their use will result in significant damage to the formation where used.

Mineralogy of Formations

Numerous authors[5, 6, 7] have investigated the impact of injected fluids on the clays contained in sandstones. The impact is negative in that it tends to reduce the native permeability of the formation. This reduction in permeability may result from clay swelling and/or mechanical breakdown. For this reason, Potassium Chloride is often added to fresh water before hydrofracturing. This procedure of adding Potassium Chloride was suggested by Black and Hower[6] and is commonly used in the Appalachian basin.

Clays are negatively charged. The density of negative charges can be measured by determining the number of positive charges required to neutralize the clay crystal. This is known as the cation exchange capacity (CEC) of the clay and is expressed in milliequivalents (ME) for 100-grams of clay. The table below lists the CEC of several clays[8]. The replacement of one cation by another on any clay is governed mainly by the

Cation Exchange Capacity of Selected Clays and Sand	
Clay	Range of Cation Exchange Capacity
Smectite	80 to 150
Illite	10 to 40
Kaolinite	3 to 15
Chlorite	10 to 40
Sand (2 to 62 microns)	0.6

Law of mass action and the valence of the cation. Generally, where monovalent and divalent cations are present in the same concentration, the divalent cation will be preferentially attracted to the clay. The physical effect of this phenomenology is that the introduction of freshwater into a clay system will result in permeability damage and a reduction in production. For this reason, Potassium Chloride is added to the fresh water. Among common monovalent cations, potassium has been shown to be more effective than sodium as a method for mitigating clay swellage and damage.

The impact on the clay contained in these formations of using formation brine as the hydrofracturing fluid is not known. In other producing areas, hydrocarbon (oil and gas) and brine from one formation are produced to the surface. The brine is separated from the produced hydrocarbons and often used in drilling and completions effort. In the Appalachian basin, wells penetrating the Middle Devonian sandstones, the hydrocarbons and brines from multiple formations are produced as a commingled stream to the surface through a common well bore. The commingled brine stream is separated at the surface and stored in steel tanks. It is this brine that is used for stimulation purposes.

Hydrofracturing a Middle Devonian Well

The brine used for Hydrofracturing a Middle Devonian well is delivered to the well to be stimulated by over the road tankers. It is pumped into an open-pit that has been lined with an impermeable plastic liner. A centrifugal pump is used to feed the suction side of the positive displacement pumps. The various chemicals and proppants are mixed and added to the brine and displaced into the well at volumetric flow rates of 800-1000 gallons/minute. At the completion of the first stage, the slurry is flowed back into the pit and the process repeated again using the same fluid. This fluid now contains a complex array of chemicals and "solid fines" that are made up of attrited proppants and shale. During each stage, additional chemicals are added and the amount of attrited proppants and shale increases.

Investigation

The purpose of the study is to determine the effect of using these brines in the stimulation process on the ultimate recovery of natural gas from Middle Devonian reservoirs located in the Appalachian basin. There are several questions that need to be answered concerning this procedure. These questions include:

- Given the fact that the mineralogy of each formation is unique, what is the impact of injecting commingled brine into these formations in terms of its impact on the clays contained therein?
- What damage to formation permeability results from the recycling of brine from one stage to the next?
- What damage to formation permeability results from the use of brine that contains micron size "solid fines"?
- What is the impact of this process on ultimate natural gas production and the economics of well development?

To answer these questions, a work plan was developed. The elements contained in the work plan are as follows:

- Five wells will be selected for the analysis. Prior to setting casing in the well bore, sidewall cores of the formations to be hydrofractured will be obtained. The mineralogy of these cores will be determined. Representative brine will be displaced through the cores and the effect on permeability of the brine evaluated.

- The flow-back from each hydrofracture stage will be collected and analyzed to determine changes in the brine given the addition of the chemicals used in hydrofracturing and the presence of solid fines.
- Historical production data will be analyzed to determine any measurable effects of stimulation on ultimate production.

It is expected that this study will be undertaken during the 2000-2001 drilling cycle. A final report is expected during the third quarter of 2001.

Summary

The recent regional drought has created a situation where water necessary for stimulating gas wells was scarce. Independent producers in the Appalachian basin replaced the freshwater used for stimulation with brine that had been produced from existing production wells in the area. The results of this replacement procedure require an assessment to determine whether the procedure impacts ultimate recovery of the natural gas contained in these reservoirs. Moreover, an evaluation of the procedure needs to be undertaken to determine whether changes to it are in order. To accomplish this analysis, a systematic study has been proposed and will be undertaken. Elements of the study include analyses of the rock cores and hydrofracture fluids, and analysis of gas production data.

Bibliography

1. United States Environmental Protection Agency, Office of Ground Water and Drinking Water, "Types of underground injection wells," EPA web site, May, 2000.
2. Adamiak, R.: "Franklin Brine Treatment Plant." Paper presented at the Ohio Oil and Gas Association Technical Meeting, October 13, 1987.
3. Atkinson, J.F., Matsumoto, M.R., Bunn, M.D. and Hodge, D.S.: "Use of Solar Ponds to Reclaim Salt Products from Brine Waters from Oil and Gas Well Operations in New Work," Proceedings of the 1992 International Produced Water Symposium held February 4-7, 1992, in San Diego, California, Edited by James P. Ray and F. Rainer Engelhardt, Plenum Press, New York and London, pp. 535-547 (1992)
4. Economides, M.J., Watters, L.T. and Dunn-Norman, S.: "Petroleum Well Construction, John Wiley & Sons Ltd, West Sussex, England, 1998, p. 473.
5. Weaver, C.E.: "The Clay Petrology of Sediments," Clays and Clay Minerals, (1970) V. 18, 165-177.
6. Black, H.N. and Hower, W.F.: "Advantageous Use of Potassium Chloride Water for Fracturing Water Sensitive Formations," API Paper No. 851-39-F presented at Wichita, Kansas, April 3, 1965.
7. Hower, W.F.: "Adsorption of Surfactants by Montmorillonite," Clays and Clay Minerals, (1970) V. 18, 97-105.
8. Modern Completion Practices, pp. 9-60 to 9-61, Halliburton Company, (1985).

Adsorption of SO_2 and NO_x by Zeolites Synthesized from Fly Ash, Cement Kiln Dust and Recycled Bottle Glass

Suman Bopaiah and Michael W. Grutzeck
Materials Research Laboratory
The Pennsylvania State University
University Park, PA 16802

Introduction

Natural and synthetic zeolites (molecular sieves) can adsorb SO_2 and NO_x from flue gases. Unfortunately their cost ($500-$800 per ton on the East Coast) has deterred their use in this capacity. It has been shown however, that zeolites are relatively easy to synthesize from a variety of natural and man-made materials. The overall objective of the current work was to evaluate the feasibility of using zeolites synthesized from fly ash, cement kiln dust and other recycled materials to adsorb SO_2 and NO_x from flue gases.

Background

Zeolites occur naturally. Normally they are associated with volcanic ash deposits such as those found in Italy, Japan and the West Coast of North America. The ash forms during explosive volcanic eruptions such as the Mount St. Helens eruption a few years ago. The ash that forms during the explosion consists of very fine-grained particles of glass that are rich in alumina and silica. Because of their nature, the ash particles are very reactive. Those that deposit into alkaline lakes will slowly convert into zeolites. In the presence of water and caustic (sodium and/or potassium), the ashes react to form a wide variety of zeolites.

The synthesis of zeolites in a commercial setting is relatively straightforward. Reactive reagents are also used (sodium aluminate, sodium silicate, silica), but in this instance higher temperatures and more concentrated caustic solutions shorten the synthesis process from hundreds of years to a matter of hours or days. If one now begins to think about the potential of using industrial waste products as a source of starting materials for zeolite synthesis, one soon begins to realize that the list can contain a wide variety of materials. For example, aluminosilicate glasses with compositions similar to volcanic ash include fly ash and recycled glass cullet. If one looks for sources of caustics one can add cement kiln dust and a variety of caustic waste streams.

Synthesis procedures are straightforward: add caustic to aluminosilicate glass, allow the mixture to soak to develop precursor gel structures, and then cure at elevated temperatures ranging from 60° to 180°C. Heating the sample causes it to crystallize. The process is well documented for fly ash. More than a dozen papers are available in the literature (1-14). In addition, LaRosa et al. (15,16) and Grutzeck and Siemer (17) found that zeolites Na-P1, X and Y tended to form readily. Adding cement kiln dust (CKD) could alter bulk compositions. The high concentration of potassium in the CKD tended to reduce the need for sodium hydroxide. Recycled bottle glass provided an inexpensive source of sodium silicate (18).

Zeolites normally form on the surfaces of the fly ash particles. Once formed, the zeolites can be used for a wide variety of applications. For example some have been tested for their ability to adsorb ammonia from solution (18). It has been proposed that they be used for wastewater clean up in storm runoff impoundments and sewage treatment plants. Once loaded, they can be used as fertilizer and soil conditioner. These zeolites are also useful for adsorbing gasses such as SO_2 and NO_x from flue gases. Experiments have shown that the proposed technology is viable. Those samples cured at 150°C normally contained analcime while those synthesized at 90°C contained zeolites X, Y and NaP-1. Results suggest that SO_2 removal is 100% efficient until breakthrough and that even after breakthrough some additional adsorption takes place for a significant amount of time. Results also suggest that uptake efficiencies improve in the presence of water vapor. This is an important finding in as much as flue gas contains approximately 10-volume % water vapor. Capacity of zeolites for SO_2 ranged from 10 mg SO_2/gram to 120 mg SO_2/gram. These values are within the range reported in the literature for natural and synthetic zeolites.

Experimental Methods

Normally zeolites were synthesized from fly ash with additions such as ground glass cullet and cement kiln dust. The chemistry is quite forgiving. Phases that form are determined by the bulk chemistry. Variations tend to cause different amounts of the phases to form rather than radically differing phases. The materials are mixed together in the dry state and ball milled with ceramic balls overnight. The resulting powder is then mixed with sodium hydroxide solution, allowed to soak, and then reacted at 90-180°C for a few days. Yields are on the order of 30%

zeolite. The remainder is mullite quench crystals, carbon, iron oxides and unreacted fly ash. The zeolites are filtered and rinsed on filter paper. Then they are ground and dried at 120°C.

Results

Uptake of SO_2 and NO_x was measured using a flow through test apparatus in which a synthetic flue gas containing 2000 ppm $SO_2$was passed through a packed bed of various zeolites. The effluent gas was analyzed for SO_2 and NO_x using a Varian 2000 UV/VIS spectrophotometer. The adsorption of SO_2 and NO_x can be followed using their characteristic adsorption band at 284 and 380 nm. Each sample (air-dried, 120°C oven dried, or microwave dried) was tested by first recording a baseline SO_2 concentration in the stack gas by passing the stack gas through the empty adsorption unit (without the zeolite sample). Glass wool was used to seat the sample within the U-tube and so that the finely ground particles of the zeolite would not get entrained in the stack gas exiting the U-tube and entering the spectrophotometer. See Figure 1. As expected, there was little significant adsorption of SO_2 by the glass wool. Second, 1g of zeolite was weighed and placed in the U-tube between two glass wool plugs. The stack gas was passed through the sample at ~ 4 cc/min and the changes in adsorbance were recorded by the spectrophotometer. The procedure was repeated for each of the three types of dried samples (air dried, oven-dried at 120° C, and microwave dried). Between runs, the system was purged with N_2 gas to establish a SO_2 free baseline. The breakthrough curves were used to theoretically estimate the amount of the SO_2 removed. In as much as SO_2 content is known and total gas passed prior to breakthrough, the amount of SO_2 adsorbed can be calculated. As a check, some of the spent samples were analyzed for total sulfur content and the results obtained were compared to the theoretical calculation of SO_2removed.

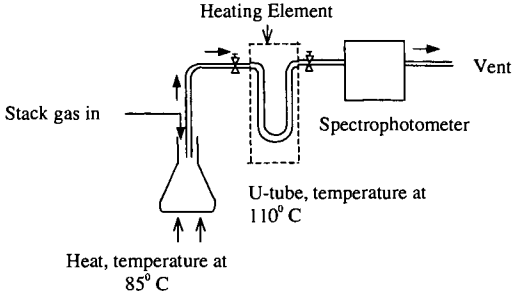

Figure 1. Details of steam generator used to mix water vapor with the simulated gas stream. Tubing running from the tanks to the glass cells was constructed of 5mm stainless steel to insure gas tightness at the ~5psi pressure needed to pass the gas through the packed bed. This set up allowed samples to be tested with or without water vapor present.

Zeolite samples that exhibited a high SO_2 capacity were also tested using the same experimental set-up with the exception that water vapor was introduced into the system. The water vapor source consisted of a 250 ml Pyrex beaker filled with a pre-weighed amount of distilled water kept at ~85°C between the flow meter and the U-tube. See Figure 1. Also, the U-tube sample holder was encased in glass wool and the temperature maintained at 110°C with heating tape to prevent any condensation of the water vapor passing through it. Once again SO_2 as ppm versus time was recorded and as a check, selected samples were chemically analyzed for their total sulfur content before and after they were tested to compare the change in sulfur content. Results are given below.

Adsorption by air-dried samples

Adsorption was first carried out in the absence of water vapor in the influent stack gas. After removing a zeolite sample from its reaction vessel, it was washed with deionized water to remove excess alkali, and then dried in room temperature air. One gram of the zeolite was weighed out and finely ground with a mortar and pestle and placed in the sample holder between plugs of glass wool. Initial tests were conducted with the background SO_2 concentration being

recorded for reference. The sample of zeolite depicted in Figure 2 showed a reasonable amount of SO_2 uptake. The break-through curve exhibited a maximum (100% SO_2) uptake for ~25 minutes.

In the next test, before introducing the sample, water vapor from the Erlenmeyer flask maintained at 85°C (Figure 1) was mixed with the gas and allowed to flow through the system. In this case, a dramatic increase in the adsorption capacity of the zeolite was seen due to the presence of water vapor. See Figure 2. Complete removal of SO_2 molecules from the influent stack gas and steam occurred for about 86 minutes after which SO_2 removal continued to occur, though 100% removal was not seen beyond that point. Sulfur analyses of the air sample tested in the presence of water vapor showed SO_2 concentrations of 10 wt% which is roughly in agreement with SO2 uptake calculated

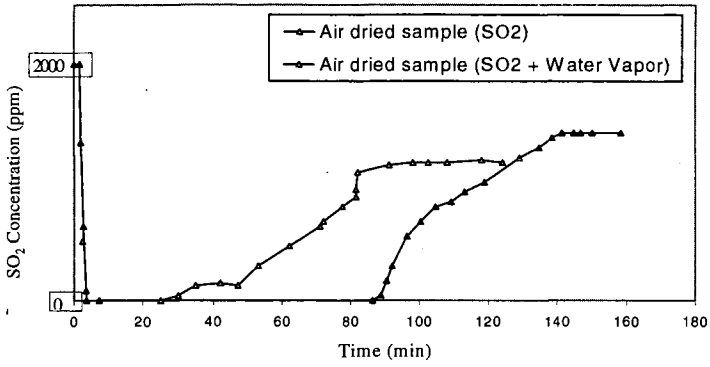

Figure 2. Breakthrough adsorption curves of air-dried zeolite sample (unknown phase) made with Class F+C fly ash, cement kiln dust and silica fume and then used to treat a simulated stack gas of (a) 2000 ppm SO_2 (~25 min to breakthrough) and (b) 2000 ppm SO_2 plus saturated water vapor (~86 min to breakthrough). Flow

from the graph in Figure 2.

Adsorption by samples dried at 120°C

Similar tests were carried out with complimentary samples that were dried at 120 °C overnight. These samples (same as above) also showed an increase in adsorption in the presence of saturated water vapor. The sample showed complete adsorption in the absence of water vapor for 8 minutes but this value increased in the presence of water vapor to 23 minutes as shown in Figure 3. This again shows the increase in SO_2 uptake in the presence of water vapor. Sulfur analyses of the oven dried sample tested in the presence of water vapor showed SO_2 concentrations of 6 wt%. Surprisingly, the degree of pre-drying had a negative impact on the adsorption capacity of the zeolite.

Discussion

In the case of the air-dried samples, the dramatic increase in adsorption in the presence of water vapor is thought to occur due to the dissolution of the SO_2 molecules in the water molecules adsorbed on the surface of the zeolite sample. Subsequently, oxidation of the SO_2 molecules to sulfate and sulfite might have occurred at the temperature of 120 °C, which was constantly maintained. This oxidation of SO2 molecules is known to be temperature sensitive as previously observed by Tsuchai et al. (19) using an absorbent prepared by coal fly ash, calcium oxide and calcium sulfate. In

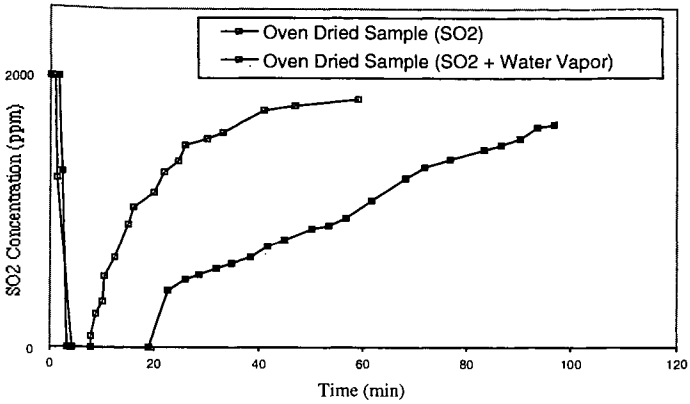

Figure 3. Breakthrough adsorption curves of same oven-dried zeolite sample with simulated stack gas of (a) 2000 ppm SO2 (~8 min to break-through) and (b) 2000 ppm SO2 and saturated water vapor (~23 min to breakthrough). Flow rate ~4 cc/s. Calculated uptake of 23 minute breakthrough sample=3 wt%.

this study, Tsuchai et al. proposed that a monolayer of water is formed at the surface of the absorbent in the presence of relative humidity. Above the monolayer, SO_2 dissolves in the layer while below the layer, SO_2 forms calcium sulfate due to the presence of NO and the chemical composition of the absorbent used.

In the case of the oven-dried samples, possibly, the structure of the zeolite might have undergone changes due to the overnight heating at 120°C. Though this might have occurred, an increase in adsorption was still seen in the case of the sample subjected to water vapor. This could be due to the sulfur dioxide oxidation occurring mainly at the surface of the sample rather than deep in the interior cages and channels as for the air dried sample.

Summary

A graphic representation of SO_2 adsorption results in milligrams SO_2 adsorbed per gram of tested zeolitic material is given in Figure 4. The results are typical of those obtained for air and microwave dried zeolites synthesized at •100°C. One sample (NaP-1) was regenerated by heating it in air. It was regeneratable, but less effective at adsorbing SO_2 the second time around. As seen in Figure 4, zeolites used to extract SO_2 from the simulated stack gas in the presence of water vapor could adsorb nearly 120 mg of SO_2/gram of sample. Also, surprisingly enough, zeolite samples that initially contained water (those that were air dried versus those that were dried at 110°C) tended to adsorb more SO_2 than their "drier" counterparts. Note, however, that microwave drying (MW in table) tended to increase SO_2 capacities for identical samples (oven versus microwave dried) of clinoptilolite and phillipsite run in a non-water vapor containing atmosphere. The effect of microwave drying is still being investigated, as data seem to be contradictory at this point in time.

One interesting observation was the fact that these fly ash-based zeolites were also able to adsorb NO_2 from a gas mixture containing 2000 ppm NO_2 (balance N_2). The sample in question was reacted at 90°C for 56 days. It was non-crystalline (X-ray amorphous) which is notable in as much as adsorption is usually correlated with crystallinity. Perhaps, short-range order is enough to capture certain gases. It was able to capture 88 mg NO_2/gram of zeolite. It is suggested that this property could turn out to be even more important than the zeolite's SO_2 adsorption capacity.

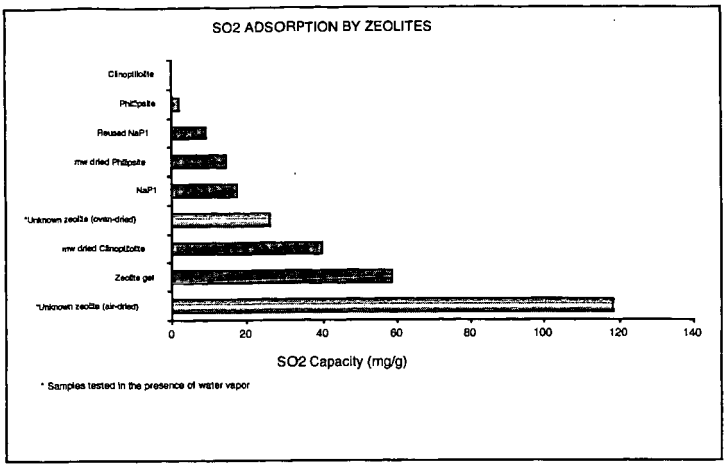

Figure 7. Relative capacities for SO_2 of samples tested with and without water vapor. Note that some of these are "dry" values and adsorption is normally two or three times higher in the presence of water vapor.

References

1. Henmi, T.*Soil Sci. Plant Nutr.* **1987**, 33, 517-521.
2. Mondragon, F.; Rincon, F.; Sierra, L.; Escobar, J.; Ramirez, J.; Fernandez, J. *Fuel* **1990**, 69, 263-266.
3. Shigemoto, N.; Shirakami,K.; Hirano, S.; Hayashi, H. *Nippon Kagaku Kaishi* **1992**, 484-92.
4. Shigemoto, N.; Hayashi, H.; Miyaura K. *J. Mat. Sci.***1993**, 28, 4781-86.
5. Chang, H.-L.;Shih, W.-H. In *Environmental Issues and Waste Management Technologies V*; Jain, V; Palmer, R., Eds.; Ceramic Transactions 61; Amer. Ceram. Soc.:Westerville, OH 1995; pp.81-88.
6. Lin, C-.F.; Hsi, H.-C. *Environ. Sci. Tech.* **1995**, 29, 1109-17.
7. Park, M.; Choi *J. Clay Sci.* **1995**,9, 219-229.
8. Querol, X.; Alastuey, A.; Fernandez-Turiel ,J.L.; Lopez-Soler, A. *Fuel* **1995**,74, 1226-31.
9. Shigemoto, N.; Sugiyama,S.; Hayashi, H.; Miyaura, K.*J. Mat. Sci.***1995**,30, 5777-83.
10. Shih, W.-H.; Chang, H.-L.; Shen, Z. Mat. Res. Soc. Symp. Proc. Vol. 371; Materials Res.Soc: Pittsburgh 1995; pp 39-44.
11. Singer, A.; Berkgaut V. *Environ. Sci. Technol.* **1995**, 29, 1748 -53.
12. Amrhein, C.; Haghnia, G.H.; Kim, T.S.; Mosher, P.A.; Gagajena, R.C.; Amanios, T.; de La Torre, L. *Environ. Sci. Tech.* **1996**, 30, 735- .
13. Suyama, Y.; Katayama, K.; Meguro, M. *Chem. Soc. Japan* **1996**, 136-40.
14. Querol, X.; Alastuey, A.; Lopez-Soler, A.; Plana, F.; Andres, J. M.; Juan, R.; Ferrer, P; Ruiz, C.R. *Environ. Sci. Tech.* **1997**, 31, 2527-13.
15. LaRosa, J.; Kwan, S.; Grutzeck, M.W. *J. Amer. Ceram. Soc.* **1992**, *75*, 1574.
16. LaRosa, J.; Kwan, S.; Grutzeck, M.W. In *Mat. Res. Soc. Symp. Proc.* 245; Mat. Res. Soc.: Pittsburgh, 1992; pp. 211-16.
17. Grutzeck, M.W.; Siemer, D.D. J. Amer. Ceram. Soc.**1997**, 80, 2449-53.
18. Grutzeck, M.W. and J. A. Marks, *J. Environ. Sci. Eng.* **1999**, 33, 312-317.
19. Tsuchiai, H., T. Ishizuka, H. Nakamura, T. Ueno, H. Hattori, *Ind. Eng. Chem. Res.* **1996**, 35, 851-855.

Acknowledgements

Support by the FETC Grant Number DE-FG22-96PC96210 is gratefully acknowledged.

SYNTHESIS AND CHARACTERIZATION OF A NOVEL MULTIFUNCTIONAL CARBON MOLECULAR SIEVE

Wei XING and Zi-Feng YAN*
State Key Laboratory for Heavy Oil Processing,
University of Petroleum, Dongying 257061, P R China

ABSTRACT Carbon molecular sieves were prepared from petroleum coke by chemical activation. The effects of activation temperature, holding time, preliminary treatments and activated agent ratio on surface area, pore structure of the carbon molecular sieves produced in our lab were investigated. The specific surface area and average pore size of the carbon are obviously increased with increasing use of activator and rise of activating temperature. The rate of elevating temperature is not specifically limited. But the heat-retaining time has much influence on the performance of the activated carbon. Suitable holding time may lead to high degree of activation, with result of increase in pore diameter of micropore and mesopore. But too long holding time can destroy pore structure and result in decrease of specific area. In addition, the effects of coke pre-oxidation on activating results were also investigated. Coke pre-oxidation leads to a remarkable decrease of mesopore volume. The carbon molecular sieves prepared in our lab are about 3000 m^2/g in BET specific area. Diffraction peaks in XRD patterns indicate the generation of a new crystalline phase of carbon. The prepared carbon molecular sieves with extremely high specific area and uniform micropore distribution are ideal materials for natural gas adsorption storage as vehicular fuel. Carbon molecular sieves differing in BET surface area were used to evaluate the natural gas storage capacity on them at different pressures by two-vessel volumetric method at 293 K and up to 5.0 MPa. In addition, this kind of carbon molecular sieve can also be used as microwave absorbent and PSA adsorbent for gas separation.

KEYWORDS Carbon molecular sieve, natural gas absorption, chemical activation

1. INTRODUCTION

Petroleum coke is a material of low volatility produced during the refining of crude oil and generally comprises carbonaceous material including elemental carbon, as well as relatively heavy hydrocarbon products including straight- and branched-chain saturated and unsaturated hydrocarbons, cyclic and polycyclic saturated and unsaturated hydrocarbons, whether unsubstituted or substituted with acyl, cyano, sulfur, or halogen constituents, and organometallic compounds. It is abundant and cheap, being widely used as fuels and for the production of graphite electrodes in electric furnace smelting.

A new value-added carbon product, a novel multifunctional carbon molecular sieve, is developed from petroleum coke, which can be widely used as natural gas adsorbent, microwave absorbent and, after pore structure modification, PSA adsorbent for gas separation.

2. EXPERIMENTAL

2.1 Preparation of Carbon Molecular Sieve

Carbon molecular sieves were prepared from petroleum coke (manufactured by ShengLi-Refinery) which mainly consists of carbon atoms, more than 90%, with minor other atoms such as S, N and heavy metals. The raw material, hard, compact and non-porous, was grounded and sieved from 100 ~ 200 mesh. The activator is prepared by mixing, slurrying and stabilizing an alkali metal hydroxide or oxide with other transition metal chlorides or nitrates. Petroleum coke powder was chemically activated using alkali metal hydroxides or oxides as the reagent, and acetone or ethanol as the surfactant. Activated agent, acetone and water were added in specific amounts to petroleum coke. The mixture was stirred homogeneously, giving slurry. The activation of petroleum coke was then carried out in a parallel stainless steel reactor at a certain temperature. The effects of activation temperature, holding time, preliminary treatments and activated agent ratio on surface area, pore structure, and methane storage capacity of the carbon produced in our laboratory were investigated. After activation, the sample was submerged in deionized water, filtered and rinsed again in deionized water to remove any activator derivatives.

In addition, the pre-oxidation of the coke powder on activating results was also investigated. The coke powder was oxidized in air at 473K for 24 hours prior to activation.

* To whom correspondence should be addressed-mail: zfyancat@sunctr.hdpu.edu.cn

2.2 Characterization of Carbon Molecular Sieve

The surface properties such as surface area, average pore diameter and pore volume were determined using an automatic ASAP2010 apparatus (Micromeritics) by N_2 absorption at 77.5K. The total pore volume, V_t, is derived from the amount of absorption at a pressure relatively close to unity, given that the pores were totally filled with the liquid absorbate. The mesopore distribution curve is obtained from the absorption branch of the N_2 isotherm by BJH method. The micropore distribution is calculated from the gas absorption using the Horvath-Kawazoe equation, with relatively pressure (P/P_0) below 0.01. Absorption isotherms of CH4 have also measured by two-vessel volumetric method in a high-pressure range (0~5.0MPa) at ambient temperature.

A BDX-3200 X-ray powder diffractometer, manufactured by Peking University Instrument Factory, was used to identify the crystal form of carbon molecular sieve. Anode Cu Kα (40kV, 20mA) was employed as the X-ray radiation source, covering 2θ between 20° and 120°. The XRD patterns were monitored and processed by a computer.

The surface morphology of carbon absorbents was observed using scanning electron microscopy (JEM 5410LV, JEOL Technologies) with the accelerating voltage of 25kV. The surface elemental composition of carbon molecular sieve was determined by energy distribution spectrum using X-ray microanalysis (ISIS, Oxford Instrument).

3. RESULTS AND DISCUSSION

3.1 Pore Structure Variation of Carbon Molecular Sieve

(1) Effect of Activated Agent Ratio on Structure Variation of Carbon Molecular Sieve

Carbon molecular sieves were prepared by chemical activation using various amounts of activated agent. A quantitative comparison of the variation of the textual structure, mesopore and micropore distribution of carbon molecular sieves is given in Table 1.

The results show that specific surface area, average pore size, average micropore size and pore volume in different size range is obviously increased with increasing use of activator. It means that the amount of activator used determine the depth of activation. The more activator is used, the more micropores are developed. It can be seen from Table 1 and Figure 1 that the volume of pore range from 7 to 30Å, which is believed to play a role for natural gas absorption in relatively low pressure, takes up about 90% in the total pore volume. The absorption isotherms of all carbon molecular sieves shown in Figure 1(b) belong to typical type I isotherm, which also indicates that carbon molecular sieve is a microporous carbon-based material.

(2) Effect of Activating Temperature on Structure Variation of Carbon Molecular Sieve

Petroleum coke was activated at different temperature, which resulted in the variation of pore structure for carbon molecular sieve. Table 2 shows that specific surface area, pore diameter and pore volume all change to be larger with the rise of activating temperature. Obviously, the mesopore (>20Å) volume increases more substantially than the micropore volume. It should be also noted that a shorter period is demanded for activation at high temperature. Excessively long period of heat retaining at high temperature may be responsible for the deviation of activation results at 1173K. It may destroy micropore structure and result in the decrease of specific area.

(3) Effect of coke preoxidation on Structure Variation of Carbon Molecular Sieve

Petroleum coke was preoxidized at 573K for 24 hours in air prior to activation. Table 3 shows the variation of pore structure on carbon molecular sieves caused by preoxidation. We can draw a conclusion from Table 3 that mesopore (>20Å) volume decreases remarkably due to preoxidation. The decline of mesopore volume range from 20 Å to 30 Å may be disadvantageous for natural gas absorptive storage. However, the decrease of mesopore(>20Å) volume results in increase of density for carbon molecular sieves, which is meaningful for natural gas storage.[1] More importantly, it provides a possible way to produce carbon molecular sieve with uniform micropore-size distribution.

3.2 XRD Characterization

Natural gas is absorbed in the micropores that is close related to the crystal structure of carbon molecular sieve. Understanding the crystal structure of carbon molecular sieve is instructive not only for structural optimization of absorbents prepared, but also for the accurate evaluation BET, porosity, etc., of absorbents.

The major crystalline phases of carbon molecular sieve were examined by XRD and the spectra were presented in Figure 2. There are 4 sharp peaks visible, which can be indexed as (100, 111, 200, 210) of a primitive cubic unit cell with a unit cell length of 2.026 Å. Assuming a disordered rhombohedral (hexagonal) cell, this calculates to a = 1.43 and c = 3.51 Å which is comparable to the distances in graphite, 3.35 Å, within and perpendicular to the layers. Although

how the carbon crystal lattice arranges to form this centralized distribution of micropore is not known exactly, it is a really interesting point worth further studying. It may be the fundamental to understand the nature of gas absorptive storage on carbon.

3.3 SEM and EDX Analysis

The microscopic appearance observation of the carbon was conducted using scanning electron microscopy. The micrographs of absorbents, derived from raw coke and preoxidized coke respectively, are illustrated in Figure 3, from which the porous structure of absorbents is clearly imaged. The markedly different surface morphology between these two absorbents indicates various reacting processes during activation. The pore shapes of absorbents prepared from raw coke look randomly, while the pore shapes prepared from preoxidized coke are circular universally. Although the formation mechanism of these circular pores is not known exactly, it is believed to be close relative with retarding the formation of mesopore, which is reflected in Table 3. After preoxidation at 473K in air for 24 hours, surface oxides generated on the surface of the coke. During activation, these surface oxides removed primarily to form rudimentary pores, which is reckoned to be in favor of subsequent activation.

The surface elemental composition of the absorbents was also characterized by energy distribution spectra using X-ray microanalysis and the results show that carbon atoms accounted for absolute majority on the surface of absorbents with only a small quantity of other atoms such as oxygen, potassium and iron.

3.4 Evaluation of Natural Gas Adsorption on Carbon Molecular Sieve

Instability in the oil markets and increase in environmental concerns have stimulated research for alternative transportation fuels. One alternative to gasoline is natural gas, which consists primarily of methane (85% ~ 95%) with minor amounts of ethane, other higher hydrocarbons, and carbon dioxide. The advantage of natural gas is that it is cheaper than gasoline and readily available in the world. Natural gas burns more cleanly than gasoline, emitting fewer toxic hydrocarbons and 90% less carbon monoxide. At present, many governments are actively making efforts to popularize natural gas-driven vehicles, mainly driven by compressed natural gas (CNG), in big city to alleviate the pollution caused by exhaust gas.

The use of natural gas as vehicular fuel, an application where storage volume is limited, has necessitated the use of high-pressure storage, which requires high pressure (20 ~ 30MPa) and an expensive multi-stage compression facility, to give an adequate if not entirely satisfactory driving range. Numerous vehicles have been adapted to use compressed natural gas (CNG) as fuel, which is stored in heavy steel cylinders. The net deliverable capacity for CNG at 1.35 atm (5 psi) is 215 standard liter per liter of storage volume. The disadvantages of such high pressures have stimulated research into the use of absorbents in an attempt to provide a similar energy density, but at relatively low pressure (typical target of 3.4 MPa, 500 psi) achievable by single-stage compression. This concept of absorbed natural gas (ANG) can reduce the highest storage pressure so those lightweight cylinders can be used. The key question is whether the net deliverable capacity of such a device can match or exceed that of CNG. Obviously, one needs a high pore volume, high surface area absorbent for this purpose. This kind of novel carbon molecular sieve produced in our laboratory is such material suitable for the application of ANG.

From above data, derived from characterization of the absorbents in previous sections, it is clear that BET surface area varies with other structural parameters, such as average pore size and microporosity, in direct proportion. Therefore, absorbents differing in BET surface area were used to evaluate the natural gas storage capacity on them by two-vessel volumetric method at 293 K and up to 5.0 MPa. Table 4 submits natural gas storage capacity on absorbents at different pressures. As seen from Table 4, with the increase of storage pressure and BET surface area, natural gas storage capacity enhanced obviously. Of interest is that, with the rise of storage pressure from 3 MPa to 5 MPa, the net increased storage capacity on an absorbent with high BET surface area is large than the one with low BET surface area. Under higher pressure, more relatively large pores play a role in natural gas absorption. Absorbents with higher surface area have more large micropores and small mesopores (20~30Å), which contribute more to natural gas absorption under high pressure than low pressure.

4. CONCLUSIONS

(1) Activated agent ratio, activated temperature and holding time have much influence on the structure of the Carbon Molecular Sieve;
(2) Coke preoxidation results in the remarkable decrease of mesopore volume;
(3) A new crystal phase is formed during activation process;
(4) Increase in pressure from previously suggested 3.4 MPa [2] to 5.0 MPa, at which relatively larger pores play a role in natural gas absorption, does allow a greater amount of natural gas to be absorptively stored on the absorbents with high surface area.

This kind of carbon molecular sieve can also be used as microwave adsorbent and PSA adsorbent for gas separation. We are extending study to these areas.

ACKNOWLEDGEMENTS

Financial supports by the Sheng-Li oilfield and Young Scientists Award Foundation of Shandong Province and Young Scientists Innovation Foundation of China National Petroleum Corporation are gratefully acknowledged.

REFERENCES

1. Matranga K. R. and Myers A. L. Glandt E. D., *Chem. Eng. Sci.* **1992**, 47 ,1569.
2. Quinn D. F. and Macdonald J. A., *Carbon*. **1992**, 30, 1097.

Table 1. Characterization of carbon molecular sieve structure

W_{ACT}/W_{coke}	S_{BET} (m^2/g)	D (Å)	D_{micro} (Å)	V (~20Å) cm^3/g	V(20~30Å) cm^3/g	V(30Å~) cm^3/g
1	909.3	20.748	8.077	0.356	0.040	0.029
2	1173.9	21.173	8.267	0.403	0.131	0.062
3	2273.5	21.048	8.786	0.636	0.428	0.150
5	2859.5	21.501	8.857	0.762	0.604	0.201

[a] D: average pore diameter D_{micro}: average micropore diameter

W_{ACT}/W_{coke}: weight ratio of activator vs. coke

Table 2. Characterization of carbon molecular sieve structure

T (K)	t (min)	S_{BET} (m^2/g)	D (Å)	D_{micro} (Å)	V (~20Å) Cm^3/g	V(20~30Å) cm^3/g	V(30Å~) cm^3/g
973	120	2257.9	20.311	8.688	0.697	0.212	0.078
1073	60	2859.5	21.501	8.857	0.762	0.604	0.201
1173	60	2304.8	23.602	9.106	0.585	0.675	0.389
1273	1	3734.9	23.620	9.136	0.925	1.121	0.640

[a] Activating conditions: W_{ACT}/W_{coke}= 5, the rate of elevating tempreture=10K /min,

N_2 flow rate=30ml/min T: activating temperature t: retaining time

D: average pore diameter D_{micro}: average micropore diameter

Table 3. Characterization of carbon molecular sieve structure

	S_{BET} (m^2/g)	D (Å)	D_{micro} (Å)	V (~20Å) cm^3/g	V(20~30Å) cm^3/g	V(30Å~) cm^3/g
Untreated	2859.5	21.501	8.857	0.762	0.604	0.201
Preoxidation	2255.8	20.293	8.626	0.667	0.304	0.084

[a] D: average pore diameter D_{micro}: average micropore diameter

Table 4. Natural gas absorption capacity on carbon molecular sieves with different surface area

S_{BET} (m2/g)	V/V (3.0MPa)	V/V (4.0MPa)	V/V (5.0MPa)
1634	86.7	115.6	132.9
2069	127.1	144.2	156.7
2745	150.3	179.8	208.3

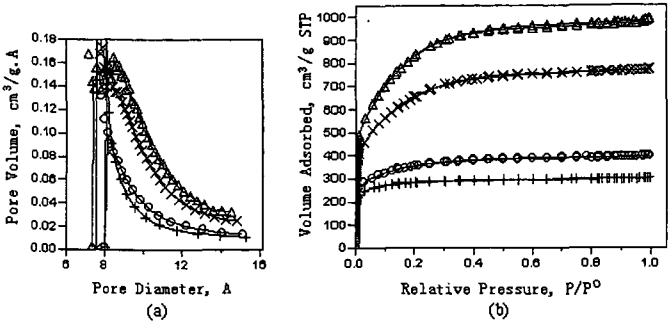

Figure 1. Characterization of carbon molecular sieve structure
(a): micropore distribution; (b): absorption isotherm

+: W_{ACT}/Wcoke=1:1; o: W_{ACT}/Wcoke=2:1; ×: W_{ACT}/Wcoke=3:1; Δ: W_{ACT}/Wcoke=5:1;

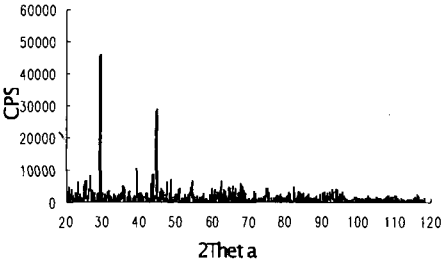

Figure 2. XRD patterns of carbon molecular sieve

(a) Derived from raw coke (b) Derived from preoxidized coke

Figure 3. The SEM photo of carbon molecular sieves

INORGANICS IN FUEL: A CENTURY OF SCIENTIFIC AND ENGINEERING PROGRESS

Constance L. Senior
Physical Sciences, Inc.
20 New England Business Center
Andover, MA 01886 USA
senior@psicorp.com

INTRODUCTION

Combustion of fossil fuels has been the backbone of the power generation, manufacturing and transportation industries in the twentieth century. Although the mix of fuels has changed, at the close of the century we find that combustion systems have not changed overmuch. Operational caused by inorganic elements in fossil fuels (corrosion, slagging, and fouling) continue to present problems in combustion systems, although substantial progress has been made in understanding and addressing such problems. In the latter half of the century, the impact of inorganic elements in fossil fuels on the environment was recognized as a potential problem. Considerable effort has therefore been directed at understanding the behavior of certain trace metals such as mercury, arsenic, nickel, chromium, and selenium during the combustion process. This paper briefly reviews the behavior of inorganic elements in practical combustion systems as well as the progress made in applying this knowledge to improvements in operational and environmental performance.

Most inorganic elements in the periodic table can be found in fossil fuels, although only a small number occur in significant concentrations to cause operational or environmental problems. Coal has by far the highest content of ash, although the chemical composition of lower ash fuels can make oil and biomass problematic in some instances. Table 1, drawn largely from Bryers,[1] summarizes the contributions of the elements in ash from various fuels to slagging, fouling, corrosion, and environmental problems. Slagging is defined as deposition of fly ash in the radiant section of the furnace, on both heat transfer surfaces and refractory surfaces. Fouling occurs in the convective heat transfer section and includes deposition of ash and volatiles as well as sulfidation reactions of ash. Fouling results in loss of heat transfer efficiency and blockage of the gas flow path. Corrosion occurs primarily on the water-wall tubes in the radiant section of the boiler and results in thinning of tubes with eventual leaks.

Table 1. Impact of Inorganic Elements in Fuel on Operational and Environmental Problems.

	Bituminous Coal	*Subbituminous Coal*	*Lignite*	*Oil and Coke*	*Biomass*
Wt% Ash	*5-20%*	*4-7%*	*5-20%*	*0.1-0.5%*	*1-3%*
Si	S		S		S
Al	S		S		
Fe	S		S		
Mg	S		S		
Ca	S	F, S	F, S		
Na	C, F	F	F	F,C	C, F
K	S				C, F
S	C, F	F	F	C,F	C,F
Cl	C				C
Ni				F	
V				C, F	
As	E	E	E	E	
Cr				E	
Hg	E	E	E	E	

Major elements are shown in **bold**
C – Corrosion
E – Environmental
F – Fouling
S - Slagging

Environmental problems include the impact of ash on the air pollution control devices (APCDs) and on the environment. Increasingly, the emission of toxic metals to the air and water from fossil fuel combustion is recognized as a problem. Mercury is the element of most concern, particularly for coal-fired power plants. Other metals (e.g., As, Cr, Ni, V) are also of concern when burning petroleum-derived fuels. There are other impacts of inorganic elements in the environmental performance of combustion systems, including operation of particulate collection

devices and the poisoning of selective catalytic reduction catalysts by arsenic. In coal-fired power plants, the sodium and sulfur contents of the fuel both affect the resistivity of the fly ash. If an electrostatic precipitator (ESP) is used to collect the ash, resistivity is the key ash parameter which influences the collection efficiency.

CHARACTERIZATION OF INORGANIC ELEMENTS IN FUEL

Coal was the first fossil fuel to be used for generation of steam applied to transportation and manufacturing, and later to large-scale power generation. Heavy oils and coke, produced from refining of petroleum have been utilized for power generation and manufacturing in the latter half of the century. Wood and agricultural wastes (biomass) have been used at a low level throughout the century, and this may increase with concerns about the use of non-renewable resources. Most of the fossil fuels used for large scale industrial use have a substantial fraction of inorganic elements, the exceptions being natural gas and transportation fuels such as gasoline and diesel oil.

Early methods for characterizing inorganic elements in coal were indirect, for example, ash content or fusibility of the ash. It acknowledged early on that the composition of coal ash strongly influenced the tendency to form deposits in the combustion system. Beginning in the 1930's, the contribution of specific minerals to slagging and fouling problems was recognized using methods of density separation to isolate mineral-rich fractions of coal.[2] With the advent of cyclone boilers for pulverized coal, viscosity measurements were made on coal ash.[3] Mineralogical characterization of coal continued, resulting in a fairly comprehensive understanding of the occurrence and formation of the major minerals in coal by techniques such as physical separation, selective leaching, and x-ray diffraction analysis. Table 2 summarizes the important minerals in coal.[1] More recently, automated techniques such as computer controlled scanning electron microscopy (CCSEM)[4] and scanning electron microscopy point count (SEMPC)[5] have been developed to provide a more accurate picture of the minerals in coal.

Table 2. Minerals occurring in coal

Quartz
Shale group
Species: illite, montmorillonite, muscovite, bravaisite
General formula: $(K, Na, H_3O, Ca)_2 (Al, Mg, Fe, Ti)_4 (AlSi_3O_8O_{20}(OH,F)_4)$
Kaolin group
Species: kaolinte, livesite, metahalloysite
Formula: $Al_2(Si_2O_5)(OH)_4$
Sulphide group
Species: pyrites, marcasite
Formula: FeS_2
Carbonate group
Species: calcite, dolomite, ankerite
Formula: $(Ca,Mg,Fe,Mn)\ CO_3$
Chloride Group
Species: sylvite, hallite
Formula: KCl, NaCl

Since the 1960's, low rank coals have become more widely used for steam generation because of their low ash and sulfur contents. Low rank fuels have a major proportion of inorganic elements organically bound to the coal matrix instead of in discrete minerals. Selective leaching (or chemical fractionation) methods have been used to identify and characterize the organically bound elements, primarily Ca, Na, and Mg in subbituminous and lignite coals.[6] Recently, selective leaching and advanced analytical methods such as X-Ray absorption fine structure spectroscopy have been applied to the problem of determining the forms of occurrence of trace elements in coal.[7,8]

Oil and coke, as well as biomass, have much lower ash contents than coal and little, if any minerals (although the inorganic elements in these fuels can still cause problems in practical combustion systems). Generally the ash content and ash composition of these fuels is all that is measured, although the mineralogy and leaching behavior of elements of some biomass fuels have been reported.[1]

IMPACT OF INORGANIC ELEMENTS ON SYSTEM OPERATION

At the start of the twentieth century, coal burned in stoker-fired units was the most common for industrial applications. In the 1920's pulverized coal was introduced and this allowed the design and implementation of new combustion system designs, including wall-fired boilers, cyclone boilers, and fluidized bed combustors. Large scale refining of petroleum in the latter half of the twentieth century introduced new fuels, heavy oils and coke, which are often burned to produce steam and/or electricity in suspension-fired and fluidized bed combustion systems.

Figure 1 illustrates the transformation of inorganic elements during coal combustion. Petroleum-derived fuels and biomass transformations are similar, although these fuels have less discrete mineral matter than coal. During the combustion process, the carbon matrix is consumed resulting in very high particle temperatures. Most of the inorganic elements (either from discrete minerals or organically associated) coalesce into ash particles in the range of 1-20 microns in diameter. A small part of the inorganic elements vaporize during the combustion process (1-5 wt%) and recondense, forming a fine (0.1-0.5 micron) aerosol. Some inorganic vapors condense on the larger ash particles, but the high specific surface area of the submicron aerosol tends to bias condensation to the smaller particles.

These ash particles reside largely in the flue gas in pulverized coal- or oil-fired combustion systems. In cyclone-fired boilers and fluidized bed systems, the majority of the ash ends up as slag or spent bed material. This fly ash, in the flue gas, deposits on heat transfer surfaces in the boiler and ultimately, on modern coal-fired combustion systems, must be removed before the gas can be emitted to the atmosphere.

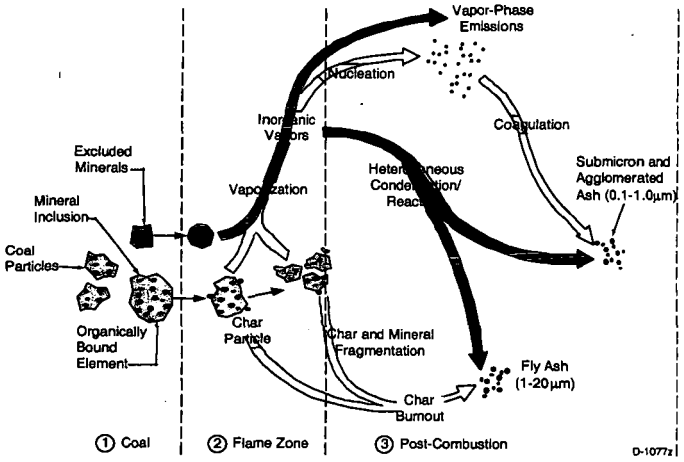

Figure 1. Transformations of Inorganic Elements During Combustion of Pulverized Coal

As discussed above, slagging, fouling and corrosion affect the operation of industrial combustion systems and are directly caused by inorganic elements in fossil fuels. Coal combustion systems are plagued by all these problems. Corrosion is the dominant problem in oil-fired boilers because of the formation of vanadium sulfate deposits which are quite corrosive. Corrosion can be a problem in some biomass combustion systems because some biomass fuels have a very high alkali content. The combination of silica and alkali can also result in slagging and fouling.

Initially, empirical indices were developed to evaluate the potential for operational problems due to the inorganics in fuels. There are many such indices,[1] but they are not specific to particular boiler designs or operating conditions. As discussed above, the realization that specific minerals in coal were responsible for slagging, fouling, and corrosion led to an explosion of research on mineralogical characterization of fuels. This was followed by attempts to create mechanistic (as opposed to empirical) models for the behavior of inorganic elements in practical combustion systems.[9,10,11] Such models are used to provide better indications of the potential effects of fuels on system operations.

IMPACT OF INORGANIC ELEMENTS ON THE ENVIRONMENT

The emission of toxic metals to the air and water from fossil fuel combustion is becoming of concern. In the United States, the potential for regulation of hazardous air pollutants, including metals, was specifically addressed in the 1990 Amendments to the Clean Air Act.

A recent report by the Environmental Protection Agency (EPA) on emission of hazardous air pollutants by electric utilities predicted that emissions of air toxics from coal-fired utilities would increase by 10 to 30% by the year 2010.[12] Mercury from coal-fired utilities was identified as the hazardous air pollutant of greatest potential public health concern. Anthropogenic emissions of mercury account for 10 to 30% of the world-wide emissions of mercury.[12] EPA has estimated that during the period 1994-1995 annual emissions of mercury from human activities in the United States were 159 tons.[12] Approximately 87% of these emissions were from combustion sources. Coal-fired utilities in the U.S. were estimated to emit 51 tons of mercury per year into the air during this period. Considerable work is in progress by the author,[13] and many other groups, which will lead to a more complete understanding of the behavior of mercury in coal-fired power plants.

Other metals (e.g., As, Cr, Ni, V) are also of concern when burning petroleum-derived fuels. Chromium and nickel are the metals of most concern for residual oil combustion. Certain compounds of Cr and Ni are highly carcinogenic. Advanced analytical methods such as XAFS have been used to identify compounds of these elements in residual oil fly ash in order to assess the potential health risks.[14] Cd and Zn in biomass fly ash have also been characterized by this technique. When considering the potential risk to human health or to the biosphere, the ability to identify specific compounds of these toxic metals becomes vitally important. Advanced analytical methods have proved useful in the past and are continually being improved.

SUMMARY

Inorganic elements are present in almost all industrially important fossil fuels and can have major impacts on operation and environmental performance of fossil fuel combustion systems. Improved analytical methods for measuring the composition and for characterizing the form of inorganic elements in fuels have been developed. These methods have led to a better understanding of the behavior of inorganic elements in combustion systems and have spurred the development of fundamentally based models which have been applied in practical systems. More recently, concerns have been raised over the impact of fossil fuel combustion systems on the environment. Advanced analytical methods are just now starting to be applied to characterization of trace metals in fossil fuel and in combustion byproducts. This will lead to an improved understanding of the behavior of trace metals in combustion systems and more effective methods to assess the potential risk to human health.

REFERENCES

1. Bryers, R.W., "Fireside Slagging, Fouling, and High-Temperature Corrosion of Heat Transfer Surface due to Impurities in Steam-Raising Fuels," *Prog.Energy Combust. Sci.*, **1996**, *22*, 29-130.
2. Moody, A.N. and Langan, D.D., "Fusion characteristics of fractionated coal ashes," *Combustion*, **1933**, *October*, 15-17.
3. Reid, W.T. and Cohen, P., "Flow characteristics of coal ash slags in solidification range," Furnace performance supplement to *Trans. ASME*, **1940**, *62*, 144-153.
4. Lee, R.J., Huggins, F.E., and Huffman, G.P., Scanning Electron Microscopy/1978/I, (ed. O. Johari), SEM Inc., 561-568, (1978).
5. Steadman, E.N., Erickson, F.A., Folkedahl, B.C., and Brekke, D.W., "Coal and ash characterization: digital image analysis applications," in *Proceedings of the Engineering Foundation Conference on Inorganic Transformations and Ash Composition During Combustion*, S.A. Benson, editor, ASME, New York, 1991, pp. 147-164.
6. Finkelman, R.B., Palmer, C.A., Krasnow, M.R., Aruscavage, P.J., Sellers, G.A., and Dulong, F.T., "Combustion and Leaching Behavior of Elements in the Argonne Premium Coal Samples," *Energy & Fuels*, **1990**, *4*, 755-766.
7. F. E. Huggins, N. Shah, G. P. Huffman, A. Kolker, S. Crowley, C. A. Palmer, and R. B. Finkelman, "Mode of occurrence of chromium in four U.S. coals", *Fuel. Proc. Technol.*, **2000**, *63(2-3)*, 79-92.
8. Kolker, A., Palmer, C.A., Crowley, S.S., Finkelman, R.B., Huggins, F.E., Shaw, N., and Huffman, G.P. "Mode of Occurrence of Arsenic in Four U.S. Coals," *Fuel. Proc. Technol.*, **2000**, *63(2-3)*, 167-178.
9. Helble, J.J., Srinivasachar, S., Senior, C.L., Wilemski, G., Baker, J., Simons, G.A., and Johnson, S.A., "A fundamentally based model of slag formation in utility boilers," presented

at the Second Australian Workshop on Ash Deposition, Brisbane, Queensland, Australia, July 13-14, 1992.
10. Erickson, T.A., O'Leary, E.M., Folkedahl, B.C., Ramanathan, M., Zygarlicke, C.J., Steadman, E.N., Hurley, J.P., and Benson, S.A., "Coal Ash Behavior and Management Tools," in The Impact of Ash Deposition on Coal Fired Power Plants, J. Williamson and F. Wigley, editors, Taylor & Francis, Washington, D.C., 1994.
11. Baxter, L.L., "Ash Deposition During Biomass and Coal Combustion: A Mechanistic Approach," *Biomass and Bioenergy*, **1993**, *4*, 85-102.
12. Keating, M.H., et al. *Mercury Study Report to Congress, Volume I: Executive Summary*, EPA-452/R-97-003, December 1997.
13. Sarofim, A.F., Senior, C.L., and Helble, J.J., "Emissions of Mercury, Trace Elements, and Fine Particles from Stationary Combustion Sources,accepted for publication in *Fuel. Proc. Technol.*, **2000**.
14. Huggins, F.E., Shah, N., Huffman, G.P., and Robertson, J.D., "XAFS Spectroscopic characterization of elements in combustion ash and fine particulate matter," presented at the Conference on Air Quality, McLean, Virginia, December 1-4, 1998.

MODES OF OCCURRENCE OF TRACE ELEMENTS IN COAL: RESULTS FROM AN INTERNATIONAL COLLABORATIVE PROGRAMME

Robert M. Davidson
IEA Coal Research - The Clean Coal Centre
Gemini House, 10-18 Putney Hill
London SW15 6AA, United Kingdom
email: robert@iea-coal.org.uk

Keywords: Coal, Trace Elements, Modes of Occurrence

INTRODUCTION

A collaborative research project on the modes of occurrence of trace elements in coal was set up within the IEA implementing agreement on Coal Combustion Sciences. Les Dale of CSIRO, Australia, coordinated the project. Participants in the project were requested to determine the modes of occurrence of trace elements of environmental significance using their chosen methodology. The aim was to determine not only the modes of occurrence but also to obtain data that could be compared and contrasted. The final reports were then sent to IEA Coal Research to form the basis of a critical review of the project (Davidson, 2000). They have been published on the CD-ROM that accompanies the overall final report.

The collaborative programme was set up because the participants believe that understanding the modes of occurrence in coal is essential for developing reliable models to predict the behaviour of elements during in-ground leaching, weathering, coal cleaning, or combustion. Modelling the behaviour of the trace elements is necessary to provide an accurate evaluation of the environmental and human health impacts, technological impacts, and economic by-product potential of coal use (Willett and others, 2000). Knowledge of the mineralogical residences or modes of occurrence of trace elements in coal is very important in the understanding of mechanisms by which trace elements are enriched in fly ash and are found in flue gas (Dale and Chapman, 1999). This is because the behaviour of the trace elements in coal-fired power stations is partly dependent on the mode of occurrence of the elements in the original coal (Wigley and others, 2000).

THE PARTICIPATING LABORATORIES

Laboratories in Australia, Canada, Spain, the United Kingdom, and the USA participated in the collaborative study:

Australia	CSIRO, Division of Energy Technology, Lucas Heights, NSW (Dale and Chapman, 1999)
Canada	Geological Survey of Canada, Energy and Environment Division, Calgary, Alberta (Goodarzi and others, 1999).
Spain	Institute of Earth Sciences "Jaume Almera", CSIC, Barcelona (Querol and others, 1999)
UK	University of Sheffield, Centre for Analytical Sciences, Sheffield (Spears and others, 1998)
UK	Imperial College of Science, Technology and Medicine, Department of Materials, London (Wigley and others, 2000)
USA	Energy & Environmental Research Center, University of North Dakota, Grand Forks, ND (Galbreath and others, 1999)
USA	University of Kentucky, Department of Chemical and Materials Engineering, Lexington, KY (Huggins, 1999)
USA	US Geological Survey, Reston, VA (Willett and others, 2000)

THE COALS SELECTED

In the initial stages of the project, three different coal samples were distributed. A fourth coal, from a mine in Nova Scotia, Eastern Canada was distributed to participants about a year after the first three coals were distributed. Not all the collaborating laboratories were able to study all four samples, but most were able to study the Australian, British, and US samples. The coals selected were:

- Wyee coal - a high volatile bituminous Australian coal,
- Gascoigne Wood - a UK bituminous coal from a 2 tonne batch from power station feed,
- Illinois No. 6 - a high volatile US bituminous coal, and an
- Eastern Canadian coal - also high volatile bituminous.

Table 1 lists some analytical data provided by Goodarzi and others (1999).

Table 1 **Proximate and ultimate analyses of the four coals** (Goodarzi and others, 1999)

	Wyee, Australia	Eastern Canadian	Gascoigne Wood, UK	Illinois No. 6, US
Proximate analysis, wt% ar				
Moisture	2.6	1.33	3.2	3.3
Ash	23.0	9.86	15.2	10.1
Volatile matter	27.1	31.96	29.6	36.1
Total sulphur	0.37	3	1.16	3.4
Ultimate analysis, wt% daf				
Carbon	63.62	75.31	69.2	69.84
Nitrogen	1.31	1.38	1.58	1.36
Sulphur	0.38	3.00	1.20	3.52
Hydrogen	3.46	4.53	4.03	4.27
Oxygen	7.62	6.12	8.25	10.57
Sulphur forms, wt%				
Sulphate S	0.01	0.30	0.08	0.08
Pyritic S	0.05	1.70	0.32	1.30
Organic S	0.31	1.00	0.76	2.02

MINERALOGY

Goodarzi and others (1999) provide a comprehensive account of the mineralogies of the coals used in these studies. Most of the collaborating laboratories analysed the mineral composition of the coals although different methods were used. The analyses of the bulk ash contents are in reasonably close agreement for all the laboratories that provided data. However, some differences emerge in the detailed data. Huggins (1999) reports values for the float/tailings fractions and their ash content for separations performed using a Denver flotation cell. Galbreath and others (1999) separated the coals using a 1.6 specific gravity solution for the Wyee coal and a 1.45 specific gravity solution for the other three. The data are compared in Table 2 that lists the percentage ash remaining in each fraction.

Table 2 **Percentage ash separation analyses** (Galbreath and others, 1999; Huggins, 1999)

	Wyee, Australia	Eastern Canadian	Gascoigne Wood, UK	Illinois No. 6, US
Density sink	73	76	73	54
Denver cell tailings	40	49	69	21
Density float	27	24	27	46
Denver cell float	60	51	31	79

The differences, except for the Gascoigne Wood coal, are considerable but most likely reflect physical differences in the separation methods. The differences in the separations by different mechanical separations could possibly lead to different assignations of the trace element modes of occurrence. It would be expected that a greater proportion of trace elements will be found in the maceral-rich fraction from Denver cell flotation except, possibly, for the Gascoigne Wood coal. Although, when at least 24% of the ash is encountered within the maceral-rich float fractions, this is scarcely evidence for 'maceral-association' rather than 'mineral-association' with minerals dispersed within the bulk of the organic matter. Galbreath and others (1999) observed that most of the minerals in their float fractions were present as tiny (< 5 μm in the longest dimension) inclusions within coal particles. Most of the trace elements are enriched to some extent in the tailings fractions (Goodarzi and others, 1999) but, even when depleted in the float compared with the coal, a greater proportion of the trace elements often remains there.

THE TRACE ELEMENTS COMPARED

Not every trace element was analysed by every laboratory so that comparisons among them have to be made using a restricted set. The eleven elements identified in the US Clean Air Act Amendments (CAAA) of 1990 as potentially 'hazardous air pollutants' with the addition of copper and zinc formed the basis of the overview report:

Beryllium, chromium, manganese, cobalt, nickel, copper, zinc, arsenic, selenium, cadmium, antimony, mercury, and lead.

A range of analytical techniques was employed in the qualitative and quantitative analysis of the elements in the coals and their fractions. Generally, the data for the concentrations of these trace elements in the whole coal were in reasonably good agreement

SAMPLE FRACTIONATION

In order to determine the modes of occurrence of the trace elements in the samples, the coals were fractionated using variants of two techniques - **physical separation** and **sequential leaching**. As noted above, Galbreath and others (1999) used a float/sink density separation method with specific gravity solutions composed of mixtures of reagent-grade tetrachloroethylene and petroleum ether. After mixing and centrifugation, the float and sink samples were separated, dried in a nitrogen-purged oven and weighed. Float fractions were composed predominantly of organic (maceral-rich) with small proportions of minerals. Most minerals in the float fractions were present as tiny (< 5 μm in the longest dimension) inclusions within the coal particles. However, as shown in Table 2, the minerals in the float fractions still accounted for about a quarter of the total in three coals (Wyee, Eastern Canadian, and Gascoigne Wood) and nearly half in the Illinois No. 6 coal. The sink fractions were composed predominantly of larger discrete mineral grains.

Querol and others (1999) also used density fractionation. They obtained seven density fractions between < 1.3 and > 2.8 g/cm^3 by using heavy liquid mixtures of bromoform, tetrachloroethylene, and xylene. It was noted that the density fractionation technique was developed for the study of high mineral matter coals. The relatively low mineral matter content of the coals in the collaborative study made complete isolation of the minerals difficult. Further, as noted above, it was also found that the mineral matter was finely dispersed in the organic matter that consequently made good density separation. It was for such reasons that chemical treatments were also used to isolate or extract mineral phases from the density fraction, specifically to extract gypsum from the 2.0-2.4 g/cm^3 fraction of the Gascoigne Wood coal and to enrich pyrite by acidic attack on calcite in the > 2.8 g/cm^3 fraction of the Illinois No. 6 coal (Querol and others, 2000). Using this separation technique, Querol and others (1999) were able to assign the trace elements into the following affinity categories:

organic matter (OM), density fraction < 1.3;
aluminosilicates, mainly clays (ALS);
sulphates (GYP);
sulphides, selenides, and arsenides (PY), density fraction > 2.8;
iron carbonate (CARB);
heavy minerals (HM); and
phosphates (PHOS).

Table 2 in Querol and others' (1999) report shows more details of the density fractions used for each coal. Querol and others (2000) later modified their density fractionation data by using a mathematical deconvolution of the chemical analyses of the whole coals and their density fractions. The mathematical deconvolution calculates the amount of organically associated elements in each density fraction. It is based on a method developed by Klika and Kolomaznik (2000) and uses the following data from the float/sink experiments:

1. mass of the coal fractions,
2. sum of crystalline phases and ash content,
3. concentrations of the trace elements in each of the coal fractions,
4. concentrations of sulphide and carbonate in each fraction.

This enables the calculation of the percentage trace element affinity to the organic part of the coal. The concentrations of the elements in the sulphide and carbonate fractions of the coal are used in a semiquantitative determination of the elemental affinities in the inorganic parts of the coal.

Huggins (1999) used a hybrid physical separation method in which the coal samples were first separated into float and tailings fractions using a Denver column flotation cell. A small fraction of the tailings product was then further subdivided by a float/sink density separation technique using bromoform with a specific gravity of 2.875. As a result of these separations, the as-received coal (RAW) was split into four fractions:

the tailings (TAILS) from the Denver cell flotation,
an "organic fraction" (ORG) representing the float fraction from the Denver cell,
a "heavy minerals" fraction (HYM) representing the fraction of the Denver cell tailings that sank in bromoform, and
a "clay" fraction (CLAY) representing the fraction of the Denver cell tailings that floated in bromoform.

The bromoform separations were not very successful. As a result, with the exception 1-2% of HYM from the Illinois No. 6 coal, the TAILS and CLAY fractions were essentially the same. The float and tailings fractions from the Denver cell were also analysed by Goodarzi and others (1999).

The other laboratories involved in the study used different sequential leaching separations. These are based on the standard method of determining the forms of sulphur in coal. Dale and Chapman (1999) used the following sequence:

1. 4.3 M hydrochloric acid (HCl) at 80°C for two hours. This dissolves oxides, carbonates, and monosulphides. The residue was then treated with
2. 0.5 M nitric acid (HNO_3) at 80°C for two hours. This dissolves sulphides (pyrite). The residue was then treated with
3. 10 ml 40% hydrofluoric acid (HF) and 1 ml concentrated HCl at 60-70°C for 1 hour. 5 ml HCl and 5 ml water were then added and the mixture heated at 60-70°C for a further 1 hour. This dissolves the silicates.

The various solutions were analysed for specific trace element concentrations and the "organic" residue was also analysed. The selectivity of the pyrite leaching (stage 2) for the Illinois No.6 coal was investigated by X-ray diffraction. It was verified that 0.5 M HNO_3 removed 100% of the pyrite.

Although not used in the study of the IEA collaborative programme coals, Dale and others (1999) later introduced an initial stage in which coal samples were treated with 1M ammonium acetate (CH_3COONH_4) at 80°C for two hours. This is similar to the first stage of the USGS sequence used by Willett and others (2000):

1. 1N ammonium acetate (CH_3COONH_4). This removes loosely bound ions that may be organically associated or ions absorbed on clays and dissolves some calcite. The residue was then treated with
2. 3N HCl. This removes carbonates, such as calcite, and monosulphides. The residue was then treated with
3. concentrated (48%) HF. This removes silicates, including quartz and clay minerals. The residue was then treated with
4. 2N HNO_3. This primarily removes disulphides such as pyrite.

It was recognised that some silicates, such as zircon, may be resistant to the HF leaching in stage 3. The residue left includes these, other insoluble minerals, and elements "shielded" from the solvents, together with the organic portions of the coal. It should be noted that the ash yield of the residual leached coal was commonly less than 0.3 wt%, suggesting little in the way of shielded and insoluble phases in most coals.

Spears and others (1998) used the sequence:

1. shake with deioinised water for up to 12 hours. This removes elements present in pore fluids and soluble minerals. The residue is shaken with
2. dilute HCl for up to 12 hours. This removes carbonates (mainly calcite), exchangeable cations and monosulphides. The residue is shaken with
3. dilute HNO_3 (5%) for up to 12 hours. This removes carbonates (mainly dolomite and ankerite) and some pyrite. The residue is shaken with
4. concentrated, cold HNO_3 and allowed to stand for up to 12 hours. This removes the remaining pyrite. The solid remaining is digested with
5. concentrated HNO_3 with microwave heating. This digests the organic matter. Any remaining solid is digested with
6. concentrated HCl and HF with microwave heating. This digests the silicates.

Unlike the other sequential leaching procedures, this method completely digests the coal sample leaving no "organic" residue. Some inherent problems in the technique were recognised by Spears and others (1998). For example, some of the pyrite is released in stage 3 but not quantitatively, the rest is removed in stage 4. The silicates and the organic matter will also have been partially attacked in the early stages. There is also the problem that mineral groups, such as carbonates and sulphides, do not behave uniformly.

Obviously, the data from the different groups are not strictly comparable since they were obtained from different of separation techniques ranging from simple fractionation into float and sink fractions to more complex fractionation either by density fractionation or selective leaching. Nevertheless, comparisons needed to be made, even at the risk of misinterpreting some of the data. The comparisons are published in the final overview report (Davidson, 2000) and some of them will be discussed in the presentation.

REFERENCES

Dale L S, Chapman J F (1999) *IEA collaborative project on the modes of occurrence of trace elements in coal (phase 1) final report.* Lucas Heights, NSW, Australia, Commonwealth Scientific and Industrial Research Organisation, Division of Energy Technology, 18 pp (Dec 1999)

Dale L S, Chapman J F, Buchanan S J, Lavrencic S A (1999) *Co-operative Research Centre for Black Coal Utilisation. Mechanisms for trace element partitioning in Australian coals. Project 4.2 - final report.* Investigation report CET/IR215, Lucas Heights, NSW, Australia, Commonwealth Scientific and Industrial Research Organisation, Division of Energy Technology, 35 pp (Sep 1999)

Davidson R M (2000) *Modes of occurrence of trace elements in coal: Results from an international collaborative programme.* London, UK, IEA Coal Research (2000)

Galbreath K C, DeWall R A, Zygarlicke C J (1999) *IEA Coal Research collaborative programme on modes of occurrence of trace elements in coal - results from the Energy & Environmental Research Center. Final report.* Grand Forks, ND, USA, Energy & Environmental Research Center, University of North Dakota, 21 pp (Nov 1999)

Goodarzi F, Pollock S, Charland J-P (1999) *Mode of occurrence of trace elements and minerals in coal.* Calgary, Alberta, Canada, Geological Survey of Canada, Energy and Environment Division, 80 pp (1999)
Huggins F E (1999) *Trace element speciation in four bituminous coals.* Lexington, KY, University of Kentucky, Department of Chemical and Materials Engineering, 56 pp (1999)

Klika Z, Kolomaznik I (2000) New concept for the calculation of the trace element affinity in coal. *Fuel*; 79 (6); 659-670 (May 2000)

Querol X, Alastuey A, Juan R, Huerta A, López-Soler A, Plana F, Chenery S R N, Robinson J (1999) *Determination of elemental affinities by density fractionation of bulk coal samples.* Barcelona, Spain, Institute of Earth Sciences "Jaume Almera", CSIC, 19 pp (Sep 1999)

Querol X, Klika Z, Weiss Z, Finkelman R B, Alastuey A, Juan R, López-Soler A, Plana F, Kolker A, Chenery S R N (2000) Determination of elemental affinities by density fractionation of bulk coal samples. To be published in *Fuel*.

Spears D A, Booth C, Staton I (1998) *Mode of occurrence of trace elements in round-robin coals: differential dissolution.* Sheffield, UK, University of Sheffield, Centre for Analytical Sciences, 31 pp (Sep 1998)

Wigley F, Williamson J, Miles N J (2000) *The distribution of trace elements in a UK bituminous coal.* London, UK, Imperial College of Science, Technology and Medicine, Department of Materials, 44 pp (2000)

Willett J C, Finkelman R B, Mroczkowski S J, Palmer C A, Kolker A (2000) *Semi-quantitative determination of the modes of occurrence of elements in coal: results from an international round robin project. Final report.* Reston, VA, USA, U.S. Geological Survey, 45 pp (2000)

STANFORD-USGS SHRIMP-RG ION MICROPROBE: A NEW APPROACH TO DETERMINING THE DISTRIBUTION OF TRACE ELEMENTS IN COAL

Allan Kolker[1], Joseph L. Wooden[2], Harold M. Persing[2], and Robert A. Zielinski[3]

[1]*U.S. Geological Survey, 956 National Center, Reston, VA 20192*
[2]*U.S. Geological Survey, Stanford-USGS Micro-Isotopic Analytical Center, Green Earth Sciences Building, Stanford University, Stanford, CA 94305-2115*
[3]*U.S. Geological Survey, 973 Denver Federal Center, Denver, CO 80225*

Key Words: Illite/Smectite in Coal; Ion Probe Analysis; SHRIMP-RG.

ABSTRACT

The distribution of Cr and other trace metals of environmental interest in a range of widely used U.S. coals was investigated using the Stanford-USGS SHRIMP-RG ion microprobe . Using the oxygen ion source, concentrations of Cr (11 to 176 ppm), V (23 to 248 ppm), Mn (2 to 149 ppm), Ni (2 to 30 ppm), and 13 other elements were determined in illite/smectite, a group of clay minerals commonly present in coal. The results confirm previous indirect or semi-quantitative determinations indicating illite/smectite to be an important host of these metals. Calibration was achieved using doped aluminosilicate-glass synthetic standards and glasses prepared from USGS rock standards. Grains for analysis were identified optically, and confirmed by 1) precursory electron microprobe analysis and wavelength-dispersive compositional mapping, and 2) SHRIMP-RG major element data obtained concurrently with trace element results. Follow-up investigations will focus on the distribution of As and other elements that are more effectively ionized with the cesium primary beam currently being tested.

INTRODUCTION

Research on the occurrence of potentially toxic trace metals in coal is fundamental to predicting the potential for distribution of these metals to the environment through coal combustion, mining, and leaching from storage piles. Microbeam instruments with good spatial resolution and element sensitivities are needed to make direct, in-situ trace-element determinations that are specific to individual coal components. The Sensitive High-Resolution Ion Microprobe with Reversed Geometry (SHRIMP-RG) at Stanford University offers these characteristics. The reversed geometry, in which the electrostatic sector is downstream of the magnetic sector of the mass spectrometer, gives the SHRIMP-RG superior mass-resolution compared to its forward geometry (FG) SHRIMP predecessor and smaller ion probes.

Our initial use of the SHRIMP-RG for coal samples focussed on the distribution of Cr and other transition metals in illite/smectite, a common inorganic clay mineral constituent of coal and other sediments. Previous work, including studies by selective leaching, electron microprobe, and XAFS spectroscopy (Huggins et al., 2000) and chemical analysis of mineral separates (Palmer and Lyons, 1996), indicates a significant residence for Cr in clay minerals in coal. This study was undertaken to confirm and quantify these results, and to demonstrate the utility of the SHRIMP-RG for studies in environmental geochemistry. Understanding the mode of occurrence of Cr in coal is especially important because the hexavalent form of the element is a known carcinogen.

SAMPLE CHARACTERIZATION AND ANALYSIS METHODS

Samples studied include three coals currently being investigated by the USGS in Phase II of a larger DOE-funded study of toxic substances from coal combustion. The three Phase II coals are a bituminous Ohio 5/6/7 blend, a sub-bituminous Wyodak sample, and a North Dakota lignite. Three additional samples were investigated, a bituminous Illinois #6 sample from Phase I of the combustion study, a Northern Appalachian (Pittsburgh) bituminous sample and a second Illinois #6 sample studied by the USGS as part of another recent contract. Each of these samples has been very well characterized by conventional coal-testing methods, bulk geochemistry, mineralogy, and element modes of occurrence, including selective leaching, electron microprobe, and for all but the Pittsburgh and second Illinois #6 samples, bulk XAFS analysis.

Preliminary work involved characterization of illite/smectites using a JEOL 8900R electron microprobe for quantitative analysis and wavelength-dispersive elemental mapping. SHRIMP-RG data were obtained in August, 1999 and February, 2000, using an O_2^- duoplasmatron source. Analysis points were initially subjected to a 1-3 minute burn-in to stabilize the response. The burn-in was followed by a "short" analysis consisting of 4, 7, or 8 elements, to confirm the identity of the grains selected and minimize the contribution of overlapping grains. In the August, 1999 runs, the short analyses were followed directly by "long" analyses in which the

initial 7 elements (Mg, Al, Ca, Si, ^{52}Cr, K, and Fe) were re-determined and combined with analyses of Sc, Ti, V, ^{53}Cr, Mn, Co, Ni, Cu, Zn, Rb, and Sr. The same procedure was used to measure these elements in reference standards. A similar procedure was followed in February, 2000, except that all the short runs were conducted successively, followed by a series of long runs for only the most promising grains. This modification minimized magnet instability caused by changes to its within-run scan range. Quantifying the concentration of Cr was the highest priority of the study, and therefore, Cr was determined twice, as ^{52}Cr and as ^{53}Cr. Using this approach, the natural ratio of $^{53}Cr/^{52}Cr$ (0.1134) was typically reproduced to three decimal places. Concentrations obtained using the two chromium isotopes were generally within 1% (absolute), for calibrations obtained using the same standard (Table 1).

A variety of aluminosilicate standard glasses were investigated, including National Institute of Standards and Technology (NIST) SRM glasses 610 and 612, glass synthetic standards GSE and GSD, prepared for the USGS by Corning Glass Works, Inc., and glass prepared from powdered USGS rock standard BHVO-1. Concentrations were obtained by determining the counts/ppm for standards and calculating the concentrations of unknowns by comparing their raw counts to the standard data. Calibration results obtained using three different standards, SRM 610, GSE, and BHVO-1, for the same Ohio 5/6/7 illite/smectite, are given in Table 1. From electron microprobe analysis, the SiO_2 and Al_2O_3 contents of illite/smectite are known to be about 50 and 30 weight percent, respectively. SHRIMP-RG results for these elements are given in weight percent to facilitate comparison to the microprobe data (Table 1). For most elements, the GSE standard gives the lowest concentrations, and these can be considered minima (Table 1). GSE is the only standard determined in every SHRIMP-RG run, providing a uniform basis for comparing data from each of the runs and for all of the samples. Table 2 shows the reproducibility of counts/concentration for the GSE standard in 4 runs over a 2-day period in February, 2000. Total deviation ranges from 5.8 to 12.5%, except for Rb (20.9%) and Sr (17.9%).

Table 1. SHRIMP-RG Data Reduction and Comparison of Standards for an Ohio 5/6/7 Illite/Smectite.

August 1999	*Raw*	Counts/ppm (Al_2O_3, SiO_2 in wt. %)			Concentration (ppm) (Al_2O_3, SiO_2 in wt. %)		
Ohio 5/6/7	*Counts*	*SRM 610*	*GSE*	*BHVO*	*Conc. 610*	*Conc. GSE*	*Conc. BHVO*
Mg	21391	9.44	13.00	13.06	2266	1645	1637
Al_2O_3	325487	10252	16810	11708	31.75	19.36	27.80
Ca	5442	12.68	15.57	14.59	429.2	349.5	393.0
SiO_2	1059325	18292	27723	19627	57.91	38.21	53.97
Sc	4163	362.6	240.5	349.6	11.48	17.31	11.91
Ti	29024	18.13	20.55	17.24	1601	1413	1683
V	13766	175.0	190.0	129.8	78.68	72.47	106.04
^{52}Cr	14022	180.2	215.9	163.0	77.82	64.95	86.01
^{53}Cr	1587	20.25	24.53	18.53	78.37	64.72	85.65
Mn	7009	200.6	303.2	253.2	34.94	23.12	27.69
Co	173	108.3	196.0	165.0	1.60	0.93	1.05
Ni	687	21.94	43.81	34.70	31.30	15.67	19.79
Rb	68370	617.4	718.8	584.2	110.74	95.12	117.02
Sr	11821	239.3	280.4	233.1	49.40	42.15	50.70

Table 2. SHRIMP-RG Results- Reproducibility of the GSE Standard.

	GSE standard counts per ppm (Al_2O_3, SiO_2 in counts/wt. %)				
Date	2 Feb 00	2 Feb 00	3 Feb 00	3 Feb 00	% Total
Run #	1	2	3	4	Deviation
^{26}Mg	236.5	227.5	230.0	222.7	5.8
^{43}AlO	48462	46832	50470	47871	7.2
^{44}Ca	44.88	43.00	46.70	44.14	7.9
^{44}SiO	81609	79596	85734	81213	7.4
^{45}Sc	762.3	738.3	799.6	728.8	8.7
^{47}Ti	63.08	60.69	66.63	61.58	9.8
^{51}V	608.0	572.0	644.1	585.8	11.0
^{52}Cr	650.5	611.0	668.6	618.6	8.6
^{53}Cr	72.98	68.83	75.45	69.67	8.8
^{55}Mn	864.3	844.1	897.6	827.7	7.8
^{55}KO	7.17	6.97	7.30	6.71	6.8
^{59}Co	475.9	474.3	493.0	446.3	9.5
^{60}Ni	103.8	104.1	107.07	96.12	11.0
^{63}Cu	165.3	166.7	176.9	151.2	11.5
^{64}Zn	84.54	87.33	85.92	76.38	12.5
^{72}FeO	15.82	15.67	16.33	14.67	10.2
^{85}Rb	1673.3	1673.4	1926.4	1523.8	20.9
^{88}Sr	736.0	723.9	866.0	710.6	17.9

SHRIMP-RG RESULTS FOR ILLITE/SMECTITE

Chromium concentrations in illite/smectite in these coals range from 11 to 176 ppm (Fig. 1a). The results are consistent with semi-quantitative estimates obtained from previous electron microprobe data, leaching results, and XAFS (Huggins et al., 2000). Results for the Ohio and Pittsburgh samples are co-linear for Cr and V, possibly indicating a similar diagenetic history for these illites from the northern Appalachian Basin. Concentration ranges for some other elements of environmental interest in illite/smectite are as follows: V (23 to 248 ppm); Mn (2 to 149 ppm); and Ni (2 to 30 ppm; Fig. 1b-d). Trace element contents generally increase with the Mg content of the illite/smectite.

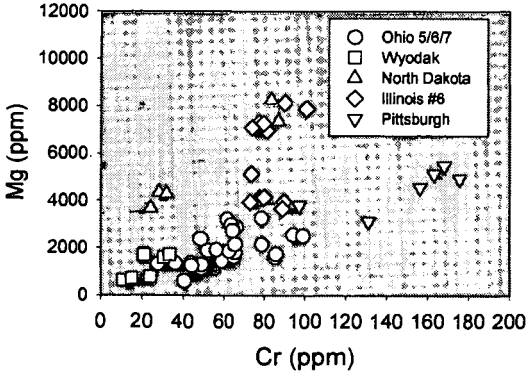

Figure 1a). Plot of Mg vs. Cr in illite/smectite from six coal samples, based on single-standard calibration using results for GSE. Illinois #6 data are for different two samples.

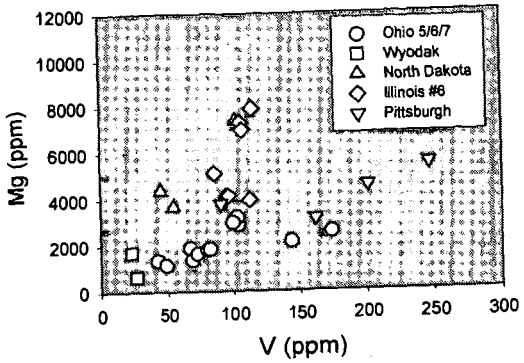

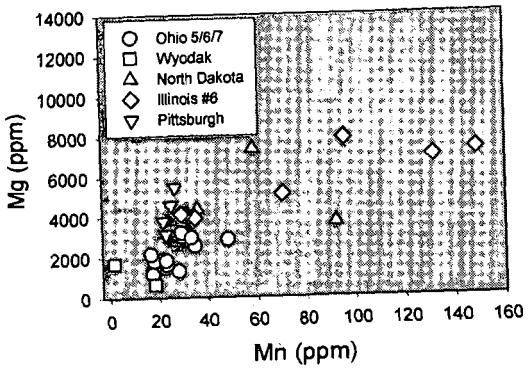

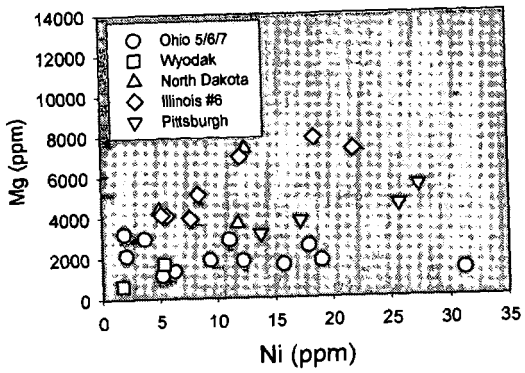

Figure 1b-d). Plots of V, Mn, and Ni vs. Mg in illite/smectite from six coal samples, based on calibration using GSE standard. Illinois #6 data are for two different samples.

PLANNED INVESTIGATIONS

The results reported here were determined using the SHRIMP-RG in its current configuration, in which oxygen (O_2^-) ions form the primary beam. Work is now being planned to take advantage of a high-energy Cs^+ ion source that is expected to be available for use in the summer of 2000. In the first planned study, the distribution of arsenic in fly ash particles will be investigated with the SHRIMP-RG. This study is prompted by evidence that moderately to slightly volatile elements such as Se and As, condense on the surface of fly ash particles as they cool, contributing to the health risk from inhaled particles and the leachability of toxic elements into the environment (EPRI, 1998). Using the oxygen source, we conducted a number of preliminary tests on fly ash from a Kentucky power plant, and on the aluminosilicate glass standards. These tests showed that the ^{75}As peak could be resolved from potential interferences in the GSE standard, whereas a mass scan on fly-ash in which ^{75}As was present also showed a larger and broader unknown peak that is not completely resolvable from the analytical peak using oxygen ions. Count rates for arsenic are expected to be an order of magnitude higher with the cesium source.

SUMMARY

This paper reports our initial use of the SHRIMP-RG ion microprobe for determining trace metal contents in illite/smectite, a common mineral constituent of coal and sediments. Results confirm and quantify the concentration of Cr in illite/smectite inferred from previous indirect or semi-quantitative studies. This knowledge is important in developing quantitative models for the behavior of Cr during coal processing and combustion. Planned SHRIMP-RG investigations will use a Cs^+ ion beam to more effectively ionize metals such as As and Hg, thereby improving their detection and analysis.

ACKNOWLEDGEMENT

Acquisition of SHRIMP-RG data in this study was supported by U.S. Department of Energy Interagency Agreement DE-AI22-95PC95145 with the U.S. Geological Survey.

REFERENCES

EPRI (Electric Power Research Institute), 1998, Indentification of arsenic species in coal ash particles, EPRI, Palo Alto, CA, Technical Report TR-109002.

Huggins, F.E., Shah, N., Huffman, G.P., Kolker, Allan, Crowley, S.S., Palmer, C.A., and Finkelman, R. B., 2000, Mode of occurrence of chromium in four U.S. coals: Fuel Processing Technology, v. 63, p. 79-92.

Palmer, C.A., and Lyons, P.C., 1996, Selected elements in major minerals from bituminous coal as determined by INAA: Implications for removing environmentally sensitive elements from coal: International Journal of Coal Geology, v. 32, p. 151-166.

DIRECT COMPARISON OF XAFS SPECTROSCOPY AND SEQUENTIAL EXTRACTION FOR ARSENIC SPECIATION IN COAL

Frank E. Huggins[1*], Gerald P. Huffman[1], Allan Kolker[2], Stanley Mroczkowski[2], Curtis A. Palmer[2], and Robert B. Finkelman[2]

[1]Chemical and Materials Engineering/CFFLS, University of Kentucky, 533 South Limestone Street, Suite 111, Lexington, KY 40506-0043, *fhuggins@engr.uky.edu

[2]Eastern Energy Resources Team, 956 National Center, U.S. Geological Survey, Reston, VA 20192

KEYWORDS: Arsenic, coal, sequential extraction, modes of occurrence, XAFS spectroscopy

ABSTRACT

The speciation of arsenic in an Ohio bituminous coal and a North Dakota lignite has been examined by the complementary methods of arsenic XAFS spectroscopy and sequential extraction by aqueous solutions of ammonium acetate, HCl, HF, and HNO_3. In order to facilitate a more direct comparison of the two methods, the arsenic XAFS spectra were obtained from aliquots of the coal prepared after each stage of the leaching procedure. For the aliquots, approximately linear correlations ($r^2 > 0.98$ for the Ohio coal, > 0.90 for the ND lignite) were observed between the height of the edge-step in the XAFS analysis and the concentration of arsenic measured by instrumental neutron activation analysis. Results from the leaching sequence indicate that there are two major arsenic forms present in both coals; one is removed by leaching with HCl and the other by HNO_3. Whereas the XAFS spectral signatures of the arsenic leached by HCl are compatible with arsenate for both coals, the arsenic leached by HNO_3 is identified as arsenic associated with pyrite for the Ohio coal and as an As^{3+} species for the North Dakota lignite. Minor arsenate forms persist in both coals after the final leaching with nitric acid. The arsenate forms extracted in HCl are believed to be oxidation products derived from the other major arsenic forms upon exposure of the pulverized coals to air.

INTRODUCTION

The techniques of sequential leaching and XAFS spectroscopy have both been used to determine modes of occurrence of elements in coal. Both methods have their advantages and disadvantages. XAFS spectroscopy is a direct probe of the occurrence of elements and is capable of providing information on how specific elements exist in coal at concentrations as least as low as 2 ppm. The major disadvantage of the technique is that only a single spectrum is obtained which is the weighted sum of all the occurrences of the element in the coal. This problem can be largely avoided by examination of different fractions of the coal separated by various physical methods, such as float/sink in heavy liquids or froth flotation [1,2]. In addition, a database of possible occurrences of the element in coal must also be established for comparative purposes [2,3]. Finally, the method is limited to a single element at a time. Sequential leaching is an indirect method and is based upon the anticipated behavior of certain mineral types in a suite of progressively stronger acidic reagents. It has the advantage that it is a multi-element technique, although depending on the analysis methods used to determine the concentrations of the elements in the residues and solutions, the analysis time can be lengthy. As with any indirect method, sequential leaching is only as good as the assumptions on which it is based and the technique may be completely misleading if the assumptions are incorrect.

In this study, we present the first direct comparison of XAFS and sequential leaching methods for determination of elemental modes of occurrence in coal. Data from both methods are presented for the speciation of arsenic in two different coals: a bituminous coal from Ohio and a lignite from North Dakota.

EXPERIMENTAL

(i) Coals Investigated

Three coals were initially considered for this study: a bituminous coal from Ohio, which is a blend of coal mined from the Ohio No. 5, 6 and 7 seams, a subbituminous coal from the Wyodak seam in Wyoming, and a lignite mined from the Hagel seam in North Dakota. All three coals are used for electrical power generation at full-scale utility operations and the samplings are representative of the coal, in both composition and particle-size (~70% -200 mesh), fed to the burners at the power plants.

The trace-element contents of the two coals were determined by a combination of instrumental neutron activation analysis (INAA), inductively-coupled plasma mass spectrometry (ICP-MS), and ICP atomic emission spectroscopy (ICP-AES). Arsenic contents determined for the Ohio bituminous coal, the North Dakota lignite and the Wyodak subbituminous coal are 18, 10, and 1.7 ppm (dry basis), respectively. Owing to its very low arsenic content, the Wyodak coal was not investigated in the detail afforded to the other two coals.

(ii) Sequential Leaching Procedure

Preparation of the coal samples and the sequential extraction analysis were performed at the U.S. Geological Survey at Reston. The procedure is described in detail elsewhere [4,5]. It consists of the following sequence of extractions: (1) 1N ammonium acetate, (2) 3N HCl, (3) 48% HF, and (4) 2N HNO_3. Each extraction is performed in 50 ml centrifuge tubes on a wrist-shaker, except for the extraction in HNO_3, which is performed in 125 ml Erlenmeyer flasks [5]. These extractions are designed respectively to solubilize (1) exchangeable cations and some readily soluble carbonate species, (2) more resistant carbonates and simple sulfides (ZnS, PbS, $CuFeS_2$), (3) clays and other silicates, and (4) iron disulfides (pyrite and marcasite, FeS_2). After each stage, the concentrations of elements in the extract were analyzed using ICP-AES and ICP-MS and portions of the residue were saved for analysis using INAA and CVAA and also for XAFS spectroscopy.

(iii) Arsenic XAFS spectroscopy

Arsenic K-edge XAFS spectroscopy was carried out at beam-line X-18B at the National Synchrotron Light Source (NSLS), Brookhaven National Laboratory, NY, during a period when the synchrotron was operated in maximum flux mode at 2.8 GeV with currents up to 400 mA. Arsenic XAFS spectra were collected in fluorescent mode using a 12-element germanium array detector [6]. The coal residue samples were suspended in the monochromatic X-ray beam by means of ultra-thin polypropylene bags. In addition to multiple scanning, both Soller slits and a 6μ Ge filter were employed to enhance the signal/noise ratio of the spectra as much as possible. XAFS spectra were typically collected at X-ray energies ranging from about 100 eV below to at least 500 eV above the arsenic K absorption edge using a rotating Si (220) double crystal monochromator to select the energy. A thin smear of As_2O_3 on scotch tape was used as the primary calibration standard; this sample was run in an absorption experiment after the fluorescence experiment so that it provided a simultaneous calibration. The major peak in the absorption spectrum of As_2O_3 was used to define the zero-point of energy for the arsenic XAFS spectra. It is assumed to occur at 11,867 eV.

The XAFS data collected at the synchrotron were returned to the University of Kentucky for analysis. The data were analyzed in the usual fashion [7,8]: after calibration of the energy scale, the spectra were split into separate X-ray absorption near-edge structure (XANES) and extended X-ray absorption fine structure (EXAFS) regions and each region was analyzed independently. The XANES region was used not only as a fingerprint for identification of the forms of occurrence of arsenic in the fly-ash samples, but also as the basis for extracting percentages of the different arsenic forms present in the coal sample. This was achieved by means of a calibrated least-squares analysis routine developed for analysis of arsenic XANES spectra [9], an example of which is shown in Figure 1. Owing to the low arsenic contents of the coal samples, neither the EXAFS region nor the radial structure function (RSF), which is derived from the EXAFS spectrum by mathematical manipulation [7,8], was useful for this study.

RESULTS AND DISCUSSION

(i) Sequential Leaching

Results from the sequential leaching will be reported in detail elsewhere; here, data will be presented and discussed only for arsenic. The arsenic contents of the residue fractions, determined by instrumental neutron activation analysis (INAA) after each extraction, are summarized in Table 1:

Table 1: As contents of residues remaining after leaching experiments

	Ohio bituminous As in ppm	Wyodak subbit. As in ppm	N. D. lignite As in ppm
After Amm. Acet. leach	19.1	1.7	11.0
After HCl leach	15.1	1.0	5.2
After HF leach	15.2	0.7	3.6
After HNO_3 leach	0.9	0.4	1.6

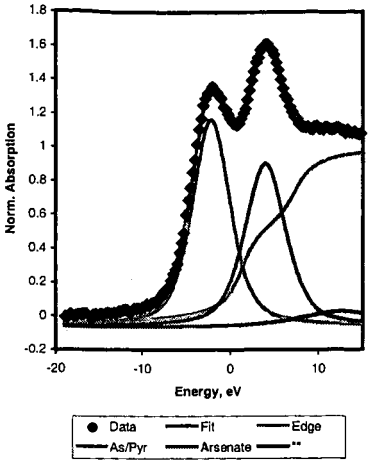

Figure 1: Least-squares fitted As XANES spectrum of Ohio bituminous coal after the ammonium acetate leach.

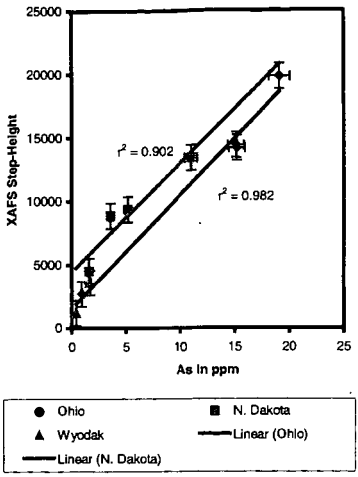

Figure 2: Correlation between the XAFS step-height and the concentration of arsenic in the leached residues.

The analytical data in Table 1 can be correlated with the step-height determined from XAFS spectra, which is also an approximate measure of the arsenic concentration. This correlation is shown in Figure 2. The correlations between the analytical data and the XAFS edge-step heights for the two coals show a reasonable approximation to a linear relationship. For the Ohio bituminous coal, the correlation coefficient (r^2) exceeds 98%, whereas it is about 90% for the North Dakota lignite. This result indicates that both analyses are consistent with each other.

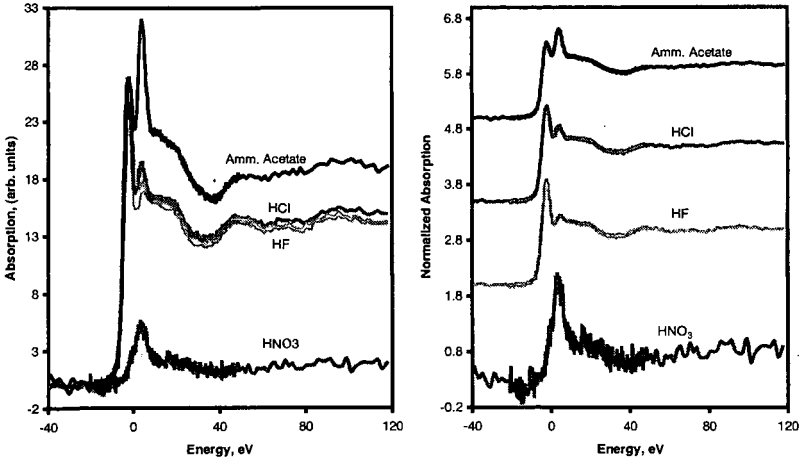

Figures 3 and 4: Unnormalized (left, Figure 3) and normalized (right, Figure 4) arsenic XANES spectra for the Ohio coal residues after different stages of the USGS leaching protocol.

(ii) XAFS Spectroscopy

Arsenic XAFS spectra were collected from the various fractions using as many as 10 scans for each sample. The spectra are shown in Figures 3 and 4 for the Ohio bituminous coal and in Figures 5 and 6 for the North Dakota lignite. Figures 3 and 5 show the unnormalized spectra, whereas Figures 4 and 6 show the same spectra normalized to the edge step and hence, these latter groupings of spectra have the effect of concentration removed from them. The data clearly show, by the reduction in intensity of the major peak at about 4.0 eV, that the HCl treatment removes principally, if not exclusively, arsenate from both the Ohio and North Dakota coals. This observation confirms more definitively the similar conclusion made in Phase 1 of this study

[4,10] based on a less direct comparison of leaching data and arsenic XAFS data for various coals. The data show also that the HF treatment has little effect, except for removing some very minor amounts of arsenate remaining after the HCl treatment. For the Ohio coal, as indicated by the reduction in intensity of the peak at about –2 eV, the HNO_3 treatment removes all of the pyritic arsenic. However, no such phase is present in the North Dakota lignite. Rather for this coal, the HNO_3 treatment appears to be removing an As^{3+} phase, as the peak that is removed is close to 0 eV. For both coals, there is a small residue of arsenic that remains after all the leachings. It is not arsenical pyrite or As^{3+}, but rather more like an arsenate phase.

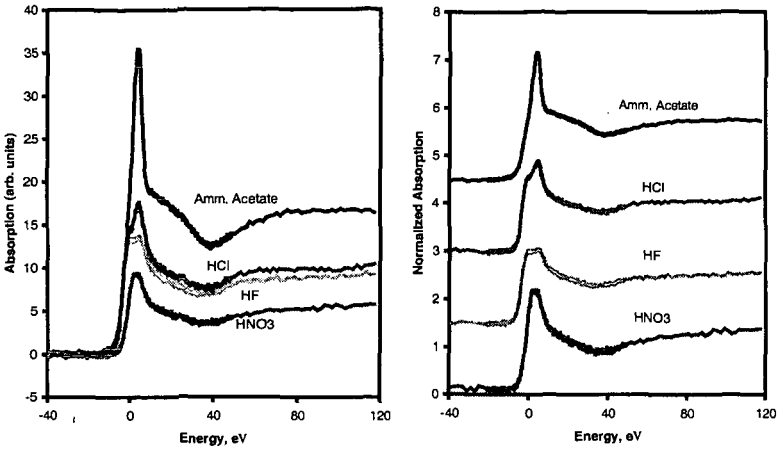

Figures 5 and 6: Unnormalized (left, Figure 5) and normalized (right, Figure 6) arsenic XANES spectra for North Dakota Lignite residues after different stages of the USGS leaching protocol.

A calibrated least-squares fitting model, developed earlier for quantifying arsenic species in bituminous coals [9], was used to quantify the arsenic speciation in the Ohio bituminous coal samples. For this coal, it was decided to fit only the two major arsenic forms present: arsenical pyrite and arsenate. Using this procedure [9], the arsenic speciation results obtained for the Ohio bituminous coal are summarized in Table 2. The least-squares fitting model has not yet been modified for application to the low-rank coals and their different arsenic species.

Table 2: Estimates of arsenic forms remaining after each leaching step in the Ohio coal

Leachant	%As as As/pyrite	%As as Arsenate	ppm As as As/pyrite	ppm As as Arsenate
Amm. Acetate 19.1 ppm As remains	75	25	14.3	4.8
HCl 15.1 ppm As remains	93	7	14.0	1.1
HF 15.2 ppm As remains	>95	<5	>14.4	<0.8
HNO_3 0.9 ppm As remains	<10	>90	<0.1	>0.8

Based on this analysis, the concentration of arsenic as As/pyrite after the first three leaching steps is approximately the same, 14 ± 1 ppm. This indicates that none of the three reagents, ammonium acetate, HCl, or HF removes significant arsenic as As/pyrite. As has been postulated previously [9], the presence of arsenic in pyrite appears to make pyrite more reactive to oxidation. However, for this particular coal, it does not appear that any arsenic associated with pyrite is leached prior to the HNO_3 treatment. The HF leach appears to remove only the minor arsenate remaining after the HCl leach. The HNO_3 leach removes all of the arsenic as arsenical pyrite and appears to leave a small residue of arsenate on the carbonaceous materials. It should be noted that the arsenate in the HNO_3 residue is higher than that remaining after the HF leach, suggesting that it has been formed during the nitric acid leach.

XAFS examination of different aliquots of the two coals about a year apart shows a significant enhancement of arsenate in both coals during this time period. The arsenate species is clearly an oxidation product of other arsenic forms in the coals. Furthermore, even though the coals are not

deliberately oxidized, such oxidation is an on-going process once the coal is crushed and exposed to air. Hence, the leaching results are likely to be found to change systematically with time, reflecting this time-dependent change in arsenic speciation.

CONCLUSIONS

The use of arsenic XAFS spectroscopy to examine arsenic in leached residues of coals from a sequential leaching protocol for elemental speciation in coals has provided unparalleled insight into the leaching characteristics of arsenic from coal and enables a rather complete assessment of the assumptions behind using sequential leaching for arsenic speciation to be made. XAFS spectroscopy shows clearly that the major fraction of arsenic leached from both coals by HCl is arsenate and that HNO_3 removes much of the remaining arsenic in both coals. Leaching with HF has little effect on the arsenic content of both coals examined and appears restricted to removing any arsenate species that remains after the HCl leach. The arsenic associated with pyrite in the bituminous coal is removed effectively by nitric acid, but a quite different form is removed from the lignite by nitric acid. The XAFS data suggest that this arsenic phase may be an As^{3+} species, but it remains yet to be positively identified. Finally, a small fraction of the arsenic (5-15%) remains in the coal after the nitric acid leach. We suspect that this is an organoarsenate formed by a side reaction between the arsenic leached from the coal and new oxygen functionality on the coal introduced by reaction of the coal macerals with nitric acid.

ACKNOWLEDGEMENTS

This work is supported by the U.S. Department of Energy through DOE Contract No. DE-AC22-95PC95101 to Physical Sciences, Inc. The U.S. Department of Energy is acknowledged for its support of the synchrotron facilities at Brookhaven National Laboratory, NY.

REFERENCES

[1] F. E. Huggins, S. Srikantapura, B. K. Parekh, L. Blanchard, and J. D. Robertson, **Energy & Fuels**, 11, 691-701, (1997).

[2] F. E. Huggins, and G. P. Huffman, **Int. J. Coal Geol.**, 32, 31-53, (1996).

[3] F. E. Huggins, and G. P. Huffman, In: **Mineral Spectroscopy: A Tribute to Roger G. Burns**, (eds. M. D. Dyar, C. A. McCammon, and M. W. Schaefer), The Geochemical Society, Houston, TX, Special Publication No. 5, 133-151, (1996).

[4] A. Kolker, S. Crowley, C. A. Palmer, R. B. Finkelman, F. E. Huggins, N. Shah, and G. P. Huffman, **Fuel Proc. Technol. (Air Toxics special issue)**, 63, 167-178, (2000).

[5] S. J. Mroczkowski, in C. L. Senior, T. Panagiotou, F. Huggins, G. P. Huffman, N. Yap, J. O. L. Wendt, W. Seames, M. R. Ames, A. F. Sarofim, J. S. Lighty, A. Kolker, R. Finkelman, C. A. Palmer, S. J. Mroczkowski, J. J. Helble, and R. Mamani-Paco, *Toxic Substances from Coal Combustion – A Comprehensive Assessment.* Appendix B. **Quarterly Report No. 11, DOE Contract No. DE-AC22-95PC95101**, U.S. Department of Energy, January 1999.

[6] S. P. Cramer, O. Tench, N. Yocum and G. N. George, **Nucl. Instrum. Meth.** A266, 586-591, (1988).

[7] P. A. Lee, P. H. Citrin, P. Eisenberger, B. M. Kincaid, **Rev. Mod. Phys.**, 53, 769-808, (1981).

[8] D. C. Koningsberger, R. Prins, **X-ray Absorption.** J. Wiley & Sons, New York, (1988).

[9] F. E. Huggins, J. Zhao, N. Shah, F. Lu, G. P. Huffman, L. E. Bool, III, and C. L. Senior, **Proceedings, ICCS '97, 9th International Conference on Coal Science, (Essen, Germany)**, (eds. A. Ziegler, K. H. van Heek, J. Klein, and W. Wanzl), 1, 381-384, P & W Druck und Verlag GMBH, Essen (1997).

[10] L. E. Bool, III, C. L. Senior, F. Huggins, G. P. Huffman, N. Shah, J. O. L. Wendt, F. Shadman, T. Peterson, W. Seames, A. F. Sarofim, I. Olmez, T. Zeng, S. Crowley, R. Finkelman, J. J. Helble, and M. J. Wornat, *Toxic Substances from Coal Combustion – A Comprehensive Assessment.* **Final Report, DOE Contract No. DE-AC22-95PC95101**, U.S. Department of Energy, July 1997.

ROUND ROBIN ON BIOMASS FUELS

Thore von Puttkamer, Sven Unterberger, Klaus R.G. Hein
Institute for Process Engineering and Power Plant Technology (IVD)
Pfaffenwaldring 23
70550 Stuttgart, Germany
Phone:+49-711/6853565, Fax:+49-711/6853491,e-mail:puttkamer@ivd.uni-stuttgart.de

Keywords: Biomass analysis, digestion, analysis methods

INTRODUCTION

In order to optimise the use of biomass as a fuel it is essential to have reliable information about its chemical composition. Therefore, it is of great significance to have useful methods for detecting the complete composition of the fuel. By means of Round Robins the commonly used methods can be evaluated and rated.

OBJECTIVES

The data gained from the Round Robin shall provide a representative overview of the common methods for biomass characterisation used in the laboratories. It will give detailed information about all analysing steps (sample preparation, digestion methods, and analysis). The evaluation will cover in first place the interlaboratory scattering of results. Laboratories using similar methods of analysis will be gathered and evaluated separately. Due to the fact that no reference samples for biomass are available it will not be possible to assess the accuracy of the analytical data.

IMPLEMENTATION

Two fuel samples of wood and straw were investigated in the Round Robin. The fuels were milled and homogenised by an independent laboratory and then checked for homogeneity by analysing for some major elements (C,N,S,K,Fe). In the Round Robin the probes were analysed for 35 parameters by 39 German and European laboratories. All participating laboratories were free to choose the analytical methods they are used to, only recommendations concerning available experience and possible problems that might occur were supplied. Moreover, the laboratories were free to use several different methods in parallel to compare the obtained results. In order to be able to compare the different methods, the laboratories should fill in a detailed questionnaire to clearly describe each step of preparation, digestion, and analysis itself. Based on this information a comparison of the influence of each single analysis step was possible.

EVALUATION

The classical evaluation of a Round Robin is based on ISO 5725. The assumption for using this standard is the Gaussion distribution of the data. A normal distribution is based on random mistakes scattering around the accurate value. In a Round Robin where each laboratory was recommended to use its own well proven analytical methods the interlaboratory mistakes will be systematic [1]. In this Round Robin the gained data is very inhomogeneous and therefore, a few data may have a big influence on the location parameters.
Consequently, a distribution free, robust method based on Hampel was used for statistical evaluation. This method does without elimination of so called outliers, which are weighted instead making the results less sensitive to extreme single values [2].
In order to illustrate the statistical calculations the results are shown in evaluation diagrams. Some of the terms mentioned can be defined as follows:
"Wiederholstandardabweichung" ,V_r, corresponds to the mean value of all intralaboratory standard deviation ,S_r, divided by the "robust" mean value.
"Vergleichstandardabweichung" ,V_R, corresponds to the mean value of the interlaboratory standard deviation ,S_R, divided by the "robust" mean value.
The values measured by the laboratories are represented in the diagrams by bars. The centreline of each bar shows the robust mean value, the standard deviation corresponds to the distance between the centreline and the outside bounds of the bar.

RESULTS

As an example for using biomass as a fuel the analysis results for chlorine and ash content that are important for the combustion and slagging/fouling behaviour in furnaces are presented..
KCl in the fuel could be released as KCl or converted into HCl, Potassium silicate and K_2SO_4. At combustion temperature KCl is released into the gas phase and condenses at the heat surfaces at lower temperatures. Condensed KCl on tube surfaces could form low melting eutectics, leading to an increased corrosion rate [4].
The ash content affects the ashing device and the ash disposal as well as the concept and the cleaning of the heat exchanger.

Figure 1 shows the evaluated chlorine contents of the straw sample. The robust mean value of all laboratories is 1263 mg/kg (db), the range between the single mean values ranges from 745 mg/kg (db) up to 2391 mg/kg (db).

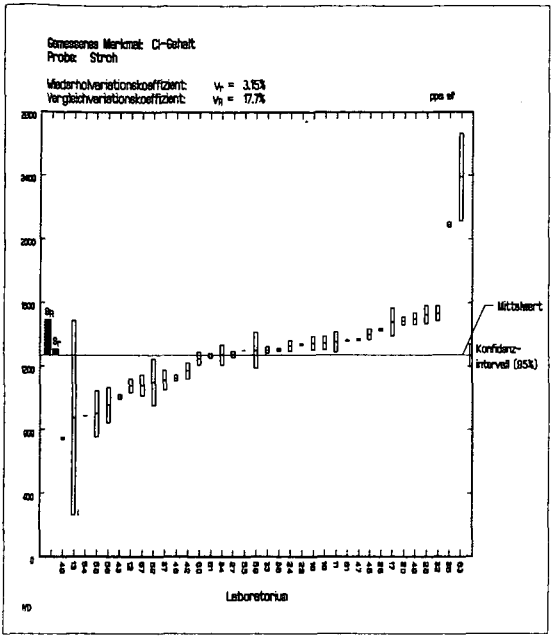

Figure 1: Chlorine in straw

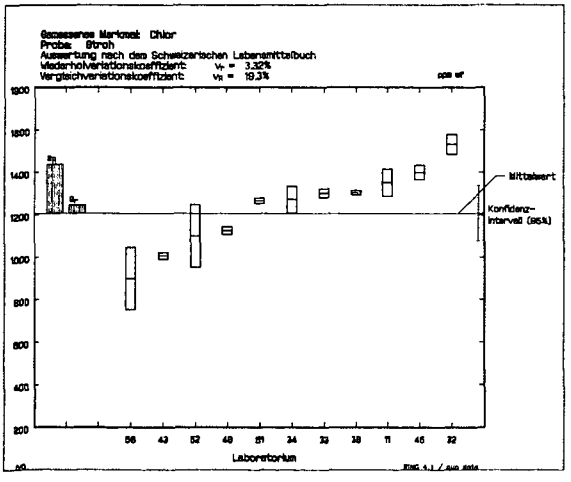

Figure 2: Chlorine in straw analysed by reduced methods

In order to evaluate some single laboratory values the sample preparation, digestion and measurement procedures are shown in Table 1 and 2. Some of the results can be explained as follows:

- Preashing the sample will lead to a loss of volatile matters (Lab 49)
- Using Eschka-mixture (Labs12,37) is also not recommended for Cl detection, because volatiles will be lost when putting the probe for 1h in an 675°C heated muffle furnace. This was also reported by [3].
- The low temperature and low pressure of the "Wurzschmitt"-Digestion (Lab 58) may lead to bad results
- Due to a single analysis the results from Lab 54 are not considered.

In order to go one step further, the laboratories were divided into several groups of similar digestion methods. This shows whether the analysis results will be more comparable for laboratories using comparable digestion methods. **This is no classification or benchmarking of the laboratories.**

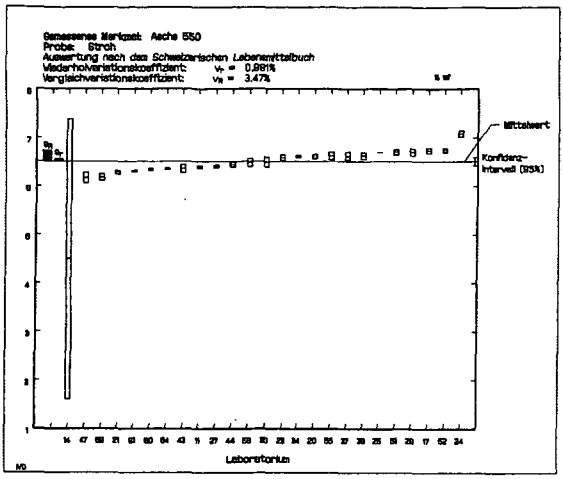

Figure 3: Ashcontent of straw at 550°C

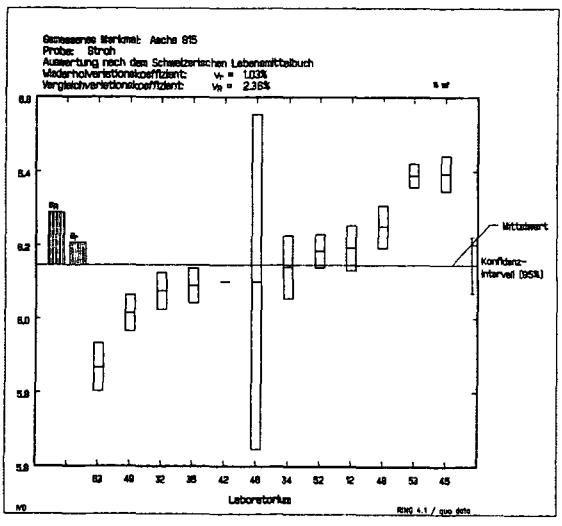

Figure 4: Ashcontent of straw at 815°C

Figure 2 shows laboratories using a combustion method collecting the combustion products in an alkali solution.
This makes it clear that reducing the analysis methods for chlorine detection does not lead to more comparable results.

Due to the free choice of analytical methods the ash content was determined in a temperature range of 550°C up to 900°C. Figure 3 and 4 show the measured results.
The high standard deviation of Laboratory 14 in figure 3 can not be explained. The results from other labs scatter in a range of ± 7% around the robust median value of 6,5% (db). The methods used are all based on the principle of ashing the probes till constant weight. They only differ in sample preparation (milled, unmilled, preashed, or humidified). The ash content determined at 815°C shown in Figure 4 has a mean value of 6,18% (db), which is significantly lower than the 550°C values.

DISCUSSION AND CONCLUSIONS

One of the major problems when analysing biomass is the non-homogeneity of the fuel and therefore, the collection of a representative probe. The reason for "outliers" is often the small sample-mass taken for the digestion.
Comparing the results from different laboratories using suitable methods for analysing chlorine in the fuel it can be seen that the values scatter in a range of ±25% around the robust mean value although they were using very different methods. Even digesting the sample by eluting it with water shows very good results. This confirms the assumption that chlorine in Biomass is mostly inorganically bound, whereas the organically bound part is very small. The elution method facilitates to use larger sample quantities for the digestion, with which a better homogeneity can be reached. Reducing the possible digestion methods does not lead to a better comparability of the results. This underlines the previously mentioned problem of the non-homogeneity of the fuel.
The ash content of the fuel is strongly connected to the ashing temperature since at higher temperatures more volatile matters are released. The amount of volatiles in biomass (>75%) is very high compared to coal (≈ 35%). It is recommended that ash content should be determined at 550°C, because the volatile elements in a combustion plant condense in the fly ash and therefore must be considered in the ash balance.

ACKNOWLEDGEMENTS

The presented work has been financially supported by the German Federal Ministry for Agriculture and Forest. FKZ:97NR055, "Standardisierung biogener Festbrennstoffe".

Table 1: Analysis Methods

Lab	Preparation	Amount	Digestion	Method	Lab	Preparation	Amount	Digestion	Method
		[mg]					[mg]		
11	1000	1100	03b	12	43	1005	300	03b	19
12	1000	1100	05	12	45	1000	20	02e	20
13	1000	200	02d	06	46	1000	20	02d	20
17	2300		03c	12	47	1000	1000	14	06
20	1000	5000	12c	06	48	1000	250	07	06
22	1000	500	20	12	49	1000	500	04	12
24	1000	10000	13	06	51	1000	700-800	03a	06
25	1303	5500	21	14	52	1000	100-200	17	06
27	1000		20	06	54	1002	1000	03c	06
29	1004		21	14	56	1000	400-600	03a	12
32	1000	400	03a	06	57	1000	1000-2000	07	12
33	2302	2-10	02e	12	58	1000	100	16	06
34	1001	15000	03b	06	59	1000	220	03c	06
35	1003	200	03a	06	60	1001	220	03c	06
36	1000	800	02	06	61	1001	1000	14	06
37	2300	1100	05	12	63	1000	130	03a	06
42	1000	2000	04	06					

Table 2: Method-Code

Digestion		**Analysis**	
2	Combustion in Oxygen	6	IC
3	Calorimetric Bomb	12	Titration $AgNO_3$
4	Wickbold	14	XRF
5	Eschka	19	Ion Sensitive Electrode, ISE
7	Eluting with HNO3	20	Mikrocoulorimeter
12	Ashing		
13	Aqueous Solution (hot) 10g/250 ml	**Chemicals**	
14	Aqueous Solution (hot) 5g/250 ml	a	Alkali Solution and H_2O_2
16	Wurzschmitt	b	Alkali Solution
17	Grote-Krekeler	c	In Water
18	Melting Digestion	d	In Aqueous H_2O_2-Solution
20	Aqueous Solution	e	In Acid and Acetate - Solution
21	Pellet		

Sample Preparation							
1	As recieved	0	20°	0	Air	0	No extra milling
2	dried	3	105°	1	N_2	1-5	Extra milling

REFERENCES

[1] Mäder, Manfred (1996): Auswertung von Ringversuchen mit Hilfe Robuster Statistik, Ph.D, University of Würzburg

[2] Schweizer Handbuch für Lebensmittelchemie, 1989

[3] Obernberger, I. et al (1996): Round Robin on biomass fuel and ash analysis, Joule III, JOR3-CT95-0001, European Commission

[4] IVD, et al (1999) „Operational Problems, Trace Emissions and By-Product Management for Industrial Biomass Co-Combustion....", JOR3-CT95-0057

USE OF CHEMICAL FRACTIONATION

TO PREDICT BIOMASS FUEL ASH BEHAVIOUR

Rob Korbee

ECN-Biomass
Netherlands Energy Research Foundation
P.O. Box 1, 17755 ZG Petten, The Netherlands

KEYWORDS: biomass, ash deposition, selective extraction

ABSTRACT

Chemical Fractionation (CF) has been proposed by several researchers as a tool to assist in the advance prediction of biomass fuel ash behaviour. In this work, the relation between CF classes and alleged behaviour during pf combustion is studied experimentally. Samples of well-analysed fuel batches - wood, straw and chicken manure - have been subjected to a scheme of selective extractions. After each extraction, a subsample of the partly extracted material was used as a fuel in a lab-scale combustion and ash deposition test. Comparison of the ash deposits obtained with original and selectively extracted fuels yielded valuable information on the practical use of selective extraction for the prediction of biomass fuel ash behaviour. Suggestions for improvement of the extraction scheme are also given.

INTRODUCTION

Chemical Fractionation (CF) is a method to discriminate inorganic classes in biomass fuels according to their solubility in a sequence of increasingly aggressive solvents [Baxter, 1996]. The parts of the fuel found as either water soluble, ion exchangeable, hydrochloric acid soluble or residual (non-soluble) are subsequently related to their alleged behaviour in a process like e.g. pulverised fuel combustion. Generally, the water soluble and ion exchangeable classes include various salts of potassium and sodium which are considered to be easily vaporised in a high temperature process. Carbonates and sulphates are expected in the hydrochloric acid soluble class [Baxter, 1996], while the oxides, silicates and sulphides are not extracted and classified as residual.
Both the hydrochloric acid soluble and residual matter are considered to be much less reactive in a thermal process.

The proportion of the elements of interest found in the first two classes is mostly interpreted as a measure for the release of reactive inorganic species to the gas phase. Their availability is subsequently related to enhanced deposition of ash on boiler and heat exchanging surfaces.
So far, ash deposition has been studied using fuels as a whole. In the current study, selective extraction has been applied to produce fuels lacking specific inorganic species. These fuels have been used in lab-scale deposition tests to verify the alleged relations with the currently used CF classes.

EXPERIMENTAL

Wood, straw and chicken manure with well-known inorganic compositions (threefold ICP-AES analysis per fuel) have been tested with respect to their ash deposition behaviour in a lab-scale combustion simulator. In Figure 1, a schematic view of the installation is given. By means of a staged gas burner and electrical furnace, the gas temperature and gas phase concentrations of O_2, CO, CO_2, H_2O, SO_2 and N_2 have been set to simulate typical combustion conditions in a pulverised fuel boiler. Fouling of superheaters was simulated by means of a temperature-controlled metal deposition surface, with a surface temperature of 600 °C at a gas temperature of 1200 °C. The surface temperature was recorded during the deposition test. The deposits were analysed off-line in 2D and 3D by means of SEM-EDX. The results serve as a reference for comparison with the deposition behaviour of partly extracted fuels.

The same fuels were subjected to a sequence of three selective extractions using water, a 1 M NH_4Ac solution and a 1M HCl solution. The procedure suggested by Baxter [1996], see Figure 2, was evaluated by a) comparing the composition of the extracted material with the extract concentrations, b) comparing parallel to sequential extraction, c) examining the effect of pH-control during the extraction and d) evaluating multiple extractions at a low L/S ratio versus a single extraction at a proportionally higher L/S ratio. From these tests, suggestions for improvement of the procedure are given. Extracted material has been taken from each extraction step to be used as a fuel in a deposition test in the facility described above. Again, SEM-EDX was used to examine the deposits and to compare the occurrence of specific species in these deposits with those obtained from burning the original fuels.

RESULTS

Extraction at a L/S ratio of 3 is not feasible for biomass such as wood or straw due to a very high water uptake. An L/S ratio of 10 or more should be used in stead.

The determination of extracted elements is much easier and cheaper by analysing the extract than by handling and opening up and analysing the extracted solid residue.

The pH-value after equilibration of the solvent with the solid phase is influenced by and depends on the biomass used. Control of the pH-value at a pre-set constant value may be considered but care must be taken not to replace a pH-influence on the extraction process by an influence of increased ion concentrations in the solvent.

Partly extracted fuels have been used in lab-scale ash deposition tests under simulated pf firing conditions. The deposits are compared to those obtained from the original fuels by means of 2D and 3D SEM-EDX analysis, identifying the presence and role of relevant species in the deposit. Heat fluxes through the growing deposit layers have been determined as a function of time as a more quantitative measure of deposit development. Definite results will be presented by the time of the symposium.

DISCUSSION AND CONCLUSIONS

- Selective extraction schemes which are currently used for predicting fuel ash behaviour have been designed - in the past - for the evaluation of leaching characteristics of soils. For a Chemical Fractionation analysis of biomassfuel inorganic matter, an adapted design should be aimed at the selective extraction of elements of interest applying specific pH-values and/or solvent ion concentrations. It may be necessary to control these conditions to eliminate effects of the fuel (biomass) matrix during the extraction. More work is needed to establish specific conditions for extracting key elements or species with a known behaviour in thermal processes.
- Up till now, only a gross difference between water soluble / ion exchangeable, strong acid soluble and non soluble inorganic species can be made using three selective extractions. A definite relation between extraction results and fuel ash behaviour can be obtained using fuels which have been partly extracted under well-controlled conditions in subsequent combustion tests aimed at ash deposition evaluation. From this, extraction schemes can be set up for the determination of specific, predefined inorganic species.

REFERENCES

L.L. Baxter, Chemical Fractionation Procedure, in: "Alkali Deposits Found in Biomass Power Plants, a Preliminary Investigation of Their Extent and Nature", Summary Report for National Renewable Energy Laboratory, by T.R. Miles, P.E., T.R. Miles jr., L.L. Baxter, R.W. Bryers, B.M. Jenkins and L.L. Oden, Golden, CO, USA (1996).

FIGURES

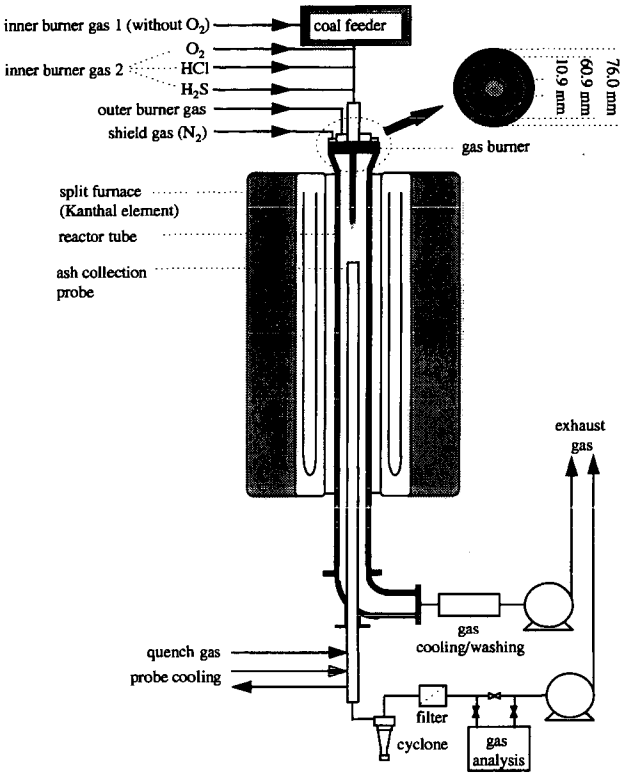

Typical particle feed rate (g/h)	1
Particle residence time (ms)	10 – 3000
Particle heating rate (°C/s)	$> 10^5$
Gas supply inner burner	CH_4, CO, CO_2, H_2, N_2, O_2, H_2S
Gas supply outer burner	CH_4, CO, H_2, O_2, H_2S
Operating pressure (MPa)	0.1
Reactor tube inner diameter (m)	0.076
Reactor tube length (m)	1.0
Max. electrical heating temperature (°C)	1600
Probes for:	gas temperature/ composition measurement; ash & deposit collection

Figure 1. Schematic overview of the Atmospheric Entrained-Flow Gasification and Combustion simulator, and its main features.

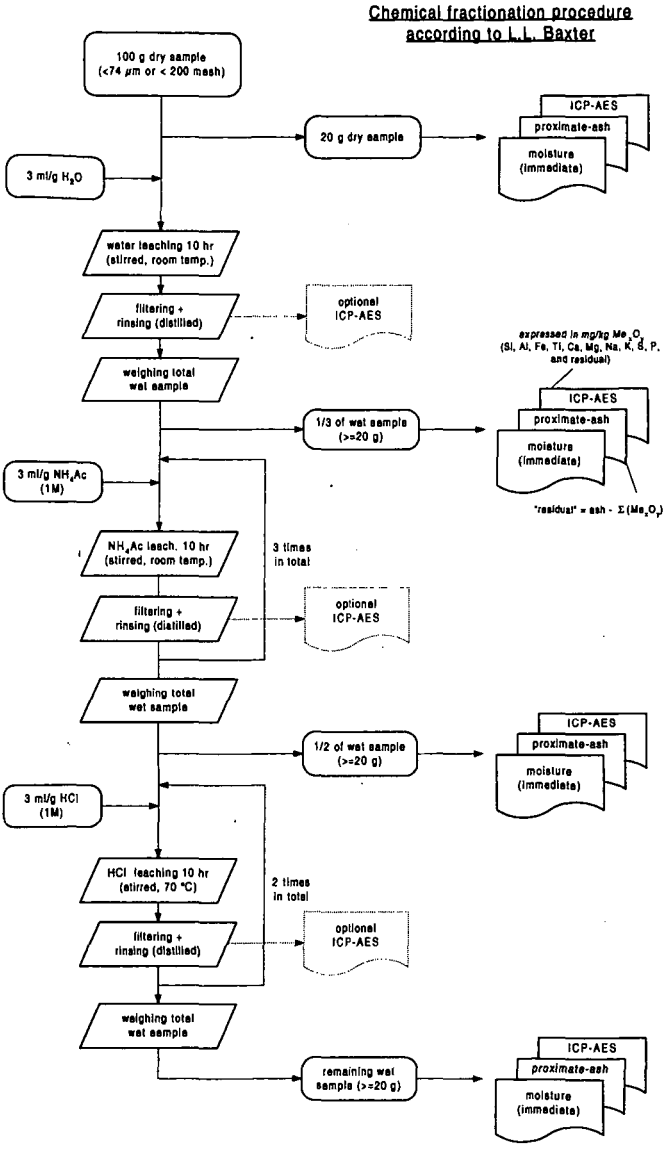

Figure 2. Extraction scheme used for Chemical Fractionation analysis of inorganic matter in biomass fuels (Baxter, 1996).

TRAPPING AND IDENTIFICATION OF OXIDIZED MERCURY SPECIES IN FLUE GAS

Edwin S. Olson, Jeffrey S. Thompson, John H. Pavlish

Energy and Environmental Research Center, University of North Dakota

Grand Forks, ND 58202

KEY WORDS: mercury measurement, speciation, gas chromatography–mass spectrometry

ABSTRACT

Current methods for speciation of vapor-phase mercury do not distinguish the inorganic forms of oxidized mercury. The assumption that Hg(II) is $HgCl_2$ or HgO for modeling behavior of oxidized mercury is unwarranted. Advances in cryogenic and solvent trapping of oxidized mercury species and their analysis by mass spectrometry led to the conclusion that surface reactions of elemental mercury with flue gas components result in more complex chemistry. Recent research demonstrated that in a simulated flue gas stream containing NO_2 and SO_2, the volatile form of the mercury emitted from the sorbent after breakthrough was determined to be mercury (II) nitrate hydrate, $Hg(NO_3)_2 \cdot H_2O$. Improvements in the sampling and analysis allowed for examination of other reaction products. Mercuric chloride and mercuric nitrate hydrate are separated by gas chromatography and identified by mass spectrometry. The eventual goal of this effort is a definitive speciation technique for determination of oxidized mercury in combustion flue gas.

INTRODUCTION

Much attention is currently focused on the air emission of trace amounts of toxic inorganic compounds during combustion of fossil fuels and incineration of waste materials. Mercury is of particular interest, owing to the high volatility of mercury and certain mercury compounds, the biological pathways that result in its concentration in fatty tissues, and its potential neurotoxic effect. To understand the complexities of its emission during combustion and dispersion throughout the environment, it is necessary to identify the mechanisms for its transformations, including capture on sorbents, scrubbers, or other control devices and release from these devices. Understanding these mechanism in turn requires identification and quantitation of the forms of mercury compounds involved. Previous and ongoing identifications or speciations of trace mercury are based mainly on distinguishing oxidized from elemental mercury forms. Often it is assumed that oxidized mercury in the gas phase is mercuric chloride, since that is the most well-known volatile mercury salt. Predictions based on this *implicit speciation* could be erroneous if one uses the thermodynamic stabilities of mercuric chloride to represent the behavior of oxidized mercury.

Characterization of trace amounts of solid-phase mercury has progressed further, especially with the application of XAFS. Mercury forms sorbed on three types of activated carbon sorbents were recently examined (1). The results for mercury chemisorbed on a lignite-derived activated carbon were consistent with a form with either a mercury–sulfur bond or a mercury–chlorine bond. This more *explicit speciation* is valuable in determining the nature of the sorption reactions.

For understanding mercury transformations between the gas and solid phases, a *definitive speciation* of mercury compounds is needed. Perhaps HgO could form in certain atmospheric conditions as a combustion gas cools, but it is unlikely that HgO desorbs from a solid phase, since the heat required to decouple the mercury–oxygen bonds in the polymer is too high; thus elemental mercury is more likely released. That simply points to a need for a method to identify not only HgO in the gas phase but also many other mercury species containing nitrogen, sulfur, oxygen, and chlorine.

Previous research at the Energy & Environmental Research Center (EERC) was successful in cryogenically trapping oxidized mercury forms from a gas stream (2). Selective desorption could separate elemental mercury from oxidized forms, but the desorption of oxidized forms was not accompanied by a selective identification method.

Recently, the EERC reported the trapping and identification of the oxidized mercury species that is released from an activated carbon sorbent after breakthrough in a simulated flue gas stream containing both SO_2 and NO_2 (3). In an extensive matrix of mercury sorption experiments with flue gas components (4), early breakthrough was observed only when NO_2 and SO_2 were both present in the gas phase. Many years ago, the reaction of NO_2 with Hg was shown to form HgO on the container surface (5). This reaction is consistent with the high sorption capacity observed on carbons

in a gas containing NO_2 and not SO_2. Later, Freeman and Gordon (6) presented evidence for mercurous nitrite and mercurous nitrate in solid products from the reaction. To understand the early breakthrough interaction when SO_2 is added to experiments, identification of the volatile oxidized mercury species was required. This was established by trapping the effluent gas in a cold organic solvent, evaporating part of the solvent, and analyzing by GC–MS. This high-confidence technique demonstrated that the released mercury product formed in the NO_2–SO_2 mixture was mainly mercuric nitrate hydrate (3). Both MnO_2 and catalytic carbons behaved similarly.

In other environments, species such as $HgCl_2$ could also be present and detectable. Work in an earlier CATM project established that $HgCl_2$ could be trapped cryogenically and subsequently desorbed readily as an oxidized mercury species, presumed to be the original $HgCl_2$ (2).

Transformations of the oxidized species in the flue gas to other oxidized species are anticipated as a result of gas-phase or gas–solid reactions. Methods for distinguishing these species, mixtures of these species, and other oxidized species are needed to understand the interactions occurring on sorbents, ash particles, and duct or filter bag surfaces.

Whether other oxidized mercury species are present in sorbent breakthrough emission or flue gas emissions in general is unknown. It is important to determine the definitive speciation of all emitted oxidized species in order to understand the reactions that occur on the sorbent that lead to inferior mercury sorbent performance in flue gas component mixtures. These interactions between mercury and gas components are also very important in understanding speciation of mercury in combustion flue gases and similar interactions that may occur on ash particles.

Organomercury compounds, as well as $HgCl_2$, have been separated and determined by GC; however, the trapping and identification of a nonhalogenated vapor-phase oxidized mercury species is a novel breakthrough in mercury research. The goal of present research is to develop cryogenic trapping and desorption methods for oxidized mercury species and to develop and apply high-confidence MS methods for identification and quantitation of oxidized mercury species.

RESULTS

In order to develop a method for determination of oxidized mercury compounds in the gas phase by cryogenic trapping coupled with desorption into a GC–MS, the volatility and stability of the mercury compounds of interest must be understood. The volatility behavior of mercuric chloride is better known, and the application to trapping and desorption appeared straightforward (2). Other mercury salts are less well understood. A recrystallized standard of $Hg(NO_3)_2 \cdot H_2O$ was prepared and vaporized in a gas flow as a source of $Hg(NO_3)_2 \cdot H_2O$ vapor. The gas flow was trapped cryogenically, and the concentration was determined by desorption, conversion to elemental mercury in a heated tube, and detection with a conventional atomic fluorescence spectrometer. This gave reproducible peak area responses. This established that a constant source for vapor phase $Hg(NO_3)_2 \cdot H_2O$ could be utilized for loading traps with this species and that trapping and desorption of this compound are feasible.

Conditions for GC–MS analysis of $HgCl_2$–$Hg(NO_3)_2 \cdot H_2O$ mixtures were investigated. Previous studies indicated that acetonitrile solutions of $Hg(NO_3)_2 \cdot H_2O$ could be injected in a standard inlet operated under splitless conditions, and the $Hg(NO_3)_2 \cdot H_2O$ eluted as a fairly sharp peak at 5.4 minutes through a nonpolar (DB5) 30-meter column. A unique mass spectrum corresponding to $Hg(NO_3)_2 \cdot H_2O$ was observed for this peak. Injection of $HgCl_2$ in acetonitrile resulted in elution of a $HgCl_2$ peak with its characteristic mass spectrum. The $HgCl_2$ peak eluted later than the $Hg(NO_3)_2 \cdot H_2O$ and was very broad. This indicates that $HgCl_2$ interacts much more strongly with the column phase than does $Hg(NO_3)_2 \cdot H_2O$, as one would expect.

During the chromatography of $Hg(NO_3)_2 \cdot H_2O$, some elemental mercury forms in the GC injector from decomposition of the $Hg(NO_3)_2 \cdot H_2O$ on the injector surfaces and elutes very early in the chromatogram. It is also likely that some mercury is vented from the inlet. Thus the response for $Hg(NO_3)_2 \cdot H_2O$ is not as high as hoped, but standard injection in a solvent is probably not the ideal way to introduce these compounds to the mass spectrometer. In fact, the injection temperature had to be lowered to get a better response for the $HgCl_2$. Except for the elemental, no other Hg-containing peaks, such as an acetonitrile complex or product resulting from decomposition, were observed.

When mixtures of $Hg(NO_3)_2 \cdot H_2O$ and $HgCl_2$ in acetonitrile were injected at an intermediate temperature, two peaks were observed at their characteristic retention times in the chromatogram (Figure 1b). Reconstructed selected ion chromatograms for the isotopic cluster at m/z 250–254 representing the $Hg(NO_3)_2 \cdot H_2O$ peak and at m/z 270–274 representing the $HgCl_2$ peak are shown

in Figures 1c and 1d, respectively. The mass spectrum of $Hg(NO_3)_2 \cdot H_2O$ representing one scan in the $Hg(NO_3)_2 \cdot H_2O$ peak is shown in Figure 1a. The base peak is at m/z 252 with a characteristic pattern for the mercury isotope ions (3). The molecular ion is very small for this compound and cannot be seen in the mass spectrum for this scan.

While it is clear that optimization of the inlet configuration and chromatography conditions are needed, these experiments establish the feasibility of observing at least two oxidized mercury species as they elute from a GC column. These two compounds appear to have no difficulty transferring through the coated columns that are necessary to maintain the vacuum conditions. Of course, other mercury compounds may not survive inlets, columns, or desorption conditions and may convert to these and other species.

Replacement of the standard GC inlet with a 1-mL glass vial for introducing oxidized mercury species was investigated. The vial was fitted with a small septum through which an inlet capillary (from the injector assembly) and outlet capillary (the GC column) were inserted through the septum. The vial was loaded with a mixture of $HgCl_2$ and $Hg(NO_3)_2 \cdot H_2O$ by injecting 1μL of the standard acetonitrile solution of $HgCl_2$ and $Hg(NO_3)_2 \cdot H_2O$ and allowed to evaporate for a minute. The septum cap was replaced and the vial placed in the GC oven. The GC oven temperature program was initiated and mass spectral data accumulated. The $HgCl_2$ and $Hg(NO_3)_2 \cdot H_2O$ were successfully desorbed from the vial into the column. Initially, a very short column (3 meter) was used, and both mercury compounds desorbed and eluted into the MS in a broad unresolved peak The spectra of both the $HgCl_2$ and $Hg(NO_3)_2 \cdot H_2O$ were evident, but the ion trap was not operating under high vacuum with the short column, so the spectra and reconstructed chromatogram were noisy, owing to excessive space charging. Use of a longer column resolved the peaks and allowed a better vacuum resulting in better spectra. The peaks were not as sharp as those obtained with a normal GC injector.

The vial was then loaded from a gas stream containing $Hg(NO_3)_2 \cdot H_2O$. The vial was cooled in an ice salt bath, and the $Hg(NO_3)_2 \cdot H_2O$ was loaded using the source described above. The vial was then transferred to the GC oven and attached to the column as described above with the septum cap. Again, the $Hg(NO_3)_2 \cdot H_2O$ peak was observed in the accumulated mass spectal data. Some decomposition to elemental mercury was evident. The reproducibility of this method has not yet been established, and further research in materials and techniques is needed. Of major concern is how to deal with trapped moisture that is eluted into the MS.

CONCLUSION

GC–MS methods were used to separate a mixture of two volatile oxidized mercury species, $HgCl_2$ and $Hg(NO_3)_2 \cdot H_2O$, and give characteristic mass spectra for the two components. The separation and analysis can occur with materials trapped from the gas phase into a solvent and subsequent injection into the GC–MS injection port or by desorption from a solid phase in a small trapping vial. Thus definitive identification and quantitation of these two species are feasible. Present efforts are focused on developing coupling hardware for interfacing larger traps to the GC–MS.

ACKNOWLEDGMENTS

The authors express their thanks to the following sponsors: North Dakota Industrial Commission; EERC Center for Air Toxic Metals Program sponsored by EPA under Assistance Agreements CR821518k CR823173, and CR824854; Otter Tail Power Company; and Northern States Power Company.

REFERENCES

1. Huggins, F.E.; Huffman, G.P.; Dunham, G.E.; Senior, C.L. *Energy & Fuels* **1999**, *13*, 114.
2. Thompson, J.S.; Pavlish, J.H. Cryogenic Trapping of Oxidized Mercury Species from Combustion Flue Gas. *Proceedings of the Air Quality Conference*; McLean, VA, Dec 1, 1998.
3. Olson, E.S.; Sharma, R.K.; Miller, S.J. Dunham, G.E. Mercury in the Environment. *Proceedings of a Specialty Conference*; VIP-91, Air & Waste Manag. Assoc., Minneapolis, MN, Sept. 15, 1999, p. 121.
4. Miller, S.J.; Dunham, G.E.; Olson, E.S. Mercury Sorbent Development for Coal-Fired Boilers. *Proceedings of the Air Quality Conference*, McLean, VA, Dec 1, 1998.
5. Pierce, W.C.; Noyes, W.A. *J. Amer. Chem. Soc.* **1928**, *50*, 2179.
6. Freeman, E.S.; Gordon, S. *J. Amer. Chem. Soc.* **1956**, *78*, 1813.

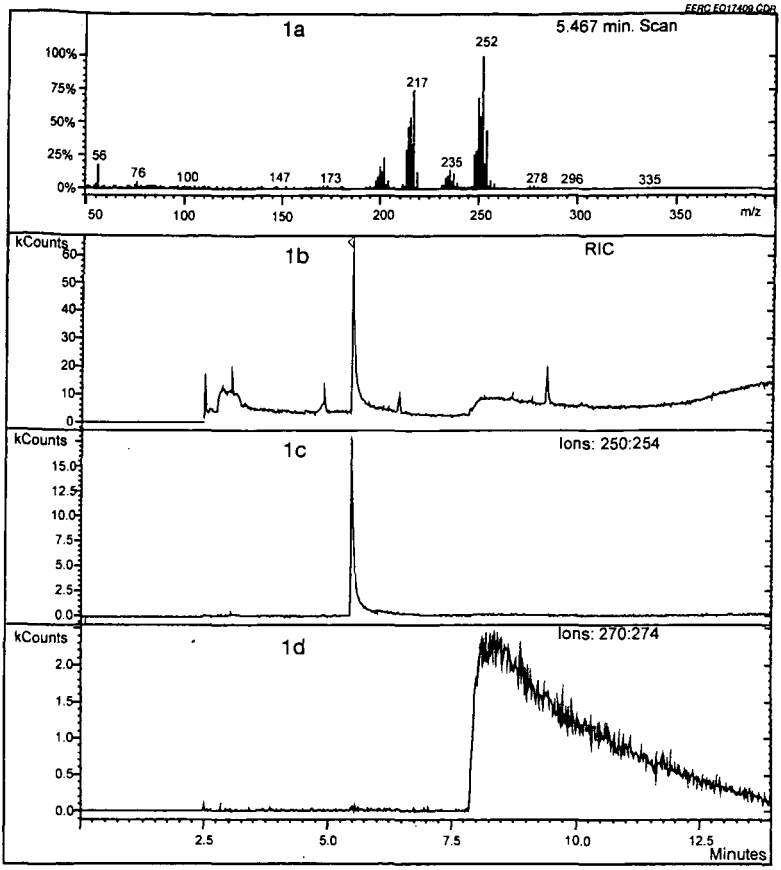

Figure 1a. Mass spectrum for Scan 329; 1b, total in chromatogram; 1c, selected ion chromatogram for m/z 250-254; and 1d, selected ion chromatogram for m/z 270-274.

ANALYSIS OF HIGH TEMPERATURE COHESION OF ASH PARTICLES USING MODEL PURE SILICA POWDERS COATED WITH ALKALI METALS

Hidehiro Kamiya, Akira Kimura, and Makio Naito*

Graduate School of Bio-Application System Engineering, BASE, Tokyo University of Agriculture & Technology, Koganei, Tokyo 184-8588, Japan
* Japan Fine Ceramics Center, Atsuta-ku, Nagoya Japan

ABSTRACT. This paper analyzes the mechanism of increasing cohesive behavior of ash powders at elevated temperatures. Model ash powders were prepared from fine pure silica powder coated on the surface with 0.5 wt% alkali metal. The cohesive behavior and deformation properties of model ash powder beds were determined by using a new split type tensile strength tester of powder beds. The behavior of fly ash collected in pulverized coal combustion and model ash powders were compared. In the high temperature range above 1100 K, a rapid increase of tensile strength and plastic deformation of the ash powder beds occurred in both the natural ash and the model silica particles. It is suggested that the coated alkali metal on the silica powders reacted with the amorphous silica phase and formed a small amount of low melting point eutectic materials.

INTRODUCTION

The increase of stickiness and adhesion force of ash powder at high temperatures hinders the stable operation and scale-up design of various high efficiency coal combustion power generation system, for example, the integrated coal gasification combined cycle (IGCC) and pressurized fluidized bed combustor (PFBC) systems. Dry ash particle deposition and the growth of a deposited ash layer on the water-cooled wall blocked the gasifier in IGCC systems and pulverized-coal combustors[1]. In PFBC systems, the operation of filter cake detachment on rigid ceramic filters by reverse-pulsing has difficulty with the increase of the adhesive force of ash[2]. These cohesive properties of ash particles at these high temperatures depend on many physical and chemical factors.

In our previous paper we measured the tensile strength of fly ash powder beds by using a diametal compression test of ash powder pellets[3] and a new split type tensile strength tester of ash powder beds[4] at high temperature at a range from room temperature to 950°C. We reported that the tensile strength of ash powder beds rapidly increased over a range of 800°C.

This paper analyzes the mechanism of increasing cohesive behavior of ash powders at elevated temperatures by using model ash powders, which were prepared from fine pure silica powder coated on the surface with 0.5 wt% alkali metal. The cohesive behavior and deformation properties of model ash powder beds were determined by using a new split type tensile strength tester of powder beds. Based on the comparison with these results of fly ash and model powders, the increasing mechanism of ash powder stickiness at high temperature is discussed.

EXPERIMENTAL PROCEDURE

Model ash powder preparation and characterization

The original powder samples used a commercial pure fused amorphous silica powder and fly ash. Fly ash powder was collected in a commercial pulverized coal combustion plant. The chemical component and particle size distribution of each sample were determined using ICP and a

centrifugal sedimentation method shown in Table 1. The total impurity such as Na, K, etc. in the high-pure amorphous silica powder was about 13 ppm. The concentration of sodium and potassium in the fly ash was about 0.5%. The mean particle diameter of each sample was similar at about 5 μm.

Table 1 Mean diameter and chemical component of pure silica and fly ash powders

Powder sample	Mean diameter	Chemical component [wt%]				
		SiO_2	Al_2O_3	Fe_2O_3	K_2O	Na_2O
Pure silica	5.3 μm	99.99	13 ppm			
Fly ash	4.75 μm	45.0	38.5	4.6	0.3	0.5

Based on the above results, model ash powders were prepared from a commercial pure fused silica powder. Firstly, pure silica powder was added to the sodium or potassium oxalate solution. The amount of silica particles added and the concentration of the oxalate solution was adjusted so that the alkali metal concentration would become 0.5 wt% (silica) after drying. The silica suspension was mixed for one minute by a planetary type mixer and dried in an oven at 120°C. After grinding with a pestle and mortar, dried silica powders with alkali oxalate were heat treated at 620°C for 1 hour, causing thermal decomposition and removal of the oxalate.

Split type tensile strength tester for powder beds

The detail of a sprit type tensile strength test at high temperatures was described in our previous paper[4]. The powders were placed in a circular cell 5 cm in diameter with a depth of 1 cm. The cell can be divided equally into a stationary and a movable part; both parts were prepared with high-purity silica glass. After fixing the mobile part using a hook, powder samples were packed into the cell and consolidated by uni-axial pressing (2.5 kPa for 600 s). Tensile testing was carried out at various temperatures ranging from room temperature to 1173 K, with an electric furnace at a heating rate of 600°C/h. After heat treatment at each temperature for 540 s before the tensile test, the hook used to fix the mobile cell is removed, and the mobile cell is pulled in each high temperature conditions. The relationship between load and displacement during loading was then measured.

RESULTS AND DISCUSSION

Tensile strength and deformation behavior of fly ash and pure fused silica

Examples of tensile load and displacement relationship at room temperature and 1123 K are shown in Fig. 1. The brittle failure of both powder beds was observed after elastic deformation at room temperature. In the case of the pure silica powder sample, the brittle failure of the powder bed appeared at 1073 K. On the contrary, in the case of fly ash samples, viscous deformation appeared near the maximum load at 1073 K. Under conditions of relatively low temperatures below 1000 K, the adhesive force of both powders increased gradually in proportion to temperature. The tensile strength of the pure silica powder bed gradually increased, even in elevated temperatures (> 1073 K). However, a rapid increase of tensile strength of fly ash powder beds was observed in the high temperature range (> 1073 K).

Model ash powders

To analyze this rapid increasing tensile strength of fly ash above 1100 K, the relationship between tensile strength and deformation behavior of alkali metal coated pure silica powder beds with

different coating condition at different temperature were measured and shown in Fig. 2. The rapid increase of tensile strength with viscous tensile deformation was observed by a coating of 0.5 % alkali metal on the surface of pure silica powders in a high temperature range above 1073 K.

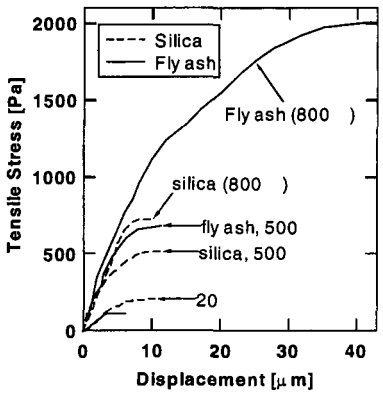

Fig. 1. Examples of tensile stress and displacement relationship of ash and silica.

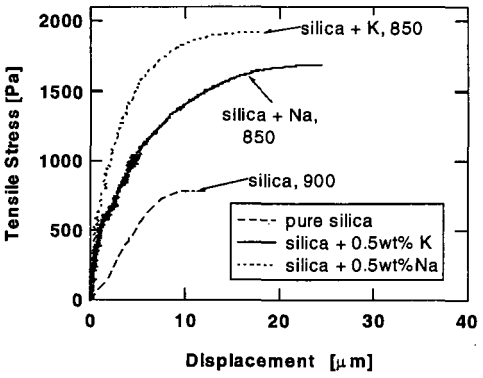

Fig. 2. An example of the tensile stress and displacement relationship of model ash powder beds prepared from pure amorphous silica powder and alkali metals.

The effect of testing temperature on the tensile strength of model ash powder beds with different alkali coating conditions is shown in Fig. 3. Regardless of the alkali metal used, the tensile strength of the model powder beds exhibited an increase with a temperature rise above 1073 K equal to that shown in the fly ash samples. This indicates that the coated alkali metal on the silica powders reacted with the amorphous silica phase and formed a small amount of low melting point eutectic materials. Hence, above 1073 K, a small amount of liquid phase formed between silica particles consisting of amorphous silica and alkali metal. It is suggested that a small amount of low melting point eutectic materials, consisting of amorphous silica and alkali metal, formed a liquid phase and this was responsible for the majority of the increase in the adhesive force mechanism of the ash powders at high temperature. This liquid phase mix was estimated from the increase in rupture displacement during tensile test of powder beds at high temperature.

CONCLUSION

Model ash powders prepared from pure amorphous silica powder and coated alkali metal were used to reproduced the rapid increasing tensile strength of ash particle stickiness and deformation behavior in high temperatures above 1073 K. We suggest that low melting point eutectic materials consisting of amorphous silica and alkali metal formed a small amount of liquid phase between particles and promoted the increase of ash adhesion behavior.

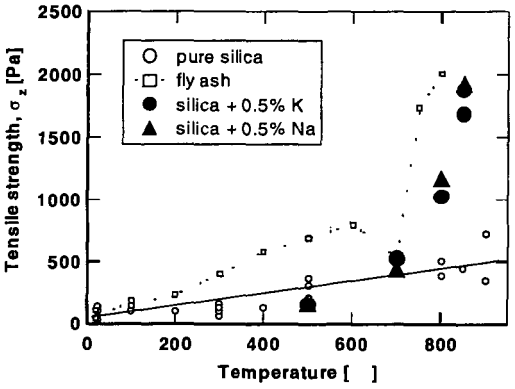

Fig. 3. The effect of temperature on tensile strength of model ash powders prepared from pure amorphous silica powders coated with sodium and potassium

Acknowledgment: This work is supported by the Proposal-Based New Industry Type Technology R&D Promotion Program from NEDO of Japan and Grant-in-Aid for Scientific Research (B), Japan.

REFERENCE

1. D.H. Smith, G.J. Haddad and M. Ferer : Energy & Fuel, 11, 1006-11 (1997)
2. H. Kamiya, K. Deguchi, J. Gotou and M. Horio : "High Temperature Gas Cleaning II" p. 111-118 (1999)
3. H. Kamiya, A. Kimura, M. Horio, J.P.K. Seville and E. Kauppinen : J. of Chem. Eng. Jpn., accepted.
4. H. Kamiya, A. Kimura, T. Yokoyama, M. Naito and G. Jimbo : Pow. Tech., to be submitted.

STUDY OF VANADIUM EMISSION CONTROL IN COMBUSTION SYSTEMS BY THERMODYNAMIC EQUILIBRIUM ANALYSES

Chang-Yu Wu and Sang-Rin Lee
University of Florida, Dept. of Environmental Engineering Sciences, Gainesville, FL 32611-6450

Key Words: Vanadium, Sorbent, Thermodynamic Equilibrium

INTRODUCTION

Toxic metal emissions from combustion sources such as vanadium are of great concerns. It is concentrated in certain types of coal, heavy oil and petroleum coke[1,2]. Once emitted, it can be transported to distance, resulting in adverse environmental and health effects[3]. It is known that vanadium may cause cardiovascular disease, bronchitis and lung carcinoma. Due to its high concentration, interest has been developed to recover vanadium from ash[4]. Vanadium, as other metals in the fuel matrix, may enter the gas stream in combustion systems by vaporization or entrainment of vanadium compounds. At high temperatures, it undergoes various chemical reactions to form various species depending on the combustion environment and composition in the system. At the cooler post combustion zone, various aerosol dynamics proceed resulting in the transformation of vanadium into particulate phase. The particle size distribution depends on the temperature history and the existing species in the system[5]. A lot of research studies have shown that metals undergoing this pathway generally form aerosols in the submicrometer regime. Unfortunately, traditional control devices have their minimum efficiency in this size regime. Thus, it is important to develop new techniques to effectively control vanadium emission.

Recently, studies have been conducted to use mineral sorbents to capture heavy metals. Heavy metals are chemically adsorbed on the injected sorbent particles. As these sorbent particles are relatively larger in size (typically greater than 10 μm), the metal-sorbent particles can be easily collected using traditional particulate control devices. Shadman and co-workers[6,7] used silica, alumina and various naturally available materials (i.e. bauxite, kaolinite and lime) to capture lead and cadmium. Venkatesh et al.[8] evaluated various mineral sorbents constituting a spectrum of alumino-silicate compounds for immobilization of several heavy metals. Biswas and co-workers[9-11] *in-situ* generated sorbents particles with very high surface area to capture lead and mercury. However, no study using sorbents to capture vanadium has been conducted.

At high temperatures, reactions are fast and equilibrium can possibly be achieved. Hence thermodynamic equilibrium methods can be applied to determine the potential sorbent materials. The objective of this study is to use equilibrium calculations to determine the effective materials that can chemically adsorb vanadium. Optimal conditions to achieve high efficiencies will be determined. The impact of various common constituents in combustion systems on the performance will be assessed. The most effective one for vanadium control will be determined.

METHODOLOGY

A computer code, STANJAN[12], was used to implement the calculations. Its principle is to minimize the system's Gibbs free energy by using the method of elemental potentials combined with atom constraints. The thermodynamic data for all the relevant species were obtained from the literature[13,14]. Table 1 lists the species that are included in the calculations. The simulation conditions are listed in Table 2. The concentrations correspond to the levels found in a typical coal combustion system[15]. Due to the lack of coal's thermodynamic data, methane (CH_4) is used in the calculations. As the metal concentration is trace in the fuel, the form of the fuel used in the system does not affect the metal's speciation.

Calculations were first conducted to determine the behavior of vanadium in a typical combustion system without sorbent as the baseline. The performance of individual sorbent was then investigated for a wide range of temperatures. Parametric analyses were then conducted to evaluate the impact of chlorine and sulfur. Finally, all the sorbents were included and competition for vanadium among the various sorbents was placed to determine the best sorbent.

Table 1. List of Species used in the Equilibrium Calculation

Reactant	Product
V	V, VCl_2, VCl_3, VCl_4, VO, VO_2, $VOCl_3$,V_2C, VCl_4, V_2O_3, V_2O_4, V_2O_5, V(g), VCl_2(g), VCl_4(g), VO(g), $VOCl_3$(g), VO_2(g)
Ca	$CaCl_2$, CaO, CaO_2, $CaSO_3$, $CaSO_4$, CaS, $CaCO_3$, **$Ca(VO_3)_2$**, **$Ca_2V_2O_7$**, **$Ca_3(VO_4)_2$**, Ca(g), $CaCl_2$(g), CaS(g)
Mg	Mg, $Mg(OH)_2$, $MgCO_3$, $MgCl_2$, MgO, $MgSO_4$, **$Mg(VO_3)_2$**, **$Mg_2V_2O_7$**, Mg(g), $MgCl_2$(g), MgOH(g)
Na	Na, NaCl, NaOH, $NaClO_4$, $NaHCO_3$, Na_2CO_3, Na_2O, Na_2O_2, Na_2SO_3, Na_2SO_4, **$NaVO_3$**, **Na_3VO_4**, **$Na_4V_2O_7$**, Na(g), NaCl(g), NaOH(g), $Na_2O_2H_2$(g), Na_2SO_4(g)
Common compound	CH_4, CO, CO_2, , Cl, HCl, HOCl, NOCl, ClO, Cl_2, H, OH, H_2O, N, NO, NO_2, N_2, N_2O,O, O_2, S, SO_2, SO_3,

Table 2. Simulation conditions for evaluating the performance of various sorbents in capturing vanadium (unit: mole).

Set.	V	Cl	S	CH_4	O_2	N_2	Na_2O	$CaCO_3$	MgO
I-1	$7x10^{-7}$	0	0	1	4	15	0	0	0
I-2	$7x10^{-7}$	0.011	0	1	4	15	0	0	0
II-1	$7x10^{-7}$	0	0	1	4	15	$4.12x10^{-4}$	0	0
II-2	$7x10^{-7}$	0	0	1	4	15	0	0.0034	0
II-3	$7x10^{-7}$	0	0	1	4	15	0	0	$9.95x10^{-4}$
III-1	$7x10^{-7}$	0.011	0.0389	1	4	15	$4.12x10^{-4}$	0	0
III-2	$7x10^{-7}$	0.011	0.0389	1	4	15	0.0778	0	0
III-3	$7x10^{-7}$	0.011	0.0389	1	4	15	0.0934	0	0
III-4	$7x10^{-7}$	0.011	0.0389	1	4	15	0	0.0034	0
III-5	$7x10^{-7}$	0.011	0.0389	1	4	15	0	0.0389	0
III-6	$7x10^{-7}$	0.011	0.0389	1	4	15	0	0.0467	0
III-7	$7x10^{-7}$	0.011	0.0389	1	4	15	0	0	$9.95x10^{-4}$
III-8	$7x10^{-7}$	0.011	0.0389	1	4	15	0	0	0.0389
III-9	$7x10^{-7}$	0.011	0.0389	1	4	15	0	0	0.0467
IV-1	$7x10^{-7}$	0	0	1	4	15	0.0389	0.0389	0.0389
IV-2	$7x10^{-7}$	0.011	0.0389	1	4	15	$4.12x10^{-4}$	0.0034	$9.95x10^{-4}$
IV-3	$7x10^{-7}$	0.011	0.0389	1	4	15	0.0389	0.0389	0.0389

RESULTS AND DISCUSSIONS

Set I : Vanadium in a Typical Coal Combustion System Without Sorbents Added.

In the first set, the behavior of vanadium in a typical combustion system is studied. The results are shown in Figure 1. As shown, the major product is divanadium pentaoxide (V_2O_5) over the entire range studied. Metal oxide aerosols formed in combustion systems are generally in the submicrometer range and hence they are not desired.[17]

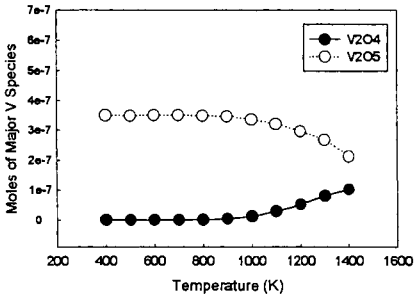

Figure 1 Partition of vanadium speciation in a typical coal combustion system without chlorine

Chlorine is known to have a strong affinity to react with many metals Therefore, its effect on vanadium speciation is also studied. The results are shown in Figure 2. As shown, vanadium oxytrichloride ($VOCl_3$) is important at medium temperatures (~500 – 1000 K) although not dominant. Compared with earlier studies on other heavy metals[5], chlorine's affinity to react with vanadium is relatively weak. Hence, it is probable that the presence of chlorine in typical combustion systems will not significantly affect vanadium's speciation.

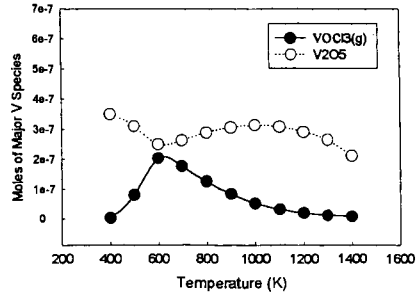

Figure 2 Partition of Vanadium species in a typical coal combustion system with chlorine

Although sulfur has been reported to be important for certain metals[5,16], calculations were not conducted in this study as there is no thermodynamic data available for vanadium-sulfur compounds.

Set II. Performance of Individual Sorbent.

Next, individual sorbent is examined for its performance. The amount of each sorbent used corresponds to the level found in typical coal. The results are shown in Figures 3a – 3c. As shown, all the sorbent materials used are very effective in almost the entire temperature range (forming sorbent-vanadium products). This indicates the high potential of using these materials. However, it should be noted that it does not necessarily guarantee the success of the process because of the influence by other constituents in the system. This will be discussed more in the next section.

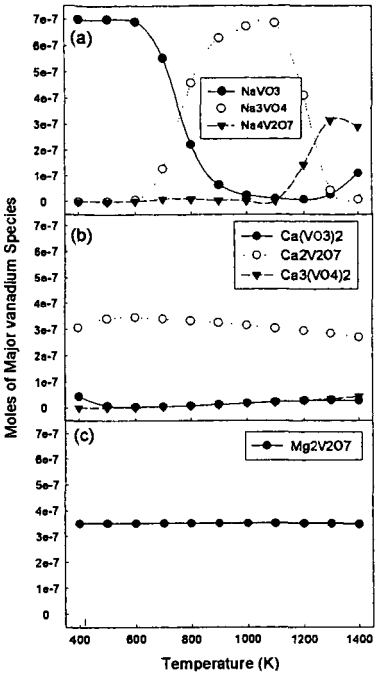

Figure 3 Partition of vanadium species using: (a) Na- based sorbent; (b) Ca-based (b) sorbent; (c) Mg-based sorbent

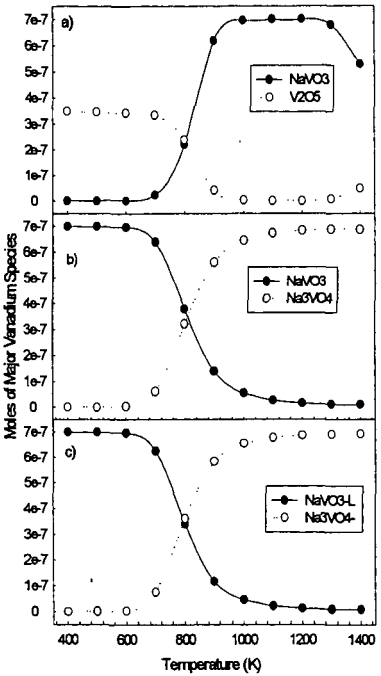

Figure 4 Impact of chlorine and sulfur on the effectiveness of Na-based sorbent: a) typical concentration in coal; b) stoichiometric amount of sorbent; c) to react with Cl and S 20% excess of sorbent than the stoichiometric amount

Set III Effects of Chlorine and Sulfur on the Performance of the Various Sorbent Used

Chlorine and sulfur are very common in coal and other fuels. They may react with vanadium to form vanadium chloride or sulfate. They can also react with the sorbent materials, for example, calcium sulfate (gypsum), thus reducing the available amount of sorbents to react with vanadium. Hence, their impact is investigated. First, calculations were performed using their concentrations in typical coal (Table 3). Then the stoichiometric amount necessary for scrubbing sulfur was used. Finally, 20% more of the sorbent than the stoichiometric amount was used. The results are shown in Figures 4 – 6 for Na-, Ca-, and Mg- based sorbent respectively.

Na-based sorbent

Figure 4a shows that V_2O_5 is dominant at lower temperatures (< 800K), indicating the ineffectiveness of the process. Examination of the products shows that the majority of sodium forms sodium sulfate (Na_2SO_4), thus depleting the available sodium. When Na_2SO_4 becomes unstable at higher temperatures (>900K), the sorbent is available again to react with vanadium. When the amount of sorbent is enough to deplete sulfur and chlorine, this process is effective (forming vanadium sorbent compound) even at lower temperatures, as shown in Figures 4b when stoichiometric amount of sorbent reacting with chlorine and sulfur is used.

Ca- based sorbent

Similar to the sodium case, Ca- based sorbent is ineffective at lower temperatures (< 1000K, Figure 5a). V_2O_5 is the dominant species and the cause is the same. When stoichiometric amount of calcium sorbent is used (Figure 5b), the temperature range for effective vanadium capture expands but V_2O_5 is still not captured effectively when the temperature is lower than 800 K. Only when excess sorbent is used (Figure 5c), calcium vanadate becomes the dominant species.

Mg- based sorbent

The similar trend is observed when Mg-based sorbent is used. However, Mg- based sorbent seems to be less effective than the other two sorbents investigated. As shown in Figure 5a, magnesium vanadates are not present even at high temperatures. The reason is due to magnesium's high affinity to form magnesium sulfate even at high temperatures. Magnesium vanadate becomes dominant only when excess amount of sorbent is used as shown in Figure 6c.

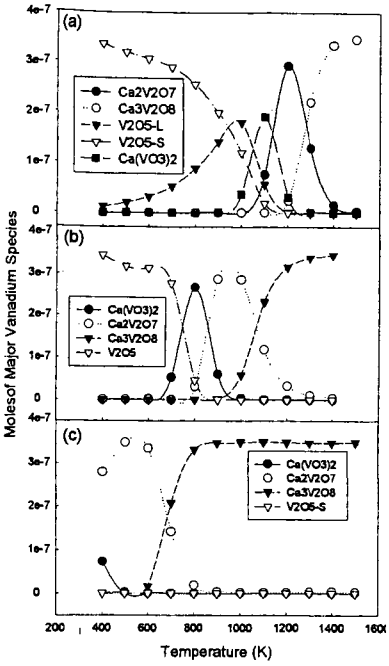

Figure 5 Impact of chlorine and sulfur on the effectiveness of Ca-based sorbent: a) typical concentration in coal; b) stoichiometric amount of sorbent to react with chlorine and sulfate; c) 20% excess of sorbent then the stoichiometric amount

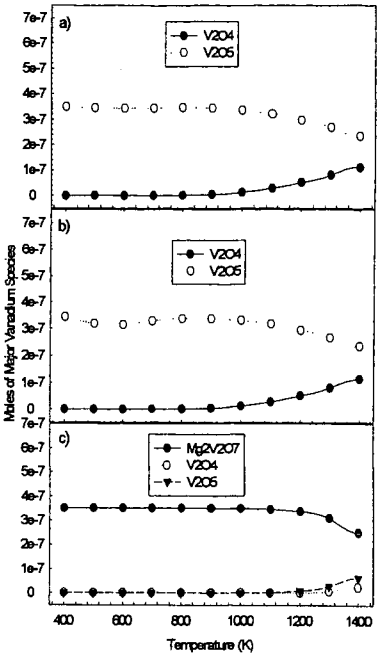

Figure 6 Impact of chlorine and sulfur on the effectiveness of Mg-based sorbent: a) typical concentration in coal; b) stoichiometric amount of sorbent to react with chlorine and sulfate; c) 20% 20% excess of sorbent then the stoichiometric amount

Set IV : Determination of the most effective sorbent.

To determine the most effective sorbent, in the final set of calculations all the sorbents were included. Calculations were first conducted for typical coal combustion assuming no chlorine or sulfur. Chlorine and sulfur concentrations in typical coal were then used. Finally, stoichiometric amounts of sorbent materials were used. The results are shown in Figures 7a-c, respectively.

Without chlorine or sulfur in the system, Na- based sorbent apparently is the most effective one in the entire temperature range investigated (Figure 7a). However, it has a stronger affinity to react with chlorine and sulfur. Hence, it becomes ineffective when chlorine or sulfur is present. On the other hand calcium is not significantly affected by the presence of chlorine. It is impaired by sulfur only at lower temperatures. Hence, Ca-based sorbent is more competent when chlorine or sulfur is present (Figure 7b). When stoichiometric amounts of sorbents are used, Ca- based sorbent is effective even at lower temperatures. This is probably due to the shielding effects of the presence of Na- and Mg- based sorbents as they are more vulnerable to chlorine and sulfur.

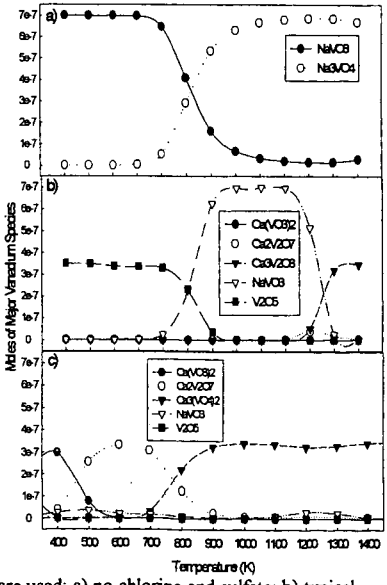

Figure 7 Partition of vanadium species when various amount of all sorbents are used: a) no chlorine and sulfate; b) typical coal combustion; c) stoichiometric amount of sorbents

CONCLUSIONS

Vanadium is concentrated in various fuels and the emission of vanadium from combustion systems is of concern. Mineral sorbents have been demonstrated to be effective to control various toxic metals in combustion systems. In this study, equilibrium calculations were conducted to identify the potential sorbent materials to chemically adsorb vanadium. Na-, Ca- and Mg- based sorbents were found to be effective. However, the presence of chlorine and sulfur in the system may affect the performance of these sorbents. Na- based sorbent is significantly impaired when chlorine or sulfur is present. Sodium chloride and sulfate are formed under this condition. Ca- and Mg- based sorbents are less affected by chlorine but sulfur substantially reduces their performance. Sulfates are formed under this condition. The formation of sulfates or chlorides diminishes the available sorbents for vanadium capture. Calculations were also performed to determine the most effective sorbent. Na- based sorbent is found to be the most effective one when no chlorine or sulfur is present. However, Ca-based sorbent becomes the most robust one when chlorine or sulfur exists.

This study provides the insight of the reactions between vanadium and sorbents as well as the impact of various operating conditions. The information obtained can be used as a basis for developing a better strategy for managing vanadium emission problems.

ACKNOWLEDGMENTS

The authors are grateful to the generous help from Dr. R. C. Reynolds, Department of Mechanical Engineering, Stanford University.

REFERENCES

1. Yee, B. H.; Rosenquist, W. A., "Petroleum Coke as an Alternative Fuel for New Generation and Repowering"; Proc. Amer. Power Conf., **(2)**, 838-841, 1996. IL Inst. Tech., Chicago, IL.
2. Bryers, R. W., "Utilization of Petroleum Coke and Petroleum Coke/Coal Blends as a Means of Steam Raising", *Fuel Processing Technology*, v 44 n 1-3 Sep 1995., p 121-141
3. Lin, C.Y.; Chiu, C.H., "Emissions of Industrial Furnaces Burning Vanadium-Contained Heavy Oils", *J. Env. Sci. Health*, A: Env. Sci. Eng. & Toxic & Haz. Sub. Ctrl, **30(1)**, 1995,133-142.
4. Tsuboi; I. K., Kunugita, S., Komasawa, E., Isao Recovery of Gallium and Vanadium From Coal Fly Ash., *J Chem Eng* Jpn, **24(1)**, 1991, 15-20.
5. Biswas, P. and Wu, C. Y., "Control of Toxic Metal Emissions from Combustors Using Sorbents: A Review", *J. Air & Waste Management Association*, **48**, 1998, 113-127.
6. Scotto, M. V., Uberoi, M., Peterson, T. W., Shadman, F. and Wendt, J. O. L., Metal Capture by Sorbents in Combustion Processes, *Fuel Proc. Technol.*, **39(1/3)**, 1994, 357-372.
7. Wu, B., Jaanu, K. K. and Shadman, F., "Multi-functional Sorbents for the Removal of Sulfur and Metallic Contaminants from High-Temperature Gases", *Environ. Sci. Technol.*, **29(6)**, 1995, 1660-1665.
8. Venkatesh, S., Fournier, D. J. Jr., Waterland, L. R. and Carroll, G. J., "Evaluation of Mineral-Based Additives as Sorbents for Hazardous Trace Metal Capture and Immobilization in Incineration Processes", *Haz. Waste. Haz. Mat.*, **13(1)**, 1996, 73-94.
9. Owens, T. M. and Biswas, P., "Reactions between Vapor Phase Lead Compounds and *In Situ* Generated Silica Particles at Various Lead-Silicon Feed Ratios: Applications to Toxic Metal Capture in Combustors", *J. Air Waste Manage. Assoc.*, **46**, 1996, 530-538.
10. McMillin, B. K., Biswas, P. and Zachariah, M., "*In Situ* Diagnostics of Vapor Phase Growth of Iron Oxide-Silica Nanocomposites", Part I: 2-D Planar Laser-Induced Fluorescence and Mie Imaging, *J. Mater. Res.*, **11(6)**, 1996, 1552-1561.
11. Wu, C. Y., Lee, T. G., Arar, E., Tyree, G. and Biswas, P., "Capture of Mercury in Combustion Environments by *In-Situ* Generated Titania Particles with UV Radiation", *Env. Eng. Sci.*, **15(2)**, 1998, 137-148.
15. Owens, T., Wu, C. Y. and Biswas, P., "An Equilibrium Analysis for Reactions of Metal Compounds with Sorbents in High Temperature Systems", *Chem. Eng. Comm.*, **133**, 1995, 31-52.
17. Wu, C. Y. and Biswas, P., "An Equilibrium Analysis to Determine the Speciation of Metals in an Incinerator", *Combust. Flame*, **93**, 1993, 31-40.
12. Reynolds, W. C., "STANJAN-Interactive Computer Programs for Chemical Equilibrium Analysis", Dept. Mechanical Engineering, Stanford Univ., 1995.
13. Chase, M. W., Davies, C. A., Downey, J. R., Frurip, D. J., McDonald, R. A. and Syverud, A. N., JANAF Thermochemical Tables, 3rd Edition, *American Chemical Society and American Institute of Physics for the National Bureau of Standards*, Midland, MI, 1986.
14. Barin, I., "Thermochemical Data of Pure Substances", 3rd Ed., *VCH*, Germany, 1995.
16. Linak, W. P. and Wendt, J. O. L., "Toxic Metal Emissions from Incineration: Mechanisms and Control", *Prog. Energy Combust. Sci.*, **19**, 1993, 145-185.

SUPERCRITICAL WATER GASIFICATION OF COAL USING CA(OH)$_2$ AS AN ADDITIVE

Jie Wang and Takayuki Takarada
(Department of Biological and Chemical Engineering,
Gunma University, Kiryu , Gunma 376, JAPAN)

KEYWORDS: supercritical water, coal gasification, calcium hydroxide

ABSTRACT

A few coals were gasified under the supercritical water conditions in an autoclave at a temperature up to 700 °C and a pressure up to 30 Mpa. Calcium hydroxide was used both as a catalyst and an absorbent for the capture of CO_2. The carbon conversion, gas and liquid productions, CO_2 sorption by calcium and calcium utilization were determined in the experiments. Without the addition of Ca, the carbon conversion of Yallourn coal was about 44% at 690 °C and 28 Mpa; whereas the addition of Ca up to a Ca/C molar ratio of 0.6, the carbon conversion increased by 22%. Correspondingly, hydrogen yield was increased from 0.23 to 0.37 NL/g-coal (daf), methane yield from 0.16 to 0.19 NL/g-coal(daf), and ethane yield from 0.015 to 0.03 NL/g-coal(daf). At a Ca/C ratio of 0.6, almost no CO_2 remained in gas phase, with a calcium utilization value of 50-60%.

INTRODUCTION

Gasification is one of the oldest coal utilization processes. The present paper is concerned with the gasification of coal in supercritical water at a temperature up to 700 °C and a pressure around 30 Mpa with the addition of calcium hydroxide. The essential idea concerning this research subject has been proposed by Lin et al [1]. They found that when several coals were gasified in supercritical water at temperatures 650-700 °C and a pressure of 60 Mpa using lime and a small amount of sodium compounds as additives, very high carbon conversion could be achieved with a high proportion of hydrogen and some CH_4 and CO in resultant gas. The following global reactions are principally taken into account in the gasification system:

$$C + H_2O \rightarrow CO + H_2 \qquad \Delta H_{900} = 140.3 \text{ kJ mol}^{-1} \qquad (1)$$

$$H_2O + CO \leftrightarrow CO_2 + H_2 \qquad \Delta H_{900} = -32.6 \text{ kJ mol}^{-1} \qquad (2)$$

$$Ca(OH)_2 \leftrightarrow CaO + H_2O \qquad \Delta H_{900} = 92.6 \text{ kJ mol}^{-1} \qquad (3)$$

$$CO_2 + Ca(OH)_2 \leftrightarrow CaCO_3 + H_2O \qquad \Delta H_{900} = -83.4 \text{ kJ mol}^{-1} \qquad (4)$$

$$CO_2 + CaO \leftrightarrow CaCO_3 \qquad \Delta H_{900} = -176.0 \text{ kJ mol}^{-1} \qquad (5)$$

Where the values of reaction heat change refers to those at a temperature of 900 K, a steam pressure of 30 Mpa and other gas pressures of 0.1 Mpa. As shown in reactions (4) and (5), lime or slaked lime can also play an important role in capturing environmentally unfriendly CO_2 and sulfur-bearing gases. As the released CO_2 gas is eliminated effectively by $Ca(OH)_2$ and/or CaO by reactions (4) and (5), CO can thus be highly transferred to hydrogen by enhancing the forward step of reaction (2).

In the present study, we aim at revealing catalytic effect of calcium hydroxide on supercritical water gasification of coal because no meticulous report has been documented regarding this interesting issue. We also would like to discuss the behaviors of calcium hydroxide for the retention of CO_2 in supercritical water.

EXPERIMENTAL

Gasification was carried out in a 20 ml batch autoclave. In each run, a 0.2 g sample of coal mixed with the desired amount of $Ca(OH)_2$ was added into the reactor with the injection of around 3.5 ml distilled water. It typically took 20 min for temperature to rise from room temperature to 690 °C.

Compositional analysis of the resultant gas was carried on a gas chromatograph, which used molecular sieve column in one channel and HaySep A column in another with TCD detectors (detectable gasses: H_2, O_2, N_2, CH_4, CO, CO_2, C_2, C_3 and C_4). The reacted slurry was filtered to collect the liquid. Some of the filtrates were analyzed on a gas chromatograph to determine BTX, PCX and naphthalene. Effort was made to collect the solid with least loss. The solid was dried at 107 °C in flowing nitrogen and then subjected to the analysis of the forms of carbon in it (total carbon content and carbon content as $CaCO_3$) through a method of acid dissolution.

Reagent-grade calcium hydroxide was purchased from Wako Co. in Japan. Table 1 lists the characteristics of coal samples used in the study. The particle size of coal samples was screened between 60 and 100 Tyler mesh.

Table 1. Characteristics of Coal Samples used in the Study

Coal sample	Proximate analysis (wt%, as-received)				Ultimate analysis (wt%, daf)				
	Moisture	VM	Ash	FC	C	H	N	S	O
Yallourn (YL)	14.3	47.3	0.8	36.6	66.1	5.3	0.6	0.3	27.7
Morwell (ML)	10.0	46.3	1.4	43.3	67.9	5.0	0.5	0.3	26.3
Tanitoharum (TN)	4.6	48.8	5.0	41.6	76.3	5.6	1.4	0.2	16.5

RESULTS AND DISCUSSION

Table 2 lists the yields of gases, carbon conversion and carbon recovery obtained at 690 °C and around 28 Mpa as functions of the Ca/C molar ratio. Runs 3 and 4 as well as runs 6 and 7 demonstrate the reproducibility of experiment. Carbon conversion refers to the sum of carbon fraction in gas phase and that in solid. No determination of liquid was considered in this series of experiment. Regardless of calcium addition, the main combustible gases produced were hydrogen and methane. With more calcium addition up to a Ca/C ratio of 0.6, an increase in the hydrogen yield concurrent with an increase in the carbon conversion was striking; whereas more CO_2 was fixed in the solid. At a Ca/C ratio of 0.6, virtually no CO_2 remained in the gas phase. In the presence of calcium, the yields of methane and ethane appeared to be somewhat larger than those in the absence of calcium. Antal and his collaborators ever made their efforts to produce a hydrogen-rich gas from biomass by supercritical water gasification at 600-650 °C and 30 Mpa [2]. In our study, it was shown that although the proportion of hydrogen in the resultant gas significantly increased, partly because of an increased carbon conversion to hydrogen via reactions (1) and (2), calcium hydroxide had no great effect on the decomposition of methane and ethane into hydrogen.

Table 2. Gas Yields and Carbon Conversion of YL coal with the Addition of $Ca(OH)_2$ (690±4 °C; 28±3 Mpa; holding time at the final temperature, 0 min)

Run No.	Ca/C molar ratio (-)	Gas yield (NL/100g-coal daf)					CO_2 fixed (NL/100g-coal(daf)	Carbon conversion (%)	Carbon recovery (%)
		H_2	CO_2	CH_4	C_2H_6	C_3H_8			
1	0	23.6	18.1	15.8	1.1	nd	-	43.9	86.5
2	0.15	24.0	8.3	15.8	2.2	0.02	16.4	52.1	87.5
3	0.30	29.0	2.4	15.7	2.4	nd	26.1	55.0	86.1
4	0.30	31.6	5.0	15.9	2.6	nd	27.7	60.8	84.6
5	0.45	35.5	0.8	16.6	2.1	nd	30.6	64.4	79.6
6	0.60	38.9	0.1	19.2	2.6	nd	37.0	69.4	82.1
7	0.60	35.4	0.02	18.5	3.2	0.03	40.1	67.6	86.8

nd, not detected (the same as below)

Because the carbon conversion was not as high as expected even with twice amount of $Ca(OH)_2$ added to coal, the reaction was prolonged to examine the gasification of remaining char and the results are listed in Table 3. Surprisingly, in the absence of catalyst, an increase in the carbon conversion was so slight even for prolonging the reaction for 20 min. At a Ca/C ratio of 0.6, hydrogen yield to some degree increased, with the increase of carbon conversion. From these data, we can see that the gasification of residual char was slow even under the supercritical water conditions and with the addition of calcium. We noticed that the molar ratio of H_2 to CO_2 was around 1, half lower than the stoichiometric ratio by reactions (1) and (2). This may be because some hydrogen can be consumed in the formation of CH_4, and also because part of CO_2 can be derived from the volatile of coal.

Table 4 shows the results of the gasification of MW coal and TN coal. It was observed that calcium hydroxide also had an effect on enhancing gasification of these two coals to produce more hydrogen. The three coals used in the study were all young coals which may be better suitable for the gasification in supercritical water. When higher-rank bituminous coals were gasified (not shown here), the carbon and hydrogen yields were relatively low as compared with those obtained for these three coals.

Table 3. Gas Yields and Carbon Conversion of YL Coal Gasified for Different Holding Times at Final Temperature (680±4 °C; 30±2 Mpa).

Run No.	Ca/C molar ratio	Holding time (min)	Gas yeild (NL/100-coal(daf)					CO_2 fixed (NL/100g-coal(daf)	Carbon conversion (%)	Carbon recovery (%)
			H_2	CO_2	CH_4	C_2H_6	C_3H_8			
8	0	0	25.8	18.0	15.7	1.4	nd	-	44.7	86.3
9	0	10	32.3	20.7	14.8	1.4	nd	-	47.2	85.8
10	0	20	36.8	18.9	17.6	1.3	0.02	-	46.0	86.7
11	0.3	0	25.5	0.8	15.4	2.4	nd	30.4	59.4	83.4
12	0.3	10	40.4	6.6	21.1	3.2	nd	27.8	69.6	82.1
13	0.6	10	43.4	0.3	20.9	2.9	0.06	43.8	71.7	87.7
14	0.6	20	46.9	1.8	23.5	2.9	0.02	42.3	74.8	86.5

Table 4. Gas Yields and Carbon Conversion in the gasification of MW coal and TN coal (688 ±2 °C; 28 ±2 °C; holding time, 0 min)

Run No.	Coal sample	Ca/C molar ratio	Gas yield (NL/100-coal(daf)					CO_2 fixed (NL/100g-coal(daf)	Carbon conversion (%)	Carbon recovery (%)
			H_2	CO_2	CH_4	C_2H_6	C_3H_8			
15	MW	0	23.2	17.1	13.3	1.7	0.004	-	47.4	79.8
16	MW	0.45	38.3	0.03	17.5	2.3	0.08	39.7	61.2	87.4
17	TT	0	21.4	14.2	14.5	2.4	0.004	-	49.7	74.7
18	TT	0.45	35.6	0.01	14.1	2.5	0.3	31.2	59.6	79.4

We noticed that the values of carbon recovery shown in Tables 2-4 were not beyond 90%. Despite a small part of carbon loss which was unavoidable in the experimental procedures, the deficient amount of carbon recovery lower than 100% might be mainly due to the excluded carbon fraction in tarry materials. However, some of the filtrates were determined in the amounts of light hydrocarbons, and the partial analysis data and the values of carbon closure through the analysis of light hydrocarbons are given in Table 5. We found that at lower temperatures, the values of carbon closure were still significantly lower than 100% but the balance was enhanced at higher temperatures. At lower temperatures, there obviously existed more BTX, PCX, with more tar that was not determined. In the visible observation, the water solutions separated after filtration were brown in color while the solution obtained at higher temperatures were essentially transparent. An important observation was that calcium oxide had a marked effect on the decomposition of coal in supercritical water. More tarry materials may be formed via promoting hydrolysis and dissolution into dense supercritical water, as well as via preventing the secondary reaction from depolymerization, under the effects of $Ca(OH)_2$ in supercritical water.

Table 5. Carbon Partition into gaseous, liquid and solid products for YL coal.

Experimental conditions				Carbon partition (% of total carbon)								Carbon closure (%)
FT (°C)	Ca/C (-)	HT (min)	P (Mpa)	gaseous CH_4	CO_2	C_2	C_3	BTX	PCX	C_6H_6	solid *	
568	0	13	24	3.3	5.4	0.5	0.1	1.0	1.0	0.1	60.9	72.3
565	0.3	13	25	3.1	0.0	1.2	nd	0.4	1.2	0.2	67.2	74.6
560	0.60	12	28	4.2	0.0	1.5	0.4	0.4	1.6	0.0	68.3	76.3
680	0	20	32	12.6	14.7	2.3	0.1	0.0	0.7	0.0	57.8	88.3
683	0.6	20	29	17.0	0.1	4.7	0.1	0.0	0.6	0.0	63.2	88.0

*, including carbon as $CaCO_3$ and organic carbon

Figure 1 displays the relation of CO_2 sorption and calcium utilization with Ca/C molar ratio. In the case of almost complete retention of CO_2, the value of calcium utilization was 50-60%. When prolonging the reaction, carbon dioxide was not effectively captured by remaining calcium, as illustrated in Figure 2. However, it remained doubtful how much the CO_2 could possibly be captured during cooling stage.

ACKNOWLEDGMENTS

We thank Drs. Lin S. Y., Hatano H. and Suzuki Y. at National Institute for Resource and Environment for their discussion and assistance in this subject of research. The financial support from CCUJ, Japan is greatly appreciated.

REFERENCES

1. Lin S. Y., Suzuki Y. and Hatano, H., Harada, M. A New Method (Hypr-RING) for Producing Hydrogen from Coal. In Prospects for Coal Science in the 21st Century (editors, Li B. Q and Liu Z. Y.). 1999. Shanxi Sic. Tech. Press: 475-478.

2. Xu X.and Antal M. J. Environmental Progress. 1998, 17, 215.

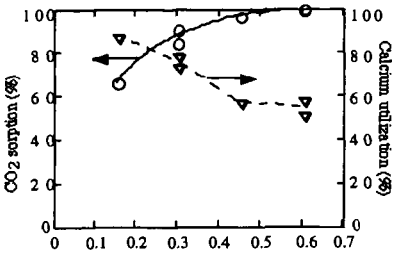

Figure 1. CO_2 sorption and calcium utilization the amount of $Ca(OH)_2$ added (690 °C, 28 Mpa, 0 min holding time).

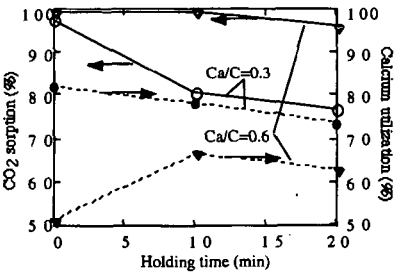

Figure 2. CO_2 sorption and calcium utilization with holding time at varying Ca/C molar ratio (680 °C, 30 Mpa).

THE IMPACT OF CHLORINE ON HEXAVALENT CHROMIUM EMISSIONS FROM A LAMINAR DIFFUSION FLAME

Bing Guo and Ian M. Kennedy
Department of Mechanical and Aeronautical Engineering
University of California
Davis, CA 95616
USA

ABSTRACT

Measurements of total chromium and hexavalent chromium have been obtained in a laminar hydrocarbon/air diffusion flame. Chlorine was added to the fuel as methyl chloride gas. A probe sampled the emissions from the flame. Particles were collected on a filter and vapor phase species were collected in impingers. Hexavalent chromium was measured with a spectrophotometric method. Total chromium added to the flame was determined by gravimetric analysis of the chromium source, chromium hexacarbonyl. The fraction of hexavalent chromium increased significantly as small amounts of chlorine were added. Partitioning between phases was also altered – much more hexavalent chromium was found in the impingers as the chlorine loading increased. Differential mobility analysis of the particles showed that the mean particle size was always in the range of 25-30 nm, whether chlorine was added or not. However, particle concentrations decreased when chlorine was present. Equilibrium calculations showed strong sensitivity to the thermochemical properties of the included species, particularly CrO_2Cl_2.

KEYWORDS: hexavalent chromium, chlorine, laminar diffusion flame

INTRODUCTION

Metals are often unavoidably introduced into combustion systems. Coal combustion ineluctably introduces metals as part of the mineral matter of the fuel. The incineration of many wastes also suffers a similar problem. Many of these metals can exist in more than one oxidation state, some are of great environmental concern. It is known that the toxicity of the metals is a strong function of the oxidation state. For example, the hexavalent form of chromium is much more toxic than the trivalent form [1, 2]. The physical state of the metal may also depend upon its chemical state, with significant implications for the selection of air pollution control equipment.

The problem of metal transformation and fate is exacerbated in waste incineration when chlorine is present. Many waste streams introduce chlorine as part of the waste itself. The presence of chlorine in the mixture will result in an increase in the emission of vapor phase metals, as the metal chlorides are generally more volatile than the metal oxides. Furthermore, Linak and Wendt [3] showed, via equilibrium calculations, that chlorine has a significant impact on the fraction of the total chromium that appears as hexavalent chromium, primarily through the enhanced formation of the hexavalent CrO_2Cl_2 at a temperature around 700K. This temperature is expected in the post flame gases, and gives rise to the possibility that hexavalent chromium may be formed in the downstream sections of an incinerator if sufficient residence time is available.

A number of earlier studies of the fate of metals in combustion systems have focused on simulations of realistic incinerator conditions [3-5]. Fewer studies have been undertaken in simple flame configurations that are amenable to theoretical or numerical modeling. Premixed flame studies, such as that of Bulewicz and Padley [6], are useful in gaining an understanding of the kinetics of metal oxidation. However, practical combustion systems generally utilize non-premixed reaction. Yoon et al. [7] studied a laminar, hydrogen/air diffusion flame that was seeded with chromium and found that high temperatures favored the formation of hexavalent chromium. They did not add chlorine to the flame.

This paper is an extension of the earlier work of Yoon et al. [7]. It considers the impact of chlorine in a laminar hydrocarbon/air diffusion flame, with particular attention to the issues of speciation of chromium and partitioning between solid and vapor phases. The measurements and equilibrium analysis reveal the impact of varying temperature and oxygen concentration on chromium speciation in the presence of chlorine.

EXPERIMENTAL

The coflow, laminar, diffusion flame system is shown in Fig. 1. The 5 mm burner nozzle was positioned in the center of a 100×100 mm duct containing flow straighteners and a series of fine-mesh screens to ensure air-flow uniformity. Methane (CH_4) was used as the primary fuel in this experiment. A small quantity of CH_3Cl was added into the fuel as a chlorine source. The flow rate of CH_4 was adjusted, according to the CH_3Cl flow rate, so as to keep the mixture flow rate constant. The mole fraction of CH_3Cl in the fuel was in the range from zero to 0.07.

Chromium hexacarbonyl ($Cr(CO)_6$), a volatile crystal that decomposes at 210 °C to produce elemental Cr, was used as a chromium source in the experiment. A glass cartridge containing chromium hexacarbonyl was added to the fuel delivery line. The CH_4/CH_3Cl mixture flowed through the cartridge at a rate of 0.160 L/min. With temperature controlled at 24 °C, the vapor pressure resulted in a chromium concentration of 60 ppmv. The concentration of chromium in the carrier gas was obtained gravimetrically by comparing the mass difference of chromium hexacarbonyl in the cartridge before and after the experiment. Chromium hexacarbonyl vapor carried in the fuel decomposed quickly in the flame to provide zero-valence chromium.

Samples of vapor and particle phases of chromium compounds emitted from the flame were obtained with a stainless steel sampling probe positioned above the flame on the centerline. The 200-mm-long, 22-mm-outer diameter sampling probe contained a 150-mm-long, 13-mm-inner diameter sintered metal tube as its inner wall. Nitrogen dilution gas was provided to the sampling probe through its inner wall and mixed with the sample to quench reactions, the development of aerosols through the sampling lines, and to minimize the transport of particles and vapors to the probe wall. The flow rate of nitrogen was fixed at 0.8 L/min, accounting for more than 25% of the total sampling flow rate, which was deemed adequate to serve those purposes mentioned above [7].

Figure 2 shows the chromium sampling system. The particle phase of chromium, and some absorbed gas phase material, was captured on a 47-mm-diameter alumina membrane filter with 20 nm pores. The temperature of the filter, and the sampling lines between the probe and the filter, was kept slightly above 100°C by heating with heating tapes, to prevent water condensation along the lines and on the filter, and avoid interconversion between Cr(VI) and Cr(III). All of the samples were obtained above the flame tip at a distance of 55 mm from the nozzle exit where the temperature was 1400 °K on the centerline. The flame tip was approximately 26 mm from the nozzle exit for all the experiments.

The impingers and liquid nitrogen trap were designed to capture the vapor phase of the chromium compounds. A $NaHCO_3$ solution was used in the impingers to prevent further conversion between Cr(VI) and Cr(III). HCl was a major product of the CH_4/CH_3Cl flame; the pH of the $NaHCO_3$ buffer solution was adjusted to accommodate the CH_3Cl concentration in the fuel and the resultant concentration of HCl in the sample.

The sampling time for each sample was 1 hour. The filter was cut into two halves, one for hexavalent chromium analysis and another for total chromium analysis. Samples from the impingers and the liquid nitrogen trap were analyzed solely for hexavalent chromium. Sampling lines before the filter were rinsed with deionized water for hexavalent chromium analysis. In the experiments reported herein, there was no measurable amount of hexavalent chromium detected in the samples from the liquid nitrogen trap and those from rinsing the sample lines.

The half filter for Cr(VI) analysis was extracted with a 0.01 N $NaHCO_3$ solution for 20 hours before the extraction solution was analyzed by a spectrophotometric method as described in EPA Method 7196A [8]. An X-ray fluorescence (XRF) method was used to measure the total chromium on the filter with a Kevex 0700/8000 energy dispersive XRF spectrometer. Total chromium consumed in the experiment was determined from the mass difference of the chromium hexacarbonyl in the cartridge before and after the experiment with a Mettler AJ100 balance.

A TSI Model 3934 SMPS (Scanning Mobility Particle Sizer) system was used for the particle size analysis. A denuder containing sodium hydroxide was added to the sampling line to eliminate H_2O and HCl from the sampled post flame gases. A post flame aerosol stream of 0.6 L/min was fed into the particle size analyzer.

RESULUTS AND DISCUSSION

A series of samples were taken at a fixed sampling point 55 mm above the nozzle to study the combustion products with varying chlorine concentrations in the fuel. With the chlorine concentrations that were used in these experiments, the flame length did not show a measurable change. Cr(VI) mass on the filter was compared with the total chromium mass on the filter. As an abbreviation, this fraction is referred to as "on-filter Cr(VI) fraction" hereafter. The total Cr(VI) mass from both the filter and the impingers was compared with the total chromium consumed in the experiment, and this fraction is referred to as "overall Cr(VI) fraction" hereafter. The Cr(VI) emitted in the vapor phase and trapped in the impingers was compared with the total chromium consumed in the experiment. This fraction is referred to as "gas-phase Cr(VI) fraction" later in this paper. Similarly, the Cr(VI) captured on the filter was compared with the total chromium consumed in the experiment, and this fraction was referred to as "solid-phase Cr(VI) fraction" hereafter. The fraction of the total input chromium that was recovered was evaluated by comparing chromium recovered on the filter and in the impingers with the total chromium supplied in the fuel. Without chlorine we found typical recoveries of input chromium

of about 10%. As chlorine was added, the recovery rate increased to up to 64%, as a result of a greater amount of Cr(VI) passing through the filter to the impingers and being detected by the spectrophotometric method.

Figure 3 shows the overall Cr(VI) fraction of the total chromium added to the flame; it is plotted against varying CH_3Cl concentrations in the fuel. Since it was possible that some of the flame emission was not collected into the sampling probe, this fraction can be interpreted as a lower limit of the Cr(VI) fraction. Nevertheless, the samples showed a clear increase in Cr(VI) with increasing CH_3Cl concentration in the fuel. This trend is consistent with measurements in practical systems. Volland [9] reported results from a variety of tests on medical waste incinerators in which stainless steel "sharps" may provide a significant source of chromium. Without chlorine in the feed, about 16% of the stack gas chromium appeared in its hexavalent state. With 8.5% chlorine in the feed, the fraction of hexavalent chromium increased to about 48%. Our results confirm the strong impact of chlorine on the propensity to form hexavalent chromium.

It was also found that the on-filter Cr(VI) fraction increased to 1 as only a small amount of chlorine was added, while the typical value for samples from experiments without chlorine was around 0.2, as illustrated in Figure 4. The increase in the on-filter hexavalent fraction was accompanied by a change in the color of the filter. Without chlorine, the filters were reddish-brown, suggestive of CrO_3. As chlorine was added, the filters changed color to green and further yielded a light green solution when extracted with water. We expect, from equilibrium calculations discussed later, and from its solubility, that the compound CrO_2Cl_2 may be responsible for the observed color change.

The presence of chlorine affects not only the chemical state of the metal, but also its physical state, largely as a result of the formation of more volatile metal chlorides that tend to yield gas phase products. Sampling at the same point above the flame showed that gas-phase Cr(VI) increased with increasing concentration of chlorine in the fuel, while the solid-phase Cr(VI) fraction remained at a steady level for all the chlorine concentrations, as shown in Figure 5. This trend is in agreement with observations from practical incinerators [9].

Differential mobility particle analysis showed some impact of chlorine on the particle size distribution in the post flame gases. While the mean particle size was always found to be in the range of 25-30 nm, not very sensitive to CH_3Cl concentration in the fuel, a decrease by a factor of 10 was observed in particle concentration when CH_3Cl concentration in the fuel increased to about 0.03. This is in agreement with the increase in gas-phase Cr(VI) associated with increasing CH_3Cl concentration in the fuel.

An equilibrium calculation considered the following species: CH_3Cl, CH_4, CO, CO_2, Cl_2, Cr, $CrOCl_2$, $CrOH_3$, CrOOH, CrO_2, CrO_2Cl, CrO_2OH, $CrO_2(OH)_2$, CrO_3, $Cr_2O_{3(s)}$, HCl, H_2O, N_2, and O_2. This list is by no means an exhaustive compilation of all possible species. As Linak and Wendt [3] and Kashireninov and Fontijn [10] pointed out, equilibrium calculations can be affected dramatically by the choice of species that are included. Nevertheless, the important species that were identified by these authors were included in the calculation. In addition to the impact of the choice of species, we have found that uncertainties in the thermochemical data, in particular that for the species CrO_2Cl_2, can be important. The enthalpy of formation for CrO_2Cl_2 reported by Ebbinghaus [12] was -519.2 kJ/mol, slightly higher than that reported by Barin [11] of -538.062 kJ/mol. Calculation showed that with these different values of enthalpy of formation, the equilibrium concentration of CrO_2Cl_2 could vary by a factor of 10. We have chosen to use the heat of formation for CrO_2Cl_2 that was reported by Barin. The results of a STANJAN calculation are presented in Fig. 6 in which Cr_2O_3 was considered to be in its solid form. The temperature was found from imposing an adiabatic condition.

The predicted equilibrium fraction of hexavalent chromium exhibits a maximum at a temperature of about 1400 °K. In contrast, Kashireninov and Fontijn [10] found a maximum in the Cr(VI) fraction at a temperature of about 1600 °K. Furthermore, these authors found that CrO_2Cl_2 was not significant down to temperatures of 1000 °K. Wu and Biswas [13] reported equilibrium results for the CH_4-air-Cl_2 system at temperatures of 1100 °K and 1500 °K. They used a combination of data from Barin [11] and Ebbinghaus [12]. The equilibrium results showed that CrO_2Cl_2 was not significant until temperatures dropped below 1000 °K. At higher temperatures, $CrO_2(OH)_2$ was the dominant hexavalent species. On the other hand, Linak and Wendt [3] showed that CrO_2Cl_2 was an important species in equilibrium over a broad range of temperatures from 500 °K to 1500 °K. The importance of CrO_2Cl_2 is apparent in Fig. 6. It is the dominant hexavalent chromium species in very lean mixtures and, of course, only appears when chlorine is present. In richer mixtures at concomitantly higher temperatures, chlorine makes little difference in the equilibrium fraction of hexavalent chromium.

The relevance of the equilibrium predictions to the measurement that we have undertaken can be understood if the equilibrium concentrations are plotted as a function of temperature and equivalence ratio. The equivalence ratio was obtained from thermocouple temperature

measurements. It was assumed that heat-releasing chemical reactions were complete at the measurement locations in the post flame gases. An adiabatic mixing calculation was performed to find the number of moles of air that were required to mix with combustion products to achieve the measured temperature. Equilibrium calculations were then run for the measured temperature and estimated equivalence ratio as a function of radial location. The temperature profile and the equilibrium mole fractions are shown in Fig. 7. It should be recalled that the sampling probe drew in most of the post flame gases. The measured hexavalent chromium fraction on the filter and in the impingers arises from streamlines that have passed through both the centerline of the flow and through peripheral regions. Temperatures and equivalence ratios in the latter regions are lower than along the centerline. The increase in Cr(VI) with chlorine addition can be understood in terms of an increase in CrO_2Cl_2 at the cooler edges of the flow. Equilibrium calculations suggest that Cl addition should have little impact on Cr speciation in the hotter gases on the centerline of the flow. The change in color of the filter with chlorine addition is consistent with this structure of the flow.

CONCLUSIONS

Chromium sampling in a CH_4/CH_3Cl flame has been performed using an N_2 dilution sampling probe, an alumina membrane filter, two impingers and a liquid nitrogen trap. All the samples were analyzed by EPA Method 7196A and X-ray fluorescence spectrometry to quantify the amounts of Cr(VI), and the partitioning of Cr(VI) phases. Flame products were analyzed with a TSI Model 3934 SMPS particle size analyzer. The results of Cr sample analysis showed a significant Cr(VI) fraction increase in the post flame gases with increasing concentration of CH_3Cl in the fuel. The fraction of Cr(VI) emitted as vapor increased with increasing CH_3Cl concentration in the fuel. It was also found that the color of the sample on the filter changed from dark brown to light yellow-green as CH_3Cl concentration in the fuel increased, which suggested there was a change in the species distribution among the combustion products. This change was attributed to the increased presence of CrO_2Cl_2 in the post flame gases. Particle size analysis showed that the particle concentration in post flame gases decreased with increasing CH_3Cl concentration in the fuel, while no significant change was found in the mean particle diameter as CH_3Cl concentration in the fuel varied. Equilibrium calculations agreed with the observed Cr(VI) fraction change with varying CH_3Cl concentration if the enhanced Cr(VI) yield is ascribed to enhanced CrO_2Cl_2 formation on the edge of the jet. The equilibrium results showed some sensitivity to the choice of thermochemical properties of CrO_2Cl_2.

ACKNOWLEDGEMENTS

This research has been supported by the Superfund Basic Research Program with Grant 2P42ES04699-14 from the National Institute of Environmental Health Sciences, NIH with funding provided by EPA. Its contents are solely the responsibility of the authors and do not necessarily represent the official views of the NIEHS, NIH or EPA.

REFERENCES

1. Flora, S. D. and Wetterhahn, K. E.: *Life Chem. Reports* 7, 169 - 244 (1989).

2. Flora, S. D., Bagnasco, M., Serra, D. and Zanacchi, P.: *Mutation Research* 238, 99 - 172 (1990).

3. Linak, W. P. and Wendt, J. O. L.: *Prog. Energy Combust. Sci.* 19, 145 - 185 (1993).

4. Fournier, D. J., W.E. Whitworth, J., Lee, J. W. and Waterland, L. R.: *The Fate of Trace Metals in a Rotary Kiln Incinerator with a Venturi/Packed Column Scrubber*, EPA/600/S2-90/043 EPA, 1991.

5. Linak, W. P., Srivastava, R. K. and Wendt, J. O. L.: *Combust. Sci. Tech.* 101, 7 - 27 (1994).

6. Bulewicz, E. M. and Padley, P. J.: *Proc. Roy. Soc. Lond. A.* 323, 377 - 400 (1971).

7. Yoon, Y., Reyes, C., Jones, A. D., Kelly, P., Chang, D. P. Y. and Kennedy, I. M.: *TwentySixth Symposium (Int.) on Combustion*, p. 1953 - 1959, The Combustion Institute, Pittsburgh,1996.

8. *Test methods for evaluating solid waste: physical/chemical methods*, U.S. EPA, Office of Solid Waste and Emergency Response, 1986.

9. Volland, C. S.: *85th Annual Meeting AWMA*, Paper 92-40.1, 1992.

10. Kashireninov, O. E. and Fontijn, A.: *Combust. Flame* 113, 498-506 (1998).

11. Barin, I.: *Thermochemical Data of Pure Substances*, VCH, Weinheim, Germany, 1993.

12. Ebbinghaus, B. B.: *Combust. Flame* 93, 119 - 137 (1993).

13. Wu, C. Y. and Biswas, P.: *Combust. Flame* 93, 31 - 40 (1993).

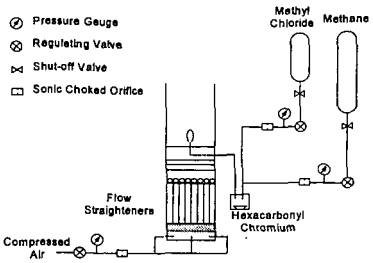

Figure 1 Schemetic of experimental apparatus

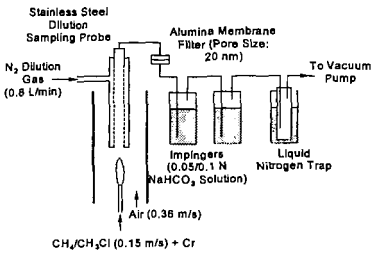

Figure 2 Schematic of chromium sampling system

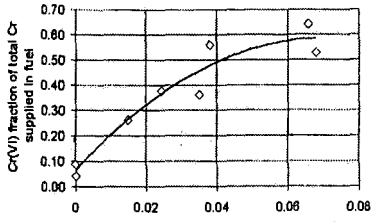

Figure 3 Cr(VI) Fraction of Total Cr Supplied in Fuel vs. CH3Cl Concentration in Fuel

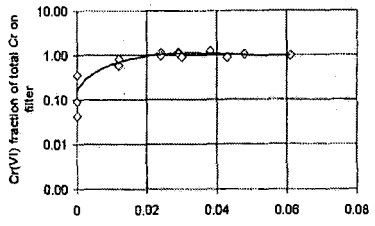

Figure 4 Cr(VI) Fraction of Total Cr on Filter vs. CH3Cl Concentration in Fuel

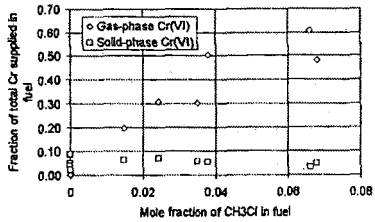

Figure 5 Gas-phase and Solid-phase Cr(VI) Fraction of Total Cr Supplied in Fuel vs. CH3Cl Concentration in Fuel

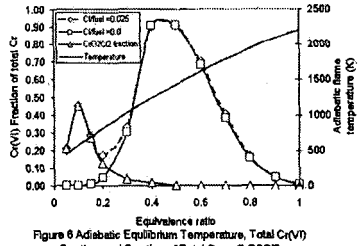

Figure 6 Adiabatic Equilibrium Temperature, Total Cr(VI) Fraction, and Fraction of Total Cr as CrO2Cl2

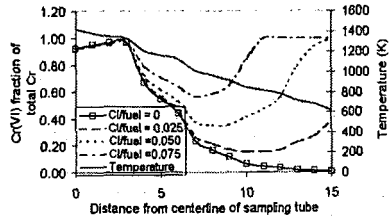

Figure 7 Measured Temperature Profile across Flame at Sampling Location and Calculated Equilibrium Cr(VI) Fraction of Total Cr

CONTROL OF HEAVY METAL EMISSIONS FROM INCINERATION OF CCA-TREATED WOODS

Chang-Yu Wu, Kenjiro Iida, John Pierman, Thabet Tolaymat and Timothy Townsend,
University of Florida, Dept. Environmental Engineering Sciences, Gainesville, FL 32611-6450

Key Words: CCA wood, leaching, emission.

INTRODUCTION

Chromium Copper Arsenate (CCA) has been used as a wood preservative since the 1970s. The production of CCA-treated woods has increased approximately 12 fold from 1970 to 1996.[1] By 1996, 79% of all the treated wood produced in the US, approximately 13 million cubic meters, was CCA-treated wood. Within Florida, 1 million pounds of the chemical were disposed during 1996.[2] Solo and Townsend[1] reported that by 2016 it would reach 6.8 million pounds. In Florida, the majority of the CCA-treated waste is processed through construction and demolition recycling facilities, resulting in a wood waste composition containing on average 6% CCA-treated wood. The primary market for wood waste is energy recovery and, therefore the majority of CCA-treated wood waste is burned for energy recovery purposes.[1]

During combustion, the heavy metals in these woods may escape from the combustion system and can be emitted into the atmosphere. Arsenic is known to be a volatile metal and is likely to enter the gas stream by vaporization.[3] Hirata *et al.*[4] performed an isothermal pyrolysis of CCA-treated wood and reported that almost all chromium and copper from the CCA woods were recovered from the ash while the majority of arsenic evolved into the gas phase. Once the metallic vapors exit the high temperature region and enter the low temperature region downstream, they may form submicrometer-sized aerosols.[5] Unfortunately, conventional air pollution control devices such as electrostatic precipitators (ESPs) have their minimum collection efficiencies at the submicrometer range.[6-8]

After combustion, the heavy metals are concentrated in the remaining ash[1]. The concentration of arsenic, chromium, and copper in the ash ranged from 8980~45000 mg/kg, 1780~22500 mg/kg, and 2720~31500 mg/kg, respectively.[1] Pohlandt *et al.*[9] conducted distilled water extraction on furnace, boiler, and fly ash produced from the combustion of CCA-treated wood. They reported that furnace ash produced the highest chromium concentrations (greater than 1,000 mg/L) and the fly ash produced the highest arsenic concentrations. Messick *et al.*[10] performed TCLP and SPLP on the ash obtained from the combustion of various retention levels of CCA-treated wood. The TCLP limits were exceeded for arsenic in almost all of their CCA ash samples. Half of their CCA ash results exceeded the TCLP limit for chromium. Once a waste is regulated as hazardous it must be disposed differently from regular wastes, which eventually increases the cost, the paperwork, and the labor needed for their disposal.

To prevent these undesirable consequences, a new technique needs to be developed. Using mineral sorbent materials to control heavy metals has been studied by a number of researchers since the late 1980s.[3, 11-13] Uberoi and Shadman[11] and Ho *et al.*[12] used silica, alumina and various naturally available materials (*i.e.*, bauxite, kaolinite and lime) to capture lead and cadmium. Mahuli *et al.*[3] demonstrated that calcium hydroxide can effectively capture volatile gaseous arsenic and confirmed the presence of calcium arsenate in the ash. Gullett and Ragnunathan[13] observed the reduction in submicrometer concentrations of arsenic when hydrated lime and limestone were injected into the combustion system. Chen and Wey[14] studied the effects of various operating conditions, such as the presence of organic chloride (PVC), inorganic chloride (NaCl), and sodium sulfide (Na_2S), on the capacity of a sorbent (limestone) to capture the heavy metals during combustion. The experiences of these researchers suggest that sorbent technology can be applied to the incineration of CCA-treated wood. The common mineral sorbents will potentially react with the heavy metals within the CCA-treated wood and also may impact the leaching behavior of these metals.

The objective of this research is to control both the emissions and leaching of heavy metals from the incineration of CCA-treated woods by using sorbent materials. Equilibrium calculations were performed to identify potential materials that can effectively bind those metals. Experiments were conducted to study their performance. The information obtained in this study will result in a better management option for CCA-treated wood disposal.

EQUILIBRIUM MODELING

In a high temperature system, reactions are generally very fast, and equilibrium conditions are possibly achieved. Hence, thermodynamic equilibrium calculations can be used to predict the behavior of a high temperature system. In this study, thermodynamic equilibrium calculations were performed to identify the sorbent materials which can potentially react with the heavy metals in the CCA-treated wood. The effects of sulfur and chlorine, on the formation of sorbent-metal compounds were also analyzed. Available thermochemical data were gathered[15, 16] and the data of any relevant reactants and possible products were included in the calculations. The calculations were performed using the software STANJAN.[17] The calculations were performed assuming 100% excess air for a wide temperature range. The simulation conditions are listed in Table 1.

Table 1. Simulation conditions in each calculation.

Calculation # or Figure #	Type of Sorbent Tested	Moles of Species Included in Calculation					
			Sorbent				
		Metal	$NaHCO_3$	KOH	MgO	S	Cl
1	Na	1	2	N/A	N/A	0	0
2		1	2	N/A	N/A	0	10
3		1	2	N/A	N/A	10	0
4	Mg	1	N/A	N/A	0.5	0	0
5		1	N/A	N/A	0.5	0	10
6		1	N/A	N/A	0.5	10	0
7	Na, Mg, K	1	2	2	0.5	0	0
8		1	2	2	0.5	10	10

Chromium-Sorbent System

Calculations were first performed for chromium. Figure 1 shows the result of using a Na-based sorbent. As shown, sodium chromate (Na_2CrO_4) is the thermodynamically most stable compound among other possible chromium compounds. The result indicates the potential use of Na-based sorbents. Chlorine and sulfur are known to have strong affinity to react with many metals and hence their impact on the sorbent's performance is investigated. As shown in Figure 2, when chlorine is present in the system, chlorine consumes all the sodium available for chromium and forms sodium chloride (NaCl) at temperatures below 500°C and above 1200°C. Between 500°C and 1200°C, hydrochloric acid is more thermodynamically stable than NaCl; therefore, Na becomes available for chromium to form Na_2CrO_4. Thus, the Na-base sorbent is effective only at that temperature range. Figure 3 shows the effect of sulfur. As shown, when sulfur is present in the system, chromium sulfate is the major chromium species up to around 550 °C. Above this temperature, Cr_2O_3 becomes the dominant chromium species. Sodium is in the form of Na_2SO_4 only above 1000°C when the sodium sorbent becomes effective.

Figure 1. Effectiveness of Sodium Sorbent on Chromium Capture

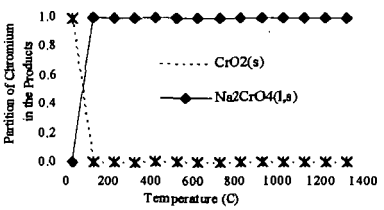

Figure 2. Effect of Chlorine on Sodium Sorbent

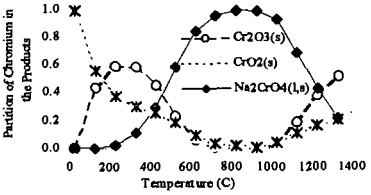

Figure 3. Effect of Sulfur on Sodium Sorbent

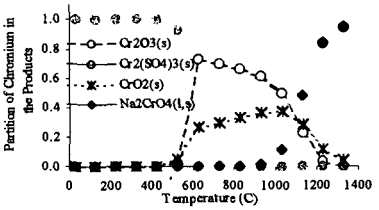

Calculations were also performed for the alkaline earth metal-based sorbents. The result for a Mg-based sorbent is shown in Figure 4. As shown, magnesium can also form stable compounds with chromium at a wide temperature range, and magnesium chromite ($MgCr_2O_4$) is the predominant chromium species. The effects of chlorine and sulfur on the Mg-based sorbent were also investigated. Figure 5 shows the effect of chlorine on the Mg-based sorbent. As shown, $MgCr_2O_4$ still remains to be the most stable chromium compound in the system even when a significant amount of chlorine is present. Magnesium has stronger affinity to react with chromium than chorine does. On the other hand, when a significant amount of sulfur is present in the system, magnesium is consumed by sulfur and forms magnesium sulfate $MgSO_4$. This trend continues up until around 700 °C, above which magnesium sulfate becomes unstable and the Mg becomes available for chromium to form $MgCr_2O_4$.

Figure 4. Effectiveness of Magnesium Sorbent on Chromium Capture

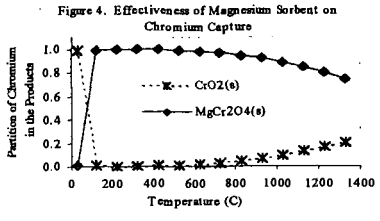

Figure 5. Effect of Chlorine on Magnesium Sorbent

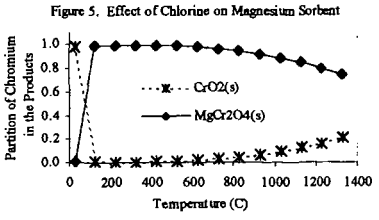

Arsenic-Sorbent and Copper-Sorbent Systems

Calculations were also performed for arsenic and have been reported by Barton and Wu.[18] In short, alkali metals and alkaline earth metals are effective though the performance may be reduced when chlorine or sulfur is present in the system. In addition, aluminum is also effective to capture arsenic. Calculations were not performed for copper due to the lack of thermochemical data for potential compounds between candidate sorbents and copper.

Considering all the modeling results for arsenic and chromium capture, alumina Al_2O_3, lime $Ca(OH)_2$, and soda ash Na_2CO_3 were chosen to be used in the combustion experiments.

EXPERIMENT

The experimental set-up is shown in Figure 6. CCA wood is combusted in a fluidized bed combustor inside the muffle furnace. The hot flue gas is directed into the heat exchanger designed to condense organic matter. The gas stream exiting the heat exchanger enters two columns of absorption spray towers. Each tower is 4 inches in diameter and 2.5 feet in height. The diameter of the column was small enough to achieve good contact between the gas stream and the spraying water without the use of packing materials. Tap water was constantly sprayed from the top of the column and was recirculated until each combustion run finished. The gas streams are further carried into a column of cotton filter to capture the remaining moisture content, volatile matter, and particulate matter in the gas stream. A glass fiber filter was used as the final particulate control device to capture the remaining micron-sized particulate matter. The flow of the gas stream was drawn by a vacuum pump at a flow rate of 30 lpm.

Figure 6: Schematic of Entire Set-Up

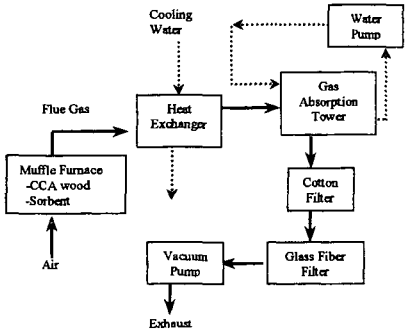

The type of CCA-treated wood combusted was type-C with 2.5 pcf (2.5 lb of chromium copper arsenate per ft^3 of dry wood). The wood was processed into sawdust, which was combusted with three different sorbents within a fluidized bed consisting of two layers of stainless steel meshes. 100 g of CCA wood was thoroughly mixed with 18 g of the selected sorbent and placed on the lower stainless steel mesh. Combustion products collected in this layer correspond to the bottom ash in general incineration systems. Another 18 g of sorbent was evenly spread on the upper steel mesh. This layer is designed to capture any vaporizing gaseous metals from the burning of CCA wood in the lower layer. Metals collected in this layer correspond to those observed in the fly ash in general incineration systems. Two sets of experiments were conducted. The experimental conditions are listed in Table 2 below. In the first set, only CCA-treated wood is combusted at three temperatures to establish the baseline. In the second set, three sorbent materials representing different groups (alkali metal, alkaline earth metal, and aluminum-based sorbents) are added to the system to investigate their performance in capturing the metals. After each combustion run, the leaching behavior and the total mass of the metals from the ash is analyzed, according to EPA Method 1311, Toxicity Characteristic Leaching Procedure. Total mass of each of these metals in the ash was analyzed according to EPA Method 3050B, Acid Digestion of Sediments, Sludges, and Soils. Acid Digestion of Aqueous Samples and Extracts for Total Metals for Analysis by FLAA or ICP Spectroscopy. The total mass of these metals in the original CCA sawdust was also analyzed by Method 3050B. Identification of the compounds in the obtained ash is done by X-ray Diffraction (XRD).

Table 2.Experimental Conditions

		Mass of Materials added (g)				
			Sorbent			Sulfur on
	Temperature	CCA Wood	Name	Bottom Layer	Top Layer	Bottom Layer
Set I	600 °C	100g	None	N/A	N/A	0 g
	750 °C					
	900 °C					
Set II	600 °C	100g	Al_2O_3	18g	18g	0g
			$Ca(OH)_2$	18g	18g	
			Na_2CO_3	18g	18g	
	750 °C		Al_2O_3	18g	18g	
			$Ca(OH)_2$	18g	18g	
			Na_2CO_3	18g	18g	
	900 °C		Al_2O_3	18g	18g	
			$Ca(OH)_2$	18g	18g	
			Na_2CO_3	18g	18g	

RESULTS AND DISCUSSIONS

In our preliminary study, four experiments have been conducted at 750°C. For the first run, 100 g of CCA wood was burnt without any sorbent. For the other three runs, 12 g of Al_2O_3, $Ca(OH)_2$, and $NaHCO_3$ were individually mixed with 100 g of CCA wood. It took two hours to reach 750°C which was then maintained for 45 minutes. After combustion the obtained ash was analyzed for the leaching behavior of heavy metals and the composition identified. The leaching levels from the TCLP tests are shown in Table 3 and the results from X-ray diffraction for NaHCO3 are given in Figures 7 and 8 (other results are not shown due to space limit).

Table 3: TCLP results for CCA Wood Combustion with and without the Addition of Sorbents.

	As (mg/L)	Cr (mg/L)	Cu (mg/L)	pH (raw)	PH (TCLP)
CCA-Only	87.0	16.9	23.2	6.3	2.9
CCA + Al_2O_3	7.9	19.0	33.0	6.9	2.7
CCA + $Ca(OH)_2$	0.8	84.3	1.0	12.5	11.5
CCA + $NaHCO_3$	3687.0	4627.0	2.1	12.6	12

The TCLP criteria for arsenic and chromium are 5 mg/L. Unfortunately, none of the ash samples passed the TCLP criteria. However, when alumina was added the arsenic leaching was 11 times lower than that without any sorbent (CCA-Only). The calcium based sorbent appears even better. The arsenic concentration drastically decreases to 0.8 mg/L, 110 times lower than the CCA-Only case. Speciation plays an important role here as the solubility varies with speciation. The potential arsenic-sorbent products ($Ca_3(AsO_4)_2$ and $AlAsO_4$) are insoluble.[19] This explains the reduced leaching level observed. Unfortunately, these species were not identified in the XRD.

It is generally known that the pH of the leachate has strong impact on the leaching behavior of heavy metals.[20-21] Warner and Solomon[22] found that copper, chromium, and arsenic were found in the leachate of both new and weathered CCA-treated jack pine, with significantly higher levels of all metals at lower pH values. One interesting phenomenon observed in our results regards this low pH effect on arsenic leaching. Although the pH of the solution after a TCLP test was low (< 3) for both CCA-Only and CCA+Al_2O_3, the addition of alumina reduced the leaching of arsenic by 11 times. This comparison proves that addition of alumina reduces the arsenic leaching under aggressive conditions. Dutre and Vandecasteele[23] have observed and also calculated that the addition of lime into a waste fly ash decreases the leaching level of arsenic. However, it is important to emphasize here the distinct difference between the addition of lime before and after the combustion. Lime captures volatile metals during the combustion, which not only reduces the leaching but also reduces the air emission of toxic metals.

Figure 7 X-ray diffractograms of CCA+Na_2CO_3 Bottom Ash

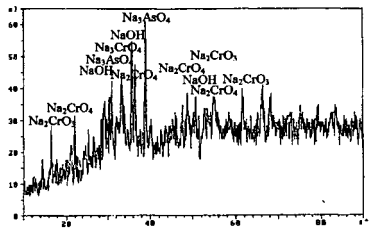

Figure 8 X-ray diffractograms of CCA+Na2CO3 Fly Ash

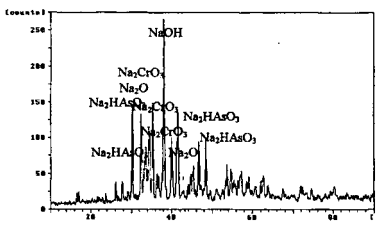

Unfortunately, neither alumina nor lime reduced the leaching of chromium. The cause of this poor result is not clear at this stage. XRD results show that chromium oxide instead of calcium chromite or aluminum chromate is the identifiable component. The result indicates that the sorbent materials are not effective in reacting with the chromium in the system. Mass transfer or reaction kinetics may be the limiting factor.

Leaching of copper was reduced by the addition of lime and sodium bicarbonate. Several studies have shown that copper is known to leach more at low pH.[24,25] The raised pH of the leachate solution most likely caused this low leaching level of copper.

The addition of sodium sorbent such as sodium bicarbonate, on the other hand, caused an incredible amount of leaching. This is due to the formation of very soluble compounds such as Na_3AsO_4 and Na_2CrO_4 identified by the XRD (Figures 7 and 8). As far as the leaching is concerned, this result is highly undesirable. However, this result can be interpreted in another way. Using these leaching levels of arsenic and chromium, a mass balance calculation was performed to obtain how much of the original amount of these metals in 100 g of wood was still present in the ash. It was found out that at least 78% of arsenic and 88% of chromium still remains in the ash after the combustion. These are very conservative values since these are derived only from a leaching test, not the total metal analysis with an aggressive acid digestion. Typically, only 20~30% of arsenic is reported to stay in the bottom ash. Hence, Na-based sorbent is very effective in retaining arsenic in the bottom ash.

CONCLUSIONS

CCA-treated wood contains a chemical preservative that consists of arsenic, chromium and copper. The majority of the recycled CCA-treated wood waste is currently burned for energy recovery purposes. There are two major problems associated with the combustion of CCA-treated wood: the emission of heavy metals as gaseous or particulate matter and the leaching of these metals from the ash. Application of sorbent technology may solve these two problems simultaneously.

Thermodynamic equilibrium calculations were performed to predict potential sorbent materials for chemically adsorbing the heavy metals in the CCA-treated wood |The results suggest that alumina, alkaline earth metals and alkali metals are effective for capturing both arsenic and chromium. However, alkali metal-based sorbents become less effective when sulfur and chlorine are present in the combustion system. According to these modeling results, alumina, lime and sodium bicarbonate were selected and their performance was examined in an experimental combustion system. The CCA wood sawdust was combusted with three different sorbents within a fluidized bed. TCLP tests were performed on the obtained ash to test the leaching behavior of heavy metals. XRD was performed on the ash sample to identify the products. The addition of alumina and lime greatly reduced the arsenic leaching. None of the sorbents reduced the leaching of chromium. The cause of this poor result is not clear at this stage. Leaching of copper was low when lime or sodium bicarbonate was added as sorbents. This is probably due to the high pH caused by lime and sodium bicarbonate in the leachate. The addition of the sodium sorbent caused an incredibly high leaching level of arsenic and chromium. It was found out that approximately 78% of arsenic and 88% of chromium still remains in the ash after the combustion, showing the sodium sorbent is very effective in retaining arsenic in the ash, which prevents the emission of arsenic.

ACKNOWDGEMENTS

This research was carried out as a part of the University Scholars Program at the University of Florida. Partial financial supports from the University and the Florida Center for Solid and Hazardous Waste Management are greatly acknowledged. The authors are also grateful to the generous support from Dr. William Wise, Dept. Environmental Engineering Sciences, University of Florida and Dr. R. C. Reynolds, Dept. Mechanical Engineering, Stanford University.

REFERENCE

1. Solo-Gabriele, H.M. and Townsend, T., **1998**, *Generation, Use, Disposal & Management Options for CCA-Treated Wood, Report #98-1;* FL CSHWM.
2. Solo-Gabriele, H.M., and Townsend, T., **1999**, *Disposal of CCA-treated Wood: An Evaluation of Existing and Alternative Management Options, Report #99-6;* FL CSHWM
3. Mahuli, R.; Agnihotri, S.; Chauk, S.; Chosh-Dastidar, A.; Fan, L.-S. *Environ. Sci. Tech.* **1997**, 31, 3226-3231.
4. Hirata, T.; Inoue, M.; Fukui, Y.; *Wood Sci. Technol.* **1993**, 24, 35-47.
5. Biswas, P.; Wu, C. Y. *J. Air & Waste Manage. Assoc.* **1998**, 48, 113-127.
6. Davison, R. L.; Natusch, D. F. S.; Wallace, K. R.; Evans, C. A. *Environ. Sci. Technol.* **1974**, 8, 1107-1113.
7. Greenberg, R.R.; Zoller, W.H.; Gordon, G. E. *Environ. Sci. Technol.* **1978**, 12, 566-573.
8. Taylor, D. R.; Tompkins, M. A.; Kirton, S. E.; Mauney, T.; Natusch, D. F. S.; Hopke, P.K. *Environ. Sci. Technol.* **1982**, 16, 148-154.
9. Pohlandt, K.; Strecker, M.; Marutzky, R., *Chemosphere* **1993**, 26, 2121-2128.
10. Messick, B.W. Graduate Thesis, University of Florida, **1999**.
11. Uberoi, M.; Shadman, F. *AIChE J.* **1990**, 32, 307-309.
12. Ho, T.C.; Chen, C.; Hopper, J. R.; Oberacker, D. *Combust. Sci. Technol.* **1992**, 85, 101.
13. Gullet, B.K.; Raghunathan, K. *Energy and Fuels* **1994**, 8, 1068-1076.
14. Chen, J.C.; Wer, M.Y. *Environment International* **1996**, 22, 743-752.
15. Brian, I. *Thermochemical Data of Pure Substances*; VCH: Germany, **1995**.
16. Chase, M.W.; Davies, C.A., Downey, J.R.; Frurip, D.J.; McDonald, R.A.; Syverud, A.N.; *JANAF Thermochemical Tables, 3rd Edition*; ACS and AIP for the NBS, Midland, MI, **1986**.
17. Reynolds, W.C. "STANJAN-Interactive Computer Program for Chemical Equilibrium Analysis," Department of Mechanical Engineering, Stanford University, **1995**.
18. Wu, C. Y. and Barton, T., Paper No. 408, *92th Annual Meeting of the Air & Waste Management Assoc.*, St. Louis, MO, June 20-24, 1999.
19. CRC Handbook of Chemistry and Physics. 58th ed., CRC Press, Cleveland, Ohio., **1977**
20. Wasay, S. A. J. *Environ. Sci. Health* **1992** A27(1), 25-39
21. Cooper, P. A. *Forest Products J.* **1991**, 41, 30-32.
22. Warner, J. E.; Solomon, K. R. *Environmental Toxicology and Chemistry* **1990**, 9, 1331-1337.
23. Dutre, V.; Vandecasteele, C. *Environ Sci. Technol.* **1998**, 15, 55.
24. Carey, P. L.; Mclaren, R.G.; Adams, J.M. *Water, Air and Soil Pollution* **1996**, 87, 189-203.
25. Chirenje, T.; Ma, L. Q. *J. Environmental Quality* **1999**, 28, 760-766

SUPPORT MODIFICATION OF COBALT BASED SLURRY PHASE FISCHER-TROPSCH CATALYSTS

J. van de Loosdrecht, S. Barradas, E.A. Caricato, P.J. van Berge, and J.L. Visagie

Sasol Technology (Pty) Ltd, PO Box 1, Sasolburg 9570, South Africa

Tel: +27-16-9603075; Fax: +27-16-9602053

KEYWORDS: Fischer-Tropsch synthesis; cobalt catalyst; support modification

INTRODUCTION

Gas-To-Liquids (GTL) processes have received widespread attention as an economically viable route to convert natural gas to liquid transport fuels[1,2]. The GTL process consists of three main steps, i.e. (i) the reforming of natural gas, (ii) the production of hydrocarbons from synthesis gas (i.e. the Fischer-Tropsch synthesis), and (iii) the optimisation to middle distillates. The Fischer-Tropsch synthesis step is preferably performed in a slurry phase bubble column reactor with a suspended cobalt Fischer-Tropsch catalyst of high intrinsic activity[3,4]. For optimum cobalt utilisation, a supported catalyst is selected. The commercial supports of choice are alumina, titania, and silica. In addition to a specification with respect to the mechanical strength of the eventual slurry phase catalyst, it is important to ensure proper cobalt anchoring during the impregnation step of the pre-shaped support material. Insufficient anchoring could result in the washing out of cobalt-rich ultra-fine particulates from the porous support material during commercial slurry phase Fischer-Tropsch synthesis.

Support modification has been reported earlier in the open literature [5-9]. Zirconia modification of silica supports was used to prevent the formation of unreducible cobalt-silicates[5]. Zr, Ce, Hf, or U modification of titania supports was reported to prevent the formation of cobalt-titanates during regeneration[6]. To increase the porosity of titania supports, they were modified with small amounts of binders, e.g. silica, alumina or zirconia[7]. Lanthanum oxide promotion of alumina was reported to be beneficial for improved production of products with higher boiling points[8], and zirconia modification of alumina supports was carried out to decrease the interaction of cobalt with alumina[9]. All these modified supports were either used for fixed bed cobalt based Fischer-Tropsch catalysts or they were used for slurry bed cobalt catalysts, but not tested under realistic Fischer-Tropsch synthesis conditions in large scale slurry bed reactors.

This paper will deal with the modification of alumina and titania supports for cobalt based slurry phase Fischer-Tropsch catalysts to ensure the successful operation of slurry phase bubble column reactors on commercial scale.

EXPERIMENTAL

Two alumina-supported catalysts were prepared by means of a two-step slurry phase impregnation method, using an aqueous cobalt nitrate solution[10-13]. After impregnation and vacuum drying, the dried intermediate was calcined in air at 250°C for 6 hours. The calcined catalyst was reduced at 380°C in pure hydrogen using a heating rate of 1°C/min. Platinum was incorporated as a reduction promoter. The catalyst compositions were: catalyst A: $30gCo/0.075gPt/100gAl_2O_3$, and catalyst B: $30gCo/0.075gPt/1.5gSi/100gAl_2O_3$.

Silicon support modification was performed, prior to the catalyst preparation, in the case of catalyst B, by means of a non-aqueous slurry phase impregnation step using Tetra Ethoxy Ortho Silicate (TEOS) as precursor. TEOS dissolved in dry ethanol was used as impregnation solution. After impregnation, the slurry was dried at 60°C under vacuum for 6 hours. The dried modified support was calcined in air at 500°C for 2 hours[11].

The dissolution behaviour of the supports were characterised by monitoring the conductivity of a support in a model acidic aqueous slurry. The support was added to an acidic aqueous medium with a pH of 2 at 25°C. The conductivity was measured continuously for 30 hours under stirring at 25°C. As the dissolution of the support will increase the pH, continuous and automatic titration with a 10% HNO_3 solution was required to fix the pH at 2.0 during the 30 hours dissolution experiment.

Laboratory Fischer-Tropsch synthesis tests were performed in a slurry phase CSTR. The pre-reduced catalyst (20-30 g) was suspended in ca 300 ml molten Fischer-Tropsch wax. Realistic Fischer-Tropsch conditions were employed, i.e.: 220 °C; 20 bar; commercial syngas feed: 50 vol% H_2, 25 vol% CO and 25 vol% inerts; syngas conversion levels in excess of 50%. Use was made of the ampoule-sampling-technique as the selected on-line synthesis performance monitoring method[14].

Larger scale Fischer-Tropsch synthesis runs were performed in a pilot plant slug-flow slurry reactor using 3-8kg catalyst as well as in a slurry phase bubble column demonstration unit using 500-1500kg catalyst. The reaction conditions were similar to those in the laboratory CSTR runs. The reactor wax production varied between 5 and 30kg per day for the pilot plant runs and up to 60bbl/day for the demonstration unit. On-line catalyst samples were taken for particle size distribution measurements and SEM analyses.

RESULTS AND DISCUSSION

The intrinsic Fischer-Tropsch activity as well as the selectivity of the supported cobalt catalysts studied in this paper (i.e. catalyst A and B) is such that these catalysts are economically viable for the GTL process (table 1). Low level silica modification of alumina supports did neither influence the acidity of the support and nor the Fischer-Tropsch synthesis behaviour of the catalysts (table 1).

Table 1: Fischer-Tropsch synthesis data for catalysts A and B, as tested under realistic reactor conditions (refer: Experimental).

	Catalyst A 30gCo/0.075gPt/100gAl_2O_3	Catalyst B 30gCo/0.075gPt/1.5gSi/100gAl_2O_3
Run number	175$	98F
Time on line (h)	15	20
Syngas conversion (%)	75	76
FT reaction rate (mol/s)	6.8×10^{-6}	7.1×10^{-6}
Productivity (gHC/gcat/h)	0.34	0.36
CH_4 selectivity (%C-atom)	4	7

Important for slurry phase Fischer-Tropsch catalysts is the mechanical strength, as catalyst break-up will result in (i) loss of catalyst, (ii) difficulties with the catalyst/wax separation, and (iii) undesired contamination of the wax product with cobalt. During extensive Fischer-Tropsch synthesis runs in both pilot plant scale reactors as well as the demonstration unit, the mechanical integrity of the catalyst was monitored by means of Particle Size Distribution (PSD) measurements as well as SEM analyses on extracted catalyst samples. The average particle size did not change even after 8 months of operation, which strongly indicates that catalyst break-up did not occur. This was in agreement with SEM analyses (figure 1).

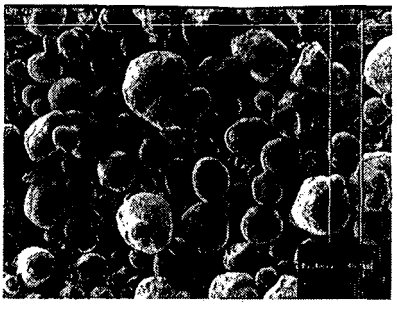

Figure 1: SEM image of alumina-supported cobalt catalyst A after Fischer-Tropsch synthesis test run in the demonstration unit.

The unmodified alumina-supported cobalt catalyst (catalyst A) was tested in the pilot plant slug-flow reactor under realistic Fischer-Tropsch conditions. The produced wax was secondary filtered over a 2 micron filter and analysed for cobalt content. Initially, clean white wax was produced without any cobalt contaminants present. After about 10 days on stream, however, the secondary filtered wax started discolouring and high levels of cobalt containing particulates were

observed (figure 2). This is very undesired, as cobalt contamination of wax may poison the downstream hydroprocessing catalysts. These cobalt containing particulates did not originate from catalyst break up.

The presence of high levels of cobalt-containing particulates in secondary filtered wax was correlated with the dissolution behaviour of the alumina support during the slurry phase impregnation steps of the catalyst preparation procedure. It was reported earlier that alumina supports could (partially) dissolve in aqueous solutions[15], even at pH values close to the isoelectric point[16]. Partial dissolution of the alumina used during the preparation of catalysts A and B was experimentally confirmed during the aforesaid model dissolution test (figure 3).

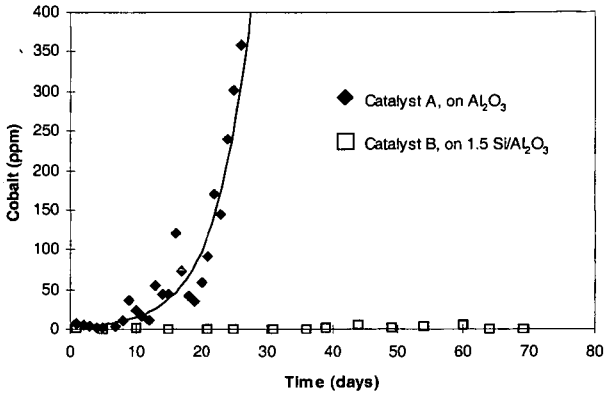

Figure 2: Cobalt content in secondary filtered wax during pilot plant scale Fischer-Tropsch synthesis runs, using catalyst A: 30gCo/0.075gPt/100gAl_2O_3 (run F102), and catalyst B: 30gCo/0.075gPt/1.5gSi/100gAl_2O_3 (run F117).

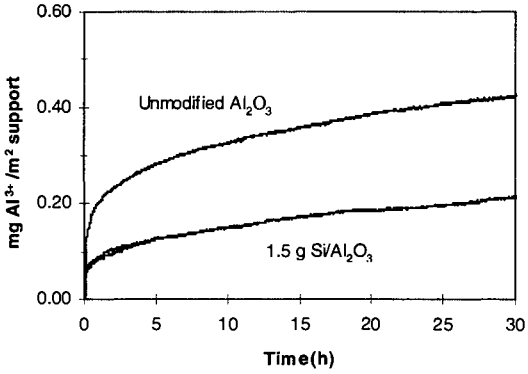

Figure 3: The dissolution behaviour of an alumina support (used to prepare catalyst A) as well as a silica modified alumina support (used to prepare catalyst B).

It can be seen that rapid dissolution occurs within the first hour, followed by a more gradual dissolution that proceeds continuously (i.e. about 30 hours). A mechanism of dissolution is reported in literature[15] (equations 1 and 2). During catalyst preparation, the dissolved aluminium ions can precipitate either as boehmite or in combination with cobalt ions as a cobalt aluminium hydrotalcite[17], producing a physically amorphous layer uniformly covering the surface of the bulk support material[16]. It is hypothesised that the presence of this amorphous layer, prior to the actual impregnation process, weakens the anchoring of the eventually catalytically active cobalt metal. The cobalt metal crystallites that are weakly anchored to the

alumina support can dislodge and be washed out during slurry phase Fischer-Tropsch synthesis, a process that is enhanced by the increased turbulence associated with large-scale reactors.

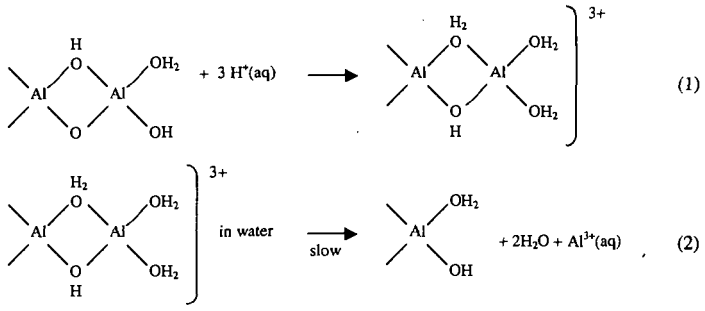

To prevent the dissolution of the alumina support during the slurry phase impregnation step of the catalyst preparation procedure, the alumina support was modified with silicon, using Tetra Ethoxy Ortho Silicate (TEOS) as precursor. The support modification step was performed as a slurry impregnation using TEOS dissolved in dry ethanol as impregnation solution. During support modification, TEOS reacts with the hydroxyl groups of the alumina surface. The three remaining ethoxy groups were thermally decomposed during a calcination step at 500°C in air. The maximum amount of silicon that can react with the alumina support depends on the surface area of the alumina support as well as the surface hydroxyl concentration. The dissolution behaviour of the silica-modified alumina was measured (figure 3), and found to be significantly inhibited.

A cobalt catalyst was prepared (catalyst B: 30gCo/0.075gPt/1.5gSi/100gAl_2O_3) on the silicon modified alumina support, using the standard aqueous slurry phase impregnation method. Catalyst B was tested in the pilot plant scale slurry reactor as well as in the semi-commercial demonstration unit under realistic Fischer-Tropsch synthesis conditions during an 8 month continuous test run. Catalyst break-up was not observed during this run, as measured by PSD and SEM analyses. Clean white wax was produced during this entire run, and the cobalt content of the secondary filtered wax remained very low (figure 2). This proved that silicon support modification successfully prevented the generation of cobalt containing ultrafines during large scale Fischer-Tropsch synthesis runs. From table 1, it can be concluded that silicon modification of alumina did not have any substantial effect on the Fischer-Tropsch synthesis performance of the catalyst.

Silicon modification of alumina supports is not only restricted to the utilisation of TEOS. Other silicon precursors can be used, e.g. Tetra Methoxy Ortho Silicate (TMOS). Besides silicon, successful modification of alumina can also be effected with other compounds.

The dissolution of titania supports was also investigated[11]. Titania also (partially) dissolves in aqueous solutions and silicon modification, using TEOS, effectively inhibited support dissolution.

CONCLUSIONS

It was demonstrated that the production of clean white wax (i.e. free of any cobalt contamination) during large scale slurry phase Fischer-Tropsch synthesis runs, was successfully effected with cobalt catalysts that were prepared on modified supports (i.e. supports displaying inhibited dissolution behaviour in aqueous environments). As an example, the silicon modification of alumina supports was discussed in detail.

REFERENCES

(1) B. Eisberg, R.A. Fiato, Studies in Surface Science and Catalysis, Vol. 119 (1998) 961.
(2) M.M.G. Senden, A.D. Punt, A. Hoek, Studies in Surface Science and Catalysis, Vol. 119 (1998) 943.
(3) J.W.A. de Swart, R. Krishna, and S.T. Sie, Studies in Surface Science and Catalysis, Vol. 107 (1997) 213.
(4) P.J. van Berge, and R.C. Everson, Studies in Surface Science and Catalysis, Vol. 107 (1997) 207.
(5) A. Hoek, J.K. Minderhout, and P.W. Lednor, EP 110449, 1983.
(6) C.H. Mauldin, S.M. Davis, and K.B. Arcuri, US 4,663,305, 1987.

(7) C.H. Mauldin, and K.L. Riley, US 4,992,406, 1991.
(8) S. Eri, J.G. Goodwin Jr., G. Marcelin, and T. Riis, US 4,880,763, 1989.
(9) F. Rohr, A. Holmen, and E.A. Blekkan, proceedings of Syngas Conversion to Fuels and Chemicals symposium, 217th ACS national meeting, Anaheim, March 21-25, 1999.
(10) R.L. Espinoza, J.L. Visagie, P.J. van Berge, and F.H. Bolder, US 5,733,839, 1998.
(11) P.J. van Berge, J. van de Loosdrecht, E.A. Caricato, and S. Barradas, WO 99/42214, 1999.
(12) P.J. van Berge, J. van de Loosdrecht, E.A. Caricato, S. Barradas, and B.H. Sigwebela, WO 00/20116, 2000.
(13) P.J. van Berge, J. van de Loosdrecht, J.L. Visagie, US 09/168604, 1999.
(14) Schultz, H., and Geertsema, A., Erdöl and Kohle, 30 (1969) 193.
(15) G. Furrer, and W. Stumm, Geochim. Cosmochim Acta, 50 (1986) 1847.
(16) J.-B. d'Espinose de la Caillerie, and O. Clause, Studies in Surface Science and Catalysis, Vol. 101 (part B) (1996) 1321.
(17) J.-B. d'Espinose de la Caillerie, C. Bobin, B. Rebours, and O. Clause, Prep. of Cat. VI (eds G. Poncelet et al, Elsevier Science B.V.) (1995) 169.

FISCHER-TROPSCH DIESEL FUEL PREPARATION AND TESTING

Paul F. Schubert, Robert Freerks, H. Lynn Thomlinson, Branch Russell

Syntroleum Corporation

1350 S. Boulder, Suite 1100, Tulsa, OK

KEYWORDS: FISCHER-TROPSCH, SYNTROLEUM, SYNTHETIC DIESEL FUEL

ABSTRACT

Synthetic diesel fuel which is sulfur and aromatic free has been produced using the Syntroleum Process. The main difference between the Syntroleum Process and traditional Fischer-Tropsch (FT) processes is the use of a nitrogen diluted syngas stream to the FT reactors. This Syngas stream is produced in an air-blown autothermal reformer using natural gas. In the FT reactors, a cobalt based catalyst is used to convert the syngas to paraffinic oils and waxes. These products are then separated, saturated, and cracked to produce the desired products.

The emissions from two diesel fuels, this FT diesel and a conventional low sulfur diesel were measured according to the Code of Federal Regulations (CFR) Title 40 specifications in a Cummins 5.9 liter heavy duty diesel engine and a 1.9 liter light duty diesel engine. The FT diesel showed substantially reduced emissions compared to the other diesel fuels.

INTRODUCTION

The Syntroleum process is a modification of the Fischer-Tropsch (FT) process originated[1] by Franz Fischer and Hans Tropsch in 1923 to convert coal to fuels and lubricants. This process was practiced in Germany[1], and Japan[2] during the Second World War, and has been practiced in South Africa since it was forced to be essentially energy self-sufficient during its apartheid era. Obviously, the drivers for these uses of the Fischer-Tropsch process were not open market economics. The first commercial development of the FT process involved fixed bed reactors using cobalt based catalysts[3]. Nine commercial FT plants were completed in Germany between 1935 and 1939. However during this same period research continued targeted at developing higher process efficiency and cost savings with three phase reactor systems[4-6].

The earliest work on three phase, liquid circulating reactor systems was conducted by Dufschmidt[7] for I. G. Farbenindustrie beginning in 1934. Initially this work involved circulating a liquid through a fixed bed of catalyst[8-10], however, a system with an expanded bed was developed and patented[11]. This work was largely interrupted by the war. However, it served as the basis for FT slurry reactor development after the war[4]. This early work taught novel features included in many current slurry type FT reactors, including external circulation loops, and inclusion of pumps and separators into those circulation loops[7-11].

The primary steps in the process are generation of synthesis gas (CO and H_2) from a hydrocarbon feed, conversion of the synthesis gas to hydrocarbons, and then refining of the desired products. The initial commercial plants all used coal as the hydrocarbon source, and cobalt catalysts in the FT reactors. The main fuel produced from the process was diesel, because of the excellent cetane number obtained from the highly paraffininc products.

Broader application of Fischer-Tropsch technology has awaited substantial improvement in process economics. In addition, the continued discovery of vast quantities of natural gas around the globe has reduced the emphasis on generating synthetic fuels from coal and "bottom-of-the-barrel" hydrocarbon sources, and emphasized the importance of gas-to-liquid (GTL) processes. It is likely that there are economically viable applications for a number of different hydrocarbon to synthetic fuels processes.

The Syntroleum Process (Figure 1) is designed to reduce costs in critical, capital intensive areas while providing excellent product yields. The critical cost reduction areas are syngas generation, Fischer-Tropsch reactor design, and process integration. In conventional FT processes, the syngas generation step can require 50% to 60% of the total capital investment for the plant. An air-blown process can reduce this to the 25% range because of a combination of the elimination of the air separation unit, use of a small autothermal reformer (ATR), and using a gas turbine to provide the air compression for the air fed to the ATR.

Syngas generation from natural gas has traditionally been done using either steam methane reforming (SMR) or partial oxidation (POX). Both of these require substantially pure oxygen streams from an oxygen plant, which adds significantly to the size and capital cost of the plant. The Syntroleum Process utilizes a proprietary catalytic ATR to convert natural gas to syngas using air as the oxygen source. The reactions occurring in the ATR are shown below.

$$CH_4 + 1.5\,O_2 \rightarrow CO + 2\,H_2O \qquad \Delta H = -519 \text{ kJ/mole} \qquad (1)$$

$$CH_4 + H_2O \rightarrow 3\,H_2 + CO \qquad \Delta H = 206 \text{ kJ/mole} \qquad (2)$$

$$CO + H_2O \rightarrow H_2 + CO_2 \qquad \Delta H = -41 \text{ kJ/mole} \qquad (3)$$

Small amounts of steam are added to the system to suppress the formation of carbon. Because the system is in heat balance, no heat transfer system is required, and the reactor is much more compact than is possible with SMR or POX. The H_2 to CO ratio of the resulting syngas is close to the approximately 2:1 ratio in the hydrocarbon products from the FT process (4).

$$n\,CO + (2n+1)\,H_2 \rightarrow C_nH_{2n+2} \qquad (4)$$

The Fischer-Tropsch products are highly paraffinic, but also contain low levels of primary olefins and alcohols. If desired, these can be saturated to produce an essentially totally paraffinic material. Generally, economics are most favored by production of the long chain hydrocarbons which are cracked to the desired products rather than maximizing the amount of product in the fuel range produced directly by the FT process. This is because the latter approach tends to produce undesirably high levels of low value C_1 to C_5 hydrocarbons. Cracking to fuel range products is done using typical refining methods. However, the conditions needed to convert this synthetic crude into products are milder than those required for traditional natural crudes, which generally contain substantial amounts of unsaturated and heterocyclic species.

Because syngas produced in this air-blown process is diluted with nitrogen relative to an oxygen-blown system, there is some increase in the size of the downstream equipment associated with gas processing. However, economic evaluations show that elimination of the entire oxygen plant can be a significantly greater savings than the costs associated with nitrogen in the synthesis gas. An air-blown system allows the use of a turbine for the air compressor thereby enhancing thermal integration as well as allowing an inexpensive method for producing electric power for resale and/or driving other processes. Furthermore, the dilute light hydrocarbon stream that typically would be flared can be used as fuel for the turbine. The air-blown system offers greater flexibility in achieving higher carbon efficiencies and energy integration over a broad range of natural gas compositions. The economic incentives for the air blown system are evident at all plant throughputs and are greatest when evaluating small to mid size plants (< 50,000 bpd).

Cost savings in Fischer Tropsch reactor design are accomplished with a moving bed system, where catalyst microspheres are suspended by the gas in circulating liquid. This system provides more effective multiphase mixing thereby enhancing catalyst productivity and selectivity while minimizing the required heat transfer area. This gives a reactor that is more efficient than tube and shell reactors that have previously been commercialized[6]. Our economic evaluations strongly indicate that the Syntroleum moving bed system with our proprietary cobalt based FT catalyst provides significant

cost savings over the three phase bubble columns previously described in the technical literature[12, 13]. The improved economic performance of the moving bed system is due to the integration of catalyst performance with reactor design. The catalyst possesses high activity, attrition resistance, excellent hydrodynamic properties and is readily separated from the hydrocarbon products. Additionally, reaction kinetics have been tailored to give the preferred selectivity in the nitrogen-diluted environment.

PILOT PLANT DESIGN AND PERFORMANCE

The ATR and moving bed FTR combination for the Syntroleum process were demonstrated using a pilot plant constructed at ARCO's Cherry Point, Washington refinery. The individual process units were modular in design, constructed in Tulsa, OK, and shipped to the site in Washington state, where they were erected. The objectives of the Cherry Point pilot plant are to confirm the commercial design basis, identify optimum operating conditions for different natural gas feed compositions, and to generate the data necessary to validate Syntroleum process models. The unit was sized to reflect the hydrodynamics and multi-phase flow processes anticipated in commercial operations. Instrumentation was installed to monitor all critical axial and radial variables associated with phase holdups, interphase transport and recirculation rates. Process conditions were varied over a broad range to determine optimal conditions for the production of fuels and/or specialty products. The pilot plant was initially designed with a nameplate capacity of 70 barrels of FT product per day. Higher catalyst productivities and selectivities have been achieved due to better than expected catalyst performance in the turbulent mixing regime associated with commercial sized moving bed reactors. The first portion of the plant started operation in April 1999, and has achieved in excess of 6000 hours of ATR operation and 4500 hours of FT operation. We have successfully demonstrated ATR operation without significant carbon formation, and the FT unit has met or exceeded all design criteria associated with multiphase mass and heats transfer as well as with hydrodynamic and phase partitioning and separation parameters.

The autothermal reformer was designed to generate sufficient syngas to support 70 barrel per day FT product yields as well as allow for production above that nameplate capacity. The ranges of operating parameters being studied involve natural gas formulations containing significant quantities of C_2^+ hydrocarbons and CO_2. After determining critical residence times and reaction rates, the unit has given excellent performance in terms of carbon conversion efficiency to CO and operating stability.

The catalyst used in the pilot plant is a powder composed of cobalt on alumina-based microspheres. This material was produced in a full commercial- sized batch in commercial manufacturing equipment. Catalyst development involved starting with preparations of gram quantities at the laboratory scale, moving to pound quantity preparation procedures in order to define commercial manufacturing procedures. The final catalyst used in the pilot plant is from a 25,000 lb lot produced using low cost commercial manufacturing equipment.

In order for the catalyst to function effectively in the process, it must first be activated (reduced), because it is cobalt metal that is the actual catalytic species, while cobalt oxide is the form produced during manufacturing. Conditions and procedures were developed and followed at commercial scale, and resulted in catalyst in service in the reactor that met or exceeded the performance requirements in terms of activity and selectivity.

As previously mentioned, catalyst attrition and catalyst-product separation are some of the critical issues to be determined in the unit. After over 4500 hours of operation under widely varying conditions, there is no evidence of significant attrition within the unit. The attrition resistance of the catalyst has been monitored using particle size analysis, the settling characteristics of the particles, and the filter/separator performance. In addition, catalyst life and activity maintenance have met or exceeded expectations.

FUELS PREPARATION AND ENGINE TESTING

Syntroleum has produced a number of fuel range materials by refining Fischer-Tropsch wax, including synthetic analogs of gasoline, JP-5, JP-8, and diesel fuel. Synthetic diesel

is currently receiving considerable attention because diesel engine emissions are under regulatory scrutiny. Syntroleum S-2 fuel is a sulfur free, aromatics free fuel with an exceptionally high cetane index. Table 1 shows S-2's properties compared to typical properties of low emissions EPA D-2 Diesel.

Unmodified Heavy Duty Diesel Engines. Numerous studies have evaluated engine emissions from conventional, unmodified diesel engines using a variety of FT fuels. Engine tests with three S-2-like fuels consistently show decreases of hydrocarbons, carbon monoxide, nitrous oxides and particulate matter emissions[14]. We have confirmed these results in work at Southwest Research Institute comparing Syntroleum S-2 with EPA #2 using an unmodified heavy duty 5.9L Cummins engine on a test stand (Table 2) and an unmodified heavy-light duty diesel vehicle with the same engine on a chassis dynamometer (Table 3)[15]. None of these tests included engine timing modifications which could have taken advantage of the significantly higher cetane of Syntroleum S-2. In both tests, the Syntroleum S-2 significantly reduced emissions from the 5.9L Cummins engine. The 40% to 45% reduction in particulate emissions using the Syntroleum S-2 is especially notable.

Although our testing did not examine emission reductions from aromatic-containing FT fuels, previous engine tests[16] have shown that those fuels do not achieve the same level of improvement achieved from the more hydrogen saturated FT fuels in this study.

Table 1
Properties of US EPA Diesel and Syntroleum S-2

Property	Test Method	Units	US EPA D-2 Diesel	Syntroleum S-2 Fuel
Specific Gravity	ASTM D-1298	g/cc	0.846	0.771
API, Max	ASTM D-1298	deg	35.9	52
Flash Point	ASTM D-93	deg F	157	148
Cloud Point	ASTM D-2500	deg F	32	<0
Color	ASTM D-1500	Inspection	-	<0.5
Sulfur	ASTM D-2622	wt. %	<0.05	nd
Aromatics	ASTM D-1319	vol %	30	nd
Olefins	ASTM D-1319	vol %	1	nd
Saturates	ASTM D-1319	vol %	69	>99
Cetane Number, min	ASTM D-613	-	45	>74

Table 2
Emissions from a 5.9 liter Cummins B engine on a test stand
Average results from 2 runs

Test (g/bhp-hr)	HC	CO	NOx	Particulates
EPA # 2 Diesel	0.10	1.30	4.00	0.10
Syntroleum S-2	0.10	0.80	3.20	0.06
% reduction for S-2	0	38	20	40

Table 3
Emissions from a Heavy light-duty truck (2000 Dodge Ram 2500) with a 5.9 liter Cummins B engine on a chassis dynamometer using the US06 test protocol
Average results from 2 runs

Test (g/bhp-hr)	HC	CO	NOx	Particulates
EPA # 2 Diesel	0.19	0.70	5.24	0.11
Syntroleum S-2	0.16	0.50	4.50	0.06
% reduction for S-2	16	29	14	45

Light Duty Diesel Engines. Emissions evaluation of Syntroleum S-2 and EPA #2 were conducted on a 1.9L Volkswagen diesel engine in a 1999 Golf GL TDI (Table 4). This is a current production model, U.S. market passenger car, and is equipped with a catalytic converter. The hydrocarbon, CO, and NOx emissions from both fuels were equivalent within the experimental error of the test. However, the particulate emissions were dramatically lower from the Syntroleum S-2 fuel.

Table 4
Emissions from a light-duty passenger car (1999 Volkswagen Golf) with a 1.9 liter engine on a chassis dynamometer using the US06 test protocol
Average results from 2 runs

Test (g/bhp-hr)	Particulates
EPA # 2 Diesel	0.42
Syntroleum S-2	0.05
% reduction for S-2	88

CONCLUSIONS

Syntroleum and ARCO have successfully demonstrated a GTL conversion process that utilizes an air blown autothermal reformer and moving bed Fischer-Tropsch reactor. The process is robust, and is ready for scale-up to commercial scale fuels production plants. Economic evaluations of such commercial plants show that production of synthetic fuels is now economically competitive with conventional fuels.

Synthetic S-2 fuel produced substantially lower emissions than EPA diesel under all of the conditions tested. This S-2 fuel has substantial advantages compared to other alternative fuels because, in addition to being environmentally acceptable, it is backward compatible with current vehicles, and is compatible with the existing fuels delivery infrastructure. Syntroleum S-2 also exceeds engine manufacturers desires for ultra-low sulfur fuel which is needed to allow use of NOx absorption catalyst in future vehicle designs.

The need for backward compatibility with little or no modification to the engine is important because owners of current vehicles will not generally volunteer to make their vehicles obsolete because the actions of non-market forces. Furthermore, since it will take considerable time from the introduction of any new engines until they represent a majority of the vehicles on the road, substantial advantage in achieving environmental goals may be made using the existing inventory of vehicles.

The need for compatibility with the existing extensive fuels delivery infrastructure is important for several reasons. It allows consumers to maintain current behavior

patterns while still adopting new technology. In addition, it allows the many fuels distributors to become partners instead of competitors in technology introduction. This eliminates the need to for the new engine and new fuels suppliers to invest billions of dollars in a delivery system (service stations, etc.) and allows existing fuels marketers to pursue their own marketing strategies. The synthetic GTL fuels facilitate this approach because they are compositionally compatible with the existing tanks and pumps in service stations and fueling facilities, and may require little more than clean out of the tanks.

ACKNOWLEDGEMENTS

The authors would like to thank Jeff Bigger, Gary Beer, and Jim Leahy of ARCO, Robert Fannick of Southwest Research Institute and Ray Huang, Cemal Ercan, and Paul Kennedy of Syntroleum for their contributions.

REFERENCES

1. Storch, H. R., Golumbic, N., Anderson, R. B. *The Fischer-Tropsch and Related Synthesis*, **1951**, John Wiley & Sons, New York, 1.
2. Stranges, A. N. *Annals of Science*, **1993**, *50*, 229-265.
3. Henrici-Olive, G. and Olive, S. *Angew Chem (Eng. Ed.)*, **1976**, 15, 136.
4. Stranges, A. N. *Annals of Science*, **1997**, *54*, 29-68.
5. Kolbel, H. and Ralek, M. *Cat Rev-Sci Eng.*, **1980**, 21(2), 225.
6. Van Vuuren, D.S. CSIR Report OENG 432, **1982**, Pretoria, South Africa.
7. Benson, H. E.; Field, J. H.; Bienstock, D.; Storch, H. H. *Ind. and Eng. Chem.*, **1954**, 46, 2278-2285.
8. Duftschmidt , F.; Linckh, E.; Winkler, F. U.S. Patent 2,159,077, **1939**.
9. Duftschmidt , F.; Linckh, E.; Winkler, F. U.S. Patent 2,207,581, **1940**.
10. Duftschmidt , F.; Linckh, E.; Winkler, F. U.S. Patent 2,318,602, **1942**.
11. Duftschmidt , F.; Linckh, E.; Winkler, F. U.S. Patent 2,287,092, **1942**.
12. Oukaci, R., Singleton, A.H. et. al., *Applied Catalysis*, **1999**, *186*, 129-144.
13. Jager, B. AICHE 1997 Spring Nat. Meeting (Houston 3/9-13/97), **1997**, N.27c 9p.
14. Ryan, T. W. and Montalvo, D. A.: Emissions Performance of Fischer-Tropsch Fuels; 1997 AIChE Spring Meeting, Houston, TX; March 9-13, 1997 (unpublished).
15. Syntroleum Corporation emissions and toxicological study comparing Syntroleum S-2 CI fuel with commercially available diesel fuels; 2000 (unpublished).
16. Thomas D. Durbin, John R. Collins, Joseph M. Norbeck, Matthew R. Smith; Evaluation of the Effects of Alternative Diesel Fuel Formulations on Exhaust Emissions rates and Reactivity; University of California (Riverside); April, 1999.

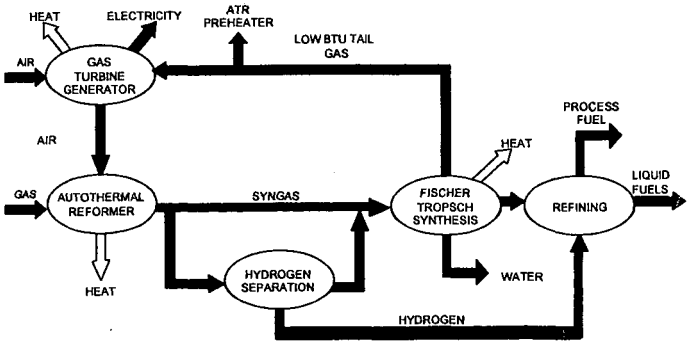

Figure 1. Process schematic for fuels production via the Syntroleum Process.

A TWO-STEP CONVERSION OF SYNGAS VIA DIMETHYL ETHER

Chang-jun Liu, Tao Jiang, and Gen-hui Xu

State Key Laboratory of C1 Chemical Technology,
Tianjin University, Tianjin 300072, China

ABSTRACT In this presentation, we present some of our experimental results of a two-step conversion of syngas into more valuable chemicals or high performance fuel additives. In the first step, dimethyl ether (DME) is formed from syngas. With the second step, the formed DME is applied for the further synthesis via an "electronic" catalysis. The conversion of DME by this way can reach a high-energy yield. The products of such conversion include oxygenates and/or alkanes. The two-step conversion of syngas via DME could lead a new synthesis from syngas. Especially, the conversion of DME in the second step can be operated at ambient condition. The synthesis reported here could lead to a new application of DME.

KEYWORDS: DME, electronic catalysis, plasma

INTRODUCTION

The formation of Dimethyl Ether (DME) from syngas conversion has recently attracted more and more attention. DME is becoming a major product, especially for the gas reserves at remote sites or coalbed methane. It is important for us to seek for more applications of DME. DME is a useful chemical intermediate for the synthesis of many important chemicals, including dimethyl sulfate, lower olefins and methyl acetate.[1-3] DME has also been proposed as an aerosol propellant to replace chlorofluoro carbons, which were found to have destroying effect on the ozonosphere.[4] In addition, DME is a promising alternative fuel to diesel.[5] Brown *et al.* had a detailed discussion on the possible fuels or fuel precursors from DME[6]. They also described some possible methodologies for the use chemically of DME, including oxidative coupling, vinylation/hydrogenation, oxidative coupling (with MTBE) and carbonylation. Compared to the utilization of DME as fuel, propellant and so on, the use of DME as a chemical intermediate is particularly attractive and needs to be investigated extensively. Especially, DME has been recognized as an alternative to methanol as a chemical building block.

Here we report a conversion of DME in a dielectric-barrier discharge (DBD) plasma reactor at ambient condition, as a two-step of conversion of syngas. The DBD used in these experiments is a high pressure, non-equilibrium discharge which is initiated when alternating voltages of sufficiently high amplitudes are applied between two electrodes separated by a non-conducting medium (dielectric barrier) in addition to a gas space. The frequency of the ac electric field can vary over a wide range from line frequency to several MHz. Glass, quartz or ceramics can be used as dielectric materials. When the amplitude of the applied ac electric field reaches a critical value, breakdown is initiated in the gas and current flows through the gas space from one electrode to the other. Once breakdown is initiated at any location within the discharge gap, charge accumulates on the dielectric resulting in an opposite electric field. This opposite electric field locally reduces the external electric field in the gap and interrupts the current flow within a few nanoseconds. By this mechanism individual current filaments called microdischarges are formed. Their duration depends on the pressure and the properties of the gases involved and the dielectrics used. A large number of such microdischarges will be generated when a sufficiently high ac voltage is applied. The principal advantages of the DBD are that non-equilibrium plasma conditions can be established at atmospheric pressure and that the entire electrode area is effectively used for discharge reactions. The unusual "electronic" catalysis of DBD for the conversion of DME at ambient condition has been confirmed in this investigation. This could lead to a two-step utilization of syngas. In the first step, dimethyl ether (DME) is formed from syngas. With the second step, the formed DME is applied for the further synthesis via such electronic catalysis. Due to the limited space, we only focus on the second step in this paper and leave the first step for the future discussions.

EXPERIMENTAL

Figure 1 illustrates the reactor system. The gas flow (pure DME) is subjected to the action of the DBD in an annular gap formed between an outer stainless steel tube maintained at constant temperature and an inner quartz tube. The radial width of the discharge space was 1 mm, its length 50mm ~ 150 mm. This reactor system is very similar to the DBD reactor for methane conversion described elsewhere.[7,8] All the experiments were conducted at atmospheric pressure. The feed and exhaust gases were analyzed by a gas chromatograph (HP 4890) with a thermal conductivity detector (TCD) and a flame ionization detector (FID). The exhaust gas from the reactor was first introduced into a condenser to separate the condensable product from the gas. A high voltage generator working at about 25 kHz applies the power. The power can be varied by

adjusting the voltage amplitude, which causes a slight change of frequency. The voltage and current measurements were conducted using a high voltage probe (Tektronix P6015) and a current probe (Tektronix CT-2) with a digital oscilloscope (Tektronix TDS 210).

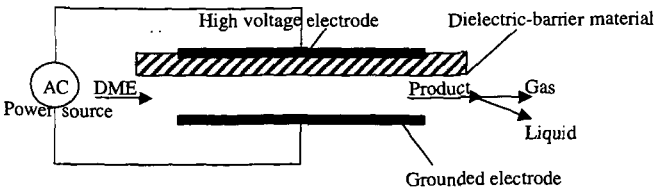

Figure 1. Schematically representative of the DBD reactor system

RESULTS AND DISCUSSION

A surprising high DME conversion has been achieved in the present reactor design. The C-O bond breakdown in a DME molecule does not require a high energy and this leads to the high DME conversion. The bond strength of C-O in DME molecule is only 81 kcal/mol at 298 K. CH_3 and CH_3O radicals can be easily obtained within DME plasmas. Hydrocarbons and ethers are expected to be formed from chain reactions initiated by CH_3 and CH_3O radicals.

Table 1 shows the composition of gaseous products observed at 60°C and different gas flowrates. The gaseous product is a mixture of hydrocarbons, ethers, H_2 and CO. Methane, ethane, propane, methyl ethyl ether, acetone, methyl isopropyl ether, ethyl ether, 1,2-dimethoxy ethane and dimethoxy methane were detected. Most of methyloxy-containing hydrocarbons have been detected in the liquid phase. The composition of gaseous products changed greatly with the variation of gas flowrate. Experimental results showed that most of gaseous products were H_2 and C_1-C_3 alkanes. The amount of oxygenates was very little in the gaseous phase but abundant in liquid product. Table 1 also shows the composition of lower alkanes in the gaseous phase increases with the decreasing flowrates. This is a typical characteristic of chain reactions. A mechanism has been presented to explain the observed phenomena. CH_3 and CH_3O radicals are first generated in the DBDs via electronic dissociation or other plasma reactions. Some of chain reactions have been proposed as the following to explain the production of part of hydrocarbons:

$$CH_3 + CH_3 \rightarrow C_2H_6$$
$$CH_3 + CH_3 + M \rightarrow C_2H_6 + M$$
$$C_2H_6 + e \rightarrow C_2H_5 + H + e$$
$$C_2H_5 + CH_3 \rightarrow C_3H_8$$
$$C_2H_5 + C_2H_5 \rightarrow C_2H_6 + C_2H_4$$
$$C_2H_5 + CH_3 \rightarrow C_2H_6 + CH_4$$
$$C_3H_8 + e \rightarrow C_3H_7 + H + e$$

$$CH_3O + CH_3 \rightarrow CH_3OCH_3$$
$$CH_3O + C_2H_5 \rightarrow C_2H_5OCH_3$$
$$C_2H_5OCH_3 \rightarrow C_2H_5O + CH_3$$
$$C_2H_5O + C_2H_5O \rightarrow C_2H_5OC_2H_5$$

$$CH_3O + C_2H_4 \rightarrow CH_3OCH_2CH_2OCH_3$$

$$CH_3OCH_3 \rightarrow H + CO$$
$$CH_3OCH_3 + CO \rightarrow CH_3COOCH_3$$
$$C_2H_4 + H_2 + CO \rightarrow CH_3COCH_3$$
$$CH_3O + C_2H_4 + CH_3O \rightarrow CH_3OCH_2CH_2OCH_3$$

In addition, the experiment has shown a formation of some paraformaldehyde, that could be induced from the reaction: $CH_3O + H \rightarrow HCHO + H_2$.

The DBD conversion of DME leads to a selective production of liquid product, that is a mixture of various ethers. Figure 2 shows the results of DME conversion and the ratio of liquid production to the total production. It is clear that higher DME conversion accompanies with more liquid products produced. More than 93% of the product is liquid at a gas flowrate of 20

ml/min. This suggests that DBDs could easily convert DME to liquid chemicals at ambient conditions. A more surprising phenomenon with this DBD DME conversion is that no carbon deposit has been observed on the dielectric, while a serious carbon deposit has been formed during plasma conversion of methane or other lower alkanes[8,9,10]. It has been considered that some aerosols would have been formed during DBD conversion of DME. It is the aerosol inhibits the formation of carbon deposit. Further investigations are being conducted.

Table 1: Effect of gas flow rate on the composition of gas product

Composition / mol%	Gas flow rate / ml/min			
	60	45	30	20
H_2	9.15	10.83	20.49	31.26
CO	4.29	4.20	8.56	17.70
CH_4	4.46	5.54	9.82	12.50
C_2H_6	2.66	3.19	5.36	6.02
C_3H_8	0.22	0.28	0.59	1.22
DME	76.48	72.87	50.63	26.71
C_2H_5 O CH_3	1.32	1.51	2.37	1.83
CH_3 CO CH_3	0.04	0.05	0.10	0.20
$C_2H_5(OCH_3)CH_3$	0.04	0.04	0.09	0.10
C_2H_5 O C_2H_5	0.02	0.03	0.05	0.07
CH_3O CH_2 OCH_3	0.19	0.22	0.32	0.23
CH_3O CH_2CH_2 OCH_3	0.14	0.15	0.14	0.07
others	1.00	1.09	1.49	2.10

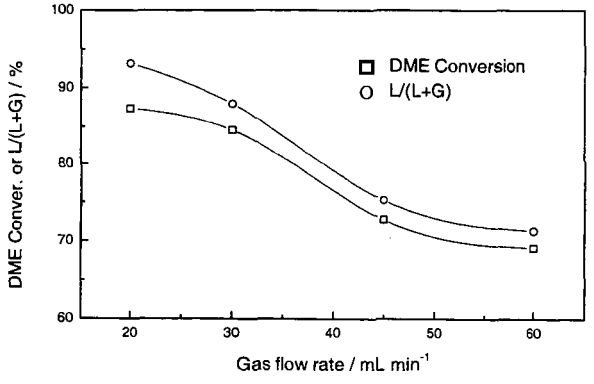

Figure 2. Effect of gas flow rate on experimental results

CONCLUSIONS

The potential of plasma conversion of DME has been demonstrated in this work. The present product from this DME conversion can be used as the high performance fuel additive. Moreover, further investigation is being conducted to produce selectively other valuable hydrocarbons. Some other potential pathways for the DME conversion via electronic catalysis are as the following:

With CO_2 plasma:

$CO_2 \rightarrow CO + DME \rightarrow$ carbonylation

$\rightarrow O + DME \rightarrow$ oxidative coupling

With hydrogen plasma:

$H_2 \rightarrow H + DME \rightarrow$ dehydrogenation (to produce ethylene)

$\rightarrow$ higher hydrocarbon formation

With oxygen plasma:

$O_2 \rightarrow O + DME \rightarrow$ oxidative coupling

With lower alkane (methane, ethane or propane) plasma:

lower alkane plasma + DME $\rightarrow$ high performance fuels or fuel precursors

With steam plasma:

steam plasma + DME $\rightarrow$ special oxygenated hydrocarbons

With syngas plasma:

syngas plasma + DME $\rightarrow$ carbonylation and others

These pathways open more doors to produce series of valuable chemicals. Especially, one of advantages of such electronic catalysis of DME plasma is her high efficiency that is able to convert DME into some special chemicals, that may be difficult to be produced using the conventional technologies. Since the plasma is a complex reactive system that contains a mixture of electrons, ions, radicals, photons, and so on. The control of plasma reactions needs special skills so that a selective conversion of DME can be achieved. We have confirmed that DBD can perform as excellent electronic catalyst for DME conversion. There are some other plasma phenomena, like corona discharge, arc discharge, gliding arc discharge and microwave discharge, that could also be useful for the DME conversion. To compare with the conventional catalysis, the controlling parameters of electronic catalysis are electron temperature, electron density, radical energy and density and so on. The gas temperature and pressure have a little influence on electronic catalysis. More fundamental investigations are necessary to understand the mechanisms. The feasibility of the two-step conversion of syngas via DME using electronic catalysis is being confirmed in our further investigations.

ACKNOWLEDGEMENT

The support from The Research Fund for the Doctoral Program of Higher Education in China is very appreciated. The assistance from Mr. Guo-liang Fang, Mr. Sen Han, Ms. Fei He, Mr. Yang Li, Dr. Zhen-hua Li, Dr. Chun-de Yao and Dr. Ming-fa Yao in Tianjin University is also appreciated.

REFERENCES

1 T. Shikada, K. Fujimoto, M. Miyauchi and H. Tominaga. Appl. Catal., **1983**,7, 361.
2 W. W. Kaeding and S. A. Butter. J. Catal., **1980**,61,155.
3 Guangyu Cai, Zhongmin Liu and Renmin Shi *et al.* Appl. Catal., A **1995**,125, 29.
4 K. Guenter, S. Guenter and T. Dieter. DE Patent 4313584
5 Alkeos C. Sofianos and Mike S. Scurrell. Ind. Eng. Chem. Res., **1991**,30, 2372.
6 D.M. Brown, B.L. Bhatt and T.H. Hsiung *et al.* Catal. Today, **1991**, 8, 279
7 Chang-jun Liu, Gen-hui Xu and Timing Wang. Fuel Processing Technology, **1999**,58, 119.
8 Baldur Eliasson, Chang-jun Liu and Ulrich Kogelschatz. Ind. Eng. Chem. Res., **2000** (to be published).
9 Chang-jun Liu, R.G. Mallinson and L. Lobban. J. Catal., **1998**, 179,326.
10 Chang-jun Liu, R.G. Mallinson and L. Lobban. Appl. Catal. A, **1999**, 178,17.

NEW CONCEPTS IN OCTANE BOOSTING OF FUELS FOR INTERNAL COMBUSTION ENGINES

Paul F. Waters
Department of Chemistry, American University
4400 Mass. Ave. NW, Washington, DC 20016
and
Jerry C. Trippe
General Technology Applications, Inc.
7400 Gallerher Road, Gainesville, VA 21055

KEYWORDS: polymer, droplet size, octane increase

ABSTRACT
The holy grail of the combustion of fuels in internal combustion engines is the perfect mixture of fuel and air. This ideal state will allow complete combustion at a uniform rate, delivering optimal power with no harmful emissions under all operating conditions. A primary objective of engine builders is to achieve engine designs that will produce a uniform distribution of very-small-diameter fuel droplets, said to be crucial to forming a mixture approaching perfection. When high molecular weight polymers are added to hydrocarbon fuels at low ppm levels, the viscoelasticity manifested during the stress of carburetion or injection precludes the formation of large numbers of fine droplets. The average droplet size of such fuels, aerosolized in air, is measurably larger than the droplets sprayed with neat fuels, and the size distribution is narrowed. Moreover, the number of droplets below the upper threshold for explosive combustion is greatly reduced. Such polymer-fortified fuels burn at substantially lower average temperatures, thereby increasing the octane rating of the fuel, the efficiency of combustion, and the power delivered to the crankshaft.

INTRODUCTION

The combustion of hydrocarbon (HC) fuel in internal combustion (IC) engines is an extremely complex event, encompassing many variables, and far from being completely understood. It is a phenomenon which is readily characterized by the adage, "The less known about a scientific or engineering process, the more measurements required to define it." In support of this view, a partial listing of topics on the combustion of gasoline in IC engines, which appeared in publications of the Society of Automotive Engineers over the last decade, includes: the properties of spray from an injector, the location and focusing of injectors, the time of injection relative to intake valve position, the flow of the air/fuel mixture in the induction channel, the liquid fuel films on the walls of the induction channel and the intake valve, the vaporization of droplets in the induction channel, the vaporization of the wall film in the induction channel, the atomization of the wall film from the induction channel caused by air flow, the fuel species which comprise the wall film of the induction channel, the effects of viscosity and surface tension on the air-stripping of fuel from the wall film of the induction channel, the fuel from one injection remaining in the induction channel through multiple cycles, the condition of the air/fuel mixture in the cylinders, the liquid fuel film on the walls of the cylinders, the spatial distribution of the fuel species in the gas in the cylinders, the effects of swirl and tumble motions in the cylinders, the presence of liquid fuel at the end of compression, the stratification of the fuel/air charge, the air/fuel ratio at the spark plug, the condition of the air/fuel mixture at ignition, the carryover of unburned fuel in the cylinders from the previous exhaust stroke, and the charge temperature. Many of these factors have been investigated over a range of operating conditions and then related to ignition, inflammation, rate of heat release, burning time, mean effective pressure, cycle variability, end-gas temperature, knock, emissions and volumetric efficiency.

The segment of the combustion process addressed in this paper is the air/fuel mixture preparation, a critical component of the overall process, which affects virtually all of the variables listed above. The air/fuel mixture preparation involves the introduction of the gasoline into the induction system from a carburetor or an injector, the mixing of the air and fuel in the induction channel, the transport of the air/fuel mixture into the cylinder during the intake stroke, the compression of the mixture, and the condition of the mixture at the time of ignition.

It is the physical properties of the gasoline which constitute the greatest single barrier to providing an optimal air/fuel charge at the spark plug at the time of ignition. A description is given here, and a model is proposed, for the manner in which polymers alter the physical properties of gasoline droplets. Polymers improve the combustion process, and lead to increases in fuel octane rating, power production and volumetric efficiency, as well as substantial emissions reductions. Analogous benefits have been found with low ppm concentrations of polymers in diesel fuel, burned in both large and small diesel engines, where the release of black particulates is greatly diminished. The most dramatic improvements have been recorded with the polymer-fortified fuels used in two-cycle engines, where the usual raw-gas emissions are significantly curtailed and noise is abated.

EXPERIMENTAL

VISCOELASTICITY

When elastomers of molecular weight, sufficient to impart a viscoelasticity at low concentrations, are added to gasoline, a hydrodynamic control is conferred upon the fuel. A quiescent viscoelastic fluid acts as an ordinary liquid. Under sudden stress, the liquid exhibits greatly increased viscosity and solid-like elastic properties. The effect of viscoelasticity on the aerosolization of fuels is shown in Figure 1, where an antimisting function, $P/(P - R)$ is plotted against both the molecular weight and the concentration of polyisobutylene in diesel fuel at 20° C (●). P is the quantity per minute of liquid pumped through a paint sprayer; R is the quantity of liquid recovered in a line-of-sight vessel, positioned two meters from the sprayer (1). In a correlative experiment, the function, h/c, is plotted against the molecular weight of polyisobutylene in toluene at 20° C (O). The term, h, is the height to which a thin stream of viscoelastic solution may be stretched before separation occurs, and c is the concentration (2). Polyisobutylene, of molecular weight 7.2 Md, was used in all of the measurements reported here.

TEMPERATURE

Table 1 contains measurements recorded at the D.A.M. engine lab in Duchess County, NY, on a four-cycle, single-cylinder Briggs & Stratton gasoline engine. The fuel contained 10 ppm of polymer. The data are representative of the temperature decreases observed in both gasoline and diesel engines using polymer-fortified fuels. A relation developed between the temperature of the unburned gas in a gasoline engine and the octane requirement, measured on a 2.2 liter, 4-cylinder, Chrysler production engine, is that for each 7° K increase in unburned gas temperature, the octane requirement of the fuel increases by a single unit (3). If a substance decreases the operating temperature of an engine, this is tantamount to increasing the octane rating of the fuel-in-use. Such a substance would not necessarily exhibit an octane increase when tested at constant temperature.

POWER

In Figure 2 are presented test data recorded on a 1990 turbodiesel Toyota Landcruiser with a 400,000 km odometer reading, in Perth, Australia. The dynamometer measurement of horsepower (BHP) was first determined without polymer in the fuel. The peak BHP was 95.7. Polymer was added to achieve a concentration of 10 ppm, and the vehicle was returned four days later for testing. The 107.2 BHP recorded represents a 12 % increase in power attributable to the polymer [in order to save space the neat fuel value was traced into Figure 2 from the DYNO DYNAMICS dynamometer graph].

EMISSIONS

As a consequence of the overall decrease in operating temperatures, and the control of the droplet size and size distribution, the emissions of the routinely-monitored pollutants from gasoline engines are reduced substantially by the addition of 10 ppm of polymer to the gasoline. The first three entries in Table 2 were measured by engineers from SNAP-ON TOOL INC., in Richmond, VA; the last two were determined at an official State of Virginia testing facility in Fairfax County, VA.

TRANSIENTS

The values given in Figure 3 were measured by engineers from EG&G AUTOMOTIVE RESEARCH, INC., in San Antonio, TX, on a 1985 Nissan 300 ZX, with a gasoline engine and an odometer reading of 180,000 miles. The dark bars show the mass of neat fuel required to attain a given MPH; the light bars, the mass of fuel containing the polymer at 10 ppm required to reach comparable speeds. The polymer has a profound effect on the efficiency of combustion during accelerations, where engines are least efficient, and the emissions of pollutant species are greatest—the conditions frequently met in urban driving.

PARTICLE SIZE AND DENSITY

Figure 4 shows photographs of aerosols, produced by a paint sprayer, taken at the University of Dayton, Dayton, OH. The probing technique used was laser light scattering. In order to avoid a possible explosion from the mist, which would be produced with raw gasoline, water and an aqueous solution of high molecular weight polyethylene oxide were sprayed. The solution was identical in viscoelastic properties to a solution of polyisobutylene in gasoline at 10 ppm, measured with the ductless siphon (2). The dark region depicts water, with its high density of minute droplets; the light region shows the droplets from the polymer solution. The marker is a 50-micron copper wire.

DISCUSSION

Gasoline contains species which vaporize at different rates, at a given temperature. In neat fuel, the "light" ends vaporize more rapidly, and concentrate near the spark plug at ignition. The "heavy" ends dominate the liquid films in the induction channel, and on the cylinder walls, and remain further from the spark plug at ignition. The "light" paraffin molecules burn more rapidly than the "heavy" aromatic molecules. The ignition of the "light" molecules causes an early temperature spike which dissociates Nitrogen molecules and generates NO_x. The predominance of the "heavy" ends in the unburned fuel causes a relatively slow flame-front advance, and these ends may persist beyond exhaust valve opening. This model leads to: knock, poor effective pressure, unburned HC, CO, partially oxidized HC, NO_x and particulates.

The viscoelastic effect displayed in Figure 1 demonstrates that, at sufficiently high molecular weight, the polymer is a strong deterrent to mist formation. Very little fuel is lost at the higher concentrations sprayed. In usable fuels, the concentration is two orders of magnitude lower, so the polymer can permit appropriate droplet formation. The polymer is able to achieve the beneficial results reported here by limiting the population of very-small-diameter droplets (Figure 4). In addition, the droplets formed possess a certain toughness. The larger size, and inelastic structure, provide the momentum for further penetration of the fuel droplets into the faster moving air mass, thereby producing an air/fuel mixture closer to the ideal. Moreover, under stress, the polymer conveys to the droplets a surface viscoelasticity which increases the surface tension, and limits the vaporization of the "light" ends from the droplets throughout the stress, and until such time as the polymer molecules relax. The composition of the fuel droplets should remain relatively uniform during the relaxation. As the droplets are heated, at the point of relaxation, the vaporization of all species, through the surface film, is likely to be spontaneous, leading to a more uniform distribution of the various gaseous species in the air/fuel mixture.

The polymer-containing fuels reduce the temperature, as reported in Table 1, and result in antiknock activity and an octane increase. This suggests that a more homogeneous blend exists at ignition, and that the high temperature spike, which causes knock, is moderated, and this implies an improved air/fuel mixture preparation. Moreover, exhaust temperatures are lower with polymer-fortified fuels. High exhaust temperatures are produced by fuels burning late into the expansion stroke. A more uniform blend of "light" and "heavy" species in the unburned gas, ahead of the flame front, results in faster flame advance, and lower exhaust temperatures. The exhaust temperature differentials, entered in Table 1, indicate better air/fuel mixture preparation. Likewise, the power increase, displayed in Figure 2, can develop only with an increase in the octane (cetane here) rating of the fuel, suggesting a more homogeneous air/fuel mixture preparation. The reduction of the pollutants HC and CO, reported in Table 2, reflects a more complete combustion, and the decrease in NO_x relates to the paucity of fine fuel droplets. These environmental improvements, together, imply an air/fuel mixture preparation nearer to the ideal.

As revealed in Figure 3, the fortified fuel is particularly effective in overcoming inefficiencies during transients. The cause of transient hesitations is the build-up of the liquid-fuel film in the induction channel. The consensus is that it is the inability of this film to vaporize rapidly enough to be readily transported into the cylinder, when the intake valve opens, that is the cause of the lean mixture and the hesitation. It is counterintuitive to believe that a substance which limits vaporization from the droplets in the cylinders, as suggested here, could improve engine performance during transients, when limited vaporization from the liquid-fuel film in the induction channel is the cause of the hesitation. The results from the EG&G tests, however, are quite convincing. A reconsideration of the problem is instructive. The paradigm proposed here is: 1) the transient hesitations arise because, with neat fuels, there is insufficient fuel, either in the liquid or vapor phase, imported into the cylinder; 2) the inelastic droplets of fortified fuels, which exist before the polymer reaches complete relaxation, rebound from the induction channel walls in sufficient numbers to reduce the portion of liquid film on the walls, and increase the concentration of liquid droplets in the air/fuel mixture; 3) the polymer limits vaporization from the fuel droplets in the air/fuel mixture flowing in the induction channel, and these fuel-dense droplets are available for transport into the cylinder when the intake valve opens. This model is satisfactory for understanding the improvement of engine performance during transients and in steady-state combustion as well.

CONCLUSIONS

High molecular weight polymers confer significant benefits when present in fuels burned in IC engines. The overall operating temperatures are decreased, imputing an octane or cetane rating increase to the fuel-in-use. The power output is increased. Fuel consumption is reduced and, while not reported explicitly here, mileage gains are substantial, particularly with diesel and two-cycle, engine-powered vehicles (4). The pollutants, HC, CO and NO_x are reduced.

ACKNOWLEDGEMENT

We thank John B. Waters for providing the computer graphics.

REFERENCES

(1) Waters, P.F., Hadermann, A.F. and Trippe, J.C., Proceedings of the Second International Conference on Reactive Processing of Polymers, pp 11-22, J.T. Lindt, Ed., U. of Pittsburgh, Pittsburgh, PA, November 2-4, 1982.

(2) Chao, K.K., and Williams, M.C., J. Rheology, 27, 451, 1983.

(3) Valtadoros, T.H., Wong, V.W. and Heywood, J.B., Division of Petroleum Chemistry Preprints, Vol. 36, No. 1, pp 66-78, 1991, Am. Chem. Soc., Atlanta Meeting, April 14-19, 1991.

(4) Trippe, J.C., Hadermann, A.F. and Cole, J.A., US Patent, 5906665, May 25, 1999.

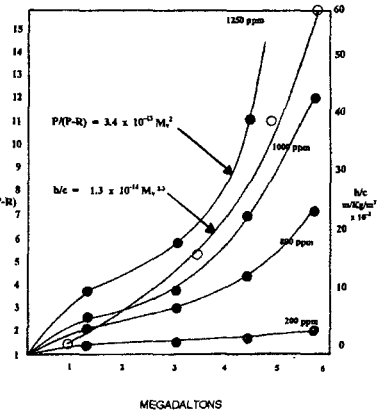

Figure 1. Antimisting function, P/(P-R) and ductless siphon function, h/c vs. molecular weight of polyisobutylene at 20°C (● in diesel fuel, ○ in toluene).

TABLE 1. ENGINE TEMPERATURES OF A 4-CYCLE, SINGLE-CYLINDER GASOLINE ENGINE

FUEL	RANGE	AVERAGE	DIFFERENCE
	CYLINDER HEAD EXHAUST		
No polymer	290-300°F	295°F	
With polymer	260-270°F	265°F	-30°F
	EXHAUST MANIFOLD		
	RANGE	AVERAGE	DIFFERENCE
No polymer	1280-1360°F	1320°F	
With polymer	1208-1248°F	1228°F	-92°F
	TAILPIPE		
	RANGE	AVERAGE	DIFFERENCE
No polymer	980-1110°F	1045°F	
With polymer	798-862°F	830°F	-215°F

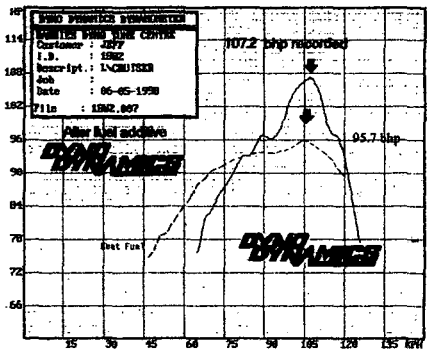

Figure 2. Brake horsepower (BHP) of a 1990 turbodiesel Toyota Landcruiser with polymer (solid line) and without polymer (broken line).

TABLE 2. VEHICLE EMISSIONS TEST RESULTS

		HC			CO			NOx		
Vehicle	Test	BEFORE (PPM)	AFTER (PPM)	LOSS %	BEFORE %	AFTER %	LOSS %	BEFORE (PPM)	AFTER (PPM)	LOSS %
'97 Jeep Wrangler	Sun Dyno	22	6	72	0.02	0.0	100	34	0.0	100
'95 Nissan Pathfinder	"	92	8	91	0.10	0.0	100	162	0.0	100
'88 Chevy Suburban	"	139	54	61	0.32	0.05	84	370	151	59
'90 Ford Bronco	Bear Static	135	0.0	100	0.90	0.0	100	not measured		
'87 Toyota Pickup	"	280	40	86	1.50	0.0	100	not measured		

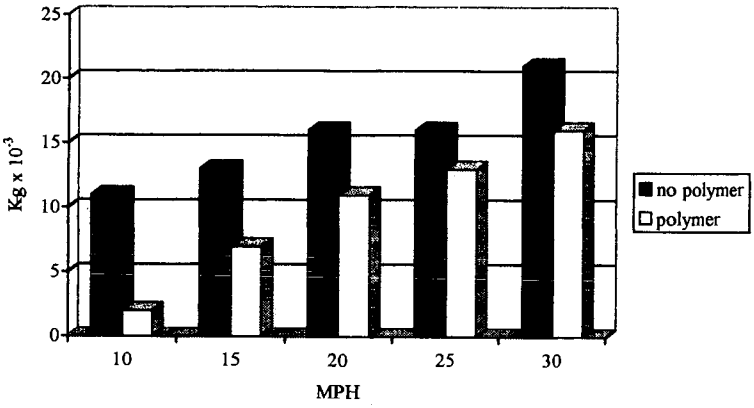

Figure 3. Acceleration tests on a 1987 gasoline-powered Nissan 300 ZX.

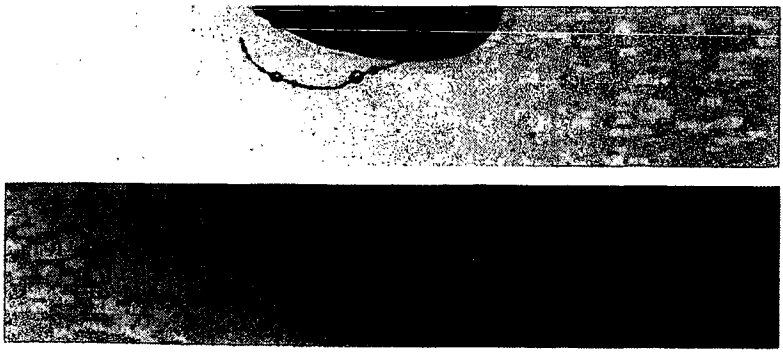

Figure 4. Laser light scattering images of droplets of an aqueous solution of polyethylene oxide (low density) and water (high density)

CARBON NUMBER CORRELATION OF OVERALL RATE CONSTANT OF PYROLYSIS OF N-ALKANES

Masaru Watanabe, Tadafumi Adschiri, and Kunio Arai
Department of Chemical Engineering, Faculty of Engineering, Tohoku University
07, Aramaki, Aoba, Sendai, 980-8579, JAPAN

KEYWORDS: n-alkane pyrolysis, kinetic model, size dependence

Introduction

A lot of studies have been reported so far on pyrolysis of n-alkanes. From the literature, the overall rate constant of pyrolysis of n-alkanes is well known to affect on reaction condition (pressure and temperature) and carbon number of n-alkane.

The pressure dependence of reaction rate can be predicted by Rice and Herzefeld theory[1]. However, carbon number dependence of overall rate constant of n-alkane has not been explained by theoretical base, yet.

For carbon number dependence of the overall pyrolysis rate constant, two correlations were reported[2,3]. Voge and Good's correlation[3] is as:

$$k_{(i)}\ [s^{-1}] = (i-1)\ (1.57i - 3.9) \times 10^{-5} \qquad (1)$$

Herein, $k[s^{-1}]$ is the pseudo first order rate constant of pyrolysis of n-alkanes and i is carbon number of n-alkane. This equation can be applied for the pyrolysis of n-C_4 ~ n-C_{16} at 773 K and 0.1 MPa. Tilicheev's correlation[2] obtained for n-C_{12} ~ n-C_{32} at 698 K and 15 MPa has a different function of i.

$$k_{(i)}\ [s^{-1}] = (2.3i - 15.6) \times 10^{-5} \qquad (2)$$

On the other hand, Yu and Eser[4] proposed the normalized expression of the overall rate constant of n-alkanes (n-C_8 ~ n-C_{16}) using the overall rate constant of n-dodecane (n-C_{12}) at 698 K and a reaction pressure (0.1 MPa ~ 15 MPa) recently, as follows

$$k_{(i)} / k_{12} = (1.89i - 12.3) \times 10^{-1}, \qquad (3)$$

where k_{12} is the overall rate constant of n-C_{12} pyrolysis at 698 K and a given pressure. This equation suggests that the carbon number dependence of the overall rate constant of n-alkane pyrolysis can be expressed by the same function for carbon number regardless of the reaction temperature and pressure (concentration).

A motivation of this study was to give a reasonable explanations for the above three correlations on the theoretical basis, and to proposed a global model for the pyrolysis of n-alkanes. In this study, we proposed the global model for pyrolysis of n-alkanes (n-C_3 ~ n-C_{32}) in a wide range of reaction conditions (572 K ~ 973 K, 6.86×10^{-3} M ~ 2.72 M). Next, we explain previously reported size dependence[2,3,4], based on the proposed model.

Model

The model is considered the following five elementary reaction groups: 1) initiation: a reaction of a C-C bond cleavage of n-C_i, 2) isomerization: an odd electron position in an alkyl radical through intra- and intermolecular H abstraction, 3) β-scission: a reaction of an alkyl radical decomposition, 4) H abstraction: a reaction of an odd electron transfer between n-C_i and an alkyl radical, 5) termination: a reaction of recombination of two alkyl radicals. Applying steady-state approximation for concentration of alkyl radical and considering the carbon number size dependence for the rate constants of bimolecular reactions (details in elsewhere[5]), the apparent first order rate constant of n-C_i pyrolysis can be expressed as

$$k_{(i)} = \frac{k_{\beta(i)} k_{H(i)} \sqrt{\frac{2k_{init(i)}[n-C_i]}{k_{term0}}}}{k_{\beta(i)} + (1/i)k_{H(i)}[n-C_i]}, \quad (4)$$

where $k_{\beta(i)}$ is the rate constant of β-scission of a radical (R_i), $k_{H(i)}$ is the rate constant of H abstraction of an alkyl radical from n-C_i, $k_{init(i)}$ is the rate constant of C-C bond cleavage of n-C_i, and k_{term0} is the rate constant of recombination of two methyl radicals. In the following, the method to evaluate each elementary reaction rate constant is shown.

1) Initiation

In the model, initiation occurs only for mother n-alkanes (n-C_i), because amount of n-C_i is much more than that of the other species at a lower conversion level. We took into account of the number of C-C bond for the overall rate constant of initiation since the rate constant of C-C bond rupture of n-C_i is assumed to be the same for any n-alkane. The activation energy of the rate constant of initiation with forming methyl radical ($k_{init(M)}$) should be 13 kJ/mol higher than that of forming the other radicals ($k_{init(O)}$)[6]. The frequency factor is the same for $k_{init(M)}$ and $k_{init(O)}$ as to be A_{init}[7]. Therefore, the overall rate constant of initiation of n-C_i, $k_{init(i)}$, should be as

$$k_{init(i)} = 2k_{init(M)} + (i-3)k_{init(O)} = A_{init} \exp\left(-\frac{E_{init}}{RT}\right)\left\{2\exp\left(-\frac{16.7\ kJ/mol}{RT}\right) + (i-3)\right\}, \quad (5)$$

where A_{init} is $10^{18.7}$ h^{-1} and E_{init} is 343 kJ/mol, which is C-C bond energy between two secondary carbons for n-butane[6,7].

2) Isomerization

Isomerization is an intramolecular H abstraction. Although this rate constant is not used in Eq. 4, this reaction is essential to determine the rate constant of β-scission, $k_{\beta(i)}$. An odd electron position on an alkyl radical is evaluated statistically, because the rate of isomerization is much faster than that of the other propagation reaction. The activation energy of rate constant of intra- and inter-molecular H abstraction from primary carbon ($k_{H(P)}$) is 16.7 kJ/mol higher than that from secondary carbon ($k_{H(S)}$)[8,9], and the frequency factor of both $k_{H(P)}$ and $k_{H(S)}$ is the same[8,9].

Isomerization of R_i produces as primary radicals, R_i^1 and R_i^i, or secondary radicals, R_i^j ($2 \le j \le i-1$). There are six possible positions on two primary carbons for an odd electron, since each of two primary carbons has three hydrogens. There are $2 \times (i-2)$ possible positions on (i–2) secondary carbons, since each of (i–2) secondary carbons has two hydrogens. Therefore, the probability of an odd electron on a primary carbon in R_i (R_i^1 or R_i^i), $P_{(Pi)}$, can be expressed as

$$P_{(Si)} = \frac{6k_{H(P)}}{6k_{H(P)} + 2(i-2)k_{H(S)}} = \frac{6\frac{k_{H(P)}}{k_{H(S)}}}{6\frac{k_{H(P)}}{k_{H(S)}} + 2(i-2)} = \frac{6\exp\left(\frac{-16.7kJ/mol}{RT}\right)}{6\exp\left(\frac{-16.7kJ/mol}{RT}\right) + 2(i-2)}. \quad (6)$$

The probability of an odd electron on a secondary carbon (R_i^j) ($2 \le j \le i-1$), $P_{(Si)}$, is as

$$P_{(Si)} = \frac{2(i-2)k_{H(S)}}{6k_{H(P)} + 2(i-2)k_{H(S)}} = \frac{2(i-2)}{6\frac{k_{H(P)}}{k_{H(S)}} + 2(i-2)} = \frac{2(i-2)}{6\exp\left(\frac{-16.7kJ/mol}{RT}\right) + 2(i-2)}. \quad (7)$$

3) β-scission

The activation energy of the rate constants of β-scission of forming methyl radical ($k_{\beta(M)}$) is 8.4 kJ/mol higher than that for forming the other radicals ($k_{\beta(O)}$)[9] and both frequency factors of the rate constants of β-scission forming methyl radical ($k_{\beta(M)}$) and that for forming the other alkyl radicals ($k_{\beta(O)}$) are the same[7]. Here, we took into account of the number of C-C bond for the overall rate constant of β-scission.

The primary radical (R_i^1 or R_i^i), which has an odd electron on a primary carbon, has one β-position and produces ethylene and R_{i-2} through β-scission. Since the probability of the

formation of R_i^1 or R_i^1 through isomerization is $P_{(Pi)}$, the rate of the formation of ethylene and R_{i-2} through β-scission from R_i is $P_{(Pi)}k_{\beta(O)}[R_i]$. For the secondary radical that has an odd electron at 2 or i-1 position in the radical (R_i^2 or R_i^{i-1}), there is one β-position in the molecule and the radical produces propylene and R_{i-3} through β-scission. The probability of j =2 or i-1 for R_i^j is $2P_{(Si)}/(i-2)$ because there are two carbons corresponding to the position of j = 2 or i-1 in i-2 secondary carbons. Thus, the formation rate of propylene and R_{i-3} through β-scission from R_i is $2P_{(Si)}/(i-2)\ k_{\beta(O)}[R_i]$. In the case of R_i^3 or R_i^{i-2}, there are two β-positions in the radical. From the one of the ways of β-scission of R_i^3 or R_i^{i-2}, methyl radical and 1-alkene has i-1 carbon (Ol_{i-1}) are produced. From the another way, butylene (Ol_4) and R_{i-3} are formed. In i-2 secondary carbons, there are two position corresponding to j = 3 or i-2. Thus, the formation rates of methyl radical and Ol_{i-1} and that of Ol_4 and R_{i-3} are $2P_{(Si)}/(i-2)\ k_{\beta(M)}[R_i]$ and $2P_{(Si)}/(i-2)\ k_{\beta(O)}[R_i]$, respectively. For the case of $4 \le j \le i-3$ of R_i^j, there are also two β-positions in the radical. The β-scission of R_i^j produces Ol_{j+1} and $R_{i-(j+1)}$ from one of the two ways and $Ol_{i-(j-2)}$ and R_{j-2} from the other. The formation rate of Ol_{j+1} and $R_{i-(j+1)}$ or $Ol_{i-(j-2)}$ and R_{j-2} from R_i^j through β-scission is thus $2(i-6)P_{(Si)}/(i-2)\ k_{\beta(O)}[R_i]$ because there are i-6 carbons that are $4 \le j \le i-3$ in R_i^j. The overall rate constant of disappearance of R_i through β-scission ($k_{\beta(i)}$) should be as follows since that rate is the summation of the above formation rate constant of 1-alkenes and alkyl radicals;

$$k_{\beta(i)} = P_{(Mi)}k_{\beta(O)} + \frac{2P_{(Si)}}{i-2}k_{\beta(O)} + \frac{2P_{(Si)}}{i-2}k_{\beta(M)} + \frac{2P_{(Si)}}{i-2}k_{\beta(O)} + \frac{2(i-6)P_{(Si)}}{i-2}k_{\beta(O)}. \qquad (8)$$

From Eqs. (6) and (7), Eq. (8) is as

$$k_{\beta(i)} = A_\beta \exp\left(-\frac{E_\beta}{RT}\right)\left\{\frac{4\exp\left(-\frac{8.4\ \text{kJ/mol}}{RT}\right)}{6\exp\left(-\frac{16.7\ \text{kJ/mol}}{RT}\right)+2(i-2)} + \frac{6\exp\left(-\frac{16.7\ \text{kJ/mol}}{RT}\right)+4(i-4)}{6\exp\left(-\frac{16.7\ \text{kJ/mol}}{RT}\right)+2(i-2)}\right\}, \qquad (9)$$

where A_β and E_β are the kinetic parameters of β-scission for R_4^1 producing Ol_2 and R_2 and $10^{15.9}$ h^{-1} and 100.4 kJ/mol, respectively[10].

4) H abstraction

In this model, H abstraction occurs only for n-C_i because n-C_i is the most abundant in the system at a low conversion level. The activation energy of rate constant of H abstraction from primary carbon ($k_{H(P)}$) is 16.7 kJ/mol higher than that from secondary carbon ($k_{H(S)}$)[8, 9], and the frequency factor of both $k_{H(P)}$ and $k_{H(S)}$ is the same. Thus, $k_{H(i)}$ is defined as below because n-C_i has 6 primary hydrogens and 2(i-2) secondary hydrogens:

$$k_{H(i)} = 6k_{H(P)} + 2(i-2)k_{H(S)} = 2A_H \exp\left(-\frac{E_H}{RT}\right)\left\{3\exp\left(-\frac{16.7\ \text{kJ/mol}}{RT}\right)+(i-2)\right\}, \qquad (10)$$

where A_H and E_H are the kinetic parameters of H abstraction of methyl radical from a secondary carbon from n-propane and 10^{12} $M^{-1}h^{-1}$ and 42.5 kJ/mol, respectively[11]. In the recent study[5], we found that the rate of H abstraction for n-C_{16} by R_j can be expressed as $(1/j)k_{H(16)}[R_j][n\text{-}C_{16}]$. The radical size dependence of H abstraction is reasonable both from the collision theory and transition-state theory[5]. Thus, for n-C_i, the H abstraction rate for n-C_i by R_j can be described as $1/j\ k_{H(i)}[R_j][n\text{-}C_i]$.

5) Termination

Since a contribution of disproportion between two alkyl radicals is negligible[11], the radical reaction network of n-C_i pyrolysis is terminated by only the recombination of two radicals. With the analogy of H abstraction, the rate constant of termination between R_i and R_m is assumed to be expressed by $(1/i)(1/m)k_{term0}$, where k_{term0} is the intrinsic rate constant and k_{term0} reported for two methyl radicals is employed ($A_{term} = 10^{14.3}$ $M^{-1}h^{-1}$ and $E_{term} = 0$ kJ/mol)[11].

Results and Discussion

1. Comparison between experimental results and calculated results

Figure 1 shows the parity plot between the experimental results and the model. In the case the experiments were conducted using flow type apparatus, the concentration was estimation from the reaction pressure and temperature by Peng-Robinson equation of state[12]. The critical constants (T_c, P_c, and ω) were from the book by Reid et al.[13] or calculated by the ABC method[14]. As shown in Fig. 1, the model described the experimental results successfully over a wide range of experimental conditions (T = 572 K ~ 973 K, $[n\text{-}C_i] = 6.86 \times 10^{-3}$ M ~ 2.72 M, and i = 3~32).

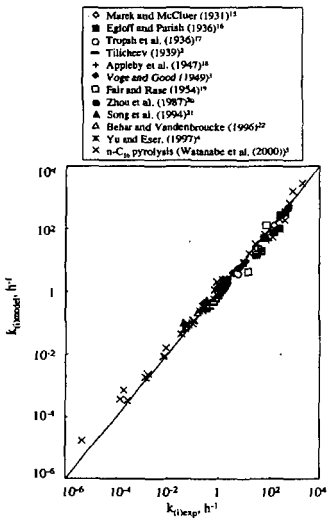

Figure 1 Parity plot of overall rate constants of n-alkanes pyrolysis

2. Correlation of the overall rate constant with carbon number of n-alkane

The rate constant of initiation (Eq. 4) can be approximated as follows because $k_{init(M)}$ is much less than $k_{init(O)}$:

$$k_{init(i)} \approx (i-3)k_{init(O)}. \tag{11}$$

From Eq. 9, the rate constant of β-scission at a long chain n-alkane (i ›› 4) can be simplified to

$$k_{\beta(i)} \approx \frac{4(i-4)}{2(i-2)} k_{\beta(O)} \approx 2k_{\beta(O)}, \tag{12}$$

since $k_{\beta(M)}$ is much less than $k_{\beta(O)}$ and $P_{(Mi)}$ is much less than $P_{(Si)}$. The rate constant of H abstraction (Eq. 10) can be simplified as

$$k_{H(i)} \approx 2(i-2)k_{H(S)}, \tag{13}$$

because the contribution of $k_{H(P)}$ to $k_{H(i)}$ is much less than that of $k_{H(S)}$. Thus, using the approximation of Eqs. 11 ~ 13, Eq. 4 can be approximated by

$$k_{(i)} \approx \frac{2k_{\beta(O)} \cdot 2(i-2)k_{H(S)}}{2k_{\beta(O)} + (1/i) \cdot 2(i-2)k_{H(S)}[n-C_i]} \sqrt{\frac{2(i-3)k_{init(O)}[n-C_i]}{k_{term0}}}. \tag{14}$$

When i is much larger than 2, i-2/i is almost equal to unity. Thus, Eq. 14 becomes

$$k_{(i)} \approx \frac{2k_{\beta(O)} \cdot 2(i-2)k_{H(S)}}{2k_{\beta(O)} + k_{H(S)}[n-C_i]} \sqrt{\frac{2(i-3)k_{init(O)}[n-C_i]}{k_{term0}}} = (i-2)\sqrt{i-3}\left\{\frac{4k_{\beta(O)}k_{H(S)}}{2k_{\beta(O)} + k_{H(S)}[n-C_i]} \sqrt{\frac{2k_{init(O)}[n-C_i]}{k_{term0}}}\right\} \tag{15}$$

Therefore, regardless to the temperature and concentration, the overall rate constant of n-alkane pyrolysis depends on $(i-2)\sqrt{i-3}$ for carbon number of n-alkane. Normalizing the rate constant of n-alkane pyrolysis by the rate constant of n-C_{16} pyrolysis at a given condition, Eq. 15 is as

$$\frac{k_{(i)}}{k_{(16)}} = \frac{(i-2)\sqrt{i-3}}{14\sqrt{13}}. \tag{16}$$

Figure 2 shows the normalized rate by Eq. 19.Tilicheev's[2], Voge and Good's[3], and Yu and Eser's[4] correlations with Eqs. 1, 2, and 3, respectively, are also shown in this figures. As shown in Fig. 2, all the plots by Tilicheev's[2], Voge and Good's[3], and Yu and Eser's[4] correlations fall on the line calculated by Eq. 16. This analysis gives the theoretical basis to their correlations.

Conclusion

We proposed a new model for overall rate constant of n-alkane pyrolysis, based on Kossiakoff and Rice theory, by taking the carbon number dependence of alkyl radical for the rate constant of bimolecular reactions into account. The model can express the experimental overall rate constant of n-alkanes (n-C_3 ~ n-C_{32}) at wide range of temperatures (572 K ~ 973 K) and concentrations (6.86×10^{-3} M ~ 2.72 M), and could explain previously reported carbon number correlation of pyrolysis rate.

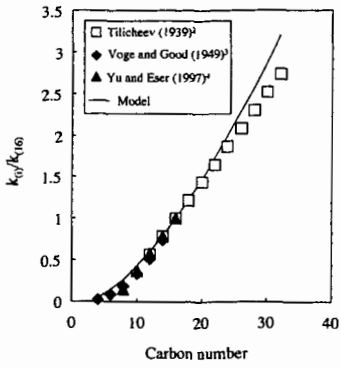

Figure 2 Normalization of carbon number dependence of Voge and Good's[3], Tilicheev's[2], and Yu and Eser's[4] correlation by the overall rate constant of n-C_{16} pyrolysis at given conditions

Acknowledgement

The authors wish to acknowledge the Ministry of Education, Science, Sports and Culture, Japan and New Energy and Industrial Technology Organization (NEDO) for financial support of this research.

Literature Cited

(1) Rice, F. O.; Herzefeld, K. F., *J. Am. Chem. Soc.* **1934**, *56*, 284-289.

(2) Tilicheev, M. D., *Foreign Petrol. Technol.* **1939**, *7*, 209-224.

(3) Voge, H. H.; Good, G. M.,. *J. Am. Chem. Soc.* **1949**, *71*, 593-597.

(4) Yu, J.; Eser, S., *Ind. Eng. Chem. Res.* **1997**, *36*, 585-591.

(5) Watanabe, M.; Tsukagoshi, M.; Hirakoso, H.; Adschiri, T.; Arai, K.,.*AIChE J.* **2000**, *46*, 843-856.

(6) Benson, S. W. *Thermochemical Kinetics, 2nd edition*; Wiley: New York, 1976.

(7) Nigam, A.; Klein, M. T., *Ind. Eng. Chem. Res.* **1993**, *32*, 1297-1303.

(8) Fabuss, B. M.; Smith, J. O.; Satterfield, C. N., *Adv. Pet. Chem. Refin.* **1964**, *9*, 157-201.

(9) Murata, M.; Saito, S.; Amano, A.; Maeda, S., *J. Chem. Eng. Jpn.* **1973**, *6*, 252-258.

(10) Doue, F.; Guiochon, G., *J. Chim. Phys.* **1968**, *65*, 395-409.

(11) Allara, D. L.; Shaw, R., *J. Phys. Chem. Ref. Data* **1980**, *9*, 523-559.

(12) Peng, D. Y.; Robinson, D. B., *Ind. Eng. Chem. Fundam.* **1976**, *15*, 59-68.

(13) Reid, R. C.; Prausnitz, J. M.; Sherwood, T. K. *The Properties of Gases and Liquids, 3rd edition*; McGraw-Hill: New York, 1977.

(14) Marano, J. J.; Holder, D., *Ind. Eng. Chem. Res.* **1997**, *36*, 1895-1907.

(15) Merek, L. F.; McCluer, W. B. *Ind. Eng. Chem.* **1931**, *23*, 878.

(16) Egloff, G.; Parrish, C. I., *Chem. Rev.* **1936**, *19*, 145-161.

(17) Tropsch, H.; Thomas, C. L.; Egloff, G., *Ind. Eng. Chem.* **1936**, *28*, 324-332.

(18) Appleby, W. G.; Avery, W. H.; Meerbott, W. K. *J. Am. Chem. Soc.* **1947**, *69*, 2279.

(19) Fair, J. R.; Rase, H. F. *Chem. Eng. Progr.* **1954**, *50*, 415.

(20) Zhou, P.; Hollis, O. L.; Crynes, B. L., *Ind. Eng. Chem. Res.* **1987**, *26*, 846-582.

(21) Song, C.; Lai, W.; Schobert, H. H., *Ind. Eng. Chem. Res.* **1994**, *33*, 548-557.

(22) Behar, F.; Vandenbroucke, M., *Energy & Fuels* **1996**, *10*, 932-940.

PREPARATION AND CHARACTERIZATION OF Co-Mo/SiO_2-Al_2O_3 CATALYSTS

Shakeel Ahmed[1] Mazen A Shalabi[2]
[1]The Research Institute, King Fahd University of Petroleum and Minerals,
Dhahran 31261, Saudi Arabia
[2]Department of Chemical Engineering

KEYWORDS: Hydrocracking catalysts, TPR/TPS/TPD, HDS

INTRODUCTION

Hydrocracking catalysts are bifunctional catalysts having both hydrogenation-dehydrogenation function and an acidic function. Proper balancing of the two functions plays a prominent role in deciding the performance of the catalyst for application in hydrocracking [1]. The cracking function is provided by an acidic support, whereas the hydrogenation-dehydrogenation function is provided by metals. The acidic support consists of (a) amorphous oxides (e.g., silica-alumina), (b) a crystalline zeolite (mostly modified Y zeolite) plus binder (e.g., alumina), or (c) a mixture of crystalline zeolite and amorphous oxides. Cracking and isomerization reactions take place on the acidic support. The metals providing the hydrogenation-dehydrogenation function can be noble metals (palladium, platinum) or non-noble metal sulfides from group VIA (molybdenum, tungsten) and group VIIIA (cobalt, nickel). These metals catalyze the hydrogenation of the feedstock, making it more reactive for cracking and heteroatom removal, as well as reducing the coking rate. They also initiate the cracking by forming a reactive olefin intermediate via dehydrogenation. The ratio between the catalyst's cracking function and hydrogenation function can be adjusted to optimize activity and selectivity. For a hydrocracking catalyst to be effective, it is important that there be a rapid molecular transfer between the acid site and hydrogenation sites in order to avoid undesirable secondary reactions. Rapid molecular transfer can be achieved by having the hydrogenation sites located in the proximity of the cracking (acid) sites [2]. Catalysts with amorphous support are in commercial use, primarily where maximizing the production of middle distillates or conversion to lube oil blending stock is the objective [3,4]. Amorphous hydrocracking catalysts contain primarily amorphous silica-alumina [5]. Other amorphous supports reported are titania-zirconia, silica-alumina dispersed in alumina, alumina-boria, and other acidic mixed oxides. Hydrocracking catalysts containing fluorinated inorganic oxides as supports have also been reported [6]. In this research work a series of CoMo-silica-alumina amorphous base hydrocracking catalysts was prepared by impregnation method. The amorphous silica alumina support was prepared in the laboratory by co-precipitation method. The effect of order of impregnation of cobalt and molybdenum on the catalyst activity was studied by specific characterization methods and model compounds reactions. In addition, γ-alumina and Y-zeolite based catalysts were also prepared and studied for comparison purposes.

EXPERIMENTAL

Catalyst Preparation: A series of silica-alumina supported CoMo hydrocracking catalysts were prepared by impregnation method. The order of impregnation of cobalt and molybdenum was varied. For catalyst HC-1, molybdenum was impregnated first and then cobalt was loaded. In catalyst HC-2, this order was reversed. On the other hand, simultaneous impregnation of cobalt and molybdenum was adopted for the preparation of catalyst HC-3. All catalysts were calcined at 500 °C for three hours in a stream of dry air. The silica-alumina supports were also prepared in the laboratory by co-precipitation method. In addition, γ-alumina and 50% mixture of γ-alumina and commercial Y-zeolite were also used as supports. Catalyst HC-4 was prepared by using commercial acidic alumina supplied by Aldrich. For the preparation of catalyst HC-5, a 50% mixture of commercial γ-alumina (Aluminum Company of America) and Y-zeolite (CATAL, UK) was used. Commercial γ-alumina and Y-zeolite were dried at 250 °C before using as catalyst support.

Catalyst Characterization: The catalysts samples were characterized by temperature-programmed desorption (TPD) of ammonia, temperature-programmed reduction (TPR), and temperature-programmed sulfiding (TPS). The details of the measurements are given elsewhere [7]. The elemental composition of the catalysts was measured by ICP. Surface area (BET method) and pore volume was measured by Quantachrome (NOVA 2000).

Catalyst Evaluation: The prepared hydrocracking catalysts were evaluated for HDS and cracking activities using thiophene and cumene as model compounds, respectively. The activity measurements were conducted in a pulse type micro reactor. The detailed experimental procedures are given elsewhere [7].

RESULTS AND DISCUSSION

Some of the physico-chemical properties of the prepared catalysts are given in Table 1. It was observed that the surface area of the catalyst was reduced as compared with the blank support, after the impregnation of the metals. This could be due the pore blocking by cobalt and molybdenum in the catalysts. This was also evident from the reduction in pore volume of the catalysts in comparison with the respective support. However, the reduction in surface area for

the γ-alumina-based catalyst (HC-4) was not as pronounced as in the case of synthesized silica-alumina-based catalysts. Similarly, the surface area of HC-5 was comparable with the average surface area of the respective support.

Temperature-Programmed Reduction: The results of temperature-programmed reduction of silica alumina and zeolite based catalysts are given in Figure 1. Almost all the catalysts show a multiple peak reduction behavior. The first reduction appear in the region of 300 to 500 °C. The variation in the peak temperature was attributed to the differences in the metal support-interactions and multiple peak pattern might be due to the presence of molybdenum at different sites of the support. The highest reduction temperature was observed for HC-1 (peak at 363 °C). On the other hand, HC-5 reduced at minimum temperature in the series giving a shoulder at 397 °C with the main peak at 462 °C. It was also observed that catalyst prepared by simultaneous impregnation of metals (HC-3) reduced at lower temperature (431 °C) as compared with its homologues. The reduction emperature indicates the metal-support interaction, which intern influences the HDS activity of the catalyst.

Temperature-Programmed sulfiding: The results of temperature-programmed sulfiding are given in Figure 2. The TPS profiles are similar to the molybdenum containing commercial catalysts. The upper curve represents the UV-detector signal, which monitors the hydrogen sulfide concentration, where the positive peak means the production of hydrogen sulfide and the negative peak means consumption. The lower curve is a response of the TCD, which monitors the hydrogen concentration, and the positive peak in this case indicates the consumption of hydrogen. The TPS profile can be divided into four regions. In the region I (25 to <100 °C) the positive peak in UV signal is due to the desorption of hydrogen sulfide, which was mainly adsorbed physically during stabilization at room temperature. The desorption of hydrogen sulfide is followed by a low-temperature sulfiding in region-II (below 200 °C). No hydrogen is consumed in this region as noticed in the lower curve. Arnoldy et al. [8] showed in their study that sulfiding in this region occurs by simple O-S exchanges on Mo^{+6}. In region-III, hydrogen sulfide is produced as a sharp peak, coupled with the consumption of hydrogen. The sharpness of the peak points to a chemically well-defined surface compound. In this region Mo^{+6}-S bond is breaking down and the free sulfur is reduced so the hydrogen sulfide is produced. This peak appeared at 134 °C for HC-5 whereas, for HC-2 it is at 218 °C. The sharpness of the peak in catalyst HC-2 also indicates the homogeneous distribution of molybdenum over the catalyst support. Note that in this sample, molybdenum was impregnated after the cobalt loading. While, catalyst HC-1 gave relatively broad peak at 199 °C in which the order of impregnation was reversed. This gives some indication that there may exists some competition between the metal ions being impregnated over the support. High temperature sulfiding (region-IV) is taking place above 250°C in all cases. In this region, most of Mo ions are already in Mo^{+4} state, sulfiding can be described mainly as O-S exchange on Mo^{+4} ions. Sulfiding appears to be completed at about 800°C in all cases. In this region, HC-4 gave a shallow peak as compared to other catalysts. On the other hand, HC-2 and HC-3 showed maximum consumption of H_2S in this region.

Temperature-programmed Desorption: Total acidity of the silica alumina and zeolite based catalysts, measured by TPD of ammonia is given in the Table 2. Figure 3 shows the TPD curves of these catalysts. The total acidity (Bronsted and Lewis) measured was in the range of 0.3 to 0.8 m mole/g. For the catalysts HC-1, -2 and -3 the order of impregnation of cobalt and molybdenum appears to be playing a role in determining the acidity. It was found to be highest in the case of simultaneous impregnation of the metals. Quite interestingly, the total acidity was lower for the catalyst containing Y-zeolite (HC-5) as compared with some of the silica-alumina based catalysts. This indicates that there might be more Lewis acid sites in silica-alumina based catalysts as compared with zeolite containing catalyst. The cracking of cumene will give more information about the acidic properties of the catalysts.

Catalytic Activity: Hydrocracking of cumene was performed to evaluate the cracking property of the catalysts. The results of cumene cracking are given in Figure 4. Maximum cracking activity was observed for HC-5 (zeolite based). This higher cracking activity was attributed to the presence of Y-zeolite in the catalyst. HC-3 catalyst showed maximum total acidity (0.765 m mol/g), but it gave lower cumene cracking (46.7%) as compared to HC-5 (97.9% cumene conversion). It was observed that total acidity measured by TPD of ammonia was not well correlating with the cracking of cumene. This indicates that Lewis acid sites are contributing more to the acidity measurement as compared to the Bronsted acidity (for silica-alumna catalysts) which is required for cracking activity. In the silica-alumina based catalyst series, maximum cumene cracking was found for HC-1 (78.5%) whereas, HC-2 gave minimum conversion (34.3%). This shows that the order of impregnation of cobalt and molybdenum plays an important role in the cracking activity of cumene. The cracking activity was higher when molybdenum was impregnated first and lower in the case where cobalt was impregnated first followed by molybdenum. Total acidity was also lower for HC-2 as compared with that of HC-1. These results show that cobalt is interacting with the acid sites and blocking them so that

the total acidity was decreased. This requires further investigations in terms of metal-acid-sites interactions.

The hydrodesulfurization of thiophene was performed to measure the HDS activity of the catalysts. Figure 5 shows the results of HDS of thiophene at different temperatures. The highest HDS activity was found in the case of HC-4 (alumina based catalyst). On the other hand, minimum HDS activity was observed for HC-1. Here also the order of impregnation of metals plays a role. In the series of silica-alumina based catalysts, the highest HDS activity was found for HC-3. In the catalyst cobalt and molybdenum were impregnated simultaneously. A trend was observed between the HDS activity and the reduction temperature measured by TPR. It was found that at lower reduction temperature higher HDS activity occurred. Figure 6 shows the correlation of thiophene conversion versus peak temperature of TPR profile. For catalyst HC-5 the average of the two peaks was used for correlation curve.

CONCLUSIONS

The order of impregnation of cobalt and molybdenum over silica-alumina based hydrocracking catalysts plays an important role in terms of catalyst activity. Maximum cracking activity was found for the catalyst prepared by impregnating molybdenum first and then cobalt in the second step over silica-alumina support. Temperature programmed methods were successfully utilized for the characterization of the prepared hydrocracking catalysts. A trend was observed for the HDS activity of the hydrocracking catalysts and reduction temperature measured by TPR method. Catalysts reducing at lower temperature performed better for HDS activity.

ACKNOWLEDGEMENT

The authors wish to acknowledge the support of the Research Institute, King Fahd University of Petroleum and Minerals, and Petroleum Energy Center, Japan, with the subsidy of the Ministry of International Trade and Industry, for this work under KFUPM-RI Project No. 21151.

REFERENCES

[1] Marcilly, C and Frank, J. P., *Stud. Surf. Sci. Cat.*, v. **5**, pp. 93-104 (1980).
[2] Franck, J.P and LePage, J.F., Proc. 7th Intern. Congr. Catal., Tokyo, p.792 (1981).
[3] Bridge, A.G., Jaffe, J., and Powell, B.E., Proc. Mtg. Jap. Petr. Inst., Tokyo, Japan, (1982).
[4] Reno, M.E., Schaefer, B.L., Penning, R.T., and Wood, B.M., NPRA Ann. Mtg. March 1987, San Antonio, TX, AM-87-60.
[5] Sullivan R.F., and Scott, J.W., *Heterogeneous Catalysis: Selected American Histories*, ACS Symposium Series 222, Washington, D.C., p.293 (1983).
[6] Adachi, M., Okazaki, H., and Ushio, M., U.S. Patent No. 4,895,822 (1990).
[7] Ahmed, S., et al., Proceedings of the Sixth Annual Workshop on Catalysts in Petroleum Refining and Petrochemicals, December 1996, pp. 223-234.
[8] Arnoldy, P., Franken. M.C., Scheffer, B., and Moulijin, J.A., *J. Catal.*, v. **92**, pp. 35-55 (1985).

Table 1. Physico-chemical properties of CoMo-supported hydrocracking catalysts

Catalyst Code	Support	Surface Area (m^2/g)	Pore Volume (cm3/g)	CoO (wt %)	MoO_3 (wt %)
HC-1	SA*	145	0.20	3.89	13.2
HC-2	SA	124	0.24	4.86	14.4
HC-3	SA	183	0.19	4.10	15.1
HC-4	γ-Alumina**	140	0.23	5.35	13.7
HC-5	γ-Alumina + Y-Zeolite**	280	0.29	3.74	14.5

* Silica-Alumina support prepared in the laboratory; surface area 376 m^2/g pore volume 0.34 cc/g
** Acidic alumina, surface area 140 m^2/g from Aldrich
** γ-Alumina surface area 216 m^2/g from Aluminum Company of America
Y-Zeolite surface area 515 m^2/g from CATAL, UK.

Table 2. Results of TPD analysis

Catalyst	Acidity (m mol/g)
HC-1	0.589
HC-2	0.288
HC-3	0.765
HC-4	0.320
HC-5	0.413

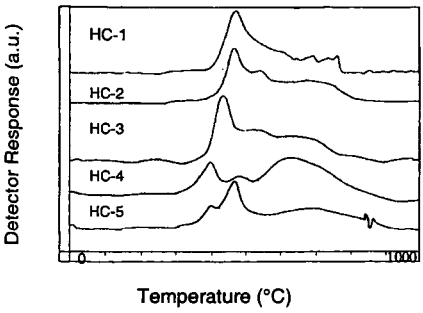

Figure 1. TPR profiles of CoMo-supported hydrocracking catalysts.

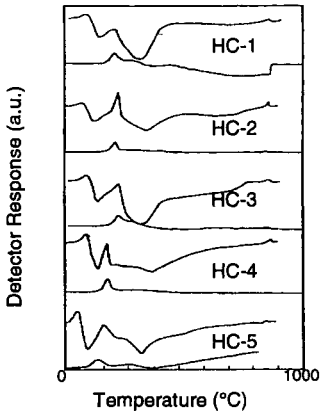

Figure 2. TPS profiles of CoMo-supported hydrocracking catalysts.

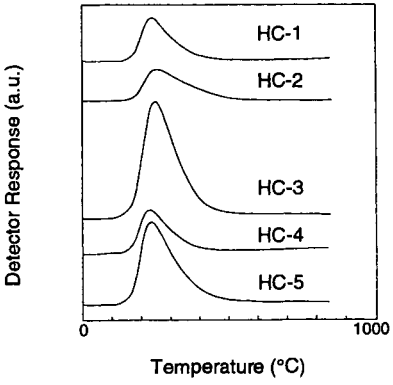

Figure 3. TPD profiles of CoMo-supported hydrocracking catalyst.

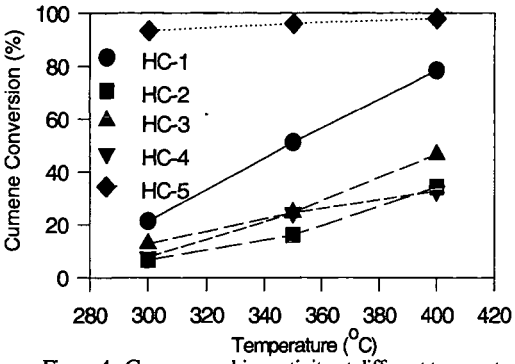

Figure 4. Cumene cracking activity at different temperatures.

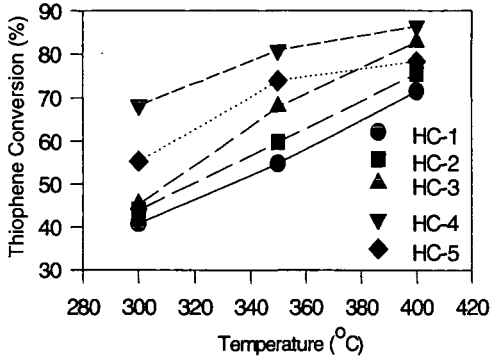

Figure 5. Thiophene HDS activity at different temperatures.

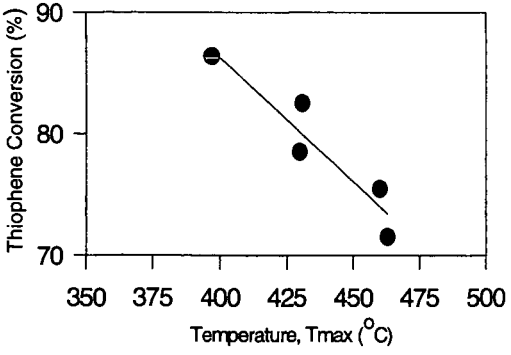

Figure 6. Correlation of thiophene conversion versus TPR Tmax

CONTROL OF SEVERITY IN VISBREAKING

J.A. Carrillo*, F. Pantoja*, G. Garzón*, H. Barrios, J. Fernández**, E. Carmona*** and J. Saavedra*****

*-ECOPETROL-Instituto Colombiano del Petróleo; **-ECOPETROL-Cartagena Management; ***-ECOPETROL- Barrancabermeja Management.

Test results of the behavior of different feeds in the visbreaking process at the pilot as well as the industrial plant level are presented, in agreement with their insoluble matter content in nC_7. The interval studied was 10%m (vacuum barrel bottoms) at 32%m (deasphalted barrel bottoms). In the processing of barrel bottoms, a correlation was found between the abrupt change in the slope of efficiency in function of severity by temperature (at the 745-760 °K interval) regarding the change in slope of the line of stability determined by means of the Merit Test, while at the interval tested for residence time (3.8-6.4 minutes) there was no change in slope found. In the processing of deasphalted barrel bottoms, no correlation was found between the abrupt change in the slope of efficiency in function of the severity by temperature (at the 749-773 °K interval) regarding the change in slope of the line of stability determined by means of the Merit Test, while at the interval of residence time tested (5-13 minutes) a change of slope was found in the Merit Test. In this type of feeds, it was observed that the severity is controlled most efficiently by temperature, without noticeably increasing coke production in the oven, while for barrel bottoms, it is preferred to control severity by means of residence time. The study shows the influence of steam and light cycle oil on the processing of DEMEX barrel bottoms in visbreaking.

In addition, correlations are shown between the Merit Test, the Coking Index using Heithaus and the Stability Factor of the feeds and products.

INTRODUCTION

Visbreaking is a process of thermal breaking of barrel bottoms that is carried out between 748-773 °K, with a residence time (in the reaction zone) of 6-10 minutes. Sometimes from 1 to 4% v of steam and from 0% to 10% of light cycle oil (LCO) is introduced.

Visbreaking is a low capital investment process and is operated at threshold conditions to produce a greater quantity of distillates and reduce the quantity of diluent used in the preparation of fuel oil from visbroken tar. The severity threshold has been studied by several researchers (Savaya, et al., 1988) and it is determined by the stability of the fuel oil and the quantity of coke deposited on the inner walls of the oven. To measure severity in the operation, techniques such as the Merit Test, the Coking Index using Heithaus (John and Adam, 1999) and the Stability Factor (S.F.) which relates oil composition to severity (Kuo, 1984).

Another important factor that limits severity measured in function of conversion is the quality of feed. The greater the quantity of insoluble matter in nC7, greater will the production of barrel bottoms be and the less the production of gas-oil (John and William, 1982).

For this study, only the coil visbreaking technology was considered, because this is the technology of the plants currently operating in ECOPETROL refineries.

EXPERIMENTAL

Simulations at the pilot level were carried out at a plant built in ECOPETROL-Instituto Colombiano del Petróleo (Carrillo and Pantoja, 1998).

The stability of the visbroken residue is determined by means of two tests developed by the IFP (Merit Test) and the WRI (Heithaus Titration Test); which consist of a paper chromatography and the precipitation of asphaltenes with i-octane, and are based on the solubility of the sample to be analyzed in a blend of aromatic and paraffin solvents of known proportions.

For the tests, asphaltenes were obtained from the deasphalted vacuum bottoms of the oil blend of the Barrancabermeja refinery (insoluble matter in n-C7 between 30 and 35%m) and vacuum bottoms of oil blend from the Cartagena refinery whose characteristics are given in Table 1.

Heithaus parameters of severity

Titration using Heithaus consists of taking a constant quantity of a visbroken barrel bottom (2 g) and diluting it in three different volumes of o-xylene: 5, 7 and 9 ml respectively. These concentrations are titrated with isooctane. The methodology is included in Schabron and Pauli.

Table 1: Characteristics of Vacuum Bottoms

Properties/Refinery	Barranca-Bermeja		Cartagena			Standard/equipment
Typo of bottom feed	DEMEX		Vacuum			
nC_7 insolubles, % wt	32.7	30.5	11.9	13.48	16.45	UOP-614
Saturates, % wt	4,0	2,7	11.2	10.8	11.2	Iatroscan Method
Aromatics, % wt	44,4	47,9	56.5	55.9	49.7	Iatroscan Method
Resins, % wt	34,2	33,0	24.1	23.5	28.3	Iatroscan Method
Asphaltene; % wt	17,5	16,4	8.2	9.7	10.8	Iatroscan Method
CCR, % m	38.8	36.5	22.2	22.46	24.53	ASTM D-4530
Merito test	—	3.0	5.0	4	4	IFP
F.E.	0.5	0,8	0.32	0.33	0.28	*
Density @ 15 °C, gr./ cm^3	1.077	1.0892	1.0196	10.254	1.0256	ASTM D-70
Viscosity @ 150 °C, cP			229	421	588	ASTM D-445
VBN	-12,8	-5.2	2.69	1.94	1.03	

* -Calculated by Kuo, 1984. F E = (Aromatics + Resins) / (Saturates * CCR)

Coking index

This index is defined as the peptizabilitation (Pa)/dilution concentration (Cmin) ratio. It is based on the considerations that Pa decreases when the parameter of solubility or the molecular weight of the asphaltenes is increased, and Cmin increases when residue stability decreases. Preliminary studies suggest that a ration near one (1) indicates a highly stable system ratio and coking begins when the ratio is near 0.3.

RESULTS AND DISCUSSION

1. Processing of vacuum barrel bottoms

1.1 Evaluation of severity based on temperature

Product efficiency for the different conditions of severity used, does not vary noticeably for temperatures below 754 °K (figure 1). For temperatures above 754 °K, coke formation is triggered and a drastic reduction in the production of barrel bottoms occurs, which reflects in the increase of gas-oil efficiency (atmospheric + LGO + HGO) and the production of gases and gasoline.

When the content of asphaltenes, resins, coke and some of their correlations are related, similar trends are observed, where the behavior of the asphaltenes that have a maximum of 756 °K stands out, while the resins and the resin/asphaltene ratio shows an opposite behavior. These trends indicate that once the maximum cracking temperature is reached for each feed, the system stops being stable, the miscellar structure is destroyed and the asphaltenes become coke precursors. This instability is confirmed by the Merit Test performed on the visbroken tar, where a change in slope at 754 °K is observed, as is shown in figure 2. At values below this temperature, the visbroken tar is stable, while at higher temperatures the colloidal state is thrown off balance.

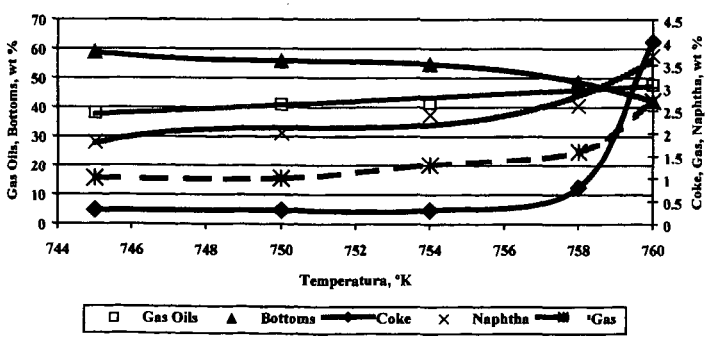

Figure 1. Severity as temperature function

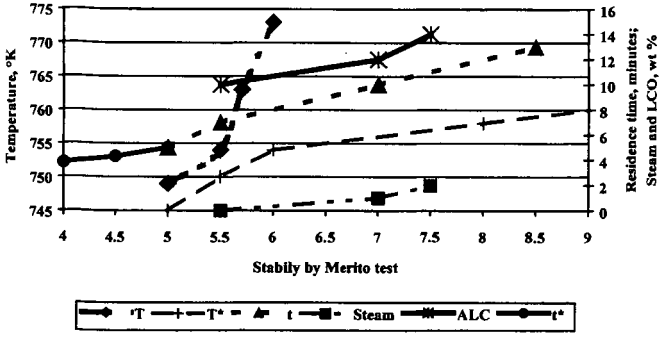

Figure 2. Stability of the visbreaking bottoms by Merite test

1.2 Evaluation of severity based on residence time

At the conditions analyzed there were no abrupt variations in the efficiency of the products. The gases, gasolines, gas-oils and coke are increased in a constant fashion with the increase in residence time, while the production of tar and the resin asphaltene ration is reduced at the same interval analyzed. The resin/asphaltene ratio is greater than that of the data with temperature variation, which explains the greater stability of the visbroken tar. This stability is shown in figure 2, where it is observed that all the values are equal to or below 6 on the Merit Test; in addition there are no changes in slope.

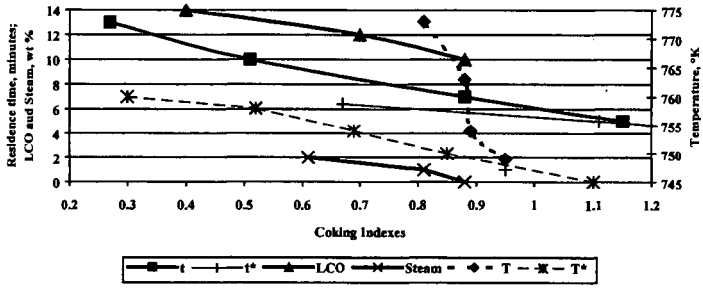

Figure 3. Coking Indexes using The Heithaus Titration and Asphaltene Solubility. Barrancabermeja Refinery

1.3 Correlations between the method of measuring the stability of the visbroken tar by means of Titration using Heithaus with the method based on the Merit Test

Figure 3 presents the titration results for different samples corresponding to variations in severity by residence time and temperature. Similarly, diagrams for steam and light cycle oil were obtained.

When the coking index is illustrated in function of severity by temperature, it is found that the recommended stability interval (0.3 - 1) does not correspond to this type of feed with the results of efficiency (figure 2) and with the Merit Test for the same evaluation. These values indicate that at a temperature of 756°K, there is a transfer from a stable area to an unstable area above this temperature. For this reason, the results seem to indicate that for this type of feed, the control interval to be recommended in the Coking Index should be 0.6-1.

A similar procedure was followed with the samples corresponding to the variation of severity by residence time.

When the modified interval of the Coking Index (0.6-1.0) is the same as in the Merit Test, all the points analyzed are within the stable interval, which supports the fact that the residence time at the interval analyzed shows less risk than the temperature in handling severity.

2. Processing desasphalting bottoms.

2.1 Evaluation of severity based on temperature.

Severity in funtion of temperature was evaluated maintaining residence time constant at 7 min, the LCO at 10% and the amount of steam supplied to the feed in 0%.

In spite of this, the system remains colloidally stable, being that the amount of resins increases and at the same time the asphaltenes decrease, becoming coke as was stated previously. Therefore, all the points analyzed by the Merit Test yield values below 7. This indicates that in the processing of this type of feeds the threshold is not found in the stability of the products, but in the amount of coke deposited on the inner walls of the oven pipes.

2.2 Evaluation of severity based on residence time.

Severity in function of residence time was evaluated keeping temperature constant at 763 °K. This value corresponds to the temperature used at the Barrancabermeja refinery. The LCO percentage was kept at 10%v and the amount of steam supplied to the feed before entering the reactor at 0% v.

Product efficiencies vary noticeably for different conditions of severity used in function of residence time, above all during periods of over seven minutes. With an increase in residence time, the production of gases, gasolines and coke is increased and the production of barrel bottoms is reduced. Just as the influence of the change in severity in function of temperature, it is expected that the increase in severity will increase the production of gas-oils, for which the production of tar would be below that illustrated. With a residence time of 7 minutes, a change is observed in the slope of coke and tar production, which coincides with the change in slope of the stability index as well as residence time. With a residence time of 13 minutes, the system is totally unstable.

The resin/asphaltene ratio shows a slight tendency toward increase as residence time is increased. It would be expected that in this order, the stability of the system increase. Nevertheless, over ten minutes of residence time, the system is unstable possibly due to the abrupt reduction in viscosity or due to the great amount of gas-oil formed in the reaction, which by dilution destabilizes the colloidal system.

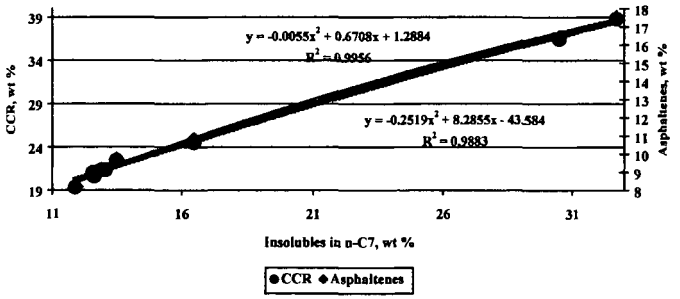

2.3 Severity in function of the percentage of steam.

For these tests, residence time (7 min.), the percentage of LCO (10% V) and temperature (763 °K) are kept constant.

This variable was kept in mind due to the fact that at the Barrancabermeja refinery, the steam is used to reduce the residence time inside the furnace.

It would be expected that by increasing the percentage of steam in the feed, the residence time would be reduced and therefore soften conversion. However, the opposite is observed. When the percentage of steam in the feed is increased, the gasoline production is increased considerably and tar production is reduced drastically. This is due to the fact that the steam helps to decrease the partial pressure of the heavy fragments, improving the distillation process, or perhaps it is a hydrogen donor in the different thermal reactions that take place inside the reactor. Within this explanation, it would be expected for coke production to be reduced, which does not occur in practice, possibly due to a change in the flow rate into two phases. It can also be observed that

the coke has a constant increase with the increase in the amount of steam and that its values are above 1% m, which is a high value and implies rapid oven coking. In spite of the fact that according to the Merit Test (figure 2) the system is within the limits of stability, a change is observed in slope for concentrations above 1% m. The quality of the visbroken tar goes through a process similar to that of the tar coming from the visbreaking of vacuum bottoms as can be seen in figure 4.

2.4 Evaluation of severity in function of the amount of LCO in the feed.

For these tests, residence time (7 min), temperature (763°K) and the amount of steam (0%) were kept constant.

Analyzing the parameters of severity in agreement with the titrations using Heithaus, it is observed that in these tests the temperature has more incidence on the stability of the visbroken star than on residence time.

To apply the corrected value of 6 instead of 0.3 on the stability threshold of Titration using Heithaus we find that the residence times of over 9 minutes give an unstable product which corresponds to two points of the interval analyzed.

In agreement with the Titration using Heithaus, values of over 12% m of LCO in the feed produce instability in the visbroken tar. The stable values in this product in agreement with the Merit Test indicate that up to 14% m of LCO in the feed is allowed. Nevertheless, this same test indicates that there is a change in slope at concentrations of 12% m, which corresponds to a value of 7 on the Merit Test. The point of the change in slope coincides with those registered for the influence of steam and residence time, which indicates that this type of feed should have not 7.5 but 7 as a control of stability on the Merit Test.

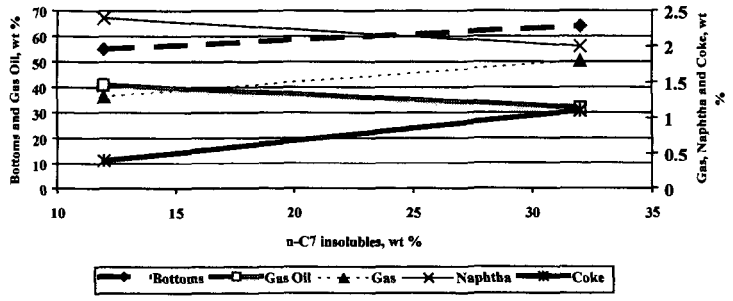

The crackability of feeds is a function of the amount of asphaltenes in it, expressed by means of the amount insoluble in C5 or C7. As this amount increases, the conversion decreases.

CONCLUSIONS

- The most important characteristic defined by cracking of a feed in visbreaking is the amount of asphaltenes it has. The higher the concentration of asphaltenes in the feed, the lower the crackability.

- For DEMEX barrel bottoms, in which the insoluble matter in nC7 are greater than 18% m, the variable that influences operational control most is temperature, which allows increases of up to 758°K reducing the production of visbroken tar by almost 4% m, the ΔVBN increases by 0.3 points and the coke increases by 22% m. At these conditions, the °API remains constant.

- With this same type of feeds, the steam as well as the ALC show similar behavior. It is recommended to use steam between 0.4 and 0.6%m, which means a reduction in tar production by 1% m and in increase in ΔVBN by 1 point and the °API by 0.4 points. Coke production is increased by 16%m. Above 0.6% m of steam, coke production can put the duration of the run at risk due to oven fouling.

- The ALC has a marked influence on the operation, which is why stricter control is recommended.

- For vacuum barrel bottoms, with concentrations of insoluble matter in nC7 below 18% m, the variable that allows the most control of severity is residence time, while for feeds with asphaltene concentrations of over 18% m, the variable that allows better control is temperature.

- The Merit Test as well as the Coking Index characterize visbreaking results well from the visbroken tar stability viewpoint, but not for the oven fouling, especially for feeds with over 18% m insoluble matter in nC7. Nevertheless, the Coking Index is more exact, which is why it is presented as a better tool for operational control.

Literature Cited:

CarrilloJ.A., Pantoja F., Barrios H., Estrada C., Alvarez N. And Chinchilla M. 1999. "Pressure control in vacuum towers". CT&F, Vol. 1 Núm. 5:25-34.

Savaya Z. F., Al-Soufi H.H., Al-Azawi I and Mohamed H.K. 1988. "The effect of Visbreaking conditions on the stability of some Iraqui Long Residues". Fuel Science and Technology INT'L., 6(3):354-366.

Maketta, Jhon and Cunnigham, William, 1982. "Encyclopedia of chemical processing and design", Ney York, Marcel Dekker

Kuo, C, J., 1984. "Effect of crude types on Visbreaking conversion". Oil & Gas Journal (Sept24):100-102.

Schabron J.F and Pauli A.T. 1999. "Coking Index using The Heithaus Titration and Asphaltene Solubility". American Chemical Society, National meeting and exposition program, Anaheim, C.A. (March 21-25): 187-193.

EFFECT OF VANADIUM POISONING AND VANADIUM PASSIVATION ON THE STRUCTURE AND PROPERTIES OF REHY ZEOLITE AND FCC CATALYST

Huai-Ping Wang*, Fang-Zhu Wang, and Wen-Ru Wu

State Key Laboratory of Heavy Oil Processing, University of Petroleum, Dongying 257061, CHINA

Keywords: REHY-zeolite, FCC-catalyst, passivator

INTRODUCTION

The effects of vanadium and nickel contaminants on the performance of cracking catalysts are well known [1,2]. These metals are deposited continuously on the catalyst during the cracking reaction and promote dehydrogenation reactions, which result in an increased formation of coke and light gases. Vanadium has an additional effect of reducing catalyst activity and selectivity by destroying zeolite crystallinity. Antimony passivation is widely practiced to control the effect of nickel poisoning [3], while vanadium poisoning is more difficult problem. Although much work has been done in the field, the exact mechanisms of the interaction of vanadium and zeolite and of the passivator for vanadium tolerance are still a matter of controversy [2,4-5]. However, application of a vanadium passivator in commercial FCC units also verified that a vanadium passivator can reduce the effect of the activity and the dehydrogenation by 30-50% and 65%, respectively [6].

Until recently, the vanadium passivation processes discussed extensively in the literature [7-9] involved addition onto the FCC catalyst of many different passivators, including rare earth metal oxides and alkali-earth metal oxides. These vanadium passivators can react with vanadium acid or V_2O_5, forming stable high melting compounds in the FCCU regenerator, so that vanadium poisoning is reduced and the crystal structure of zeolite is well protected.

In this paper, the mechanism of vanadium poisoning and vanadium passivation is proposed. The crystal structure of zeolite and its activity were well correlated with cracking activity.

EXPERIMENTAL

Catalyst Preparation and Evaluation

The RHZ-300 type cracking catalyst used in this work is a commercial heavy oil FCC catalyst composed of more than 30% REHY zeolite imbedded in 65-70% SiO_2-Al_2O_3-Kaolin matrix. The RHZ-300 catalyst and REHY (rare earth HY) zeolite were supplied by the Catalyst Factory of Qilu Petrochemical Company, Zibo, Shandong, China.

The vanadium poisoning of cracking catalyst procedure is used to impregnate RHZ-300 catalysts to the desired vanadium level with ammonium metavanadate solutions of different concentrations. The RHZ-300 catalysts contained 6000 ppm vanadium were then impregnated respectively with an acetate (such as lanthanum, magnesium, calcium, and so on) at various mole ratios of the passivator metal element to vanadium. After drying for 24 h at120• and calcination at 550°C for 4 h in air, the metal-loaded catalysts were aged at 760°C for 6h in 100% steam. The catalysts without vanadium passivators experienced the same procedure.

The catalyst's cracking activity was evaluated by a MAT test similar to one described by the RIPP-92-90 procedure [10] of The Research Institute of Petroleum Processing, China. The conditions of the MAT testing were 460°C for 70 s, catalyst-to-oil ratio = 3.2, WHSV (h-1) = 16,

*To whom correspondence should be addressed.

5.0 g catalyst, and the feedstock was a 1.56 g Dagang straight-run light diesel oil boiling range 230-350°C. The compositions of the products were analyzed using SQ-206 gas chromatography.

Catalyst Characterization

The relative crystallinity of the zeolite in the catalyst was obtained from the peak intensities of (533) plane of Y zeolite by XRD method with a Rigaku D/max IIIA X-ray diffractometer using Cu Kα radiation. The surface acid sites were characterized by NH_3-TPD-TG technique with a CAHN-200 thermal balance in the presence of a nitrogen atmosphere. The heating rate was 8°C /min. Analysis of the BET surface area and pore volume was measured by liquid nitrogen adsorption static state capacity method with an ASAP 2010 Multifunction Physisorption Instrument. Coke deposition on the catalyst was carried out in a micro fixed-bed reactor.

RESULTS AND DISCUSSION

The Effect of Vanadium Poisoning on the Cracking Activity and the Coke Formation of the RHZ-300.

The different effects of vanadium on the RHZ-300 cracking activity and coke formation are illustrated in Table 1. As shown in Table 1, microactivity monotonically decreased and the coke formation increased gradually with vanadium levels deposited on the catalyst. Little effect of MAT was observed up to 4000 ppm as vanadium, but above that amount, the activity decreased markedly with vanadium. Particularly, the coke formation on the catalyst was high when the deposition of vanadium reached 6000 ppm, a result consistent with the findings in the literature [11]. It is well known that the deposited vanadium reduces catalyst activity and selectivity and has catalytic activity towards dehydrogenation after aging at hydrothermal conditions, so that the dehydrogenation increases with vanadium levels, leading to an increase in the coke formation and a decrease in selectivity.

TABLE. 1. Microactivity and coke formation vs vanadium deposition on the catalyst.

$V/\times10^3$ppm	0	2	4	6	8	10
MAT/wt%	80.40	76.12	72.01	54.32	51.47	31.53
Coke yield/wt%	0.54	0.61	0.72	0.96	1.35	1.72

Vanadium Passivator Study

The effectiveness of one and two active constituent passivators prepared by loading on RHZ-300 individuality and mixture of rare earth oxides and alkali-earth oxides is shown in Table 2. As shown in Table 2, all active constituents are effective for vanadium passivation. However, vanadium passivation of performance of any one and two active constituent passivators was inferior to that of the pure lanthanum type. The vanadium passivator with a rare earth as the active constituent has an advantage over others in microactivity of RHZ-300, but the vanadium passivator with alkali-earth oxides as the active constituent greatly decreased the coke yields of RHZ-300. The phenomenon is primarly that the rare earth is weaker than alkali-earth oxide in neutralizing strong acidic sites of the catalyst, but greatly improves vanadium tolerance, whereas alkali-earth oxides easily neutralize excessively acidic sites, including weak acid sites and middle strong acid sites, owing to having strong basicity, leading to difference in activity and selectivity of RHZ-300.

TABLE 2 Vanadium passivation performance of the active constituents of passivators

Samples	Blank	La	Mg	Ca	La-Mg	La-Ca	La-Ce	La-Sr
MAT/wt%	54.32	72.88	67.34	64.46	69.87	67.56	71.74	67.76
Coke yield/wt%	0.96	0.75	0.53	0.56	0.65	0.67	0.73	0.69

The Effect of Vanadium Poisoning and Introduction of Passivator on the Structure and Microactivity of RHZ- 300

It is shown in Table 3 that after poisoning of the RHZ-300 catalyst by vanadium, the crystallinity of the REHY zeolite in the catalyst decreased from 10.5 % to 4.7%, a 55.2% reduction. Similarly, the BET surface area and pore volume of catalyst decreased respectively 55.3% and 7.8 %. This could indicate that the crystal structure of REHY zeolite in RHZ-300 was severely destroyed. Zeolite is often the cracking activity center of an FCC catalyst, and the activity drop could certainly be due to the destruction of zeolite structure. The reaction data from the MAT cracking testing (Table 3) verified that the microactivity of catalysts decreased from 80.4% to 54.32 %, while the coke formation increased from 0.80% to 0.96 %, as compared before and after poisoning with vanadium. These results agree with the conclusion made by Occelli et al [2]. The addition of passivator could prevent vanadium from poisoning the activity and selectivity of a FCC catalyst, so that the physicochemical and catalytic properties of RHZ-300 improved markedly, and the crystal structure of zeolite was recovered partially.

TABLE 3. Crystal Structure and Activity of Three Samples as Measured by Surface Area (BET), Pore Volume, XRD, Coke Formation, and Microactivity after Calcination at 550• and Hydrothermal Treatment at 760°C

Sample	RHZ-300	RHZ-300+V	RHZ-300+V+Passivator
MAT/wt%	80.4	54.32	75.60
Coke yield/wt%	0.80	0.96	0.65
BET S.A /$m^2.g^{-1}$	135.7	60.6	130.9
Pore volume/$cm^3.g^{-1}$	0.192	0.177	0.182
Crystallinity/%	9.7	4.7	7.2

Effect of Vanadium Poisoning and Introduction of Passivator on the Acidity of and Catalyst

Amounts of desorbed NH_3 were determined with the NH_3-TPD-TD method. The data of Table 4 show that total acidity of catalyst decreased from 2.21 to 1.08 after vanadium poisoning, indicating that over 50% of acid sites were destroyed. The distribution of acid intensity also indicated that acid sites destroyed were primarily weak acid sites and middle strong acid sites, over 65% of acid sites were destroyed whereas the middle strong acid sites have middle intensity adsorption, offer primary acid sites of catalytic activity. Cracking catalytic activity decreased greatly with the amounts of middle strong acid sites. In contrast, the amounts of strong acid sites increased from 0.37 to 0.45, so that the selectivity to coke formation could have an adverse effect (Table 4), since the coke is formed on the strong acid sites by polymerization of the unsaturated hydrocarbon molecules. The introduction of passivator (La_2O_3) can protect some of the acid sites leading to an increase in the number of acid sites of catalyst.

TABLE 4: Effect of Introduction of Vanadium and Passivator on Acidity of FCC Catalyst after Calcination at 550°C and Hydrothermal Treatment at 760°C

Sample	Acid sites (Desorbed NH_3 Amounts / $mmol.g^{-1}$ Cat.)			
	Weak acid sites	Middle strong acid sites	Strong acid sites	Total acid sites
RHZ-300	1.29	0.55	0.37	2.21
RHZ-300+V	0.45	0.18	0.45	1.08
RHZ-300+V+La_2O_3	0.94	0.55	0.38	1.87

Mechanism of Vanadium Poisoning and Passivation

In order to investigate interaction of zeolite and vanadium, steam-aging (at 760°C) experiments of REHY zeolite (with and without vanadium) were carried out in a flowing tube reactor. Fig. 1a shows the XRD pattern of REHY zeolite without vanadium; the crystal structure of zeolite is

completely retained without loss of crystallinity. Fig. 1c shows XRD pattern of the 2% vanadium-loading REHY zeolite. As evidenced by Fig. 1c, the zeolite completely loses crystallinity after vanadium poisoning, as the zeolite structure collapses with the formation of mullite ($Al_6Si_2O_{13}$), silica (tridymite) and rare earth vanadate ($CeVO_4$). The X-ray diffractograms for RHZ-300 catalysts with vanadium in the presence of steam at 760°C for 6 h are shown in Fig. 2a. It is very similar to the vanadium-loading REHY zeolite structure collapse with the formation of mullite. The above results and literature [2] suggest that the vanadium first deposits on the outside of the zeolite and catalyst particles, then migrates to pores, channels, or cages of the zeolite and catalyst and reaches acid sites during steaming at high temperature, where besides neutralized acid sites vanadium is trapped as cationic VO_2^+ species poisoning the catalyst according to the following reactions:

$$V_2O_5 + 2H^+\text{-}Y = 2VO_2^+\text{-}Y + H_2O \qquad [1]$$
$$VO_2^+\text{-}Y + 2H_2O = H^+\text{-}Y + H_3VO_4 \qquad [2]$$

Vanadic acid is a strong acid, P_K= 0.05 [20]. It behaves as a catalyst in the hydrolysis of the framework Al-O and Si-O tetrahedra and contributes to the accelerated destruction of the zeolites, causing zeolite de-alumination and lattice collapse with total loss of catalytic activity. The amorphous product recrystallizes then into mullite and the excess silica forms tridymite (Figs. 1c, 2a, 2b).

In REHY crystals it is believed that Ce^{4+} ions, present as an oxycerium complex, is preferentially loaded near the supercages, where it can more readily react with the stable oxyvanadyl cations (VO_2^+ or VO^{2+}) and form $CeVO_4$ (Fig. 4c).

The deleterious effects of vanadium deposits on zeolite-containing FCC can be greatly reduced by addition of certain materials (vanadium passivators) capable of minimizing V-FCC interactions by selectively (and irreversibly) sorbing migrating vanadium compounds such as H_3VO_4 (Figs. 1b, 2b). Since vanadic acid is not consumed as a catalyst in the hydrolysis reaction of framework. When a basic species exists in this system, it will compete with the zeolite for vanadic acid to form stable orthovanadates. The rare earth oxides such as La_2O_3 and alkali-earth metal such as MgO have basicity and react with vanadic acid to form orthovanadates, which are stable even at the highest temperatures reached in the regenerator unit.

Fig. 3 shows DTA thermograms of La_2O_3, V_2O_5, and the mixture of La_2O_3 and V_2O_5. There is a strong endothermic peak at 668°C in Fig. 3b, indicating the melting of V_2O_5. The strong exothermic peak at 670°C in Fig. 3c is probably an indication that a new compound is formed from the reaction of La_2O_3 and V_2O_5 as the melting point of V_2O_5 was reached. The XRD pattern (Fig. 4) verified the above observation that $LaVO_4$ indeed formed via the reaction, exhibiting the vanadium passivation by La_2O_3.

The DTA thermograms of MgO and V_2O_5 are shown Fig. 5, which were similar to Fig. 3. A strong exothermic reaction between MgO and V_2O_5 occurred at 670°C, and the reaction product characterized by XRD was MgV_2O_6 and $Mg_2V_2O_7$ (Fig. 6).

CONCLUSIONS

This study shows that when vanadium is deposited on a REHY zeolite and a RHZ-300 catalyst, the surface area, pore volume, crystallinity, acidity, and cracking activity of the vanadium-loading catalyst decrease with vanadium levels after aging at hydrothermal condiotion. In addition, vanadium forms a volatile vanadic acid during steaming at high temperature, which then catalyzes the hydrolysis of the framework Al-O and Si-O tetrahedra causing the collapse of the zeolite structure with the formation of mullite ($Al_6Si_2O_{13}$), silica (tridymite) and rare earth vanadate ($CeVO_4$). The activity and acidity of catalyst is completely lost at the same time. In contrast, the deleterious effects of vanadium deposits on zeolite-containing FCC catalyst can be greatly reduced by addition of certain vanadium passivators. The rare earth oxides and alkali-earth metal oxides are efficient passivators because they trap vanadium in form of vanadates, which are stable high melting compounds. Vanadium passivation reduces the

hydrolysis of zeolite framework, preserves the crystal structure of zeolites and acidity of FCC catalysts, and enhances the activity and selectivity of FCC catalyst. The optimum La/V mole ratio among the vanadium and La impregated catalysts (0.75) was obtained at the highest microactivity (72.88 wt%).

REFERENCES

1. Ritter, R. E., Rheaume, L., Welsh,W. A.,and Magee, J. S., Oil & Gas J.,103 (July 6,1981).
2. Occelli ,M. L., Catal. Rev. Sci. Eng., 33, 241 (1991).
3. McKay, D.L., Hydrocarbon Process, 97 (1987).
4. Pine, L. A., J .Catal.125,514(1990).
5. Trujilo, C. A., Uribe, U. N., Knops-Gerrits., et al., J. Catal.1, 186 (1997).
6. Barlow, R . C., et al., "NPRA Annual Meeting, 1986" AM-86-57.
7. Feron, B., Gallezot, P., and Bourgogne, M., J. Catal. 134, 469 (1992).
8. Chao, K. J., Lin, L. H., and Ling, Y. C., Appl. Catal. 121, 217 (1995).
9. Wormsbecher, R. F., Peters, A.W., and Maselli, J. M., J. Catal.100, 130 (1986).
10. Cuiding, Yang., et al., The Methods of Petroleum Processing, Science Press, Beijing, 1990.
11. Boock, L.T., Petti, T. F., and Rudesill, J. A., Preprints, ACS Div. Petrol. Chem., 40, 421, (1995).
12. Pope, M. T., in "Comprehensive Coordination Chemistry" (G. Wilkinson, Ed). Vol.3, p. 1026, Pergamon. Oxford.1987.

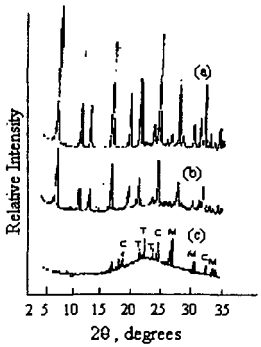

Fig. 1 X-ray diffractograms of REHY crystals steam-aged: (a) REHY, (b) REHY + 2%V + Passivator, (c) REHY + 2%V
M-Mullite ($Al_6Si_2O_{13}$), T-Sillica (tridymite)
C-Cerium vanadate ($CeVO_4$)

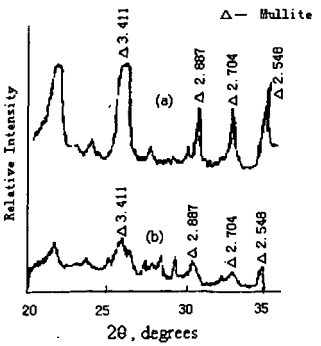

Fig. 2 X-ray diffractograms of catalysts with or without V-passivator: (a) no passivator, (b)passivator added

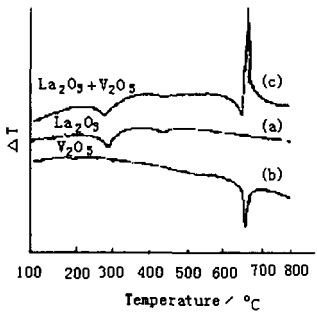

Fig. 3 DTA thermograms of La_2O_3, V_2O_5 and mixture of La_2O_3+V_2O_5 = 1 (mole ratio)

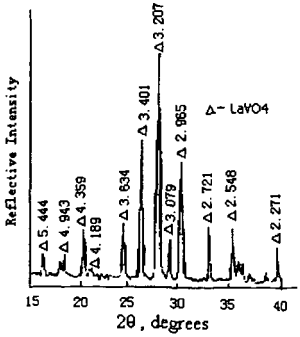

Fig. 4 X-ray diffractogram of the reaction product of La_2O_3 with V_2O_5

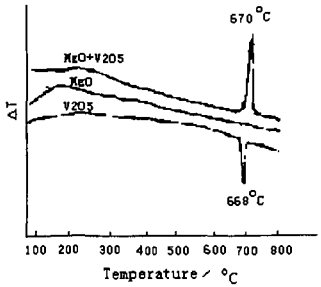

Fig. 5 DAT thermograms of MgO, V_2O_5 and mixture of $MgO/V_2O_5 = 1$ (mole ratio)

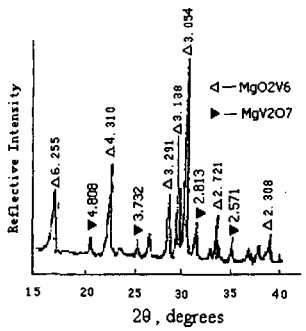

Fig. 6 X-ray diffractogram of the reaction product of MgO with V_2O_5

MOLECULAR DESIGN OF USY ZEOLITES USED FOR THE FCC PROCESS*

Xin-Mei Lui, Zi-Feng Yan**, Ling Qian, and Chun-Min Song

State Key Laboratory for Heavy Oil processing, University of Petroleum, Dongying 257062, CHINA

ABSTRACT USY zeolites, ultrastablized in hydrothermal treatment, were further modified by orthogonal design method with tartaric acid in an unbuffered system. The crystal structure, surface area and pore distribution, B acid sites and L acid sites, stability, and the activity for catalytic cracking of the modified samples were characterized by XRD, N_2 adsorption, FT-IR, DTA, and MAT. The research shows that the Si/Al ratio and the relative crystallinity of modified samples are both reasonably increased. Moreover, the pore system is developed further and the secondary mesopores are significantly greater than in the parent zeolites. The study has also shown that modified zeolites are preferable to deep cracking catalyst for producing lighter olefins and diesel oil with good yield and selectivity.

Keywords: USY; modification; tartaric acid; Si/Al ratio; pore distribution; activity; selectivity; lighter olefins

INTRODUCTION

Catalytic cracking process has been one of major techniques for lightening heavy oil. It not only plays an important role in petroleum refining, but also it is one focus that people pay close attention to. The success of the catalytic cracking is mostly attributed to the development or modification of the catalyst. With the cracking gasoline octane number boost, environmental concerns and deeper conversion of residual and heavy oils, especially the employment of reformulated gasoline, and the requirement for lower carbon olefins is dramatically increased. It is an effective way to produce much lighter olefins by further modification of zeolites existing in mordent FCC industry. Simultaneously, it is useful to the research of the design or modification of the catalyst structure.

Our efforts have been devoted to strengthening of the acidity and expanding of the mesopore of the USY zeolite by extraction of aluminum with tartaric acid whose negative ions has great complexing ability for Al^+. The negative ions and proton ions act in concert to Al-O band, which can achieve the de-alumination from the framework of the zeolites. The samples were prepared by orthogonal design (OD). The crystal structure parameter, physical adsorption property, stability, catalytic property of the modification zeolites was researched systematically by XRD, N_2 adsorption, FT-IR, DTA and MAT. The weight factors of effecting on the modification USY zeolites and optimum amount of each factor were explored.

EXPERIMENTAL

Materials and instruments

The parent USY zeolites were provided by Zhoucun Catalyst Company with the Si/AI ratio of 8.3, the unit cell constant of 24.528 Å and the relative crystallinity of 68.2%. Its crystal lattice was basically complete in the unbuffered acid system with the pH value above 2.0.
Type 79-1 magnetic heating agitator was purchased from Zhongda Instrument Plant in Jiangsu.

* This program is financially supported by Natural Science Foundation of Shandong Province.

** To whom correspondence should be addressed

Sample Preparation

A series of modified USY samples were synthesized by sol-gel method according to a L_4^5 orthogonal design table, in which the strong interactions among the parameters, such as addition volume of tartaric acid, solvent pH value, solvent volume and temperature were practically considered. The modified zeolite was washed by the distilled water to pH = 7, then filtered and dried for 14 hours at the temperature of 200°C.

Characterization of the Samples

The Si/Al ratio, unit cell constant, and relative crystallinity of the modified zeolite were determined by XRD with a Ricoh D/Max-IIIA X-Ray diffractometer using Cu Kα radiation. The pure NaY zeolite was used as calibration material. The Si /Al ratio was estimated from angles of 31~32 (2θ) XRD peaks.

The temperature of zeolite structure collapse was determined by DTA, with a CDR-1 DTA instrument of Shanghai Balance Instrument Plant.

The surface area and pore size distribution of modified samples were monitored by N_2 adsorption with a Macromectics ASAP 2010 unit.

Activity for catalytic cracking of Shenghua heavy oil (343°C-515°C) was carried out at 823 K near atmospheric pressure in a fixed-bed stainless steel reactor. The catalyst, which consists of 30% modified zeolites and 70% pretreated kaolin, was heated at 1073 K in a flow of water vapor for 4 h prior to introducing into reactor. The gaseous products were analyzed by HP-5890II gas chromatography equipped with a FID and a 50 m fused silicon capillary column. The liquid part was identified from simulated distribution on a HP-5880A with a FID and a 508mm fused UCW-982 column.

The number of acid sites was determined by FT-IR.

RESULTS AND DISCUSSION

The relation of the weight factors

The L_4^5 OD table is employed to find out the optimum synthesis conditions and investigate the interactions among factors. The SiO_2/Al_2O_3 ratio, mesopore (20 ~ 80 Å) volume and micro-activity are used to evaluate the performance of the modified USY zeolites. It is found that the order of the weight factors for above parameters employed is tartaric acid volume > pH value > solvent volume > temperature > reaction time.

The crystal parameters

The results of XRD show that the Si/Al ratio of the modified samples is obviously increased compared to the parent zeolites because the crystal unit cell content dramatically decreased, as observed in Table 1. This means that nearly only Al is extracted and therefore the skeletal Si/Al ratio is increased. The extracted Al dissolves in diluted de-alumination reagent solution and only partially remains in the zeolites. Owing to the stereo effect of the de-alumination acid, the frameworks Al is first depleted in the surface or subsurface and subsequently dissolves in solution. A similar transformation has been observed as a consequence of $(NH_4)_2SiF_6$ used for the treatment of a NaY zeolite [1]. Here, the higher relative crystallinity value of the de-alumination samples when compared to the parent zeolite may suggest that part of the framework be rebuilt. It can also be attributed to some changes in the physico-chemical properties (Si/Al ratio and extraction of the non-framework aluminum), which may influence the relative intensities of the X-ray diffraction peaks in the characteristic region of 2θ [2]. In addition, we also observed that when the relative crystallinity reaches the maximum, the content of crystal silicon of zeolite sample will amount to the maximum too, but the largest Si/Al ratio may not be obtained at this moment. This indicates that there is a portion of non-framework silicon existing in the zeolite. Furthermore, with the increase of silicon to aluminum ratio and decrease of crystal unit cell, the thermal stability of the modified zeolites is improved. This has been confirmed by the results of DTA. According to the OD results, it is postulated that the optimum modification conditions could be that the tartaric acid volume is 40 ml, pH value of solution is 1, the solvent volume is 40 ml, and the reaction time is 4 h.

Pore distribution

We always hope that the active component of FCC catalyst should possess structure with developed secondary mesopore. On the one hand, the larger reactant molecules may enter the pore channels of zeolite. On the other hand, it can decrease the molecular diffusion resistance to the zeolite cages. Thus the speed of the molecular diffusion is faster than the chemical reaction speed in the pores, which makes the activity sites of the pore be effectively used and the activity of the catalyst increased. This results in the catalyst efficiency improved. Fig.1 shows that the pore distribution of modified samples displays remarkable variation as a result of the tartaric acid treatments. The amount of secondary mesopores is distinctly increased. This refers not only to the mesopore volume, but also to the content of mesopore (20 ~ 80 Å). It reveals that the de-alumination is accompanied by the formation of some skeletal vacancies or defects. This vacancy or defect can be replenished by non-framework Si to complete the substitution of Al with Si. It can also be used to enlarge the pore mouth to form secondary mesopore. The enlarging of the pore mouth is attributed to the connection among the framework vacancies or defects by the interruption points created by the extraction of aluminum. All this leads to an increase of the amount of the secondary mesopores. Here the secondary mesopore formation is superior to silicon substitution because of the less enough silicon sources. It is worth mentioning that the amount of micropores is also increased, moreover, the micropore volume is enlarged. This may be achieved not only from the rebuilding of the framework, which leads to the larger mesopore changing into several micropores, but also from the enlarging of existing micropore (such as hexagonal column cages) that can not be tested by nitrogen adsorption. The optimum pore diameter of USY zeolite for processing heavy or residual oil should be in 20 ~ 80 Å, because the average van der Waal radius of the molecule residual and heavy oil, is 25 Å. Thus, the pore of 20 ~ 80 Å might be employed to evaluate the OD performance. The superior OD conditions are deduced as follows: the tartaric acid volume is 20 ml, pH value of solution is 3, the solvent volume is 40 ml, the temperature is 363 K and the reaction time is 6 h.

Acid property

The active sites of catalytic cracking reaction are acid components of the zeolites. Catalytic acidity of USY zeolites is attributed to acidic aluminum sites in both framework structure and non-framework debris [3]. Thus the extraction of the aluminum either from framework or non-framework of the zeolites should decrease the number of acid sites. The results of FT-IR really prove that the number of acid sites of the modified samples is decreased with the increase of Si/Al ratio. The Bronsted acid lies in the 1540 $cm^{-1}$and Lewis acid is in 1450 cm^{-1}, which is accordance with the literature [4,5]. The results are shown in Fig. 2.

Activity and selectivity

The MAT data reveal considerable changes as a result of the tartaric acid treatments. The results are shown in Fig. 3and Fig. 4. From the above results, it can be seen that the modified USY samples possess the more reasonable pore system structure, the greater SiO_2/Al_2O_3 ratio, and better distributed aluminum, which leads to the selectivity of all kinds of object product improved. The acidity of USY zeolites governs their activity. So with the de-aluminating, the active sites are decreased. But with the increase of the secondary mesopores and the enlarging of average total pore openings, the activity sites are effectively used. Though the acid sites are decreased, the catalyst total activity is not dropped clearly; conversely, some catalyst's activity is improved. This change is exhibited by the conversion change as the results of Fig.3. Moreover, the extraction of aluminum results in the increase of acid strength, which restrains the inter-molecular hydrogen migration of hydrocarbon intermediates. So the selectivity to the $C^{=}_3$ ~ $C^{=}_6$ hydrocarbons in the gas is raised, however, due to the difference of the gas selectivity of each catalyst, the yield of the $C^{=}_3$ ~ $C^{=}_6$ hydrocarbons is less even if selectivity of some catalysts is greater. The deep conversion is a tendency for FCC process. It is controlled by accumulation of coke on catalyst surface not by activity of catalyst. Thus, the selectivity of the coke is the principal focus to which attention is paid. In order to prolong the catalyst life span and reduce the load of its regeneration, we always hope that the coke yield is as low as possible in the case of satisfying our need for the object products. Fortunately, our goal is achieved. The decrease of the coke has two reasons. One is the increase of the acid strength; this leads to the reduction of the speed of condensation reaction. The other is the decrease of the external

surface area; this cuts down the chances of the inter-molecular hydrogen migration reaction that can produce coke. According to the results, it is postulated that the optimum modification conditions are the same as the pore distribution conditions. Using this modified zeolites, the products distribution are as follows: the light oil yield is 69.4%, the coke yield is decreased from 3.73% to 3%, the selectivity and the yield of $C^{=}_{3}-C^{=}_{6}$ are respectively 51.7% and 15.53%.

CONCLUSIONS

The results indicate that it is a new effective method to modify USY zeolites with tartaric acid in the unbuffed system. In this way, the thermally more stable samples with higher SiO_2/Al_2O_3 ratio, higher relative crystallinity, more well developed secondary mesopore system can be prepared. These samples may be benefit to heavy oil and residual oil deeper cracking. Furthermore, lighter olefins with good yield and selectivity may be obtained in the FCC procedure.

References

[1] P. Xie, Y. Zh. Zhang, L.B. Zheng, CUI HUA XUE BAO, 1991, p.

[2] R. Le Van Mao, S. T. Le, D. Ohayon, F. Caillibot, L. Gelebart, and G. Denes, Zeolites, 1997, p.270.

[3] Xiaolin Yang and Ralph E. Truitt, Zeolites, 1996, p.249.

[4] R. Beaunmont and D. Barthomeuf, J. Catal., 1972, p.218.

[5] G. T. Kerr, R. J. Mikovsky, U.S. Patent, 3,493,519 (1970).

Table 1. The crystal structure parameters of zeolites

Experiment order	Si/Al ratio	relative crystallinity C_{RX}%	crystal unit cell param. a_o/Å	content of crystal silicon S
1	10.2	64	24.463	157.6
2	10.1	65	24.466	159.7
3	10.4	66	24.460	162.7
4	10.6	67	24.455	165.8
5	11.6	68	24.435	170.4
6	11.6	67	24.435	167.9
7	12.6	68	24.419	172.1
8	10.4	69	24.461	170.1
9	12.9	68	24.415	175.1
10	12.8	66	24.416	167.4
11	10.8	77	24.451	191.1
12	11.0	74	24.448	184.0
13	11.9	75	24.431	188.4
14	12.2	77	24.427	194.0
15	11.9	72	24.431	180.9
16	12.2	77	24.426	194.1
Parent sample	8.3	68	24.528	161.0

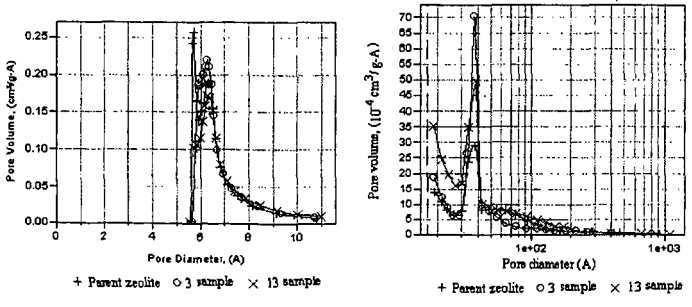

Fig.1 Profile of the pore size distribution of modification samples

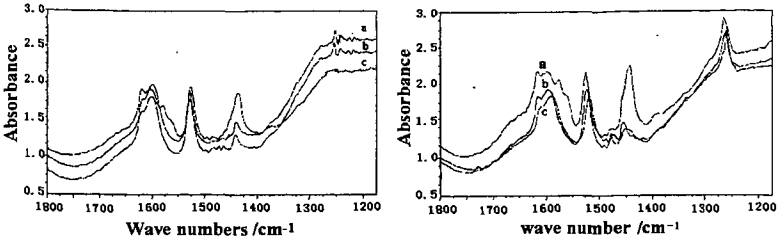

Fig.2. Profile of the acid site of modification samples. a---423K; b----523K; c-----623K

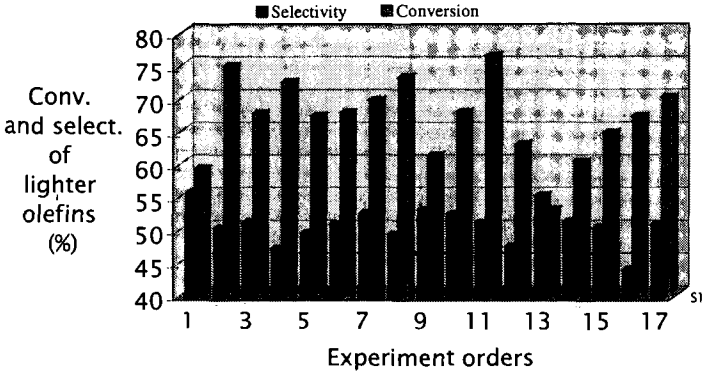

Fig.3 Profile of the conversion and selectivity of $C^{=}_{3}$-$C^{=}_{6}$

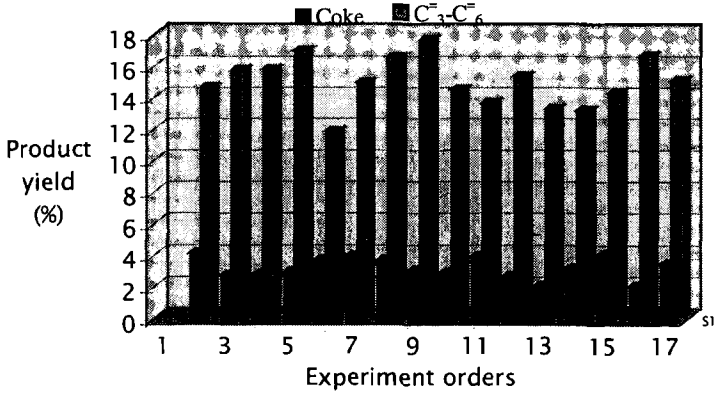

Fig.4 Profile of the product yield

EXTRACTING NUCLEAR ENERGY FROM HEAVY WATER WITH THE AID OF ELECTROCHEMISTRY

Andrew C. Angus,
Absolute Foundation,
2117 Wendover Lane, San Jose, California 95121, U.S.A.,
E-mail: andrewangus@yahoo.com.

KEYWORDS: heavy water, electrochemistry, low-energy fusion

INTRODUCTION

Heavy water, chemically known as **deuterium oxide**, is usually used as a moderator in nuclear reactors. However, two chemists, Stanley Pons and Martin Fleischmann, reported excess heat four times the energy output by electrolysing heavy water with the use of Palladium and Platinum electrodes and Lithium Deuteroxide as electrolytes. They believed that nuclear fusion occurred in their experiments. (Pons and Fleischmann, Ref.#3)

Did the two chemists made a mistake in their experiments? Or did Ernest Rutherford made a mistake in his theory of thermo-nuclear fusion reaction? Should experiments fit into a conventional theory? Or should theory fit experimental results?

What are the principles underlying nuclear fusion at low temperature?

In this paper, the author explains the theoretical foundations of nuclear fusion at low temperature with the aid of electricity and the new models of nuclear fusion.

METHOD

Electrolysis

The electrolysis of heavy water will yield two deuterium ions (D^+1) and oxygen ions (O^-2). Electrolysis is an endothermic reaction. About 118 kilojoules of energy must be supplied to form one gram of hydrogen. (Masterton p.97)

$$\text{Electricity} + \quad D2O \rightarrow (2D+) + O\text{-}2 \qquad \text{eq.1}$$

RESULTS

Electrochemical Reactions

The following are electrochemical reactions that occur in the Platinum anode and Palladium cathode in the Pons-Fleischmann experiment using the electrolyte Lithium Deuteroxide:

1. Deuterium Oxide (D2O)

$$\text{Anode} : O^{-2} \rightarrow O + 2e^- \qquad \text{eq.2}$$
$$\text{Cathode:} \ 2(D^{+1}) + 2(e^-) \rightarrow D^*2 \qquad \text{eq.3}$$

2. Lithium Deuteroxide (LiOD)

$$\text{Anode} : (OD^-) \rightarrow O + (D) + 1e^- \qquad \text{eq.4}$$
$$\text{Cathode:} \ (Li^{+1}) + e^- \rightarrow Li \qquad \text{eq.5}$$

3. Lithium Deuteroxide (LiOD) and Deuterium Oxide (D2O)

$$\text{Anode:} \ O\text{-}2 + (OD^-) \rightarrow 2O + D + 3e^- \qquad \text{eq.6}$$
$$\text{Cathode:} \ 2(D^{+1}) + (Li^{+1}) + 3(e^-) \rightarrow D^*2 + Li \qquad \text{eq.7}$$

Note: D*2 refers to a diatomic deuterium molecule.

Pons and Fleischmann reported excess heat energy four times the energy output. (Pons and Fleischmann, Ref#3) How is nuclear fusion possible in the Palladium cathode at low temperature/low energy?

DISCUSSION

A. What is the most important factor involved in Low-Energy Fusion?

In **muon-catalyzed nuclear fusion,** the muon (which is more massive than the electron) replaces the electron and induces the fusion of two nuclei. (Steven Jones, Ref. #2). In **electron-catalyzed nuclear fusion,** the electron must have an effective mass which will induce the fusion of two nuclei. (Barbara Levi, Reference #4)

K Capture is an important nuclear process which involves the increase of electron mass. Hence, K Capture is an essential process in electron-catalyzed nuclear fusion. K Capture, therefore, is the most important factor involved in Low-Energy Fusion.

B. What is K Capture?

K Capture *is the nuclear process whereby the nucleus absorbs its electron in the K Shell,* the nearest energy shell. (Weber p. 868)

C. When does K Capture occur?

Conventional theory states that heat induces K Capture. The author gives an alternative theory whereby electricity induces K Capture.

The author theorizes that K Capture occurs when electricity increases the mass of electron in the K shell at a critical level that the binding energy (hf) needed in maintaining the massive electron in the K shell is not sufficient anymore. Consequently, the repulsive force barrier of the nucleus collapses and the electron is absorbed by the nuclear proton forming a new neutron or, **neo-neutron** (n-1) to differentiate it from the old neutron in the nucleus. Meanwhile, if deuterium undergoes K Capture, the by-product is called **di-neutron** (n-2) which is simply a fused neutron pair.

D. How does K Capture occur?

Let us use Hydrogen as our example. The energy that prevents the absorption of electron by the nucleus is the binding energy of the photon (hf) possessed by the atom. If the Hydrogen atom is treated with electricity, the electron mass will increase in direct proportion to the current amperage and time. The resulting electron that increased in mass is called a **superelectron** or **heavy electron.** As the electron's mass increases, the atom's binding energy (hf) needed in maintaining the heavy electron at the K shell is not sufficient anymore since the kinetic energy of the heavy electron has increased due to an increase of electron mass. The kinetic energy (1/2 mv^2) of the heavy electron has become greater than the atom's binding energy (hf). At a certain critical electronic energy (qV) and critical mass (m) of the electron, the atom's repulsive force will collapse and the heavy electron will be absorbed by the nuclear proton to form a new neutron or **neo-neutron** (n-1). When the nucleus absorbs the heavy electron, the binding energy (hf) will be emitted by the nucleus.

E. An example of K Capture Equation

The reaction-equation of the K Capture of Deuterium is as follows:

$$3MeV + D \longrightarrow n\text{-}2 \qquad \text{eq. 9}$$

Legend: D stands for deuterium, n-2 stands for dineutron particle.

F. What are the Laws of K Capture?

The author formulates mathematical equations called the Laws of K Capture to explain the mechanism of K Capture as induced by electricity.

i). First Law of K Capture: The new electron mass (m) is equal to amperage (I) multiplied by time (t), then, multiplied by J.J. Thomson's ratio (k) of electronic mass to electronic charge (q).

$$I \times t \times k = m. \qquad \text{eq. 10}$$
$$q \times k = m \qquad \text{eq. 11}$$

The first Law of K Capture was derived as follows:

$m \alpha I$ eq. 12
$m \alpha t$ eq. 13
$m \alpha It$ eq. 14
$m / It = constant$ eq. 15
$It = q$ eq. 16
$m / q = constant$ eq. 17
$m / q = k$ eq. 18
$q \times k = m$ (eq. 11)

The first Law of K Capture is called the **Law of Electron Mass Accretion**.

ii). Second Law of K Capture: The net kinetic energy of the absorbed electron is equal to the electronic energy (qV) minus the energy (W) needed to overcome the repulsive energy barrier of the nucleus.

Net K.E. (absorbed electron) = qV– W eq. 19

The Second Law of K Capture is called the **Law of Electronuclear Effect.**

iii). Third Law of K Capture: The net kinetic energy of the absorbed electron is transferred to the new neutron formed. Thus, the net kinetic energy of the new neutron is equal to the net energy of the absorbed electron.

Net K.E.(neo neutron) = Net K.E.(absorbed electron) eq. 20

iv). Fourth Law of K Capture: The net kinetic energy of the neo-neutron formed is equal to the electronic energy (qV) minus the energy (W) needed to overcome the repulsion barrier. From eqs. 12 and 13, we derive:

Net K.E. (neo neutron) = q V – W. eq. 21

v). Fifth Law of K Capture

Now, the following condition show when K Capture will occur or will not occur.

i). If qV = W, then K Capture will not occur. eq. 22
ii), If qV < W, then K Capture will not occur. eq. 23
iii). If qV >W, then K Capture will occur. eq. 24

The author introduced the Laws of K Capture in a paper presented in an international conference in Sta. Fe, New Mexico, U.S.A. (See Reference #1.)

G. What are electro-nuclear fusion models?

K Capture can be used to explain and unify the diverse unconventional results obtained in deuterium-related experiments by Steven Jones, Stanley Pons, Martin Fleischmann, Japanese scientists Yoshiaki Arata and Yue-Chang Zhang, etc.

Let us now introduce the new models of nuclear fusion. These are **K Capture-based nuclear reactions** called **electro-nuclear reactions** to differentiate it from Rutherford's thermo-nuclear reaction models of nuclear fusion:

a.) 3 MeV (electricity) + D*2 → n-2 + D → H-4 → T + n + 6.2 MeV eq. 25
b.) 3 MeV (electricity) + D*3 → n-2 + D2 → He-6 → 2T + 12.4 M eV eq. 26
c.) 3 MeV (electricity) + D*3 → n-2 + D2 → He-6 → He-4 + n-2 + 25 MeV eq. 27
d.) 3 MeV (electricity) + D*3 → n-2 + D2 → He-6 → He-3 + 3n + 4.15 MeV eq. 28

Note the following: **Eq. 9** shows that neutrons are formed but no excess nuclear energy is produced, thereby, explaining the negative energy result in the experiments of **Steven Jones.** (See Ref.#2) Eqs.18 shows that Tritium and neutrons are formed and nuclear energy is produced. **Eq. 26** shows that the energy output is four times the energy input which is exactly reported by **Stanley Pons and Martin Fleischmann** in March 1989. (See Ref. #3.) **Eqs. 27 & 28** show that Helium-4 and Helium-3 and excess energy are produced which explain the experiments of **Yoshiaki Arata and Yue-Chang Zhang.** (See Ref. #5)

H. What about the conventional thermo-nuclear fusion models?

The conventional thermo-nuclear reaction models of nuclear fusion of Ernest Rutherford cannot unify and explain the diverse experimental results of Steven Jones, Stanley Pons, Martin Fleischmann, Yoshiaki Arata and Yue-Chang Zhang.

Perhaps, we have to say good-bye to the following thermo-nuclear fusion reactions:

$D + D \rightarrow T + p + 4.03\ MeV$	eq. 29
$D + D \rightarrow He\text{-}3 + n + 3.27\ MeV$	eq. 30
$D + T \rightarrow He\text{-}4 + n + 17.59\ MeV$	eq. 31

I. Why is Plasmic State - Hot Fusion unsustainable?

Plasmic State - Hot Fusion Theory is feasible but not sustainable in accordance to the following argument:

a. Let us review the **Ideal Gas Law** which is well-known to chemists and physicists alike (equation 32) :

$$PV = nRT \qquad \text{eq. 32}$$

b. Let us derive "concentration density" from the Ideal Gas Law. How?

Let us define **concentration density** as the number of moles of an element per unit volume. We use the symbols C or n/V for concentration density.

$n / V = P / R\,T$	eq. 33
$C = n / V$	eq. 34
$C = P / RT$	eq. 35

R is the Rydberg Constant,
P is Pressure,
T is temperature,
n is the number of moles,
V is the Volume.

c. Equation 34 and 35 are called the **Laws of Concentration Density** which is one of the underlying principles of the Low-Temperature Nuclear Fusion Theory or Low-Energy Nuclear Fusion Theory.

d. High Concentration density is more achievable for hydrogen in a gaseous state in a solid state medium rather than hydrogen in a plasmic state confined in a magnetic bottle.

e. Plasmic state- Hot Fusion Theory is a **physical violation** of Equations 34 and 35. Plasmic state- Hot Fusion Theory can never achieve a sustainable nuclear fusion because the high temperature of a plasmic state induces a very low concentration density. Consequently, the probability of nuclear fusion is very low.

Consequently, the physics world must accept the Low-Temperature Nuclear Fusion Theory or Low-Energy Nuclear Fusion Theory.

CONCLUSION

The controversial claims of chemists Stanley Pons and Martin Fleischmann that they achieved nuclear fusion at low temperature in the historic year 1989 is clearly justified on the basis of new models of nuclear fusion called electro-nuclear reactions. Hence, physicists and chemists must welcome the theory of low energy - nuclear fusion and the new electro-nuclear reaction models of nuclear fusion.

We have to say good-bye to Rutherford's thermo-nuclear reaction models of nuclear fusion since the energy input, energy output, reactants and by-products observed in deuterium-related experiments do not commensurate if we use Rutherford's thermo-nuclear reaction models of nuclear fusion.

Indeed, heavy water is a good source of nuclear energy with the help of electrochemistry. Eventually, mankind is assured of a cheap, limitless and clean source of energy.

REFERENCE

1. Angus, Andrew (1999). "Mathematical Model of K Capture and Its Implications", paper presented as poster in the *10th International Symposium on Capture Gamma Ray and Spectroscopy* in Sta. Fe, New Mexico, U.S.A. last August 30-September 3, 1999.

2. Jones, S., Palmer, E.P. et. al. (1989). "Observation of Cold Nuclear Fusion in Condensed Matter. In: *Nature*, Vol **338**, April 27, 1989, pp. 737-740.

3. Fleischmann, M. and S. Pons. (1989). "Electrochemically Induced Nuclear Fusion of Deuterium". In: *J. Electroanalytical Chemistry*. **261.**

4. Levi, Barbara (1989). "Doubts Grow as Many Attempts at Cold Fusion Fail". In: *Physics Today*, June 19, 1989. p.19.

5. Arata, Y. and Y-C Zhang (1997). "Helium (He-4, He-3) Within Deuterated Pd-Black". In: *Proc Japan Acad.* Ser. B, 1997, 73.

6. Masterton, W. , Slowinski, Emil J. and Stanitski, C. (1985). *Chemical Principles,* 6th Edition. USA: Saunders College Publishing.

7. Weber, R., Manning, K., White, M. and George Weygand (1977). *College Physics*, 5th ed., New York: McGrawHill Book Co.,. P. 868.

CHEMICAL BONDING OF NEW ALLOTROPES OF HYDROGEN AND ITS IMPLICATIONS TO FUEL SCIENCE

Andrew C. Angus
Absolute Foundation
2117 Wendover Lane, San Jose, CA 95121, U.S.A.
angusandrew@yahoo.com

KEY WORDS: chemical bond, polyatomic allotropes of hydrogen, nuclear fusion

INTRODUCTION

The author predicts that polyatomic allotropes of hydrogen such as triatomic deuterium (D*3) and quadratomic deuterium (D*4) are formed inside the core of the sun.

The theoretical existence of triatomic deuterium molecules and other polyatomic allotropes of hydrogen in general is necessary in order to account nuclear fusion in the sun.

The theoretical existence of triatomic deuterium molecules and polyatomic allotropes of hydrogen if confirmed experimentally is important in fuel science since polyatomic allotropes of hydrogen increase the probability of nuclear fusion by virtue of their close distance to one another.

This paper explains the chemical bonding of *triatomic* and *quadratomic deuterium atoms* which can be applied to polyatomic hydrogen atoms in general.

MODELS OF CHEMICAL BONDS

1. Lewis Model of Chemical Bond

G. N. Lewis, an American physical chemist was the first to suggest that a **chemical bond** is composed of an "**electron pair**". (Masterton, p. 267)

The **Lewis model of chemical bond** in molecules or between atoms shows an electronic structure of a molecule or ion in which electrons are shown by dots or dashes (electron pairs). The Lewis model of chemical bonds does not show the actual physical models of the atoms. For example, the Lewis model of a diatomic hydrogen is *illustrated as:* $H : H$ *or* $H\text{-}H$.

The Lewis model of chemical bond does not explain the possible existence of triatomic molecule of hydrogen or polyatomic allotropes of hydrogen in general.

2. Angus Model of Chemical Bond

The author proposes a chemical bond called "**single electron sharing**" between two atoms to explain the theoretical existence of a triatomic deuterium molecule, quadratomic deuterium molecule and higher polyatomic hydrogen molecules. This bond that is based on a "single electron sharing" is called "**mono-electron bond**" or "**alpha bond**". Hydrogen bonds between water molecule is a good example of an alpha bond or mono-electron bond.

Chemists failed to realize that the hydrogen bonding in water molecules and protein molecules could probably involve a "single electron sharing" bond.

The author coins the term "***di-electron bond***" *as a synonymous term to Lewis' chemical* bond of "**pair electron sharing**". The sigma bond is a good example of a "di-electron bond".

The "**quadri-electron bond**" is a "four-electron sharing" bond such as the chemical bond in an Oxygen diatomic molecule. The "quadri-electron bond" is synonymous to the "double bond".

The "**hexa-electron bond**" is a "six-electron sharing" bond such as the chemical bond in a Nitrogen diatomic molecule. The "hexa-electron bond" is synonymous to the "triple bond".

ILLUSTRATIONS

The author gives the illustrations of the allotropes of Hydrogen namely, **monatomic** hydrogen, **diatomic** hydrogen, **triatomic** hydrogen and **quadratomic** hydrogen:

1. Monatomic Hydrogen (H)

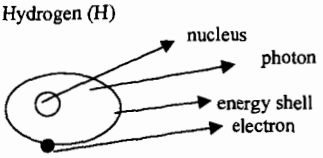

Monatomic Protium

Monatomic Deuterium

2. Diatomic Hydrogen (H*2)

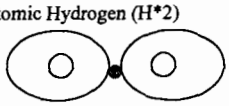

i).. **alpha bond**: single electron sharing

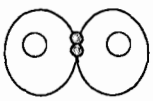

ii). **sigma bond**: pair electron sharing

3. Triatomic Hydrogen (H*3)

i). Chain structure of a triatomic protium molecule (H*3) and triatomic deuterium molecule (D*3).

2 alpha bonds in H*3 ion

2 alpha bonds in D*3 ion

ii). Ring structure of a triatomic protium molecule (H*3) and triatomic deuterium molecule (D*3).

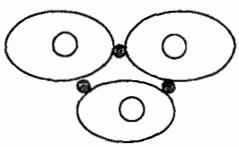

3 alpha bonds in H*3 molecule

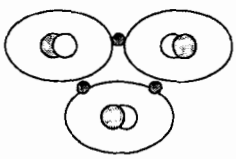

3 alpha bonds in D*3 molecule

4. Quadratomic Hydrogen (H*4)

i). Chain structure of a quadratomic protium molecule (H*4) and quadratomic deuterium molecule (D*4)

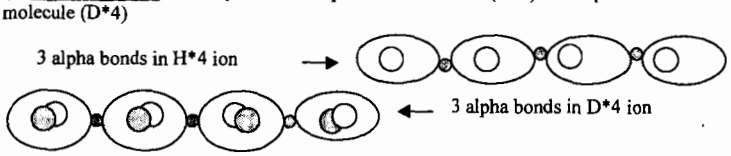

ii). Ring structure of a quadratomic protium molecule (H*4) and quadratomic deuterium molecule (D*4)

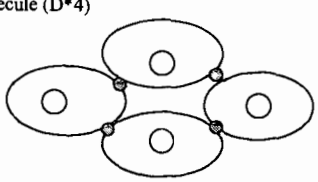

4 alpha bonds in H*4 molecule

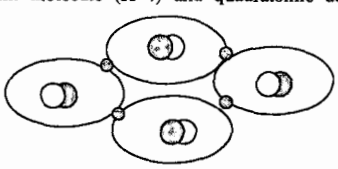

4 alpha bonds in D*4 molecule

DISCUSSION

A. Angus Model of an Atom

1. **Description.** The **Angus Model of the Atom** depicts atoms that looks like a "biological cell" with a central nucleus. The nucleus is surrounded by a quantum of energy or photon. The electron is at the surface of the photon. The **atom's energy realm** refers to the total area or volume occupied by the photon in an atom. The periphery of the photon is called the **atom's energy shell.** (See Illustration #1)

2. **Energy Barrier.** The electron cannot penetrate the nucleus because of the **photon energy barrier (hf).** The photon energy barrier (hf) is equal to the force (F) between the proton and the electron multiplied by the radius (r) distance between the nucleus and the electron.

$$F \times r = hf \qquad \text{eq.1}$$

3. **Photon Force.** The new model of the atom proposes that the force (F) between proton and electron is exerted through the medium of a photon energy (hf) that binds the electron and the nucleus at a certain distance (r). The force exerted by the proton on the electron through an photon energy medium is called a **photon force.**

$$hf / r = F \qquad \text{eq.2}$$

B. Angus Model of Chemical Bond

The Lewis Model of chemical bond of a **"pair electron sharing"** cannot account the new allotropes of Hydrogen namely the triatomic deuterium molecule (D*3) and the quadratomic deuterium molecule (D*4). The author's theory of chemical bond of **"single electron sharing"** called "alpha bond or mono-electron bond" can account the existence of new polyatomic allotropes of Hydrogen (such as D*3, D*4, D*5, etc.).

The concept of a "single electron sharing" of a diatomic hydrogen molecule was discussed thcoretically in physics textbook . (Kenneth Krane, p. 360-364.) But the author did not use it to explain the possible existence of polyatomic allotropes of hydrogen molecules/ions. Furthermore, the author claimed that the attractive force of the electron **is greater** than the repulsive force exerted by the protons on the electron. (Krane p.360)

I believe: If the electron's attractive force is greater than the repulsive force of the two protons (as claimed by Krane p.360), then the two protons will fuse towards the electron. Therefore, physicist's analysis of a "single electron sharing" between two atoms would make a mono-electron bond an unstable bond.

Is a mono-electron bond (or alpha bond) stable or unstable? I offer an alternative analysis of a "single electron sharing bond". The two protons are both attracted to the single electron. The attractive force of this single electron shared by two protons **is equal** to the two protons' repulsive force exerted on the electron. The electron maintains its distance equally to the two protons. The electron stays in the middle of the two protons. The electron is not absorbed by the two protons. Thus, a mono-electron bond is stable.

attractive force of electron on proton = $(1/4\pi\varepsilon)[e^2/(R)^2]$ eq. 3
attractive force of electron on 2 protons = $2(1/4\pi\varepsilon)[e^2/(R)^2]$ eq.4
repulsive force of proton on electron = $(1/4\pi\varepsilon)[e^2/(R)^2]$ eq.5
repulsive force of 2 protons on electron = $2(1/4\pi\varepsilon)[e^2/(R)^2]$ eq.6
attractive force of e- on two protons = repulsive force of two protons on e- eq.7
$2(1/4\pi\varepsilon)[e^2/(R)^2] = 2(1/4\pi\varepsilon)[e^2/(R)^2]$ eq.8

In Illustration #2, it can be gleaned that a diatomic hydrogen can either have an alpha bond (mono-electron bond) or a sigma bond (di-electron bond).

In the Illustration #3 (triatomic hydrogen) and #4 (quadratomic hydrogen), it can be gleaned that polyatomic allotropes of hydrogen in general can either have a chain structure or a ring structure.

In Illustration #3, triatomic deuterium has two alpha bonds since the K shell of deuterium can carry a maximum of two electrons. Instead of deuterium sharing the two electrons to one atom, deuterium is sharing one electron to each of the two atoms.

The nature of hydrogen bonding is a mystery to chemists. The author theorizes that hydrogen bonding occurs in water molecules when oxygen atom "share a single electron" to a neighboring hydrogen atom bonded to another oxygen atom.

C. Source of Polyatomic Hydrogen

I predict that triatomic deuterium (D*3) and quadratomic deuterium (D*4) and other polyatomic deuterium molecules exists in the sun. I believe that triatomic, quadratomic allotropes of hydrogen or polyatomic hydrogen atoms in general are the main fuel of the sun.

The sun has a high density 1.5 x 10^5 kg/m^3 about 13 times the density of lead, a high central pressure (approximately 2 x 10^11 atmosphere) and a central temperature of 1.5 x 10^7 Kelvin. (Halliday p. 1317)

The high pressure due to the gravitational pressure or the electromagnetic pressure in the sun could be the major factor in creating polyatomic hydrogen atoms such as triatomic deuterium (D*3), quadratomic deuterium (D*4), pentatomic deuterium (D*5), etc.

$$D + D + D + D + \text{pressure} + \text{electricity} \rightarrow D^*4 \qquad \text{eq. 9}$$

If nuclear fusion reactions occur in the sun, then hydrogen atoms must be close to each other as in a "chain of polyatomic hydrogen atoms" or a "ring of polyatomic hydrogen atoms". Nuclear fusion reactions would be difficult to occur if hydrogen atoms exist as monatomic atoms. Thus, to facilitate nuclear fusion, polyatomic hydrogen must exist in the sun since polyatomic allotropes of hydrogen consists of hydrogen atoms that are very close to each other.

The high density of the sun is probably due to helium atoms and polyatomic allotropes of hydrogen. Monatomic hydrogen atoms tend to be far apart when heated to extreme high temperatures. An abundance of monoatomic hydrogen atoms will create a low-density sun. An abundance of polyatomic allotropes of hydrogen will help in creating high-density sun.

D. Energy Mechanism of the Sun

Hans Bethe made a theory explaining the energy mechanism of the sun based on thermonuclear model of nuclear fusion whereby heat initiated nuclear fusion.

However, I believe Bethe's Theory cannot be totally correct for the following arguments: 1). Extreme heat will encourage the formation of monatomic hydrogen ions rather than triatomic and polyatomic allotropes of hydrogen atoms. 2). Monatomic hydrogen ions are so far apart that the probability of nuclear fusion will be greatly decreased. 3). Pure monatomic hydrogen atoms will create a low-density sun. 4). Nuclear reactions can occur in proto-stars or actual stars even at low energy or low temperature (as will be explained in the next paragraph).

An alternative energy mechanism of the sun (without resorting to high temperature) involves high pressure to create polyatomic allotropes of hydrogen and electricity applied on these polyatomic allotropes of hydrogen as follows:

Phase 1

$H + \text{pressure} + \text{electricity} \rightarrow n\text{-}1$ (K Capture of Hydrogen) eq.10

$H + H + \text{pressure} + \text{electricity} \rightarrow H^*2$ eq.11

$H^*2 + \text{pressure} + \text{electricity} \rightarrow n\text{-}1 + H \rightarrow D + 2.22\ \text{MeV}$ eq.12

Phase 2

$D + \text{pressure} + \text{electricity} \rightarrow n\text{-}2$ (K Capture of Deuterium) eq.13

$D + D + D + \text{pressure} + \text{electricity} \rightarrow D^*3$ eq.14

$D^*2 + \text{pressure} + \text{electricity} \rightarrow n\text{-}2 + D \rightarrow \mathbf{H\text{-}4} \rightarrow T + n + 6.2\ \text{MeV}$ eq.15

$D^*3 + \text{pressure} + \text{electricity} \rightarrow n\text{-}2 + D^*2 \rightarrow \text{He-}6 \rightarrow 2T + 12.4\ \text{MeV}$ eq.16

$D^*3 + \text{pressure} + \text{electricity} \rightarrow n\text{-}2 + D^*2 \rightarrow \text{He-}6 \rightarrow \text{He-}3 + 3n + 4.15\ \text{MeV}$ eq.17

$D^*3 + \text{pressure} + \text{electricity} \rightarrow n\text{-}2 + D^*2 \rightarrow \text{He-}6 \rightarrow \text{He-}4 + n\text{-}2 + 25\ \text{MeV}$ eq.18

(Note: **Protium** is defined as a proton with an orbiting electron. **Hydrogen** is defined as an element with a single proton. Protium (H), Deuterium (D), Tritium (T), Quadrium (Q) are the four isotopes of Hydrogen. **Quadrium (H-4 or Q)** occurs in the reaction in equation 15.)

K Capture is a nuclear process that involves the absorption of orbital electron in the K Shell. K Capture is a key factor in overcoming repulsive energy barrier of atoms at low temperature with the help of electricity. The process of K Capture with the help of electricity

converts Protium (H) into neutron (n-1) as shown in eq. 10. The process also converts Deuterium atom (D) into a di-neutron (n-2) as shown in eq. 13. (Angus 1999)

K Capture as induced by electricity is represented by the mathematical equation 19 called **Law of Electro-nuclear Effect** (Angus 1999):

$$\text{Net K.E. of electron} = qV - W \qquad \text{eq.19}$$

Meanwhile, the high pressure (Pb) in the sun will force the atoms to get closer to each other. Then, electrcity (qV) can increase the effective mass of orbital electron to produce neutrons or di-neutrons that will induce nuclear fusion of deuterium atoms. The repulsive energy barrier of the atoms can be overcome by the following equation whereby the orbital electron is subjected to the pressure (Pb) and the electricity (qV) in the sun:

$$\text{Net K.E. of electron} = (Pb + qV) - W \qquad \text{eq.20}$$

P is the pressure, b is the volume of the electron, q is the electronic charge, V is the voltage and W is the energy needed to overcome the repulsive energy of the atom.

Equation 20 is called the **Law of Piezo-electro-nuclear Effect** which explains K Capture as induced by pressure and electricity. This Law explains K Capture as a key factor in the energy mechanism of the sun or proto-suns at low energy or low temperature.

We can simulate the energy mechanism of the sun here on earth by creating polyatomic allotropes of hydrogen with the aid of electricity and pressure, then subjecting the polyatomic allotropes of hydrogen to further pressure and electricity to induce nuclear fusion or nuclear transmutations.

The extreme heat of the sun is most likely a by-product of the nuclear fusion reactions in the sun rather than heat as an initiating mechanism of nuclear fusion reaction.

CONCLUSION

The existence of triatomic deuterium molecule or polyatomic allotropes of hydrogen in general is significant to fuel science because these polyatomic allotropes of hydrogen increase the probability of nuclear fusion and therefore, a sustainable production of nuclear energy through nuclear fusion will be available to mankind.

We have to invent the concept of "alpha bond" or "mono-electon bond" to account the theoretical existence of polyatomic allotropes of hydrogen and in order to account nuclear fusion reactions in the high-density sun. Nuclear fusion in the sun is not possible if only monoatomic atoms exist in the sun since monoatomic atoms are very far apart. There has to be polyatomic allotropes of hydrogen in the sun since polyatomic allotropes of hydrogen (D*3, D*4, D*5, etc.) increase the probability of nuclear fusion by virtue of the close distance of hydrogen atoms in a polyatomic structure.

Perhaps, we have to say good-bye to Hans Bethe's theory of energy mechanism of the sun and replace it by the author's new energy mechanism of the sun.

REFERENCE

1. Angus Andrew (1999). "A Mathematical Model of K Capture and Its Implications". Paper presented as poster in the *10th International Symposium on Capture Gamma Ray and Spectroscopy* in Sta. Fe, New Mexico, U.S.A. last August 30-September 3, 1999.

2. Krane, Kenneth (1983). "The Hydrogen Molecule Ion". In: *Modern Physics.* U.S.A.: John Wiley and Sons. pp. 360-364.

3. Krane, Kenneth (1983). "The Stellar Evolution". In: *Modern Physics.* U.S.A.: John Wiley and Sons. pp. 446-449.

4. Halliday, David and Resnick, Robert (1986). "Thermonuclear Fusion in the Sun and Other Stars". In: *Physics Part 2.* U.S.A.: John Wiley and Sons. pp.1317-1321.

5. Masterton, William L., Slowinski, Emil J., Stanitski C. (1985). *Chemical Principles.* 6th edition. U.S.A.: Saunders College Publishing. p.267